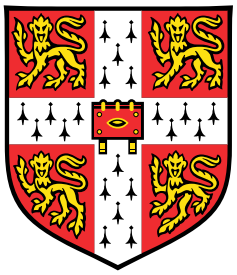

Investigating the effects of tau mutations in induced pluripotent stem cell-derived neurons

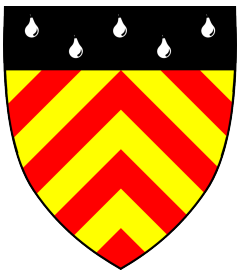

Janine Louise Ostick

Department of Clinical Neurosciences
University of Cambridge

This dissertation is submitted for the degree of
Doctor of Philosophy

Clare Hall

December 2018

I would like to dedicate this thesis to the memory of my dad, Grenville John Ostick.

Declaration

This dissertation is the result of my own work and includes nothing which is the outcome of work done in collaboration except as declared in the Preface and specified in the text. It is not substantially the same as any that I have submitted, or, is being concurrently submitted for a degree or diploma or other qualification at the University of Cambridge or any other University or similar institution except as declared in the Preface and specified in the text. I further state that no substantial part of my dissertation has already been submitted, or, is being concurrently submitted for any such degree, diploma or other qualification at the University of Cambridge or any other University or similar institution except as declared in the Preface and specified in the text. This dissertation contains fewer than 60,000 words excluding bibliography, figures, appendices and tables.

Janine Louise Ostick
December 2018

Acknowledgements

This PhD would not have been possible without my supervisor, Professor Maria Grazia Spillantini, who I would like to thank for the opportunity to work in her laboratory, for her multitude of ideas, for the responsibilities she gave me, and for teaching me the importance of a good mentor. My project was greatly enriched by my second supervisor, Dr Madeline Lancaster, who I would like to thank for her patience and for teaching me to make cerebral organoids. I am grateful to the MRC/Sackler Prize PhD programme which funded my PhD, travel to conferences, and a work placement, all of which expanded my horizons. I would also like to thank Yichen Shi of Axol Bioscience, for his generosity in allowing me to use the three isogenic iPSC lines described in Chapter 6.

I have been lucky to work with many former and present members of the Spillantini lab, and I would like to thank each of them for their invaluable scientific advice, their enthusiasm, and their friendliness. In particular, I would like to thank Dr Laura Calo for her endless patience whilst introducing me to basic laboratory techniques, guiding me - particularly during the first year of my PhD - and teaching me cell culture. My bench work was made possible by Dr Laura Calo, Dr Michal Wegrzynowicz, Dr. Maria Eugenia Herva Moyano, Dr Aviva Tolkovsky, and Dr Jack Brelstaff, who each helped me by answering my questions, discussing experiments with me, and by sharing their insights, knowledge and reagents. My cell culture work would not have been possible without Dr Aviva Tolkovsky, Dr Laura Calo, Dr Jessica Santiváñez Pérez, Dr Mariagrazia Paonessa and Joana Domingues, who each kindly kept my cell cultures alive when I could not. I would also like to thank Emma Carlson, Olga Sauchanka, and Mercy Danga, who helped everything run smoothly.

I am deeply grateful to my fellow PhD students Dr Jessica Santiváñez Pérez, who taught me the monolayer neuron culture techniques used in Chapters 3 and 4; Dr Mariagrazia Paonessa, who helped me screen iPSC clones following CRISPR; and Dr Sylvia Agathou, who guided Dr Laura Calo and I through our trials by iPSC-derived neuron. More importantly, I am grateful to each of them, and as well as Dr Mayen Briggs, Dr Antonella Poggiani, Maria Ajmone Marsan, and Joana Domingues, for their moral support and laughter in times of extreme stress and tissue culture.

Finally, I would like to thank my friends Samantha Conlon, Danny Boag and Jeffrey Shen, who distracted me from the frustration, exhaustion and loneliness of PhD life. I am especially grateful for the support and kindness of my partner Christoph Eigen, and for my family, Alexandra Ostick and Denise Ostick, for their kind, rational words. Without them, I would have given up by now.

Abstract

Investigating the effects of tau mutations in induced pluripotent stem cell-derived neurons

By Janine Louise Ostick

Microtubule-associated protein tau (MAPT) is a neuronal protein which promotes microtubule assembly and stabilisation. The MAPT gene is alternatively spliced to give six tau isoforms: three with 3 microtubule-binding repeats (3R, excluding exon 10) and three with 4 microtubule-binding repeats (4R, including exon 10). MAPT mutations cause the progressive, degenerative disorder fronto-temporal dementia with Parkinsonism linked to chromosome 17 (FTDP-17T), in which tau becomes abnormally phosphorylated and aggregates. FTDP-17T related MAPT mutations can either alter exon 10 splicing and the 3R:4R tau isoform ratio (such as N279K), or affect tau's biochemical properties (such as P301L and V337M).

In this project, I differentiated induced pluripotent stem cells (iPSCs) derived from control subjects and people with the N279K or V337M MAPT mutations to monolayer neurons. There was an increase in the proportion of neurons containing tau phosphorylated at the AT8 epitope in N279K cultures after 50 days, and more 4R tau was detected earlier in the N279K cultures than in controls, confirming the action of the N279K mutation. All monolayer neural cultures matured at similar rates in terms of synapse formation, neuronal marker expression and astrocyte production, and I did not detect other FTDP-17T-relevant phenotypes in MAPT-mutant cultures, perhaps due to the time points (50 and 80-100 days) at which I examined them.

To investigate the effects of the N279K mutation independent of iPSC line genetic background, I attempted to create isogenic iPSC lines using CRISPR. This was not successful, but I obtained isogenic control and P301L iPSCs from Axol Bioscience, from which, along with the patient-derived P301L MAPT-mutant iPSCs, I made cerebral organoids (COs). Similar amounts of neuronal, astrocyte, and synaptic proteins were detected in the control and MAPT-mutant COs, as were cortical layer markers indicating a forebrain-like fate.

Phosphorylation at the AT8 epitope was detected in the control and MAPT-mutant COs, as was tau misfolding, detected using the MC-1 antibody.

In conclusion, some alterations similar to those observed in FTDP-17T brains can be observed in monolayer iPSC-derived neurons and perhaps in iPSC-derived COs. However, some phenotypes may be masked by experimental variability which needs to be addressed in the future.

Table of contents

List of figures

List of tables

Abbreviations

2D 2 dimensional

3D 3 dimensional

0N No N-terminal inserts

1N 1 N-terminal insert

2N 2 N-terminal inserts

3R 3 repeat tau

4R 4 repeat tau

AA Ascorbic acid

ACE A/C rich splice enhancer

AD Alzheimer's disease

AGD Argyrophilic grain disease

AIS Axon initial segment

ANOVA Analysis of variance

AP Action potential

ASCL1 Achaete-scute homolog 1

ATP Adenosine triphosphate

BCA Bicinchoninic acid

BDNF Brain-derived neurotrophic factor

BiP Binding immunoglobulin protein

BMP Bone morphogenic protein

bp Base pairs

BPS Branch-point sequence

BSA Bovine serum albumin

C9ORF72 Chromosome 9, open reading frame 72

Cas9 CRISPR-associated protein 9

Cas9n Cas9 nickase

Cas9wt Cas9 wild-type

CBD Cortico-basal degeneration

CC Corpus callosum

CCK Cell culture kitchen

Cdk5 Cyclin-dependent kinase 5

ChAT Choline acetyltransferase

CHMP2B Charged mulitvesicular body protein 2b

CJD Creutzfeldt-Jakob disease

CNS Central nervous system

CO Cerebral organoid

Con6 non-isogenic control 6

CP Caudate putamen

CRISPR Clustered regularly-interspaced short palindromic repeats

crRNA CRISPR RNA

CTRL control

DAPI 4',6-diamidino-2-phenylindole

DAPT N-[N-(3,5-Difluorophenacetyl)-L-alanyl]-S-phenylglycine t-butyl ester

db-cAMP Dibutyl-cyclic adenosine monophosphate

dd Double-distilled

DM-1 Differentiation medium 1

DM-2 Differentiation medium 2

DM-3 Differentiation medium 3

DMEM Dulbecco's modified Eagle's medium

DMSO Dimethyl sulfoxide

DNA Deoxyribonucleic acid

DSB Double-stranded break

DSBR Double-stranded break repair

E8 Essential 8 medium

EB Embryoid body

EDTA Ethylenediaminetetraacetic acid

EEA1 Early Endosome Antigen 1

EGFP Enhanced green fluorescent protein

EPSC Excitatory post-synaptic current

ERK2 Extracellular signal-regulated kinase 2

ESE Exon splicing enhancer

(h) (m) ESC (human) (mouse) embryonic stem cell

ESS Exon splicing silencer

FACS Fluorescence-activated cell sorting

FBS Fetal bovine serum

FGF Fibroblast growth factor

FoxG1 Forkhead box protein G1

FTD Frontotemporal dementia

FTDP-17T Frontotemporal dementia with parkinsonism, linked to chromosome 17 and tau mutations

FTLD Frontotemporal lobar degeneration

FTLD-ni Frontotemporal lobar degeneration, no inclusions

FUS Fused in sarcoma

G3BP Ras GTPase-activating protein-binding protein 1

GABA Gamma-aminobutyric acid

GDNF Glial derived neurotrophic factor

GFAP Glial fibrillary acidic protein

GFP Green fluorescent protein

GGT Global glial tauopathy

GL Granule layer

gRNA guide RNA

GSK-3β Glycogen synthase kinase 3β

HC Hippocampus

HDR Homology-directed repair

HEK293 Human embryonic kidney cells

HR Homologous recombination

HRP Horseradish peroxidase

HSF Human splicing finder

IF Immunofluorescence

iN Induced neuron

Indel Insertion-deletion mutation

iPSC Induced pluripotent stem cell

ISM Intron splicing modulator

IsoCon isogenic control

ISS Intron splicing silencer

KANSL1 KAT8 regulatory NSL complex subunit 1

kDa kilodaltons

Klf4 Kruppel-like factor 4

KO Knock-out

KSR Knock-out serum replacement

LAMP-1 Lysosomal-associated membrane protein 1

LD Lysogeny broth

LDH Lactate dehydrogenase

LRM Laboratory of Regenerative Medicine

LTD Long-term depression

LTP Long-term potentiation

LVA Lateral ventricular area

MAP Microtubule associated protein

MAPT Microtubule associated protein tau

MEF Mouse embryonic fibroblast

mRNA messenger RNA

MSA Multi-system atrophy

MT Microtubule

NDM Neuronal differentiation medium

NEAA Non-essential amino acids

NEC Neuroepithelial cell

NeuroD1 Neurogenic differentiation 1

NF-M Neurofilament-medium

NFT Neurofibrillary tangle

Ngn2 Neurogenin 2

NHEJ Non-homologous end-joining

NI Neural induction medium

NIM Neuronal induction medium

NMR Nuclear magnetic resonance

NPC Neural precursor cell

NPM Neuronal proliferation medium

OCT Optimum cutting temperature

Oct4 Octamer-binding transcription factor 4

P301Lhet P301L heterozygous

P301Lhom P301L homozygous

P301Lpat P301L heterozygous, patient derived

PAM Protospacer-adjacent motif

Pax6 Paired box 6

PBS Phosphate buffer saline

PCR Polymerase chain reaction

PD Parkinson's disease

pen-strep Penicillin and streptomycin

PFA Paraformaldehyde

pFTAA Pentameric formyl thiophene acetic acid

PGRN Progranulin

PiD Pick's disease

P/L Poly-L-ornithine and laminin

PP1, PP2A, PP2B, PP5 Protein phosphatase 1, 2A, 2B, 5

PPE Polypurine enhancer

p-PERK Phosphorylated protein kinase RNA-like ER kinase

PPT Polypurine tract

PSC Pluripotent stem cell

PSD-95 Post-synaptic density protein 95

PSP Progressive supranuclear palsy

PUMA P53-upregulated modulator of apoptosis

RD Repeat domain

RIPA Radioimmunoprecipitation assay

RNA Ribonucleic acid

rpm Revolutions per minute

ROCK Rho-associated coiled-coil containing protein kinase

SatB2 Special AT-rich sequence-binding protein 2

SC35 SC35-like binding sequence

SD Standard deviation

SDS-PAGE Sodium dodecyl sulphate-polyacrylamide gel electrophoresis

SDSA Synthesis-dependent strand annealing

Ser Serine

SFEBq Serum-free floating culture of embryoid body-like aggregates with quick reaggregation

Shh Sonic hedgehog

shRNA Short hairpin RNA

SN Substantia nigra

SNP Single-nucleotide polymorphism

Sox2 Sex determining region Y box 2

SRp Serine/arginine-rich protein

ssDI Single-strand DNA incorporation

SSEA-4 Stage-specific embryonic antigen-4

ssODN Single-stranded DNA oligomer

STP Short-term plasticity

TALENs Transcription activator-like effector nuclease

Tbr1 T-box brain 1

Tbr2 T-box brain 2

TBS Tris-buffered saline

TBST Tris-buffered saline with Tween

TDP-43 TAR DNA binding protein 43

TGFβ1 Transforming growth factor β

Th Tyrosine hydroxylase

Thr Threonine

TIA-1 T-cell intracytoplasmic antigen 1

tracrRNA Transactivating CRISPR RNA

TRS Tandem repeat sequence

UPR Unfolded protein response

UPS Ubiquitin proteasome system

VCP Valosin containing protein

VTA Ventral tegmental area

VTN-N Truncated recombinant human vitronectin

WB Western blot

WT Wild-type

ZFN Zinc-finger nuclease

Chapter 1

Introduction

1.1 Tau in a normal brain

1.1.1 Isoforms and alternative splicing

Microtubule-Associated Protein Tau (MAPT) is encoded by the MAPT gene on chromosome 17q21 (Neve et al., 1986). Due to a 970kB inversion encompassing MAPT, there are two tau haplotypes (H1 and H2), in which MAPT lies in opposite orientations (Baker et al., 1999, Figure 1.1). MAPT encodes 16 exons: eight are constitutively expressed (1, 4, 5, 7, 9, 11, 12, 13) and three are alternatively spliced (2, 3 and 10). In the peripheral nervous system, inclusion of exons 4a, 2, 3 and 10 generates big tau, a 110 kDa protein expressed in peripheral neurons (Georgieff et al., 1993; Goedert et al., 1992).

In the central nervous system, alternative splicing of exons 2 and 3 results in the inclusion or exclusion of a 29 amino acid (exon 2) or 58 amino acid (exons 2 and 3) insert towards tau's N-terminus (Goedert et al., 1989a). Exon 10 inclusion adds a microtubule-binding repeat in addition to the three encoded by the constitutively expressed exons 9, 11 and 12 (Goedert et al., 1989b). The three tau isoforms lacking exon 10 have three microtubule-binding repeats and are known as 3 repeat (3R) tau, whilst the three isoforms including exon 10 have four microtubule-binding repeats and are known as 4 repeat (4R) tau. Alternative splicing of exons 2, 3 and 10 gives six tau isoforms: 0N3R, 0N4R, 1N3R, 1N4R, 2N3R and 2N4R (Goedert and Jakes, 1990a; Figure 1.1).

Tau isoform expression is developmentally regulated: only the shortest isoform (0N3R) is present in fetal brains, whereas all six isoforms are expressed post-natally (Goedert and Jakes, 1990; Goedert et al., 1989a,b). In a healthy adult human brain 3R and 4R tau are

present in a 1:1 ratio (Goedert and Jakes, 1990). 0N, 1N and 2N tau make up approximately 37%, 54% and 9% of total tau, respectively (Hong, 1998).

1.1.2 Structure

In a healthy brain, tau is a soluble protein with an unfolded structure (Mukrasch et al., 2009). The addition of N-terminal inserts encoded by exons 2 and 3 makes the N-terminal more acidic and negatively charged, whereas the proline-rich region, microtubule binding repeats and C-terminal regions have more basic residues and a net positive charge (Goedert et al., 1989a). The N-terminal is referred to as the projection domain (Steiner et al., 1990), because it projects away from microtubules when tau is bound to them (Hirokawa et al., 1988; Figure 1.1). The proline rich region, the microtubule binding repeats, and 10 downstream residues bind with negatively charged microtubules, so this region is known as the assembly domain (Sillen et al., 2007; Steiner et al., 1990).

Post-translational modifications

Tau is subject to many post-translational modifications, including acetylation, cleavage or truncation, glycation, glycosylation, nitration, oxidation, phosphorylation, polyamination, prolyl-isomerisation, sumoylation and ubiquitination (reviewed by Martin et al., 2011). Of these, phosphorylation is the most frequently occurring, and is discussed below.

The roles of these modifications in diseased and normal states are many and varied: some affect tau-microtubule interactions, and many have been implicated in tau accumulation during disease. For example, ubiquitination targets tau for degradation under normal conditions, but in disease states, tau filaments are thought to be ubiquitinated after they have been phosphorylated and glycated. Glycation is an age-related modification that may make tau more resistant to degradation, leading to tau accumulation, whereas phosphorylation alters tau's binding to microtubules (reviewed by Mietelska-Porowska et al., 2014).

Tau phosphorylation

Tau has 85 serine, threonine and tyrosine residues which are potential phosphorylation sites, although not all of them are phosphorylated: up to 16 phosphorylated residues have been found in control brains and 45 have been identified in brains from people with Alzheimer's disease (AD; reviewed by Hanger and Noble, 2011). However, Matsuo et al. (1994) report that adult human tau from rapidly analysed brain biopsy tissue is more highly phosphorylated

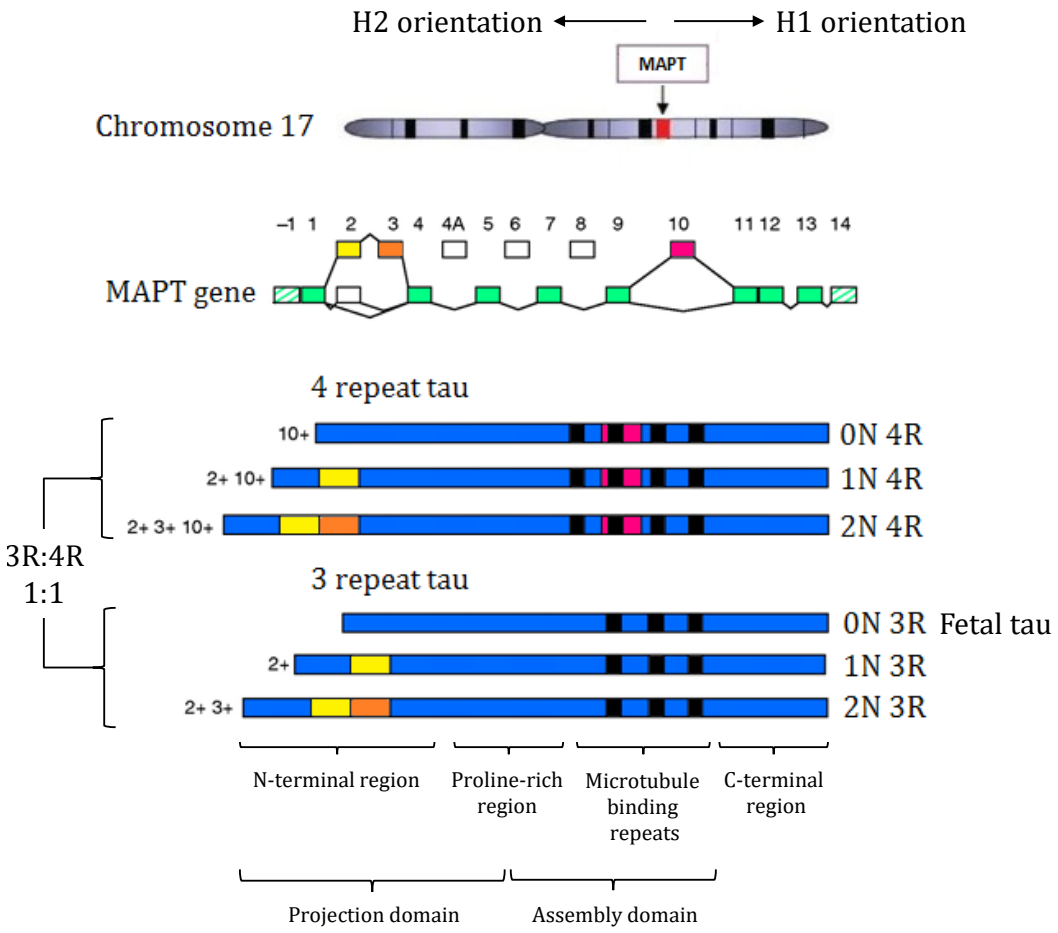

Fig. 1.1 **Tau gene expression and alternative splicing.** The position of microtubule-associated protein tau (MAPT) on chromosome 17 is shown in red and the orientations of a chromosomal region including tau are shown by arrows (H1 and H2). Green boxes represent constitutively expressed exons and green shaded boxes represent exons -1 and 14 which are transcribed but not translated. White boxes represent exons which are not included in tau central nervous system transcripts: exon 4a is expressed in the peripheral nervous system in big tau but exons 6 and 8 are not expressed in human tau proteins. Exons 2 (yellow), 3 (orange) and 10 (red) are alternatively spliced to give six tau isoforms. Exon 3 is not included in tau mRNA without exon 2. Inclusion of exon 10 gives three tau isoforms with 4 microtubule-binding repeats (4 repeat or 4R tau) and exclusion of exon 10 three tau isoforms with 3 microtubule-binding repeats (3 repeat or 3R tau). Alternative splicing of exons 2 and 3 adds N-terminal inserts (0N, 1N or 2N). Tau without exon 2, 3 or 10 is the fetal isoform, 0N3R, which also persists in the adult brain. The microtubule binding repeats interact with microtubules and (along with part of the proline-rich region) promote microtubule assembly (Sillen et al., 2007; Steiner et al., 1990). The N-terminal part of tau projects out when tau is bound to microtubules and is therefore named the projection domain. Diagram altered from Warren and Burn (2007).

than tau from post-mortem brain tissue, indicating that tau is dephosphorylated after death, which may make estimates of tau phosphorylation in the normal living brain inaccurate.

Tau phosphorylation is developmentally regulated: fetal 0N3R tau is heavily phosphorylated (Goedert and Jakes, 1990) at epitopes including AT8 (Brion et al., 1993; Matsuo et al., 1994; Milenkovic et al., 2018) and PHF-1 (Bramblett et al., 1993; Kenessey and Yen, 1993; Matsuo et al., 1994), which are also detected in brains from people with tauopathies (Table 1.1).

Tau phosphorylation and dephosphorylation are mediated by a balance of kinase and phosphatase activity. At least 24 kinases which phosphorylate tau have been identified (reviewed by Wang et al., 2012), including serine/threonine kinases, such as GSK-3β (Hanger et al., 1992) and tyrosine kinases, such as Fyn (Lee et al., 2004). At least four phosphatases which dephosphorylated tau have been identified, including the serine/threonine protein phosphatases PP1, PP2A, PP2B and PP5 (Wang et al., 2017). Kinases and phosphatases are implicated in tau phosphorylation in normal and disease states, and their activity can be altered by other post-translational modifications of tau, indicating a complex and highly regulated system (Wang et al., 2012).

1.1.3 Distribution

Tau is predominantly expressed in neuronal axons, where it binds to microtubules (Binder et al., 1985) and other cytoskeletal proteins including actin (Griffith and Pollard, 1982) and spectrin (Carlier et al., 1984), as well as motor proteins such as dynactin (Magnani et al., 2007) and kinesin, whose motility is modulated by competition with tau to bind microtubules (Dixit et al., 2008). Neuronal tau has also been detected bound to the plasma membrane via its N-terminus (Brandt et al., 1995), bound to ribosomes (Papasozomenos and Binder, 1987) and in nuclei (Loomis et al., 1990; Thurston et al., 1996).

Low levels of phosphorylated tau have been found in dendrites (Papasozomenos and Binder, 1987; Tashiro et al., 1997), where tau targets the tyrosine kinase Fyn to the post-synaptic density (Ittner et al., 2010). Both isoform-specific sorting and dendritic translation of tau mRNA have been shown to contribute to dendritic tau in mouse models (Kobayashi et al., 2017; Zempel et al., 2017), although it is not clear whether tau's presence in dendrites is linked to overexpression and disease (Ashe and Zahs, 2010).

In addition, tau has been detected in non-neuronal cells: at low levels in astrocytes (Papasozomenos and Binder, 1987) and in oligodendrocytes in some species (LoPresti et al.,

1995), where tau interacts with Fyn and may have a functional role in myelination (Klein et al., 2002). However, this is still debated (Ossola et al., 2016).

Area specific variations in tau expression across the brain have been reported. For example, a study of tau expression in five brain regions from 12 control brains found the most tau protein in the frontal cortex, with lower tau protein levels in the white matter, occipital cortex, putamen and cerebellum. Protein levels were correlated with total tau mRNA levels in these regions (Trabzuni et al., 2012). The same study found that tau isoform expression did not differ between the frontal cortex, white matter, occipital cortex or putamen, but found significantly less 0N3R tau in the cerebellum.

Other studies have found different patterns in tau isoform expression. For example, Majounie et al. (2013) examined brain samples from control and PSP subjects with H1/H1 or H1/H2 haplotypes and found higher 4R tau mRNA levels in the pons and cerebellum than the temporal and frontal cortices, regardless of haplotype and disease status. Tau protein levels in these brain areas were not quantified. In another study, Caffrey et al. (2006) measured the ratio of 4R to 3R tau mRNA transcripts in 14 control brains and found 1.3 to 3.5 times more 4R tau mRNA in the globus pallidus than the frontal cortex in 13 of the brains. However, whether the difference in mRNA transcript levels resulted in different protein expression levels was not assessed.

Differences in tau isoform distribution have also been detected at the cellular level. Goedert et al. (1989b) found both 3R and 4R mRNA in cerebral cortex pyramidal cells, but in the hippocampus 3R mRNA was present in both pyramidal and granule cells, whereas 4R mRNA was detected in most, though not all, pyramidal cells and not in granule cells. Since adult neurogenesis may occur in the dentate gyrus of the hippocampus where granule cells are located, the expression of 3R but not 4R tau may indicate the relative immaturity of newly-born neurons (Bullmann et al., 2007). Alternatively, this could indicate that tau mRNA (and possibly tau protein) is expressed in a cell-specific manner.

Tau is also released into the extracellular space and is detectable in cerebrospinal fluid from healthy individuals (reviewed by Blennow and Hampel, 2003). However, the release mechanism and role of extracellular tau is unclear (reviewed by Wang and Mandelkow, 2015).

Finally, tau expression has been reported in peripheral tissues including the heart, skeletal muscle, lung, kidney, and testis in rat (Ashman et al., 1992; Gu et al., 1996) and in the nuclei of cells including fibroblasts and lymphocytes (Loomis et al., 1990; Thurston et al., 1996).

1.1.4 Functions

Tau has many binding partners including microtubules, motor proteins, kinases, phosphatases, chaperones, and membrane proteins (reviewed by Wang and Mandelkow, 2015).

As a microtubule-associated protein (MAP), tau promotes the assembly of tubulin into microtubules (Weingarten et al., 1975) and decreases the rate of tubulin depolymerisation, thereby stabilising microtubules (Drubin and Kirschner, 1986) which form part of the cytoskeleton. Tau's microtubule binding is isoform- and phosphorylation-dependent, with phosphorylation decreasing tau's microtubule binding ability and as a consequence decreasing microtubule stability (Drechsel et al., 1992). Tau isoforms with three microtubule binding repeats have a lower affinity for microtubules than tau isoforms with four repeats (Dayanandan et al., 1999; Goedert and Jakes, 1990). The N-terminal inserts (which are part of tau's projection domain that does not bind to microtubules) may regulate the spacing of microtubules (Chen et al., 1992), or bind to the plasma membrane (Brandt et al., 1995).

The switch from highly phosphorylated 0N3R tau in fetal human brains to a 50:50 mix of less phosphorylated 3R and 4R isoforms in adult human brains suggests that modulating tau's function has an important developmental role. The low microtubule binding ability of phosphorylated fetal 0N3R tau may increase microtubule dynamics and allow the plasticity needed for the outgrowth and synaptic connection of neurons (Goode and Feinstein, 1994).

As part of the cytoskeleton, tau is involved in neurite and axon outgrowth (Black et al., 1996; Dawson et al., 2001; Liu et al., 1999) and neurite polarisation (Caceres and Kosik, 1990), as well as in axonal transport, in which motor proteins move cellular cargo along microtubules. Tau interacts with the motor protein dynein (Magnani et al., 2007) and modulates the motility of both dynein and kinesin by competing with them to bind microtubules (Dixit et al., 2008). In addition, tau binds to proteins with SH3 domains, such as Fyn (Lee et al., 2004), suggesting that tau may have a role in neuronal signalling (reviewed by Wang and Liu, 2008).

Tau has also been reported in the nucleus, where it may have a role in chromosome stability (Granic et al., 2010; Rossi et al., 2008) and DNA protection, since tau increases DNA melting temperatures *in vitro* (Hua and He, 2000) and protects against heat-induced DNA damage *in vivo* (Sultan et al., 2011).

1.2 Tau in disease

Tau aggregates in diseases known as tauopathies which include AD, corticobasal degeneration (CBD), chronic traumatic encephalopathy, Pick's disease (PiD), progressive supranuclear palsy (PSP), fronto-temporal dementia with Parkinsonism linked to chromosome 17 and tau mutations (FTDP-17T), and many others (Ghetti et al., 2015). Although tau pathology varies between tauopathies, there are some unifying features: in diseased brains, tau becomes hyperphosphorylated, insoluble and aggregated (reviewed by Spillantini and Goedert, 2013). The mechanism by which tau dysfunction results in tauopathies is still unknown.

1.2.1 FTDP-17T: fronto-temporal dementia with Parkinsonism linked to chromosome 17 and MAPT mutations

Mutations in MAPT cause the progressive, degenerative disorder FTDP-17T. FTDP-17 was defined at an international conference which discussed 13 familial dementias linked to chromosome 17q21-22 that shared symptoms, genetic linkage and some neuropathology (Foster et al., 1997). At the time, tau pathology had been described in brains from four of the families, but tau mutations were later discovered in nine of the 13 families, showing that MAPT mutations are sufficient to cause neurodegeneration (Hutton et al., 1998; Poorkaj et al., 1998; Spillantini et al., 1998b). The remaining four families had mutations in progranulin (PGRN) (Baker et al., 2006; Cruts et al., 2006), sub-dividing FTDP-17 into FTDP-17T (linked to MAPT mutations) and FTDP-17 GRN (linked to PGRN mutations).

1.2.2 Classification of FTDP-17T and other fronto-temporal dementias

FTDP-17T is defined by the presence of MAPT mutations, and is part of the wider group of fronto-temporal lobar degeneration (FTLD), which encompasses the clinical diagnoses of fronto-temporal dementia (FTD), progressive non-fluent aphasia, and semantic dementia (Neary et al., 1998).

FTLD can be divided into subtypes based on the protein aggregates present. Subtypes include FTLD-tau (tau positive inclusions), FTLD-TDP (TAR DNA binding protein-43 (TDP-43) and ubiquitin positive inclusions), FTLD-UPS (inclusions of ubiquitin proteasome system (UPS) proteins, which are TDP-43 negative), FTLD-FUS (fused in sarcoma (FUS) inclusions), and FTLD-ni (no inclusions) (Mackenzie et al., 2011, 2009).

Most occurrences of FTD are sporadic: only about 10-25% of cases have evidence of a dominantly inherited mutation (Rohrer et al., 2009; Seelaar et al., 2008). To date, mutations linked to FTLD have been found in *PGRN* (Baker et al., 2006; Cruts et al., 2006), valosin-containing protein (*VCP*) (Watts et al., 2004), charged multivesicular body protein 2b (*CHMP2B*) (Skibinski et al., 2005), *FUS* (Broustal et al., 2010), *TDP-43* (Synofzik et al., 2014), a hexanucleotide repeat in the intronic region of chromosome 9, open reading frame 72 (*C9ORF72*) (DeJesus-Hernandez et al., 2011; Renton et al., 2011) and MAPT (Hutton et al., 1998; Poorkaj et al., 1998; Spillantini et al., 1998c).

FTLD-tau

The FTLD-tau subtype includes PiD, CBD, PSP, argyrophilic grain disease (AGD), globular glial tauopathy (GGT) and neurofibrillary tangle predominant dementia (NFTPD) (Forrest et al., 2018; Mackenzie et al., 2009). FTLD-tau (sporadic, without MAPT mutations) and FTDP-17T (familial, with MAPT mutations) are often classified separately, even though FTLD-tau and FTDP-17T cases have similar disease durations, similar neuropathology, and can be classified into the FTLD-tau subtypes (Forrest et al., 2018). For example, MAPT mutations have been identified in people suffering from PSP, CBD and AGD (reviewed by Sieben et al., 2012). MAPT mutations account for 30-40% of FTLD-tau cases (Zempel and Mandelkow, 2014), and about 5% of FTD cases (Goedert, 2016).

Tau haplotype as a tauopathy risk factor

Although many tauopathy cases are sporadic, tau haplotype (the orientation of MAPT, Baker et al., 1999) is a genetic risk factor: being homozygous for the H1 haplotype is associated with sporadic PSP (Baker et al., 1999), CBD (Houlden et al., 2001), and Parkinson's disease (PD) (Pastor et al., 2000). The latter association is surprising since PD brains do not contain much tau (reviewed by Irwin et al., 2013). Association with the H1 haplotype could implicate genes other than MAPT which characterise the H1 and H2 haplotypes, including those for corticotropin releasing hormone receptor 1 and N-ethylmaleimide-sensitive factor (Stefansson et al., 2005). However, the presence of tau aggregates in PSP and CBD brains (Arai et al., 2001) suggests that tau may be the culprit.

The increased risk may be due to an increase in 4R tau mRNA from the H1 relative to the H2 haplotype, which has been shown in human brain (Caffrey et al., 2006) and human induced pluripotent stem cell (iPSC)-derived neurons (Beevers et al., 2017). However, Trabzuni et al. (2012) contend that observed differences in H1- and H2-specific tau mRNA expression

are artefacts, caused by qPCR problems. Specifically, these are preferential probe binding to H1 mRNA (from whose sequence the probes were designed) and decreased binding to H2 mRNA, due to H2-specific single-nucleotide polymorphisms and insertion-deletion mutations.

An alternative explanation is a protective effect of the H2 haplotype, which may increase tau exon 3 expression (Caffrey et al., 2008; Trabzuni et al., 2012). Inclusion of exon 3 in tau protein increases the minimal concentration needed to cause aggregation *in vitro* by 1.5-fold and decreases the extension rate of filaments (Zhong et al., 2012). By comparison, inclusion of exons 2 or 10 increase the filament extension rate and decrease the minimal tau concentration required for aggregation.

1.2.3 Symptoms of FTDP-17T

FTDP-17T symptoms vary between people with different mutations and even between individuals with the same mutation, suggesting the existence of other genetic or environmental influences (Foster et al., 1997). Most FTDP-17T patients exhibit at least two of the three main symptom groups, which are behaviour and personality changes, motor dysfunction, and cognitive impairment (reviewed by Ghetti et al., 2015). However, memory and visuospatial skills are usually somewhat preserved until very late stages of the disease (Neary et al., 1998).

1.2.4 Neuropathology of FTDP-17T

In FTDP-17T, the frontal and temporal lobes atrophy, and other brain areas can also be affected. These include the parietal cortex, caudate nucleus, entorhinal cortex, amygdala and hippocampus in the cerebrum; the substantia nigra and basal ganglia in the midbrain; parts of the pons, medulla and cerebellum; and the anterior horn of the spinal cord (reviewed by Ghetti et al., 2015; Figure 1.2). Neuronal loss in the substantia nigra and basal ganglia is consistently observed in N279K cases (Slowinski et al., 2007), which may contribute to the early parkinsonism reported in patients with this MAPT mutation (reviewed by van Swieten et al., 1999).

Cellular neuropathology

At autopsy, brains from people with FTDP-17T contain insoluble aggregates of abnormally phosphorylated tau in neurons and sometimes in glia, alongside neuronal loss and gliosis (Foster et al., 1997; Spillantini et al., 1998a) (Figure 1.2).

Both tau inclusion morphology and isoform composition vary between individuals with different MAPT mutations (Section 1.2.5). Mutations which increase exon 10 inclusion, such as N279K (Hong, 1998), lead to 4R tau inclusions (Ogaki et al., 2013), whereas mutations which alter tau's properties (such as P301L and V337M) result in inclusions containing 3R and 4R tau (Spillantini et al., 1996a, 1998b).

Inclusions in neurons can be intraneuronal (in the cell body) or neuropil threads (in neuronal processes). Intraneuronal tau deposits can appear dot-like, resembling the pre-tangles of AD, or can be neurofibrillary tangles (NFTs) which may leave ghost tangles when a neuron dies. Inclusions can also resemble Pick bodies found in PiD, or the intraneuronal inclusions (known as cortico-basal bodies) found in CBD (reviewed by Reed, 2001).

Glial inclusions are sometimes present: mutations in exons 9, 11, 12 and 13 are associated with mainly neuronal tau deposition, whereas mutations in exon 1 and 10 or introns 9 and 10 are associated with neuronal and glial tau aggregates (Ghetti et al., 2015). Individuals with the P301L mutation can have oligodendrocytic inclusions which are globular, or inclusions known as coiled bodies (Forrest et al., 2018), which have also been observed in the presence of the N279K mutation (Arvanitakis et al., 2007; Slowinski et al., 2007). Tau aggregates in astrocytes can be dot-like, thread-like or globular inclusions, all of which have been observed in the presence of the P301L mutation (Forrest et al., 2018; Tacik et al., 2017). Tau deposits in astrocytes also include astrocytic plaques, found in CBD, and tufted astrocytes, characteristic of PSP (Forrest et al., 2018).

Astrogliosis occurs in cortical and sub-cortical areas in FTDP-17T, including in people with the N279K (Arvanitakis et al., 2007; Slowinski et al., 2007), P301L (Miyasaka et al., 2001), and V337M mutations (Spina et al., 2017). Astrogliosis is a response to a brain injury or insult, and can range from astrocyte hypertrophy to astrocyte overgrowth and astrocytic scar formation. Reactive astrocytes release molecules including neurotrophic and inflammatory factors, which can have neuroprotective or neurotoxic effects (reviewed by Phatnani and Maniatis, 2015).

Balloon neurons have been reported in FTDP-17T (Foster et al., 1997), including in P301L (Forrest et al., 2018) and N279K cases (Arvanitakis et al., 2007; Delisle et al., 1999; Wren et al., 2015), Figure 1.2. Balloon neurons are recognisable by their swollen cell bodies and displaced nuclei, and are usually positive for αB-crystallin and phosphorylated neurofilament (reviewed by Aoki et al., 2003). Balloon neurons are observed in various neurodegenerative diseases including PiD, CBD, PSP, AGT and Wernicke's encephalopathy (Freiesleben et al., 1997; López-González et al., 2014) but their role in neurodegeneration is unclear.

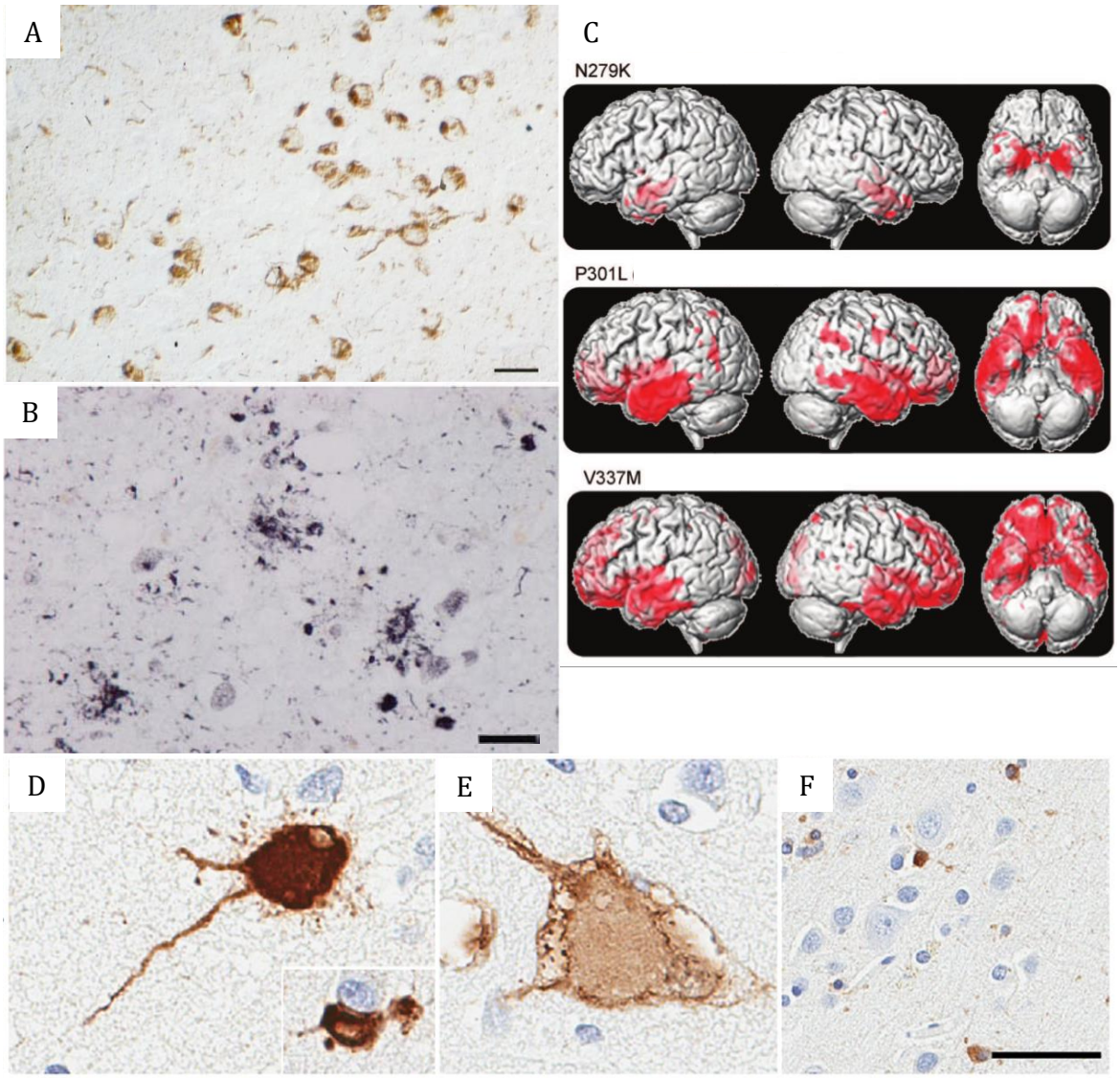

Fig. 1.2 **Pathology and atrophy in FTDP-17T brains.** **A** Tau-positive neurons in the temporal cortex of a FTDP-17T patient with the P301L mutation, detected with the AT8 antibody which detects tau phosphorylated at Ser202 and Thr205. Scale bar = 66 µM (Spillantini et al., 1998b). **B** Tau-positive astrocytes with granular inclusions in a FTDP-17T patient with the P301L mutation, detected by the AT8 antibody. Scale bar = 25µM (Ferrer et al., 2014). **C** 3D renderings of grey matter loss (shown in red) in FTDP-17T patients with the N279K (n=3), P301L (n=4) and V337M (n=3) mutations, in relation to controls (Whitwell et al., 2009). **D, E, F** αB-crystallin positive balloon neurons in the frontal (**D**) and temporal (**E**) cortex and αB-crystallin positive glia (**F**) in the brain of a FTDP-17T patient with the N279K mutation. Scale bar = 25µM (Wren et al., 2015).

Molecular neuropathology

Tau inclusions contain tau filaments, which can be paired helical filaments, like those found in AD (Goedert et al., 1988; Grundke-Iqbal et al., 1986; Wischik et al., 1988), straight filaments, or twisted ribbon-like filaments (reviewed by Ghetti et al., 2015).

Tau is a phosphoprotein and 85 potential phosphorylation sites have been described (reviewed by Hanger and Noble, 2011). Tau is abnormally phosphorylated in FTDP-17T and in other tauopathies (Goedert et al., 1992; Spillantini et al., 1996b) and several antibodies have been developed against epitopes phosphorylated in AD or FTDP-17T brains (Table 1.1). However, there is some overlap between tau phosphorylation in disease and tau phosphorylation during development: phosphorylated tau has been detected with the AT8, AT270, AT180, PHF-1 and 12E8 antibodies in both human fetal brain and brains from tauopathy sufferers (Table 1.1). Tau phosphorylation during development may have a functional role, by decreasing tau binding to microtubules (Drechsel et al., 1992) and potentially increasing plasticity (Goode and Feinstein, 1994), but the significance of fetal-like phosphorylation in tauopathies is unknown. Epitopes of other antibodies, such as AT100 or AP422, have not been detected in fetal brains and may be more specific for pathological tau (Hasegawa et al., 1996; Ksiezak-reding et al., 2000; Matsuo et al., 1994; Milenkovic et al., 2018; Morishima-Kawashima et al., 1995).

There is also overlap between tau phosphorylation in disease and tau phosphorylation under physiological circumstances. For example, Preuss and Mandelkow (1998) detected tau phosphorylation with the AT8, AT180, and PHF-1 antibodies during mitosis, but not in the parent or daughter cells. Phosphorylated tau has also been detected with the AT8, AT180, and 12E8 antibodies in the brains of hibernating ground squirrels, although phosphorylation is reversed after hibernation (Arendt et al., 2003).

The abnormal nature of tau phosphorylation in tauopathies may be the degree of phosphorylation, as well as the epitopes phosphorylated. In Western blotting experiments, autopsy-derived aggregated tau from AD brains has been found to be more highly phosphorylated at epitopes including AT8, PHF-1, AT270 and AT180 as compared to fetal tau, brain biopsy-derived adult tau and autopsy-derived adult tau (Matsuo et al., 1994). Fetal and biopsy-derived adult tau were phosphorylated to similar levels, whereas autopsy-derived adult tau was mostly dephosphorylated at the epitopes measured, suggesting that rapid post-mortem dephosphorylation may explain the differences in phosphorylation observed between fetal brains, control adult brains and tauopathy brains found in other studies.

Table 1.1 **Tau phosphorylation in development and FTDP-17T**

Antibody	Epitope	In human fetal brain	In FTDP-17T brain
AT8 [1]	pSer202+pThr205 [2]	Y [3,4,5,20♦]	Y [6,7,8,9,10,18]
AT270 [11]	pThr181	Y [4,20,♦]; low [5]	Y [6,8]
AT180 [11]	pThr231+pSer235	Y [4,20,♦]; low [5]	Y [6,8,18]
PHF-1	pSer396+pSer404 [12]	Y [4,13,14,♦]	Y [6,8,18]
12E8 [15]	pSer262 and/or pSer356 [15]	Y [15]	Y [6,18]
AT100 [1]	pThr212+pSer214 [19]	N [4,16]; low [5]	Y [6,8,18]
MC-1 [17]	7-9, 312-342 [17]	No data	Y [6]
AP422 [21]	pSer422 [21]	N [22]; low [21]	Y [23]

Tau antibodies which bind to phosphorylated or conformational epitopes found in developing brains, or in brains of people with FTDP-17T. The symbol ♦ indicates that phosphorylation at this epitope was detected in brain biopsy-derived adult human tau but not in post-mortem human tau by Matsuo et al. (1994). The MC-1 antibody is conformational; the AT100 antibody requires both phosphorylation and a conformation change. References: [1]: Mercken et al. (1992); [2]: Goedert et al. (1995); [3]: Brion et al. (1993); [4]: Matsuo et al. (1994); [5]: Milenkovic et al. (2018); [6]: Spillantini et al. (1996a); [7]: Spillantini et al. (1998b); [8]: Rizzini et al. (2000); [9]: de Silva et al. (2006); [10]: Arvanitakis et al. (2007); [11]: Goedert et al. (1994); [12]: Lang et al. (1992); [13]: Bramblett et al. (1993); [14]: Kenessey and Yen (1993); [15]: Seubert et al. (1995); [16]: Ksiezak-reding et al. (2000); [17]: Jicha et al. (1996); [18]: van Swieten et al. (1999); [19]: Zheng-Fischhöfer et al. (1998); [20]: Goedert and Jakes (1990); [21]: Hasegawa et al. (1996); [21]: Morishima-Kawashima et al. (1995); [23]: Miyasaka et al. (2001).

1.2.5 MAPT mutations in FTDP-17T

More than 60 MAPT mutations have been linked to FTDP-17T (Goedert, 2016; Figure 1.3). My project focuses on three of them: N279K and P301L in exon 10, and V337M in exon 12. These mutations are described in detail in this section and in Table 1.3.

The main evidence for a causative role of MAPT mutations in FTDP-17T is the co-segregation of mutations with the disease, and their absence in unaffected family members and control subjects (Poorkaj et al., 1998; Hutton et al., 1998; Spillantini et al., 1998; Clark et al., 1998; Malkani et al., 2006; McCarthy et al., 2015; and many others). In addition, expression of wild-type or mutant human tau in mouse models can lead to tau pathology, neurofibrillary tangles, neuronal loss, behavioural phenotypes, and sometimes premature death (reviewed by Götz and Ittner, 2008).

Tau mutations can be divided into two types: those altering exon 10 splicing and the 3R:4R tau ratio, and those affecting tau's biochemical and physiological properties (although some mutations may do both). Tau mutations are thought to cause tau dysfunction by two main mechanisms: a toxic gain-of-function model and a toxic partial loss-of-function.

1.2.6 Toxic gain-of-function

Several lines of evidence support the idea that tau mutations result in a toxic gain of function: almost all known MAPT mutations are autosomal dominant (Ghetti et al., 2015) (apart from S352L: Nicholl et al., 2003); tau knock-out in mice does not cause neurodegeneration (Dawson et al., 2001; Fujio et al., 2007; Harada et al., 1994; Tucker et al., 2001); and microduplication of 17q21.31 (including MAPT) in humans increases MAPT RNA 1.6-1.9 fold and results in a tauopathy (Le Guennec et al., 2017). In addition, it has been speculated that a loss-of-function affecting only 25% of total tau (caused by heterozygous tau mutations in exon 10) is unlikely to cause the neurodegeneration seen in FTDP-17T (Goedert, 2016).

The toxic function gained may be aggregation, which might damage cells (Mandelkow et al., 2003). Aggregation could occur due to mutations increasing tau's propensity for aggregation (Alonso et al., 2004; Combs and Gamblin, 2012; Hasegawa et al., 1998; Nacharaju et al., 1999). An increase in tau phosphorylation, or mutations increasing tau's propensity for phosphorylation (Alonso et al., 2004; Han et al., 2009), may also contribute to the toxic gain of function aggregation, since phosphorylation at some sites can enhance tau aggregation (Despres et al., 2017; Haase et al., 2004). Phosphorylation itself may also be a toxic gain of function: tau phosphorylation may enhance the spreading of tau pathology (Hu et al., 2016),

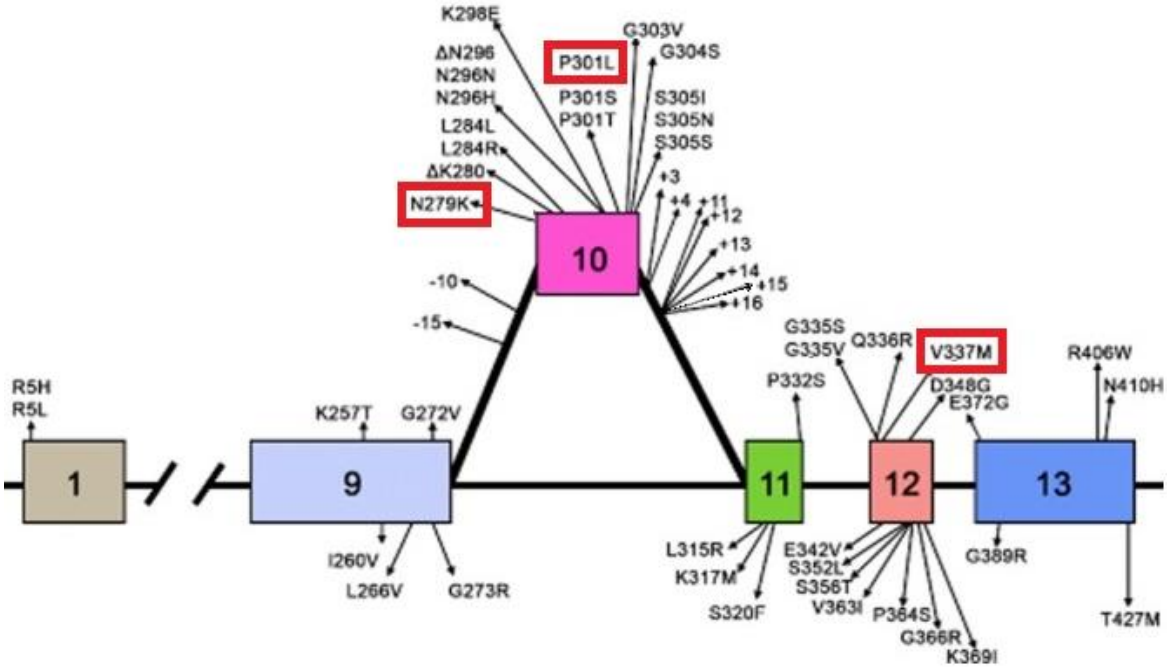

Fig. 1.3 **Mutations in the MAPT gene linked to FTDP-17T.** The N279K, P301L and V337M mutations which this project focuses on are highlighted in red. Adapted from Ghetti et al. (2015).

and it can contribute to tau toxicity in mouse (Le Corre et al., 2006; Shahani et al., 2006) and Drosophila models of tau dysfunction (Steinhilb et al., 2007) (Section 1.3.2).

A tau isoform imbalance favouring 4R tau may also lead to tau aggregation, since 4R isoforms are more aggregation-prone (Adams et al., 2010). In addition, a tau isoform imbalance may itself be a toxic gain of function, since increasing the amount of 4R to 3R tau in mice expressing human tau increased tau phosphorylation at epitopes including Ser202 and Thr205, decreased tau solubility, and increased the severity of induced seizures (Schoch et al., 2016).

1.2.7 Toxic partial loss-of-function

Tau mutations may also cause dysfunction due to a partial loss of physiological function. One deletion affecting just MAPT in humans has been reported: a heterozygous deletion of exons 6-9 (including the *Saitohin* gene in MAPT intron 9) in a person with FTD (Rovelet-Lecrux et al., 2009). The deletion would remove a microtubule binding repeat, and recombinant tau with the same deletion was less able to bind microtubules than wild-type tau *in vitro*, with no effect on tau aggregation. These results suggest that a loss of microtubule binding function could also be involved in causing FTD. However, abnormal binding of the deletion mutant

tau to MAP-1B was also reported, suggesting a possible alternative toxic gain of function (Rovelet-Lecrux et al., 2009). This remains speculation, since brain tissue from the FTD patient with the deletion was not available for analysis, so tau pathology in the brain of this individual could not be confirmed.

Other evidence suggests that heterozygous deletion of tau does not cause problems in humans. Heterozygous tau deletion has been reported in 17q21.31 microdeletion syndrome (Shaw-Smith et al., 2006), in which a region encompassing MAPT, four flanking genes and two putative genes was absent in individuals with developmental delay and intellectual disability. Although this could suggest a crucial role for tau in brain development, Zollino et al. (2012) and Koolen et al. (2012) reported two individuals with 17q21.31 microdeletion syndrome but with heterozygous loss-of-function mutations in KANSL1, indicating that KANSL1 loss-of-function is sufficient to cause 17q21.31 microdeletion syndrome, and indicating that tau does not play a role.

Tau knock-out mice offer some evidence of a tau loss-of-function phenotype. Five knock-out lines have been created, and their phenotypes are summarised in Table 1.2. Young mice are viable and reportedly appear normal, but adult mice develop deficits in muscle strength, balance, movement and behaviour from three (Ikegami et al., 2000) or 12 months of age onwards (Lei et al., 2012; Ma et al., 2014; Morris et al., 2013). Quantification of MAP proteins indicates that elevated MAP1A levels may compensate for tau's absence in young mice, and to a lesser extent in mice older than three months (Dawson et al., 2001; Fujio et al., 2007; Harada et al., 1994; Ma et al., 2014). These results suggest that tau is required for normal neuronal function, although its absence can be compensated for during early life.

The tau knock-out mice show limited evidence of a neurodegenerative phenotype. Although Lei et al. (2012) reported decreased brain weight, neuronal loss and iron accumulation in 12 month-old mice, Van Hummel et al. (2016) found no change in brain volume and no neuron loss in 16 month-old mice from a different line. Similarly, Ma et al. (2014) reported decreased levels of the post-synaptic proteins PSD-95 and drebrin, but no change in levels of the pre-synaptic synaptophysin in 19-20 month-old mice from one line, but PSD-95 and drebrin levels were unchanged in 22 month-old mice from a different line (Van Hummel et al., 2016). These results suggest that tau knock-out may not be sufficient to cause neurodegeneration, although further investigation may be warranted.

The toxic gains-of-function aggregation and phosphorylation could lead to toxic losses of normal physiological function, since both aggregated and phosphorylated tau are less able to bind and stabilise microtubules (Drechsel et al., 1992). This loss of function could be enhanced by mutations which decrease tau's affinity for microtubules. Loss of tau's

microtubule binding function could create a pool of unbound tau, which may be necessary for aggregation (Goedert and Spillantini, 2001). Alternatively, loss of function could be caused by aggregation depleting soluble tau, and by phosphorylation decreasing microtubule binding.

Decreased binding of tau to microtubules may decrease microtubule stability, since tau stabilises microtubules (Drubin and Kirschner, 1986). This could lead to cytoskeletal disruptions, disrupting cellular functions such as axonal transport, leading to retrograde degeneration and synaptic loss, and even cell death (reviewed by Rossi and Tagliavini, 2015, Rovelet-Lecrux et al., 2009). Loss of tau's normal physiological function could also contribute to DNA damage, since tau may have a role in genome stability in the nucleus (Rossi and Tagliavini, 2015), and to post-synaptic dysfunction, since dendritic tau may have a role at the post synaptic density (Ittner et al., 2010).

Another potential toxic loss of function is unbalancing of the 1:1 3R:4R ratio. Changes in the 3R:4R tau ratio can alter and impair axonal transport in PSC-derived neurons (Iovino et al., 2015; Lacovich et al., 2017) and in mice (Dawson et al., 2007). Correspondingly, in a mouse expressing all six isoforms of human tau, but preferentially expressing 3R isoforms, restoring a 1:1 3R:4R tau ratio decreased cognitive impairment and decreased the amount of tau phosphorylated at Ser202 and Thr231/Ser235 (Espíndola et al., 2018).

1.2.8 Mutations altering the 3R:4R tau ratio

Tau mutations disrupting the 1:1 3R:4R tau ratio to favour 3R (Anfossi et al., 2011; Stanford et al., 2003) or 4R (Hong, 1998) tau production can both lead to neurodegenerative disease, suggesting that upsetting the 3R:4R tau balance is sufficient to cause neurodegeneration in humans.

The 3R to 4R tau ratio may vary from the 1:1 ratio in some areas of the human brain. For example, Majounie et al. (2013) measured tau mRNA levels in different brain regions in control subjects, and found that 4R tau mRNA was approximately 35-65% of total tau mRNA, depending on the brain area. However, the tau ratio across the whole brain was not measured. In addition, the 3R to 4R tau ratio varies across species. Mice, for example, express the three 4R tau isoforms in adulthood, and express 0N3R tau only early in development (Takuma et al., 2003), indicating that changes in the 3R:4R isoform ratio without neurodegenerative disease are possible.

The idea that upsetting the 3R:4R tau balance can cause neurodegeneration is supported by *in vivo* evidence. For example, Espíndola et al. (2018) used trans-splicing to correct

Table 1.2 **Summary of findings from tau knock-out mouse lines**

Original mouse line and method	**Harada et al. (1994)**, Neo replacing exon 1	**Dawson et al. (2001)**, Neo replacing exon 1	**Tucker et al. (2001)**, EGFP-Neo in exon 1
MAP1A: young mice	↑ [1]	↑ [2], → [3]	- ↑ •
MAP1A: adult mice	↑ [1]	→ [2], ↑ [5]	- → •
MAP1B: young mice	-	→ [2,3]	-
MAP1B: adult mice	→ [1]	→ [2], ↑ 8-9m [5], ↓ 19-20m [5]	-
MAP2: young mice	-	→ [2,3]	-
MAP2: adult mice	-	→ [2]; ↑ 8-9m, → 19-20m [5]	-
Cultured neurons	→ axon extension [1]	↓ neurite length; slow maturation [2]	-
Structural brain changes	PF small axons: ↓ MT number, ↓ density [1]	↓ brain weight [12]	→ brain volume [13]
	PF large axons: → MT number, → density [1]	↑ LVA, CP area [12]	-
	PF axons: ↓ MT cross-bridges	↓ CC, GL thickness [12]	-
	-	↓ total and Th neurons in SN, VTA [12]	→ total neurons in SN [13]
	-	↓ striatal dopamine [12], → [9]	-
Iron accumulation	-	In cortex, HC, SN [12], none [9]	none [13]
Synaptic transmission (HC slices)	-	→ LTP [14]	→ EPSCs [11,16]
	-	-	→ STP; ↓ LTP [11]
	-	-	↓ insulin-induced LTD [16]
Synaptic proteins	-	→ NR1 [5], synaptophysin [2,5,12]	→ NR2A [16], NR2B, drebrin, PSD95, NR1 [13,16]
	-	↓ NR2B, drebrin, PSD95, Fyn [5]	-
Spatial learning			
Morris water maze	→ [6]	→ [7,8,9]; → 8-9m, ↓ 19-20m [5]	→ [10,11,13]; → ★
Radial water maze	→ [6]	→ [8]	-
Y-maze	→ [7]; ↓ [12]	-	-
Other learning and memory tests			
Novel object recognition	→ [9]	-	-
Activity in novel environment	↑ [6]	→ [7]	-
Activity in open field	-	→ [9]; → 6m, ↓ 12, 24m [12]	→ [11,13]
Activity in elevated plus maze	-	→ [7]	→ [11,13]
Fear conditioning	↓ contextual [6]	-	↓ cued, contextual [11]
Movement and strength			
Wire hanging	↓ [6]	-	→ [13]
Rod walking/balance beam	↓ [6]	↓ [9]	-
Rotarod	-	→ [8], ↓ [9]; → 6m, ↓ 12, 24m [12]	→ [11,13]
Pole test turn time	-	→ 6m, ↑ 12, 24m [12]	-
Pole descent time	-	↑ [9]	-
Motor score	-	→ <8m, ↑ >9m [5]	-

Two other mouse lines have been created: Fujio et al. (2007) replaced exon 1 with Neo, and their findings in this line are marked •; Tan et al. (2018) deleted tau exon 1 with CRISPR, and their findings are marked ★. All findings are relative to controls in mice more than 2 months old, unless otherwise stated. Young mice are less than 2 weeks old. Abbreviations: CC: corpus callosum; CP: caudate putamen; EGFP: enhanced green fluoresent protein; EPSC: excitatory post-synaptic current; GL: granule layer; HC: hippocampus; LTD: long-term depression; LTP: long-term potentiation; LVA: lateral ventricular area; m: months old; MAP: microtubule-associated protein; MT: microtubule; Neo: neomycin; NR: NMDA receptor subunit; PF: parallel fibre; PSD: post-synaptic density; SN: substantia nigra; STP: short-term plasticity; Th: tyrosine hydroxylase; VTA: ventral tegmental area. References: [1]: Harada et al. (1994); [2]: Dawson et al. (2001); [3]: Rapoport et al. (2002); [4]: Fujio et al. (2007); [5]: Ma et al. (2014); [6]: Ikegami et al. (2000); [7]: Roberson et al. (2007); [8]: Dawson et al. (2010); [9]: Morris et al. (2013); [10]: Tan et al. (2018); [11]: Ahmed et al. (2014); [12]: Lei et al. (2012); [13]: Van Hummel et al. (2016); [14]: Shipton et al. (2011); [15]: Marciniak et al. (2017); [16]: Ittner et al. (2010).

the over-production of 3R tau in mice transgenic for all six tau isoforms. Aged transgenic mice developed tau phosphorylation and cognitive deficits, which were reduced when trans-splicing equalised the 3R:4R human tau ratio.

Since recombinant 3R tau promotes microtubule assembly at a lower rate than 4R tau (Goedert and Jakes, 1990) and 3R tau is less able to stabilise microtubules than 4R tau (Panda et al., 2003), an 3R:4R imbalance may alter microtubule assembly and stabilisation. Additionally, since 4R tau is more aggregation-prone than a 3R and 4R tau mixture (Adams et al., 2010), an isoform imbalance towards 4R tau may favour tau aggregation.

N279K

The N279K mutation is a T→G mutation in exon 10 which results in an asparagine instead of a lysine residue (Clark et al., 1998). Although the mutation causes an amino acid change, it has its main effect at the mRNA level where it alters a polypurine enhancer (PPE) sequence, one of several splice enhancers in exon 10 (D'Souza et al., 1999). The T→G base change increases splicing factor binding (D'Souza and Schellenberg, 2006), either by increasing the number of GA-purine repeats, or by increasing the number of AAG repeats (D'Souza and Schellenberg, 2002). This increases exon 10 inclusion in RNA by approximately 80% in splicing assays (D'Souza et al., 1999). In soluble tau from the frontal cortex of individuals with the N279K mutation, there is a two-fold increase in the 4R:3R ratio relative to control (Hong, 1998), and tau inclusions contain 4R (but not 3R) tau protein (Clark et al., 1998).

Most evidence indicates that the N279K mutation leads to increased expression of functionally normal 4R tau, but there is limited evidence that the mutation also alters tau's properties (Table 1.3). For example, the N279K mutation may also decrease tau aggregation over a period of minutes (Yao, 2003) but increase aggregation over a period of days (Barghorn et al., 2000). In addition, N279K tau is reported to be less able to promote microtubule assembly than wild-type tau, and to be less able to bind microtubules than wild-type tau at low tau concentrations, but more able at high concentrations (Barghorn et al., 2000). This is in direct contrast to several other studies, which found that N279K tau does not alter microtubule binding or assembly (D'Souza et al., 1999; Hasegawa et al., 1999; Hong, 1998). The discrepancy between these results may be due to the different amounts of tau used: Barghorn et al. (2000) used a maximum of 50μM of tau, compared to a maximum of 3μM used in the other studies.

1.2.9 Mutations altering tau's physical properties

Mutations which alter tau's physical properties can increase tau's aggregation rate (Alonso et al., 2004; Combs and Gamblin, 2012; Nacharaju et al., 1999), increase the size of tau filaments (Combs and Gamblin, 2012), decrease (Hong, 1998) or increase (Pickering-Brown et al., 2004) microtubule binding, decrease microtubule assembly (Hasegawa et al., 1998; Hong, 1998), and alter the rate and extent of tau phosphorylation (Alonso et al., 2004; Han et al., 2009).

P301L

P301L is a missense C→T mutation in exon 10. Multiple studies have shown that it decreases microtubule assembly (Barghorn et al., 2000; Hasegawa et al., 1998, 1999; Hong, 1998), increases tau's propensity to aggregate (Aoyagi et al., 2007; Barghorn et al., 2000; Hong, 1998; Nacharaju et al., 1999), and increases tau's propensity for phosphorylation (Alonso et al., 2004; Han et al., 2009), but does not alter the 3R:4R tau ratio (Hasegawa et al., 1999; Hong, 1998; Hutton et al., 1998) (Table 1.3). Some studies report a decreased ability to bind microtubules (Hong, 1998), decreased chaperone-assisted stabilisation of tau (Gunawardana et al., 2015), and increased elongation rate and length of tau filaments (Combs and Gamblin, 2012).

Since the P301L mutation is heterozygous and is only present in 4R tau, only 25% of total tau carries the mutation. In the brains of FTDP-17T sufferers with this mutation, P301L mutant tau is sequestered into insoluble inclusions, which contain mostly 4R P301L tau and some 3R tau (Miyasaka et al., 2001; Rizzu et al., 2000; Spillantini et al., 1998b). This depletes soluble P301L tau but the ratio of 3R:4R soluble tau is unchanged, suggesting that 4R tau synthesis is upregulated to maintain a 1:1 3R:4R ratio (Rizzu et al., 2000). In addition, P301L and wild-type 4R tau mRNA levels remain equal, indicating that the lack of soluble P301L tau is not caused by decreased stability or increased degradation of P301L tau mRNA (Miyasaka et al., 2001).

V337M

V337M is a missense G→A mutation in the constitutively expressed exon 12, meaning that it affects all 6 tau isoforms (Poorkaj et al., 1998). Since the mutation is heterozygous, 50% of total tau in people with this mutation is mutant. Several studies have demonstrated that the mutation decreases microtubule assembly (Barghorn et al., 2000; Hasegawa et al., 1998; Hong, 1998; Pickering-Brown et al., 2004), increases tau's propensity to aggregate (Barghorn

et al., 2000; Nacharaju et al., 1999), and increases tau's propensity for phosphorylation (Alonso et al., 2004; Han et al., 2009) (Table 1.3). Individual studies indicate that the V337M mutation decreases tau's microtubule binding (Hong, 1998), has no effect on exon 10 splicing (Hong, 1998) and does not affect tau filament formation dynamics (Combs and Gamblin, 2012).

Table 1.3 **Effects of MAPT mutations N279K, P301L and V337M**

Mutation	Exon 10 inclusion	MT interactions	Aggregation	Other changes
N279K Exon 10 Affects 4R isoforms	↑ in RNA [1,2,3] ↑ 4R tau protein [4]	→ MT binding [1,4] → MT assembly [1,3,4]; ↓ [5]	↑ over 11 days (hep.) [5] ↓ over 30 minutes (hep.) [6]	
P301L Exon 10 Present in 4R isoforms (25% of total tau)	→ [3,4,7]	↓ MT binding [4] ↓ MT assembly [3,4,5,8]	↑ over 4 -11 days (hep.) [5,9,10] ↑ over 12 hours (a.a.) [11] ↑ filament length [11] ↓ nucleation rate [11] ↑ elongation rate [11]	↑ phosphorylation [12,15] ↑ mol phosphate incorporated [12] ↓ chaperone-assisted stabilisation [13]
V337M Exon 12 Present in all isoforms (50% of total tau)	→ [4]	↓ MT binding [4] ↓ MT assembly [4,5,8,14]	↑ over 4 -11 days (hep.) [5,10] → over 12 hours (a.a.) [11] → filament length [11] → nucleation rate [11] → elongation rate [11]	↑ phosphorylation [12,15] ↑ mol phosphate incorporated [12]

The experiments in this table were cell-free *in vitro* experiments. Changes in tau's biochemical properties are relative to wild-type tau. →: no change; ↑: increased; ↓: decreased; a.a: arachidonic acid; hep.: heparin; MT: microtubule. Tau aggregation *in vitro* requires the addition of polyanions (Goedert et al., 1996), in these studies either heparin or arachidonic acid was used. References: [1]: D'Souza et al. (1999); [2]: Delisle et al. (1999); [3]: Hasegawa et al. (1999); [4]: Hong (1998); [5]: Barghorn et al. (2000); [6]: Yao (2003); [7]: Hutton et al. (1998); [8]: Hasegawa et al. (1998); [9]: Aoyagi et al. (2007); [10]: Nacharaju et al. (1999); [11]: Combs and Gamblin (2012); [12]: Alonso et al. (2004); [13]: Gunawardana et al. (2015); [14]: Pickering-Brown et al. (2004); [15]: Han et al. (2009).

1.3 Tau dysfunction

In the brains of FTDP-17T sufferers, tau becomes abnormally phosphorylated and forms aggregates (Goedert and Spillantini, 2001). However, the toxic form of tau is not definitively known, and neither is the mechanism by which tau leads to cell death.

1.3.1 Tau aggregation

Tau aggregation is dependent on two motifs in the second and third microtubule binding repeats, which have a high propensity to form β-sheets (von Bergen et al., 2000). In the tau filaments found in AD, the filament core consists of two protofilaments which are arranged differently to give either straight or paired helical filaments. Each protofilament consists of tau residues 306-378, which form a C-shape due to the interaction of 8 β-sheets (Fitzpatrick et al., 2017). Tau fibrils made in cell-free experiments follow a pattern of nucleation and elongation, suggesting that they are constructed by addition of monomers to a growing fibril after a "nucleus" of aggregation has formed (reviewed by Goedert, 2016). In the brains of people with AD, tau monomers have been found assembled into oligomers (Lasagna-Reeves et al., 2012), but it is not clear if these soluble oligomers are the precursors to insoluble filamentous tau (Mudher et al., 2017).

The trigger for tau aggregation in the brain is unknown, but aggregation can be promoted by factors including truncation, some tau mutations, polyanions, and aggregated tau acting as seeds (reviewed by Cowan and Mudher, 2013), and requires a critical tau concentration (Goedert et al., 1996).

Tau phosphorylation in aggregation

Tau hyperphosphorylation is thought to occur before aggregation, but there is little evidence that phosphorylation causes aggregation (Goedert and Spillantini, 2001). Recombinant tau isoforms, hyperphosphorylated with brain extract-derived kinases, can assemble into filaments *in vitro* (Alonso et al., 2004, 2001), but this may be caused by factors other than kinases in the brain extract, since filament formation *in vitro* has been shown to be independent of phosphorylation, but dependent on polyanions (Goedert et al., 1996; Pérez et al., 1996).

Although phosphorylation is not sufficient to cause aggregation, it has been shown to influence the degree of aggregation *in vitro* (in the presence of polyanions). For example, phosphorylation or pseudo-phosphorylation at some epitopes (including Ser214, Ser262,

Ser324, Ser356, and Ser320) prevents aggregation *in vitro* (Haase et al., 2004; Schneider et al., 1999), although Ser214, Ser262 and Ser356 can also be phosphorylated after *in vitro* filaments have formed, indicating that the timing of phosphorylation is crucial (Schneider et al., 1999). Phosphorylation or pseudo-phosphorylation at other epitopes promotes aggregation. These epitopes include Ser422 and other residues in tau's C-terminus (Haase et al., 2004), as well as the combination of Ser202, Thr205 and Ser208 (Despres et al., 2017).

1.3.2 Toxic tau species

Tau species include monomers, dimers and trimers, various oligomers, filaments and aggregates, which may be interconverted in *in vitro* or *in vivo* models (Cowan and Mudher, 2013). Evidence from several animal models suggests that the toxic tau species is either a small soluble, or small insoluble tau species.

The core of a tau filament is composed of two protofilaments, each consisting of tau residues 306-378, which form a C-shape due to the interaction of 8 β-sheets (Fitzpatrick et al., 2017). Formation of β-sheets may be necessary for neurodegeneration, since Drosophila expressing β-sheet incompetent tau (tau without a hexapeptide repeat encoded by nucleotides 306-311) did not develop an age-related rough-eye phenotype, and had lifespans approaching those of Drosophila not expressing any exogenous tau. In comparison, Drosophila expressing wild-type tau which was β-sheet competent developed an age-related rough-eye phenotype and had a significantly reduced lifespan relative to that of Drosophila expressing β-sheet incompetent tau (Passarella and Goedert, 2018).

In some mouse models, such as in one expressing human tau but not mouse tau, cell death and dysfunction precede the detection of sarkosyl-insoluble tau filaments and thioflavin-S positive tau inclusions, implicating soluble tau species (Andorfer et al., 2005). Similarly, Drosophila expressing wild-type or mutant human tau have cell death and a reduced lifespan, but tau filaments are not detectable in sarkosyl-insoluble tau preparations, suggesting that soluble tau species are toxic (Wittmann, 2001).

However, in another model, a mouse over-expressing 0N3R human tau, a decrease in tau solubility was detected at the same time as neurodegeneration-like changes, such as silver-positive tau inclusions and axon degeneration (Ishihara et al., 1999), suggesting that less soluble tau species may be to blame.

Other studies support a protective role for tau aggregation. For example, in mice over-expressing 2N4R P301L tau under an inducible promotor, Santacruz et al. (2005) showed that tau-mediated behavioural deficits could be reversed and neuron loss could be halted by

reducing tau over-expression. When tau expression was decreased, tau aggregates continued to accumulate whilst tau-related behavioural deficits were reversed, suggesting that toxic tau species were being sequestered into harmless aggregates.

In support of this idea, Andorfer et al. (2005) reported that in aged mice expressing human tau but no mouse tau, most dying cells identified by electron microscopy did not contain large tau inclusions, whereas some apparently healthy neurons with tau inclusions aggregates were visible. This is supported by findings in AD. For example, mathematical modelling of hippocampal neuron loss in AD patients suggests that NFT-containing neurons can live for approximately 20 years, indicating that NFTs alone may not be sufficient to cause cell death (Morsch et al., 1999). In addition, the number of hippocampal neurons lost in AD far exceeds the number of NFTs, indicating that NFT formation might not be required for cell death and suggesting that smaller tau aggregates may be to blame (Kril et al., 2002). However, AD is not a pure tauopathy since amyloid-β is also involved, meaning that results in AD may not generalise to FTDP-17T.

Nevertheless, Gallyas silver-positive, aggregated tau has been reported in the brains of young, apparently healthy individuals (Braak and Del Tredici, 2011), and in non-demented older people (Lagui et al., 1995), suggesting that a small number of NFTs can exist without disease, although it is possible that all of these people would have gone on to develop a tauopathy had they lived longer.

Toxic phosphorylated tau species

Although some mutations increase tau's propensity for phosphorylation (Alonso et al., 2004; Han et al., 2009), no mutations create new phosphorylation sites (with the possible exception of P301S), suggesting that phosphorylation is unlikely to be the primary driver of tauopathies (Ghetti et al., 2015). However, tau phosphorylation may have deleterious effects, as many other post-translational modifications, including acetylation, glycosylation, glycation, deamidation and isomerisation, which are not covered here (reviewed by Wang and Mandelkow, 2015).

For example, in mice expressing human P301L tau, Le Corre et al. (2006) found that treatment of pre-symptomatic animals with an inhibitor of the tau kinase ERK2 decreased tau phosphorylation, which correlated with a decrease in motor impairments, although the number of tau inclusions was not affected. This suggests that abnormally phosphorylated tau contributes to motor impairments, but other tau species were not considered in the study and cannot be excluded. In addition, inhibition of ERK2 may also affect other pathways.

Evidence for the toxicity of phosphorylated tau has also been found in Drosophila. For example, expression of human wild-type tau in Drosophila retina causes a "rough-eye" phenotype (disorganised eye cells), but this phenotype is decreased in Drosophila expressing pseudo-dephosphorylated tau (where 14 serine/proline and threonine/proline sites were replaced with alanine and therefore could not be phosphorylated). Correspondingly, the rough-eye phenotype is increased in Drosophila expressing tau pseudo-phosphorylated at the same 14 sites (Steinhilb et al., 2007).

In another study, pseudo-phosphorylated wild-type tau (but not normal wild-type tau) expressed in mouse hippocampal slice cultures was reported to increase cell death, as measured by LDH release and live imaging (Shahani et al., 2006). Pseudo-phosphorylated tau was also less soluble than normal wild-type tau, suggesting that phosphorylated insoluble tau species may be toxic.

Phosphorylation may also influence the spreading of tau pathology. Hu et al. (2016) found that injecting phosphorylated tau extracted from AD brains into the brains of mice expressing all six human wild-type tau isoforms induced phosphorylated tau inclusions after six months. However, when the AD brain extracts were (incompletely) dephosphorylated before injection, fewer tau inclusions were found in injected mouse brains, and some inclusions had a different morphology. This suggests that tau phosphorylation may have roles in seeding, and in the morphology of the resulting inclusions.

1.3.3 Spreading of tau pathology

Spreading of tau pathology between cells has been shown in both *in vitro* and *in vivo* models. For example, Clavaguera et al. (2009) took brain homogenate from aged mice which expressed human P301S-mutant 0N4R tau and had developed argyrophilic filamentous tau inclusions, and injected the brain homogenate into the brains of mice expressing human wild-type 2N4R tau. The injected mice developed filamentous tau inclusions which contained wild-type human tau, and the inclusions seemed to spread from the injection site to more distal brain regions in a time-dependent manner. Mice expressing wild-type human 2N4R tau did not develop tau aggregates without a brain homogenate injection, nor when the brain homogenates were depleted of tau before injection, indicating that aggregated tau can act as a seed for further aggregation.

Similar induction and spreading of tau pathology has been shown using recombinant tau fibrils injected into the brains of pre-symptomatic mice expressing human P301S tau (Iba

et al., 2013), and using filamentous tau extracted from the brains of AD patients injected into the brains of mice expressing mouse tau but not human tau (Guo et al., 2016).

Spreading of tau pathology may also take place in the human brain. Braak and Braak (1991) proposed "staging" of AD tau pathology: spreading between synaptically connected parts of the brain, starting in the entorhinal cortex and eventually progressing to the neocortex. However, since staging is based on post-mortem brain tissue it is only circumstantial evidence; another explanation of tau's apparent spreading could be that tau pathology develops autonomously within vulnerable cells over time (Mudher et al., 2017). This seems unlikely, since tau extracted from different regions of AD brains seeded aggregation in a cell-based assay in a manner positively correlated with Braak stage (Furman et al., 2017). Moreover, in transgenic mice expressing the tau transgene specifically in the entorhinal cortex, tau aggregates can be found in the hippocampal formation of 22 month-old mice (de Calignon et al., 2012; Liu et al., 2012), supporting the idea that tau pathology may spread.

Tau seeds

Spreading of tau pathology necessitates a tau seed, which might not be the same as the toxic tau species. Neuronal loss after injecting tau fibrils into a mouse brain has only been reported in one study (Peeraer et al., 2015); other studies report the appearance and apparent spreading of tau inclusions, but do not report detectable cell death (Clavaguera et al., 2009, 2014; Dujardin et al., 2014; Iba et al., 2013), suggesting that the toxic and seed species may be different.

Possible tau seeds have been identified in some models. For example, using symptomatic mice expressing human P301S-mutant tau, Jackson et al. (2016) found that short tau filaments, which were nitrated, phosphorylated at the AT8 epitope, and made up of at least 10 tau monomers, were able to induce tau aggregation when injected into the brains of pre-symptomatic mice. Smaller tau species, including monomers and smaller aggregates were not sufficient to induce aggregation. Other studies have reported that AD brain-derived or recombinant tau species of at least three, but up to 20, tau monomers can be taken up by cells and seed tau aggregation (Mirbaha et al., 2015). In contrast, tau monomers did not cause seeding (Mirbaha et al., 2015).

Tau uptake and release

As well as a tau seed, spreading of tau pathology between brain regions requires tau to be taken up from the extracellular space, cause aggregation intracellularly, and be released and

taken up by other cells (reviewed by Goedert, 2016). Potential mechanisms for tau uptake and release have been identified, which may have a role in the spreading of tau pathology.

In cultured cells, tau fibrils can be taken up by macropinocytosis (Falcon et al., 2015; Holmes et al., 2013) or endocytosis (Wu et al., 2013). Uptake *in vitro* and *in vivo* has been reported to be dependent on heparan sulphate proteoglycans: cell surface receptors with multiple known ligands (Holmes et al., 2013). However, it is not known how tau taken up by these mechanisms escapes endosomes (Mudher et al., 2017).

Tau release has also been demonstrated in culture. For example, control iPSC-derived neurons release tau into the media under normal conditions (Chai et al., 2012), although the mechanism behind tau release remains unclear (reviewed by Wang and Mandelkow, 2015). Tau is also present in cerebrospinal fluid from both AD patients and control subjects, mostly as free tau but also in exosomes (Blennow and Hampel, 2003; Wang et al., 2017).

Some studies have shown that aggregated tau can be transferred from cell to cell. For example, Wang et al. (2017) showed that RFP-labelled exosomes containing GFP-labelled tau were taken up by neurons in one side of a microfluidic device, and transferred to neurons in the other side of the device. Uptake of labelled endosomes containing tau was only observed when the neurons made synaptic connections (detected by immunofluorescence) and not before, suggesting that the transfer of these endosomes was trans-synaptic rather than through release into the media and subsequent uptake. Furthermore, Polanco et al. (2016) have shown that exosomes isolated from cells containing aggregated tau (which was seeded using brain lysates from mice expressing human P301L-mutant tau) but not exosomes from cells without aggregated tau (seeded with brain lysates from control mice) could cause aggregation in cells from the same line (all of which expressed tau's repeat domain fused to CFP or YFP for detection of aggregation by FRET).

1.4 iPSC-derived neural cells

Human induced pluripotent stem cell (iPSC)-derived neurons provide a way to study tau toxicity in a human system.

iPSCs are made by reprogramming somatic cells to a pluripotent state from which they can be differentiated to multiple cell types. iPSCs are donor-specific, with the same DNA as the tissue donor but without age-associated markers and most epigenetic markers (Rouhani et al., 2014). This specificity means that iPSCs derived from a donor with a neurological disease can be differentiated into cell types such as neurons and astrocytes, which are usually inaccessible in a living patient, to study disease-related processes. iPSCs can also be modified

using gene-editing technologies such as CRISPR (clustered, regularly interspaced, short palindromic repeats, Chapter 4) to correct or introduce genetic aberrations linked to a disorder, so that a specific genetic change can be studied without confounding genetic background effects.

iPSC-derived neurons have been used to model numerous diseases and disorders of the brain including AD, amyotrophic lateral sclerosis, Dravet Syndrome, PD, Rett Syndrome, schizophrenia and Huntington's Disease (reviewed by Ichida and Kiskinis, 2015). They may provide a particular advantage over mouse-derived neurons for studying the effects of tau mutations, since adult human brains express six tau isoforms (three 3R and three 4R; Goedert and Jakes, 1990), whereas adult mice express only 4R tau (Götz et al., 1995).

1.4.1 iPSC origins

Gurdon (1962) first demonstrated reprogramming of differentiated cells to a totipotent state when he put Xenopus somatic cell nuclei into enucleated Xenopus oocytes, which developed into tadpoles. Later, Campbell et al. (1996) repeated this feat in mammalian cells, using somatic nuclear transfer to clone Dolly the sheep. These results showed that the nuclei of differentiated cells still contain the genetic information required for developmental programs and this concept, along with the discovery of master transcription factors like MyoD in mice (Davis et al., 1987), and the first embryonic stem cells (ESCs) made from human blastocysts (Thomson et al., 1998), led to attempts to make mammalian somatic cells into pluripotent cells using transcription factors.

The first iPSCs were made by Takahashi and Yamanaka (2006), who transduced mouse fibroblasts with 24 factors necessary for ESC pluripotency. Takahashi and Yamanaka identified the factors Oct3/4, Sox2, c-Myc and Klf4 (now known as Yamanaka factors) as sufficient to reprogram fibroblasts to iPSCs, which had ESC-like morphology, expressed ESC markers, and were pluripotent - able to differentiate into the three germ layers: mesoderm, endoderm and ectoderm. Within a year, Takahashi et al. (2007) and Yu et al. (2007) reported the reprogramming of human fibroblasts to iPSCs. Since 2007, other methods of making iPSCs have been developed.

1.4.2 Reprogramming somatic cells to pluripotent cells

iPSCs have been made from cells including fibroblasts, lymphocytes, keratinocytes, neural cells and melanocytes (Hochedlinger and Jaenisch, 2015) and can be generated using several reprogramming methods. The necessary transcription factors were first expressed using

retroviruses, which integrate their DNA into the host cell's genome. However, this can lead to incomplete reprogramming in which the cell's endogenous pluripotency programs are not sufficiently activated and the cells remain dependent on the continued high expression of the added transcription factors (Takahashi and Yamanaka, 2006). Continued expression of one factor in particular (c-Myc) would be a barrier to transplant of iPSC-derived cells, since c-Myc is an oncogene whose over-expression can cause cancer (Miller et al., 2012). To counteract this, non-integrating vectors for transcription factor expression have been used, such as non-integrating adenovirus, plasmids, or RNA viruses. Alternatively, transcription factors can be delivered to cells as RNA or recombinant proteins, or can be replaced by small molecules to make iPSCs free from reprogramming factors (reviewed by (Hochedlinger and Jaenisch, 2015).

Reprogramming does not completely remove epigenetic modifications: several studies have shown that certain epigenetic modifications in somatic cells are retained by their iPSC progeny (reviewed by Brix et al., 2015). For example, Hargus et al. (2014) made iPSCs from different somatic cell types, differentiated them to NPCs, then compared their gene expression to that of fetal NPCs. Hargus et al. found a separation in gene expression between NPCs whose parent iPSCs were mesoderm-derived and those whose parent iPSCs were neuroectoderm-derived. The neuroectoderm-derived iPSCs produced NPCs with gene expression profiles more similar to those from fetal NPCs, suggesting that neuroectoderm and mesoderm programs were not fully removed during reprogramming.

In addition, reprogramming itself can introduce mutations, at an estimated density of six protein coding mutations per exome, which could decrease the genetic similarity between an iPSC model and the individual from whom the iPSCs were derived (Gore et al., 2011).

iPSCs and ESCs

Despite coming from different sources, iPSCs are similar to ESCs. Both cell types have similar morphology, express pluripotency markers, can differentiate into all three germ layers (Takahashi and Yamanaka, 2006; Yu et al., 2007) and, when used to form tetraploid blastocysts, mouse iPSCs can contribute to the birth of live mice (Kang et al., 2009). iPSC and ESC lines have different gene expression profiles, but the differences between iPSC and ESC lines is no bigger than the difference between different ESC lines, suggesting that iPSC and ESC lines are overlapping populations (Bock et al., 2011). There is also epigenetic variation between iPSC and ESC lines, but the relevance of this, and of the genetic differences, is unknown (Colman and Dreesen, 2009). However, there may be some functional differences between iPSCs and ESCs: Hu et al. (2010) have reported that ESCs and iPSCs differentiated

to neurons using the same protocol develop over the same time course and express the same neural markers, but iPSCs differentiated with lower efficiency and with considerable variation between lines.

1.4.3 Monolayer or 2D culture of iPSC-derived neural cells

Neurons can be produced from iPSCs in 2D cultures by either directed differentiation or transdifferentiation. Directed differentiation uses the timed application of morphogens to recreate aspects of development, producing neurons via NPCs. The addition of different morphogens or morphogen-mimicking small molecules recapitulates the morphogen environment in different parts of the rostral-caudal and dorsal-ventral axes, to give region-specific cells. Alternatively, transdifferentiation uses over-expression of transcription factors to take cells from their current state (somatic or iPSCs) straight to neurons, without passing through intermediate states such as NPCs.

Morphogen-directed neuron differentiation *in vivo*

Body axes in the developing embryo are determined by morphogen gradients. In the developing vertebrate CNS rostral-caudal identity is determined first, and other axes are determined later by factors such as Wnt and retinoic acid (rostral-caudal), as well as by bone morphogenetic protein (BMPs), Wnt and Shh (dorsal-ventral) (reviewed by Astick and Vanderhaeghen, 2018). Initial rostral-caudal identity is thought to be established according to the neural-default model, in which ectodermal cells develop towards a rostral (forebrain) identity if they receive no signals to the contrary (Wilson and Houart, 2004). The intrinsic rostral fate is inhibited by BMP signalling, and BMP signalling itself is inhibited in the nascent forebrain by ligands such as Noggin, follistatin and chordin, which bind BMPs (Bachiller et al., 2000; Muñoz-Sanjuán and Brivanlou, 2002).

PSC-derived neurons via directed differentiation

Differentiation of pluripotent stem cells (PSCs, either iPSCs or ESCs) *in vitro* also follows the neural default model: culturing ESCs without caudalising factors results in NPCs with a forebrain fate (Tropepe et al., 2001; Watanabe et al., 2005). Morphogens such as Wnt and Nodal can be produced in culture, where they can cause caudalisation and promote ectoderm differentiation (Eiraku and Sasai, 2012), so inhibitors of these morphogens are often added to increase the induction of a forebrain fate (Watanabe et al., 2005).

The developmental signals to produce NPCs from PSCs can be recreated in culture in a method known as dual SMAD inhibition. BMPs are bound by the artificial ligand Dorsomorphin, or by the natural ligand Noggin, preventing binding to receptors ALK1, 2, 3 and 6. This prevents phosphorylation of the SMAD proteins 1, 5, 8 and 9. Small molecules, such as SB431542, fulfil the role of Lefty *in vivo* and inhibit the Activin/Nodal/TGFβ signalling pathway via the receptors ALK4, 5 and 7, which prevents phosphorylation of SMAD2 and 3. Blocking SMAD signalling via both the BMP and Activin/Nodal/TGFβ pathways gives the method the name dual SMAD inhibition, and prevents the activation of transcription factors which lead to mesodermal and epidermal fates (reviewed by Muñoz-Sanjuán and Brivanlou, 2002).

PSC-derived NPCs form neural rosettes, which are self-organising radial structures around a central ventricle-like cavity, like a 2D-recreation of the neural tube. Rosette-forming NPCs have a default rostral identity after dual SMAD inhibition (Chambers et al., 2009; Elkabetz et al., 2008), but this can be altered by the addition of morphogens such as Shh (which induces ventralisation), and retinoic acid, Wnts, or FGFs (inducing caudalisation) (Chambers et al., 2009; Kirkeby et al., 2012). Rosette-forming PSCs with a forebrain fate left to spontaneously differentiate produce temporally restricted neuronal populations expressing cortical layer markers, and also astrocytes, according to the inside-out model of cerebral cortex formation *in vivo* (Elkabetz et al., 2008; Gaspard et al., 2008; Shi et al., 2012a) (Section 6.2.1 in Chapter 6). As an alternative to spontaneous differentiation, PSC-derived NPCs can be driven out of the cell cycle by inhibiting Notch signalling (using small molecules such as DAPT), which results in differentiation of NPCs to neurons (Lowell et al., 2006; Pierfelice et al., 2011).

Neurons from transdifferentiation

Neurons can also be produced from somatic cells or iPSCs by transdifferentiation (also called lineage reprogramming or direct conversion) which is similar to the method used to generate iPSCs from somatic cells. In transdifferentiation, forced expression of transcription factors activates existing pathways and redirects cell fate to produce neurons (called induced neurons, iNs) without passing through precursor intermediates.

Single transcription factors, including Neurogenin 2 (Thoma et al., 2012), NeuroD1 (Zhang et al., 2013), and ASCL1 (Chanda et al., 2014) can be expressed in human or mouse fibroblasts or ESCs to drive differentiation to iNs. iNs produced by these methods are excitatory, electrophysiologically active, express neuronal and synaptic markers, and are present in homogenous cultures (Chanda et al., 2014; Thoma et al., 2012; Zhang et al., 2013). Expression of other transcription factors, alone or in combination, can produce a wide range

of neuronal subtypes, including dopaminergic, GABAergic, cholinergic, hypothalamic, and striatal medium spiny neurons, as well as astrocytes and oligodendrocytes (reviewed by Ichida and Kiskinis, 2015).

Comparing transdifferentiation and directed differentiation

Transdifferentiation allows some cell types to be produced more quickly than directed differentiation. For example, Caiazzo et al. (2015) made induced astrocytes (which showed similar gene expression and function to primary astrocytes) from fibroblasts in 21 days, as compared to 100-180 days for directed differentiation. Since transdifferentiation bypasses the developmental stages mimicked in directed differentiation, transdifferentiation can be used to produce cell types whose developmental origins are unclear. This is because transdifferentiation uses the forced expression of transcription factors which are active in the target cell type, making it (theoretically) easier to identify and express the relevant transcription factors to identify each of the developmental stages and develop a directed differentiation method (Ichida and Kiskinis, 2015).

However, there are distinct advantages to mimicking developmental conditions in culture. Directed differentiation produces neurons via NPCs, which can be expanded in culture, whereas transdifferentiation does not give proliferative intermediates, and therefore produces fewer neurons (Ichida and Kiskinis, 2015). Directed differentiation also produces related cell types (for example, forebrain neurons and astrocytes), whereas transdifferentiation produces pure cultures of a particular cell type (for example, forebrain neurons). Producing astrocytes alongside neurons can be advantageous, since they support neuron survival and function (Johnson et al., 2007). Indeed, pure iN cultures produced by transdifferentiation often have primary astrocytes added to them (Zhang et al., 2013).

Neurons made by transdifferentiation of cells from aged people maintain some features of aged cells. For example, Mertens et al. (2015) found that fibroblasts transdifferentiated to neurons by Ascl1 and Ngn2 expression had transcriptome signatures which depended on the donor's age. However, reprogramming these fibroblasts to iPSCs before directed differentiation to neurons removed the age-related signatures from the transcriptomic profiles. Retaining age-related transcriptomes may be important for modelling age-related disease with iNs. Hu et al. (2015) produced iNs by transdifferentiation of fibroblasts from AD sufferers and found that iNs from three out of four AD-affected donors had higher expression of Aβ40 or Aβ42 than iNs from non-affected donors.

Despite this, cells produced by directed differentiation may more closely resemble the target cells than those produced by transdifferentiation, according to gene expression studies

(Cahan et al., 2014). Transdifferentiation does not completely silence gene expression patterns of the initial cell population, but this thought to be because some non-converted cells remain in otherwise lineage-converted cultures (Li et al., 2014c). Therefore, Cahan et al.'s findings may be due to heterogeneous cultures rather than individual mixed-property cells.

Non-converted cells can remain in culture because transdifferentiation is not completely efficient. Different transgene expression levels can contribute to this: Treutlein et al. (2016) suggest that, in MEFs transdifferentiated to neurons using Ascl1 alone, some cells are not differentiated because Ascl1 expression is reduced and remains low, whereas in cells which become neurons, Ascl1 expression is higher. Heterogeneity in the starting cells may also impact transdifferentiation efficiency: Francesconi et al. (2019) report that differences in Myc expression in pre-B cells predicts their capacity to be transdifferentiated to macrophages. In addition, fibroblasts which have been grown in culture for longer are converted to neurons with lower efficiency (Sun et al., 2014), meaning that the number of neurons which can be produced from one batch of human cells may be limited.

Methods to produce neurons by either directed differentiation or transdifferentiation can both suffer from variability. Different PSC lines vary in their response to directed differentiation protocols (Bock et al., 2011; Hu et al., 2010; Wu et al., 2007) and different fibroblast lines can be converted to neurons by transdifferentiation with different efficiencies (McCoy et al., 2018). These differences may be due to the genetic background of the cell lines.

1.4.4 Organoids and 3D culture of iPSC-derived neural cells

Monolayer or 2D neuronal cultures obtained by directed differentiation have a degree of self-organisation, since NPCs form neural rosettes, although these are lost with extended time in culture (Chambers et al., 2009). The 3D cerebral organoid (CO) cultures, described below, have a higher degree of self-organisation: 3D rosette-like structures are maintained, and produce neurons and glia in a manner similar to that *in vivo* (discussed in detail in Section 6.2 in Chapter 6). Some culture techniques are reported as 3D, but lack the self-organising component of COs, making them more akin to thick monolayers. These cultures involve embedding NPCs in thick layers of matrigel or hydrogel, and allowing them to differentiate into neurons (Choi et al., 2014; Zhang et al., 2016).

Self-organising 3D culture of iPSC-derived neural cells: cerebral organoids

Organoids are organ-like tissues, made from PSCs or organ-specific progenitors, which produce multiple organ-specific cell types that self-organise into organ-like structures and recapitulate (to some degree) organ-specific function (Lancaster and Knoblich, 2014b). COs hold great potential, and their future uses may be as platforms for drug testing in a more physiologically relevant environment than 2D cultures, modelling patient-specific diseases, or even as replacement tissues (Lancaster and Knoblich, 2014b). Although many organoid types have been generated, this section focuses on COs, which provide a model of the brain.

COs can be divided into two main types: those grown without patterning factors, which produce a variety of brain areas within the same structure (Lancaster et al., 2013), and those grown with patterning factors, which restrict cell fate to give brain area-specific organoids. Patterning factors have been used to produce COs specific to various brain areas including the forebrain (Lancaster et al., 2017; Mariani et al., 2015), which is of most interest in FTDP-17T.

As a model of the developing human brain, COs have been used to investigate developmental diseases and disorders, including Zika virus infection (Qian et al., 2016, and others), microcephaly (Lancaster et al., 2013), and autism spectrum disorders (Mariani et al., 2015). COs have also been used to model diseases and disorders of the adult brain, including AD (Raja et al., 2016, and others), but only one study to date has used COs to study FTDP-17T-relevant MAPT mutations (Seo et al., 2017).

Self-organising 3D iPSC-derived neuronal cultures may be more physiologically relevant than their 2D counterparts, since the microenvironment for each cell is more like that in the brain (reviewed by Ranjan et al., 2018). In addition, 3D culture may increase neuron maturity with respect to tau splicing (Choi et al., 2014), electrophysiological activity (Zhang et al., 2016), and glial cell differentiation (Choi et al., 2014), although this has not yet been studied in self-organising COs. The potential advantages of 3D COs over 2D monolayer cultures are further discussed in Section 6.2 in Chapter 6.

1.4.5 Advantages and disadvantages of iPSC-derived neuronal cultures for modelling the human brain

iPSCs allow human-specific brain diseases and disorders to be modelled using human-derived cells, and these models hold great promise for determining disease mechanisms, for drug discovery and even for transplant. However, as discussed in this section, iPSC-derived neural cultures do not recapitulate all aspects of the brain: they lack certain cells types, are relatively

Table 1.4 **Published studies using iPSC-derived neurons with the N279K MAPT mutation**

Cell type	Tau			Main findings	Paper
	mRNA	Protein	Phosphorylation		
2 iPSC clones d40 neurons: $GABA^+$ 40-45% $ChAT^+$ 2-5% Th^+ 40-50%	↑ 4R, → 3R	-	↑ AT8 (all neurons) ↑ AT8 (Th^+ neurons)	↓ neurite outgrowth ↑ tau fragmentation ↑ caspase cleaved tau ↑ LDH w. rotenone ↑ UPR: p-PERK, BiP ↑ pro-apoptosis: PUMA	Ehrlich et al. (2015)
2 iPSC lines d30-100 neurons Glutamatergic	Earlier 4R → 3R	Earlier 0N4R (d55) Low 0N3R (d150) Low 1N3R (d150)	↑ AT8 (d55) AT100 puncta (d150) Earlier 4R (cell bodies) Earlier 4R (processes)	Thicker processes ↓ anterograde transport ↑ stationary mitochondria ↑ mature, repetitive APs ↑ Na^+ current	Iovino et al. (2015)
2 iPSC lines d21-28 NPCs Glutamatergic	↑ 4R, → 3R	-	-	↓ NPCs to neurons Neurons degenerate rapidly ↑ flotillin-1 ↑ EEA1: early endosomes ↑ CHMP2B: late endosomes ↓ LAMP-1: lysosomes ↑ LDH release ↑ caspase 3/7 activity ↑ stress granules: G3BP, TIA-1	Wren et al. (2015)

Neurons were generated by directed differentiation using dual SMAD inhibition. Changes are relative to control iPSC-derived neurons. →: no change; ↑: increased; ↓: decreased. Abbreviations: AP: action potential; BiP: binding immunoglobulin protein; ChAT: choline acetyltransferase; CHMP2B: charged multivesicular protein 2B; D: day; EEA1: Early Endosome Antigen 1; GABA: gamma-aminobutyric acid; G3BP: Ras GTPase-activating protein-binding protein 1; :LAMP-1: lysosomal-associated membrane protein 1; LDH: lactate dehydrogenase; p-PERK: phosphorylated protein kinase RNA-like ER kinase; PUMA: p53-upregulated modulator of apoptosis; TIA-1: T-cell intracytoplasmic antigen 1; Th: tyrosine hydroxylase; UPR: unfolded protein response.

Table 1.5 **Published studies using iPSC-derived neurons with the P301L or V337M MAPT mutations**

Cell type	Tau			Main findings	Paper
	mRNA	Protein	Phosphorylation		
P301L					
2 iPSC lines d30-150 neurons Glutamatergic	$\rightarrow$ 4R, $\rightarrow$ 3R	Some 0N4R (d55)	$\uparrow$ AT8 (d55)	Thicker processes $\downarrow$ anterograde transport $\downarrow$ retrograde transport $\uparrow$ stationary mitochondria $\uparrow$ varicosities w. α synuclein, tau $\uparrow$ mature, repetitive APs $\uparrow$ Na^+ current	Iovino et al. (2015)
1 iPSC line d80 COs	-	-	-	$\uparrow$ p25/p35	Seo et al. (2017)
V337M					
2 iPSC clones d40 neurons $GABA^+$ 40-45% $ChAT^+$ 2-5% Th^+ 40-50%	$\rightarrow$ 4R, $\rightarrow$ 3R	-	$\uparrow$ AT8 (all neurons)	$\downarrow$ neurite outgrowth $\uparrow$ tau fragmentation $\uparrow$ caspase cleaved tau $\uparrow$ LDH w. rotenone $\uparrow$ UPR: p-PERK, BiP $\uparrow$ pro-apoptosis: PUMA	Ehrlich et al. (2015)

Monolayer neurons were generated by directed differentiation using dual SMAD inhibition; COs were made from embryoid bodies, patterned with dorsomorphin. Changes are relative to control iPSC-derived neurons. $\rightarrow$: no change; $\uparrow$: increased; $\downarrow$: decreased. Abbreviations: AP: action potential; BiP: binding immunoglobulin protein; ChAT: choline acetyltransferase; CO: cerebral organoid; D: day; EEA1: Early Endosome Antigen 1; GABA: gamma-aminobutyric acid; LDH: lactate dehydrogenase; PUMA: p53-upregulated modulator of apoptosis; TIA-1: T-cell intracytoplasmic antigen 1; Th: tyrosine hydroxylase; UPR: unfolded protein response.

immature, and different differentiation methodologies make comparisons between studies difficult (reviewed by Ranjan et al., 2018). iPSC lines themselves are highly variable due to the genetic variability between the many and diverse somatic cell donors from whom the lines originate. Therefore, it is important that phenotypes revealed using iPSC-derived neural cells are corroborated by multiple studies, and that sufficient controls lines are used.

Immaturity of iPSC-derived neural cultures

Several studies indicate that iPSC-derived neurons are more representative of the fetal than the adult brain. For example, 72 day-old iPSC-derived cortical neurons had similar RNA expression profiles to primary human fetal neurons cultured for 28 days, but less similarity to fresh fetal neurons or adult neurons (Handel et al., 2016). Likewise, 56 day-old hESC-derived midbrain-like neurons were more similar to fetal brain than adult substantia nigra in terms of gene expression (Patani et al., 2012). Transdifferentiated neurons are also immature: motor iNs had similar gene expression profiles to their primary fetal counterparts (Son et al., 2011). Even COs are more similar to the fetal than adult brain, as demonstrated by several gene expression studies which found similarities between COs and the 8-9-week-old (Dang et al., 2016), 12-13-week-old (Camp et al., 2015), or 19-24-week-old (Qian et al., 2016) fetal brain.

Immaturity with respect to tau expression

Six tau isoforms are expressed in the adult human brain, as compared to one in the fetal brain (Goedert and Jakes, 1990). However, iPSC-derived neurons express mostly the fetal 0N3R tau isoform until around day 50 in culture (Iovino et al., 2015; Sposito et al., 2015), with expression of up to six tau isoforms being reported at day 150 (Iovino et al., 2015), day 190 (Beevers et al., 2017), and day 365 (Sposito et al., 2015). In addition, 0N3R tau predominates in younger cultures (Iovino et al., 2015), indicating high numbers of immature neurons. The extended culture times necessary to recapitulate adult-like tau splicing is a limit to modelling the full effects of MAPT mutations.

Genetic background effects in experimental models

In FTDP-17T, variation in symptoms and neuropathology between people with the same mutation suggests the presence of as yet unknown genetic or environmental modifiers (Foster et al., 1997). Similar effects are also seen in animal studies. For example, the expression of truncated human tau in two rat strains led to significantly different NFT loads (measured by AT8 staining) and microglial responses, although astrogliosis was similar between the rat

strains (Stozicka et al., 2010). Although this study used truncated, not mutated, human tau and although immune cells would not be present in iPSC-derived neuron models of tauopathy, it still suggests that differences in tau phosphorylation at the AT8 epitope could be attributed to genetic variation.

As well as disease-related neuropathology, the genetic background of iPSCs has been shown to influence their gene expression, DNA methylation profiles, and capacity for differentiation to other cells types (Bock et al., 2011; Boulting et al., 2011). These results demonstrate the importance of controlling for genetic background, particular in experiments using iPSC-derived neurons which typically only have iPSC lines from a small number of donors. CRISPR is a powerful tool to do this: it can be used to rescue or introduce specific mutations, creating a pair of iPSC lines sharing a genetic background and differing at the chosen mutation locus (Chapter 4).

1.4.6 iPSC-derived neurons as models of tauopathy

iPSC-derived neurons have been used to model the effects of several MAPT mutations, and findings from published studies on iPSC-derived neurons with the N279K, P301L or V337M tau mutations are summarised in Tables 1.4 and 1.5. The extent to which FTDP-17T-relevant phenotypes are recapitulated in iPSC-derived neural cultures is discussed in detail in Section 4.1 in Chapter 4.

The experiments using iPSC-derived neurons described in Tables 1.4 and 1.5 did not use isogenic controls, which can minimise the contribution of genetic background effects to subtle phenotypes (Section 1.4.5). This project aims to fill that gap, by making iPSC lines isogenic for the N279K mutation and using them to investigate tau splicing, phosphorylation and aggregation.

In addition, the experiments described in Tables 1.4 and 1.5 were all conducted in monolayer culture (except for that of Seo et al., 2017). Since 3D culture may increase neuronal maturity (Choi et al., 2014) and would provide neurons with a more brain-like environment, this project will also use cerebral organoid cultures with the aim of increasing neuronal maturity with respect to tau splicing.

1.5 Aims

The aim of my PhD project was to investigate the extent to which FTDP-17T-relevant phenotypes caused by the MAPT mutations N279K, P301L and V337M can be recapitulated

in forebrain-specific monolayer neurons and COs derived from FTDP-17T patient and control subject iPSCs. The overall aim is sub-divided as follows:

1. Differentiate forebrain-specific monolayer neuronal cultures from control subject iPSCs and FTDP-17T patient-derived iPSCs with the MAPT mutations N279K and V337M. The neuronal cultures will be maintained for up to 100 days to allow the neurons to mature and:
    - Determine the proportion of neuronal and glia cells in each culture, as a measure of the cultures' maturity and to check for FTDP-17T-relevant astrogliosis
    - Determine which tau isoforms are present, to establish the cultures' maturity with respect to tau expression, and to observe the previously established effect of the N279K mutation: an increase in 4R tau relative to 3R tau
    - Investigate if and at what time point FTDP-17T-relevant tau phosphorylation or misfolding is detectable. Tau misfolding has not previously been detected in iPSC-derived neural cultures without the addition of exogenous tau
    - Investigate whether other FTDP-17T-relevant phenotypes are present in neurons with MAPT mutations.
2. Decrease variability between iPSC lines by using CRISPR to produce isogenic iPSC lines. This will be done by correcting the N279K mutation in FTDP-17T patient-derived iPSCs, or inducing the N279K mutation in control subject-derived iPSCs
    - Ensure that gene-edited iPSC lines express the desired mutations and establish if off-target mutations or karyotypic defects are present.
3. Differentiate isogenic iPSC lines to 3D COs, to investigate the effects of MAPT mutations in a more brain-like environment by:
    - Examine which tau isoforms are present, to determine maturity with respect to tau expression, and to investigate whether 3D culture can accelerate neuronal maturation with respect to tau expression
    - Investigate if and at what time point FTDP-17T-relevant tau phosphorylation or misfolding is detectable, or if it is enhanced by 3D culture, as observed by Choi et al. (2014) using AD-relevant cells
    - Compare my findings in monolayer neurons with those in COs, to determine if CO culture is advantageous in terms of tau expression or the appearance of FTDP-17T-relevant changes.

Chapter 2

Materials and Methods

2.1 General Materials

Materials and reagents used in culture and differentiation of induced pluripotent stem cells (iPSCs), where they were purchased from, and their stock concentrations (if appropriate) are listed in Table 2.1.

2.2 iPSC culture

2.2.1 Media and solutions for iPSC maintenance

Indicated recipes are for 50ml of each solution. All media and solutions were filtered under sterile conditions with a 0.22µm filter and stored at 4°C.

MEF media: 44ml DMEM/F12, 5ml FBS, 500µl pen-strep (10,000 U/ml stock solution), 500µl L-glutamine (200mM stock solution).

Knockout Serum Replacement (KSR) Medium: 39ml Advanced DMEM/F12, 10ml Knockout Serum Replacement, 500µl L-glutamine (200mM stock solution), 500µl pen-strep (10,000 U/ml stock solution), 3.5µl β-mercaptoethanol (50mM stock solution). KSR medium was purchased from the CCK.

Essential 8 (E8) Medium: 49ml DMEM/F12, 1ml Insulin-Transferrin-Selenium (100x stock solution), 360µl sodium bicarbonate (7.5% stock solution), 500µl L-ascorbic acid (200mM stock solution in ddH_2O), 500µl pen-strep (10,000 U/ml stock solution). E8

Table 2.1 **Materials used and where purchased**

Material or reagent	Supplier	Stock concentration
β-mercaptoethanol	Life Technologies	50mM
γ-irradiated mouse embryonic feeder cells (MEFs)	Globalstem	-
Accutase	Innovative Cell Technologies	1x
Advanced DMEM/F12	Invitrogen	-
B27 supplement without vitamin A	Invitrogen	50x
B27 supplement with vitamin A	Invitrogen	50x
Bovine serum albumin (BSA)	Europa Bioproducts	-
Dispase powder	Life Technologies	-
DMEM/F12	Invitrogen	-
Dulbecco's phosphate buffered saline (DPBS)	Gibco	-
EDTA in H_2O	Invitrogen	0.5M
ES Cell Qualified Fetal Bovine Serum (FBS)	Gibco	-
FBS	Fisher Scientific	-
Fibroblast growth factor 2 (FGF2)	CCK	4mg/ml
Gelatine in sterile H_2O	CCK	0.1%
GlutaMAX	Gibco	100x
Heparin	Sigma	100mg/ml
Karyomax Colcemid solution	Gibco	10µg/ml
Knockout Serum Replacement	Invitrogen	-
Insulin	Sigma	10mg/ml
Insulin-Transferrin-Selenium	Gibco	100x
L-ascorbic acid powder	Sigma	200mM (diluted in ddH_2O)
L-glutamine	Gibco	200mM
Laminin	Invitrogen	1mg/ml
N2 supplement	Invitrogen	100x
Neurobasal	Invitrogen	-
Non-Essential Amino Acids (MEM-NEAA)	Sigma	100x
Penicillin and streptomycin (pen-strep)	Gibco	10,000 U/ml
Poly-L-ornithine	Sigma	0.1mg/ml
Sodium bicarbonate	Gibco	7.5%
Transforming growth factor beta 1 (TGFβ-1) powder	R&D	2mg/ml (diluted in ddH_2O)
Trypsin/EDTA solution	Invitrogen	0.05%
Trypsin inhibitor	Sigma	1x
Vitronectin	Gibco	500µg/ml
CoolCell freezing container	BioCision	-
Coverslips: tissue culture treated plastic	Thermo Fisher	-
Cryovials	Thermo Scientific Nunc	-
Plates: low-attachment 24-well	Costar	-
Plates: low-attachment 96-well round-bottomed	Costar	-
Vicryl polyglactin 910 surgical sutures	Ethicon	-

.

Table 2.2 **iPSC lines used**

Line name	Diagnosis	Source	References
CTRL1	none	LRM	BBHX in [1]
CTRL2	none	LRM [3]	CRL in [1,2]
N279K1	FTDP-17T	Coriell	[1]
N279K2	FTDP-17T	Coriell	[1]
V337M	FTDP-17T	Coriell	-
P301Lpat	FTDP-17T	[4]	[1]
IsoCon	none	Axol	-
P301Lhet	n/a: heterozygous knock-in	Axol	-
P301Lhom	n/a: homozygous knock-in	Axol	-

All iPSC lines were derived from fibroblasts. "Coriell" indicates that the NINDS Coriell Repository provided fibroblasts with MAPT mutations, which were re-programmed to iPSCs at the Laboratory for Regenerative Medicine (LRM). The P301Lhet (P301L heterozygous knock-in) and P301Lhom (P301L homozygous knock-in) lines were generated from the IsoCon (isogenic control) line using CRISPR by Horizon Discovery Group and obtained as part of a collaboration with Axol Bioscience. Abbreviations used in this table: FTDP-17T: frontotemporal dementia with Parkinsonism, linked to chromosome 17 and tau mutations. References: [1]: Iovino et al. (2015); [2]: Shi et al. (2012b); [3]: Vallier et al. (2009); [4]: Alberici et al. (2004).

medium was purchased from the MRC Laboratory of Regenerative Medicine Cell Culture Kitchen facility (CCK).

1mg/ml collagenase IV: 40ml Advanced DMEM/F12, 10ml Knockout Serum Replacement, 500µl L-glutamine (200mM stock solution), 0.35µl β-mercaptoethanol (50mM stock solution), 50mg collagenase IV powder. Collagenase solution was purchased from the CCK.

Collagenase-dispase mix: Dispase powder was dissolved in DPBS to make a 10mg/ml stock, which was diluted to 1mg/ml in Advanced DMEM. Equal volumes of 1mg/ml collagenase solution and 1mg/ml dispase solutions were mixed to make a 0.5mg/ml solution of both enzymes.

2.2.2 Induced pluripotent stem cell (iPSC) culture conditions

Nine iPSC lines were used (Table 2.2). The feeder-dependent iPSC lines CTRL1, CTRL2, N279K1, N279K2, V337M and P301L-patient (P301Lpat) were cultured on γ-irradiated mouse embryonic feeder cells (MEFs). Six-well plates were coated with 0.1% gelatine in

sterile H_2O for at least 1 hour before MEFs were seeded. MEFs were maintained in MEF media (Section 2.2.1) overnight before thawing or passaging iPSCs. iPSCs were maintained in KSR medium (Section 2.2.1) with 4ng/ml FGF2 (4mg/ml stock solution). Differentiated colonies (Figure 2.1) were marked under the microscope and removed by aspiration. iPSCs were passaged when they reached approximately 70% confluency, using collagenase-dispase (Section 2.2.1). If the iPSCs did not reach sufficient confluency for splitting within 1 week, more MEFs in KSR media were added to support iPSC growth. iPSCs were kept in a humidified incubator at 37°C with 5% CO_2.

Some iPSCs were grown in feeder-free conditions. These were the P301L-heterozygous knock-in (P301Lhet), P301L-homozygous knock-in (P301Lhom), and isogenic control (IsoCon) iPSC lines. They were cultured on 6-well plates coated with 5µg/ml vitronectin (500µg/ml stock solution) in DPBS for at least 1 hour at room temperature. iPSCs were maintained in E8 medium (Section 2.2.1) with 25ng/ml FGF2 (4mg/ml stock solution) and 2ng/ml TGFβ-1 (2mg/ml stock solution). Differentiated colonies (Figure 2.1) were marked under the microscope and removed by aspiration. Cells were passaged at about 70% confluency with 0.5mM EDTA in DPBS (0.5M stock solution) and kept in a humidified incubator at 37°C with 5% CO_2.

2.2.3 iPSC cryopreservation

iPSCs were cryopreserved both at low passage numbers and after karyotyping showed a normal complement of chromosomes and no genetic re-arrangements. Confluent iPSCs were lifted from the culture plate with either EDTA or collagenase-dispase, depending on the culture system (Section 2.2.2). Colonies were then added to 10ml of culture medium and centrifuged for 3 minutes at 300g in a Sorvall ST-16 centrifuge. The medium was removed and a mixture of 20% DMSO and 80% culture medium (KSR or E8) was added dropwise to the iPSC colonies. The colonies were transferred to a sterile, labelled cryovial and immediately frozen at -80°C in a CoolCell freezing container. The following day, vials were moved to liquid nitrogen for long term storage.

2.2.4 iPSC thawing

Vials containing cryopreserved iPSCs were thawed in a 37°C water bath until a ball of ice approximately 0.75cm in diameter remained. One ml of media (KSR or E8) was added dropwise to the vial, then the colonies were added to 10ml of culture medium and centrifuged for 3 minutes at 300g in a Sorvall ST-16 centrifuge. One ml of culture medium supplemented

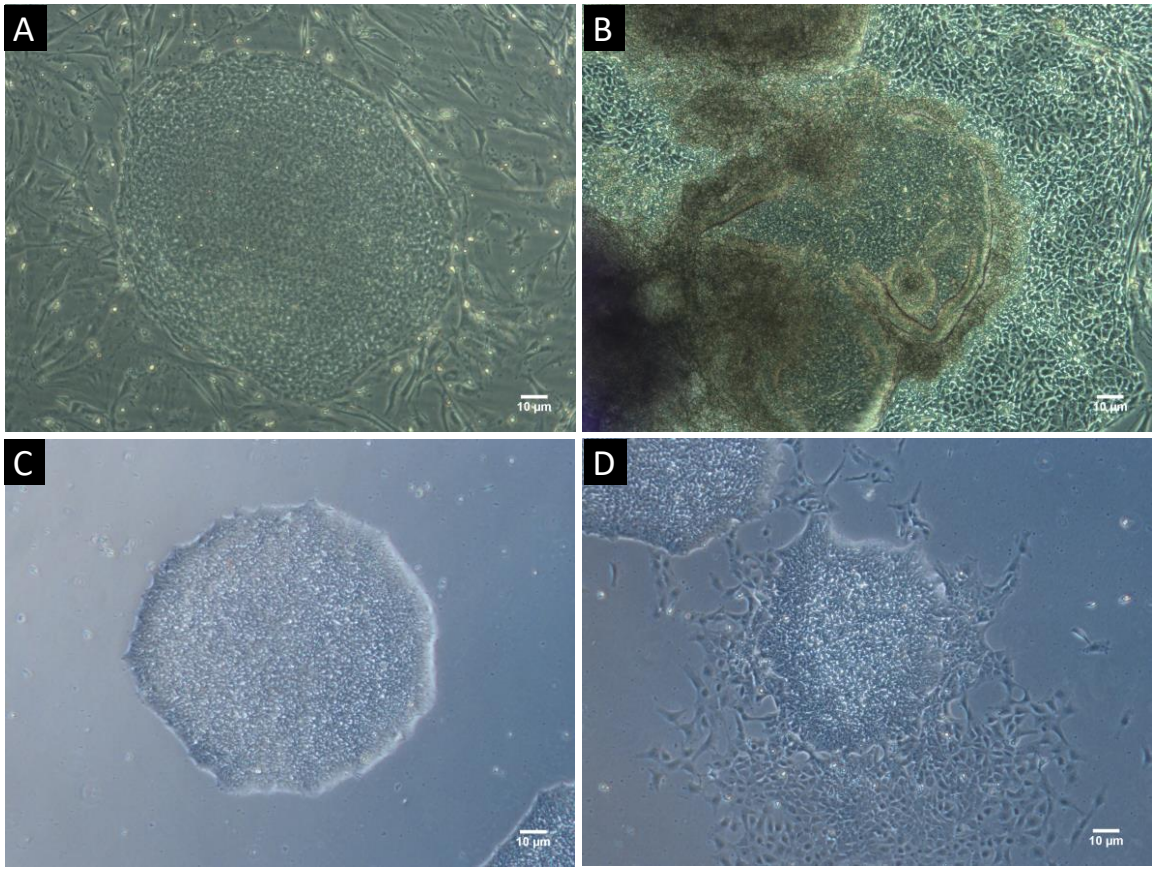

Fig. 2.1 **Pluripotent and differentiated iPSC colonies.** Pluripotent **(A)** and differentiating **(B)** iPSC colonies cultured on MEFs with KSR media supplemented with 4ng/ml FGF2. Pluripotent **(C)** and differentiating **(D)** iPSC colonies cultured on vitronectin with E8 supplemented with 25ng/ml FGF2 and 2ng/ml TGFβ-1. Scale bar = 10µm.

with 10µm ROCK inhibitor (10mM stock) to reduce cell death was added to the iPSC colonies, and colonies were gently plated on MEFs or vitronectin-coated plates. The medium was changed to KSR or E8 media without ROCK inhibitor 24 hours after plating.

2.2.5 Karyotyping

Karyomax Colcemid solution was diluted to 0.1µg/ml (from the 10µg/ml stock solution) in KSR and added to a non-confluent well of iPSCs. The plate was incubated at 37°C for 3 hours, then the colcemid solution was removed and the iPSCs were washed with DPBS. iPSC colonies were lifted from the culture plate with collagenase-dispase and added to 10ml of culture medium. The cell pellet was collected by centrifugation at 1200rpm for 7 minutes in a Sorvall ST-16 centrifuge, the supernatant was removed and a hypotonic 0.055M KCl solution was gently mixed with the iPSC colonies, to obtain chromosome spreading by swelling the cells without lysing them. The cell pellet was collected by centrifugation at 1200rpm for 7 minutes in a Sorvall ST-16 centrifuge, then fixed with 100% methanol and acetic acid in a 3:1 ratio. The fixed cell suspension was sent for karyotypic analysis.

2.3 Differentiation of iPSCs to monolayer neurons

Differentiation of iPSCs to neural precursor cells (NPCs) followed a protocol developed for human embryonic stem cells by Kirkeby et al. (2012), which was modified for iPSCs by a previous lab member (Santiváñez Pérez, 2017). Santiváñez Pérez made NPCs and plated them for terminal differentiation to neurons in 3D droplets, whereas I plated NPCs for terminal differentiation as a 2D monolayer. The method is summarised in Figure 2.2. CTRL1, CTRL2, N279K1, N279K2 and V337M iPSCs were differentiated to monolayer neurons in three independent differentiations.

2.3.1 Media recipes and growth factors for monolayer neurons

Neuronal Induction Medium (NIM): 25ml DMEM/F12, 25ml Neurobasal, 500µl N2 supplement (100x stock solution), 1ml B27 supplement without vitamin A (50x stock solution), 500µl L-glutamine (200mM stock solution), 100µl pen-strep (10,000 U/ml stock solution).

Neuronal Proliferation Medium (NPM): 25ml DMEM/F12, 25ml Neurobasal, 250µl N2 supplement (100x stock solution), 500µl B27 supplement without vitamin A (50x stock solution), 500µl L-glutamine (200mM stock solution), 100µl pen-strep (10,000 U/ml stock

solution).

Neuronal Differentiation Medium (NDM): 50ml Neurobasal, 1ml B27 supplement with vitamin A (50x stock solution), 500µl L-glutamine (200mM stock solution), 100µl pen-strep (10,000 U/ml stock solution).

Table 2.3 **Reagent for iPSC maintenance and neuronal differentiation**

Reagent	Supplier	Stock concentration	Dilutant
ROCK inhibitor (Y-27632)	Tocris	10mM	ddH_2O
Noggin	R&D	100µg/ml	0.1% BSA in DPBS
SB431542	Tocris	10mM	DMSO
Ascorbic acid	Sigma	200mM	ddH_2O
BDNF	R&D	20µg/ml	0.1% BSA in DPBS
GDNF	R&D	20µg/ml	0.1% BSA in DPBS
db-cAMP	Sigma	50mM	ddH_2O
DAPT	Sigma	40mM	DMSO
CHIR (CT99021)	Axon	10mM	DMSO

Factors were aliquoted and stored at -20°C. Abbreviations used in this table: BDNF: brain-derived neurotrophic factor; BSA: bovine serum albumin; DAPT: N-[N-(3,5-Difluorophenacetyl)-L-alanyl]-S-phenylglycine t-butyl ester; db-cAMP: dibutyl-cyclic adenosine monophosphate; DPBS: Dulbecco's Phosphate Buffered Saline; GDNF: glial cell-derived neurotrophic factor; ROCK: p160-rho-associated coiled kinase.

2.3.2 Protocol for differentiation to monolayer neurons

On day 0, confluent iPSC colonies were released from the MEFs with collagenase-dispase, added to 10ml of a 50-50 mixture of DMEM/F12 and Neurobasal media and allowed to fall by gravity for approximately 2 minutes. The medium was removed neuronal induction medium (NIM) was added, with 100ng/ml Noggin and 10µM SB431524 for neuronal differentiation by dual Smad inhibition, and 10µM ROCK inhibitor for the first 2 days to reduce cell death. The cells were cultured in low-attachment 24-well plates (coated with a hydrogel that decreases cell attachment to the plate surface) for embryoid body (EB) formation. Large clumps of cells were separated by gentle pipetting with a P1000 Gilson pipette.

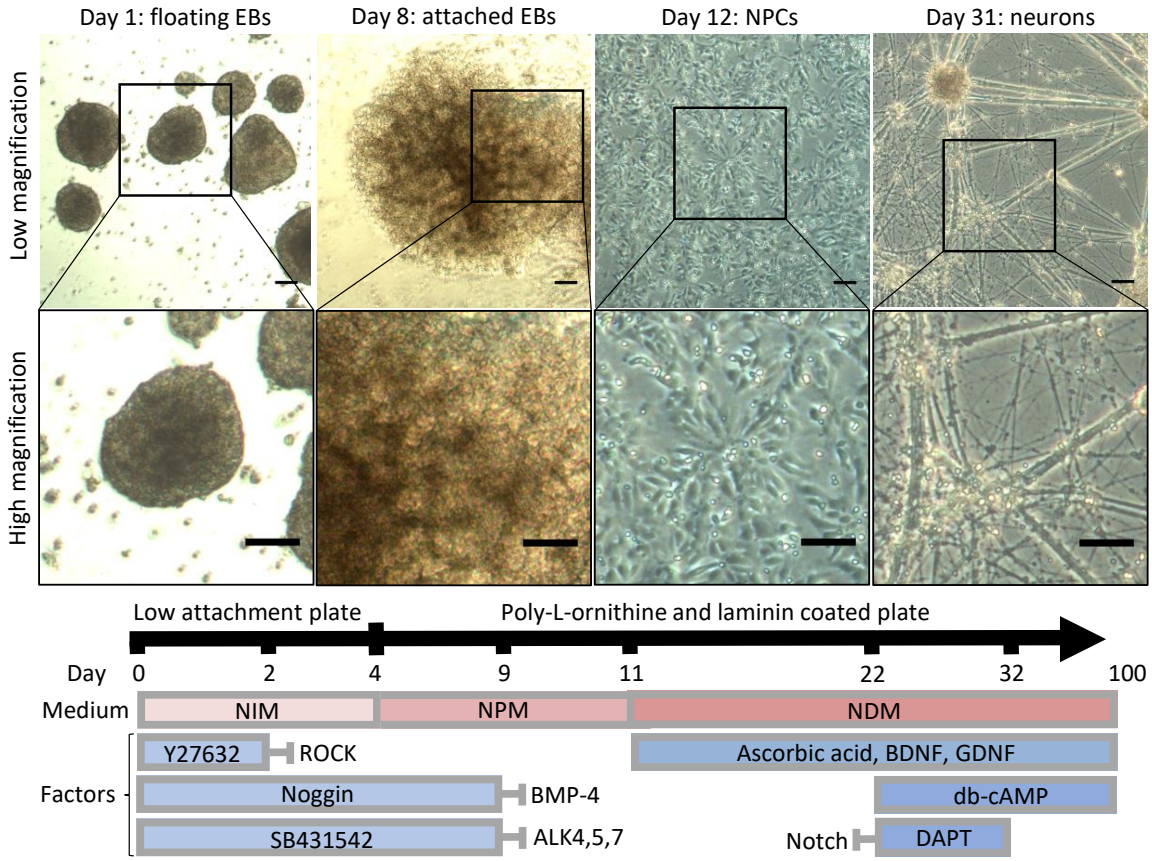

Fig. 2.2 **Neuronal differentiation of iPSCs.** Images show the stages of differentiation at high (first row) and low (second row) magnification. Scale bar = 10µm. Left to right: floating embryoid bodies (EBs) at day 1; attached EBs with circular neuronal rosettes at day 8; neuronal precursors (NPCs) from dissociated neuronal rosettes at day 12; neurons at day 31. The black bar indicates the day of differentiation, starting from iPSCs at day 0. Text above the black bars indicates the cell culture surface: low-attachment plates were used for EBs, poly-L-ornithine and laminin coated plates were used for attached cells. Pink bars indicate the medium in which differentiating cells were maintained: neuronal induction medium (NIM), neuronal proliferation medium (NPM) or neuronal differentiation medium (NDM). Blue bars show factors added to the differentiation media, and grey sideways "T" shapes show inhibition by added factors. Cells were maintained in media containing BDNF and GDNF to induce terminal neuronal maturation, as described by Kirkeby et al. (2012). BDNF: brain-derived neurotrophic factor; BMP: bone morphogenic protein; DAPT: N-[N-(3,5-Difluorophenacetyl)-L-alanyl]-S-phenylglycine t-butyl ester; GDNF: glial-derived neurotrophic factor; db-cAMP: dibutyl-cyclic adenosine monophosphate; ROCK: rho-associated protein kinase.

Prior to day 4, a poly-L-ornithine and laminin (P/L) coated 24-well plate was prepared, to culture the EBs as attached cells. Poly-L-ornithine (50µg/ml, from a 0.1mg/ml stock solution) was added to each well and incubated overnight at 37°C. The poly-L-ornithine was removed, replaced with laminin diluted in DPBS (5µg/ml, from a 1mg/ml stock solution) and incubated overnight at 37°C. On day 4, the laminin was removed and the EBs were re-plated in P/L coated wells in neuronal proliferation medium (NPM) with 100ng/ml Noggin and 10µM SB431524. On day 9, the medium was changed to NPM without SB431524 or Noggin.

Prior to day 11, P/L coated 24-well plates were prepared as described above. On day 11, laminin was removed from the P/L coated plates and each well was dried thoroughly by aspiration. The cells were incubated with 1x Accutase for 10 minutes, triturated to a single-cell suspension and transferred to a falcon tube containing 10ml Neurobasal medium. The cell pellet was collected by centrifugation at 300g in a Sorvall ST-16 centrifuge for three minutes, then the medium was removed and the cells were re-suspended in neuronal differentiation medium (NDM) at a concentration of 15000 cells/µl and plated on the dried P/L coated plates in 10µl droplets. The plates were placed in the incubator for one hour to allow the cells to attach, then NDM with 20ng/ml BDNF, 10ng/ml GDNF and 0.2mM ascorbic acid was added to each well. By day 16, neuronal precursors (NPCs) were visible as radially arranged rosette-like formations.

Prior to day 20, P/L coated plates were prepared. To grow neurons for immunofluorescence, tissue culture treated plastic coverslips were placed in 24-well plates and P/L coated as described above. To grow neurons for protein extraction, 24-well plates without coverslips were P/L coated and to collect conditioned media, 96-well plates were P/L coated. On day 20, NPCs were incubated with 1x Accutase for 10 minutes, triturated to a single-cell suspension and transferred to a falcon tube containing 10ml Neurobasal medium. The cell pellet was collected by centrifugation at 300g for three minutes, then the medium was removed and the cells were re-suspended in NDM at a concentration of 15000 cells/µl. Immediately before plating, laminin was removed from the coated plates and a minimal volume of NDM was added to each well. The cells were plated at 80000 cells/cm^2 and the plates were gently shaken to ensure an even coverage of cells over each well.

On day 22, the medium was changed to NDM with 20ng/ml BDNF, 10ng/ml GDNF, 0.2mM ascorbic acid, 500µM db-cAMP and the γ-secretase inhibitor DAPT (1µM), which inhibits Notch signalling and promotes neuronal differentiation. The medium was replaced every two days. From day 32 onward, DAPT was removed and the neurons were maintained in NDM with 20ng/ml BDNF, 10ng/ml GDNF, 0.2mM ascorbic acid and 500µM db-cAMP

until day 50, 80-100. To prevent the neurons peeling off the coverslips, laminin (1µg/ml) was added to NDM every 10 days, starting at day 30.

2.4 iPSC differentiation to cerebral organoids

Differentiation of iPSCs to forebrain-specific cerebral organoids (COs) followed the method described by (Lancaster et al., 2017) (Figure 2.3).

2.4.1 Media for cerebral organoids

Low FGF medium: 40ml DMEM/F12, 10ml Knockout Serum Replacement, 1.5ml ES Cell Qualified FBS, 500µl GlutaMAX (100x stock solution), 500µl MEM-NEAA (100x stock solution). Non-scaffold method: 0.35µl β-mercaptoethanol (50mM stock solution). Scaffold method: 100µl β-mercaptoethanol (50mM stock solution). 50µM ROCK inhibitor (10mM stock solution) and 4ng/ml FGF2 (4mg/ml stock solution) were added immediately before use.

Neural Induction Medium (NI): 50ml DMEM/F12, 500µl N2 supplement (100x stock solution), 500µl GlutaMAX (100x stock solution), 500µl MEM-NEAA (100x stock solution), 50µl heparin (100mg/ml stock solution).

Differentiation Medium Without Vitamin A, scaffold method (DM-1): 25ml DMEM/F12, 25ml Neurobasal, 250µl N2 supplement (100x stock solution), 1ml B27 supplement without vitamin A (50x stock solution), 500µl GlutaMAX (100x stock solution), 250µl MEM-NEAA (100x stock solution), 12.5µl insulin (10mg/ml stock solution), 50µl β-mercaptoethanol (50mM stock solution), 500µl pen-strep (10,000 U/ml stock solution).

Differentiation Medium With Vitamin A, scaffold method (DM-2): 25ml DMEM/F12, 25ml Neurobasal, 250µl N2 supplement (100x stock solution), 1ml B27 supplement with vitamin A (50x stock solution), 500µl GlutaMAX (100x stock solution), 250µl MEM-NEAA (100x stock solution), 12.5µl insulin (10mg/ml stock solution), 50µl β-mercaptoethanol solution (50mM stock solution), 667µl sodium bicarbonate solution (7.5%), 100µl ascorbic acid solution (200mM stock solution), 500µl pen-strep (10,000 U/ml stock solution).

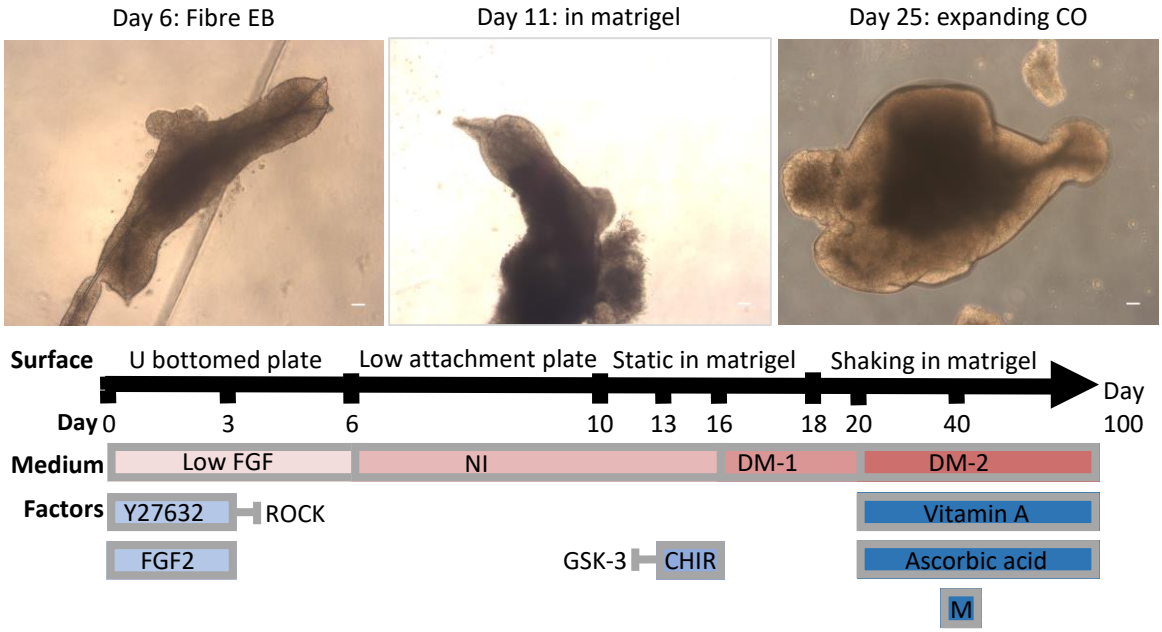

Fig. 2.3 **Differentiation of iPSCs to cerebral organoids.** Images show the stages of differentiation. Left to right: an EB formed around a fibre scaffold; an EB with brightening edges, indicating neuroectoderm tissue; a CO with growing neuroepithelial buds after embedding in matrigel. Scale bar = 10µm. The day of differentiation was counted from iPSCs at day 0. Pink bars indicate the culture medium: low FGF medium, neuronal induction medium (NI) or neuronal differentiation medium (DM-1 or 2; Section 2.2.1). Blue bars show factors added to the media; vitamin A was added as part of the B27 supplement. FGF2: fibroblast growth factor 2; GSK-3: glycogen synthase kinase 3; ROCK: rho-associated protein kinase. ”M” indicates addition matrigel, dissolved in cold DM-2 medium, at day 40.

2.4.2 Protocol for forebrain-specific cerebral organoids

Vicryl polyglactin 910 surgical sutures were untwisted to fray the end of the suture. Fibres of approximately 1mm were shaved from the frayed suture with a sterile razor blade and collected in low FGF medium with a cut P1000 pipette tip. The concentration of fibres was estimated by counting with a haemocytometer.

On day 0, confluent feeder-free iPSC colonies were washed with DPBS and lifted from the culture surface with EDTA as described in Section 2.2.2. Confluent feeder-dependent iPSC colonies were lifted from the feeder layer with collagenase-dispase as described in Section 2.2.2. iPSC colonies were then incubated with 1ml 1x Accutase for 4 minutes at 37°C. The iPSCs were triturated to a single-cell suspension, added to 9ml of E8 medium and centrifuged at 300g for 3 minutes in a Sorvall ST-16 centrifuge to collect the cell pellet. The medium was removed, then the cells were re-suspended in low FGF medium containing fibres to make a cell suspension of 9000 cells/150µl, with approximately 2 fibres/150µl. Fifty µM ROCK inhibitor and 4ng/ml FGF2 were added, then 150µl of cell suspension was pipetted with a cut P200 tip into each well of a 96-well round-bottomed low-attachment plate. On day 4, the medium was changed to low FGF medium without ROCK inhibitor or FGF2. On day 6, when EBs were brightening and had smooth edges, EBs were transferred to neural induction (NI) medium in a low-attachment 24-well plate, or cultured in the same round-bottomed plate in NI medium. NI medium was replaced every other day until day 10, when translucent neuroepithelial buds became visible. EBs were embedded in 10-20µl matrigel droplets and incubated NI medium until day 13, when 3µM CHIR was added (Table 2.3). On day 16, the medium was changed to differentiation medium 2 without vitamin A (DM-1, Section 2.4.1) and the EBs were transferred to an orbital shaker moving at 60rpm on day 18. On day 20, the medium was changed to differentiation medium 3 with vitamin A (DM-2, Section 2.4.1). The medium was replaced every 7-10 days until day 40, when the medium was replaced with cold DM-2 containing Matrigel diluted 1:50. Subsequently, DM-2 medium without matrigel was replaced every 7-10 days until day 100.

2.5 Immunocytochemistry

2.5.1 Preparation of cells for immunocytochemistry

Monolayer neurons were washed with DPBS, fixed with 4% paraformaldehyde in DPBS for 20 minutes at 4°C and washed twice with DPBS, before storage at 4°C in DPBS with 0.1% sodium azide.

COs were washed with DPBS, fixed with 4% paraformaldehyde in DPBS for one hour at 4°C, then washed once with DPBS and incubated with fresh DPBS at 4°C for 1 hour. COs were cryoprotected by incubation in 30% sucrose with 0.01% sodium azide in DPBS at 4°C overnight. The next day, COs were embedded in OCT (Thermo Scientific) and frozen in isopropanol cooled with dry ice. Embedded COs were stored at -80°C until cryosectioning into 15µm sections using a Bright OFT5000 cryostat. Sections were collected on SuperFrost Plus slides (VWR International) and stored at -20°C until immunostaining was performed.

2.5.2 Immunofluorescence protocol

For both monolayer neurons and COs, blocking of non-specific sites and cell permeabilisation was performed with 5% normal goat serum or normal donkey serum (Vector Labs) in DPBS with 0.3% Triton X-100 (Sigma) for one hour at room temperature. Primary antibodies and their dilutions are listed in Table 2.4. Primary antibodies were diluted in DPBS with 0.3% Triton X-100 (Sigma) and incubated at 4°C overnight. The next day, the samples were washed three times (for five minutes each time) with DPBS and incubated with the appropriate Alexa Fluor secondary antibodies (1:500, Invitrogen) at room temperature for two hours.

Samples were then incubated with 1µg/ml DAPI (Roche) in DPBS for 20 minutes and washed three times (for five minutes each time) with DPBS. A drop (approximately 100 µl) of Fluoromount-G (Southern Biotech) was placed on each sample and a coverslip was placed on top. After drying, the slides were stored at 4°C.

2.5.3 Tau antibodies and signal amplification

Blocking was not performed when using tau antibodies and incubation with additional primary antibodies (such as βIII tubulin) was performed sequentially over the following night. Signal amplification was required for 4R tau and AT8 antibodies: after incubation with the primary antibody, samples were washed three times with DPBS and incubated with biotinylated anti-mouse IgG (Vector Laboratories) diluted 1:250 in DPBS at room temperature for two hours. Samples were washed three times (for five minutes each time) with DPBS, then incubated with streptavidin Alexa Fluor conjugate (Invitrogen) diluted 1:500 in DPBS at room temperature for one hour.

2.5.4 Use of the dye pFTAA

The dye pentameric formyl thiophene acetic acid (pFTAA), which recognises filamentous β-sheet tau aggregates, was diluted to 3µM in ddH_2O and incubated on the samples for 30 minutes at room temperature prior to incubation with DAPI. Samples were then washed three times (for five minutes each time) with DPBS and incubated with DAPI as described above.

2.5.5 Imaging

Images were taken with a Leica DMI4000 B inverted microscope, or a Leica TCS SP8 laser-scanning confocal microscope. Where possible, the same microscope settings were used for each antibody across all differentiation rounds. Images were analysed with LAS AF software and ImageJ (from the National Institues of Health).

Table 2.4 Primary antibodies for Immunofluorescence and Western Blot

Protein target	Species	Type	Dilution		Source
			IF	WB	
3 repeat (3R) tau, RD3	Mouse	monoclonal	1:500	-	Millipore 05-803
4 repeat (4R) tau, RD4	Mouse	monoclonal	1:500	-	Millipore 05-804
$\alpha\beta$crystallin	Rabbit	polyclonal	1:1000	-	Stressgen SPA-223
βactin	Rabbit	polyclonal	1:500	1:5000	Abcam Ab8227
βIII tubulin	Rabbit	polyclonal	1:1000	-	Abcam Ab18207
βIII tubulin	Mouse	monoclonal	-	1:5000	Sigma T8660
βIII tubulin	Chicken	polyclonal	1:1000	-	Abcam Ab107216
Ankyrin-G	Mouse	monoclonal	1:200	-	NeuroMab N106/36
Anti-FLAG M2	Mouse	monoclonal	1:200	-	Sigma F1804
AT8 (tau pSer202 and pThr205)	Mouse	monoclonal	1:500	1:1000	Thermo Scientific MN1020
Cux1/2	Rabbit	polyclonal	1:50	-	Santa Cruz Biotechnology sc-13024
FoxG1	Rabbit	polyclonal	1:500	-	ProSci 8089
Glial fibrillary acidic protein (GFAP)	Chicken	polyclonal	1:1000	1:10 000	Abcam Ab4674
Human tau, HT7	Mouse	monoclonal	1:500	1:1000	Thermo Scientific Mn1000
Ki67	Rabbit	polyclonal	1:500	-	Abcam Ab16667
MC1 (misfolded tau)	Mouse	monoclonal	1:1000	-	a gift from Dr Peter Davies
Nestin	Rat	monoclonal	1:2000	-	EMD Millipore MAB353
Oct4	Rabbit	polyclonal	1:500	-	Abcam Ab19857
Otx2	Goat	polyclonal	1:1000	-	R&D AF1979
Pan Na (pan sodium channel)	Mouse	monoclonal	1:1000	-	Sigma S8809
Pax6	Rabbit	polyclonal	1:500	-	BioLegend PRB-278P-100
S100β	Rabbit	polyclonal	1:500	-	Abcam 868-500
Sox2	Rabbit	polyclonal	1:500	-	Abcam Ab97959
SSEA4	Mouse	monoclonal	1:500	-	Abcam Ab16287
Synaptophysin IV	Rabbit	polyclonal	1:500	1:1000	Abcam Ab14692
Tbr1	Rabbit	polyclonal	1:500	-	Abcam Ab31940
Tbr2	Rabbit	polyclonal	1:500	-	Abcam Ab23345
Tra-1-60	Mouse	monoclonal	1:500	-	Abcam Ab16288
Total tau	Rabbit	polyclonal	1:500	1:2500	DAKO A0024

Abbreviations used in this table: IF: immunofluorescence; WB: Western blotting.

2.6 Western blotting

2.6.1 Reagents and solutions for Western Blotting

10% Running Gel: 4ml ddH_2O, 3.3ml 30% acrylamide (Sigma), 2.5ml 1.5M pH 8.8 Tris HCl (Sigma), 100µl 10% SDS in H_2O, 100µl 10% APS (ammonium persulphate) in H_2O, 4µl TEMED (tetramethylethylenediamine).

Stacking Gel: 2.1ml ddH_2O, 500µl acrylamide; 350µl M Tris HCl, 30µl SDS in H_2O, 30µl 10% APS in H_2O, 3µl TEMED.

Running Buffer (10x) : 10g SDS, 30g Trizma Base, 144g glycine (all Sigma), dissolved in 1L H_2O.

Transfer Buffer (3x): 9.09g Trizma Base, 43.23g glycine, 300ml methanol (Sigma), dissolved in 1L H_2O.

Stripping Buffer (1x): 50mM Tris HCl pH 7.4, 2% SDS, 100mM β-mercaptoethanol.

2.6.2 Sample preparation

Monolayer neurons were collected at day 50 or 80-100 by incubation with 500µl 1x Accutase for 2 minutes at 37°C. The sheets of cells were collected in falcon tubes containing 15ml of DPBS to dilute the Accutase and centrifuged at 300g for 3 minutes in a Sorvall ST-16 centrifuge. The cell pellets were washed with DPBS and frozen at -80°C.

At least 6 COs were collected at day 100. COs were transferred to falcon tubes containing 15ml of DPBS with a cut P1000 pipette tip and centrifuged at 300g for 3 minutes in a Sorvall ST-16 centrifuge. The cell pellets were washed with DPBS and frozen at -80°C.

2.6.3 Protein extraction

Cell pellets were thawed on ice, then centrifuged for 3 minutes at 300g in a Heraeus Megafuge centrifuge. Remaining DPBS was removed and each pellet was re-suspended in 50µl (monolayer neurons) or 100µl (COs) of ice-cold Pierce RIPA buffer (Thermo Scientific), containing 1x complete EDTA-free protease inhibitor cocktail (Roche) and phosphatase inhibitor (1mM sodium orthovanadate, Sigma). The cells were lysed for 20 minutes on

ice, vortexing every 2 minutes. The cells were then sonicated (4 x 30 second cycles) in a Diagenode Bioruptor sonicator and the cell lysate was cleared by centrifugation at 14000g for 15 minutes at 4°C in a Heraeus Megafuge centrifuge. The supernatant was removed to a clean Eppendorf tube and both the pellet and supernatant were stored at -20°C.

2.6.4 Determination of protein concentration

A bicinchoninic acid (BCA) assay was performed to quantify the protein concentration in the cell lysate, and is described here. Two mg/ml bovine serum albumin (BSA, Europa Bioproducts) was serially diluted 1:2 in DPBS as a protein concentration standard. Cell lysate samples were diluted 1:5 in DPBS and added to a 96-well plate in triplicate. BCA buffer solution was prepared by mixing BCA solution with 4% cupric sulphate (1:50, both from BCA protein assay kit, Novagen). 200µl of BCA buffer solution was added to each well and the plate was incubated at 37°C for 30 minutes, protected from light. Absorbance was read at 562nm with an Infinite M200 Pro Tecan plate reader. The BSA protein standards were used to make a standard curve in Excel, from which the concentration of the samples was calculated.

2.6.5 Sodium dodecyl sulphate-polyacrylamide gel electrophoresis (SDS-PAGE)

Ten µg of protein was diluted in ice cold RIPA buffer containing protease and phosphatase inhibitors, such that all samples were the same volume. Four x NuPAGE LDS Sample Buffer and 10x NuPAGE Sample Reducing Agent (both Invitrogen) were added to the samples, which were incubated at 95°C for 5 minutes. Samples were loaded into the wells of a NuPAGE Novex Bis-Tris 4-12% 1.5mm gel (Invitrogen) alongside SeeBlue Plus2 Pre-Stained Protein Standard (Life Technologies). Loaded samples were run in NuPAGE MES buffer at 120mV. Proteins were transferred to 0.2µm nitrocellulose membrane (Bio-Rad) at 0.3A for 3 hours at 4°C, in 1x Transfer Buffer (Section 2.6.1). Non-specific binding of the primary antibody to the membrane was blocked by incubating the membrane with 5% BSA in TBS-Tween (TBST, 0.05%) for 1 hour at room temperature before incubation with the primary antibody overnight at 4°C (Table 2.4). The next day, the membrane was washed with TBST (3 x 5 minutes) and incubated with the appropriate HRP-conjugated secondary antibody (DAKO, GE Healthcare) diluted 1:5000 in 5% BSA in TBST for 2 hours at room temperature. The membrane was washed again with TBST (3 x 5 minutes) and primary

antibody binding was visualised using SuperSignal West Dura Extended Duration Substrate (Thermo Scientific) on a Biorad ChemiDoc. Band intensity was quantified using ImageJ.

2.6.6 Stripping and re-probing membranes

When membranes were probed with more than one antibody, bound primary and secondary antibodies were removed from the membrane by incubation with Stripping Buffer (Section 2.6.1) for 45 minutes at 55°C. The membrane was then washed with ddH_2O (20 x 5 minutes). Non-specific binding of the primary antibody to the membrane was blocked as described in Section 2.6.5, and the membrane was incubated with a second primary antibody as described in Section 2.6.5.

2.6.7 Western blotting for tau isoforms

To visualise tau isoforms, dephosphorylated samples were run next to their phosphorylated counterparts. To dephosphorylate samples, 15µg of protein was dephosphorylated by incubation with 16 units of alkaline phosphatase from E. coli (Sigma), in 50mM pH 7.4 Trizma HCl (Sigma), and 5mM $MgCl_2$ at 65°C for 4 hours. For the phosphorylated samples, 5µg of protein was diluted with ddH_2O, such that all samples were the same volume. Four x NuPAGE LDS Sample Buffer and 10x NuPAGE Sample Reducing Agent were added to the samples, which were incubated at 70°C for 10 minutes. Samples were then loaded into the wells of a 10% 1.5mm polyacrylamide gel (Section 2.6.1), alongside SeeBlue Plus2 Pre-Stained Protein Standard. Protein extract from control human cortex was included as a positive control for all six tau isoforms (one lane contained phosphorylated protein, one lane dephosphorylated protein). Recombinant tau protein (all 6 isoforms, rPeptide) was diluted 1:800 and included as a molecular weight marker for human tau isoforms. SDS-PAGE was performed in 1x Running Buffer (Section 2.6.1) at 90mV until the 36kDa marker ran off the gel. Transfer of proteins onto a membrane, blocking of non-specific background and incubation with primary and secondary antibodies were performed as described in Section 2.6.5.

2.7 Statistical analysis

Statistical analysis was performed with GraphPad Prism 7. To determine whether the data was normally distributed, a D'Agostino-Pearson K2 omnibus test or a Shapiro-Wilk test was performed. Equality of variance was assessed with Bartlett's test or the Brown-Forsythe test. For normally distributed data, a one-way or two-way repeated measures ANOVA

was used to compare means with one or two variables, followed by a Bonferroni post-hoc correction. Repeated measures ANOVAs were used because cultures were made from each iPSC line three times in non-concomitant differentiation rounds. This is a "randomised block" experiment, in which the blocking factor is the differentiation round. Matching the data by differentiation round (using a repeated measures ANOVA) decreases the contribution of variation by differentiation round. When data did not follow a normal distribution, a Friedman test was used to compare the means with one variable, followed by Dunn's post test. Mean values were calculated from three independent differentiations. When two groups were compared, a paired, two-tailed Student's t-test was used, or non-parametric Mann-Whitney tests if the data was not normally distributed.

Chapter 3

Characterisation of iPSC-derived neurons with MAPT mutations

3.1 Aims

FTDP-17T predominantly affects the frontal and temporal lobes of the brain. In FTDP-17T, neurons and sometimes astrocytes contain abnormally phosphorylated tau, which forms insoluble aggregates. Cultures containing both neurons and astrocytes can be made by directed differentiation of iPSCs by applying development-mimicking cues. Patterning factors can also be applied to direct the neurons towards a forebrain-like fate, making the neuronal cultures a relevant model in which to examine FTDP-17T-like changes.

Although the control and N279K iPSC lines described in this Chapter have been used to make monolayers of forebrain-specific neurons by Iovino et al. (2015), I used a different differentiation method. Therefore, characterisation of the iPSC-derived neurons was repeated.

The aim of the work described in this Chapter is to make forebrain-specific neurons from control and MAPT-mutant iPSCs, and then to characterise them, examining the maturation of the cultures over time in terms of tau isoform expression, synapse formation and the appearance of astrocytes. This aim will be fulfilled by:

1. Differentiating iPSCs to NPCs, then confirming their forebrain fate and proliferative capacity

2. Differentiating NPCs to neurons, then determining the proportion of astrocytes and neurons in the cultures, to examine maturation with respect to the appearance of astrocytes, and to check for FTDP-17T-relevant astrocyte overgrowth

3. Examining synaptic protein expression as a proxy for synapse formation, to determine whether neurons are forming synaptic connections and if there is FTDP-17T relevant synapse loss

4. Assessing tau isoform expression as a measure of neuronal maturity and to confirm that the effect of the N279K mutation (an increase in 4R tau relative to 3R tau) can be seen in these cultures.

3.2 Introduction

Directed differentiation of iPSCs to forebrain neurons provides neural cultures which mature over time, and in which neurons and glial cells are generated in a manner similar to cerebral cortex development (Angevine and Sidman (1961); Shi et al. (2012c), Chapter 1). In this Chapter I will describe the characterisation of control and MAPT-mutant iPSC-derived neural cultures over three timepoints, during which NPCs are generated, differentiate into neurons with synaptic connections, and eventually produce astrocytes.

3.2.1 Tau isoform expression in iPSC-derived neurons

Tau protein expression is developmentally regulated: of the six tau isoforms, the shortest 0N3R isoform is expressed during development, and the remaining five isoforms are co-expressed with the 0N3R isoform in the adult brain (Goedert and Jakes, 1990; Goedert and Spillantini, 1990). Tau isoform expression can therefore be used as a measure of a neuronal culture's maturity relative to the adult human brain. However, some of the MAPT mutations which cause FTDP-17T alter tau isoform ratios by either increasing or decreasing exon 10 splicing (Hutton et al. (1998); Spillantini et al. (1998b); and many others).

Maturation of tau isoform expression in control iPSC-derived neuronal cultures over time

In control iPSC-derived neural cultures, 0N3R tau expression usually predominates (Beevers et al., 2017; Iovino et al., 2015; Sposito et al., 2015), suggesting a large proportion of immature neurons in culture. 4R tau mRNA has been reported in control cultures from day 30 (Iovino et al., 2015) or day 40 (Ehrlich et al., 2015) onwards. At day 50, 0N3R tau protein is strongly expressed, and 0N4R tau is starting to become visible in Western blots for tau isoforms using control cells (Iovino et al., 2015; Sposito et al., 2015). Extended time in

culture increases the number of tau isoforms visible. Sposito et al. (2015) have demonstrated the presence of 0N3R, 0N4R and at least two higher molecular weight tau isoforms by Western blot in 365 day-old cultures, whereas Iovino et al. (2015) have shown 0N3R, 0N4R, 1N3R and 1N4R tau isoforms, and very weak 2N3R and 2N4R tau isoforms in control 150 day-old forebrain iPSC-derived neural cultures. Similarly, Beevers et al. (2017) report the expression of all six tau isoforms in control midbrain-like iPSC-derived neural cultures after 190 days in culture, as detected by antibodies against all six tau isoforms, against 4R tau isoforms, and against isoforms with two N-terminal inserts.

Splicing mutations and tau isoforms ratios

In addition to adult-like tau splicing in aged cultures, the effects of MAPT mutations which alter tau splicing are recapitulated in iPSC-derived models. Cultures with mutations such as N279K have been shown to escape the developmental regulation of tau splicing, resulting in the earlier expression of 4R tau (Iovino et al., 2015). Neural cultures with MAPT mutations which do not alter tau isoform ratios *in vitro* or in the human brain (such as V337M or P301L), express tau isoforms in a pattern similar to control neuronal cultures (Ehrlich et al., 2015; Iovino et al., 2015).

In iPSC-derived cultures with the N279K mutation, 4R tau mRNA has been detected from day 1 of differentiation onwards, whereas it was absent in control cultures until day 30 (Iovino et al., 2015). Four repeat tau mRNA has also been detected in N279K NPCs, at higher levels than in control NPCs (Wren et al., 2015). In 40 day-old neurons, 4R tau mRNA has been detected in N279K iPSC-derived neural cultures, but was not detected in control cultures (Ehrlich et al., 2015). This alteration in the ratio of 3R:4R tau mRNA has also been observed in cultures of iPSC-derived neurons with the intron 10+16 (Sposito et al., 2015) and intron 10+14 mutations (Imamura et al., 2016), both of which increase exon 10 inclusion in tau mRNA.

As would be expected given the early appearance of 4R tau mRNA, 0N4R tau protein is expressed earlier in iPSC-derived neurons with the N279K mutation than in controls (Iovino et al., 2015). In addition, iPSC-derived neurons with the N279K, 10+16, or 10+14 mutation show lower 0N3R tau protein expression than controls, indicating a change in the 4R:3R ratio, such that relatively more 4R tau is expressed (Imamura et al., 2016; Iovino et al., 2015; Sposito et al., 2015).

3.2.2 Synapses in FTDP-17T and in iPSC-derived neurons

Synapse loss in FTDP17-T

Several studies have found that synapse number declines in the brains of people with tauopathies. For example, Bigio et al. (2001) found lower synaptophysin levels in the frontal and temporal lobes of brains from people with PSP and AD, Masliah et al. (1989) found fewer synaptophysin puncta in Pick's disease and AD brains, and Callahan and Coleman (1995) found decreased synaptophysin levels in neurons containing tau inclusions, compared neurons without tau inclusions in AD brains. Synapse loss has also been shown to correlate with cognitive decline in AD (Koffie et al., 2011; Terry et al., 1991), indicating the relevance of synapse loss to AD symptoms.

Synapses are also lost in animal models of tauopathy. In the ventral striatum of aged mice expressing human V337M tau, Warmus et al. (2014) found decreased post-synaptic density area and thickness, lower PSD-95 protein levels, and decreased synapse function. Lower synaptophysin and PSD-95 levels have been observed from 1.3 months onwards in mice expressing 0N4R human tau lacking 20 C-terminal amino acids to mimic caspase cleaved tau (Kim et al., 2016), and in mice expressing R406W mutant tau with several pseudo-phosphorylated residues (Di et al., 2016).

In some mouse models, synapse loss is an early sign of disease. For example, in a mouse transgenic for human P301S tau, Yoshiyama et al. (2007) reported decreased hippocampal synaptophysin levels in three month-old mice, before tau phosphorylation and tau filaments were observed at six months, and before neuronal loss at nine months. Xu et al. (2014) observed a similar pattern in another P301S mouse, which had decreased dendritic spine density and length in the hippocampus at 2.5 months, before phosphorylated and filamentous tau was detected at five months, and before cell death at six months. Synaptic loss has also been observed in other mouse lines expressing mutant tau, including in mice expressing the P301L MAPT mutation (Kopeikina et al., 2013).

These results indicate that synaptic loss is a feature present alongside tau pathology, but it has only been investigated in a few studies of iPSC-derived neurons with MAPT mutations. Silva et al. (2016) measured the levels of PSD-95, synapsin-I and synaptophysin by Western blot in 35 day-old iPSC-derived control and A152T tau neurons, and found no differences in expression level. The other studies investigating synapse density in relation to tau have added exogenous tau. For example, Usenovic et al. (2015) found fewer synaptophysin and synapsin I positive puncta in control iPSC-derived neurons which were exposed to fibrils made of recombinant full-length human tau for two weeks. Similarly, Reilly et al. (2017) expressed

the tau repeat domain with the P301L and V337M mutations in control iPSC-derived neurons, and found a decrease in synapsin I puncta density.

The presence of synapses in iPSC-derived neurons

iPSC-derived neurons express synaptic proteins, which have been detected from as early as day 21 (Birnbaum et al., 2018). Synapse number, measured by PSD-95 and synaptophysin immunofluorescence, continues to increase over time: from day 60 to day 90 (Bergström et al., 2016), and from day 112 to 300 (Odawara et al., 2016). At least some of these synapses are also functional, which has been demonstrated by electrophysiological recordings from day 28 onwards (Iovino et al., 2015; Shi et al., 2012c).

The expression of synaptic proteins can therefore serve as a marker of a culture's maturity, but synapse number has been shown to decrease in both human and animal brains in the presence of mutant tau. iPSC-derived neural cultures of MAPT-mutant and control neurons will be used to investigate whether MAPT mutations affect synapse formation and number.

3.2.3 Astrocytes

In iPSC-derived neural cultures and the developing brain, astrocytes begin to appear after neurons, starting at approximately day 45 in iPSC-derived neural cultures (Shi et al., 2012a), and making the appearance of astrocytes another indication of a culture's maturity.

In the brain astrocytes secrete gliotransmitters, neurotrophic factors and synaptogenic factors, as well as maintaining the extracellular environment by controlling potassium ion concentration and removing excess glutamate, amongst other roles (reviewed by Kettenmann and Verkhratsky, 2016). The extent to which astrocytes fulfil all of these roles in iPSC-derived neural culture is not known, but there is some evidence that astrocytes are beneficial to neurons in culture, and support synapse formation as part of a tri-partite synapse (reviewed by Chung et al., 2015).

ESC-derived neurons co-cultured with embryonic mouse astrocytes have been shown to express synaptic proteins sooner, and to form electrophysiologically active synapses before cultures without astrocytes (Johnson et al., 2007). ESC-derived neurons cultured with astrocyte-conditioned media (but without astrocytes) also expressed higher synaptic protein levels than neurons in non-conditioned media, but Johnson et al. only detected an increase in electrophysiological activity in co-cultured neurons, suggesting that cell-to-cell contact is important for functional maturity.

The relative immaturity of the astrocytes themselves may also be for their role in synapse formation, since Christopherson et al. (2005) have demonstrated that immature (but not mature) astrocytes release synaptogenic factors, such as thrombospondin.

The abundance and appearance of astrocytes in iPSC-derived neuronal cultures with tau mutations has not yet been studied in published papers. It is of interest because it reflects not only maturation of the culture, but could also reflect astrogliosis, which is observed in cortical and sub-cortical areas in the brains of patients with the N279K (Arvanitakis et al., 2007; Slowinski et al., 2007), P301L (Miyasaka et al., 2001), and V337M mutations (Spina et al., 2017). Features of astrogliosis include astrocyte hypertrophy, overgrowth, and release of factors which can have neuroprotective or neurotoxic effects (reviewed by Phatnani and Maniatis, 2015). NPC-derived astrocytes from N279K mutant and control iPSC lines have been studied in the absence of neurons (Hallmann et al., 2017): the N279K astrocytes were found to be larger, and to express more 4R tau mRNA than control astrocytes. Although the larger size of N279K astrocytes indicates they may be hypertrophic, their tau expression raises questions about their astrocytic identity, since astrocytes do not express tau in the human brain, nor in the mouse brain (Forman, 2005).

3.3 Materials and Methods

I was unable to differentiate iPSCs to neurons following the protocol published by Shi et al. (2012a), which was previously modified by Iovino et al. (2015) to differentiate the CTRL and N279K iPSC lines used in this thesis. Instead, I used a protocol developed for ESC differentiation by Kirkeby et al. (2012) and adapted for iPSC differentiation by a Spillantini lab member (Santiváñez Pérez, 2017). The protocols differ substantially (Figure 3.1 and Table 3.1). Therefore, I repeated the previously published characterisation of tau isoforms (in this Chapter) and investigated tau phosphorylation using the anti phospho-tau antibody AT8 (in Chapter 4) in neurons obtained using the Kirkeby et al. (2012)/Santiváñez Pérez (2017) protocol.

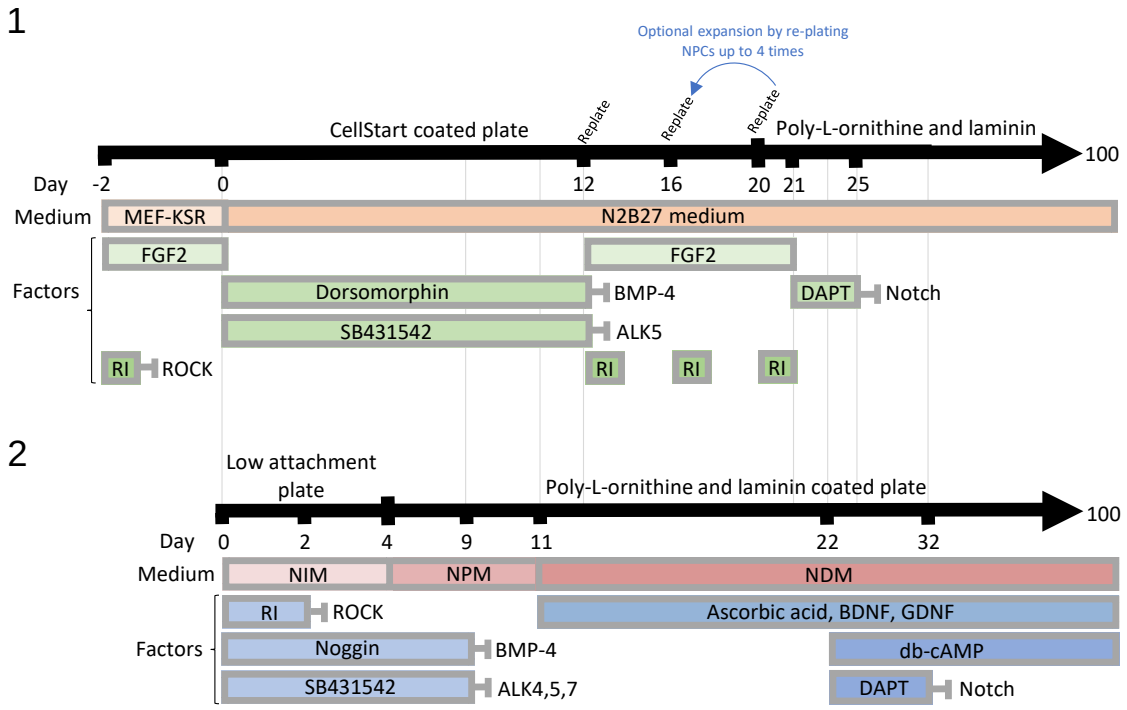

Fig. 3.1 **Comparison of the protocols developed by 1) Shi et al. (2012a) and 2) Kirkeby et al. (2012)/Santiváñez Pérez (2017) for iPSC differentiation to neurons.** Black bars indicate the day of differentiation, starting from dual Smad inhibition at day 0. Text above the black bars indicate the cell culture surface: low attachment plates were used for embryoid bodies, CellStart or poly-L-ornithine and laminin coated plates were used for attached cells. Orange (1) or pink (2) bars indicate the medium in which differentiating cells were maintained: neuronal induction medium (NIM), neuronal proliferation medium (NPM) neuronal differentiation medium (NDM), mouse embryonic fibroblast-conditioned KSR medium (MEF-KSR), or N2B27 medium. Green (1) or blue (2) bars show factors added to the differentiation media. Protocol 1 has a step before the induction of Smad inhibition: on day -2, iPSCs were dissociated to a single-cell suspension with Accutase and plated as a monolayer. iPSCs were maintained with MEF-conditioned KSR-medium and 20ng/ml FGF until they reached confluency on day 0, when SMAD inhibition began. No factors to block proliferation were added to neuronal cultures. Abbreviations: BDNF: brain-derived neurotrophic factor; BMP: bone morphogenic protein; DAPT: N-[N-(3,5-Difluorophenacetyl)-L-alanyl]-S-phenylglycine t-butyl ester; db-cAMP: dibutyl-cyclic adenosine monophosphate; GDNF: glial-derived neurotrophic factor; NPCs: neural precursor cells; RI: ROCK (rho-associated protein kinase) inhibitor.

Table 3.1 Comparison of the protocols developed by Shi et al. (2012a) and Kirkeby et al. (2012)/Santiváñez Pérez (2017) for iPSC differentiation to neurons

	Differences between the two methods	
Differentiation step	**Shi et al. (2012a)**	**Kirkeby et al. (2012)/Santiváñez Pérez (2017)**
Initial iPSC plating	Single-cell monolayer	Embryoid bodies
Smad inhibitor exposure	12 days	9 days
Smad inhibitors	SB, Noggin (protein)	SB, Dorsomorphin (small molecule)
NPC expansion	Up to 4 passages	None
DAPT exposure	4 days	10 days
Factors in neural media	N2, B27	N27, B27, AA, BDNF, GDNF, db-cAMP

Comparison of the protocols developed by Shi et al. (2012a) and Kirkeby et al. (2012)/Santiváñez Pérez (2017) for iPSC differentiation to neurons. Abbreviations: AA: ascorbic acid; BDNF: brain-derived neurotrophic factor; DAPT: N-[N-(3,5-Difluorophenacetyl)-L-alanyl]-S-phenylglycine t-butyl ester; db-cAMP: dibutyl-cyclic adenosine monophosphate; GDNF: glial-derived neurotrophic factor; iPSC: induced pluripotent stem cell; NPC: neural precursor cell; SB: small molecule SB431542.

3.3.1 iPSC culture and differentiation

iPSCs were thawed, cultured, prepared for karyotyping and differentiated to neurons as described in Chapter 2.

3.3.2 Immunostaining, Western blotting and statistical analysis

Immunostaining was performed as described in Section 2.5.1 and Western blots were performed as described in Section 2.6. Statistical analysis was performed as described in Section 2.7.

Quantification of immunostaining

Quantification was carried out using ImageJ (image analysis software developed at the National Institutes of Health). DAPI-positive nuclei were counted, then an appropriate threshold was applied to the images showing the cells with the marker of interest (Ki67 or S100β), to minimise background staining. The cells of interest were counted in the same way as the DAPI-positive nuclei. Cells were counted in three technical replicates from each of three independent differentiation rounds.

3.4 Results

3.4.1 Suitability of iPSC lines for differentiation to neurons

To determine that the iPSC lines were pluripotent before differentiation, I immunostained for the nuclear pluripotency markers Oct4 and Sox2, and the cytoplasmic pluripotency markers Tra-1-60 and SSEA4 (Figure 3.2). Oct4 and Sox2 are both transcription factors needed for pluripotency (Niwa et al., 2000; Pierfelice et al., 2011), and Sox2 is a marker for both iPSCs and NPCs (Ellis et al., 2004). SSEA4 is a glycolipid and Tra-1-60 is a keratan sulfate, both of which are expressed on the surface of human iPSCs and ESCs, and whose expression decreases during differentiation (The International Stem Cell Initiative, 2007).

All lines were positive for the pluripotency markers, which were expressed in the appropriate cellular compartment: Sox2 and Oct4 staining were co-localised with DAPI staining, indicating their presence in the nucleus, and both Tra-1-60 and SSEA4 staining were visible outside the DAPI staining in the merged image, suggesting their presence on the cell surface. All lines also exhibited iPSC-like morphology: iPSCs formed uniform colonies with clean edges, which lacked differentiating cells and were not overgrown (Figure 3.2). Based on immunostaining and morphology, the iPSCs were pluripotent and suitable for differentiation to neurons.

To ensure that the iPSC lines had a normal karyotype, karyotyping was performed on fixed cell suspensions by members of the Spillantini lab or Axol Bioscience. A late passage of the CTRL2 line had a deletion (-15) and a translocation t(15;18)(q21;q21) (Figure 3.2). This likely occurred because multiple passages over extended time in culture can result in the accumulation of karyotypic abnormalities (Lund et al., 2012). These iPSCs were discarded. CTRL2 iPSCs from an earlier passage were thawed and karyotyped, which revealed a normal karyotype (Figure 3.2).

In addition, the presence of the N279K mutation in the N279K1 and N279K2 iPSC lines was confirmed by Sanger sequencing (Figure 3.3).

3.4.2 Regional specificity of neural precursors

The iPSC lines CTRL1, CTRL2, N279K1, N279K2 and V337M were differentiated to NPCs as described in Section 2.3. Pluripotent stem cells (PSCs - either ESCs or iPSCs) differentiate towards a forebrain fate in minimal media (Tropepe et al., 2001; Watanabe et al., 2005). Since neither caudalising factors nor ventralising factors were used, iPSC-derived NPCs

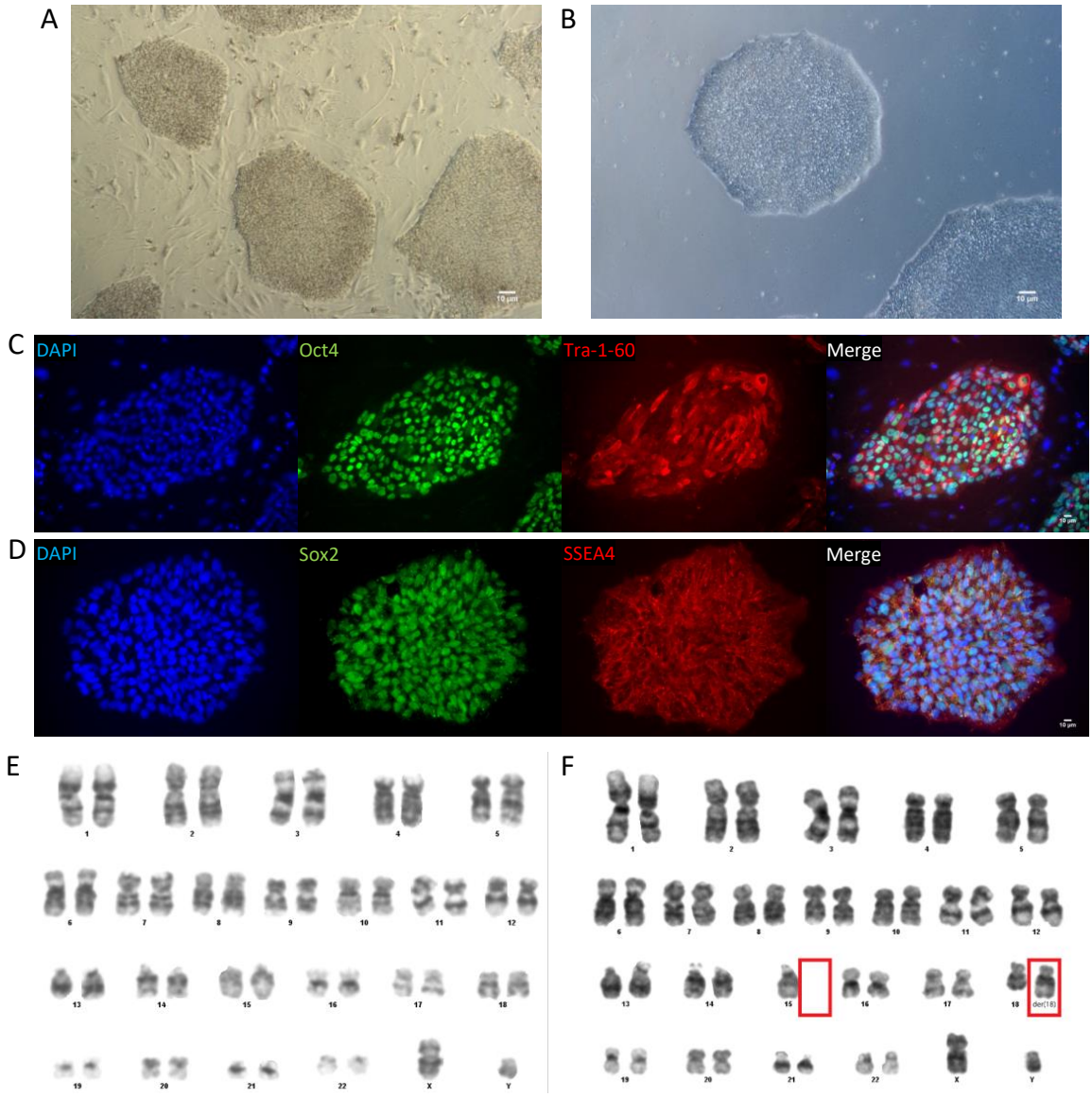

Fig. 3.2 **Pluripotent iPSCs with a normal karyotype.** Normal morphology in **A)** V337M iPSCs on MEFs and **B)** IsoCon iPSCs in feeder-free culture. **C)** Representative immunostaining of N279K2 iPSCs (on MEFs) for Oct4 and Tra-1-60. MEF nuclei are visible alongside iPSC nuclei in the DAPI image. **D)** Representative immunostaining of IsoCon iPSCs (feeder-free) for Sox2 and SSEA4. Scale bar = 10µm. **E)** Representative normal karyotype from CTRL2 iPSCs. **F)** The abnormal karyotype in CTRL2 iPSCs found at high passage number. Red boxes indicate the deleted chromosome 15 and the translocation on chromosome 18. These CTRL2 iPSCs were discarded, and an earlier passage of CTRL2 iPSCs with a normal karyotype was used instead.

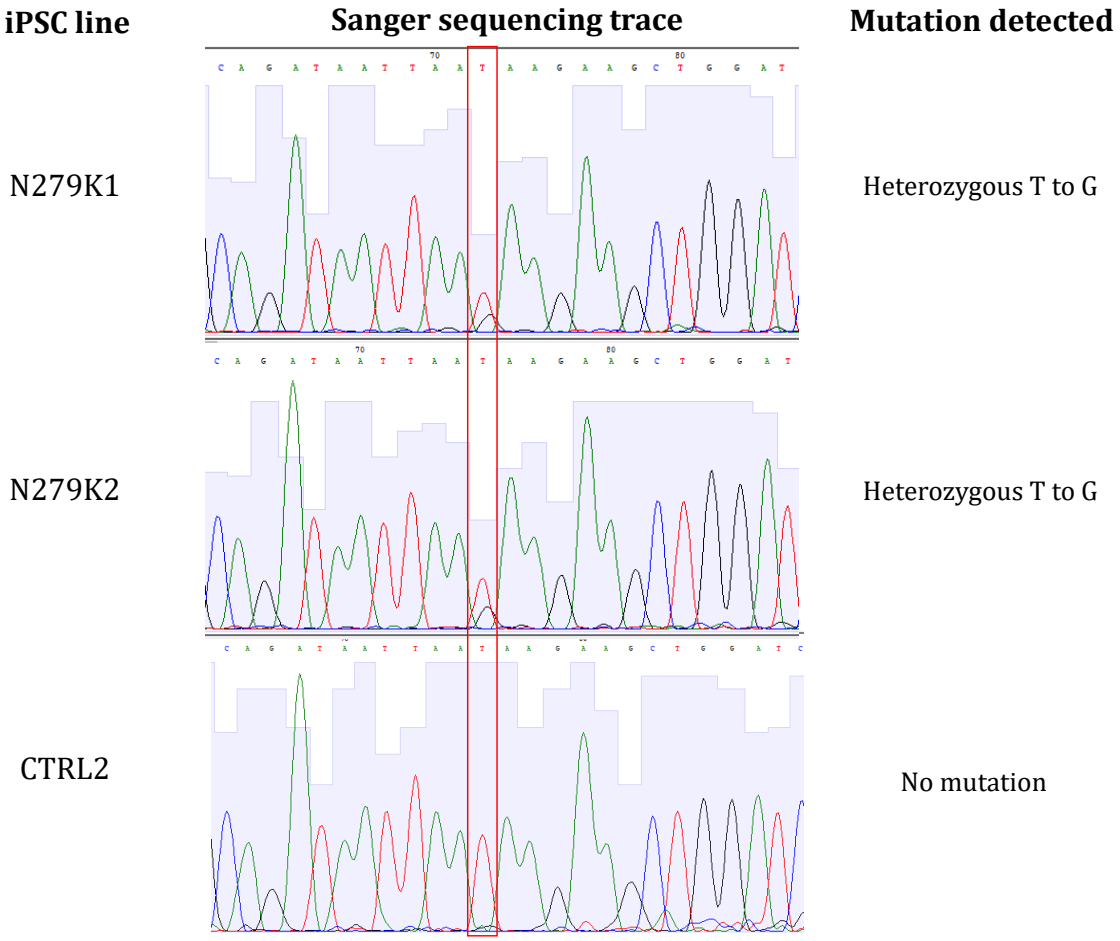

Fig. 3.3 **Sanger sequencing to show the N279K mutation in the N279K1 and N279K2 iPSC lines.** Sanger sequencing traces showing the 5' end of tau exon 10. The heterozygous N279K mutation (a base change from T to G) is visible as a double peak, outlined in red, in the N279K1 and N279K2 lines, but not in the control CTRL2 line.

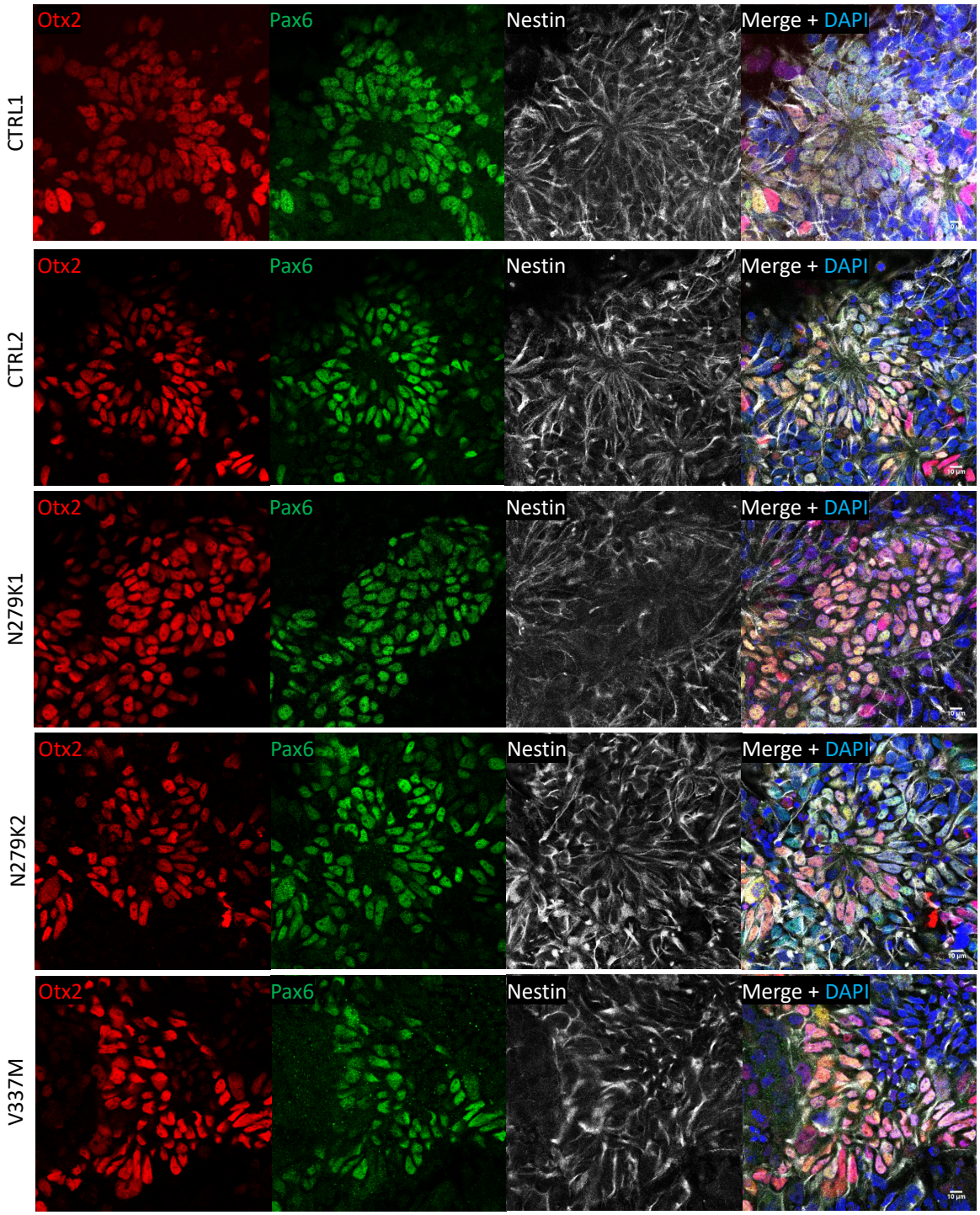

Fig. 3.4 **Neural precursors express forebrain markers Pax6, Nestin and Otx2 at day 16.** Immunostaining for the forebrain markers Pax6, Nestin and Otx2 and at day 16 in NPCs derived from CTRL1, CTRL2, N279K1, N279K2 and V337M iPSCs. The expected staining pattern was observed with Pax6, Nestin and Otx2 antibodies, indicating that the NPCs had a telencephalic or diencephalic fate. Representative images were taken to show that neural rosettes were positive for forebrain markers, but were not quantified. Scale bar = 10µm.

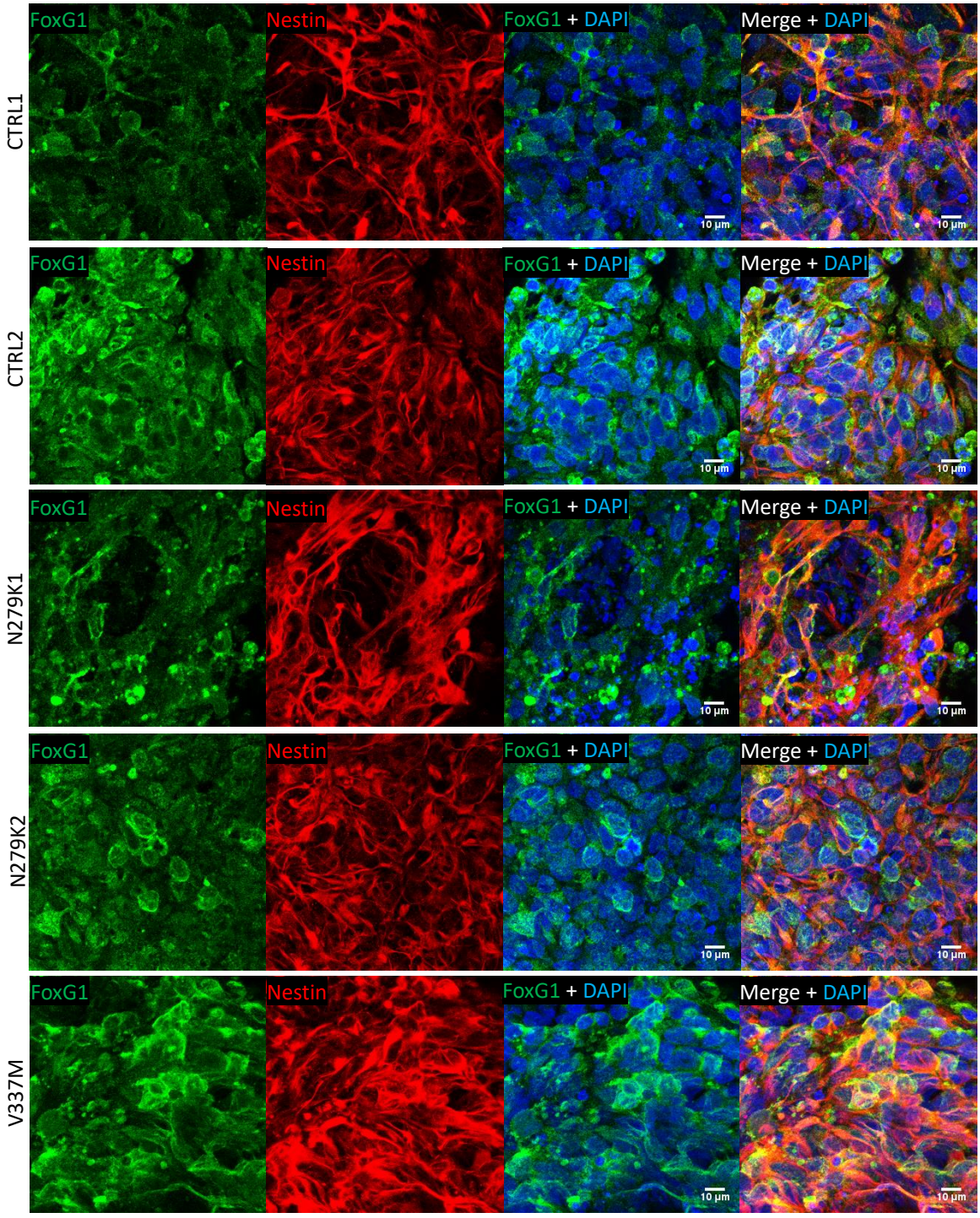

Fig. 3.5 **Neural precursors express forebrain markers FoxG1 and Nestin at day 16.** Immunostaining for the forebrain markers FoxG1 and Nestin at day 16 in NPCs derived from CTRL1, CTRL2, N279K1, N279K2 and V337M iPSCs. The expected staining pattern was observed with the Nestin antibody. FoxG1 staining was expected to be nuclear, since FoxG1 is a transcription factor, but cytoplasmic staining was observed. Cytoplasmic FoxG1 staining may indicate that the NPCs are already differentiating towards neurons, or it may be caused by non-specific antibody staining. Scale bar = 10µm.

generated via the Kirkeby et al./Santiváñez Pérez protocol are expected to have a forebrain fate.

To determine the fate of the NPCs, I immunostained for the transcription factors Pax6, Otx2 and FoxG1, and the intermediate filament Nestin at day 16, when neural rosettes were visible (Figure 3.4 and Figure 2.2). Nestin is expressed in NPCs throughout the developing human brain (Hockfield and McKay, 1985; Takano et al., 1996). Pax6 is expressed in NPCs and radial glia in the ventricular zone of the diencephalon (which becomes the thalamus, hypothalamus, epithalamus and subthalamus) and telencephalon (which becomes the cerebral cortex, basal ganglia, hippocampus, amygdala, and hypothalamus), as well as in the developing medulla oblongata, spinal cord and eye of 6-week old human embryos (Terzić and Saraga-Babić, 1999). Otx2 is expressed in the telencephalon, diencephalon, mesencephalon (which becomes the midbrain) and choroid plexus in 7-14 week-old human embryos (Larsen et al., 2010). FoxG1 is expressed in NPCs of the telencephalon, but not the diencephalon in embryonic day (E) 11.5 rats, as well as in the olfactory placode, auditory vesicle and pharyngeal pouches (Tao and Lai, 1992). Together, expression of these markers would indicate NPCs with a forebrain fate.

In all five lines, Pax6 and Otx2 staining overlap with DAPI, indicating their nuclear expression. Nestin is distributed outside DAPI-positive nuclei, suggesting its presence in the cytoplasm (Figure 3.4). FoxG1 staining does not overlap with DAPI, even though FoxG1 is a transcription factor and therefore expected to be expressed in nuclei. This suggests that FoxG1 expression is mostly cytoplasmic. FoxG1 staining still appeared to be nuclear in day 14 NPCs, and after antigen retrieval methods recommended for other FoxG1 antibodies (data not shown). A search of the literature revealed that FoxG1 is able to alternate between the nucleus and cytoplasm (Pancrazi et al., 2015), and that cytoplasmic FoxG1 has been observed in NPCs which are starting to differentiate towards neurons (Regad et al., 2007). Some βIII-tubulin positive neurons were visible in cultures by day 16, which may explain the cytoplasmic localisation of FoxG1 in these cultures.

NPCs from all lines formed neural rosettes, which is a stage of differentiation analogous to formation of the neural tube (Elkabetz et al., 2008). These are visible in Figure 3.4, but less clearly visible in Figure 3.5, since images in the latter were obtained with an epifluorescent microscope, whereas images in the former are from a confocal microscope, which can take a picture of a single slice from the NPC 3D culture, as compared to the epifluorescent microscope, which does not. The rosettes in Figure 3.4 are similar to those visible with live microscopy in Figure 2.2.

The expression of Pax6, Otx2, FoxG1 and Nestin, and the formation of neural rosettes, suggests that the iPSC-derived neurons have a forebrain fate. Since FTDP-17T is characterised by neuronal loss in the frontal and temporal lobes of the cortex (Foster et al., 1997), the neurons produced from these NPCs should provide a relevant model for observing MAPT mutation related changes.

3.4.3 Proliferative capacity of neural precursors

To investigate whether the MAPT mutations N279K and V337M influenced NPC proliferation or differentiation to neurons, I immunostained for the proliferation marker Ki67 (Figure 3.6), which is detectable during cell division but not in non-dividing cells (Gerdes et al., 1984).

As can be seen in Figure 3.6, Ki67 staining overlaps with DAPI, indicating the presence of Ki67 in the nucleus. Individual cells are differently labelled with the Ki67 antibody: some nuclei are completely labelled, whereas others contain puncta. This is because Ki67 can be detected at all stages of cell division and is localised to the surface of chromosomes (Cuylen et al., 2016), whose arrangement in the nucleus changes during the cell cycle. The various chromosomal arrangements are detected by Ki67 staining, which appears as different staining patterns. For example: during interphase Ki67 positive puncta are visible in the nucleus; during metaphase the chromosomes are visible as one Ki67 positive central mass; and during anaphase the Ki67 positive chromosomes are form two distinct masses (Gerdes et al., 1984; Scholzen and Gerdes, 2000).

DAPI stained nuclei and Ki67-positive nuclei were counted using Fiji, and the proportion of proliferating cells was calculated and compared between lines using a one-way ANOVA. There was no significant difference in the mean proportion of proliferative NPCs between iPSC lines ($F(4, 8)=2.049$, $p=0.1800$). This suggests that the NPCs derived from control or MAPT-mutant iPSC have a similar proliferative capacity, and are not spontaneously differentiating to neurons at different rates at day 16.

3.4.4 βIII-tubulin in iPSC-derived neuronal cultures over time

βIII-tubulin positive neurons were first visible at day 16, although these cultures contained mostly proliferative NPCs (Figure 3.6). βIII-tubulin positive neurons were also visible at day 50 and day 80-100, as can be seen in Figure 3.10. I assessed the proportion of neurons in day 50 and day 80-100 cultures by Western blotting, using an antibody against βIII-tubulin (Figure 3.8).

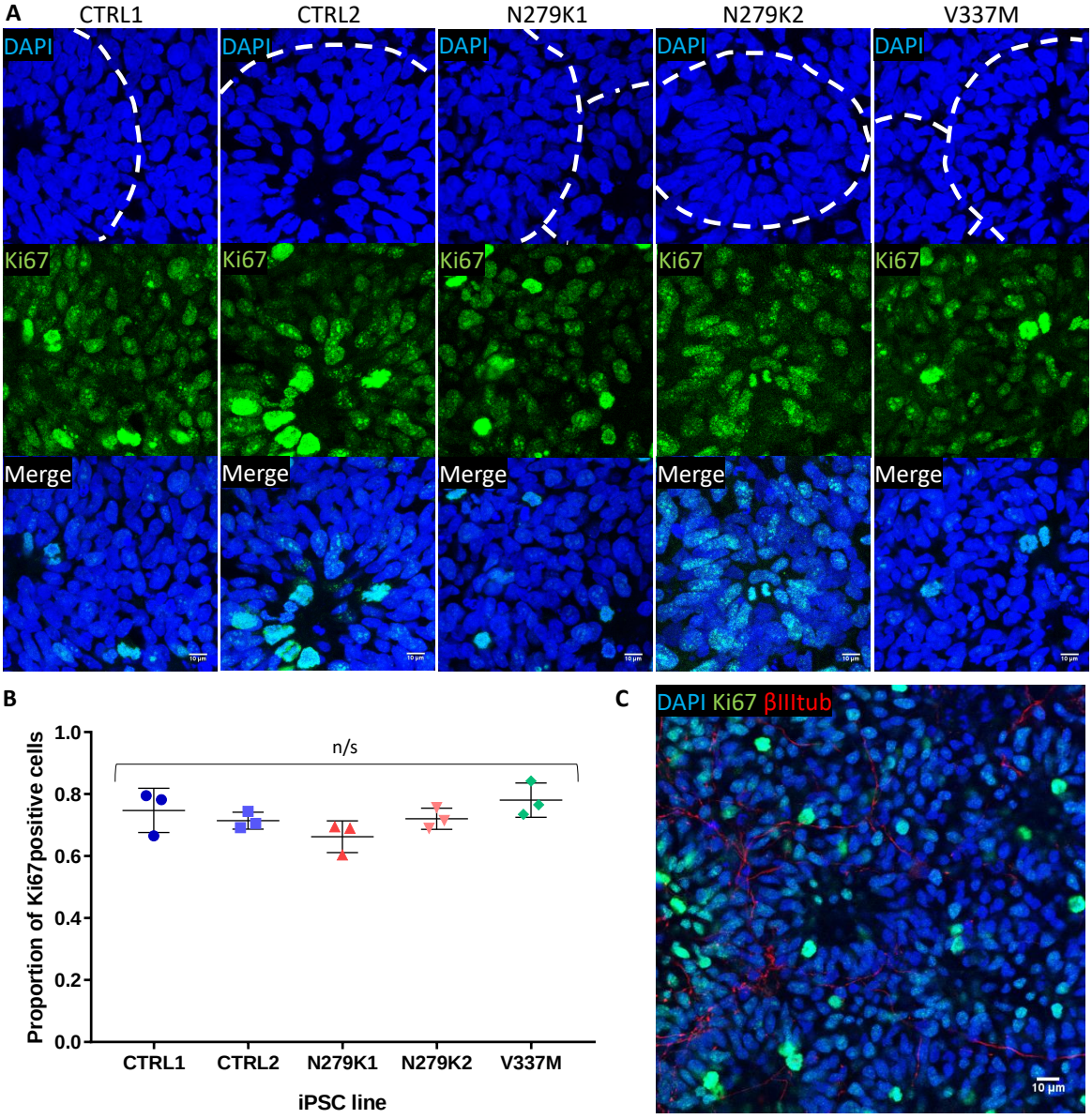

Fig. 3.6 **There is no significant difference in the proportion of proliferating neural precursor cells made from CTRL1, CTRL2, N279K1, N279K2 and V337M iPSC lines at day 16. A)** Day 16 CTRL1, CTRL2, N279K1, N279K2 and V337M NPCs immunostained for Ki67. Neural rosettes are highlighted by white dotted lines in the DAPI images. Scale bar = 10µm. **B)** The proportion of Ki67-positive NPCs was not significantly different between NPCs from the CTRL1, CTRL2, N279K1, N279K2 or V337M iPSC lines, which was an expected result. The proportion of Ki67 positive cells was determined by quantification of immunofluorescence images. For every iPSC line, each point represents the mean of one of three independent differentiations. Values represent mean±SD. **C)** Rosette-like formations of Ki67 positive NPCs and βIII-tubulin positive young neurons.

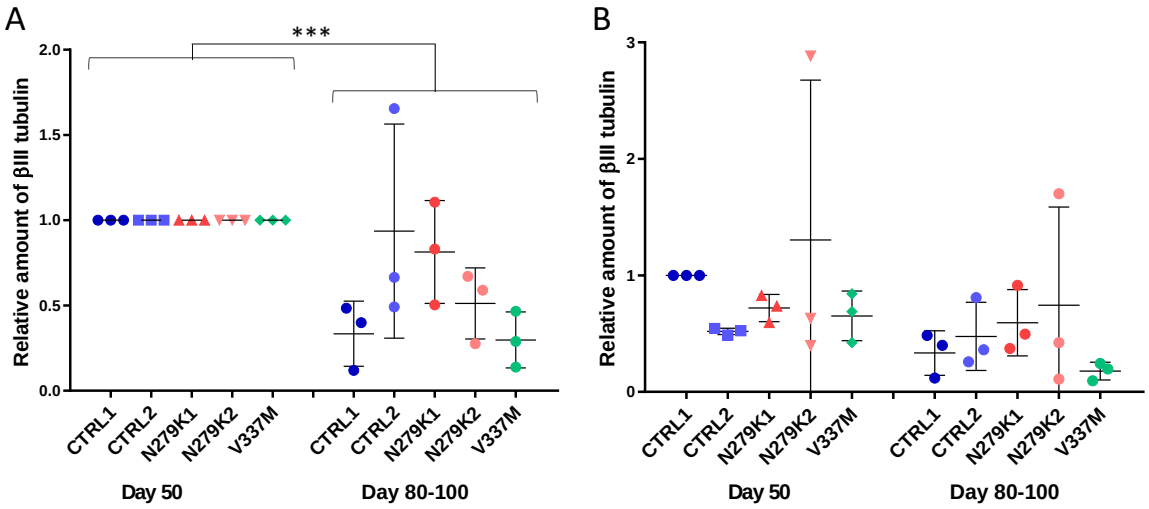

Fig. 3.7 **The amount of βIII-tubulin in iPSC-derived neuronal cultures decreased from day 50 to day 80-100, as measured by Western blot. A)** The fold change in the amount of βIII-tubulin between day 50 and day 80-100 in CTRL1, CTRL2, N279K1, N279K2 and V337M cultures. A decrease in the amount of βIII-tubulin over time was not the expected result, and may be due to neuronal loss or an increase in the proportion of non-neuronal cells. The amount of βIII-tubulin at day 80-100 has been normalised to the amount of βIII-tubulin at day 50 in the same cell line, which is set to 1. Data is from the quantification of three Western blots, using protein from cultures generated in three independent differentiations. Error bars show the SD and mean; significance bars show the results of a two-way ANOVA: there was a significant main effect of time, *** = $p \leq 0.001$. **B)** The data shown in **A)** is presented as the amount of βIII-tubulin normalised to the amount of β-actin at day 50 and day 80-100 in CTRL1, CTRL2, N279K1, N279K2 and V337M cultures. Again, a decrease in the amount of βIII-tubulin over time can be seen. All results are relative to the amount of βIII-tubulin in CTRL1 cultures at day 50, which was set to 1. Each point shows βIII-tubulin normalised to β-actin from one of three independent differentiations; error bars show the SD and mean.

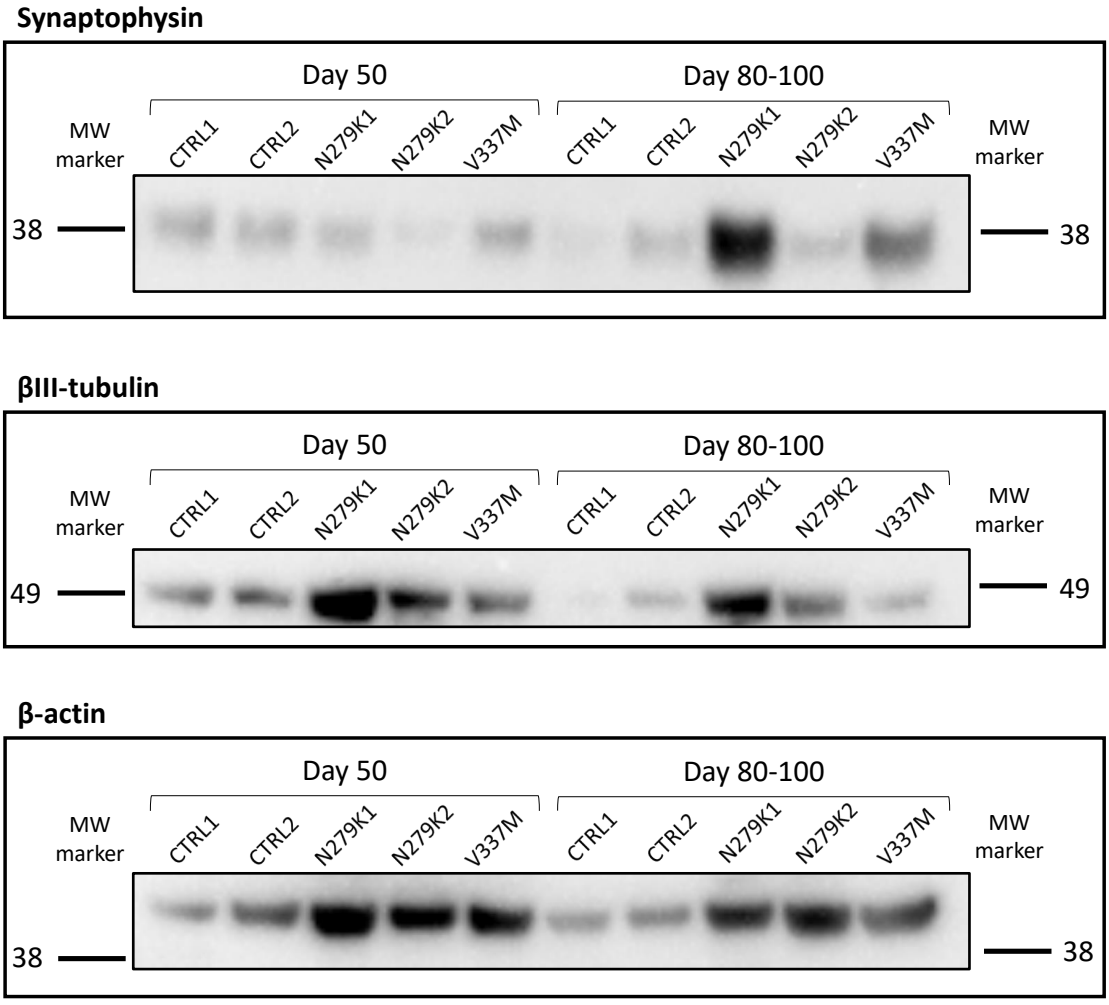

Fig. 3.8 **Representative Western blots of synaptophysin, βIII-tubulin, and βactin in iPSC-derived neuronal cultures at day 50 and day 80-100.** Representative blots showing cultures from one differentiation of CTRL1, CTRL2, N279K1, N279K2 and V337M cultures, at day 50 and day 80-100. Protein weight in kDa is indicated. The amount of protein run in each lane was determined by measuring protein extract concentration using a BCA assay, then calculating the volume needed for 10µg of protein. Volumes were equalised using ice cold RIPA buffer containing protease and phosphatase inhibitors. Despite this, differing amounts of protein were detected in each lane

To visualise the change in the amount of βIII-tubulin in each iPSC line over time, I normalised the day 80-100 levels to those at day 50 (Figure 3.7A). Figure 3.7A shows a decrease in βIII-tubulin levels between day 50 and day 80-100 in all but two cases. The same decrease in βIII-tubulin levels between day 50 and day 80-100 can be seen when the data is shown relative to the amount of in β-actin, in Figure 3.7B. The data in Figure 3.7A was analysed by a two-way ANOVA. This found a significant main effect of time, meaning that the amount of βIII-tubulin was significantly different between all cultures at day 50 and all cultures at day 80-100 ($F(1,10)=22.45$, $p=0.0008$, Figure 3.7). There was no significant main effect of iPSC line (the amount of βIII-tubulin did not vary significantly between the cultures derived from the five iPSC lines: $F(4,10)=2.069$, $p=0.1601$), and there was no significant interaction effect (time has the same effect on the amount of βIII-tubulin in cultures derived from all five iPSC lines: $F(4,10)=2.069$, $p=0.1601$). I analysed the decrease in the amount of βIII-tubulin in cultures from each iPSC line (for example: CTRL1 at day 50 versus CTRL1 at day 80-100; CTRL2 at day 50 versus CTRL2 at day 80-100, and so on) using two-tailed t-tests. These found no significant difference in the amount of βIII-tubulin between day 50 and day 80-100 in CTRL2, N279K1, N279K2 or V337M cultures, but there was a significant decrease in CTRL1 cultures ($p=0.0264$).

These results suggest that the number of βIII-tubulin positive neurons decreased over time, although the effect was not big enough to be statistically significant in all cultures when comparing day 50 and day 80-100 cultures from the same iPSC line. βIII-tubulin staining in some day 80-100 cultures derived from each of the five iPSC lines appeared broken and blobby rather than smooth and continuous, which can be seen to a small extent in Figure 3.10. This may have contributed to the decrease in the relative amount of βIII-tubulin at day 80-100 relative to day 50.

However, a decrease in the amount of βIII-tubulin protein does not necessarily reflect a decrease in the absolute number of neurons over time. An alternative or concurrent factor could be the proliferation of non-neuronal cells in culture, which would decrease the proportion of cells which were neurons and thereby decrease the contribution of βIII-tubulin protein to total protein in older cultures. The proliferation of one non-neuronal cell type (astrocytes) is further explored in Section 3.4.7.

In summary, these results suggest that the amount of βIII-tubulin positive neurons in each culture was variable, and that there was an overall decrease in the amount or proportion of βIII-tubulin positive neurons over time.

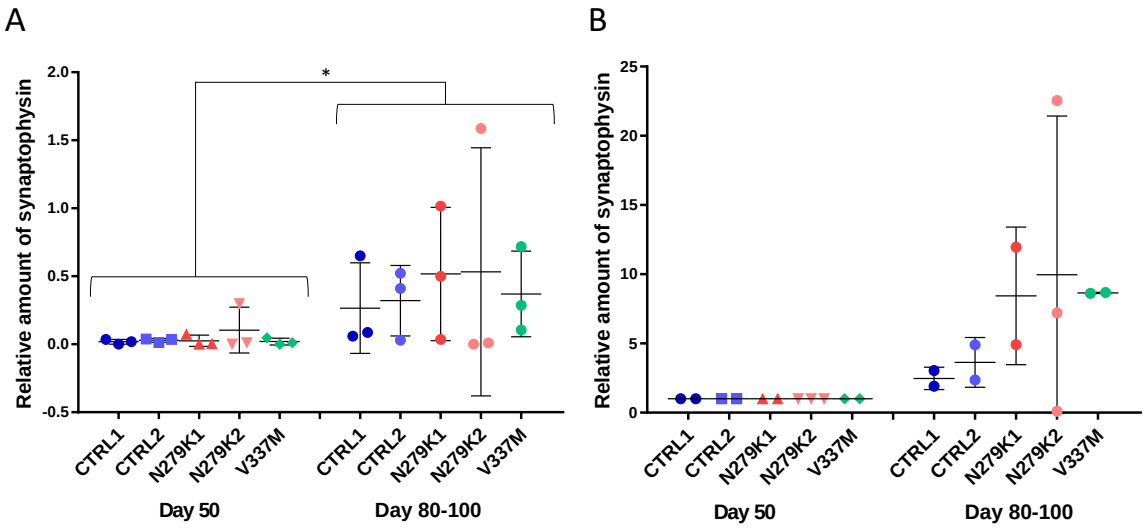

Fig. 3.9 **The amount of synaptophysin in iPSC-derived neuronal cultures increased relative to the amount of βIII-tubulin from day 50 to day 80-100, as measured by Western blot. A)** The amounts of synaptophysin in CTRL1, CTRL2, N279K1, N279K2 and V337M cultures at day 50 and day 80-100, normalised to the amount of βIII-tubulin in the cultures. The amount of synaptophysin increased over time, which was an expected result, and may reflect synapse formation in the cultures. All results are relative to the amount of synaptophysin (normalised to βIII-tubulin) in an external control (mouse brain, not shown) which was set to 1 for normalisation between blots. Each point shows synaptophysin normalised to βIII-tubulin from one of three independent differentiations; protein from each differentiation was run on a separate Western blot. Bars mean$\pm$SD. Significance bars show the results of a two-way ANOVA: there was a significant main effect of time, * = $p<0.05$. **B)** The fold change in synaptophysin between day 50 and day 80-100. The amount of synaptophysin at day 80-100 has been normalised to the amount of synaptophysin at day 50 in the same cell line, which is set to 1. No synaptophysin was detected in one differentiation round in cultures from CTRL1, N279K1 and V337M at day 50, and N279K2 at day 100. Since no ratio can be taken for these cultures, the graph has two, instead of three, points.

3.4.5 Synaptophysin in iPSC-derived neuronal cultures over time

To establish if MAPT mutations influenced synapse number, I used the amount of the pre-synaptic vesicle protein synaptophysin as a proxy measure for the number of synapses. I chose synaptophysin because it is the most abundant synaptic protein (Takamori et al., 2006), has been used to estimate synapse number in both mouse and human brain, and is reported to be an accurate marker for synapse number (Bigio et al., 2001).

I assessed the amount of synaptophysin in day 50 and day 80-100 cultures by Western blotting, using antibodies against synaptophysin and βIII-tubulin (Figure 3.8). To quantify the Western blots, the synaptophysin band in each lane was normalised to the βIII-tubulin

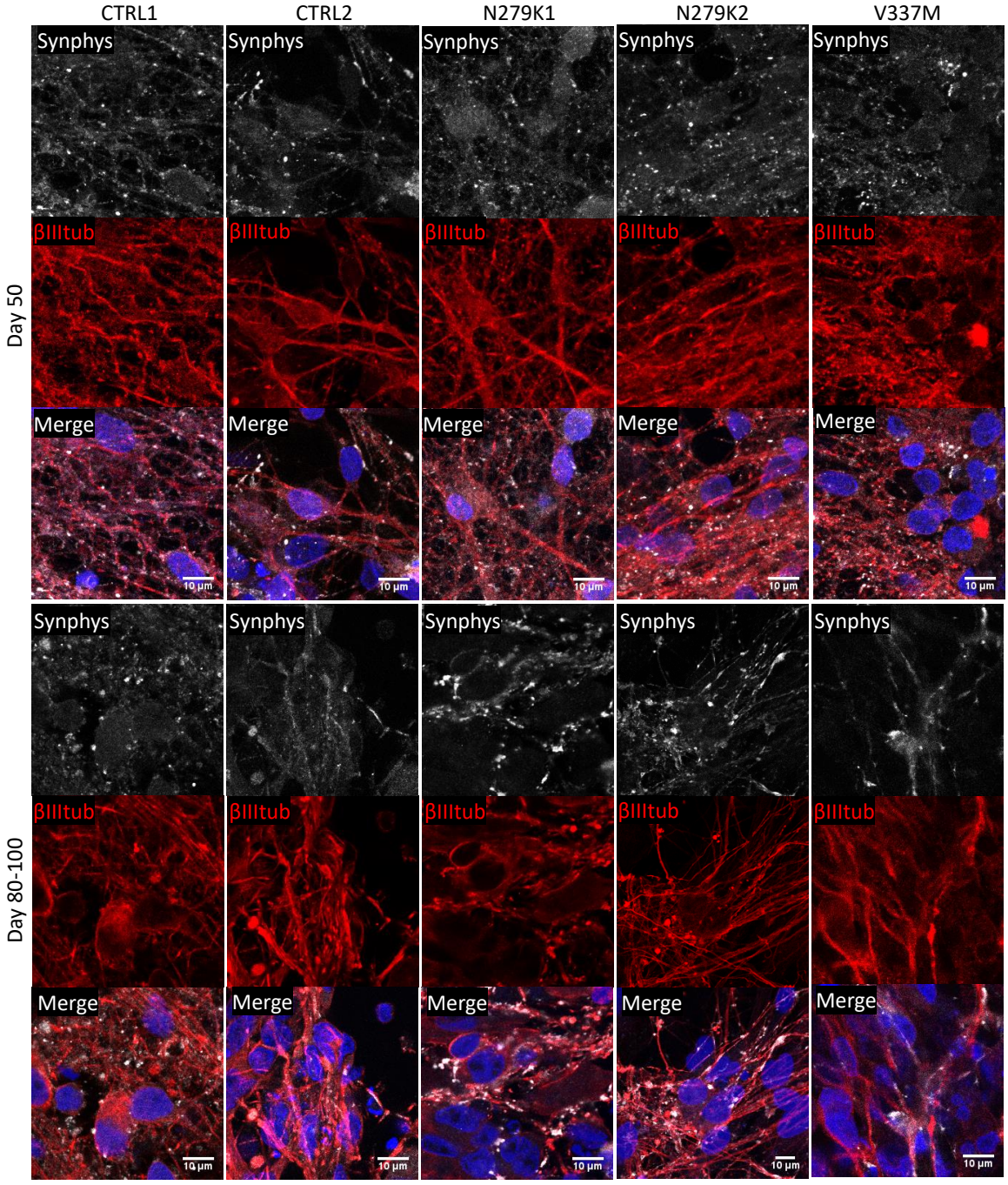

Fig. 3.10 **Representative images of synaptophysin positive puncta associated with βIII-tubulin positive neurons in iPSC-derived neuronal cultures at day 50 and day 80-100.** CTRL1, CTRL2, N279K1, N279K2 and V337M iPSC-derived neural cultures at day 50 and day 80-100 stained for the pre-synaptic marker synaptophysin and the neuronal marker βIII-tubulin. Synaptophysin positive puncta (in white) overlap with βIII-tubulin positive neurons (in red) in the merged images, suggesting that the puncta are synapses. Representative images were taken, but the amount of synaptophysin present was quantified by Western blot, since definitively assigning synaptophysin puncta to a neuronal process and counting individual puncta was difficult. Although the amount of synaptophysin relative to βIII-tubulin increased over time when measured by Western blot, this increase is not clear by eye. Scale bar = 10µm.

band in the same lane. In Figure 3.9A, the amount of synaptophysin is shown relative to the amount in an external control (mouse brain, not shown), which was set to one for normalisation between the blots. Figure 3.9A shows that the amount of synaptophysin is highly variable between differentiation rounds at day 80-100, but less variable at day 50.

To visualise the change in the amount of synaptophysin in each iPSC line over time, I normalised the day 80-100 levels to those at day 50 for each differentiation round (Figure 3.9B). However, synaptophysin was not detected in protein extracts from some cultures in one differentiation round (day 50 CTRL1, N279K1, V337M; day 100 N279K2), so ratios could not be calculated between the day 50 and day 80-100 values for cultures. Therefore, two (instead of three) points are displayed for cultures derived from these iPSC lines in Figure 3.9B.

I analysed the data in Figure 3.9A with a two-way ANOVA, which found a significant main effect of time, meaning that the amount of synaptophysin increased significantly between day 50 and day 80-100 ($F(1,10)=6.447$, $p=0.0294$). There was no significant main effect of iPSC line (the amount of synaptophysin did not vary significantly between the cultures derived from the five iPSC lines: $F(4,10)=0.2538$, $p=0.9008$), and there was no significant interaction effect (time has the same effect on the amount of synaptophysin in cultures derived from all five iPSC lines: $F(4,10)=0.09714$, $p=0.9810$).

I stained day 50 and day 80-100 neural cultures for synaptophysin and βIII-tubulin to see the distribution of synaptophysin staining in these cultures. Representative images are shown in Figure 3.10, in which cultures derived from all five iPSC lines at both day 50 and day 80-100 have synaptophysin positive puncta, overlapping with βIII-tubulin positive cell bodies and processes.

In summary, these results suggest that synapse number increases over time in cultures from all five iPSC lines. Since neuronal maturation should lead to an increase in synapse formation, the synapse number increase shown here is as expected.

3.4.6 Expression of tau isoforms

To assess the maturity of my cultures in terms of tau isoform expression, and to confirm the action of the N279K mutation on exon 10 splicing in my cultures, I detected tau isoforms by Western blotting. To do this, I dephosphorylated protein extracts with alkaline phosphatase from E.coli, since tau is phosphorylated in cells and runs as a smear on Western blots, whereas dephosphorylated tau isoforms can be seen as distinct bands. I used recombinant human tau isoforms to determine the identity of the various isoforms, and human brain extract as a

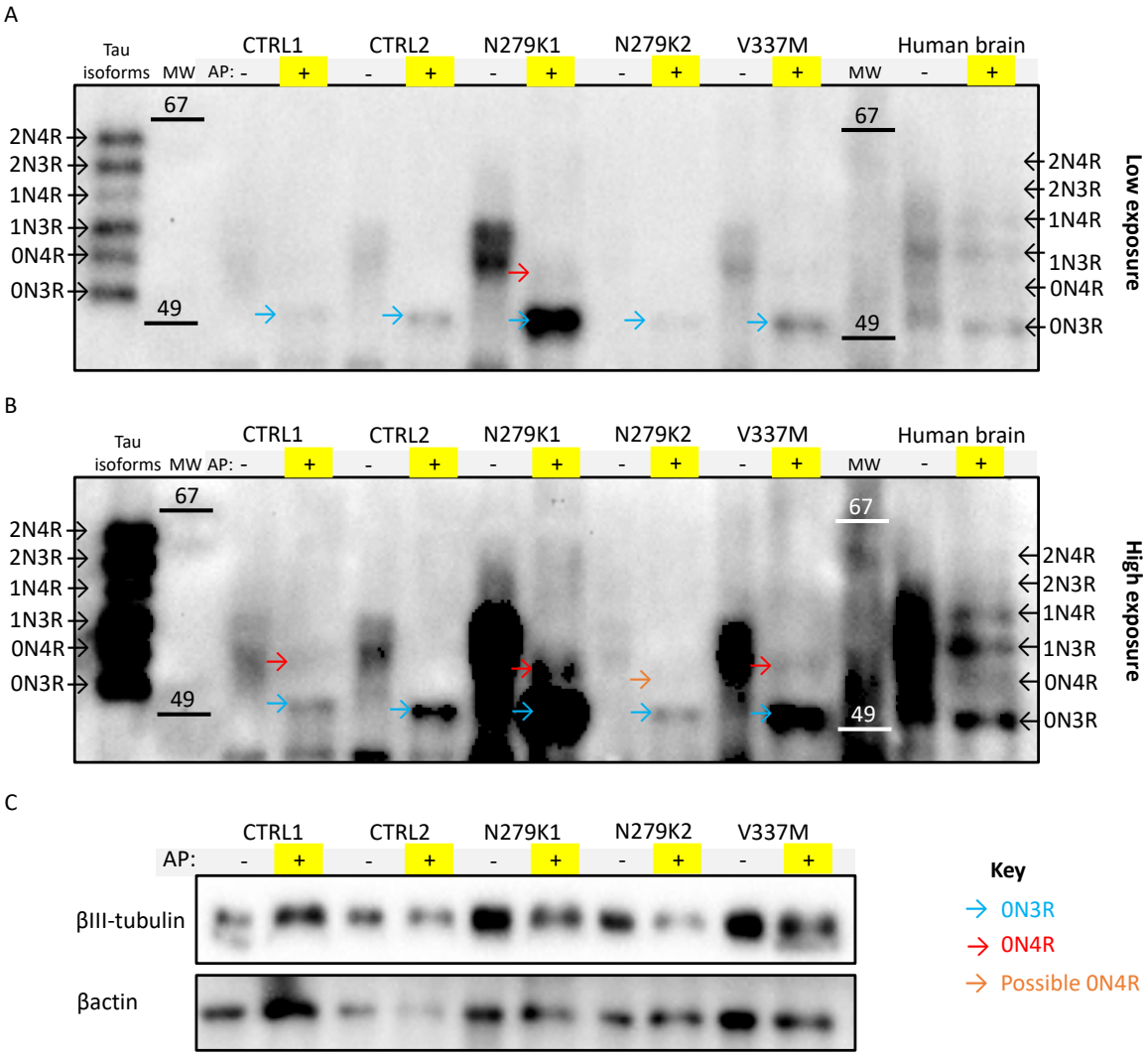

Fig. 3.11 **Western blots for tau show expression of 0N3R tau and some 0N4R tau at day 50.** A representative blot performed with protein extract from 50 day-old CTRL1, CTRL2, N279K1, N279K2 and V337M neural cultures. Lanes in which alkaline phosphatase (AP) has been used to dephosphorylate tau and produce distinct isoform bands are marked "+" and highlighted in yellow. Lanes in which the protein extract was not treated with alkaline phosphatase, in which phosphorylated tau runs as a smear, are marked "-". The identity of recombinant tau isoforms and tau isoforms from dephosphorylated human brain are indicated, as is the size and position of molecular weight markers. **A)** is a low exposure image of the membrane probed with an antibody against all tau isoforms (tau DAKO). Arrows indicate the position of tau isoform bands, visible after dephosphorylation in the lanes marked with a "+" on a yellow background. 0N3R tau bands (blue arrows) of varying intensity are visible in each of the dephosphorylated lanes ("+"). In addition, a 0N4R band (red arrow) is visible in the N279K1 dephosphorylated lane ("+"). **B)** is a high exposure image of the membrane shown in **A)**. Arrows mark the position of tau isoform bands. 0N3R tau bands (blue arrows) are visible at higher intensities in each of the dephosphorylated lanes ("+"). 0N4R tau bands (red arrows) are visible at low intensity in the CTRL1 and V337M dephosphorylated lanes ("+"), and at high intensity in the N279K1 dephosphorylated lane ("+"). A shadow which may be a low intensity 0N4R tau band (orange arrow) is visible in the N279K2 dephosphorylated lane ("+"). **C)** shows the same blot stripped and re-probed for βIII-tubulin and β-actin as loading controls. Although equal amounts of protein were loaded (according to a BCA assay), unequal amounts of βIII-tubulin and β-actin were detected.

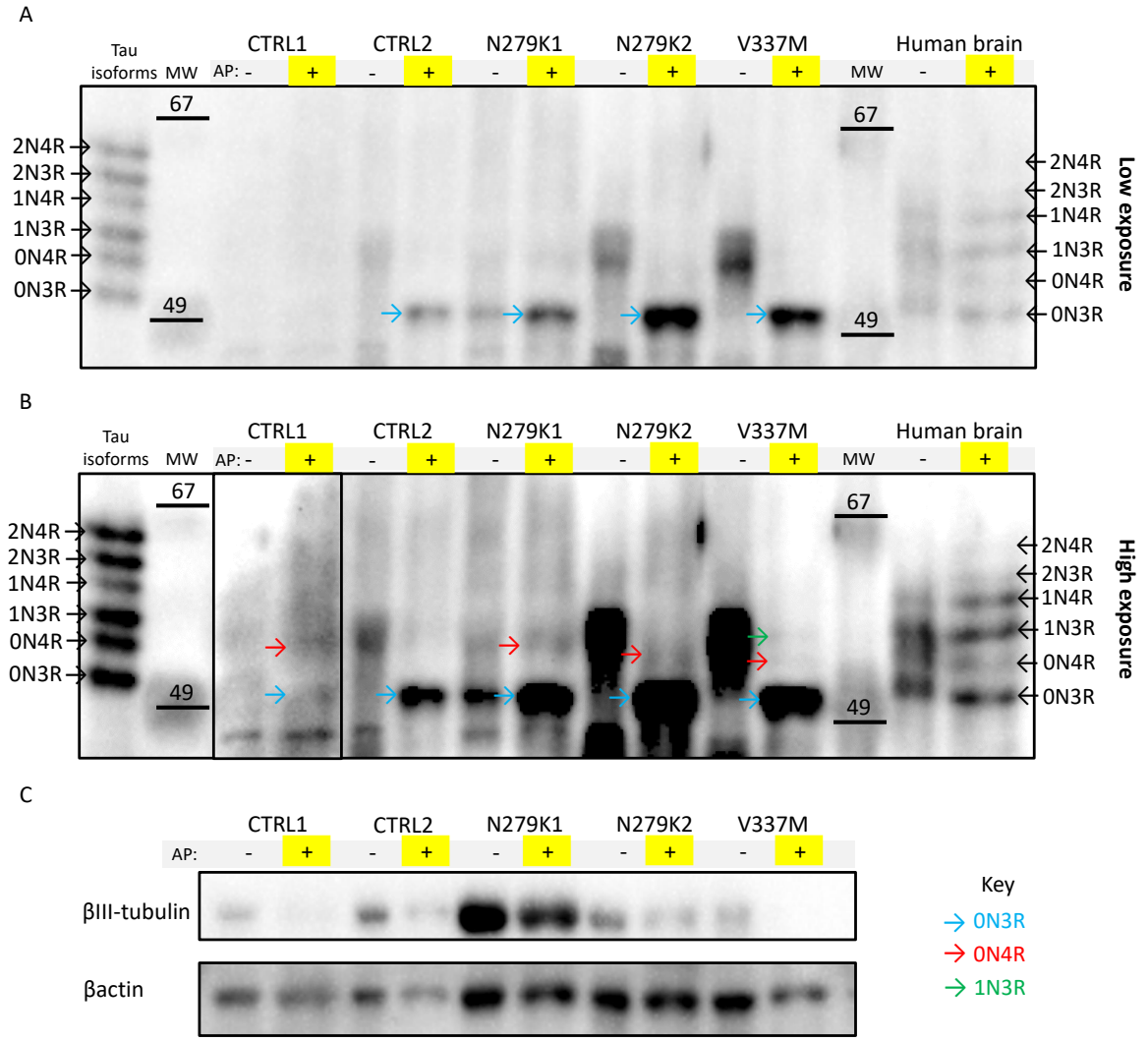

Fig. 3.12 **Western blots for tau show expression of 0N3R tau, some 0N4R tau, and occasional 1N3R tau at day 80-100.** A representative blot performed with protein extract from 80-100 day-old CTRL1, CTRL2, N279K1, N279K2 and V337M neural cultures. Lanes in which alkaline phosphatase (AP) has been used to dephosphorylate tau and produce distinct isoform bands are marked "+" and highlighted in yellow. Lanes in which the protein extract was not treated with alkaline phosphatase, in which phosphorylated tau runs as a smear, are marked "-". The identity of recombinant tau isoforms and tau isoforms from dephosphorylated human brain are indicated, as is the size and position of molecular weight markers. **A)** is a low exposure image of the membrane probed with an antibody against all tau isoforms (tau DAKO). Arrows indicate tau isoform bands, visible after dephosphorylation in the lanes marked with a "+" on a yellow background. 0N3R tau bands (blue arrows) of varying intensity are visible in the dephosphorylated lanes ("+") for CTRL2, N279K1, N279K2 and V337M. **B)** is a high exposure image of the membrane shown in **A)**. Arrows mark tau isoform bands. The box around the two CTRL1 lanes shows an even higher exposure of the same membrane, in which the 0N3R tau isoform is visible (blue arrow). 0N3R tau bands (blue arrows) are visible at higher intensities in the CTRL2, N279K1, N279K2 and V337M dephosphorylated lanes ("+"). 0N4R tau bands (red arrows) are visible at low intensity in the CTRL1, N279K1, N279K2 and V337M dephosphorylated lanes ("+"). There is an additional 1N3R band visible at low intensity (green arrow) in the V337M dephosphorylated lane ("+"). **C)** shows the same blot stripped and re-probed for βIII-tubulin and βactin as loading controls. Although equal amounts of protein were loaded (according to a BCA assay), unequal amounts of βIII-tubulin and β-actin were detected.

Table 3.2 **Tau isoforms in day 50 and day 80-100 iPSC-derived neurons detected by Western blotting**

	CTRL1		CTRL2		N279K1		N279K2		V337M	
	50	**100**	**50**	**100**	**50**	**100**	**50**	**100**	**50**	**100**
0N3R	2	3	3	3	3	3	3	3	3	3
0N4R	1	1	-	1	2	2	1	2	2	1
1N3R	-	-	-	-	-	-	-	-	-	1

The summarised results of Western blotting experiments to detect the tau isoforms present in day 50 and day 80-100 cultures. Blots were performed individually for day 50 and day 80-100 cultures, and either once or twice for each of the three independent differentiation rounds. The table indicates which tau isoforms were observed in each iPSC line and each time point over the three differentiations, although the isoform bands in the blots were not always clear. For example, 2 means the isoform was seen in two differentiations, 3 means the isoform was seen in all three differentiations, - means the isoform was not seen in any differentiations.

positive control. Tau isoforms were detected with a total tau antibody, then the membrane was stripped and probed for βIII-tubulin and βactin as loading controls (Figures 3.11 and 3.12). Western blots were run for day 50 and day 80-100 of each differentiation round, and the results of these blots are summarised in Table 3.2. Western blots were performed for each of three differentiation rounds at day 50, and at day 80-100. Each blot was performed once or twice.

Tau isoform expression at day 50

A representative blot using day 50 cultures is shown in Figure 3.11. At low exposure (3.11A), 0N3R tau bands are visible, although the relative intensity of the bands is highly variable. At high exposure (3.11B) some of the 0N3R tau bands are saturated, but higher molecular weight bands (corresponding to 0N4R tau) are visible, indicating that 0N4R tau is present in lower amounts than 0N3R tau in these cultures. Further over-exposure of the membrane caused more areas to be saturated and did not clearly reveal more tau isoform bands.

The tau isoforms detected at day 50 in cultures from all three differentiation rounds are summarised in Table 3.2. Although I attempted to identify the tau bands, their identity was not always clear due to high background after long exposure.

The 0N3R tau isoform was detected in cultures from all five lines in the three differentiation rounds, with one exception: in the day 50 CTRL1 culture from the third differentiation round, no tau bands were visible and the amount of βIII-tubulin detected was low, although

the amount of β-actin was comparable to that in other lanes (not shown). This suggests that the culture contained mostly non-neuronal cells, or that the proteins did not transfer from the gel to the membrane correctly. Unfortunately, this blot could not be repeated because there was not enough protein extract remaining. The 0N4R tau isoform was detected in one of the control cultures in one differentiation round, as well as in N279K cultures in two differentiation rounds, and in V337M cultures in two differentiation rounds.

Tau isoform expression at day 80-100

A representative blot using day 80-100 cultures is shown in Figure 3.12. At low exposure (3.12A), 0N3R tau bands are visible, and the relative intensity of the bands is variable. At high exposure (3.12B) some of the 0N3R tau bands are saturated, but higher molecular weight bands (corresponding to 0N4R and 1N3R tau) are visible. The box around the CTRL1 lanes indicates an even higher exposure, to visualise the low amount of 0N3R tau in this lane.

The tau isoforms detected at day 80-100 in cultures from all three differentiation rounds are summarised in Table 3.2. The 0N3R tau isoform was detected in cultures from all five lines in the three differentiation rounds, and predominated, even when other isoforms were also expressed. The 0N4R tau isoform was detected in the control cultures in one differentiation, and 0N4R tau, with occassional 1N3R tau, was detected in cultures with the N279K or V337M MAPT mutations.

As can be seen in Table 3.2, the proportion of cultures in which 0N4R or 1N3R tau isoforms were detected increases between day 50 and day 80-100 overall, suggesting that the cultures were maturing over time. In the N279K1 cultures, the 0N4R isoform was detected in two of the three differentiation rounds at day 50 and day 80-100, which is in agreement with the effects of the N279K mutation - an increase in exon 10 splicing and therefore an increase in 4R relative to 3R tau (Hong, 1998; Iovino et al., 2015). In the N279K2 cultures, 0N4R tau was detected at day 50 in one differentiation, and 0N4R tau was detected in two differentiation rounds at day 80-100. In V337M cultures, 0N4R bands were detected in two of the three differentiation rounds at day 50, and 0N4R and 1N3R tau were detected in one of the three differentiation rounds at day 80-100.

However, the results in Table 3.2 must be interpreted with caution, since it is difficult to establish the identity of tau isoforms visible in the Western blots due to over-exposure increasing the background. To help corroborate the findings from Western blots, I stained my iPSC-derived neural cultures for 3R and 4R tau using the exon-junction specific antibodies RD3 and RD4. RD4 signal was amplified with fluorescent streptavidin, as done by Iovino et al. (2015).

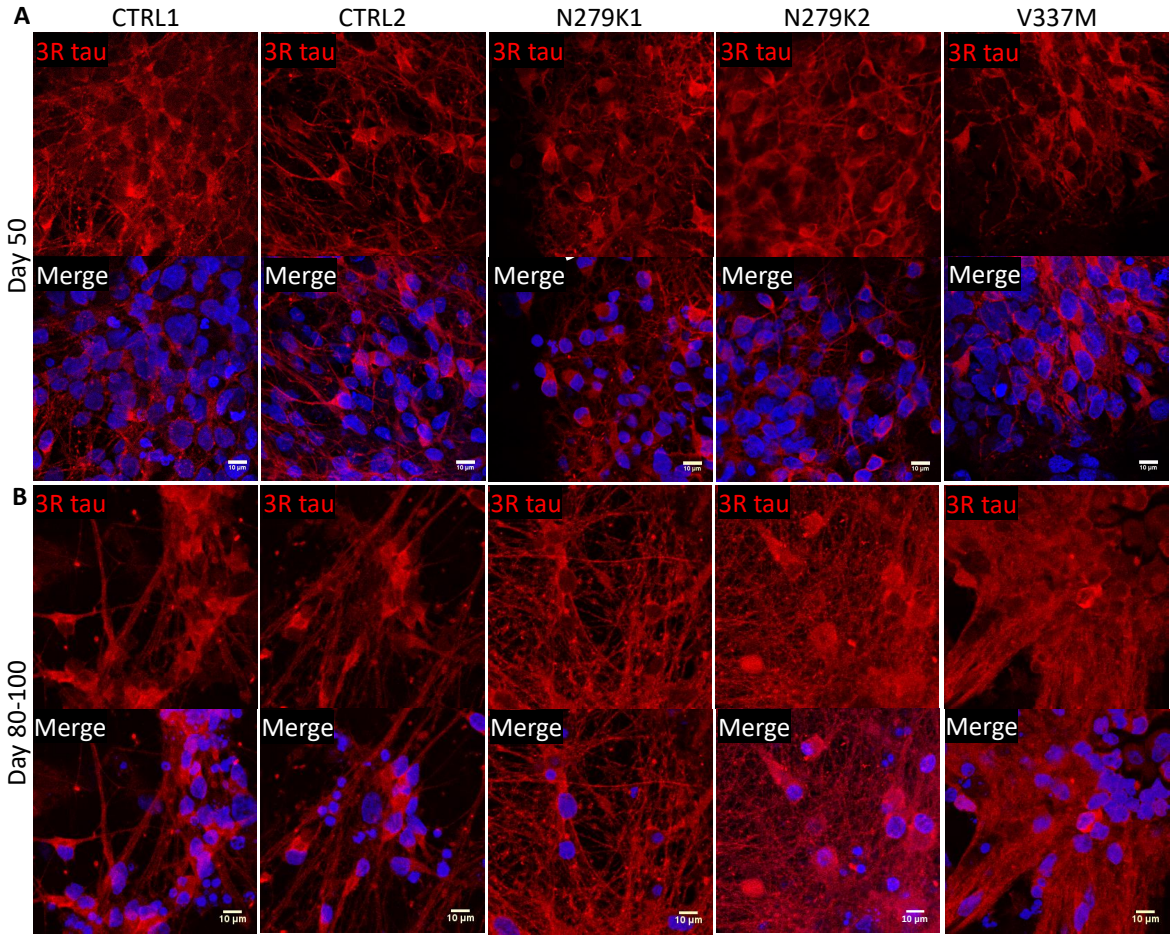

Fig. 3.13 **3R tau is expressed in iPSC-derived neurons at day 50 and 80-100.** Representative immunofluorescence images showing CTRL1, CTRL2, N279K1, N279K2 and V337M neural cultures stained for the RD3 antibody, which detects 3R tau. 3R tau is visible in the cell bodies and processes of neurons in all five cultures at day 50 and day 80-100. This is an expected result and staining pattern. Most of the 3R tau protein detected is likely to be 0N3R tau (which is expressed in fetal human neurons, as well as in the post-natal human neurons alongside the other five isoforms), since 0N3R tau was the main isoform detected by Western blot. Scale bar = 10µm.

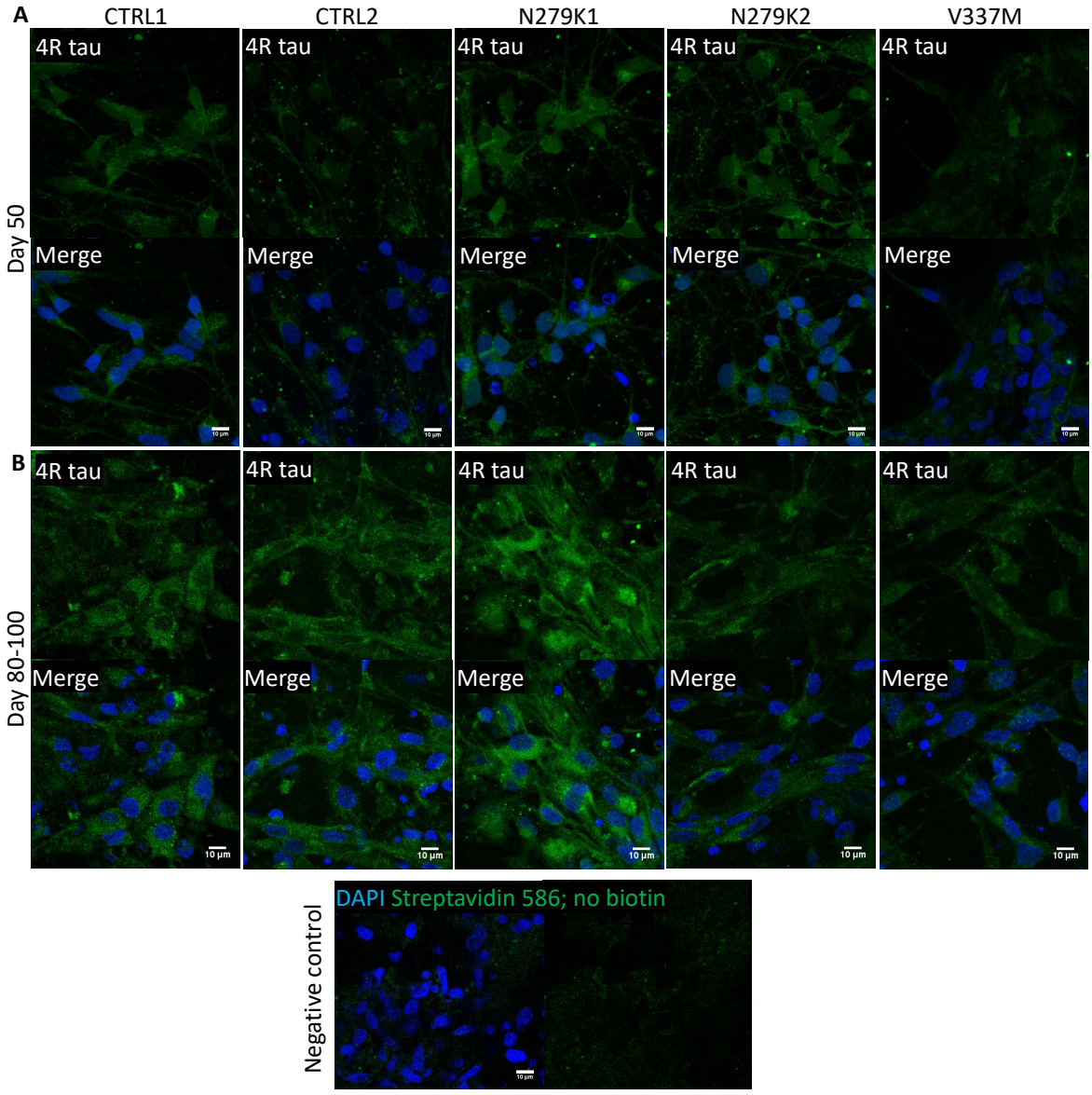

Fig. 3.14 **4R tau is expressed in iPSC-derived neurons at day 50 and 80-100.** Representative immunofluorescence images showing CTRL1, CTRL2, N279K1, N279K2 and V337M neural cultures stained for the RD4 antibody, which detects 4R tau. Faint 4R tau staining is visible in the cell bodies and in some processes in all five cultures at day 50 and day 80-100. Faint 4R tau staining is expected, since 0N4R tau is not expressed until later in development (post-natally in human neurons). The 4R tau protein detected is likely to be mostly 0N4R, since low amounts of 0N4R tau were detected by Western blotting. 4R tau staining was brighter in some cultures, particularly in N279K1 cultures at day 80-100. This may reflect a larger amount of 4R tau protein, or it may reflect variability in immunostaining. Two images at the bottom of the figure show the background introduced by streptavidin 586, in a staining performed without biotin. The lack of green fluorescence indicates that streptavidin 586 contributes little non-specific staining. Scale bar = 10μm.

Figure 3.13 shows that 3R tau was detected in neuronal processes and cell bodies in cultures from all five iPSC lines at day 50 and 80-100, with no noticeable differences in staining intensity. This supports the prominent 0N3R tau detected by Western blotting in all of the cultures at both day 50 and day 80-100. Four repeat tau was detected at a much lower level than 3R tau in day 50 and 80-100 cultures (Figure 3.14). At day 50, some staining is visible in cell bodies and to a lesser extent in processes in cultures from all five lines. At day 80-100 4R tau staining is visible in cell bodies and some processes in all cultures, but more brightly stained individual neurons are visible in the N279K1 and N279K2 cultures, suggesting a higher level of 4R tau expression.

Overall, my results indicate that 3R tau is strongly expressed in neurons from all iPSC lines at day 50 and day 80-100, whilst 4R tau expression is lower than 3R tau expression, and increases over time. In the N279K cultures, particularly N279K1, 0N4R tau is more abundant than in control cultures, possibly due to the action of the N279K mutation. Unexpectedly, tau isoforms expression in V337M cultures is more similar to that in N279K1 cultures than to that in control cultures. Since the V337M mutation does not affect tau splicing, this result may be due to variability in Western blots, or the different genetic background of the control and V337M iPSC lines.

3.4.7 Appearance of astrocytes in aged cultures

To assess the maturity of my iPSC-derived cultures in another way, and to investigate possible astrocyte overgrowth in MAPT-mutant cultures, I stained for the astrocyte marker S100β. S100β is a calcium binding protein expressed by a subset of mature astrocytes. I chose S100β rather than GFAP as an astrocyte marker because S100β is expressed only in mature astrocytes, whereas GFAP is expressed in both mature astrocytes and radial glia cells: the precursors in the developing brain which divide to produce neurons and glia (Raponi et al., 2007). In COs, radial glia are identifiable from their arrangement in culture (Chapter 6), but the monolayer iPSC-derived neural cultures used in this Chapter contained a disorganised arrangement of cells, making it impossible to exclude radial glia by eye.

At day 50, a small number of S100β positive cells are visible in each of the lines (Figure 3.15A). By day 100, more S100β positive cells are visible, and the cells are larger, with longer processes. To quantify this, I counted the number of S100β positive astrocytes and the number of DAPI positive nuclei, then compared the proportion of S100β positive cells between iPSC lines using a two-way ANOVA (Figure 3.15B). There was a significant main effect of time: the proportion of S100β positive astrocytes in all cultures at day 80-100 was

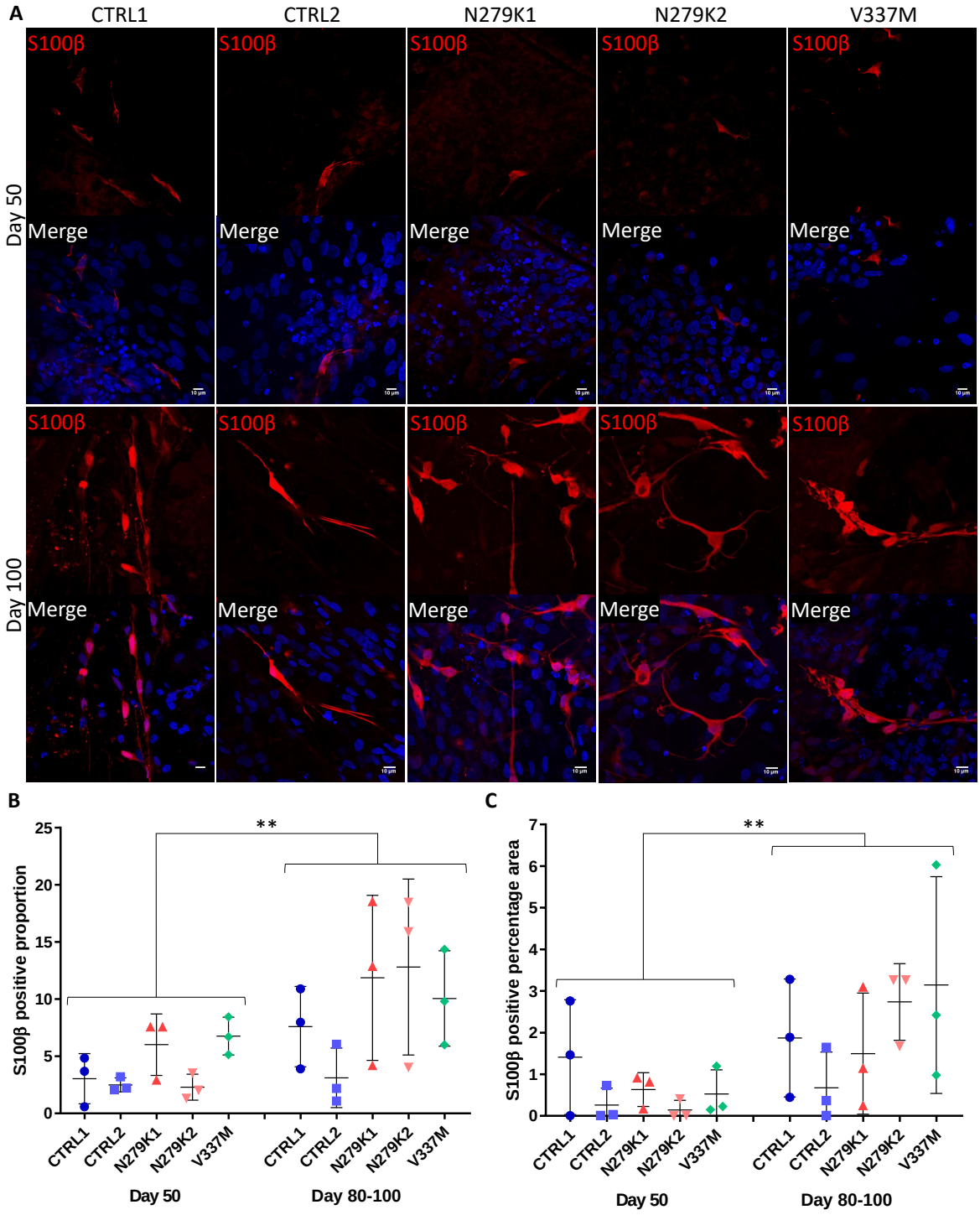

Fig. 3.15 **The proportion of S100β positive astrocytes in neuronal cultures increases from day 50 to day 80-100.** **A)** CTRL1, CTRL2, N279K1, N279K2 and V337M neural cultures stained for S100β. The proportion of astrocytes increased over time, indicating maturation of the culture. This was an expected result, since astrocytes are produced by the last division of neural precursors. Scale bar = 10µm. **B)** The proportion of S100β positive astrocytes in the cultures, counted in immunofluorescence images. For every iPSC line, each point represents the mean of one of three independent differentiations. Each mean was calculated from at least six fields of view (three from each of two or three coverslips). Bars show mean±SD; ** is p≤0.01 . **C)** The percentage area covered by S100β positive astrocytes. For every iPSC line, each point represents the mean of one of three independent differentiations. Each mean was calculated from at least eight fields of view. Bars show mean±SD; ** is p≤0.01 .

significantly higher than the proportion of S100β positive astrocytes in all cultures at day 50 (F(1,10)=17.9, p=0.0017, Figure 3.15A and B). There was no significant main effect of iPSC line (the proportion of S100β positive cells did not vary significantly between the cultures derived from the five iPSC lines: F(4,10)=1.712, p=0.2234), and there was no significant interaction effect (time has the same effect on the proportion of S100β positive cells in cultures derived from all five iPSC lines: F(4,10)=1.939, p=0.1804). After a visual inspection of the difference in the proportion of S100β positive cells between day 50 and day 80-100 in each of the iPSC lines, I performed further statistical analysis using t-tests to compare the proportion of astrocytes in day 50 and day 80-100 cultures from the same iPSC line. No statistically significant differences were observed when comparing day 50 and day 80-100 cultures from each of the iPSC lines.

In addition, I measured the area of each field of view covered by S100β positive cells, and compared between iPSC lines using a two-way ANOVA (Figure 3.15C). This too showed a significant main effect of time: the area covered by S100β positive astrocytes in all cultures at day 80-100 was significantly higher than the area covered by S100β positive astrocytes in all cultures at day 50 (F(1,10)=10.08, p=0.0099, 3.15A and C). There was no significant main effect of iPSC line (the area covered by S100β positive cells did not vary significantly between the cultures derived from the five iPSC lines: F(4,10)=1.11, p=0.4042), and there was no significant interaction effect (time has the same effect on the area covered by S100β positive cells in cultures derived from all five iPSC lines: F(4,10)=1.314, p=0.3293). In addition, I used t-tests to compare the area covered by astrocytes at day 50 and day 80-100 in cultures from each iPSC line. No statistically significant differences were observed when comparing day 50 and day 80-100 cultures from each of the iPSC lines.

These results show that the proportion of S100β positive astrocytes increases over time in iPSC-derived neural cultures, with no detectable effect of the MAPT mutations N279K and V337M. This suggests that the astrocytes are appearing in culture due to the division of late precursors.

3.5 Discussion

The results described in this Chapter indicate that my iPSC-derived neural cultures have a forebrain fate, and are maturing over time. The cultures express the neuronal marker βIII-tubulin and the pre-synaptic marker synaptophysin with no significant differences in expression level between the control and MAPT-mutant iPSC lines. The neural cultures also contain an increasing number of astrocytes over time, with no difference in astrocyte prolifer-

ation between cultures derived from the control and MAPT-mutant iPSC lines. Examination of tau isoforms present in these cultures suggests maturation of the cultures over time, with the action of the N279K mutation inducing an increase of 4R tau, as previously described using a different differentiation method (Iovino et al., 2015).

The results also show variability between the three differentiation rounds, which is particularly clear in the quantification of Western blots for synaptophysin at day 80-100, and in Western blots for tau isoforms at day 50 and day 80-100. A contributor to this variability could be that I derived NPCs from iPSCs three times, and differentiated the NPCs to neurons. This means that small stochastic differences arising during NPC differentiation, or differences in my tissue culture skills over time, for example, could cause variability between cultures obtained from the three differentiation rounds. One way to decrease variability would be to produce a large number of NPCs, freeze some, and differentiate them to neurons in three independent differentiations. However, this method would not control for the process of neuralising the iPSCs.

3.5.1 Differentiation of iPSCs to NPCs

In day 16 NPCs, I observed clear staining with the Otx2, Pax6 and Nestin antibodies. However, FoxG1 expression was mostly cytoplasmic, despite FoxG1 being a transcription factor expected to be present in the nucleus. This may be because FoxG1 can be present in the cytoplasm of differentiating NPCs (Regad et al., 2007), indicating that I should have stained for FoxG1 at an earlier timepoint. Indeed, (Watanabe et al., 2005) observed nuclear FoxG1 staining on day 10 when differentiating ESCs to NPCs using a similar method. However, the cytoplasmic FoxG1 staining could observed could have been due to non-specific antibody staining. Whether or not the FoxG1 staining was specific could have been confirmed using a positive control, such as embryonic mouse brain (provided that the antibody detected both mouse and human FoxG1).

Alternatively, I could have stained for cortical layer markers, which would confirm the cerebral cortex specificity of the neurons produced. Since the differentiation method I used did not employ caudalising or ventralising factors, the default model (in which PSCs cultured in minimal media differentiate towards a rostral forebrain fate) predicts predominantly glutamatergic neurons (Chambers et al., 2009; Elkabetz et al., 2008). No papers have been published on the identity and proportion of cell types produced using the Kirkeby et al. (2012)/Santiváñez Pérez (2017), but Jessica Santiváñez Pérez, who adapted the method for

iPSCs, found that the resulting iPSC-derived neurons were predominantly glutamatergic, with a small numbers of tyrosine hydroxylase positive and GAD65/67 positive cells.

Not all cells in the day 16 NPC cultures were Otx2, Pax6 and Nestin positive, indicating that not all of them were neuronal precursors. By day 16, a small number of NPCs had spontaneously differentiated to neurons, as can be seen in Figure 3.6. Therefore, other cell types intermediate between NPCs and neurons may have contributed to the number of Otx2, Pax6 and Nestin negative cells in NPC cultures. For example, intermediate progenitor cells (Tbr2 positive, Pax6 negative) are produced from the asymmetric division of (Pax6 positive) radial glial cells (Englund, 2005; Hansen et al., 2010; Kriegstein and Alvarez-Buylla, 2009). It is also possible that cells from other germ layers may have been present in the cultures. These could have been detected by immunostaining for ectoderm, mesoderm and endoderm markers, to determine the proportion of the cells not differentiating towards the ectoderm lineage, which could not contribute to the neuroectoderm.

Proliferation of NPCs

I observed no significant difference in the proliferative capacity of my control and MAPT-mutant NPC cultures at day 16, indicating that there was not a significant difference in spontaneous differentiation at this stage. To confirm this, I could have performed the same staining and quantification during a time course, allowing the NPCs to spontaneously differentiate over an extended time in culture, as opposed to re-plating the NPCs on day 21 and adding DAPT to induce neuronal differentiation. Since I added DAPT to my cultures at day 21, NPCs were forced out of the cell cycle at this time point, preventing the detection of differences in spontaneous NPC differentiation to neurons between the control and MAPT-mutant cultures, if they were present.

Future work could include further examination of spontaneous differentiation in control and MAPT-mutant NPCs, since there is some evidence that MAPT-mutant iPSC-derived NPCs do not behave in the same way as controls.

For example, Wren et al. (2015) reported that N279K iPSCs were less able to differentiate into ectoderm, and produced fewer Nestin and βIII tubulin positive neurons as compared to controls. Similar features have not been reported by groups making iPSC-derived neurons and NPCs from different N279K mutant iPSC lines (Ehrlich et al., 2015; Iovino et al., 2015), suggesting a problem with the N279K iPSC clone or differentiation methods used by Wren et al..

In addition, a study of iPSC-derived NPCs with three MAPT mutations (N279K, P301L and intron 10+16) showed a (non-significant) trend for a lower proportion of proliferative

NPCs than in controls (García-León et al., 2018). However, it is unclear if this is a cumulative effect of three MAPT mutations (which may not be detectable in NPCs with only one MAPT mutation), or the effect is caused by a single one of the three MAPT mutations.

3.5.2 Differentiation of NPCs to neurons

The amount of βIII-tubulin in my iPSC-derived neural cultures decreased from day 50 to day 80-100, as determined by Western blot. This may be due to an increase in the number of non-neural cells, which would decrease the proportion of total protein which was βIII-tubulin. Since the proportion of astrocytes in the cultures increased over time, this is a possible explanation. To prevent non-neural cells from proliferating in culture, I could have used DAPT to force NPCs out of the cell cycle, and then added an anti-mitotic agent such as mitomycin C to prevent proliferative cells from dividing further, as was done by Schwartzentruber et al. (2018).

The decrease in the amount of βIII-tubulin may also have been caused by cell death, which is explored further in Chapter 4. I observed more condensed pyknotic nuclei in day 80-100 cultures as compared to day 50 cultures regardless of the parent iPSC line, although this does not necessarily mean that more cells died at later timepoints.

As mentioned above, some day 80-100 cultures derived from each of the five iPSC lines had discontinuous, blobby-looking βIII-tubulin staining, as compared to the relatively smooth and continuous staining in day 50 cultures (Figure 3.10). This may be an artefact of how the cultures changed over time, since processes in some areas of day 80-100 cultures formed dense mat-like surfaces where it was difficult to see individual processes. In areas of the same culture, processes formed thick bundles, where it was again difficult to distinguish individual processes. These areas both had a higher density of blobby-looking βIII-tubulin staining despite repeated washing during staining, suggesting that primary and secondary antibody might have become trapped in these densely packed areas. A dense neuropil-like mesh has also been observed in 112 and 300 day-old neuronal cultures by Odawara et al. (2016), suggesting that the changes described above can commonly occur in iPSC-derived monolayer cultures over time. This did not occur in 3D culture, and is discussed in Chapter 6.

The amount of βIII-tubulin in the cultures was assessed by Western blot. Although the concentration of protein extracts was measured by BCA, and although protein extract volumes were calculated such that the same amount of protein was run in each lane, this was not reflected in the results. This can be seen in Figure 3.8, where the amount of β-actin is

lower in the control lanes than the MAPT-mutant lanes, bringing into question the reliability of this result. The results of this blot could have been confirmed using a more quantitative method, such as qPCR, although this method, like Western blotting, would not distinguish an absolute change in neuron number from a decrease in the proportion of neurons in the culture.

Synaptophysin expression

The levels of synaptophysin, detected by Western blotting, increased in my iPSC-derived neural cultures over time. This may indicate ongoing synaptogenesis, as it has previously been reported that the number of synapses formed by iPSC-derived neurons increases with age, even after 100 days in culture (Bergström et al., 2016; Odawara et al., 2016). The amount of synaptophysin staining was highly variable between cultures at day 80-100. This may reflect unintended variation between the differentiation rounds, or even between different individual cultures generated in the same differentiation round.

There was no effect of parent iPSC line on the amount of synaptophysin detected, suggesting that there was no MAPT mutation dependent synapse loss in the MAPT-mutant cultures. This is similar to the findings of Silva et al. (2016), who found no difference in expression of PSD-95, synapsin-I and synaptophysin proteins in 35 day-old iPSC-derived control and A152T mutant neurons. However, the neurons examined were relatively young at 35 days old, and A152T has not yet been confirmed as an FTDP-17T-linked mutation (Kara et al., 2012).

In addition, studies of neurons derived from iPSCs from AD patients, with either sporadic AD or with mutations in amyloid precursor protein, also found no change in synaptic protein levels relative to control cultures (Birnbaum et al., 2018; Israel et al., 2012; Nieweg et al., 2015). Together, these data suggest that synapse loss is not observed in iPSC-derived cultures without the addition of exogenous stressors.

If synapse loss had been detected at such an early timepoint relative to human brain development, it may have represented synaptic pruning, or a failure to make synaptic connections rather than a neurodegenerative phenotype. Studies using iPSC-derived neurons to examine the effects of diseases with a developmental component suggest that this may be the case, since synapse formation deficits have been detected in iPSC-derived neuron models of autism spectrum disorders and schizophrenia (reviewed by Habela et al., 2015).

Synaptophysin levels were measured by Western blot, but the amount of protein detected in each Western blot lane was not equal (Figure 3.8) despite calculating and loading the same protein concentration. The variability in the amount of protein detected means that results

from these Western blots may not be reliable. To confirm the increase in synaptophysin levels over time, I could have used additional techniques. For example, I could have measured synaptophysin mRNA levels by qPCR.

Another alternative would be quantification of immunostaining images. To ensure that synaptophysin puncta were specific to synapses, I could have used an antibody against a post-synaptic protein such as PSD-95 alongside the synaptophysin antibody. Counting the number of puncta that were both synaptophysin and PSD-95 positive would confirm that synapses with both pre- and post-synaptic membranes were identified, and would give an estimate of synapse number.

Alternatively, I could have confirmed my Western blotting results by measuring synapse function using electrophysiological techniques. For example whole cell patch-clamping, in which the voltage or current can be held constant, can be used to classify neuronal maturity and to identify neuronal subtypes (Belinsky et al., 2014). One drawback of this method is that it is time consuming, and each measurement is performed on a single cell for period of seconds to minutes. An alternative to this is multi-electrode arrays, which can be used to measure the electrophysiological activity of an entire culture over a period of days to weeks (Odawara et al., 2016).

However, electrophysiological activity has already been measured in neurons derived from the same control and N279K iPSC lines I used, albeit using a different method for iPSC differentiation. Iovino et al. (2015) observed faster electrophysiological maturation in iPSC-derived neurons with the N279K or P301L mutation relative to in the control neurons: neurons with N279K or P301L mutations fired regenerative, sodium channel blocker-sensitive action potentials (APs) at day 50-79, whereas control neurons did not fire comparable regenerative, sodium channel blocker-sensitive APs until day 100.

The appearance of astrocytes

The number of astrocytes in my iPSC-derived neural cultures increased over time, and the lack of difference between control and MAPT-mutant cultures suggests that there was no MAPT mutation related astrocyte overgrowth. The appearance of astrocytes in my neural cultures at 50 days (small, rounded and with few processes) and at later time points (larger, with many processes) is similar to that described in ESC-derived neural cultures (Johnson et al., 2007), suggesting that my cultures developed normally in this respect. However, astrocytic growth may have been enhanced by the use of BDNF in the maintenance media, since BDNF is thought to be pro-neural when it signals via the full length trkB receptor (which is expressed by NPCs early in development), but pro-glial when it signals via the

truncated trkB receptor (expressed later in brain development) (Cheng et al., 2007). However, BDNF probably had a small effect, since the proportion of astrocytes in my cultures remained less than 20%.

I chose S100β as an astrocyte marker since it is expressed in a subset of mature astrocytes, but not by radial glia (Raponi et al., 2007). However, it is not a perfect marker for excluding other cell types, since it is also expressed in oligodendrocyte precursors (Deloulme et al., 2004), and myelinating oligodendrocytes during development (Hachem et al., 2005). Therefore, some S100β negative astrocytes may have been undetected by my analysis, and some S100β positive oligodendrocyte precursors may have been included. Full characterisation of the astrocytes present in my neural cultures was beyond the scope of my project, and would have required an in-depth study considering the variety of astrocytes which exist (reviewed by Krencik and Ullian, 2013). Although the analysis I performed is superficial relative to what could have been done in a comprehensive characterisation, it is informative, since it shows a maturation-related increase in astrocyte number over time, and no differences between the control and MAPT-mutant cultures.

I did not examine the presence of cell types other than neurons and astrocytes in the day 50 and day 80-100 cultures, but other cell types may have been present. For example, the radial glia that generate astrocytes after neurogenesis also produce oligodendrocyte precursors (Kriegstein and Alvarez-Buylla, 2009; Rakic, 2003), suggesting that these too may have been present in my cultures. Further characterisation of these cultures could have included immunostaining for these cells.

3.5.3 Tau isoforms detected

I assessed the maturity of my iPSC-derived neural cultures and the action of the N279K mutation in these cultures by Western blotting to examine tau isoforms. In the control cultures 0N3R isoforms and occasionally 0N4R isoforms were visible at day 50, whereas 0N3R tau, some 0N4R tau, and occassional 1N3R tau were visible in one of the three differentiation rounds at day 80-100, suggesting a degree of maturation over time. Likewise, other studies have found 0N4R tau isoforms in control neural cultures after 50 days (Iovino et al., 2015; Sposito et al., 2015). Since some 4R tau immunoreactivity is visible in control neural cultures at day 50 and day 80-100, it is possible that insufficient 0N4R tau protein was present for detection by Western blot in all of the differentiation rounds, or that the quality of the blots did not allow detection.

The N279K1 neural cultures demonstrate the action of the N279K mutation, since 0N4R tau is visible in cultures from two differentiation rounds at day 50 and day 80-100. In addition, 1N3R tau is visible at both day 50 and day 80-100, and a faint band which may correspond to 1N4R tau is visible at day 50. The early appearance of 0N4R tau in this line has also been observed by Iovino et al., and the bright appearance of N279K1 neurons stained for 0N4R tau at day 80-100 corroborates the results observed by Western blot.

The 0N4R tau isoform was detected in N279K2 cultures at day 50 (one differentiation round) and day 80-100 (two differentiation rounds). In addition, brighter 4R tau immunoreactivity can be seen in N279K2 cultures relative to control cultures. Not detecting 0N4R tau as frequently in the N279K2 cultures as in the N279K1 culture led me to check that the N279K mutation was present in both lines, which was confirmed by Sanger sequencing (Figure 3.3). The relative lack of 0N4R tau isoforms in the N279K2 cultures may therefore be due to less neuronal content in the N279K2 cultures, which can be seen as less βIII-tubulin and 0N3R tau in the Western blots for tau isoforms. Lower levels of tau isoforms would make them more difficult to detect by Western blot.

Notably, 0N3R tau predominated in cultures from all iPSC lines at both timepoints, even when other isoforms were visible. This has also been reported by other groups (Iovino et al., 2015; Sposito et al., 2015), and suggests a high proportion of immature neurons in the cultures. However, Iovino et al. (2015) found that 0N3R tau protein levels were reduced relative to control in the presence of the N279K mutation, and groups studying iPSC-derived neurons from intron 10+14 and intron 10+16 mutant iPSCs (which also alter tau splicing) have found a similar effect (Imamura et al., 2016; Sposito et al., 2015).

In the V337M cultures, 0N4R tau was visible in Western blots from at day 50 (two differentiation rounds) and day 80-100 (one differentiation round). In addition, faint bands which may correspond to 1N3R and 1N4R tau were visible at day 80-100 (in one differentiation round). This could suggest that the V337M cultures either matured more quickly with respect to tau isoform expression than the control cultures. Published studies of V337M-mutant iPSC-derived neurons have shown that 3R and 4R tau mRNA expression is comparable to that in control cultures at day 40 (Ehrlich et al., 2015). This is expected, since the V337M mutation does not alter exon 10 inclusion in splicing assays (Hong, 1998), and tau inclusions in the brains of individuals with the V337M mutation consist of both 3R and 4R tau (Spillantini et al., 1996a), indicating that the V337M mutation does not alter exon 10 splicing.

Previous published examinations of tau isoforms from the Spillantini lab have used perchloric acid to selectively solubilise and extract tau from iPSC-derived neural cultures (Iovino et al., 2015; Lindwall and Cole, 1984). This method may make the tau present more

visible, since the selective solubility of tau in perchloric acid means that other proteins which contribute to background signal are removed. However, protein extract in perchloric acid cannot be used to measure the quantities of other proteins, so further cultures would be needed from each differentiation to obtain this information. To avoid these problems, I made protein extracts in RIPA buffer, to examine both tau isoforms and other proteins using the same extract. Although some tau isoforms can be detected in my Western blots, a better approach might have been to use a method for generating NPCs which allowed extensive NPC expansion, in order to make large enough neural cultures to perform perchloric acid extraction.

The amounts of protein detected in Western blots varied between cultures derived from different cell lines. This is apparent in Figures 3.8, 3.11 and 3.12 when looking at the amount of β-actin present, and could account for differences in the number of tau isoforms detected in each cell line. This discrepancy was despite measuring the concentration of protein extracts by BCA before Western blotting, and loading the same amount of protein extract in each lane. To avoid this, tau isoform expression could have been confirmed at the mRNA level by qPCR, as was done by Iovino et al. (2015), since this method would provide a quantitative result.

Although I observed brighter 4R tau staining in some day 80-100 N279K cultures as compared to controls, differences in staining intensity may have been caused by factors other than the amount of protein. For example, factors during staining, such as the degree of antibody penetration which could be affected by the density of neurons and other cells in the culture, could affect staining intensity. Factors after staining, such as photobleaching caused by exposure to light whilst imaging, could decrease the brightness of the last image taken relative to that of the first image taken. Careful quantification, rather than judging by eye, would have been required to determine whether there was a difference in tau staining intensity between the N279K and control neurons. In addition, positive and negative controls for 3R and 4R tau should have been used, to determine whether 3R and particularly 4R tau staining was specific.

Another factor which likely prevented me from detecting more tau isoforms is the amount of time I maintained the iPSC-derived neural cultures for. Initially, I intended to maintain my cultures for over 100 days, to observe more adult tau isoforms as seen after 150 days by Iovino et al. (2015). However, cultures in 12- 24- and 96-well plates began to detach from the plate surface at around day 100, despite the measures I took to prevent this. These included adding laminin every 10 days to aid adherence to the culture surface, using tissue-culture treated plastic coverslips (instead of glass) additionally treated with poly-L-ornithine and

laminin, and changing the culture media as gently as possible (Chapter 2). I fixed cultures for staining and collected others for protein extraction as soon as the first signs of detachment were visible in any of the iPSC lines, and for this reason my late timepoint is a range: 80 to 100 days. A possible solution to this problem could be using an anti-mitotic agent such as mitomycin C to prevent the continued proliferation of non-neural cells in culture Schwartzentruber et al. (2018). Other groups have overcome this problem using a matrigel layer on top of the cultures (Choi et al., 2014), and by culturing iPSC-derived neurons in suspension as cerebral organoids (Lancaster et al., 2013), which is explored in Chapter 6. The above points could explain the variability in tau isoform expression that I observed.

3.5.4 Advancing the maturity of iPSC-derived neurons

One of the biggest challenges in using iPSC-derived neurons to model neurodegenerative conditions is culturing neurons which resemble those in a mature, rather than developing brain. There are several methods which I could have used to advance the appearance of adult-like tau isoforms.

For example, making induced neurons (iNs) may provide a more mature neuron more quickly. According to one study, iNs produced from iPSCs with the intron 10+16 mutation express 0N4R tau after 7 days, and the mature MAP isoforms MAP2A/B after 14 days (Imamura et al., 2016). In addition, another study showed that iNs produced from fibroblasts with the K298E mutation and iNs from control fibroblasts both expressed 3R and 4R tau after 30 days in culture (Iovino et al., 2014). However, tau isoform expression in iNs has not yet been extensively characterised.

Tau exon 10 splicing can also be controlled by trans-splicing, in which a pre-trans-splicing cassette is introduced into the cells, then transcribed to make RNA. To control tau exon 10 splicing, an RNA strand coding for exons 10, 11, 12 and 13 would bind to intron 9 of endogenous tau pre-mRNA, replacing the endogenous exons 10 (if present), 11, 12 and 13. The inclusion of exon 10 in the trans-splicing RNA would cause expression of 4R tau. This has been demonstrated in both ESC-derived neurons (Lacovich et al., 2017) and mice expressing human tau (Avale et al., 2013), although it does not recapitulate the splicing of all six tau isoforms as seen in the adult human brain. This strategy would be useful to study mutations which do not alter tau splicing, and occur only in exon 10.

The 3D culture of neurons has also been shown to enhance neuronal maturity, in terms of βIII-tubulin expression, synaptic protein expression and synaptic function (Choi et al., 2014; Liedmann et al., 2012; Ortinau et al., 2010; Seidel et al., 2012; Zhang et al., 2016).

Most importantly for studying MAPT mutations, 3D culture may also enhance maturity with respect to tau isoform expression (Agholme et al., 2010; Choi et al., 2014). A 3D culture system is explored further in Chapter 6.

3.5.5 Summary

In this Chapter, I:

1. Differentiated iPSCs to NPCs. The NPCs' forebrain fate was confirmed by seeing the expected staining pattern using Pax6, Otx2 and Nestin antibodies. Staining with the FoxG1 antibody did not show the expected pattern (cytoplasmic instead of nuclear). This may be due to the antibody itself, or the differentiation of NPCs towards a neuronal fate. NPCs from all five iPSC lines were similarly proliferative, as confirmed by counting Ki67 positive proliferative cells at day 16.

2. Differentiated NPCs to neurons, and maintained them in culture until day 50 or day 80-100. The proportion of neurons in the cultures was measured by Western blotting, which found a decrease in the amount of βIII-tubulin from day 50 to day 80-100. This was not an expected result, and may have been caused by neuron death, or by an increase in the number of non-neural cells in the cultures over time. In support of the latter, the number of astrocytes in the cultures increased from day 50 to day 80-100. This was expected, since astrocytes emerge in maturing cultures from the last divisions of neural precursor cells.

3. Examined synaptic protein expression by Western blotting and immunostaining. There was an increase in the amount of synaptophysin (relative to the amount of βIII-tubulin) from day 50 to day 80-100. This was an expected result, since synaptogenesis has been observed to increase over time in iPSC-derived neuronal cultures.

4. Assessed tau isoform expression by Western blotting and immunostaining. The 0N3R tau isoform predominated in all cultures at day 50 and day 80-100, which was result given the age of the cultures, since 0N3R tau is the only isoform expressed in the fetal brain. 0N4R and 1N4R tau isoforms were observed, with higher frequency at day 80-100 as compared to day 50, suggesting that the cultures matured with respect to tau splicing over time. 0N4R tau was observed at higher abundances in day 50 N279K cultures as compared to day 50 control cultures, indicating the action of the N279K mutation.

In this Chapter, I found no significant difference between the control and MAPT mutant cells when measuring the proportion of proliferating NPCs, the amount of βIII-tubulin, the proportion of astrocytes, or the amount of synaptophysin. In the next Chapter, I will explore potential FTDP-17T-relevant differences between the control and MAPT mutant cultures.

Chapter 4

Pilot search for morphological and phenotypic changes in MAPT-mutant iPSC-derived neurons

4.1 Introduction

4.2 Aims

In Chapter 3, I established that the control and MAPT-mutant iPSC-derived cultures matured over time with respect to synapse formation, the growth of βIII-tubulin positive neurons, and astrocyte proliferation.

In the brains of individuals with FTDP-17T, and in the brains of some animal tauopathy models, tau is abnormally phosphorylated and forms insoluble aggregates. There is also neuronal loss, and, in the case of human FTDP-17T sufferers, αB-crystallin positive balloon neurons can be found. These changes do not occur in the brains of people without neurodegenerative diseases.

The aim of the work described in this Chapter is to investigate the presence of phenotypic and morphological FTDP-17T-relevant changes in iPSC-derived neurons with the MAPT mutations N279K and V337M, as compared to controls. This aim will be fulfilled by:

1. Examining the degree of tau phosphorylation at the AT8 epitope (Ser202 and Thr205). Iovino et al. previously detected increased AT8 staining in N279K neurons made from the same iPSCs but using a different method. I will establish whether this result can be repeated using neurons produced from a different differentiation method.

2. Looking for changes in tau's conformation using the antibody MC-1 (against hairpin-like conformation of tau) and the dye pFTAA (which detects AT100 positive, MC-1 positive tau). MC-1 positive, misfolded tau has not previously been detected in iPSC-derived neural cultures without the addition of exogenous tau.

3. Assessing the appearance of αB-crystallin positive balloon neuron-like cells. Swollen cells, which may be balloon neurons, were visible in some cultures at day 80-100. Immunostaining with αB-crystallin will help to determine the identity of these cells.

4. Comparing the appearance of sodium channels between MAPT mutant and control cultures. Iovino et al. found an increase in sodium currents in N279K neurons as compared to controls. Examining sodium channel expression may provide an explanation for this result.

5. Measuring differences in spontaneous cell death. A decrease in the amount of βIII-tubulin over time was observed in Chapter 3. This decrease may have been caused by neuronal death in the cultures, or increased numbers of non-neuronal cells. Measuring cell death will help to determine the relative contributions of these two explanations.

4.2.1 Tau phosphorylation and misfolding

Tau phosphorylation at the AT8 epitope

Tau is a phosphoprotein, with 85 potential phosphorylation sites, although not all of these are phosphorylated *in vivo* (reviewed by Hanger and Noble, 2011). Whilst tau in the normal adult human brain is phosphorylated, aberrant phosphorylation occurs in FTDP-17T and other tauopathies (Goedert et al., 1992; Spillantini et al., 1996b). Several antibodies have been produced which detect tau phosphorylated to a greater extent in tauopathies than in normal brains (Chapter 1). These include the AT8 antibody, whose epitope is the phosphorylated Ser202 and Thr205 residues. AT8 positive tau is found in the brains of people with tauopathies such as FTDP-17T, including those with the N279K or V337M mutations (Han et al., 2009; Miklossy et al., 2007; Spillantini et al., 1996b).

Tau phosphorylation is also developmentally regulated: phosphorylated 0N3R tau from fetal brains is normally hyperphosphorylated compared to tau in adult brains, and is stained by several phosphorylation-dependent antibodies including AT8 (Goedert et al., 1993), AT270, AT180, PHF-1 and 12E8 (Table 1.1 in Chapter 1). Some development-like tau phosphorylation might be expected in iPSC-derived neurons, since iPSC-derived neurons

more closely resemble those from a fetal than an adult brain according to gene expression studies, even after 59-180 days in culture (Handel et al., 2016; Patani et al., 2012).

Phosphorylation at the AT8 epitope has been investigated by several groups in MAPT-mutant iPSC-derived neural cultures. Increased phosphorylation at the AT8 epitope relative to control neurons has been reported in N279K (Ehrlich et al., 2015; Iovino et al., 2015), P301L (Iovino et al., 2015), V337M (Ehrlich et al., 2015) and A152T (Fong et al., 2013; Silva et al., 2016) MAPT-mutant iPSC-derived neurons, indicating that AT8 phosphorylation of MAPT-mutant neurons can be recapitulated in culture. The proportion of AT8 positive control neurons was variable between these studies: Iovino et al. (2015) and Ehrlich et al. (2015) found that 10-20% of control neurons were AT8-positive at day 55 and 40 respectively, whereas Fong et al. (2013) found that less than 1% of control neurons were AT8 positive at approximately day 60, and Silva et al. (2016) detected significantly lower AT8 levels in control neurons by Western blot after approximately 40 days, suggesting a variable degree of developmental-like AT8 phosphorylation.

Tau protein misfolding

A change of tau conformation can be detected by various antibodies including MC-1. The MC-1 epitope is tau amino acids 7–9 and 312–342, and immunoreactivity with this antibody is thought to represent the folding of a single tau molecule (Jicha et al., 1996). MC-1 immunoreactivity has been observed in several animal models of FTDP-17T (Decker et al., 2015; Maeda et al., 2016; Xu et al., 2014), and in the brains of people with tauopathies including AD (Bouras et al., 2003), where it is thought to represent a pathological form of tau prior to aggregation (Jeganathan et al., 2008).

In iPSC-derived neurons, MC-1 positive misfolded tau has not been reported to appear spontaneously in aging neurons, but it has been shown in neurons exposed to cues such as tau fibrils, tau overexpression, or a neurodegenerative environment. For example, Espuny-Camacho et al. (2017) observed MC-1 positive control and intron 10+16 iPSC-derived neurons after the neurons had been grafted into an AD mouse brain, and left for 180 days. Espuny-Camacho et al. did not observe MC-1 positive tau in control or intron 10+16 iPSC-derived neurons grafted into control mouse brains, indicating the importance of the environment for the conformation and phosphorylation state of both mutant and wild-type tau. MC-1 positive neurons have also been observed in control iPSC-derived neurons seven days after exposure to 2N4R wild-type tau oligomers (Usenovic et al., 2015), and in control iPSC-derived neurons overexpressing 2N4R P301L tau 14 days after exposure to fibrils made from a tau repeat domain (RD) fragment containing the P301L mutation (Medda et al., 2016).

Tau aggregation

Tau forms insoluble aggregates in FTDP-17T, AD and other tauopathies. However, this has only been recapitulated in iPSC-derived neuronal models to a limited extent.

Experiments in which iPSCs derived from FTDP-17T patients' tissues have been made into neurons rely on the endogenous mutation to produce a disease-relevant phenotype. So far, the spontaneous emergence of tau aggregates over time has been reported in a limited number of studies. For example, Imamura et al. (2016) detected punctate staining with anti-oligomeric TOC antibody in iNs with the intron 10+16 MAPT mutation, which increases the amount of 4R relative to 3R tau. TOC binds to mis-folded tau dimers, oligomers, or polymers (Ward et al., 2013), suggesting that tau dimers or larger oligomers form spontaneously in the presence of the intron 10+16 mutation. In addition, Iovino et al. (2015) detected AT100 positive tau in 150 day-old iPSC-derived neurons with the N279K MAPT mutation. The AT100 epitope requires a filament-like conformation (Zheng-Fischhofer et al., 1998), suggesting the spontaneous formation of tau filaments in the presence of the N279K mutation.

However, other studies have found no indication of tau aggregation. For example, Silva et al. (2016) found that A152T iPSC-derived neurons were thioflavin-S negative after 55 days in culture, and Verheyen et al. (2018) found that 100 day-old P301S iPSC-derived neurons did not have a detectable increase in alpha-LISA signal (alpha-LISA measures the distance between tau monomers and is used to quantify tau aggregation).

Tau aggregation has been induced in iPSC-derived models using non-physiological mutations, tau overexpression or tau fibrils. For example, Reilly et al. (2017) detected SDS-insoluble tau, as well as thioflavin-T and Gallyas silver positivity in control iPSC-derived neurons following overexpression of tau RD with the P301L and V337M mutations. Similarly, Usenovic et al. (2015) observed thioflavin-S positive cells, detected an increase in sarkosyl-insoluble tau, and saw an increase in alpha-LISA signal in control iPSC-derived neurons seven days after exposure to 2N4R wild-type tau oligomers. García-León et al. (2018) observed an increase in alpha-LISA signal in 70 day-old iPSC-derived neurons with the three tau mutations P301L, N279K and intron 10+16, after exposure to tau RD fibrils. Verheyen et al. (2018) found an increase in alpha-LISA signal in iPSC-derived neurons homozygous for the intron 10+16 and P301S mutations exposed to tau RD fibrils with the P301L mutation, but these aggregates are likely to be small, since they detected no sarkosyl-insoluble tau.

4.2.2 Sodium channels

Iovino et al. (2015) observed faster electrophysiological maturation in neurons made from iPSCs derived from patients with the MAPT mutations N279K and P301L. They also found an increase in peak sodium channel current in N279K and P301L neurons compared to controls, which coincided with regenerative, sodium channel blocker-sensitive action potential (AP) firing by MAPT-mutant neurons, but not by control neurons, which did not fire regenerative, sodium channel blocker-sensitive APs until a later timepoint. When control neurons did fire these APs, the peak sodium channel current reached similar levels to that initially observed in N279K and P301L neurons.

Earlier electrophysiological maturity has also been observed in iPSC-derived neurons with the all three of the N279K, P301L and intron 10+16 mutations (García-León et al., 2018), although sodium channel currents were not measured. In addition, neuronal hyper-excitability has been detected in hippocampal slice cultures from mice expressing human P301L mutant tau (Crimins et al., 2012).

Furthermore, increased electrophysiological activity may also be relevant to human tauopathies. People with Alzheimers disease have a 6- to 10-fold higher risk of seizures than age matched controls, and dementia severity correlates with seizure risk (reviewed by Pandis and Scarmeas, 2012). Likewise, people with FTD have a 6-fold higher risk of seizures (Beagle et al., 2017), and seizures have been reported in individuals with the FTDP-17T-relevant mutation P301S (Sperfeld et al., 1999).

Since I was using the same control and N279K iPSC lines as Iovino et al., I wanted to investigate differences in sodium channel expression between the iPSC-derived neurons, which might contribute to their early excitability.

Sodium channels are expressed in neurons throughout the cell soma, dendrites and axon at low levels, and are most densely clustered in the axon initial segment (AIS): a length of axon with a high density of sodium and potassium channels where APs are initiated (reviewed by Kole and Stuart,2012). AIS assembly is cell autonomous and dependent on Ankyrin G, which also anchors the AIS proteins in place (reviewed by Rasband, 2010). Four sodium channel subunits are expressed in the brain ($Na_v1.1$, 1.2, 1.3, and 1.6) and three of these ($Na_v1.1$, 1.2, and 1.6) are found in the AIS, with variations depending on cell type and region (Kole and Stuart, 2012; Lorincz and Nusser, 2008). The AIS in developing neurons and in adult unmyelinated neurons contains sodium channels made of $Na_v1.2$ subunits. In developing myelinated neurons levels of the $Na_v1.6$ subunit (the predominant subunit in the adult AIS) increases over time (Boiko et al., 2003).

The AIS has been detected using a pan-sodium channel antibody in iPSC-derived neurons. For example, Higurashi et al. (2013) observed AIS-like sodium channel clustering by 36 days after NPCs (analogous to approximately day 56 in my cultures) in a population of mostly GABAergic neurons. With this in mind, I set out to investigate sodium channel distribution in my iPSC-derived neurons.

4.2.3 Balloon neurons

Balloon neurons are enlarged neurons with eccentrically positioned nuclei which are found in the brains of people with various neurodegenerative diseases including the tauopathies PiD, CBD, PSP and FTDP-17T (López-González et al., 2014). Although balloon neurons are sparsely distributed in the brains of control subjects over 90 years old, they are not present in younger control brains (Iwaki et al., 1990) and their role in neurodegeneration is unclear. As well as being morphologically distinct from normal neurons, balloon neurons stain for a number of antibodies (summarised in Table 4.1) including αB-crystallin.

Table 4.1 **Proteins detected in balloon neurons found in the brains of people with neurodegenerative diseases.**

Protein detected in balloon neurons	Disease
αB-crystallin	AD [1,2], AGD [1], CBD [3,4,5], CJD [5,6,7] Diffuse Lewy body disease [6], FTDP-17T [4] MSA [6], PD [1], PSP [4,6,8,9], old age >90 years [6]
Total tau	Variable in PSP [9]
Phosphorylated tau: AT8	AGD, PD, AD [1]
Phosphorylated tau: PHF-1	AGD, PD, AD [1], variable in AD [2]
Phosphorylated neurofilament	AGD, PD, AD [1], CBD [3,5], PSP [9], CJD [5,7]
Non-phosphorylated neurofilament	AGD, PD, AD [1]
Ubiquitin	Variable in AGD, PD, AD [1], variable in PSP [9]
Synaptophysin	Weak in AGD, PD, AD [1], strong in CBD [3]
Nestin	CJD [7]

References: [1]: Tolnay and Probst (1998); [2]: Fujino et al. (2004); [3]: Matsumoto et al. (1996); [4]: Dabir et al. (2004); [5]: Sakurai et al. (2000); [6]: Iwaki et al. (1990); [7]: Mizuno et al. (2003); [8]: Togo and Dickson (2002); [9]: Mori et al. (1996).

Balloon neurons have been identified in at least four FTDP-17T cases with the N279K mutation (Arvanitakis et al., 2007; Delisle et al., 1999; Slowinski et al., 2007; Wren et al., 2015), and in at least four cases with the P301L mutation (Forrest et al., 2018; Reed, 2001). Of balloon neurons identified in brains of people with the N279K mutation, two cases were stained for αB-crystallin (Delisle et al., 1999; Wren et al., 2015); other balloon neurons were detected by their distinct appearance. In addition to balloon neurons, some astrocytes and oligodendrocytes in PSP, CBD and FTDP-17T (with the K317M, N279K or intron 10+16 MAPT mutation) have been found to be αB-crystallin positive (Dabir et al., 2004; López-González et al., 2014).

αB-crystallin is part of the small heat shock protein (HSP20) family: a group of proteins whose expression can be induced by heat shock or cell stress (Klemenz et al., 1991; Leak, 2014). αB-crystallin is expressed in the heart, muscle and brain of rats (Bhat and Nagineni, 1989), and in normal human subject brain tissue it is expressed in oligodendrocytes, a subset of astrocytes (approximately 5%), and at low levels in neurons (López-González et al., 2014).

αB-crystallin can act as a chaperone and prevent unfolded proteins aggregating (Jakob et al., 1993; also reviewed by Bloemendal et al., 2004). However, αB-crystallin does not renature denatured, misfolded or aggregation-prone proteins itself, instead it holds them until they are renatured by another chaperone, or broken down by proteolysis (Bloemendal et al., 2004; Horwitz, 2003).

The expression of αB-crystallin in so many neurodegenerative diseases and its role as a chaperone suggests αB-crystallin may be part of a protective mechanism. This is supported by findings in the brains of PD sufferers, in which most neurons expressing αB-crystallin do not contain Lewy bodies, and most neurons with Lewy bodies do not contain αB-crystallin (Braak et al., 2001), suggesting that neurons in which αB-crystallin expression is high are able to prevent α-synuclein aggregation. In addition, there is a positive correlation between tris-buffered saline soluble tau and αB-crystallin expression, and negative correlation between small insoluble tau species and αB-crystallin expression in the frontal and temporal lobes from brains of people with tauopathies, suggesting that αB-crystallin (and other small heat shock proteins) help prevent tau aggregation (Sahara et al., 2007). However, this evidence is only circumstantial.

Balloon neurons have been observed in an ex-vivo model of AD. Shahani et al. (2006) expressed wild-type human tau or pseudo-phosphorylated human tau (in which ten serine and threonine residues were replaced with glutamate to mimic phosphorylation) in cultured mouse hippocampal slices, and found some neurons with swollen balloon-like cell bodies in the presence of pseudo-phosphorylated tau. However, Shahani et al. did not further

characterise the balloon neurons, so it is unknown if they would stain for the same antibodies as balloon neurons in human tauopathy brains.

To my knowledge, balloon neurons have not been studied in iPSC-derived neural cultures to date, but αB-crystallin has been studied in iPSC-derived neurons used as a model of Alexander's disease, which is caused by GFAP mutations. Kondo et al. (2016) found small αB-crystallin puncta in some cell bodies, near areas of abnormal GFAP.

4.2.4 Cell death

The brains of people with FTDP-17T atrophy over time, and there is neuron loss (reviewed by Ghetti et al., 2015). Neuronal loss is also observed in the brains of several animal models of FTDP-17T. For example, mice expressing P301S mutant human tau show cortical neuron loss after 3 months of age (Hampton et al., 2010; Yang et al., 2016), and mice expressing N279K mutant human tau show substantia nigra neuron loss after 12 months of age (Dawson et al., 2007).

Cell death has also been observed in iPSC-derived neuronal cultures with MAPT mutations, and is often detected by an LDH (lactate dehydrogenase) assay. LDH is an enzyme present in the cytoplasm of most cells, which is released into the media when a cell dies. LDH is relatively stable in the media, and is a commonly used method for detecting cell death in culture (Chan et al., 2013).

Wren et al. (2015) found that N279K iPSC-derived NPCs spontaneously released more LDH into the media than control NPCs. However, since Wren et al. were unable to differentiate N279K NPCs into neurons, the high rate of cell death may have been due to a problem with the NPCs unrelated to the N279K mutation.

Other groups have observed cell death in iPSC-derived neuronal cultures following the addition of exogenous tau or toxic substances. For example, Ehrlich et al. (2015) found that N279K and V337M midbrain-like iPSC-derived neurons were more vulnerable to cell death following rotenone-induced complex I inhibition leading to oxidative stress, as measured by an increase in LDH release. In addition, Usenovic et al. (2015) observed increased cell death following the addition of recombinant 4R2N tau oligomers to control iPSC-derived neurons, using both a live cell dye and an LDH assay.

As mentioned in Chapter 3, I observed more condensed pyknotic nuclei in day 80-100 neural cultures relative to day 50 cultures, with no clear differences between MAPT-mutant and control cultures, as determined by a superficial observation. However, since I observed pyknotic nuclei after several washing steps during staining, these nuclei must have remained

adhered to the coverslips despite washing, so it is likely that pyknotic nuclei were not washed away during media changes, and instead accumulated over time. To get some information on spontaneous cell death in culture, I examined cell death at several points during differentiation, using an LDH assay.

4.3 Materials and Methods

4.3.1 iPSC culture and differentiation

iPSCs were thawed, cultured, prepared for karyotyping and differentiated to neurons as described in Chapter 2, and cultured as described in Section 2.3.

4.3.2 Immunostaining, Western blotting and statistical analysis

Immunostaining and imaging was performed as described in Section 2.5.1, Western blotting was performed as described in Section 2.6, and statistical analysis was performed as described in Section 2.7. AT8, MC-1, and αB-crystallin staining was quantified using ImageJ.

AT8

Cultures were co-stained with the AT8 and βIII-tubulin antibodies. I counted the number of neurons which were AT8 positive by hand, and recorded this as a proportion of the total number of βIII-tubulin positive neurons. To facilitate counting of AT8 positive cells, images were converted to binary images (Image→Adjust→Threshold in ImageJ) with the Threshold value adjusted such that background staining was eliminated. Cells were counted manually with the Plugins→Analyse→Cell Counter tool in ImageJ. Neurons were counted in two, or more commonly three, different wells from the same differentiation round (as technical replicates). The total number of neurons counted in two or three technical replicates was at least 100, and frequently 200-300. Neurons were counted in a total of three independent differentiation rounds.

To account for the presence of AT8 positive processes as well as AT8 positive cell bodies, I measured the area of each image that was AT8 positive using ImageJ, and normalised to the number of βIII-tubulin positive neurons in the same image.

MC-1

Cultures were co-stained with the MC-1 antibody and an antibody (tau DAKO) which detects all six tau isoforms independent of their phosphorylation state.

αB-crystallin

Cultures were co-stained with the αB-crystallin and βIII-tubulin antibodies. I counted the number of neurons which were αB-crystallin positive, and recorded this as a proportion of the total number of βIII-tubulin positive neurons.

4.3.3 LDH assay

To assess spontaneous cell death at days 30, 50, 70 and 100, NPCs were plated at the same density in a 96-well plate, as described in Section 2.3. Cells were maintained with 300µl per well of NDM (Section 2.2.1), which was replaced every other day. On day 28, 48, 68 or 98, media was removed from all wells and replaced with 300µl per well of NDM, which was collected after 2 days (on day 30, 50, 70, and 100) and stored immediately at -80°C.

LDH in the collected media was measured using a Bioluminescent LDH assay (Promega). Three media dilutions were tested (1:10, 1:20, 1:100), of which 1:20 gave the highest signal to background ratio. Media samples were diluted 1:20 with DPBS, and 20µl of each sample was added to a white 96-well plate (Costar), along with media alone (negative control) and media from cells lysed with 0.5% Triton X-100 in NDM (positive control). Reductase substrate was diluted 1:200 in LDH assay buffer and 20µl of this mixture was added to each sample. Samples were incubated at room temperature and protected from light for 30 minutes, then luminescence was read on an Infinite M200 Pro Tecan plate reader (integration time: 1 second, settle time: 150ms). One experiment was performed, using media from three differentiations of each cell line at four time points each. Two technical replicates were performed and averaged.

4.4 Results

4.4.1 Tau phosphorylation at Ser202 and Thr205; the AT8 epitope

I determined the proportion of AT8 positive neurons in N279K and V337M mutant cultures as compared to the controls. Although AT8 phosphorylation in N279K neurons derived from the same iPSCs has been investigated by Iovino et al. (2015), I used a different method

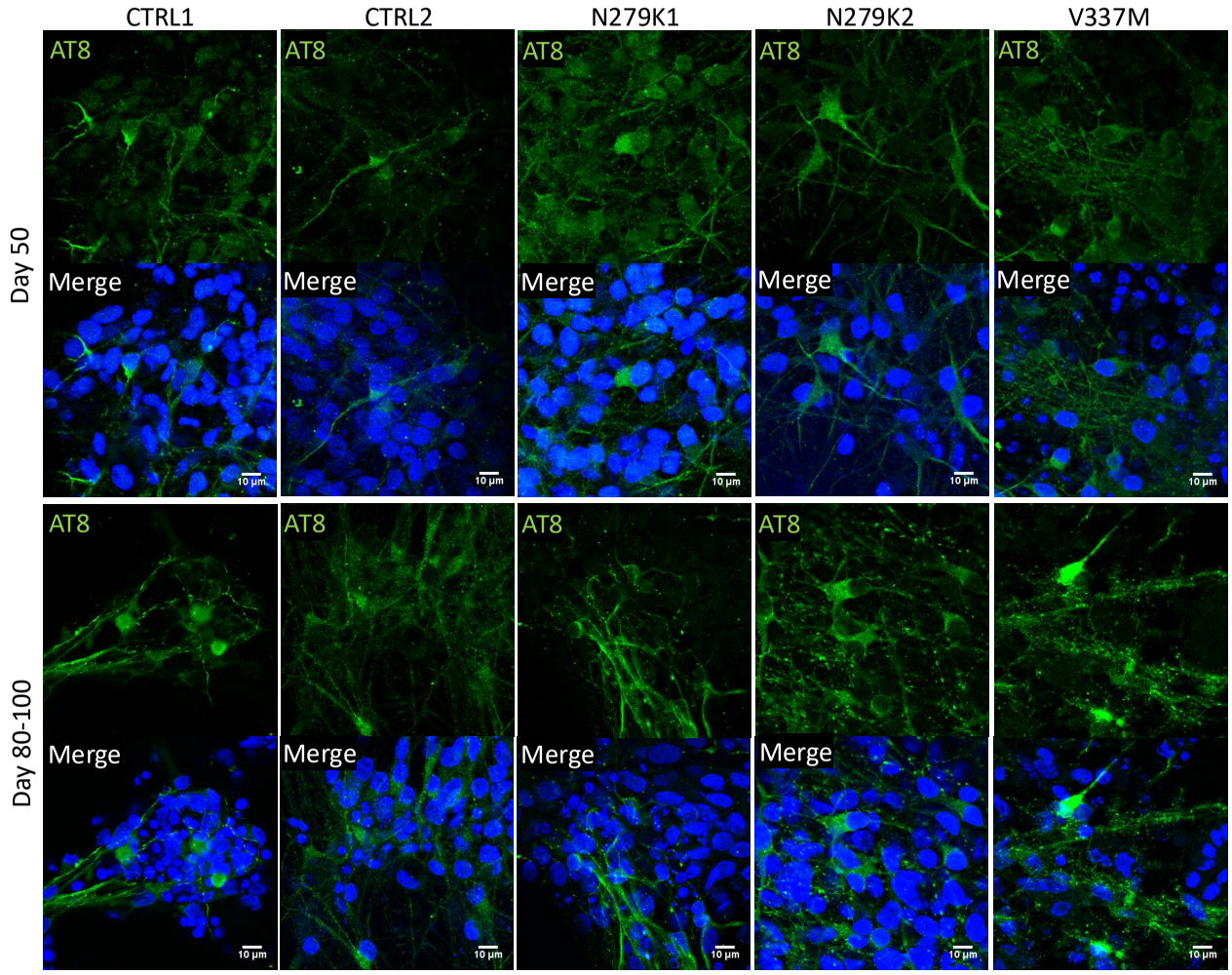

Fig. 4.1 **Tau phosphorylated at Ser202 and Thr205 (detected with the AT8 antibody) is present in some neurons at day 50 and day 80-100.** AT8 positive tau is visible in some cell bodies and processes in cultures from the CTRL1, CTRL2, N279K1, N279K2, and V337M iPSC lines at day 50 and 80-100. Quantification of these and other images showed an increase in the proportion of AT8 positive neurons over time. This was not an expected result, but some AT8 positive neurons were expected in all cultures, since AT8 is expressed in neurons in the fetal human brain, as well as in adults with FTDP-17T, but not in control adult brains. Scale bar = 10µm.

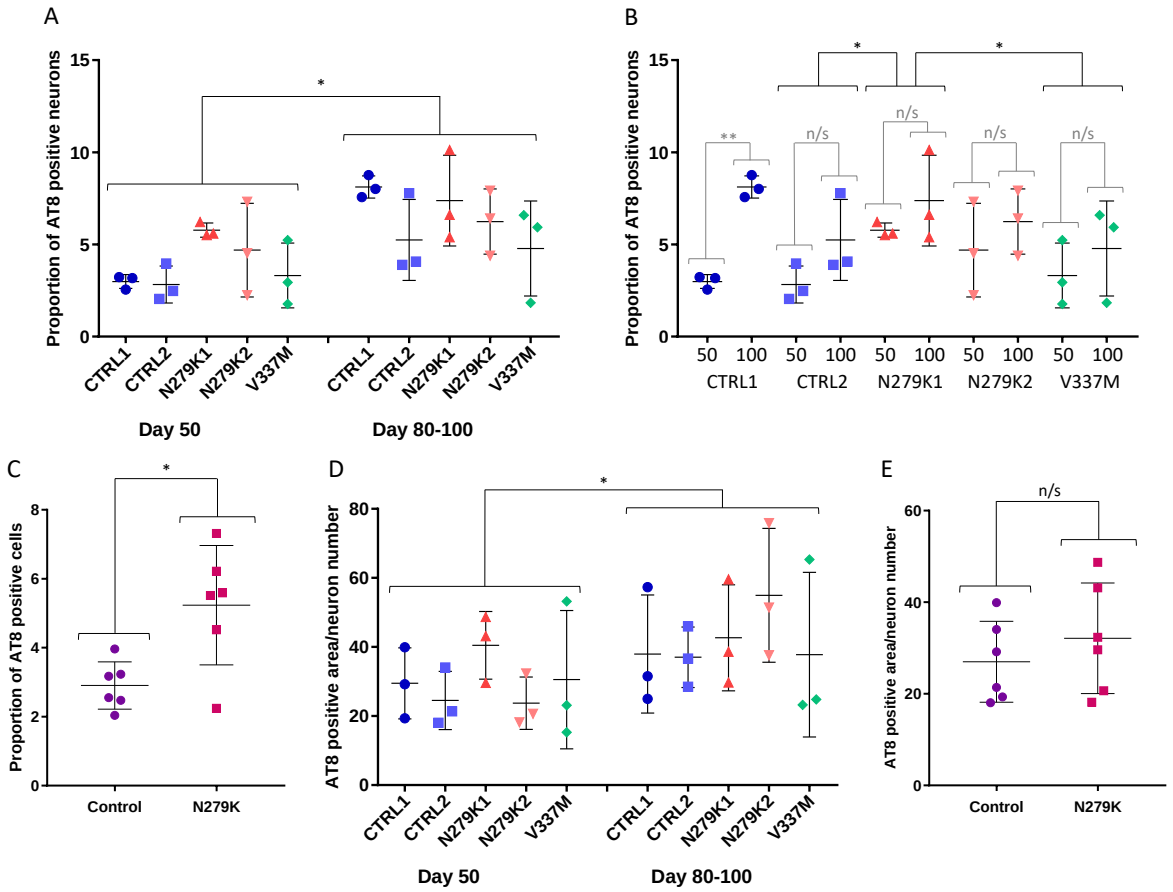

Fig. 4.2 **The proportion of AT8 positive neurons is significantly higher at day 80-100 than at day 50, and there is a significantly higher proportion of AT8 positive N279K neurons as compared to control neurons at day 50. A)** The proportion of AT8 positive neurons was counted in CTRL1, CTRL2, N279K1, N279K2 and V337M cultures at day 50 and 80-100. Cultures produced from three independent differentiations were assessed. Each point represents the mean measurement from one independent differentiation with at least two, and usually three technical replicates. At least 100 cells from each cell line were counted per differentiation. Bars show mean±SD. Significance bars show the results of a two-way ANOVA: there was an increase in the proportion of AT8 positive neurons over time (* indicates $p<0.05$). **B)** The data presented in **A)** re-organised by iPSC line. Significance bars in black show the results of a post-hoc test following a two-way ANOVA: there was a higher proportion of AT8 positive neurons in N279K1 cultures than in CTRL2 or V337M cultures (* indicates $p<0.05$). Significance bars in grey show the results of paired t-tests comparing the difference in the proportion of AT8 positive cells in cultures derived from each iPSC line at day 50 and day 80-100. There was a significantly higher proportion of AT8 positive neurons in day 80-100 CTRL1 cultures as compared to day 50 CTRL1 cultures (** indicates $p<0.01$). Comparisons between day 50 and day 80-100 cultures were not significant for other iPSC lines. **C)** The proportion of AT8 positive neurons in cultures from both CTRL1 and CTRL2 iPSC lines (control) and in both N279K1 and N279K2 cultures (N279K) at day 50. Significance bars show the results of Student's t-test. There was a higher proportion of AT8 positive N279K neurons than control neurons at day 50 (* indicates $p<0.05$). **D)** The area covered by AT8 positive cell bodies and processes was quantified in cultures derived from each iPSC line at day 50 and day 80-100. Significance bars show the results of a two-way ANOVA. There was an increase in the AT8 positive area over time (* indicates $p<0.05$). **E)** The area covered by AT8 positive cell bodies and processes in cultures from both CTRL1 and CTRL2 iPSC lines (control) and in both N279K1 and N279K2 cultures (N279K) at day 50. Significance bars show the results of Student's t-test. There was no significant difference in the AT8 positive area between N279K and control cultures at day 50.

for neuronal differentiation (summarised in Table 3.1, Chapter 3) and wanted to see if comparable results were obtained. AT8 phosphorylation in iPSC-derived neurons with the V337M and N279K mutations has also been previously investigated by Ehrlich et al. (2015), who differentiated N279K and V337M iPSCs to GABAergic and dopaminergic neurons to make midbrain-like cultures. However, my iPSC-derived neurons have a forebrain fate (Chambers et al., 2009; Kirkeby et al., 2012), since neurons in the frontal and temporal lobes are most affected by FTDP-17T (reviewed by Ghetti et al., 2015).

To determine the proportion of AT8 positive neurons, I stained for AT8 at day 50 and day 80-100 (Figure 4.1). At day 50, AT8 positive cell bodies and some processes were visible in both control and MAPT-mutant cultures; at day 80-100, more extensive AT8 staining was visible in both cell bodies and processes in all cultures.

I quantified this data in two ways: by counting the proportion of AT8 positive neuronal cell bodies, presuming that this would also account for the AT8 positive processes (Figure 4.2A), and by quantifying the AT8 positive area, to account for both AT8 positive cell bodies and AT8 positive processes (Figure 4.2D).

When counting the number of AT8 positive neuronal cell bodies, a two-way ANOVA found a significant main effect of iPSC line ($F(4,10)=7.662$, $p=0.0043$) meaning that the number of AT8 positive neurons was significantly different between cultures derived from different iPSC lines. This difference was assessed with a post-hoc multiple comparisons test, with a Bonferroni correction, in which the proportion of AT8 positive neurons in cultures derived from each iPSC line was compared. The post-hoc test found significant differences in the proportion of AT8 positive neurons between CTRL2 and N279K1 ($p=0.0106$), and between N279K1 and V337M ($p=0.0110$); in Figure 4.2, it is clear that the significant difference is an increase in AT8 positive neurons in N279K1 neurons as compared to CTRL2 and V337M neurons. This is shown in Figure 4.2B with black bars.

The two-way ANOVA also found a significant main effect of time $F(1,10)=8.283$, $p=0.0164$), meaning that the proportion of AT8 positive neurons was significantly increased between day 50 and day 80-100 (Figure 4.2A and Figure 4.1). The two-way ANOVA found no significant interaction effect between time and iPSC line ($F(4,10)=0.6965$, $p=0.6114$), meaning that time had the same effect on the number of AT8 positive cells derived from all five iPSC lines.

To compare my results directly to those of Iovino et al. (2015), I grouped day 50 CTRL1 and CTRL2 results as control, and day 50 N279K1 and N279K2 results as N279K, then performed the same analysis: Student's t-test. This revealed a significant difference in the

proportion of AT8 positive neurons between N279K and control cultures at day 50 (p=0.0120, Figure 4.2C).

In addition, I used t-tests to compare the change in the proportion of AT8 positive neurons in cultures from each iPSC line at day 50 and day 80-100. The t-tests showed no significant difference between the proportion of AT8 positive neurons at day 50 and day 80-100 in neurons from the CTRL2, N279K1, N279K2 and V337M iPSC lines. There was a significant difference (paired t(2)=12.96, p=0.0059) in the proportion of AT8 positive neurons derived from the CTRL1 iPSC line between day 50 and day 80-100. These results are shown in Figure 4.2B with orange bars.

AT8 staining was present in both cell bodies and processes (Figure 4.1). Since counting the number of AT8 positive cell bodies may not have captured differences in the number of AT8 positive processes, I quantified the AT8 positive area of each image, and normalised to the number of neurons (Figure 4.2D). A two-way ANOVA found a main effect of time (F(1,10)=5.459, p=0.0416), meaning that the AT8 positive area per neuronal cell body was significantly increased between day 50 and day 80-100. The two-way ANOVA also found no main effect of iPSC line (F(4,10)=0.4735, p=0.7546; the AT8 positive area per neuronal cell body was not significantly different between cultures derived from different iPSC lines), and no interaction effect (F(4,10)=0.9025, p=0.4982; time had the same effect on the AT8 positive area per neuronal cell body in cultures derived from all five iPSC lines).

I also represented these results in the same was as those in Figure 4.2C), by grouping day 50 CTRL1 and CTRL2 results as control, and day 50 N279K1 and N279K2 results as N279K, then performing Student's t-test. There was no significant difference in the area covered by AT8 positive neurons and processes between N279K and control cultures at day 50 (p=0.4219, Figure 4.2E).

In conclusion, there was an increase in the proportion of AT8 positive neurons over time, when AT8 phosphorylation in all cultures at day 50 was compared to AT8 phosphorylation in all cultures at day 80-100. There was also an increase in the proportion of AT8 positive neurons in both N279K cultures at day 50, as compared to both control cultures at day 50. When comparing cultures derived from different iPSC lines at day 50, there was an increase in the proportion of AT8 positive neurons in N279K1 cultures, as compared to CTRL2 and V337M cultures.

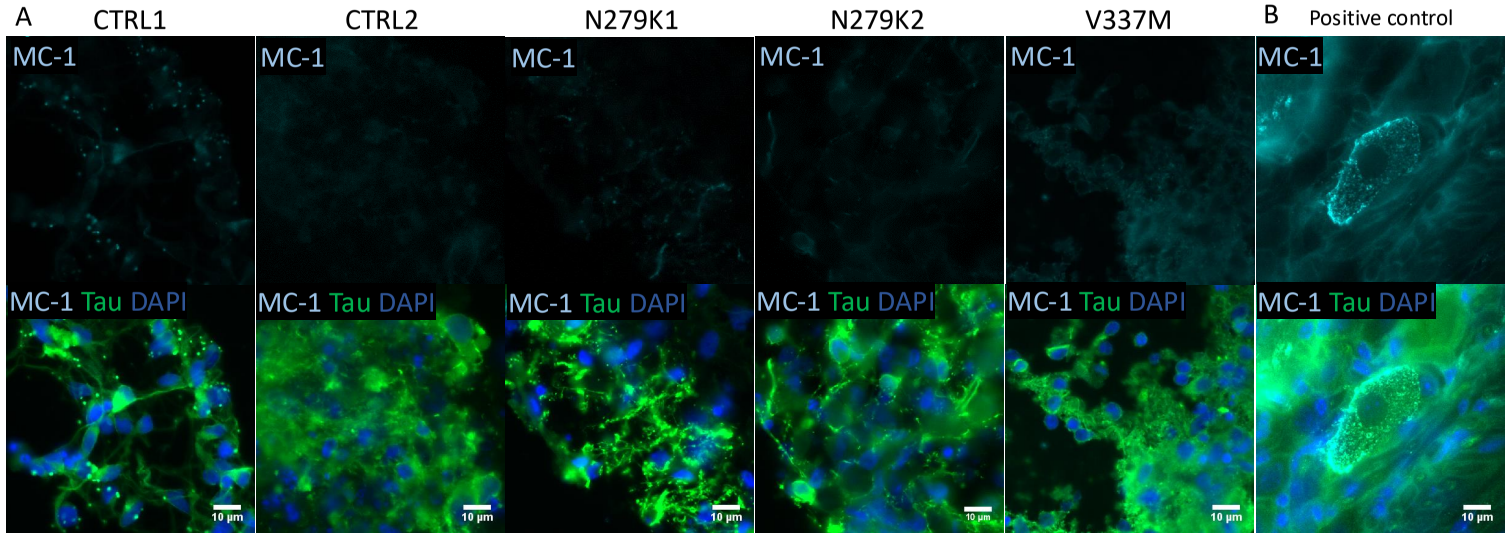

Fig. 4.3 **MC-1 positive misfolded tau is not detectable in day 80-100 neural cultures. A)** Day 80-100 neural cultures derived from the CTRL1, CTRL2, N279K1, N279K2 and V337M iPSC lines were immunostained with the MC-1 antibody and an antibody that detects all tau isoforms (Tau DAKO, labelled as tau). The expected staining pattern (in cell bodies and neuronal processes) was observed with the tau DAKO antibody. Very low levels of MC-1 staining were detected in cultures derived from all iPSC lines, indicating that misfolded tau was not present. This was an expected result, since only small differences in tau phosphorylation at AT8 were detected between control and MAPT-mutant neurons. Scale bar=10 µm. **B)** The positive control, immunostained with the MC-1 antibody and a total tau antibody (tau DAKO), is neuronal cell bodies in a dorsal root ganglion from a 5 month-old P301S mouse. MC-1 positive tau in the positive control shows the expected staining pattern, and indicates that the staining method and antibody were sufficient to detect misfolded tau.

4.4.2 Conformational changes in tau

To see if misfolded tau was detectable in day 80-100 cultures, I used the MC-1 antibody, whose epitope (tau amino acids 7–9 and 312–342; Jicha et al. (1996)) detects misfolded tau prior to aggregation. To ensure that MC-1 immunoreactivity identified was not background staining, I co-stained with an antibody that detects all six tau isoforms (Tau DAKO) and used secondary antibodies fluorescent at 488nm (Tau DAKO) and 647nm (MC-1). Images were then taken in at 488, 568, and 647nm, and the absence of fluorescence at 568nm confirmed that there was no bleed-through between the two stainings.

MC1 staining was bright in the positive control (adult P301S mouse dRG, Figure 4.3B), indicating that the staining was sufficient to detect misfolded tau. However, very little MC-1 immunoreactivity was visible in cultures derived from both control and MAPT-mutant iPSC lines (Figure 4.3A), suggesting that tau was not misfolded in day 80-100 iPSC-derived neurons.

This result was expected, since there was little difference in the proportion of AT8 positive cells between controls and N279K or V337M cultures, indicating that FTDP-17T-relevant abnormal phosphorylation was not present in the N279K or V337M cultures. Abnormal phosphorylation is thought to precede tau misfolding and aggregation (Goedert and Spillantini, 2001), so MC-1 positive, misfolded tau would only be expected after abnormal phosphorylation had been observed.

4.4.3 Preliminary results: probing for filamentous tau

To see if filamentous tau was present in the oldest neuronal cultures (at day 100), I used the dye pentameric formyl thiophene acetic acid (pFTAA). pFTAA has been shown by Brelstaff et al. (2015) to co-label AT8 positive neurons in AD patient's brains, and as well as AT100- or MC1-positive dorsal root ganglion neurons from mice expressing P301S mutant tau.

I co-stained day 100 cultures with an antibody that detects all tau isoforms (tau DAKO, referred to as total tau), to ensure that pFTAA staining detected was also tau positive. As a positive control, I used a cryosectioned dorsal root ganglion from a 5 month-old P301S mouse.

Visualising pFTAA staining required strong illumination, and this induced a high level of background fluorescence, which can be seen in the negative control of Figure 4.4. The high background fluorescence makes it difficult to attribute fluorescence in the samples to pFTAA staining, although some areas of higher fluorescence are visible in the V337M and CTRL2 cultures. The areas of higher intensity staining do not overlap with total tau staining in the

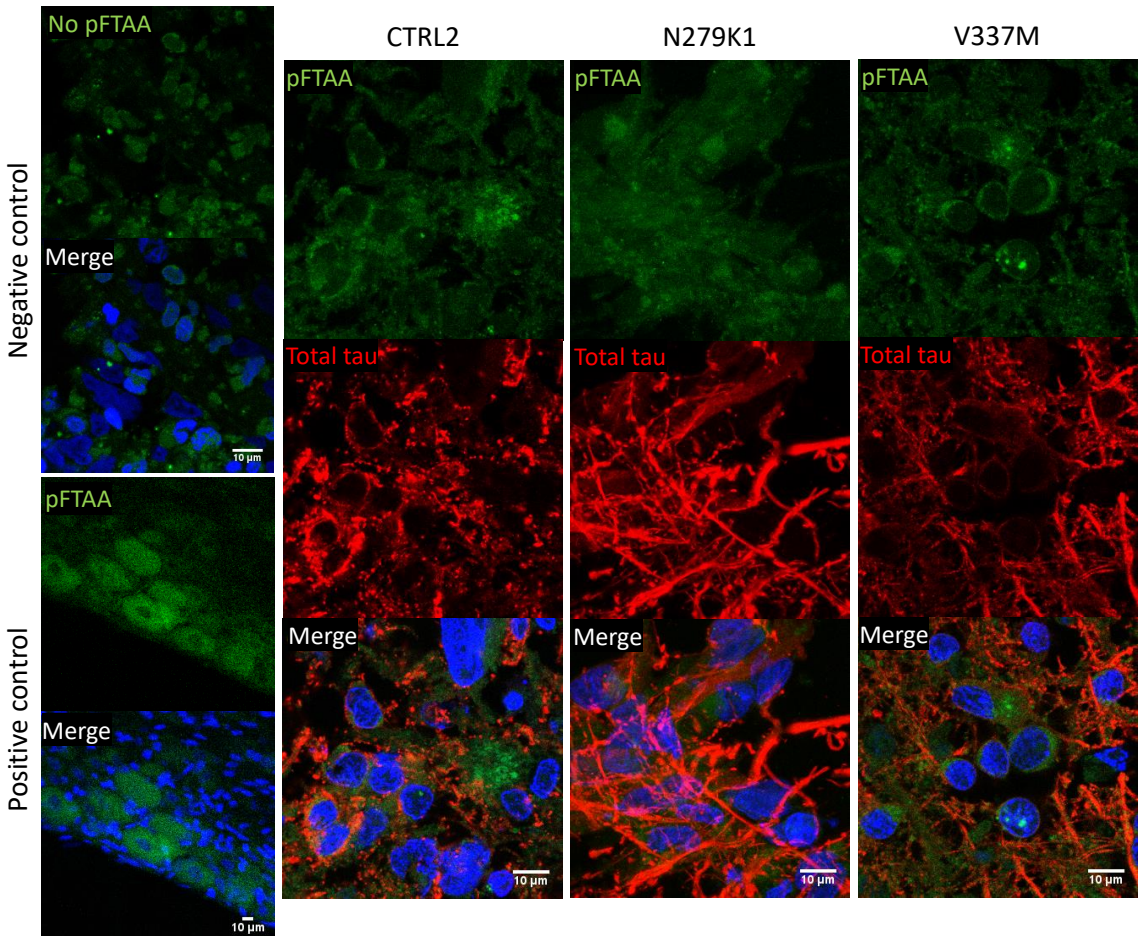

Fig. 4.4 **Filamentous tau was not detected in day 100 neural cultures using the dye pFTAA.** Day 100 neural cultures derived from the CTRL2, N279K1 and V337M iPSC lines were stained with the dye pFTAA (which detects filamentous tau) and the tau DAKO antibody (which detects all six tau isoforms). The expected staining pattern was observed with the tau DAKO antibody, but pFTAA staining in CTRL2, N279K and V337M cultures did not overlap with tau staining, suggesting that the pFTAA staining visible was not specific for tau. Dorsal root ganglion cells from a 5 month old P301S mouse were used as a positive control, and the expected staining pattern with pFTAA (brightly stained cell bodies) was seen under an epifluorescent microscope. However, this bright staining was not well detected in the confocal microscope images shown, even when exposure was high. High exposure led to autofluorescence in the green channel, as shown in the no-pFTAA control. Scale bar = 10 µm.

merged images, indicating that pFTAA is not bound to tau. In the areas that are total tau positive in the merged images, the high level of background fluorescence makes it difficult to distinguish between negative and potentially positive staining.

This staining was only performed on cultures from one differentiation round, and cultures derived from the CTRL1 and N279K2 iPSC lines were washed off the coverslips during staining. This result is therefore preliminary, and suggests that pFTAA-positive tau was not present in cultures at day 100. Given that only small differences in the proportion of neurons containing AT8 positive tau were detected between control and MAPT mutant cultures, and given that no MC-1 positive tau was detected, the lack of fibrillar tau detected with pFTAA was an expected result.

4.4.4 Balloon neurons

Some swollen cells were visible in day 80-100 cultures from all cell lines, so I stained for αB-crystallin to see if these neurons were balloon neuron-like. αB-crystallin positive neurons (which also stained for the neuronal markers βIII-tubulin or tau) were observed mostly in N279K1, N279K2 and V337M cultures (Figure 4.5). αB-crystallin was visible in cell bodies and occasionally in processes. Morphologically, αB-crystallin positive cells resembled αB-crystallin positive balloon neurons in human brains from FTDP-17T patients with the N279K mutation, as shown in Figure 4.8.

αB-crystallin-positive neurons were also positive for 4R tau (Figure 4.7A, n=1). Co-staining for αB-crystallin and AT8 showed that the majority of αB-crystallin positive neurons were AT8 negative, with a few being AT8 positive (Figure 4.7B, n=1). However, these two stainings were only performed on neurons from one differentiation round.

The proportion of αB-crystallin positive neurons in cultures from each of three independent differentiations is quantified in Figure 4.6. A relatively low proportion of αB-crystallin positive neurons were detected in the second differentiation round so, Figure 4.6B shows the data in Figure 4.6A normalised to the values for N279K2, which were set to one. A low proportion of αB-crystallin positive neurons detected in the second differentiation round in part because the cultures detached from their cover slips during staining, and were rescued on glass slides. This lead to lower-quality staining, and low numbers of neurons stained. The staining could not be repeated due to a lack of remaining cultures. A one-way ANOVA revealed no significant difference between the mean proportion of αB-crystallin positive neurons derived from the different iPSC lines.

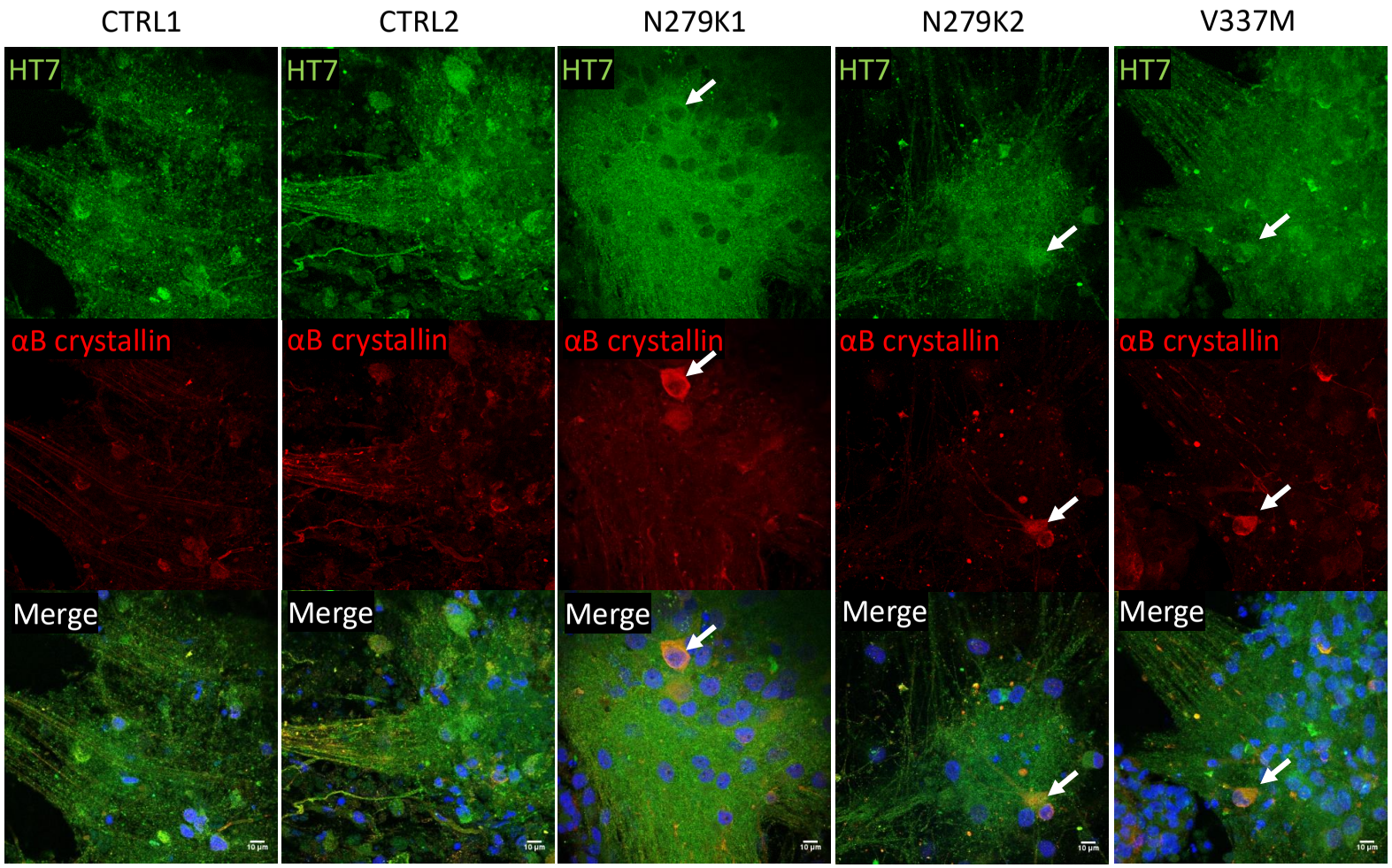

Fig. 4.5 **αB-crystallin positive neurons, resembling balloon neurons, were detected at day 80-100.** Representative images of CTRL1, CTRL2, N279K1, N279K2, and V337M cultures at day 80-100, stained for αB-crystallin and total tau (HT7). A small number of cells (indicated with white arrows) were positive for αB-crystallin and HT7, indicating that they are neurons, and may be balloon neurons. Scale bar = 10µm.

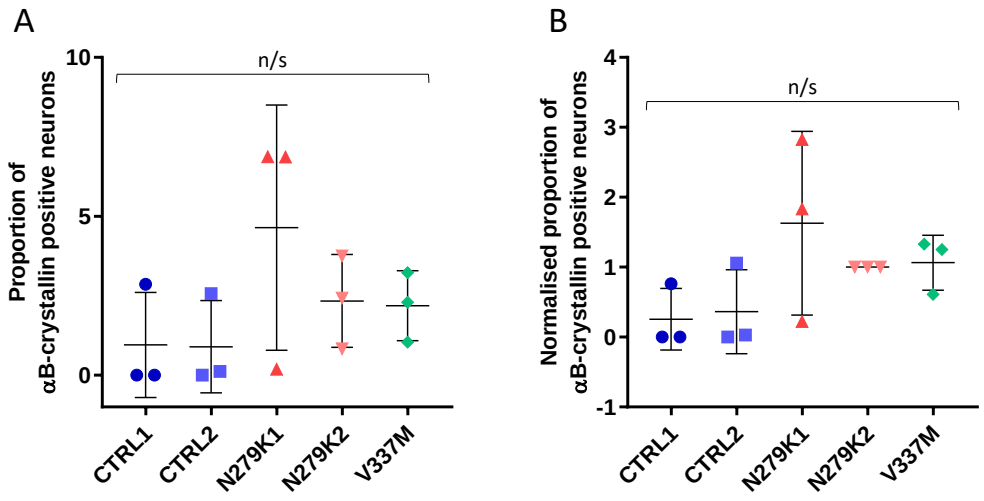

Fig. 4.6 **The number of αB-crystallin positive balloon neuron-like neurons was not significantly different between control and MAPT mutant cultures at day 80-100. A)** The proportion of αB-crystallin positive neurons in CTRL1, CTRL2, N279K1, N279K2 and V337M cultures at day 80-100 was counted by hand in cultures from three independent differentiations. There was no sigificant difference in the proportion of αB-crystallin positive neurons between the cell lines, as determined by a one-way ANOVA. **B)** The same data as shown in **A)** is normalised to the values for N279K2 cultures, which were set to one. In both **A)** and **B)**, bars show mean$\pm$SD and points show the mean proportion of αB-crystallin positive neurons in cultures from each of three differentiations.

In conclusion, some αB-crystallin positive neurons were present in day 80-100 neural cultures, although there was no significant difference in the number of αB-crystallin positive neurons between cultures derived from control and MAPT-mutant iPSC lines.

4.4.5 Markers of the AIS

To investigate differences in sodium channel expression between iPSC-derived MAPT mutant and control neurons, I immunostained day 50 and 80-100 neurons using a pan-sodium channel antibody (PanNa), raised against an epitope in the intracellular III-IV loop which is conserved between sodium channels. Staining in differentiation rounds one and two, at day 50 and day 80-100 gave diffuse, faint staining of the cell soma and processes. This staining may be specific for sodium channels even though an AIS was not detected, since sodium channels are expressed throughout the cell body, dendrites and axon (Kole and Stuart, 2012).

Potential AIS-like staining was visible in day 50 N279K1 neurons from the third differentiation round (Figure 4.9A), although neurons from the same differentiation round at day 80-100 and day 16 did not show the same pattern of staining. The average length of

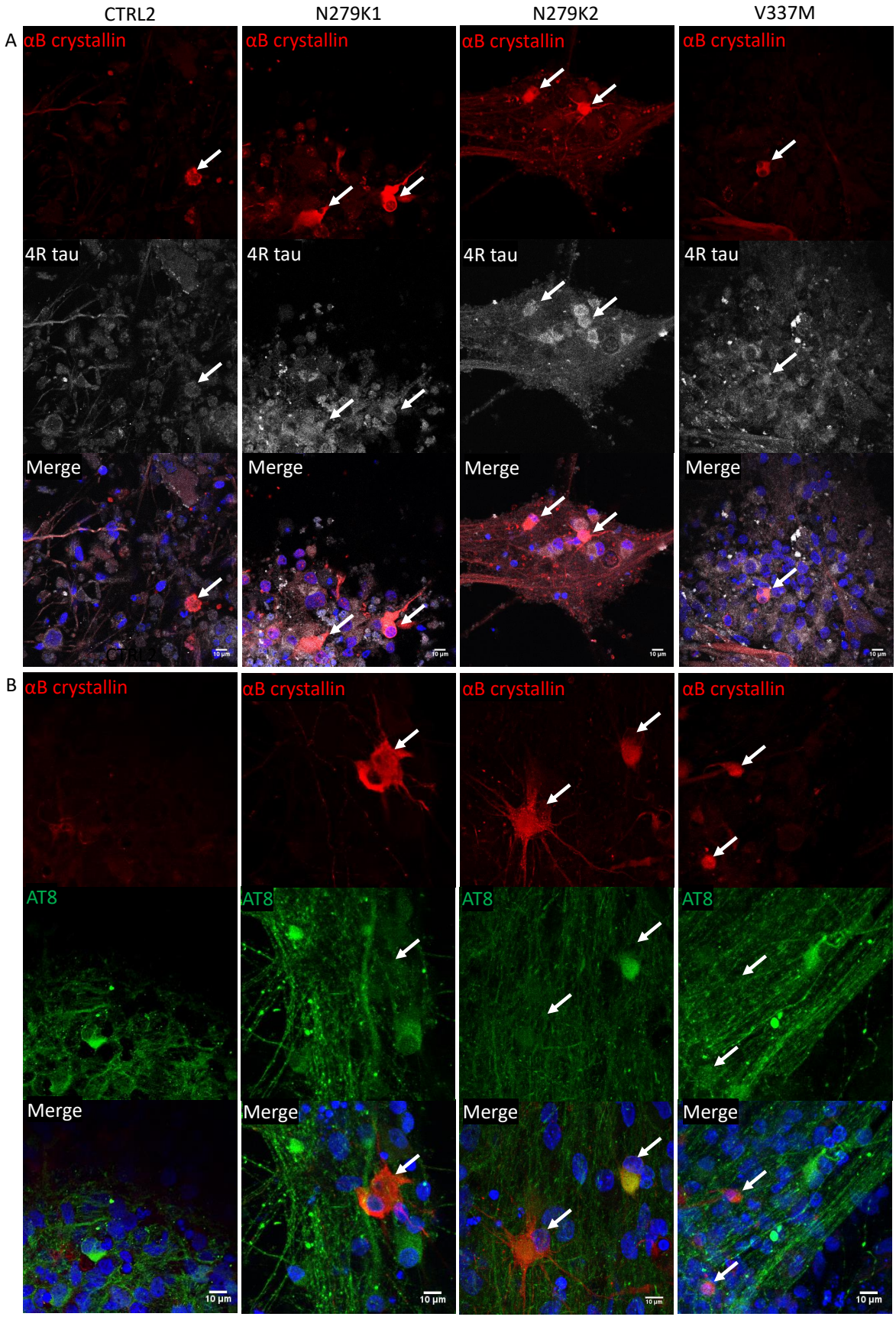

Fig. 4.7 **αB-crystallin positive balloon neuron-like neurons in cultures at day 80-100 were 4R tau positive, but most were not AT8 positive.** Representative images of αB-crystallin positive neurons from one differentiation of CTRL2, N279K1, N279K2, and V337M cultures at day 80-100, co-stained for **A)** 4R tau, and **B)** tau phosphorylated at Ser202 and Thr205 (detected with AT8). Scale bar = 10µm.

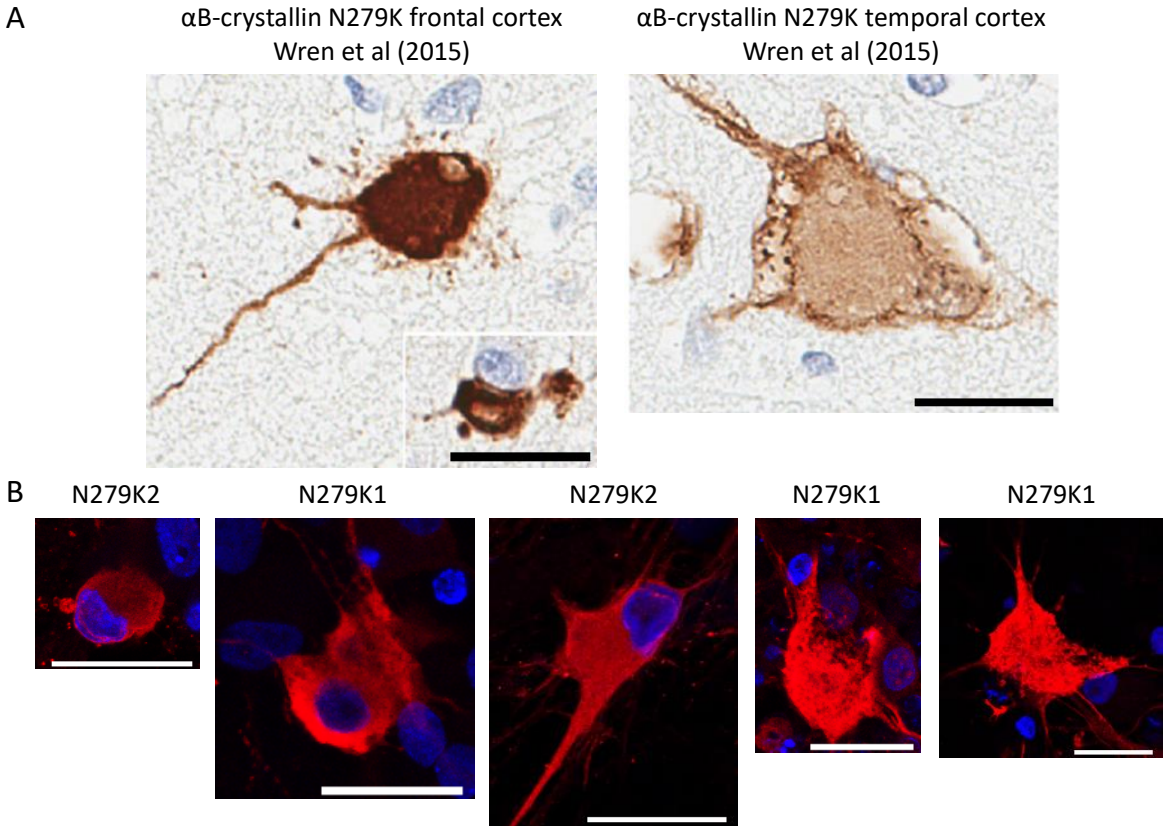

Fig. 4.8 **αB-crystallin positive balloon-neuron-like neurons at day 80-100 compared to αB-crystallin positive balloon neurons in human FTDP-17T brain. A)** shows αB-crystallin positive balloon neurons in the frontal and temporal cortex of two human FTDP-17T patients with the N279K mutation, taken from Wren et al. (2015) and Delisle et al. (1999). Scale bars = 10µm. No scale bars were provided in the Delisle et al. paper. **B)** shows representative αB-crystallin positive balloon-neuron-like neurons from N279K1 and N279K2 cultures at day 80-100. Scale bar = 10µm, and all images are resized such that the scale bars in the images are the same length.

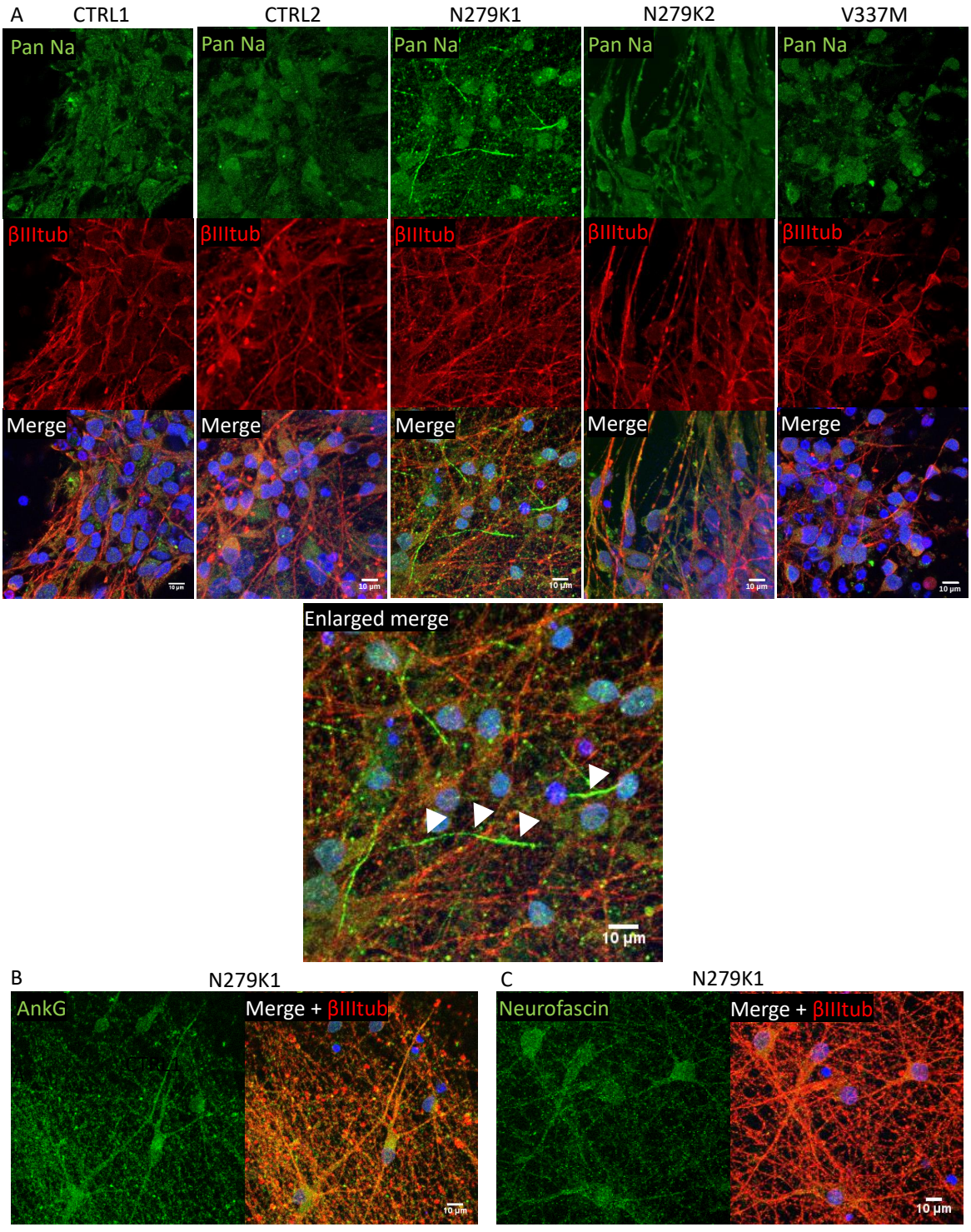

Fig. 4.9 **Sodium channel staining in day 50 cultures was not specific for the AIS. A)** Diffuse sodium channel staining (Pan Na) was visible throughout the cell soma and processes in cultures from the CTRL1, CTRL2, N279K1, N279K2, and V337M iPSC lines from three independent differentiation rounds at day 50. Potential AIS-like staining was visible in an N279K1 culture at day 50 (marked with white arrowheads in the enlarged merge). To confirm the presence of an AIS, the same N279K1 cultures were immunostained with **B)** ankyrin G or **C)** neurofascin. Ankyrin G and neurofascin antibodies gave diffuse staining, indicating that an AIS was not present. Scale bar = 10µm.

the AIS-like staining was 16.1±2.2µm, which is within the range of reported AIS lengths: 10-60µm (Kole and Stuart, 2012; Rasband, 2010).

To confirm the sodium channel staining was AIS staining, I stained the same cultures for ankyrin G, which detects a scaffold protein restricted to the AIS that is vital for AIS integrity (Rasband, 2010), and for βIII-tubulin, but no AIS-like staining was detected (Figure 4.9B). I also stained the same cultures for neurofascin, which detects the cell adhesion molecule neurofascin that binds to Ankyrin G at the AIS (Rasband, 2010), and co-stained for βIII-tubulin and MAP2, which is present in dendrites but not axons (Kosik and Finch, 1987). However, no AIS-like staining was detected: all neurofascin staining overlapped with dendritic MAP2 staining. Both of these stainings were done once.

Together, the results of staining with pan-sodium channel, ankyrin G and neurofascin antibodies suggests that no AIS was detected.

4.4.6 Cell death

To measure spontaneous cell death in iPSC-derived neural cultures, I collected media at day 30, 50, 70, and 100 from each of three differentiations. Since media were changed every two days, the data represents spontaneous LDH release occurring over two days in culture. In order to maintain the neurons in culture until day 100, NPCs were plated at the same low density in 96-well plates and the same amount of media was added prior to every media collection. Media was frozen at -20^{o}C following collection and analysed together (in two technical replicates) when all the media had been collected using a chemiluminescent LDH kit.

The data are presented in Figure 4.10. LDH release was normalised to the value at day 70 in CTRL2 cultures, which was set to one for each differentiation. This approach to normalising LDH release has also been used by Ehrlich et al. (2015) and Usenovic et al. (2015) in their experiments with iPSC-derived neurons. A positive control was made by lysing a culture with 0.5% Triton X-100 in NDM, and used alongside the other samples to show maximal LDH release.

In Figure 4.10A, the change in LDH release over time is shown for each iPSC line, and a positive control indicates maximum LDH release. In one day 100 culture derived from the N279K1 line there is a high level of LDH in the media which is very similar to that of the positive control. High values were recorded in two technical replicates, indicating that the values are not measurement errors, and suggesting that they were specific to high LDH

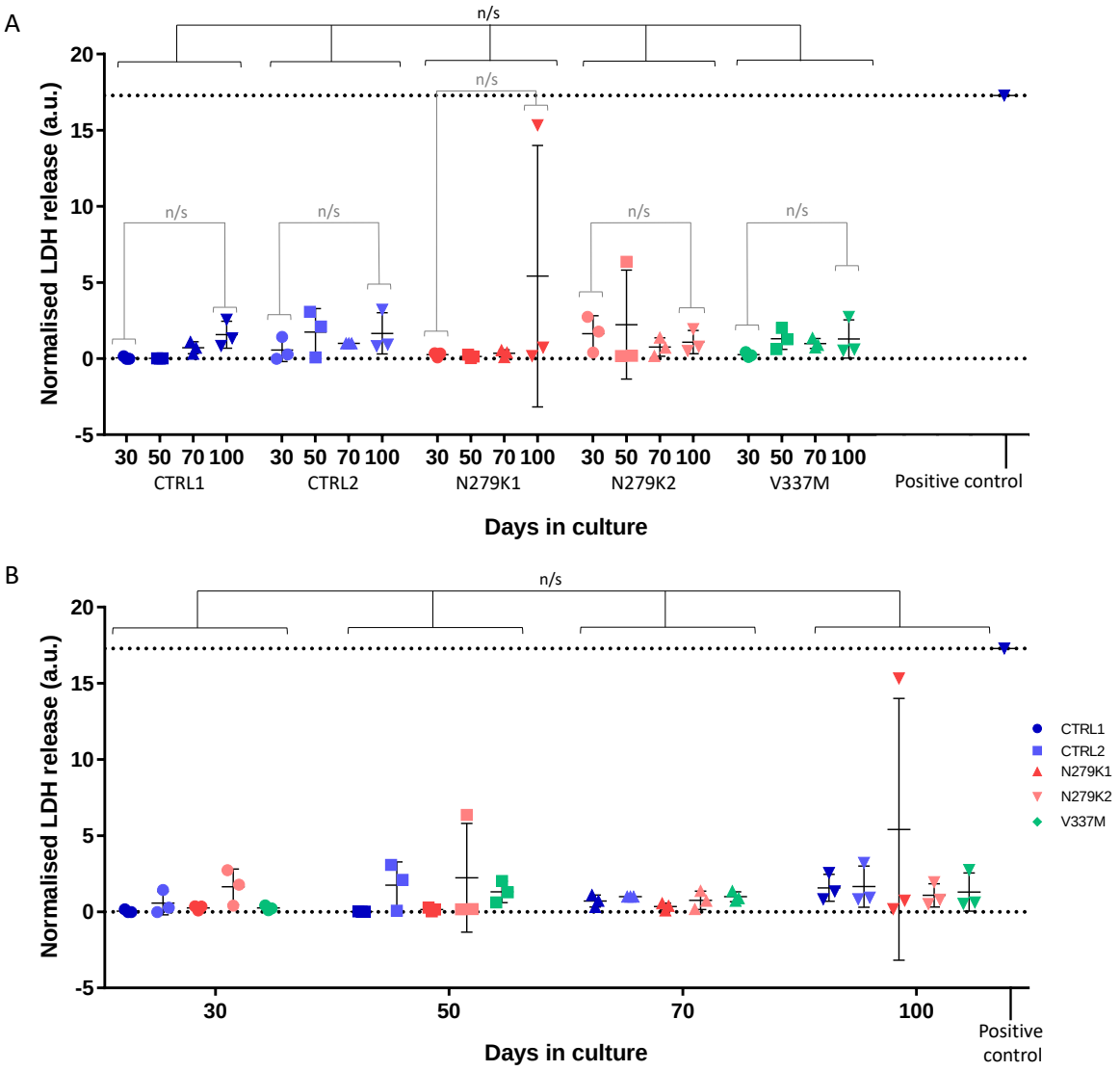

Fig. 4.10 **There was no significant change in cell death over time as measured by spontaneous LDH release into the media.** Spontaneous LDH release at day 30, 50, 70, and 100, measured in the media of CTRL1, CTRL2, N279K1, N279K2, and V337M cultures from three independent differentiations. Measurements are normalised to the reading at day 70 in CTRL1 cultures for each differentiation. Each point represents the normalised LDH release measured at one time point in one of the three differentiation rounds, and as an average of two technical replicates. The positive control indicates maximal LDH release from one culture, following lysis. Bars indicate the mean±SD. The same data are presented in **A)** and **B)**. **A)** shows data organised by parental iPSC line to show the change in LDH release in each culture over time. Significance bars in black show the results of a two-way ANOVA: there was no significant difference in cell death when comparing between the parental iPSC lines. Significance bars in grey show the results of paired t-tests comparing LDH release at day 30 and day 100 in each iPSC line: there was no significant change in LDH release comparing day 30 and day 100 for cultures from each iPSC line, although there may be a trend. **B)** shows data organised by timepoint. Significance bars in black show the results of a two-way ANOVA: there was no significant change in LDH release over time. Overall, no significant differences in cell death were detected.

release. This high level in a single culture could have been related to detachment of the cells from the plate surface.

The data were analysed by a two-way ANOVA. This found no significant main effect of time, meaning that the amount of LDH released is not significantly different between day 30, 50, 70, and 100 ($F(3,30)=1.723$, $p=0.1833$), although there is a trend towards a difference. This is shown by a black bar in Figure 4.10B. There was no significant main effect of iPSC line, meaning that the amount of LDH release did not vary significantly between the cultures derived from the five iPSC lines ($F(4,10)=0.3391$, $p=0.8435$), which is shown by a black bar in Figure 4.10A. Finally, there was no significant interaction effect (time has the same effect on LDH release in cultures derived from all five iPSC lines: $F(12,30)=0.8427$, $p=0.6087$).

To see if there was a significant change in LDH release over time in each culture, I performed paired t-tests comparing LDH release at day 30 and day 100 in each iPSC line. The results of these tests are shown by orange bars in Figure 4.10A: all the t-tests showed no significant change.

Together, these results indicate that there was no significant change in cell death in culture over time or between cultures from each of the iPSC lines. As can be seen in Figure 4.10, there is little variation in LDH level release between the cultures, with the exception of one near-maximal point at day 100 in N279K1, and one slightly higher point at day 50 in N279K2.

4.5 Discussion

4.5.1 Tau phosphorylation at the AT8 epitope

There was an increase in the number of AT8 positive neuronal cell bodies over time when I compared the cultures at day 50 to the cultures at day 80-100 (two-way ANOVA, $p=0.0164$). To investigate this further, I used t-tests to compare the difference in the proportion of AT8 positive neurons derived from each iPSC line at day 50 and day 80-100. No significant differences were detected, except for in the CTRL1 line, in which there was a significant increase in the proportion of AT8 positive neurons between day 50 and day 80-100.

These results are not easy to interpret, since the time-course of AT8 phosphorylation in embryonic human brains has not been determined, although it is higher in fetal brains than in the adult human brain (Brion et al., 1993; Goedert and Jakes, 1990). In chick optic lobes, the amount of AT8 positive tau increases between embryonic days 8 and 14 (Rösner et al., 1995), suggesting that an increase in AT8 positive neurons could be expected in iPSC-derived

cultures, representing a development-like process. Since iPSC-derived neurons are similar to human fetal neurons in terms of their gene expression (Handel et al., 2016; Patani et al., 2012), a development-like process may explain the significant increase in the proportion of AT8 positive CTRL1 neurons over time.

However, Verheyen et al. (2018) found no change in the amount of AT8 positive tau by Western blot between day 51 and day 80 in control or intron 10+16 MAPT-mutant neural cultures. This is in agreement with my findings of no significant change in the proportion of AT8 positive neurons between day 50 and day 80-100 in CTRL2, N279K1, N279K2, and V337M cultures.

With only two control iPSC lines and no data about how tau phosphorylation at the AT8 epitope proceeds over time in the human fetal brain, the meaning of this result is unclear.

Comparing the proportion of AT8 positive cells derived from the various iPSC lines, I found a significant difference in the proportion of AT8 positive neurons between CTRL2 and N279K1 cultures (two-way ANOVA, p=0.0106), and a trend towards a difference between CTRL2 and N279K2 cultures (two-way ANOVA, p=0.2838). There was no significant difference between N279K1 or N279K2 and CTRL1, or between V337M and CTRL1 or CTRL2 according to the two-way ANOVA. The reason for the variability between neurons derived from the two control and two N279K lines is unclear. It may be due to genetic background differences, which highlights a weakness of many iPSC-derived neuron studies: a small number of subjects and a lack of appropriate controls. This variability could have been controlled for using isogenic iPSC lines.

When the control and N279K line data from day 50 was grouped, there was a significant difference in the proportion of AT8 positive cells (according to Student's t-test): more AT8 positive neurons were found in the N279K cultures, which is in agreement with the findings of Iovino et al. (2015). However, the proportion of AT8 positive neurons observed was lower in my cultures than in those of Iovino et al. This may be because my neural cultures were differentiated from iPSCs using a different method, with different steps and media, and the resulting cells were maintained in media containing cAMP and BDNF (amongst other factors), both of which support neuronal survival in culture (Dugan et al., 1999; Yoshii and Constantine-Paton, 2010), whereas Iovino et al.'s cultures were not.

This increase in the proportion of N279K-mutant AT8 positive neurons at day 50 is also in agreement with the findings of Ehrlich et al. (2015), who found significantly more AT8 positive midbrain-like N279K-mutant neurons at day 40 as compared to control. However, Ehrlich et al. also found an increase in the proportion of AT8 positive V337M-mutant neurons as compared to control, whereas I did not detect a difference between V337M and CTRL1 or

CTRL2. This discrepancy may be due to the difference in neuronal types generated, since I generated neurons with a forebrain, glutamatergic fate, where Ehrlich et al. generated GABAergic and catecholaminergic neurons.

To determine the proportion of AT8 positive neurons present in each culture, I counted the number of AT8 positive cell bodies. This was difficult when cells were closely packed (since antibodies sometimes failed to penetrate the centre of a large clump of cell bodies), or when one of the z-stack images contained a large number of AT8 positive processes which obscured cell bodies (in this case a higher or lower image in the z-stack was used, in which cell bodies were clearly visible). To overcome these problems, I did not include these non-representative fields of view, and I re-counted fields of view at least twice. In addition, the age of the neural cultures hampered this process, as discussed below.

I could have validated the results obtained with AT8 by immunostaining using antibodies against other phosphorylated tau epitopes, such as PHF-1. In addition, I could have confirmed this result with Western blotting, ideally using fluorescent secondary antibodies, so that AT8 and total tau could be detected simultaneously. However, epitopes of antibodies such as AT8 and PHF-1, which are commonly used to detect tau phosphorylation in iPSC-derived neuronal cultures, are present in both FTDP-17T and during fetal development (Matsuo et al., 1994; Rizzini et al., 2000; Spillantini et al., 1996a). Therefore, a better alternative would be to use antibodies against epitopes which are present in FTDP-17T but not fetal brain, such as AP422 (Morishima-Kawashima et al., 1995), or AT100 (Ksiezak-reding et al., 2000).

4.5.2 Conformational changes in tau

I did not detect MC-1 positive tau in neurons from control or MAPT mutant cultures at day 80-100. This is in agreement with the findings of other groups using iPSC-derived neurons, since MC-1 positive tau has only been reported in neurons transplanted into the brain of a AD mouse model after 180 days (Espuny-Camacho et al., 2017), after exposure to tau oligomers (Usenovic et al., 2015), or after tau overexpression and exposure to tau fibrils (Medda et al., 2016). MC-1 positive tau has also been found in non-iPSC-derived neuronal models, including in control hESC-derived neurons over-expressing pseudo-phosphorylated 2N4R tau (Mertens et al., 2013), and in 3D-cultured neurons derived from SHSH-5Y cells expressing the P301L tau mutation, following exposure to okadaic acid (Seidel et al., 2012).

The tau conformation detected by MC-1 may be preceded by phosphorylation at the AT8 and PHF1 epitopes, since pseudo-phosphorylation at these epitopes has been shown to bring the repeat domain and N-terminus of tau closer together, and to increase MC-1

immunoreactivity (Jeganathan et al., 2008). Since phosphorylation at the AT8 epitope was detected, it is possible that longer time in culture would have produced MC-1 positive tau. MC-1 positive tau has been observed relatively early in another model: in 2.5 month-old mice expressing human P301S-mutant tau (Brelstaff et al., 2015; Xu et al., 2014). However, as already discussed, neurons detached from their coverslips at around day 100, making extended timepoints impossible.

Similarly, pFTAA-positive neurons were not detected at day 100. Since pFTAA binds to AT100 and MC-1 positive neurons in the dorsal root ganglia of mice expressing P301S tau, and recognises a β-sheet structure, pFTAA detects filamentous tau (Brelstaff et al., 2015).

The lack of misfolded or filamentous tau detected in day 100 cultures is in agreement with the lack of MC-1 positive misfolded tau detected, and with low levels of phosphorylation at the AT8 epitope. Since abnormal phosphorylation is thought to occur before misfolding and aggregation (Goedert and Spillantini, 2001), and may contribute to these processes (Despres et al., 2017; Haase et al., 2004), a lack of misfolded or fibrillar tau in my cultures is not surprising. It also echoes the results from other groups using FTDP-17T MAPT-mutant iPSC derived neurons: other groups have used thioflavin-S and alpha-LISA (which measures the distance between tau monomers) to detect tau aggregation in iPSC-derived MAPT-mutant neurons, and found none (Silva et al., 2016; Verheyen et al., 2018). However, some groups have found evidence for spontaneously occurring tau aggregation in iPSC-derived neurons. For example, in neurons with the intron 10+16 MAPT mutation, Imamura et al. (2016) observed staining using the anti-oligomeric TOC antibody which detects mis-folded tau dimers, oligomers, or polymers (Ward et al., 2013). In addition, Iovino et al. (2015) have observed AT100 positive tau in cultures of iPSC-derived neurons with the N279K MAPT mutation.

3D culture may be one way to observe tau aggregation in iPSC-derived neurons. Choi et al. (2014) cultured hESC-derived neurons overexpressing amyloidβ and/or presenilin 1 with familial AD mutations in either monolayers or a thick, 3D matrigel layer. They observed amyloidβ deposits and Gallyas-silver positive material in the 3D cultures. 3D culture of iPSC-derived neurons is explored further in Chapter 6.

4.5.3 αB-crystallin-positive balloon-type neurons

Staining with αB-crystallin revealed some αB-crystallin positive neurons in day 80-100 cultures. There was no significant difference in the proportion of αB-crystallin positive neurons between the control and MAPT-mutant cultures, but there was a slight trend towards

an increase. The detection of αB-crystallin positive neurons in iPSC-derived neurons with the N279K MAPT mutation is in agreement with findings in human brain, where αB-crystallin positive balloon neurons have been identified (Delisle et al., 1999; Wren et al., 2015). However, the detection of a low number of αB-crystallin positive control iPSC-derived neurons contrasts with findings in human brain, since control brains do not contain αB-crystallin positive balloon neurons, with the exception of brains from people over 90 years old (Iwaki et al., 1990). This suggests that cell culture conditions may have contributed to the appearance of αB-crystallin positive neurons in control cultures, since these are not expected to be present in the brain of the donor from whom the iPSCs originated. This could be confirmed using post-mortem brain tissue from the control fibroblast donors.

The αB-crystallin positive neurons in my cultures were morphologically similar to those in the brains of people with the N279K MAPT mutation: some had eccentrically positioned nuclei, some had a strongly αB-crystallin positive process, and others were enlarged. In addition, αB-crystallin positive thread-like processes were detected in some cultures, which have also been observed in tauopathy brains (Dabir et al., 2004).

Since αB-crystallin positive balloon neurons in human brains often co-stain with other antibodies, a possible extension to this work would be to look for immunoreactivity with antibodies such as synaptophysin (strongly expressed in αB-crystallin positive neurons in CBD Matsumoto et al., 1996), or phosphorylated neurofilament, which is expressed in αB-crystallin positive neurons in several diseases, including AD, CDB and PSP (Matsumoto et al., 1996; Mori et al., 1996; Tolnay and Probst, 1998).

The αB-crystallin expressing neurons were positively identified as neurons by co-staining with a total tau antibody (HT7) or with an antibody against 4R tau. However, αB-crystallin positive astrocytes and oligodendrocytes have also been reported in the brains of people with PSP, CBD and FTDP-17T (with the K317M, N279K or intron 10+16 MAPT mutation) (Dabir et al., 2004; López-González et al., 2014). I observed a small number of αB-crystallin positive cells which were not stained with neuronal markers, which may have been αB-crystallin positive astrocytes. Further studies would be needed to identify the nature of these αB-crystallin positive structures, but they were outside the scope of my thesis.

Co-staining with αB-crystallin and AT8 antibodies showed that few αB-crystallin positive neurons were also AT8 positive. It has previously been suggested that high levels of αB-crystallin expression are part of a protective mechanism which prevents the pathological accumulation of proteins in neurons: in PD sufferers, high expression of αB-crystallin and Lewy bodies are almost mutually exclusive in neurons (Braak et al., 2001). This may explain why few AT8 positive αB-crystallin positive neurons were identified in my cultures.

However, this staining was only performed on neurons from one differentiation round, so these findings are preliminary and need to be validated. In addition, the co-staining of cells for AT8 and αB-crystallin has only been performed in glia from PSP brains (López-González et al., 2014), making the relevance of AT8 and αB-crystallin co-staining in neurons with MAPT mutations unclear.

Counting the number of αB-crystallin positive neurons is a superficial way to assess a potential balloon neuron phenotype, and there is scope to investigate this phenotype further. For example, there is a decrease in αB-crystallin solubility in CBD in PSP brains as compared to control, which correlates with an increase in insoluble tau (Dabir et al., 2004). Both of these phenomena could be investigated simultaneously in aged iPSC-derived MAPT mutant neurons. In addition, αB-crystallin is subject to post-translational modifications following stressful stimuli, which make it a less effective chaperone (López-González et al., 2014). These modifications include phosphorylation at Ser19, 45 and 59, which could be investigated in future experiments; time constraints did not allow me to pursue this further.

4.5.4 Sodium channel expression and the lack of an AIS

Potential AIS-like sodium channel staining was detected in N279K1 neurons at day 50 from one differentiation round, but no AIS-like sodium channel staining was detected in any other cultures at day 16, 50 or 80-100, and no AIS-like staining was detected using the Ankyrin G or neurofascin antibodies.

It is possible that my iPSC-derived neurons were too immature for these proteins to be expressed and localised to the AIS. Galiano et al. (2012) found that ankyrin G is not present at the AIS in axons migrating through the cortical plate at embryonic time points in mice. Instead, ankyrin G is first detected at postnatal day 1, when most neurons had reached their destinations within the cortex. However, this explanation is unlikely, since Higurashi et al. (2013) detected AIS-like sodium channel staining in iPSC-derived neurons at day 56, and I detected AIS-like sodium channel staining at day 50 in one differentiation round, but not at day 80-100.

Alternatively, the AIS may not be detectable in the majority of my iPSC-derived neural cultures because the neurons are not healthy. Schafer et al. (2009) found that neuronal injury (90 minutes of middle cerebral artery occlusion leading to ischaemia in mice, or optic nerve crush in mice, or oxygen and glucose deprivation in culture) results in AIS loss, with the AIS was no longer being detectable with ankyrin G, βIV spectrin, or sodium channel antibodies. Schafer et al. (2009) demonstrated that AIS loss was due to the specific, calcium-dependent

proteolysis of ankyrin G and βIV spectrin by the protease calpain, which occurred rapidly after injury and before cell death, and which was not reversible in neurons kept for eight days in culture.

Although Schafer et al. cultured cells in media containing no glucose, causing damage, it is possible that my iPSC-derived neural cultures suffered a lesser degree of glucose deprivation. To determine if this was the case, I could have measured glucose levels in the fresh and spent media, using a glucose oxidase/peroxidase assay, for example. It is less likely that my cultures suffered oxygen deprivation, since they were stored in a normoxic incubator.

A stressor not mentioned by Schafer et al. (2009) which may have contributed to non-optimal culture conditions is pH. I changed the culture media every other day, but the cells were densely packed and the media was often orange, indicating a decrease in pH measured by phenol red. Kwolek and Kepski (2015) have shown that rat primary cortical neurons are vulnerable to low pH induced cell death, which increases with increasing acidity and increasing time in an acidic environment. Kwolek and Kepski also found that primary neurons were unable to maintain their normal pH when the extracellular pH was 6.8 of lower. It is possible that a chronically lower than optimal pH was a sufficient injury to cause AIS loss, although this has not been investigated in published work. To determine whether the pH of cell culture media could have had a deleterious effect, I could have measured the pH of spent media, although a more practical alternative would have been to plate neurons at a lower density in larger wells, in order to give them a larger volume of medium. Due to time constraints and the non-promising nature of these results, I did not investigate sodium channel expression or the presence of an AIS further.

4.5.5 Spontaneous cell death measured by LDH release

I found no significant increase in cell death over time. When measuring cell death in my cultures, I normalised LDH release to that at day 70 in CTRL2 cultures for each of the three differentiation rounds. Day 70 was chosen for normalisation because the range of luminescence values at day 70 was the smallest, and because at earlier time points some values were close to zero. A similar approach (normalising to control LDH release) has also been taken by Ehrlich et al. (2015) and Usenovic et al. (2015) in their investigations of cell death in iPSC-derived MAPT-mutant neurons, but it does not take into account a potential increase in cell number over time. Since I plated the same number of NPCs, which were then exposed to DAPT to cause differentiation to neurons, the increase in cell number over time is likely to have been similar between cultures. However, to take this into account I could

have normalised LDH release to the protein concentration in the cell lysate, as was done by Wren et al. (2015). This method requires separate wells of cells for each timepoint, whereas I collected media from the same well over time.

In addition, the method I used to detect dying cells provided only a short snapshot of the number of cells dying in the 48 hours between media changes. This may not have been sufficient time to find differences in cell death between control and MAPT-mutant cultures. As an alternative, I could have used a live-cell neuron marker such as NeuO (Er et al., 2015) to mark neurons, and a live/dead dye. Live imaging over several timepoints would then allow me to quantify the proportion of living neurons, the proportion of living cells (neurons and non neurons) and the proportion of dead cells over time. This would have required a large number of live cultures, and time constraints prevented me from producing these.

No change in cell death over time has also been observed by Medda et al. (2016), who measured by ATP levels (as a proxy for cell viability) in control iPSC-derived cultures from day 22-39, and found a non-significant trend towards decreased viability. Since iPSC-derived neural cultures are more like neurons in the developing brain than those in the adult brain (Handel et al., 2016; Patani et al., 2012), some cell death over time is to be expected, since cell death takes place during brain development (Kuan et al., 2000). Alternatively, the low levels of cell death may be due to the artificial cell culture environment: I maintained my cultures with media containing cAMP and BDNF, both of which support neuronal survival (Dugan et al., 1999; Yoshii and Constantine-Paton, 2010).

I found no change in LDH release between cultures derived from control or MAPT-mutant iPSC lines. This suggests that longer culture periods may be needed to observe spontaneous cell death in MAPT-mutant cultures, if present. Neuron loss in FTDP-17T is only documented post-mortem, in brains at an advanced disease stage which contain aberrantly phosphorylated and filamentous tau (Spina et al. 2017; Slowinski et al. 2007), and it is difficult to determine the progression of neuron loss from the onset of pathological changes in the brain. In mice expressing mutant human P301S tau, cortical neuron loss is detectable as early as 3 months of age (Hampton et al., 2010; Yang et al., 2016), and mice expressing N279K mutant human tau show substantia nigra neuron loss after 12 months of age (Dawson et al., 2007). Longer culture might therefore be required for tau aggregate toxicity to cause cell death. However, longer culture times were not possible, since the neurons began to detach from their coverslips around day 100.

Since little cell death was detectable in my cultures, it is likely that the decrease in the amount of βIII-tubulin observed between day 50 and day 80-100 by Western blot (Chapter 3)

was not caused by neuronal death. A more likely explanation is an increase in the proportion of non-neuronal cells in culture, such as astrocytes, as explored in Chapter 3.

It is possible that FTDP-17T-relevant cell death was occurring in my cultures, but that the experimental set up could not detect it. The neural cultures contained neurons from NPCs with a forebrain fate, but I did not determine which layer markers the neurons expressed. Layer identity may be important to detect a disease-relevant difference in cell death between control and MAPT-mutant neurons, since layer II neurons may be particularly vulnerable to cell death in FTDP-17T (Brandt et al., 2005). To explore this further I could have differentiated iPSCs to layer II neurons, for example by Ngn2 over-expression, which has been shown to give a pure population of layer 2/3 excitatory induced neurons (Zhang et al., 2013), and then measured LDH release in control and MAPT-mutant neurons over time. However, time constraints did not allow cell death to be investigated in more depth.

4.5.6 Experiments on iPSC-derived neural cultures at day 80-100

In conclusion, the N279K and V337M MAPT-mutant iPSC-derived neural cultures showed limited pathological changes. An increase in tau phosphorylation at the AT8 epitope was detected at day 50 in N279K relative to control cultures, but tau misfolding was not detected and nor was tau aggregation. No detectable synapse loss was observed (Chapter 3), and there was no MAPT-mutant specific increase in cell death under the conditions used. Some of these phenotypes are further explored in Chapter 6, in which 3D cultures (cerebral organoids) are made from control, N279K and P301L iPSCs.

Culturing iPSC-derived neurons until day 100 was challenging, as previously discussed in Chapter 3. Stainings had to be repeated several times due to detachment of cells from the coverslips, and in some cases βIII-tubulin staining had a broken appearance, suggesting the breakdown of neuronal processes, or non-specific binding of antibodies to the thick layer of processes. The amount of cell death in the cultures was low and constant over time, indicating that cultures were viable until they were either fixed or collected for analysis, or detached from the culture surface. However, the lack of detectable AIS in all but one differentiation round suggests that the cultures were not in optimal conditions.

4.5.7 Summary

In this Chapter I:

1. Examined the degree of tau phosphorylation at the AT8 epitope (Ser202 and Thr205). There was an increase in the proportion of AT8 positive neurons over time, which may

reflect normal maturation of young neurons, since AT8 is detected in the fetal human brain, as well as in FTDP-17T. There was a higher proportion of AT8 positive N279K neurons as compared to control neurons at day 50, when both N279K1 and N279K2 cultures were compared to both CTRL1 and CTRL2 cultures, although the proportion of AT8 positive neurons was small. This was similar to the results of Iovino et al. and may reflect FTDP-17T-relevant abnormal phosphorylation.

2. Looked for changes in tau's conformation using the antibody MC-1 (against hairpin-like conformation of tau) and the dye pFTAA (which detects AT100 positive, MC-1 positive tau). No MC-1 positive or pFTAA positive tau was detected, indicating that misfolded or fibrillar tau were not present. This fits with the finding that AT8 levels were low and similar between control and MAPT mutant cultures, since abnormal phosphorylation is thought to precede tau misfolding and aggregation.

3. Assessed the appearance of αB-crystallin positive balloon neuron-like cells. Some αB-crystallin positive cells were detected, and the majority of these were neurons, since they co-stained for tau. However, there was no significant difference in the proportion of αB-crystallin positive cells between the cultures.

4. Compared the appearance of sodium channels between MAPT mutant and control cultures. Diffuse sodium channel staining was detected, but no AIS-specific staining was detected with a pan-sodium channel antibody, a neurofascin antibody, or an ankyrin G antibody. The lack of AIS detected suggests that the neurons may have been in sub-optimal conditions.

5. Measured differences in spontaneous cell death. There were no significant differences in cell death over time, or between cultures from different iPSC lines, although there was a slight trend towards an increase in cell death over time. This result, and the finding that the proportion of astrocytes increased over time (Chapter 3) suggests that the decrease in βIII-tubulin over time was due to an increase in the proportion of non-neuronal cells, rather than neuron death.

I found minimal phenotypic changes in MAPT mutant iPSC-derived neurons as compared to control iPSC-derived neurons. This may be due in part to the genetic background differences between the five iPSC lines. Therefore, in Chapter 5, I will use the gene editing technology CRISPR to make two isogenic iPSC lines which differ only at the N279K mutation locus. In Chapter 6, I will use these isogenic iPSCs to make 3D cerebral organoids, since

3D culture may increase neuronal maturity, and may enable the detection of disease-relevant phenotypes (Choi et al., 2014).

Chapter 5

Gene editing by CRISPR to make isogenic iPSC lines

5.1 Aims

One barrier to studying the effects of the N279K mutation in iPSC-derived neurons is the genetic variability between iPSC lines derived from an FTDP-17T patient with the N279K mutation and a control subject with no MAPT mutations. This barrier can be avoided by making isogenic iPSC lines, share the same genetic background, differing only at the N279K mutation. Isogenic iPSC lines are also more suitable than non-isogenic iPSC lines for making 3D cultures such as cerebral organoids, in which variability between cultures derived from different iPSC lines can be high (see Chapter 6).

This Chapter describes the attempt to use CRISPR to produce isogenic iPSC lines by correcting the N279K mutation in FTDP-17T patient-derived iPSCs and to induce the N279K mutation in control subject-derived iPSCs.

5.2 Introduction

5.2.1 The origins of CRISPR

"CRISPR" stands for clustered regularly-interspaced short palindromic repeats and refers to short DNA sequences in prokaryotes which were first found by Ishino et al. (1987) in E. coli. The significance of these sequences was confirmed when Barrangou et al. (2007) showed that bacteria exposed to bacteriophages incorporated bacteriophage DNA fragments (named "spacers") into their genomes, between CRISPR sequences. When the spacers were removed

from bacteria resistant to a particular bacteriophage, the bacteria became vulnerable to the bacteriophage again, indicating that inclusion of foreign DNA into the CRISPR array plays an active role in prokaryote adaptive immune systems.

CRISPR systems have since been discovered in a range of archea and prokaryotes and can be divided into two classes (Makarova et al., 2015). Class 1 (types I, III and IV) CRISPR systems are defined by their multi-protein complexes which bind to and cleave the target DNA, whereas Class 2 systems (types II and V) have a lone effector protein. The type II CRISPR system is most commonly used in gene editing and is discussed here.

The CRISPR defence mechanism has three stages: adaptation, expression and interference (reviewed by Sternberg and Doudna, 2015). In prokaryotes with type II CRISPR systems, a library of protospacer sequences, interspaced with CRISPR sequences, is acquired during the adaptation phase. On transcription (the expression phase), CRISPR RNA (crRNA) is produced and base-pairs with transactivating CRISPR RNA (tracrRNA) (Figure 5.1). The crRNA-tracrRNA hybrid complexes with the effector CRISPR-associated protein 9 (Cas9) nuclease, targeting Cas9 to DNA sequences complementary to the protospacer. If these sequences directly precede a protospacer-adjacent motif (PAM), Cas9 cuts both DNA strands, completing the interference phase. Thus, exogenous DNA sequences are specifically disrupted, conferring resistance against invading viruses and plasmids.

5.2.2 CRISPR for gene editing

CRISPR has been adapted for gene editing because it can make predictable DNA breaks at specifically targeted sequences. CRISPR-Cas9 technology for gene editing is derived from the Streptococcus pyogenes adaptive immune system (reviewed by Ran et al., 2013). To edit DNA, guide RNA (gRNA) is designed complementary to a target DNA sequence, with minimal homology between the gRNA and the rest of the genome, to avoid off-target DNA editing. gRNA is then inserted into an RNA backbone which combines aspects of tracrRNA and crRNA. The gRNA complexes with Cas9 protein and directs Cas9 to cut the DNA at the target site (Figure 5.1), provided that the DNA target directly precedes a PAM (bases NGG in the S. pyogenes system, where N is any base). Wild-type Cas9 (Cas9wt) makes a double-stranded DNA break (DSB) but a modified version, Cas9 nickase (Cas9n), which has a D10A mutation in the RuvC catalytic region, can be used to make a single-stranded cut on the strand complementary to the gRNA (Jinek et al., 2012). A Cas9n pair targeted to the sense and anti-sense strands makes an offset DSB, which reduces the chance of off-target

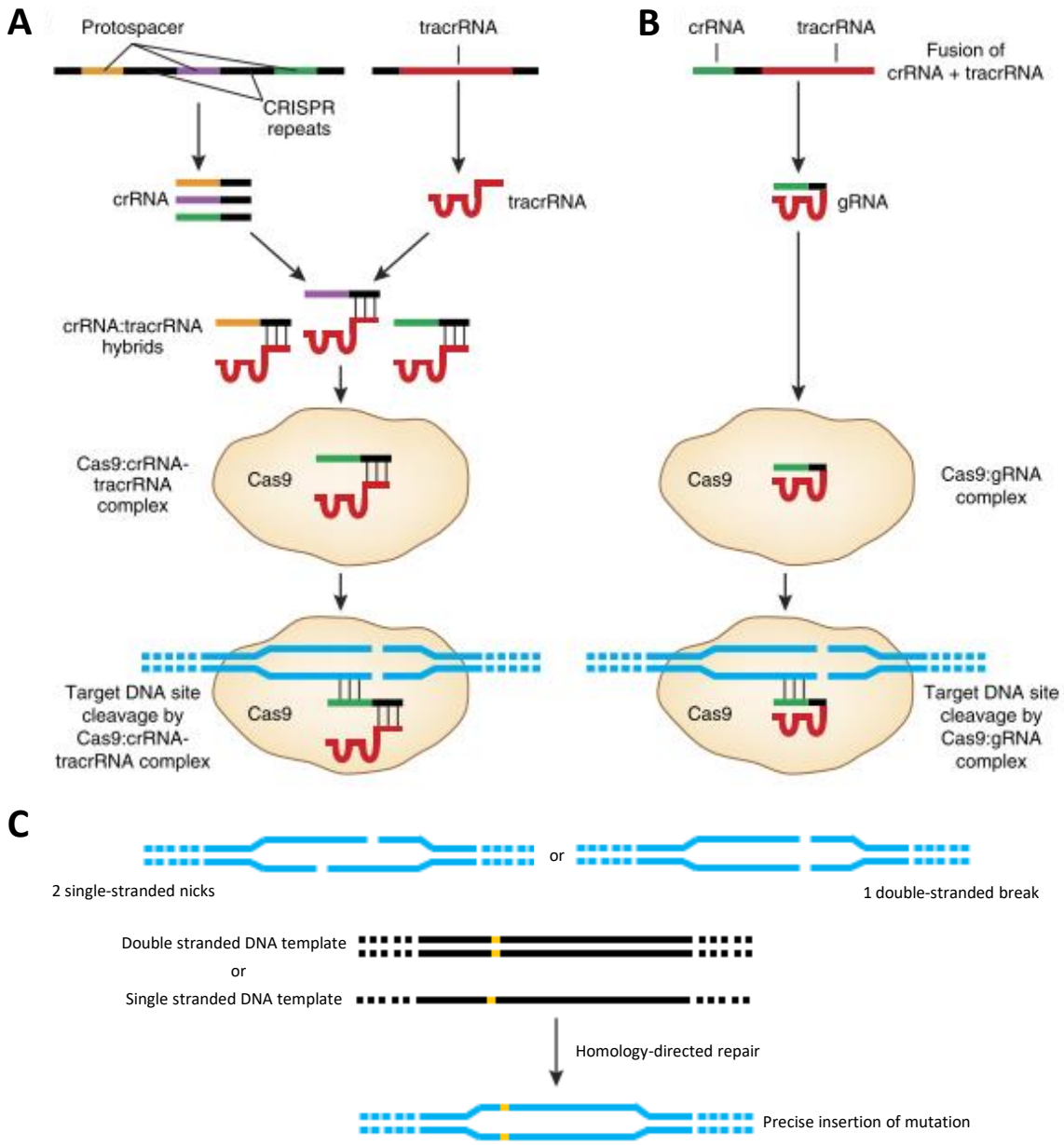

Fig. 5.1 **The S. pyogenes CRISPR system in immunity and in gene editing. A)** The type II CRISPR system in S. pyogenes. Fragments of exogenous DNA are incorporated as protospacers between CRISPR repeats. tracrRNA and crRNA are transcribed, then hybridise with each other and Cas9 nuclease. The crRNA targets the Cas9-crRNA-tracrRNA complex to its complementary DNA and Cas9 makes a double-strand break (DSB). **B)** The type II S. pyogenes CRISPR system adapted for gene editing. gRNA, a fusion of crRNA (designed complementary to a target DNA sequence) and tracrRNA, is transcribed and hybridises with Cas9. gRNA targets Cas9 to its complementary DNA sequence and Cas9 makes a DSB. **C)** A DSB can be made by wild-type Cas9 (right) or Cas9 nickase (left) which makes two neighbouring single-stranded breaks, constituting an off-set DSB. The DSB is repaired by homology-directed repair with a single- or double-stranded DNA template containing the desired mutation. The mutation is precisely inserted into the endogenous DNA. Diagram adapted from Sander and Joung (2014).

DNA cutting since the homologous region required for a DSB is twice as long as that of Cas9wt.

DSBs are then repaired by non-homologous end joining (NHEJ) or homologous recombination (HR). NHEJ makes insertion and deletion mutations (indels) of varying lengths, which can result in a premature stop codon and gene knockout (reviewed by Chang et al., 2017). In HR, homologous DNA acts as template for precise reconstruction (reviewed by Ranjha et al., 2018). Providing a double- or single-stranded DNA template with the desired insertion, deletion or point mutation can hijack the HR pathway for gene editing to make precise mutations, in a process known as homology-directed repair (HDR) (Figure 5.1).

5.2.3 Mechanisms of DNA repair by homologous recombination

HR can occur via one of several mechanisms (Figure 5.2): double-strand break repair (DSBR), synthesis-dependent strand-annealing (SDSA), or single-strand DNA incorporation (ssDI). Kan et al. (2014) showed that HR with a double-stranded DNA repair template takes place via DSBR in human cells: 5' cut DNA ends are resected to leave 3' single-stranded DNA, which invades the double-stranded template. New DNA is synthesised, forming double Holliday junctions. These are resolved, then the endogenous DNA and repair template separate, producing either cross-over or non-cross-cover products.

HR with a single-stranded DNA oligomer (ssODN) template occurs preferentially via SDSA in human cells, although ssDI is also possible (Kan et al., 2017). In SDSA, 5' cut DNA ends are resected, then the 3' single-stranded DNA end extends along the homologous complementary sequence of the ssODN. The newly synthesised strand disengages from the ssODN and anneals to the complementary DNA strand. After the resolution of remaining gaps, the result is a non-cross over product: the break is repaired by newly synthesised DNA (Nassif et al., 1994). This contrasts with ssDI, in which the ssODN itself is incorporated into the DNA at the break site (Radecke et al., 2006).

5.2.4 Off-target editing with CRISPR

Cas9 is guided to its target locus by gRNA binding to complementary DNA but off-target editing can still occur despite the specificity of nucleotide binding. The extent of reported off-target editing with CRISPR varies considerably (reviewed by O'Geen et al., 2015). For example, Fu et al. (2013) used CRISPR to edit DNA at four loci in HEK293 (human embryonic kidney), U2OS (human osteosarcoma) and K562 (human leukaemia) cells, then sequenced these loci and the most similar off-target loci. Fu et al. found high on- and

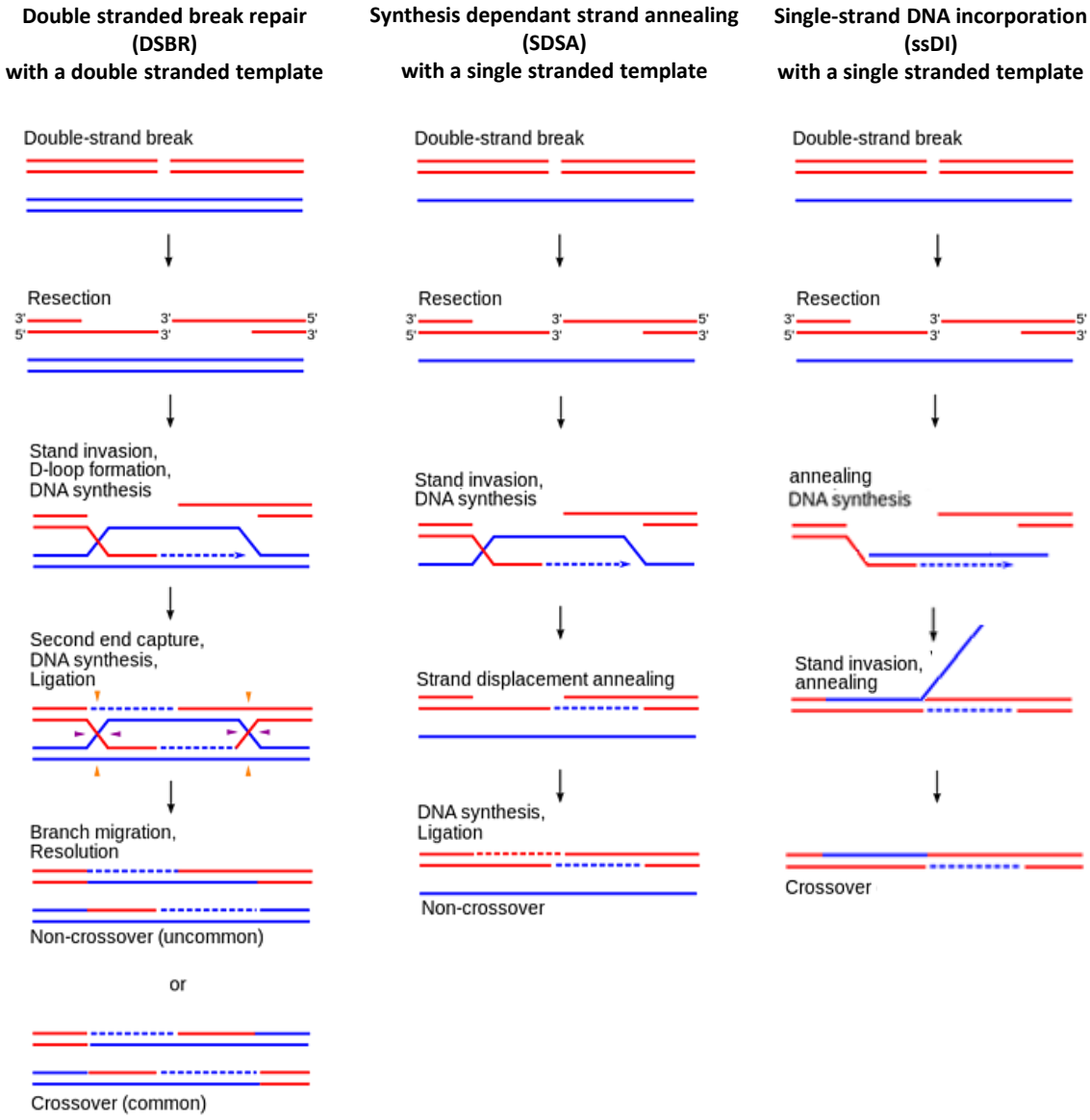

Fig. 5.2 **Mechanisms of DNA repair by homologous recombination.** Mechanisms of DSBR, SDSA and ssDI are shown. Red lines indicate endogenous DNA which has a double stranded break, blue lines indicate double- or single-stranded repair template DNA. Repair of the double-stranded break with a single-stranded template can lead to the incorporation of the template (in ssDI) or the synthesis of new DNA, without the incorporation of the template (in SDSA). The figure was adapted from https://blog.addgene.org/crispr-101-homology-directed-repair (DSBR and SDSA), Liang et al., 2017 and Kan et al., 2017 (ssDI).

off-target editing rates: the off-target loci examined had between one and four mismatches with the target locus but off-target and on-target editing rates were comparable.

Other groups report low levels of off-target modification. Hsu et al. (2013) found off-target modifications after CRISPR in HEK293 cells at a rate two orders of magnitude below that of on-target editing and Cho et al. (2014) found off-target editing at a frequency of 0.01% in K562 cells, compared to an on-target frequency of 60-75%. The differing extent of reported off-target editing might be explained by targeting different loci, or by varying dosages of Cas9 since on- and off-target editing increases as the concentration of transfected Cas9 increases (Hsu et al., 2013).

Gene editing efficiency is lower in iPSCs than in other cell types, such as HEK293 or K562 cells (Mali et al., 2013). If off-target effects occur approximately 100 times less often than on-target editing (as suggested by Hsu et al., 2013 and Cho et al., 2014), off-target editing may be near undetectable in iPSCs. Indeed, whole-genome sequencing of two CRISPR-edited iPSC lines and their parental line gave an estimate of 7-12 indels and 217-281 point mutations in each iPSC genome after editing (Smith et al., 2014). However, these mutations did not overlap with off-target sites predicted by sequence homology and were unique to each edited iPSC line, suggesting that they may have occurred spontaneously during iPSC clone expansion, not because of off-target Cas9 cutting. Veres et al. (2014) performed a similar experiment with six CRISPR-edited human embryonic stem cell (ESC) lines, and found indels, structural variants and point mutations but the modification locations could not be predicted by off-target gRNA binding, again suggesting that they may have emerged during clonal expansion. These results indicate that gene editing by CRISPR appears to be highly specific in iPSCs, but the isogenic iPSC lines generated can contain mutations arising during clonal expansion which may remain undetected unless whole-genome sequencing is performed.

5.2.5 Minimising unwanted CRISPR activity

CRISPR is reported to be highly specific in iPSCs (Smith et al., 2014; Veres et al., 2014) but off-target editing is possible (Cho et al., 2014; Fu et al., 2013; Hsu et al., 2013) and the magnitude of off-target effects may depend on the gRNA used (Fu et al., 2013; Tsai et al., 2015). In addition to off-target editing, unwanted CRISPR modifications can also occur at the target site, for example when the repaired DNA is re-cut by Cas9. The CRISPR design strategies discussed in this section decrease the chances of unwanted CRISPR activity.

Cas9 nickase (Cas9n)

Cas9n makes a single-stranded DNA break and a Cas9n pair can be used to make an offset DSB. Compared to Cas9wt, Cas9n decreases the probability of off-target mutations since the homologous sequence required for two adjacent single-stranded DNA breaks (Cas9n) is twice that required for one DSB (Cas9wt). The requirement for a longer homology region decreases the chance of similar off-target sequences in the genome and paired Cas9n sites without meaningful off-target homology are easy to find (Sections 5.4.1 and 5.4.2).

Furthermore, unpaired (off-target) single-stranded breaks created by Cas9n are repaired seamlessly, unlike DSBs, which are repaired by error-prone NHEJ (Cong et al., 2013; reviewed by Dianov and Hübscher, 2013). This results in fewer off-target indels. Cho et al. (2014) measured off-target cleavage induced by Cas9wt and Cas9n pairs at six off-target sites, which differed from the target site by one or two nucleotides. Cas9wt produced off-target indels at a frequency of 0.5-10%, as compared to no indels above the detection limit of 0.01% for Cas9n. Similarly, Ran et al. (2013b) used deep sequencing to compare off-target cleavage at five loci after editing by either Cas9wt or Cas9n. Both Cas9wt and Cas9n had similar on-target activity but the specificity (the ratio of on- to off-target indel formation) was 100-fold higher for Cas9n than for Cas9wt.

Another advantage of Cas9n is that it may favour HDR over NHEJ, increasing the probability of making precise mutations with a repair template. Mali et al. (2013) compared the effects of transfecting HEK293 cells with a repair template and either Cas9wt or a Cas9n pair and observed decreased NHEJ with Cas9n but similar levels of HR. Later, Gopalappa et al. (2018) reported that paired Cas9n are at least as efficient for making on-target modifications as Cas9wt and are sometimes more efficient.

Altered gRNA length

Truncating gRNAs from the usual 20 nucleotides reduces off-target modifications. Fu et al. (2014) used gRNAs between 15 and 20 nucleotides long to target Cas9 to four sequences in one gene and found that 17 or 18 nucleotide-long gRNAs had similar on-target activity to 20 nucleotide gRNAs but made fewer off-target cuts. gRNAs with 15 or 16 nucleotides produced either undetectable or significantly reduced on-target activity. Fu et al. suggest that the counter-intuitive increase in activity with shorter gRNAs occurs because the last two nucleotides are not essential for on-target gRNA binding but they could compensate for other mismatches between the DNA and gRNA at off-target sites.

Counterintuitively, adding two guanine nucleotides (GG) to the 5' end of gRNA can also increase specificity. The standard format for gRNA is GX_{19}, where X is any nucleotide and G is guanine, which is required for RNA transcription (Ran et al., 2013b). Cho et al. (2014) compared four $GGGX_{19}$ gRNAs with four corresponding GX_{19} gRNAs and found that all four $GGGX_{19}$ gRNAs caused fewer off-target indels in K562 cells. One $GGGX_{19}$ gRNA resulted in fewer on-target indels than the corresponding GX_{19} gRNA, suggesting that the additional GG decreases off-target indels by decreasing gRNA-DNA binding at all loci.

Single-stranded repair templates

Single-stranded ssODN repair templates may lead to fewer off-target effects than double-stranded plasmid repair templates. Chen et al. (2011) measured random integration of single- and double-stranded repair templates into cell line DNA after CRISPR and detected randomly integrated plasmid DNA but ssODNs were randomly integrated at a low enough frequency to be undetectable.

Studies comparing the efficiency of single- and double-stranded DNA templates for inducing precise mutations have given varied results. ssODNs are reported to be more efficient for small insertions in K562 cells (Chen et al., 2011), or for point mutations in HEK293 cells (Liang et al., 2017). However, plasmids are reported to be more efficient for point mutations in iPSCs (Flynn et al., 2015) and HEK293 cells (He et al., 2016). These results indicate that both ssODNs and plasmids can be used for HDR and suggest that their relative efficiency is context dependent. The discrepancy in editing efficiency could be caused by different target loci, transfection methods, ssODN or plasmid production methods or the effective template concentration at the repair site in each of the studies. Since both ssODNs and plasmids can induce precise mutations, eschewing plasmids for ssODNs to reduce the possibility of random integration will not necessarily decrease on-target editing efficiency.

Minimising homology between on- and off-target loci

DNA cleavage by Cas9 relies on homology between the gRNA and target DNA. Therefore, off-target cleavage can be reduced by using gRNA design programs to maximise the number of mismatches between the target locus and the rest of the genome. Single nucleotide mismatches are most effective when they are in the gRNA seed sequence: the 8-13 nucleotides closest to the PAM (Jinek et al., 2012). Mutations outside this region are better tolerated by Cas9, which can still cut the DNA (Hsu et al., 2013).

Single nucleotide mismatches are not always sufficient to prevent off-target cleavage. Cho et al. (2014) measured indels at loci which differed from the target site by one nucleotide and detected off-target activity at a frequency of 1.6-43% across three gRNA. When the mismatch was increased to two nucleotides, off-target editing was reduced to 0.1-1.8%. Although only three gRNAs were compared, this study shows that the number of mismatches needed to significantly reduce off-target editing varies between gRNAs, even at the same gene locus.

The positioning of mismatches relative to the PAM and to each other can also alter the rate of off-target cleavage. Hsu et al. (2013) quantified indels at three loci, using multiple gRNAs which had two, three or five mismatches with the target locus. Hsu et al. found that DNA cleavage occurred at lower rates when mismatches were: consecutive or less than four base pairs (bp) apart; at least two mismatches were in the seed region; and there were at least three mismatches. Two mismatches between the gRNA and DNA decreased indel formation but three mismatches reduced indel formation to near undetectable levels unless the mismatches were all distal to the PAM. Five mismatches provided little advantage over three mismatches, suggesting that three mismatches should be the minimum acceptable difference between on- and off-target loci.

Cas9-mediated DNA cleavage also depends on the presence of an NGG PAM sequence 3' of the gRNA binding site. A single nucleotide mismatch in a potential (off-target) PAM sequence can reduce off-target DSBs almost 500-fold (Cho et al., 2014), underlining the importance of the PAM sequence. However, Cas9 can cleave DNA with an NAG PAM sequence, as well as the NGG sequence, increasing the number of off-target sites with a potential PAM (Hsu et al., 2013).

Off-target gRNA-DNA binding is possible even with mismatches: gRNA can bind DNA with up to three (Mali et al., 2013) or up to five (Li et al., 2014b) non-matching bases. However, gRNA binding does not necessarily result in DNA cleavage. Wu et al. (2014) mapped DNA binding to four different catalytically inactive gRNA-dead Cas9 complexes in mouse ESCs and found binding at 26-6000 loci, depending on the gRNA. Repeating the experiment with catalytically active gRNA-Cas9 complexes resulted in an off-target mutation at only one locus, indicating that requirements for Cas9 cutting are more stringent than for Cas9 binding. Programs such as the CRISPR Design Tool (http://crispr.mit.edu/), which predict off-target cleavage sites by homology with the target sequence, may therefore over-estimate the number of potential off-target cutting sites.

Blocking mutations

Silent blocking mutations, in the PAM or gRNA target sequence, can be introduced in the repair template to prevent Cas9 re-cutting DNA after HDR. The introduction of blocking mutations follows the same principle as minimising homology between on- and off-target sites: a blocking mutation in the PAM sequence (Cho et al., 2014), or between one and three blocking mutations in the gRNA binding sequence (Cho et al., 2014; Hsu et al., 2013), preferably in the seed region (Jinek et al., 2012), reduce re-cutting most efficiently. However, blocking mutations must be silent, to avoid altering the target protein.

Blocking mutations increase the number of correctly edited clones. Using a repair template with a mutant PAM sequence increases editing efficiency in iPSCs 10-fold (Flynn et al., 2015), or between two- and 10-fold, depending on the locus (Paquet et al., 2016). Similar results have been found in HEK293 cells (He et al., 2016; Paquet et al., 2016).

Blocking mutations can also reduce unwanted on-target modifications. Merkle et al. (2015) found that 18% of sequencing reads from iPSC clones with an insertion had on-target indels but when the insertion site was altered to destroy the gRNA binding site, on-target indels fell to 0.08% of sequencing reads in edited clones.

5.2.6 Maximising on-target editing

Mutation locus proximity to the double-stranded break (DSB)

The distance between the DNA break and the desired mutation locus is a major factor in causing a point mutation. Elliott et al. (1998) measured point mutation induction in mouse ESCs after DSBs were made by I-SceI endonuclease and found higher mutation induction closer to the DSB: 83% of clones which underwent HDR resulting in a correction at the cut site also had a point mutation 7bp away and 40% of clones corrected at the cut site had a point mutation 45bp away. In iPSCs, Paquet et al. (2016) had similar findings: 50% of clones which underwent HDR incorporated a point mutation 10bp from the DSB, 25% of edited clones incorporated a point mutation 20bp from the DSB and 10% of edited clones incorporated a point mutation 30bp away. Paquet et al. (2016) observed similar results in HEK293 cells.

These high percentages (the proportion of edited clones which also contain point mutations) can be misleading since the proportion of edited clones out of all clones screened can be very low. For example, after CRISPR to cause a point mutation less than 10bp from the DSB, Yang et al. (2013) found that 1% of all iPSC clones sequenced incorporated the mutation. When the mutation was 20bp from the DSB, only 0.2% of all clones screened had

the mutation. Together, these results indicate that point mutation induction is more likely when the distance between the DSB and the mutation locus is lower.

5.2.7 Advantages of CRISPR for gene editing

CRISPR has several advantages over the gene editing systems zinc-finger nucleases (ZFNs) and transcription activator-like effector nucleases (TALENs).

Firstly, CRISPR components are relatively quickly designed and synthesised compared to ZFNs or TALENs. CRISPR relies on DNA-RNA base pairing, so Cas9 can be targeted to a particular locus by finding a sequence with a neighbouring PAM, then inserting the gRNA sequence into a Cas9 and gRNA expression plasmid (Ran et al., 2013b).

In contrast, ZFNs and TALENs rely on DNA-amino acid pairing, making their design and synthesis more complex and time consuming. ZFNs are based on zinc fingers: eukaryotic DNA binding domains in which groups of amino acids recognise different nucleotide triplets. Zinc fingers recognising every possible nucleotide triplet are available, so ZFN dimers can be targeted to a locus by combining the appropriate zinc fingers with a Fok1 cleavage domain. At the target site, the Fok1 nuclease domains dimerise and cleave the DNA (Vanamee et al., 2001). However, ZFNs cannot be targeted to every locus. TALENs are based on TALE DNA-binding domains, which are repeat sequences that recognise one nucleotide. Like ZFNs, TALENs are also designed as dimers, by combining appropriate DNA binding domains which are fused to FokI nuclease (reviewed by Gaj et al., 2013).

Secondly, Cas9 makes a blunt-ended DSB 3bp upstream of the PAM Jinek et al. (2012), whereas TALENs cut DNA non-specifically in the 12 to 24bp space between the TALEN binding sites (Miller et al., 2011). Predicting the cut position matters for small mutation induction by HDR since mutations closer to the DSB are more likely to be included (Elliott et al., 1998; Yang et al., 2013).

Perhaps most importantly, CRISPR is reported to have higher, or at least equal, gene editing efficiency compared to TALENs in iPSCs. Yang et al. (2013) targeted seven sequences at one gene locus in iPSCs with Cas9 or TALENs, and found that Cas9 resulted in more edited clones. Similarly, Ding et al. (2013) compared Cas9- and TALEN-mediated gene knock-down at seven loci and mutation knock-in at one locus in iPSCs: Cas9 gave more edited clones for both knock-out and knock-in. Ding et al. suggest that Cas9 is better tolerated by iPSCs than TALENs since the GFP marker in TALEN and CRISPR plasmids was expressed earlier and in a higher proportion of iPSCs electroporated with Cas9 than with TALENs.

Other groups report comparable activity between TALENs and CRISPR in iPSCs: Li et al. (2014a) used two TALEN and one CRISPR strategy to cause gene knock-out and knock-in and found similar indel and insertion rates induced by each method.

Overall, CRISPR is easier to design than ZFNs or TALENs, makes more predictable cuts than TALENs and is at least as efficient at gene editing in iPSCs as TALENs.

5.2.8 Using CRISPR to make isogenic iPSC lines

CRISPR, ZFNs and TALENs have increased the potential use of iPSCs to make iPSC-derived disease models since they allow isogenic lines to be created, which differ only at a disease-relevant mutation. Isogenic iPSC lines can be used to observe the disease-relevant effects of a mutation without the intrusion of unpredictable changes caused by the genetic background. Avoiding differing genetic backgrounds between control and mutant iPSC lines is advantageous because different iPSC lines have different gene expression and DNA methylation profiles (Bock et al., 2011) and have variable capacities to differentiate into other cells types, such as motor neurons (Boulting et al., 2011).

The efficiency of CRISPR-mediated gene editing is lower in iPSCs than in other human cell lines, such as HEK293 cells (Mali et al., 2013). The reported indel efficiency ranges from 51-79% (Ding et al., 2013) to 1% (Miyaoka et al., 2014) and point mutation efficiency ranges from 23% (Flynn et al., 2015) to 1% (Yang et al., 2013).

At least 11 isogenic iPSC lines with MAPT mutations have been produced using CRISPR or TALENs and these are listed in Table 5.1. Other MAPT mutant iPSC lines or iPSC-derived cells are available through repositories or commercially, but have not yet been described in any publications.

Table 5.1 **iPSC lines and iPSC-derived cells with MAPT mutations induced by gene editing.**

Cell type	Initial mutation → edited population	Editing method	References
iPSCs	Het A152T → Hom A152T	TALENs	[1]
iPSCs	Het A152T → Isogenic control	TALENs	[1]
NPCs	Het A152T → tau knockdown	CRISPR	[2]
NPCs	Het N279K → isogenic control	CRISPR	[3]
iPSCs	Het P301L → isogenic control	CRISPR	[4]
iPSCs	Het intron 10+14 → isogenic control	CRISPR	[5]
iPSCs	R406W → isogenic control	CRISPR	[5,6,7]
iPSCs	Control → Hom N279K, P301L, intron 10+16	CRISPR-FokI	[8]
iPSCs	Control → Het intron 10+16	ZFNs	[9]
iPSCs	Control → Hom intron 10+16	ZFNs	[9]
iPSCs	Control → Hom P301L, intron 10+16	ZFNs	[9]

Abbreviations: het: heterozygous mutation; hom: homozygous mutation; iPSC: induced pluripotent stem cell; NPC: neural precursor cell. References: [1]: Fong et al. (2013); [2]: Silva et al. (2016); [3]: Hallmann et al. (2017); [4]: Nimsanor et al. (2016a); [5]: Imamura et al. (2016); [6]: Nimsanor et al. (2016b); [7]: Nimsanor et al. (2016c); [8]: (García-León et al., 2018); [9]: (Verheyen et al., 2018).

Gene editing in proliferative versus non-proliferative iPSCs and iPSC-derived cells

Gene-editing is usually performed on proliferative cells, which can be amplified by passaging. In the case of iPSC-derived neurons, iPSCs or neural precursor cells (NPCs) are usually edited, then differentiated to neurons. This is because relying on HDR to induce a precise mutation after a DSB requires efficient DNA repair machinery. Saleh-Gohari (2004) found that HDR of DSBs in a human cell line was 24 times higher in cells arrested in S (synthesis) phase as compared to those arrested in G0 (resting) or G1 phases, suggesting that actively dividing cells are more likely to use the HR pathway for DNA repair than cells in a resting state.

Furthermore, the dominant repair mechanism for DSBs switches from HDR in proliferative NPCs to NHEJ in post-mitotic neurons. Orii et al. (2006) showed that, in embryonic day 14.5 mice with defective NHEJ machinery and normal HR machinery, differentiated neurons were more vulnerable to DNA damage-induced apoptosis as compared to the control mice. This suggests that DNA damage in neurons is repaired mainly by NHEJ but not HR. Orii et al. also noted that mouse embryos with inactive HR machinery and normal NHEJ

capability had widespread DNA damaged-induced apoptosis in proliferative NPC regions throughout the brain and did not survive beyond embryonic day 10, indicating that DNA repair takes place mainly by HR, not NHEJ, in NPCs. For gene-editing by CRISPR, these findings suggest that precise mutations by HDR are most likely to occur in proliferative cells, whereas indels are more likely in post-mitotic cells.

5.3 Materials and Methods

5.3.1 Design and assembly of Cas9 nickase and Cas9 wild-type plasmids

Three CRISPR strategies, two using Cas9 nickase (Cas9n) and one using Cas9 wild-type (Cas9wt), were designed to target the N279K mutation locus in tau exon 10, following the protocol of Ran et al. (2013b). For both the Cas9n strategies, two gRNA sequences ("left" and "right") were chosen using a CRISPR design tool (http://crispr.mit.edu/). The input sequence was 242bp centred on tau exon 10: 80bp of intron 9, exon 10 (93bp) and 45bp of intron 10. The Cas9wt gRNA location was chosen by inspection of the DNA sequence of tau exon 10 and checked with the CRISPR design tool to check for off-target matches. The choice of gRNA sequences was limited by the need for: a PAM sequence (bases NGG, where N is any base) immediately downstream of the gRNA sequence; DSB proximity to the N279K mutation locus; and a 0-20bp offset between the gRNA sequences for Cas9n (Ran et al., 2013b).

For both Cas9n strategies, four single-stranded DNA oligomers (left and right, sense and anti-sense) were obtained (Sigma). The anti-sense strand of the left pair and the sense strand of the right pair would act as gRNA in the left and right Cas9n plasmids. For the Cas9wt strategy, two single-stranded DNA oligomers were required, in which the sense strand would act as the gRNA (Table 5.2).

The oligomers were diluted to 100µM with ddH_2O. One µl sense and anti-sense oligomers were mixed with 8µl of ddH_2O and annealed (95ºC for five minutes, cooling down to 25ºC at 5ºC/minute). This formed left and right gRNA oligomers with overhanging sequences for ligation into Cas9 plasmids. One µl of 1µg/µl Cas9n plasmid (#48141, Addgene, pSpCas9n(BB)-2A-Puro from Ran et al., 2013) or Cas9wt plasmid (#62988, Addgene, pSpCas9(BB)-2A-Puro from Ran et al., 2013) was digested with 1µl Bbs1, 2µl 10x Buffer 2.1 (both New England Biolabs) and 16µl ddH_2O for three hours at 37°C. 1 µl of either left or right annealed oligomers (for Cas9n) or the annealed oligomers (for Cas9wt), 1.5µl T4

Table 5.2 **Oligomer sequences for incorporation into Cas9 plasmids.**

CRISPR strategy	gRNA	Strand	Sequence
1 (nickase)	Left	Sense	AAACGTCCAAGTGTGGCTCAAAGGC
		Anti-sense	CACCGCCTTTGAGCCACACTTGGAC
	Right	Sense	CACCGAATATCAAACACGTCCCGGG
		Anti-sense	AAACCCCGGGACGTGTTTGATATTC
2 (nickase)	Left	Sense	AAACTGCGAGCAAGCAGGCGGGTCC
		Anti-sense	CACCGGACCCGCCTGCTTGCTCGCA
	Right	Sense	CACCGGTGTCACTCATCCTTTTTTC
		Anti-sense	AAACGAAAAAAGGATGAGTGACACC
3 (wild-type)	-	Sense	CACCGGCAGATAATTAATAAGAAGC
		Anti-sense	AAACGCTTCTTATTAATTATCTGCC

Sequences are written 5' to 3'. Underlined bases are sequences for ligation, which were digested with the restriction enzyme Bbs1. Each gRNA sequence contains 19 nucleotides homologous to the DNA target, the 1st base in each gRNA is G, which is part of the U6 promotor.

DNA ligase and 1 x T4 ligase buffer (both New England Biolabs) were added to the digestion mixture for three hours at 37°C.

One Shot Stbl3 Chemically Competent E.coli (Invitrogen) were transformed with 1µl left-Cas9n, right-Cas9n or Cas9wt plasmids by heat shock at 42°C for 45 seconds as described in the manufacturer's instructions. Transformed bacteria were streaked on agar plates containing ampicillin (100µg/ml, Sigma) and incubated overnight at 37°C. Cas9n plasmids contained ampicillin-resistance genes for selection of plasmid-containing bacteria. Single colonies were picked and incubated in 5ml LB medium (Invitrogen) with ampicillin at 37°C, shaking at 225rpm overnight. Plasmid DNA was extracted using a Qiagen miniprep kit: a bacterial cell pellet was collected by centrifugation at 13000g for three minutes and re-suspended in 250µL re-suspension buffer. The cells were lysed and their DNA denatured with 250µL lysis buffer, containing sodium hydroxide and sodium dodecyl sulfate (SDS). Cell debris were precipitated with 350µL high-salt buffer and pelleted by centrifugation at 17000g for 10 minutes. The supernatant, containing plasmid DNA, was centrifuged at 17000g for 60 seconds in a spin column. DNA bound to the spin column was washed with 750µL PB buffer, then with 750µL PE buffer and centrifuged at 17000g for 60 seconds to remove remaining high salt buffer. Bound DNA was eluted with 30µL water and stored at -20°C. gRNA incorporation into the Cas9n plasmids was confirmed by Sanger sequencing (Source Bioscience) with the primer U6-Fwd (Table 5.3).

Table 5.3 **Primers used for PCR and sequencing.**

Primer name	Sequence	F/R	Reference
U6-Fwd	GAGGGCCTATTTCCCATGATTCC	F	[1]
073	GGGGTACCAATCCCAGCTTCGTAAAGCCCGCT	F	[2]
074	CGGGATCCTCATCTGCCCTATTCTGTCCACACA	R	[2]
E75	TCGAAAGTGGAGGCGTCCTT	F	-
REV83	GCATGGGACGTGTGAAGGTA	R	-

Sequences are written 5' to 3'. All primers were ordered from Sigma. References: [1]: Source Bioscience (www.sourcebioscience.com); [2]: Anfossi et al. (2011).

For transfection, DNA was amplified from 50ml overnight cultures of transformed bacteria. Plasmid DNA was purified using an endonuclease-free maxiprep kit (Qiagen): a bacterial cell pellet was collected by centrifugation at 6000g for 15 minutes at 4°C and re-suspended in 10ml re-suspension buffer. The cells were lysed and their DNA denatured with 10ml lysis buffer, then cell debris were precipitated with 10ml high-salt buffer and removed by filtration. The lysate was incubated on ice for 30 minutes with 2.5ml endotoxin removal buffer to prevent bacterial lipopolysaccharides binding to the DNA-binding column. The lysate was filtered through a Qiagen column by gravity to bind plasmid DNA. Bound DNA was washed and subsequently eluted with 15ml high-salt buffer. Plasmid DNA was precipitated with isopropanol and collected by centrifugation at 15000g for 10 minutes. The DNA pellet was washed with endotoxin-free ethanol, centrifuged at 15000g for 10 minutes and then air-dried. Plasmid DNA was re-suspended in 50µL ddH_2O and stored at -20°C.

5.3.2 Homology directed repair templates

Single-stranded repair template for CRISPR 2

A 153bp sense ssODN (sequence below), centred on the right nick site, with the N279K mutation (red nucleotide) and the left PAM mutation (green nucleotide), was ordered from Integrated DNA Technologies as a 4nM, desalted, non-PAGE purified ultramer and diluted under sterile conditions with ddH_2O to 10µM for transfection. The position of the N279K mutation locus relative to both PAM sites is shown in Figure 5.6.

ssODN sequence:

5'-TCCAGGGTGGCGCATGTCACTCATCGAAAGTGGAGGCGTGCTTGCGAGCAAGCAGG

CGGGTCCAGGGTGGCGTGTCACTCATCCTTTTTTCTGGCTACCAAAGGTGCAGATAATT
AAGAAGAAGCTGGATCTTAGCAACGTCCAGTCCAAGTG-3'

Single-stranded repair template for CRISPR 3

Two 100bp sense ssODNs (sequences below), centred on the N279K mutation, were ordered from Integrated DNA Technologies as 4nM, desalted, non-PAGE purified ultramers. One ssODN had the N279K mutation (red nucleotide):

5'-TGGCGTGTCACTCATCCTTTTTTCTGGCTACCAAAGGTGCAGATAATTAAGAAGA
AGCTGGATCTTAGCAACGTCCAGTCCAAGTGTGGCTCAAAGGATAA-3'

The other ssODN had the control sequence (blue nucleotide):

5'-TGGCGTGTCACTCATCCTTTTTTCTGGCTACCAAAGGTGCAGATAATTAATAAGA
AGCTGGATCTTAGCAACGTCCAGTCCAAGTGTGGCTCAAAGGATAA-3'

ssODNs were diluted under sterile conditions with ddH_2O to 10µM for transfection.

5.3.3 iPSC transfection by electroporation

iPSCs were transfected by electroporation, using the Amaxa electroporation system as described by Petersen et al. (2017). Petersen et al. used program CA137, whereas Byrne et al. (2014b) and Yang et al. (2014) used program CB150 for iPSCs. To optimise electroporation conditions, programs were compared by electroporating CTRL2 iPSCs with either the CRISPR 2 plasmids and ssODN, or without CRISPR components and allowing the iPSCs to recover without puromycin selection. Twenty-four hours after electroporation, the number of attached iPSCs was compared: there were more attached iPSCs in the CA137 wells than the CB150 wells, so program CA137 was chosen for electroporation.

ssODN concentration was optimised by comparing the number of attached iPSCs 24 and 48 hours after electroporation with 50pmol or 100pmol ssODN. There was no difference in the number of surviving cells between these ssODN concentrations, as judged by eye.

Puromycin selection was optimised by electroporating CTRL2 iPSCs with CRISPR plasmids (+) or without plasmids (-), then dividing each batch of electroporated iPSCs into four wells. After recovery for 24 hours, + and - iPSCs were exposed to 0.5, 0.25 or 0.125 µg/ml puromycin for 48 hours. The fourth wells of + and - iPSCs were left without selection

as controls. Four days after puromycin selection ended, some iPSC colonies were present in all + wells and in the 0.25 and 0.125µg/ml - wells. No iPSC colonies were present in the - 0.5µg/ml puromycin well, indicating that 0.5µg/ml puromycin is sufficient to kill iPSCs electroporated without plasmids but does not kill iPSCs expressing the plasmids.

Twenty-four hours before transfection, iPSC medium was changed to KSR without pen-strep and with 10µM ROCK inhibitor to improve iPSC survival. On the day of transfection, iPSCs were lifted from the MEF layer with collagenase-dispase, as described in Section 2.2.2 and dissociated to 2-3 cell clumps with Accutase. For each transfection $2x10^6$ iPSCs, 100µl P3 solution plus Nucleofector supplement (Lonza Transfection Kit) and 8µg of 1µg/µl DNA were mixed in a plastic cuvette. The DNA mixture contained 100pmol (1µl 10µM) ssODN, with either 8µg of 1µg/µl Cas9wt or 4µg of 1µg/µl or each of left and right Cas9n. Electroporation was performed with an Amaxa Nucleofector, program CA 137. After electroporation, cells were left to recover for 5 minutes at room temperature and then plated onto neomycin- and puromycin-resistant irradiated MEFs (DR4, Applied StemCell) in pen-strep-free KSR with 10µM ROCK inhibitor (Figure 5.3). Twenty-four hours later, the medium was changed to KSR with FGF2 (4ng/ml). Forty-eight hours after transfection, puromycin (0.5µg/ml, Life Technologies) was added to the media for 48 hours, to select for iPSCs transfected with Cas9 plasmids, which contain puromycin-resistance cassettes. Puromycin also killed the MEFs, so new MEFs were added after puromycin selection to support iPSC colony growth. When colonies became visible, they were picked and transferred to 48-well plates for expansion, then picked again and transferred to 48-well plates to create duplicates. After picking, transfected iPSCs were detached from the MEF layer with collagenase-dispase, as described in Section 2.2.2 and cell pellets were collected by centrifugation. DNA was extracted with 10µl QuickExtract solution (Epicentre) by incubation at 65°C for 30 minutes, then at 90°C for 15 minutes. DNA in QuickExtract was diluted 1:10 in ddH_2O as a PCR template.

5.3.4 PCR for mutation screening

The primers 073 and 074 (Table 5.3) were used to amplify a 642bp region including tau exon 10 from genomic DNA extracted from edited iPSC colonies. Five µl 10x Pfu buffer with Mg^{2+}, 1µl Pfu DNA polymerase (both Thermo Scientific), 1µl 10mM dNTPs (Invitrogen), 2.5µl each of 10µM forward and reverse primers, 1µl DNA template (DNA in QuickExtract, diluted 1:10 in ddH_2O) and 37µl ddH_2O were mixed in a PCR tube. The PCR cycle was

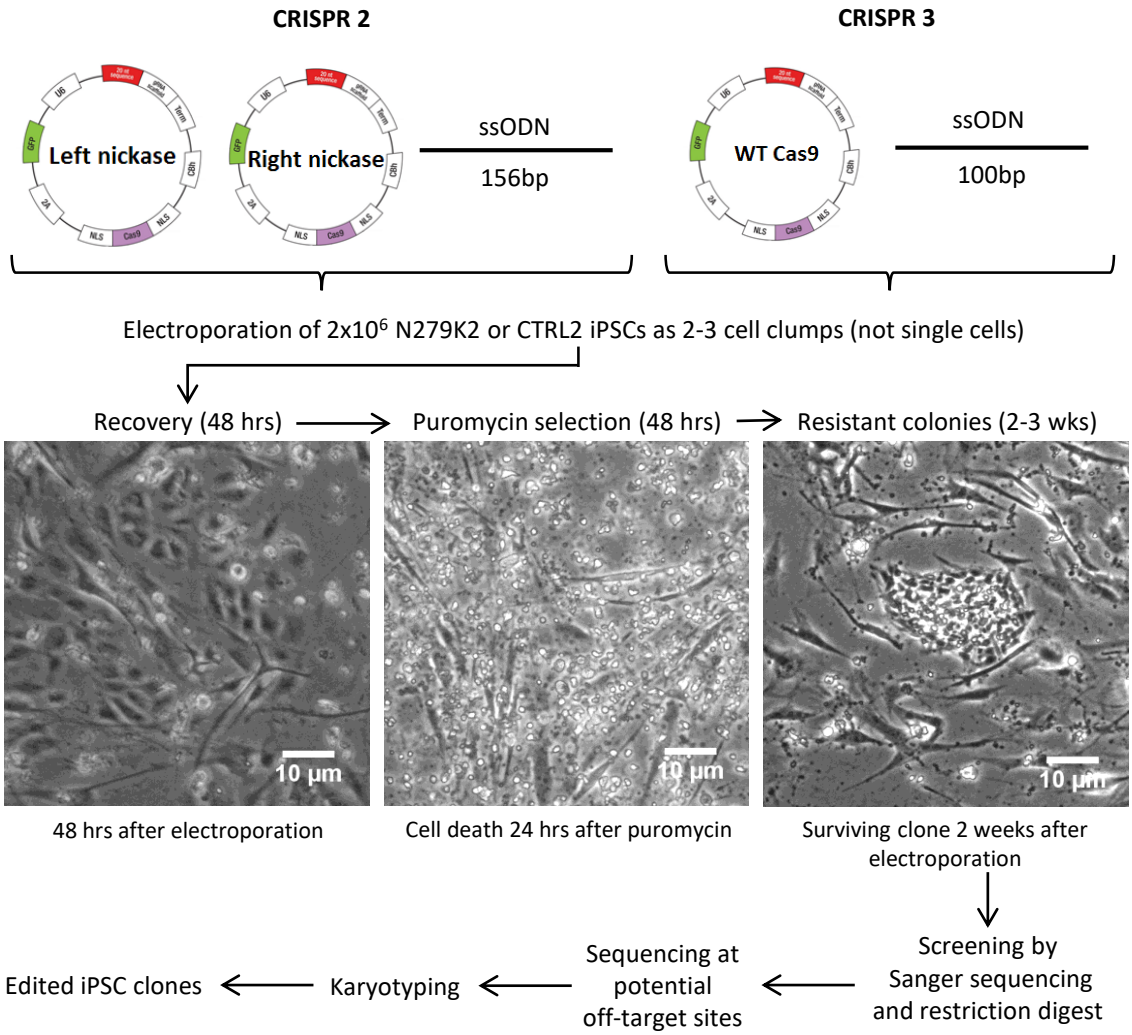

Fig. 5.3 **Workflow for gene editing in iPSCs using CRISPR.** The left and right Cas9n plasmids (CRISPR 2) or the Cas9wt plasmid (CRISPR 3) and the ssODN repair template, were electroporated into a suspension of iPSCs consisting of 2-3 cell clumps. Cas9n and Cas9wt plasmids contained a puromycin resistance cassette for antibiotic selection. iPSCs were then plated onto MEFs and allowed to recover for 48 hours before selection with puromycin. Images (left to right) show iPSCs on MEFs after electroporation; high levels of cell death following puromycin selection, after which new MEFs were added to support iPSC colony growth; the emergence of a surviving CTRL2 iPSC colony after selection. The surviving colonies were then screened by sequencing DNA with Sanger sequencing or restriction digest. Edited colonies would be checked for a normal karyotype and off-target edits. Scale bar = 20µm.

4 minutes at 95°C, then 35 cycles of 1 minute at 95°C, 1 minute at 60°C and 3 minutes at 72°C, followed by 10 minutes at 72°C.

5.3.5 Mutation screening by restriction digest

After PCR, DNA was purified using a Qiagen Gel Extraction kit. The PCR product was mixed with three 150µl of high-salt buffer QG and 50µl of isopropanol. The sample was centrifuged in a QIAquick column at 17000g for one minute to bind the DNA to the column. The DNA was washed with 500µL buffer QG and centrifuged at 17000g for one minute to remove excess agarose, then washed with 750µL buffer PE and centrifuged at 17000g for one minute to remove remaining salts. DNA was eluted by incubation with 10µL ddH_2O and centrifugation at 17000g for one minute, then the DNA concentration was measured with a Nanodrop spectrophotometer (Thermo Fisher).

One µg purified DNA was added to 1µl BsaH1 (for CRISPR 2) or 1µl AseI (for CRISPR 3) in 5µl 10x CutSmart buffer (all New England Biosciences) and ddH_2O up to 50µl. The mixtures were incubated for 3 hours at 37°C, then 16 hours at 18°C for digestion. 15µl digestion mixture was mixed with 6x DNA Loading Dye (Fermentas) and loaded into the wells of a 0.8% agarose gel in 1x Tris-Borate-EDTA buffer for gel electrophoresis at 120mV for one hour. Digested products were run next to their undigested counterparts. For CRISPR 3, a positive control (N279K2 iPSCs) and negative control (CTRL2 iPSCs) were also included. After electrophoresis, colony genotype was established by comparing the digested and non-digested lanes. For CRISPR 3, 642bp band intensity was compared to 358bp and 284bp band intensity using ImageJ, as described for Western Blot quantification in Section 2.6.5.

5.3.6 Mutation screening by Sanger Sequencing

PCR products were mixed with 6x DNA Loading Dye and loaded into the wells of a 0.8% agarose gel in 1x Tris-Borate-EDTA buffer (Merck) for gel electrophoresis at 120mV for one hour. The 642bp band was excised and DNA was extracted using a Qiagen Gel Extraction kit. The gel was dissolved in high-salt buffer QG and isopropanol. The amount of high-salt buffer QG buffer was calculated by weighing the excised gel, then adding 3µl of buffer for every mg of gel. The amount of isopropanol used was 1µl for every mg of gel. For example, a gel weighing 100mg required 300µl of high-salt buffer QG and 100µl of isopropanol. Gel extraction was then performed as described in Section 5.3.5.

For CRISPR 3, Mariagrazia Paonessa performed approximately 25% of the PCR reactions and gel electrophoreses.

The DNA concentration was measured with a Nanodrop spectrophotometer and adjusted to 10ng/µl with ddH_2O. DNA was sequenced with primers E75 and Rev83 (Table 5.3) by Source Bioscience (www.sourcebioscience.com).

5.4 Results

5.4.1 CRISPR nickase strategy 1

The first CRISPR strategy I designed (CRISPR 1 in Table 5.2) targeted tau exon 10 with Cas9 nickases, to increase the chance of HDR (Mali et al., 2013) and to reduce the chance of off-target mutations (Cho et al., 2014; Ran et al., 2013b). The gRNA sequences were chosen with the MIT CRISPR design tool (http://crispr.mit.edu/), which constrains and ranks possible gRNA sequences: 1) the target sequence has minimal similarity to other sequences in the genome; and 2) off-target sequence cleavage is unlikely because similar sequences are either not next to an NGG or NAG PAM, or contain PAM-proximal mismatches (Hsu et al., 2013).

I chose the gRNA pair with the fewest off-target matches that was closest to the N279K mutation locus since proximity to the (offset) DSB is an important factor in point mutation correction (Elliott et al., 1998; Liang et al., 2017; Paquet et al., 2016; Yang et al., 2013). Each gRNA had predicted off-target sequences which could result in single-stranded off-target DNA nicks but together, the gRNA pair had no predicted off-target sites (Figure 5.4). Counting the first nucleotide of exon 10 as nucleotide 1, the gRNA targeted nucleotides 42-61 (left) and 64-83 (right). This gives a 5' overhang required for efficient nicking and a 2bp offset between the sequences, which is within the optimal 0-20bp (Ran et al., 2013; Figure 5.4). The nickases would make cuts between nucleotides 80 and 81 on the anti-sense DNA strand (right nick) and between nucleotides 44 and 45 on the sense strand (left nick), 29 base pairs from the N279K mutation locus.

To precisely induce the N279K mutation, I designed a repair template consisting of tau exon 10 DNA in a pcDNA3 plasmid. The repair template contained sequences complementary to the gRNA and therefore could be cut by the left and right nickases. To prevent this, I added blocking mutations which block Cas9n from recognising the gRNA sequence after it has been corrected. I added a silent mutation at the left PAM, because PAM mutations decrease Cas9 cleavage approximately 500-fold (Cho et al., 2014). The mutation (39C→G,

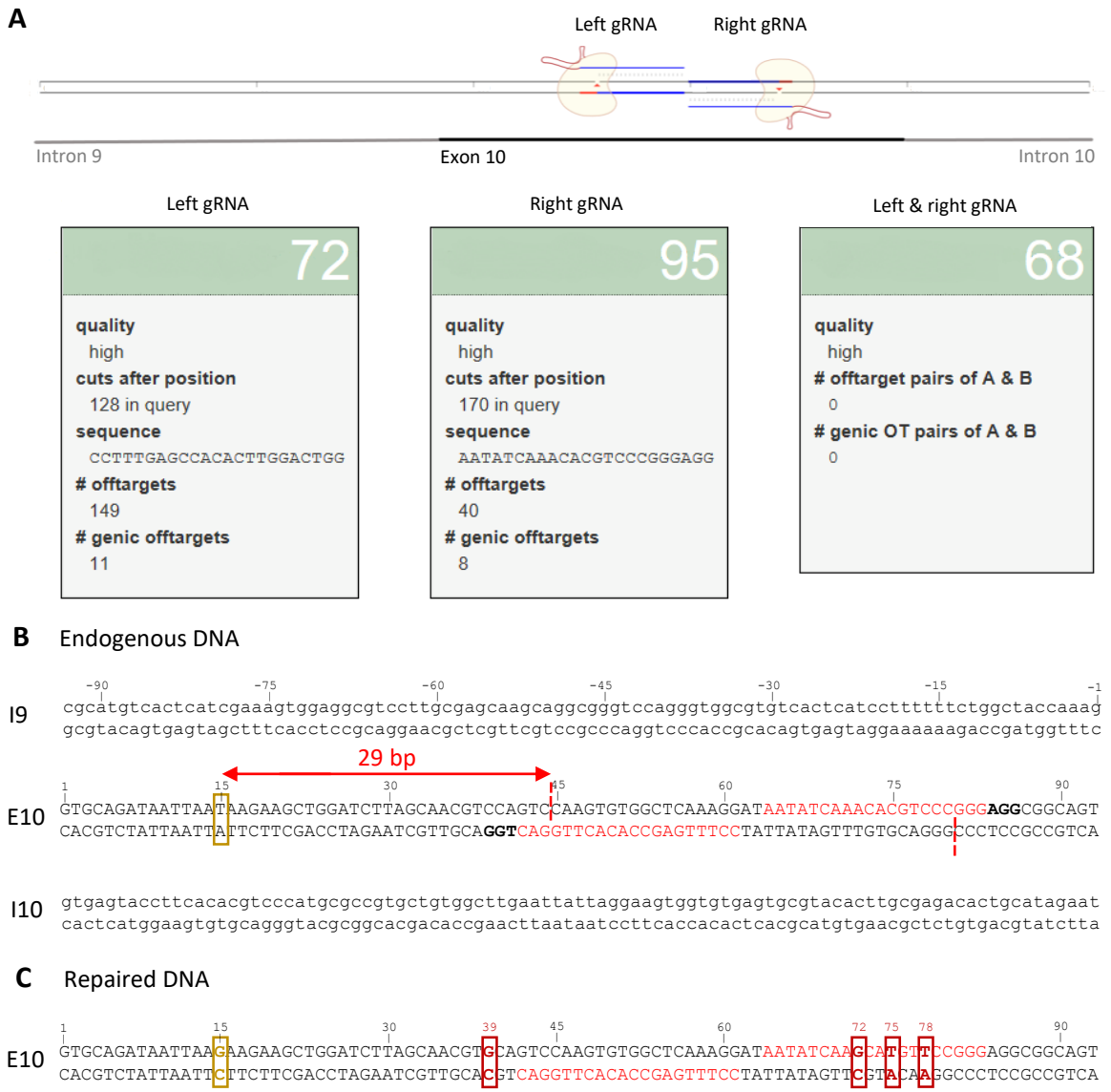

Fig. 5.4 **gRNA sequences for CRISPR 1. A)** Schematic diagram of two gRNA sequences for CRISPR 1 on the antisense (left gRNA) and sense (right gRNA) DNA strands. Red arrows indicate DNA cut sites. Green boxes show gRNA sequences, the number of off-target sites with sequence homology to each gRNA and the number of off-target sites for the gRNA pair. Diagram from the MIT CRISPR design tool. **B)** and **C)** Detailed representation of CRISPR 1. Double-stranded DNA of exon 10 (E10, upper case) and flanking regions of introns 9 and 10 (I9 and I10, lower case) are shown. Nucleotides in exon 10 are numbered, counting the first nucleotide as 1. **B)** Control DNA with the N279K mutation locus at nucleotide 15 in exon 10 (yellow box). The 20bp gRNA target sites (red nucleotides) match the gRNA: the left gRNA matches the anti-sense strand and is complementary to the sense strand, whilst the right gRNA matches the sense strand and is complementary to the anti-sense strand. Nickase cut sites (red dotted lines) are 3bp upstream of the PAM (bold font) on the complementary DNA strand. A red arrow indicates the distance (29bp) between the Cas9n cut site and the N279K mutation locus. **C)** Control DNA after editing. The induced N279K mutation is at nucleotide 15 (yellow box), the left PAM mutation is at nucleotide 39 (dark red box) and prevents repaired DNA being recut by the nickase. The right gRNA mutations are at nucleotides 72, 75 and 78 (dark red box) where they prevent the right gRNA binding.

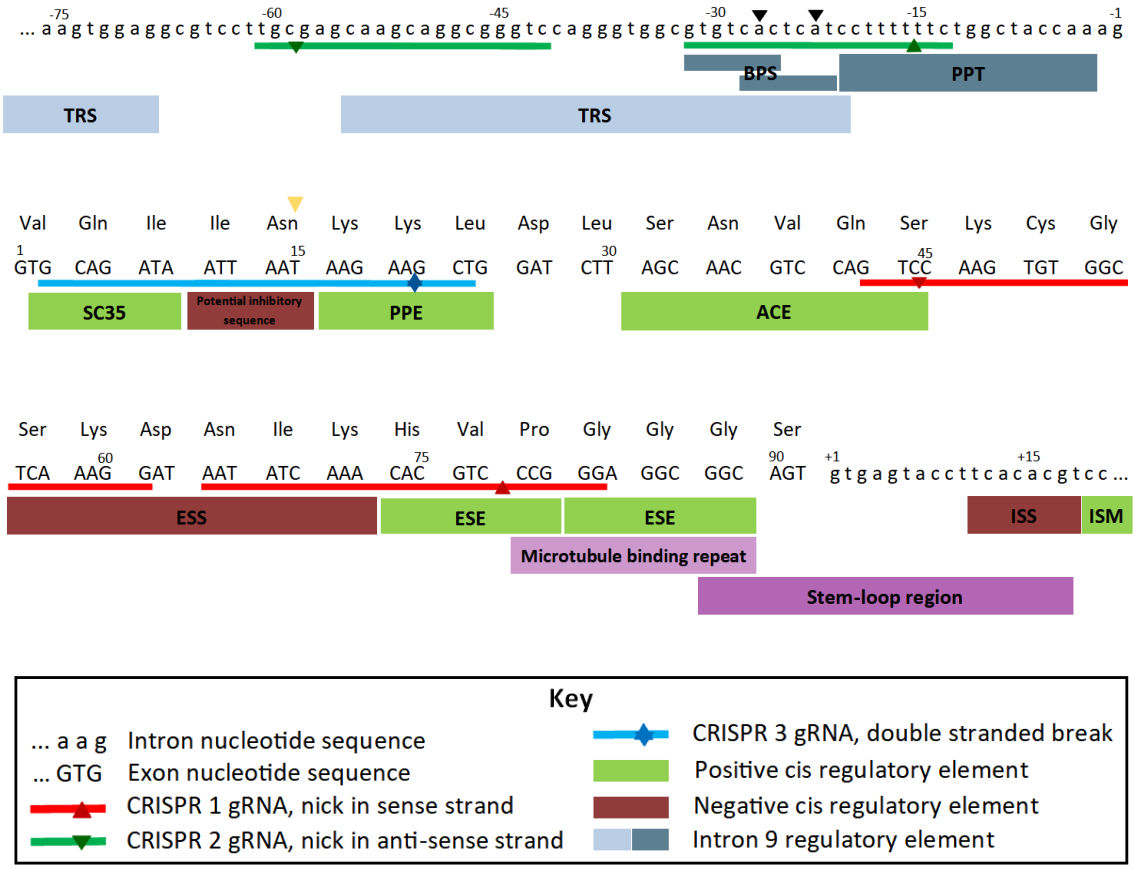

Fig. 5.5 **Cis regulatory sequences in tau exon 10.** Introns 9 and 10 are lower case, exon 10 is upper case. Nucleotides are numbered, counting the first nucleotide of exon 10 as 1, the first nucleotide upstream of exon 10 in intron 9 as -1 and the first nucleotide downstream of exon 10 in intron 10 as +1. Exon 10 amino acids are shown above the corresponding codons. Labelled bars represent nucleotide sequences that influence exon 10 splicing. Intron 9 contains two tandem repeat sequences (TRS, blue bars), two possible branch point sequence sites (BPS, teal bars) with critical "a" nucleotides indicated by black arrowheads, and a polypurine tract (PPT, thick teal bar). Exon 10 contains four splicing enhancers (green bars): a SC35-like binding sequence (SC35), a polypurine enhancer (PPE), an A/C rich element (ACE), two exon splicing enhancers (ESEs), a potential inhibitory sequence (maroon bar), and an exon splicing silencer (ESS, maroon bar). Exon 10 also a microtubule binding repeat (grey-purple bar). The stem loop region (purple bar) spans the exon 10/intron 10 boundary. Intron 10 contains a potential intron splicing silencer (ISS, maroon bar) and an intron splicing modulator (ISM, green bar). The N279K mutation locus (nucleotide 15) is marked with a yellow arrowhead. gRNA target sites are shown by red (CRISPR 1), green (CRISPR 2) or blue (CRISPR 3) lines. Arrows on these lines indicate Cas9 nicking sites: downwards arrows show a nick site on the sense DNA strand, upwards arrows show a nick on the anti-sense strand.

Figure 5.4) would be a non-coding mutation in valine 287 (using numbering for the longest 4R tau isoform).

The right PAM site could not be silently mutated, so I added three silent blocking mutations in the right gRNA recognition sequence since having three non-consecutive mismatches between the DNA and gRNA is reported to reduce Cas9 cleavage (Hsu et al., 2013). The three mutations (72A→G, 75C→T, and 78C→T, Figure 5.4), would be non-coding mutations in lysine 298, histidine 299, and valine 300 (using numbering for the longest 4R tau isoform).

Although the planned silent mutations were not known MAPT mutations, they were in sequences which regulate exon 10 splicing (Figure 5.5). The left PAM 39C→G mutation was in the A/C rich splice enhancer (ACE), in which the conserved sequence is two or three repeat motifs: either CAA, CCA, or CA (D'Souza and Schellenberg, 2000). A left PAM mutation would decrease the C content of the ACE and disrupt a potential CCA repeat motif, which could decrease exon 10 inclusion in tau mRNA transcripts. However, the effect of mutating this nucleotide on exon 10 inclusion has not been tested.

The right gRNA recognition sequence mutation 72A→G was in an exon splicing silencer (ESS), which was detected in deletion experiments by D'Souza and Schellenberg (2000), between 55T and 72A. Simultaneous mutation of 70A→G, 71A→C and 72A→T significantly increased exon 10 inclusion in a splicing assay, indicating that the ESS purine content is important for exon silencing (D'Souza and Schellenberg, 2000). This result suggests that the 72A→G mutation could also increase exon 10 inclusion, although this mutation has not been tested.

The right gRNA recognition sequence mutations 75C→T and 78C→T were in two adjacent exon splicing enhancers (ESEs), which were detected when their deletion decreased exon 10 inclusion in a splicing assay (D'Souza and Schellenberg, 2000, 2002). However, the 75C→T and 78C→T mutations have not been specifically tested for their effects on tau splicing.

I checked these potential mutation sites against the single nucleotide polymorphism (SNP) database (dbSNP, https://www.ncbi.nlm.nih.gov/snp/), to determine if any were common SNPs not linked to FTDP-17T, even if they occurred in exon 10 splicing regulatory sequences. The 72A→G and 78C→T mutations are not SNPs but 75C→T and 39C→G are. 75C→T is SNP rs147401702, which occurs in 0.00051230% of genomes in dbSNP and it is not reported as clinically significant, although this does not mean it has no effects on exon 10 splicing. 39C→G is SNP rs1275756209, which has no associated frequency information in dbSNP and is also not reported as clinically significant.

All the silent blocking mutations I planned had the potential to alter tau exon 10 splicing, which would alter the 3R to 4R tau ratio in CRISPR-edited iPSC-derived neurons. To avoid this, I designed a second CRISPR strategy.

5.4.2 CRISPR nickase strategy 2

I re-designed the CRISPR nickase strategy by using the MIT CRISPR design tool to choose a gRNA pair which did not overlap with exon 10 (CRISPR 2 in Table 5.2) and chose the pair with the fewest off-target matches, which made nicks closest to the N279K mutation locus (Figure 5.6). CRISPR 2 targeted nucleotides -61 to -43 (left gRNA) and -32 to -13 (right gRNA) in intron 9, counting nucleotides backwards from the start of exon 10, which gave a 5' overhang required for efficient nicking and an 11bp offset between the gRNAs, which is within the optimal 0-20bp (Ran et al., 2013b). The nickases would cut between nucleotides -58 and -59 (left nickase) and between nucleotides -16 and -15 (right nickase), 30bp from the N279K mutation locus. Although each gRNA had off-target sequence matches (Figure 5.6), the gRNA pair had no off-target matches.

The right gRNA sequence overlapped with two intron 9 regulatory elements: the poly-purine tract (PPT) and branch point sequence (BPS), which are present in mammalian intron 3' splice sites (D'Souza and Schellenberg, 2002). Right PAM mutations in the repair template were therefore not possible without potentially altering exon 10 splicing (Figure 5.5). Furthermore, the right PAM sequence (nucleotides -10, -11 and -12) includes two loci associated with exon 10 splicing: a G→T mutation at nucleotide -10 has been found in three individuals with FTDP-17T (Malkani et al., 2006) and a G→T mutation at -11, in combination with mutations of G→T at -10 and A→T at -7 causes constitutive exon 10 inclusion in a splicing assay (D'Souza and Schellenberg, 2002). In addition, there are no SNPs reported at position -11 in dbSNP.

The left gRNA sequence overlapped with part of an intron 9 tandem-repeat sequence which spans nucleotides -21 to -55 and -69 to -116 (D'Souza and Schellenberg, 2002; Poorkaj et al., 2001; Figure 5.5). The significance of this sequence is unclear but its exclusion does not alter exon 10 splicing in a splicing assay: D'Souza and Schellenberg (2002) transfected COS-7 cells, PC12 cells and rat neurons with constructs encoding either 1) 567bp of intron 9, plus exon 10 and 190bp of intron 10; or 2) 33bp of intron 9, plus exon 10 and 51bp of intron 10; and found that exon 10 expression was the same with both constructs. The left PAM (on the anti-sense strand) contains two C nucleotides (G on the anti-sense strand) at positions -63 and -64, neither of which have associated SNPs, according to dbSNP. A left

Fig. 5.6 **gRNA sequences for CRISPR 2.** **A)** Schematic diagram of two gRNA sequences for CRISPR 2 on the antisense (left gRNA) and sense (right gRNA) DNA strands. Red arrows indicate DNA cut sites. Green and yellow boxes show gRNA sequences, the number of off-target sites with sequence homology to each gRNA, and the number of off-target sites for the gRNA pair. Diagram from the MIT CRISPR design tool. **B)** and **C)** Detailed representation of CRISPR 2. Double-stranded DNA of exon 10 (E10, upper case) and flanking regions of introns 9 and 10 (I9 and I10, lower case) are shown. Nucleotides in exon 10 are numbered, counting the first nucleotide as 1. **B)** shows control DNA with the N279K mutation locus at nucleotide 15 in exon 10 (yellow box), the gRNA target sites (green nucleotides) and nickase cut sites (green dotted lines) 3bp upstream of the PAM (bold font) on the complementary DNA strand. The green arrow shows the distance (30bp) between the cut site and the N279K mutation locus. **C)** shows control DNA after editing. The induced N279K mutation is at nucleotide 15 (yellow box) and the left PAM mutation is at nucleotide -64 (dark green box), to prevent Cas9n re-cutting the repaired DNA.

A

Potential splice sites | Potential Branch Points | Enhancer motifs | Silencer motifs | Other motifs

HSF Matrices

Sequence Position	cDNA Position	Splice site type	Motif	New splice site	Wild Type	Mutant	If cryptic site use, exon length variation	Variation (%)
37	-67	Acceptor	cgtccttgcgagca	cgtgcttgcgagCA	73.98	72.07	+55	-2.58

B

Potential splice sites | Potential Branch Points | Enhancer motifs | Silencer motifs | Other motifs

ESE Finder matrices for SRp40, SC35, SF2/ASF and SRp55 proteins

Threshold values:
SF2/ASF: 72.98 SF2/ASF (IgM-BRCA1): 70.51 SRp40: 78.08 SC35: 75.05 SRp55: 73.86
Variation expresses the difference between reference and mutant values. Wild Type value is taken as reference.

Sequence Position	cDNA Position	Linked SR protein	Reference Motif (value 0-100)	Linked SR protein	Mutant Motif (value 0-100)	Variation
35	-69	SRp55	ggcgtc (78.15)			Site broken -100

RESCUE ESE hexamers

Predicted PESE Octamers from Zhang & Chasin

Sequence Position	cDNA Position	Reference motif	Motif value (0-100) reference sequence	Mutant motif	Motif value (0-100) mutant sequence	Variation
36	-68	gcgtcctt	30.36			Site broken -100
37	-67	cgtccttg	25.02			Site broken -100

Fig. 5.7 **Potential changes in tau exon 10 splicing which may be caused by a PAM mutation in intron 9.** Results from Human Splicing Finder (HSF) comparing wild-type tau intron 9 with intron 9 plus the left PAM mutation. The sequences input were 103bp of intron 9, exon 10 and 87bp of intron 10. **A)** shows the disruption of a splice acceptor site; **B)** shows the destruction of an ESE and two pESEs.

PAM mutation (C→G at nucleotide -64) would fall between the tandem-repeat sequences and since the smaller construct tested by D'Souza and Schellenberg excluded intron 9 nucleotides upstream of nucleotide -33 without altering exon 10 splicing, the left PAM mutation seems unlikely to alter exon 10 splicing.

To further investigate the potential effects of the left PAM mutation, I used Human Splicing Finder (HSF, http://www.umd.be/HSF/) to predict changes it could cause in splice sites, BPSs, ESEs and ESSs. HSF's predictive ability has been validated with mutations which have been shown to alter splicing *in vivo*: it correctly predicted all 84 mutations tested which disrupt splice sites, 13 out of 14 mutations which inactivated BPSs, 20 out of 20 mutations which altered ESEs or ESSs, and could discriminate between a different set of 36 experimentally validated ESE or ESS altering mutations and 220 SNPs which do not alter ESEs or ESSs (Desmet et al., 2009). HSF is therefore a reasonable tool to predict the splicing effects of a mutation.

HSF detected no significant splicing motif alterations, indicating that the left PAM mutation is unlikely to alter splicing. The four potential changes HSF found are show in Figure 5.7. A potential splice acceptor site was altered, giving a variation of -2.59% between the wild-type and mutant sequences. According to HSF's validation with experimentally determined splice sites, variation of less than 10% is not enough to significantly alter splicing Desmet et al. (2009).

A potential ESE which binds the splicing factors serine/arginine-rich protein 55 (SRp55) and 9G8 was destroyed by the mutation. The reported effects of SRp55 on exon 10 splicing are mixed. Yin et al. (2012) transfected four cell lines with a tau minigene and found that SRp55 expression increased exon 10 inclusion but did not identify SRp55's binding site beyond indicating several possible sites in exon 10. Contrary to this, Wang et al. (2005) expressed SRp55 and a smaller tau minigene in COS cells and reported a decrease in exon 10 inclusion. When Wang et al. deleted nucleotides 8-15 (counting from the first nucleotide of exon 10), SRp55 expression did not decrease exon 10 inclusion, suggesting that SRp55's binding site is in the potential inhibitory sequence identified by D'Souza and Schellenberg (2000), rather than in intron 9.

Finally, two putative ESEs (pESEs) were altered by the left PAM mutation. pESEs were identified by Zhang et al. (2005) by statistical comparison of human exon and intron sequences; out of 2000 identified, 30 have been tested experimentally and 28 were shown to increase exon inclusion, although the pESEs altered by the left PAM mutation have not been tested.

Analysing the effect of the left PAM mutation did not find strong evidence for a critical role in exon 10 splicing, which would be grounds to avoid this mutation. The analysis did indicate potential splicing alterations, so I decided to introduce the left PAM mutation into the HDR template alongside the N279K mutation and to test its effects in CRISPR-corrected iPSC-derived neurons.

To induce the N279K mutation I designed a single-stranded DNA template since ssODNs are less likely to be randomly inserted into the genome than double-stranded plasmid templates (Chen et al., 2011). Since homology between the DNA and ssODN is required for efficient editing, I sequenced DNA from CTRL2 iPSCs to check for SNPs in the region covered by the ssODN that could act as blocking mutations. This revealed one SNP (rs41543317) at position -176 (counting backwards from the 3' end of intron 9 as -1) which was outside the homology region.

ssODNs for inserting small insertions or point mutations are most efficient when centred on the mutation, with homology arms between 40bp (Chen et al., 2011; Liang et al., 2017) and 35bp (Yang et al., 2013) on each side. Therefore, I designed a 153bp sense ssODN, with the left PAM mutation and the N279K mutation. The ssODN position with respect to the mutation loci was determined by comparing the predicted homodimer and hairpin formation of six similar ssODNs, using Oligo Analyser (https://www.idtdna.com/calc/analyzer), to select the ssODN least likely to form secondary structures. The ssODN was longer than the optimal 70-90 nucleotides determined by Yang et al. (2013) but the extra length allowed homologous sequences of 39 nucleotides before the PAM mutation and 35 nucleotides after the N279K mutation locus.

The ssODN was sense rather than anti-sense to minimise ssODN cleavage by Cas9n. The ssODN was complimentary to the left gRNA, so the two sequences could bind but the left PAM mutation would prevent cutting. The ssODN and the right gRNA could not bind, as both sequences were sense.

5.4.3 Transfection of iPSCs with CRISPR 2 nickase components

I chose to transfect iPSCs rather than NPCs because HDR is more likely to occur in dividing cells (Orii et al., 2006; Saleh-Gohari, 2004) and because isogenic iPSCs would give a large supply of cells for differentiation to neurons. Although NPCs are also proliferative and suitable for transfection, repeated transfections would be needed to produce neurons from three independent differentiations, making this a less practical solution.

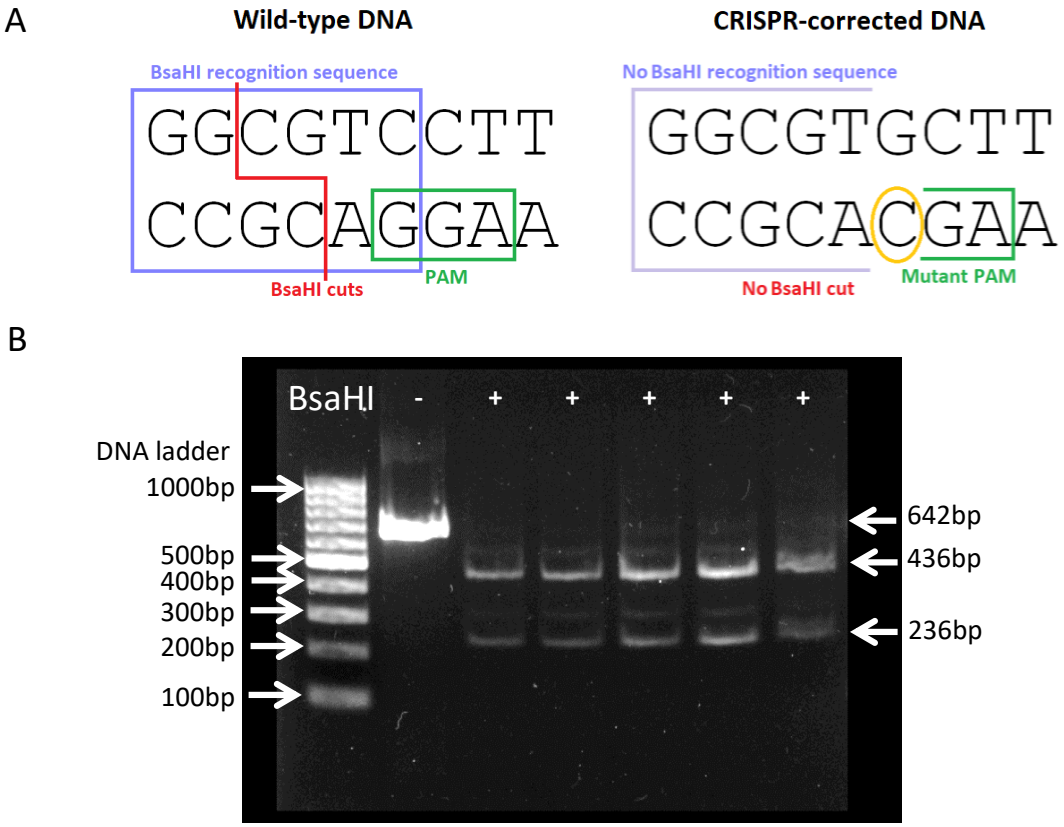

Fig. 5.8 **Screening for CRISPR-corrected iPSC colonies by restriction digest following CRISPR 2. A** The BsaHI recognition sequence (purple box) is present in wild-type DNA, so the DNA is digested (red line). A PAM mutation (yellow circle) disrupts both the PAM (green box) and the BsaHI recognition sequence (purple box), so CRISPR-corrected DNA is not cut. **B** A 642bp segment of DNA containing tau exon 10 and part of the flanking introns 9 and 10 was amplified from iPSC colonies which survived antibiotic selection. The DNA was digested with BsaHI (+) or incubated in the digestion mixture without the enzyme (-) and separated by gel electrophoresis. Representative results are shown: DNA from all colonies was cut by BsaHI.

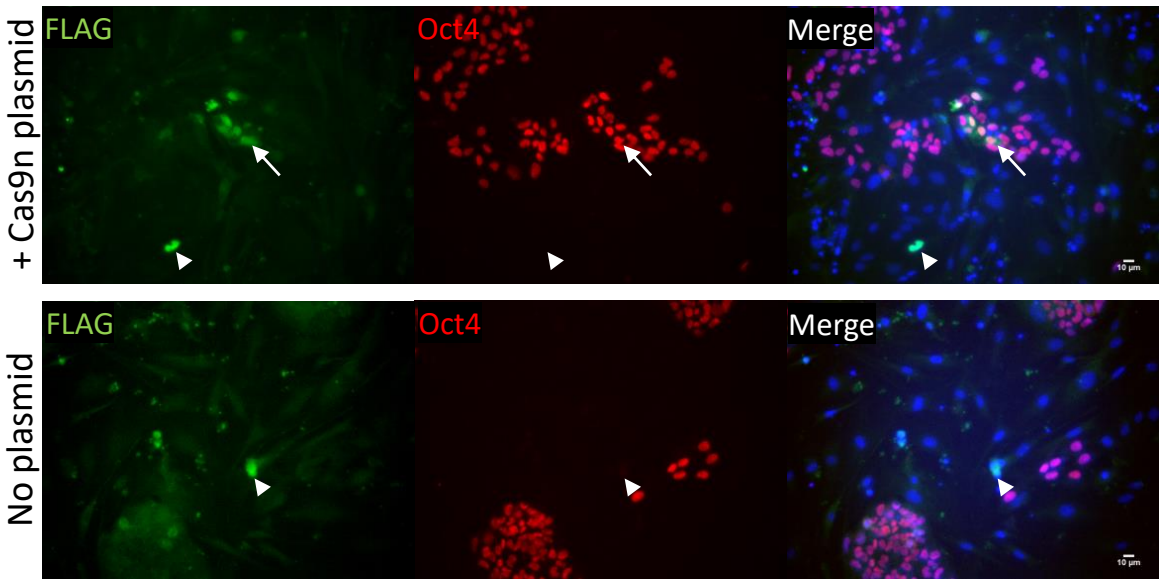

Fig. 5.9 **Immunostaining with the FLAG-M2 antibody was not specific enough to detect FLAG-tagged Cas9 in transfected iPSCs.** iPSC colonies two days after electroporation with either Cas9n or no plasmid. iPSCs are immunostained with the FLAG-M2 antibody to detect the FLAG tag on Cas9n (green) and Oct4 to detect iPSC colonies (red). In the upper panel, an Oct4 positive, FLAG-M2 positive iPSC colony is marked by an arrow. FLAG-M2 staining of iPSCs suggests that the iPSCs had been successfully transfected with Cas9n. In both panels, FLAG-M2 positive, Oct4 negative cells are marked by arrowheads. These cells were either MEFs (which were not transfected with Cas9n) or differentiated iPSCs. The presence of FLAG-M2 immunostaining in the lower panel, where Cas9n had not been introduced, indicates that FLAG-M2 immunostaining was not specific for the FLAG tag, and was therefore not a reliable indication that iPSCs had been successfully transfected with Cas9n. Scale = 10μm.

I chose to transfect CTRL2 iPSCs by electroporation, using the Amaxa electroporation system as described by Petersen et al. (2017), since electroporation gives higher efficiency than lipofection with ssODNs (Ran et al., 2013b). The Amaxa electroporation program, ssODN concentration, and puromycin selection concentration were determined (5.3.3) and the iPSCs were electroporated with the ssODN repair template and the left and right Cas9n plasmids, then transfected iPSCs were selected with puromycin since the Cas9n plasmids contained puromycin-resistance cassettes. Surviving colonies were expanded, DNA was extracted and a 642bp region was amplified by PCR. DNA was subjected to restriction digest using BsaH1, which cuts the wild-type intron 9 sequence but not the introduced G→C PAM mutation. Digested samples were run next to a non-digested control on an agarose gel to visualise mutation insertion. Representative results are shown in Figure 5.8, in which all the DNA samples have been digested, indicating that the PAM mutation was not introduced.

To determine why no left PAM mutations were detected in the edited iPSCs, I checked for Cas9n expression. To do this, I electroporated iPSCs with Cas9n or with no vector, plated them on mouse embryonic feeder cells (MEFs) and allowed colonies to grow without puromycin selection. Two days after electroporation I immunostained for FLAG (since Cas9n had a FLAG-tag) and the pluripotency marker Oct4 to label the iPSCs (Figure 5.9). Some FLAG-M2 immunoreactivity was visible in transfected iPSCs positive for Oct4, although background staining in the green (FLAG-M2) channel was high in the non-transfected iPSCs. In addition, cells with bright fluorescence in the green channel were visible in both transfected and non-transfected wells (arrows in Figure 5.9). These cells were not Oct4 positive, suggesting that they were MEFs or differentiated iPSCs and their presence in both the transfected and non-transfected wells suggests that the FLAG-M2 antibody lacked the specificity to determine whether Cas9n was expressed.

After screening at least 30 colonies by restriction digest and finding them all to be wild-type, I discussed the method with Manousos Koutsourakis and re-designed the CRISPR strategy to maximise DSB proximity to the N279K mutation locus.

5.4.4 Wild-type CRISPR strategy design

I designed a third CRISPR strategy, targeting wild-type Cas9 to tau exon 10 (Figure 5.10). The gRNA sequence was chosen by searching for the closest PAM (NGG) sequence to the N279K mutation locus since mutation efficiency increases with proximity to the DSB (Elliott et al., 1998; Liang et al., 2017; Paquet et al., 2016; Yang et al., 2013). In this case, the DSB would be 5bp from the N279K mutation locus which is within the 8-10bp where DNA editing

is most efficient (Elliott et al., 1998; Liang et al., 2017; Paquet et al., 2016; Yang et al., 2013). The gRNA was checked with the MIT CRISPR design tool for off-target sites, which found 347 potential off-targets, 25 of which were in genes. The chromosomal location, sequence and number of mismatches from the gRNA of the 20 most similar off-target sites are shown in Appendix 1.

The gRNA targeted nucleotides 3 to 23, including the N279K mutation locus at nucleotide 15 (counting the first nucleotide of exon 10 as 1). The PAM was nucleotides 24-26, making the N279K mutation the 9th nucleotide from the PAM, which is at the boundary of the 8-13 nucleotide PAM-proximal seed region (Jinek et al., 2012), in which single nucleotide mismatches between target DNA and gRNA are most effective at preventing Cas9 cleavage Hsu et al. (2013).

I used dbSNP to look for potential blocking mutations in the gRNA seed sequence. There are two SNPs in the PAM sequence at positions 25 (rs1284201310) and 24 (rs1449406929), counting the first nucleotide of exon 10 as 1. Rs1284201310 is a missense mutation but no information on its frequency or clinical significance was available, which discounts it as suitable blocking mutation since it may be a rare, unidentified pathological mutation. Rs1449406929 is a silent mutation at the end of the PPE (Figure 5.5), without frequency or clinical significance listed on dbSNP. Deletion of any of the three nucleotide triplets that make up the PPE decreases exon 10 inclusion (D'Souza and Schellenberg, 2000) and deletion of the first triplet (nucleotides 16-18, Δ280K) causes FTDP-17T (Momeni et al., 2009). Deletion of the second triplet (nucleotides 19-21) is reported as a potentially deleterious SNP on dbSNP (rs1168968788)and SNPs are reported at positions 16 (rs1369606320), 17 (rs755156853), 18 (rs182024939), 22 (rs1340490783), and 24 (rs1449406929), counting from the beginning of exon 10. Deletion of the second triplet and the mutations at positions 17 and 18 are rare, with no information on their pathogenicity. Mutations at positions 16, 22 and 24 have no available data on their frequency or pathogenicity. Given that these SNPs are rare and overlap the PPE, I judged them unsuitable as blocking mutations.

Therefore, I designed two ssODN repair templates: one with the N279K mutation and one wildtype. No blocking mutations were included, depending instead on the single nucleotide difference at the N279K mutation locus to prevent ssODN cutting and re-cutting of edited DNA. The ssODNs were 100 nucleotides long, sense, and centred on the N279K locus.

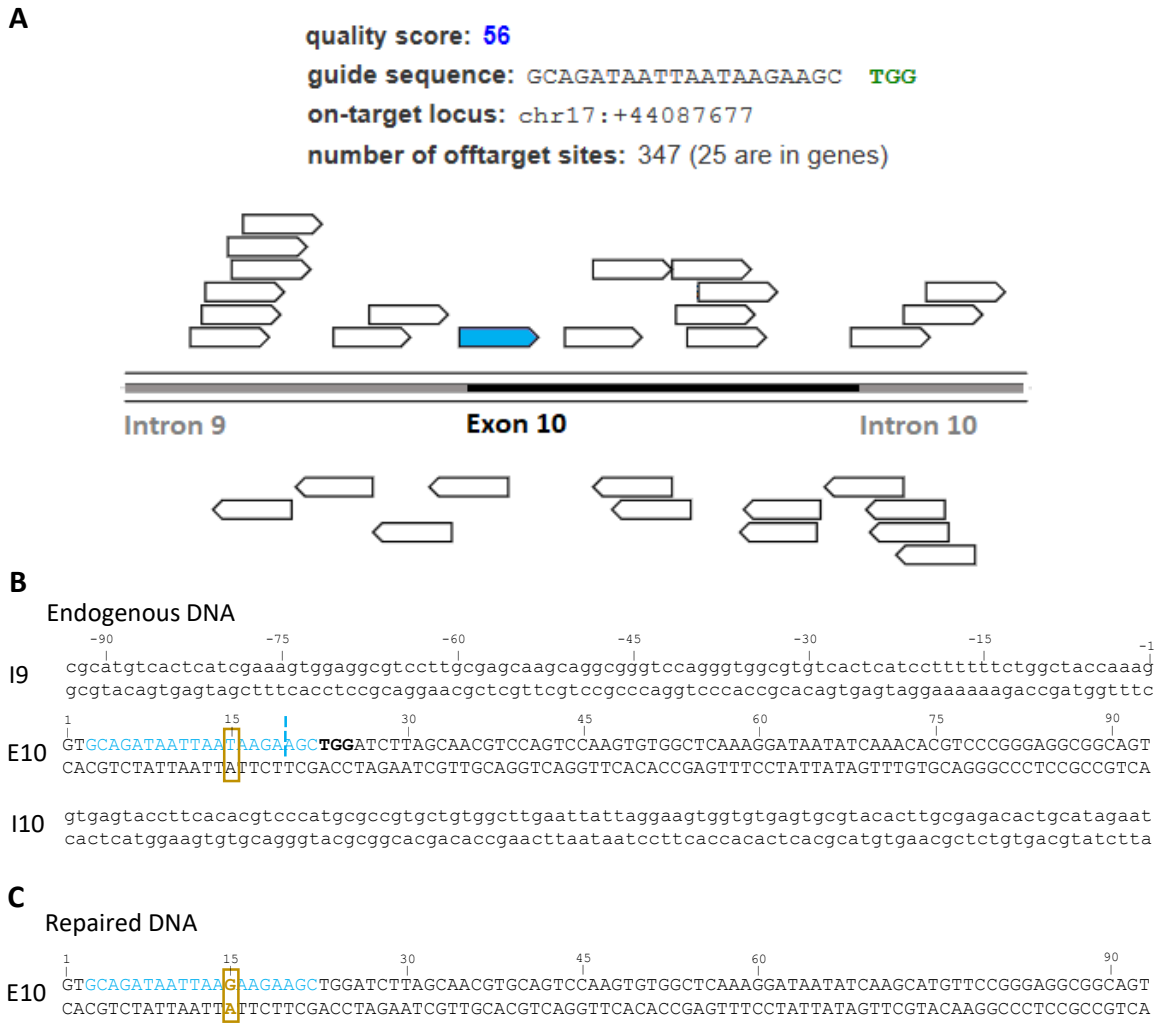

Fig. 5.10 **gRNA sequences for CRISPR 3. A)** Schematic diagram of 30 potential gRNA sequences for CRISPR 3, targeting Cas9wt to the antisense (arrows pointing right) and sense (arrows pointing left) DNA strands. The gRNA closest to the N279K mutation locus is marked in blue. Text shows the gRNA sequence and the number of off-target sites with sequence homology. Diagram from the MIT CRISPR design tool. **B)** and **C)** Detailed representation of CRISPR 3. Double-stranded DNA of exon 10 (E10, upper case) and flanking regions of introns 9 and 10 (I9 and I10, lower case) are shown. Nucleotides in exon 10 are numbered, counting the first nucleotide as 1. **B)** shows control DNA with the N279K mutation locus at nucleotide 15 in exon 10 (yellow box), the gRNA target sites (blue nucleotides), the PAM sequence (bold font) and Cas9 cut site (blue dotted line). **C)** shows control DNA after editing. The induced N279K mutation is at nucleotide 15 (yellow box).

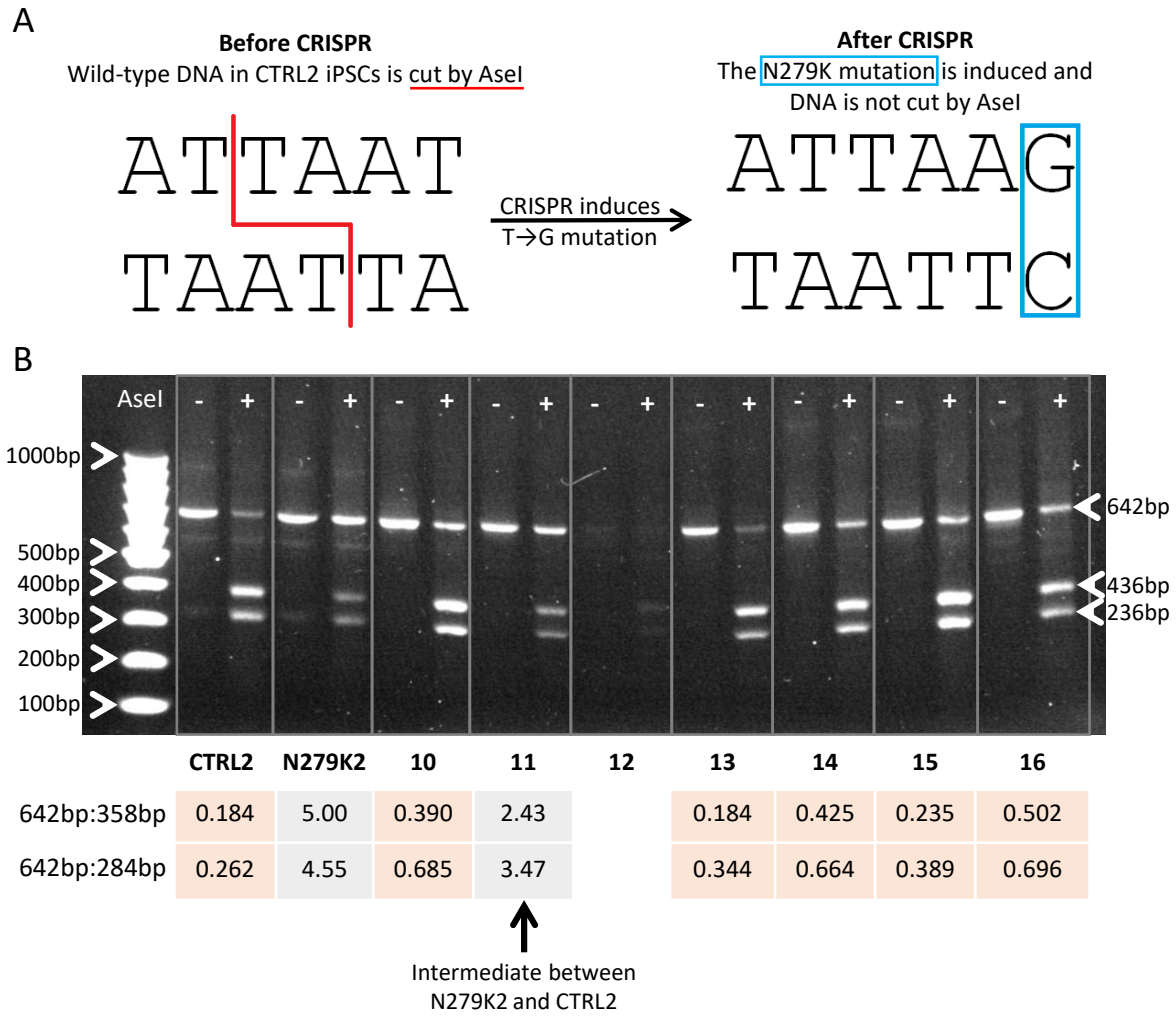

Fig. 5.11 **Screening for CRISPR-corrected iPSC colonies by restriction digest following CRISPR 3. A)** The AseI recognition sequence is present in wild-type DNA, so the DNA is digested (red line). The N279K mutation (blue box) disrupts the AseI recognition sequence, so CRISPR-mutated DNA is not cut. The N279K mutation is heterozygous, so half of the DNA is cut and half is not. **B)** CTRL2 iPSCs were electroporated with CRISPR 3 components and DNA was extracted from colonies which survived antibiotic selection. A 642bp segment of DNA containing tau exon 10 and part of the flanking introns 9 and 10 was amplified and the DNA was digested with AseI (+) or incubated in the digestion mixture without the enzyme (-), then separated by gel electrophoresis. N279K2 and CTRL2 DNA was included as positive and negative controls for the restriction digest. Representative results (samples 10-16) are shown. The ratio between the uncut (642bp) and cut (358bp or 284bp) bands was calculated and ratios from the transfected iPSC colonies were compared to those calculated for wild-type and N279K DNA.

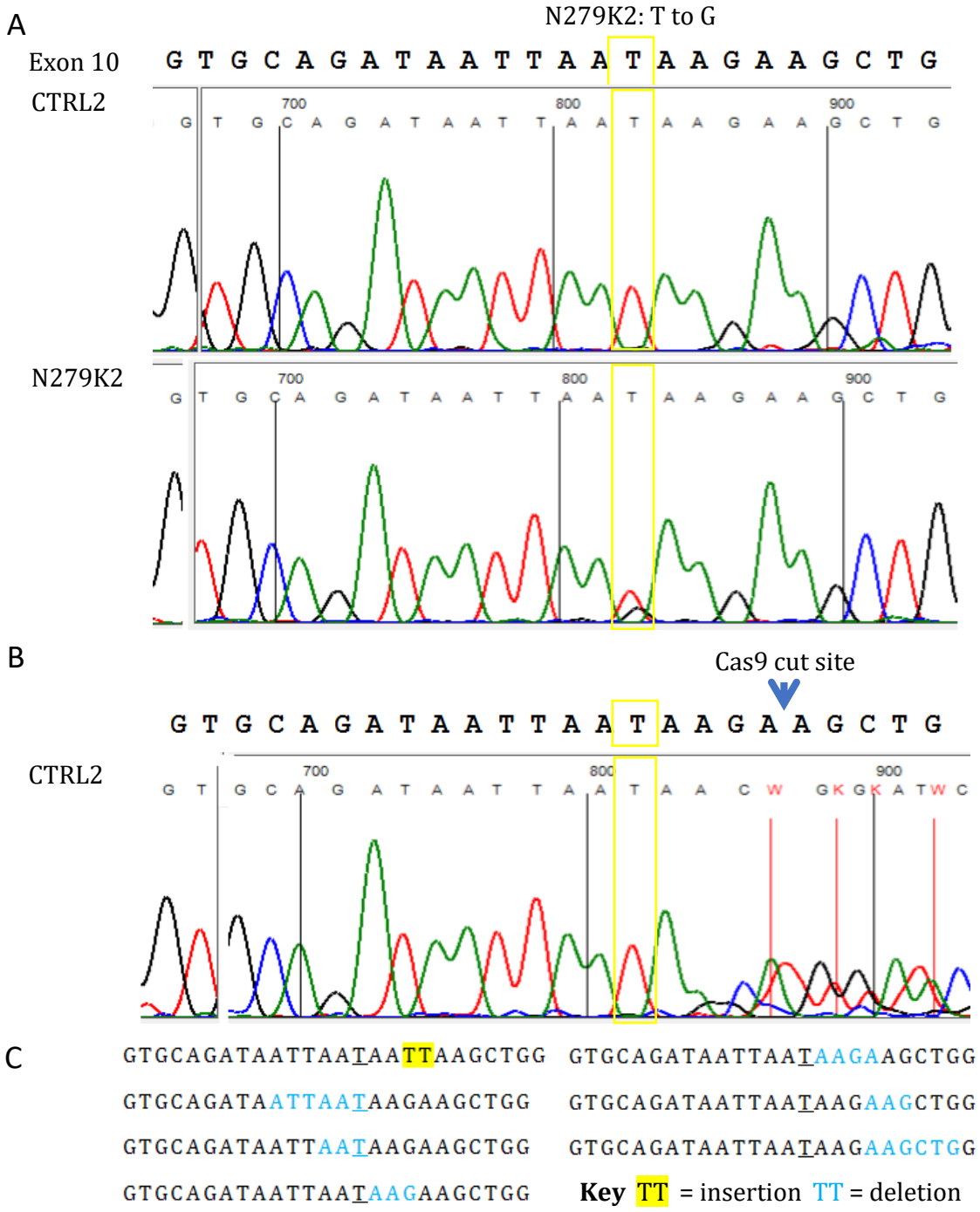

Fig. 5.12 **Screening by Sanger sequencing following CRISPR 3. A)** Sanger sequencing reads from CTRL2 (wild-type) and N279K2 (heterozygous) iPSCs. The N279K mutation locus is highlighted with a yellow box. **B)** Sanger sequencing reads from one CTRL2 iPSC colony after CRISPR. The Cas9 cut site is marked with an arrow. Mixed sequencing reads are visible, starting around the cut site. **C)** Sequences reconstructed from the mixed reads: small deletions and insertions were detected but the N279K mutation was not induced in CTRL2 iPSCs, nor corrected in N279K2 iPSCs.

5.4.5 Transfection of iPSCs with CRISPR 3 components

iPSCs were electroporated with the Cas9wt plasmid and the appropriate ssODN repair template: an ssODN with the N279K mutation was used to induce the N279K mutation in CTRL2 iPSCs, and the wild-type ssODN was used to correct the N279K mutation in N279K2 iPSCs. Following electroporation and recovery, iPSCs were selected with puromycin treatment (5.3.3). Surviving colonies were expanded and then picked: half of each colony was seeded into a new plate and half was kept for DNA extraction. A 642bp DNA region including exon 10 was amplified by PCR, then DNA was purified from the PCR mixture. DNA was subjected to restriction digest using AseI, which cuts wild-type exon 10 but not exon 10 with the T→G N279K mutation. Fifty-two digested samples were run next to their non-digested counterparts on an agarose gel to visualise mutation insertion or correction, alongside non-transfected CTRL2 and N279K2 DNA: the parental iPSC line was a negative control and the other iPSC line (either N279K2 or CTRL2) was a positive control. Most colonies had a digestion pattern like that of the parental iPSC line but some samples had a digestion pattern suggesting that the N279K mutation had been induced (in the CTRL2 iPSCs) or corrected (in the N279K iPSCs).

When the digestion pattern suggested editing, I calculated the ratio of the uncut (642bp) band intensity to the cut (358bp and 284bp) band intensity using ImageJ and compared this ratio to that of the positive and negative control. This identified four N279K2 and eleven CTRL2 colonies with digestion patterns suggesting some editing at the N279K mutation locus, like sample 11 in Figure 5.11. Sanger sequencing of DNA from these colonies revealed parental sequences in all but three N279K2 and four CTRL2 colonies, which had mixed sequencing reads, indicating that the iPSCs in the colonies were not edited in the same way.

Since electroporation was performed on 2-3 cell clumps rather than single cells, it was possible that surviving colonies had a mixed population of cells, rather than being clonal. Therefore, I split the duplicates of the three N279K2 and four CTRL2 colonies with mixed DNA sequences into 2-3 cell clumps and re-plated them sparsely in an attempt to create clonal colonies, or colonies which contained a mixture of fewer types of edited cells. This was similar to the protocol of Miyaoka et al. (2014), who repeated this method to isolate rare mutations from edited iPSCs. When the colonies were big enough, I picked them and seeded half of each into new plates, then extracted DNA from the other half. All the surviving colonies were sequenced. Twenty-nine N279K2 colonies survived and DNA could be extracted from 19: 10 began to differentiate after picking and could not be recovered. Sequencing showed that all the N279K2 colonies contained the N279K mutation and there were no mixed reads. Thirty-three CTRL2 colonies survived and DNA could be extracted

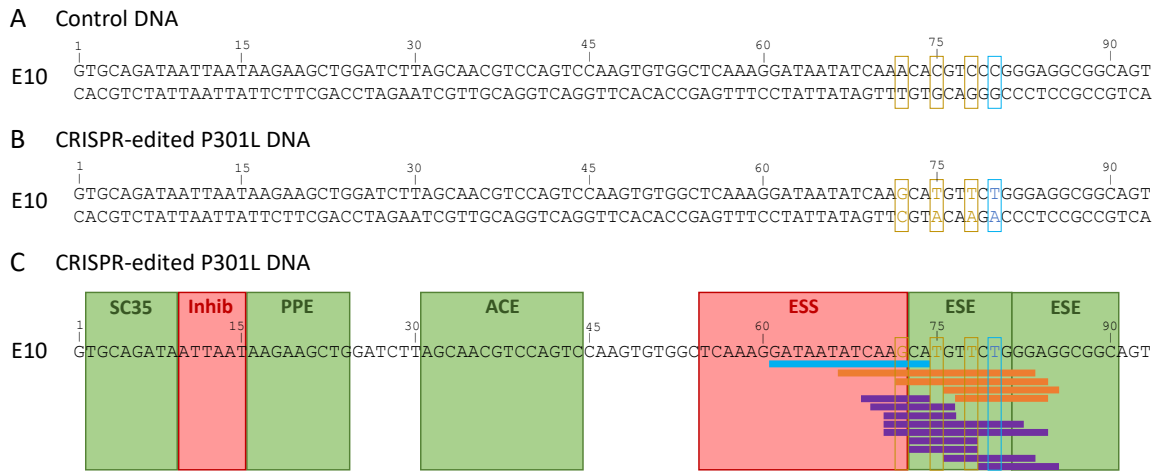

Fig. 5.13 **The position of silent blocking mutations and the P301L mutation in tau exon 10 DNA from P301L heterozygous and homozygous iPSCs created using CRISPR.** Nucleotides in double-stranded DNA from tau exon 10 (E10) is shown. Nucleotides are numbered, counting the first nucleotide of exon 10 as 1. **A)** Control DNA with the P301L mutation locus at nucleotide 80 in exon 10 (blue box). The loci of the three silent mutations are marked with yellow boxes. **B)** CRISPR-edited DNA in P301Lhom and P301Lhet iPSCs. The induced P301L mutation is at nucleotide 80 (blue box and text), and the three silent mutations are at nucleotides 72, 75, and 78 (yellow box and yellow text). **C)** CRISPR-edited DNA in P301Lhom and P301Lhet iPSCs. Boxes show sequences which affect splicing. Exon 10 contains five splicing enhancers (green boxes): a SC35-like binding sequence (SC35), a polypurine enhancer (PPE), an A/C rich element (ACE), and two exon splicing enhancers (ESEs); and two splicing silencers (red boxes): a potential inhibitory sequence (Inhib), and an exon splicing silencer (ESS). Bars show the positions of altered sequences detected by HSF: one potential splice acceptor was created (blue bar); four potential ESS sites were created (orange bars); nine potential ESE sites were disrupted (purple bars).

from 28: 22 colonies were wild-type and six had mixed reads (Figure 5.12), from which I reconstructed the DNA sequences present manually. In these colonies, the N279K locus was not altered but small insertion and deletion mutations (indels) were present upstream and downstream of the cut site.

In summary, I was not able to correct the N279K mutation in the N279K2 iPSC line, nor was I able to induce the N279K mutation in the CTRL2 iPSC line, meaning that no isogenic iPSC lines were created.

5.4.6 The effect of silent mutations in isogenic P301L iPSC lines

When I was unable to make a pair of isogenic iPSC lines with and without the N279K mutation, I used a set of isogenic iPSCs from Axol Bioscience which consisted of an isogenic control and knock-in P301L heterozygous and homozygous lines. The P301L iPSC lines

were generated from control iPSCs using a DNA template containing the P301L mutation and three silent blocking mutations to increase point mutation efficiency (Cho et al., 2014; Hsu et al., 2013; Jinek et al., 2012). The location of the three silent mutations and induced P301L mutation are shown in Figure 5.13B. In this section they are referred to according to their position relative to the first nucleotide of exon 10 (designated as one). The silent mutations are 72A→G, 75C→T, 78C→T; and the P301L mutation is 80C→T.

As discussed in this Chapter, tau exon 10 contains multiple regulatory elements (Figure 5.13C and Figure 5.5) and their disruption can alter tau splicing, as demonstrated by FTDP-17T-related MAPT mutations including N279K (Hong, 1998; Hutton et al., 1998; Spillantini et al., 1998b). Potential disruption of regulatory elements was one reason I did not use blocking mutations when trying to generate isogenic N279K iPSCs using CRISPR.

To predict possible effects of the blocking mutations on tau splicing, I checked the three silent mutation sites against the SNP database dbSNP (https://www.ncbi.nlm.nih.gov/snp/) to determine if these mutations were linked to FTDP-17T, or were known SNPs. The nucleotide changes 72A→G and 78C→T are not listed in dbSNP. 75C→T is SNP rs147401702, which is of unknown significance with low representation in the cohorts investigated (less than 0.06%).

I then used Human Splicing Finder (HSF, http://umd.be/HSF3/, Desmet et al., 2009), to predict changes caused by the three silent mutations in regions altering tau splicing. HSF predicts possible changes to splice site acceptors and donors, BPSs, ESSs, and ESEs. HSF's predictive ability has been validated with mutations which have been shown to alter splicing *in vivo*, as described in Section 5.4.2 (Desmet et al., 2009).

The three silent mutations caused several potential changes. One new potential splice acceptor site was created by the 72A→G mutation (the blue bar in Figure 5.13C). Activation of this cryptic splice site by the silent mutation could provide an alternative to the natural splice acceptor site at the 3' end of intron 9. If the cryptic splice site was used instead, the resulting tau mRNA would contain truncated exon 10 (effects of cryptic splice sites reviewed by Caminsky et al., 2014). However, the human genome contains many pseudo splice sites which do not take part in splicing (Sun and Chasin, 2000). Since the effect of this specific mutation on tau splicing has not been tested experimentally (to my knowledge), it is impossible to know what effect it has.

In addition, four potential new ESSs were detected by HSF in a region overlapping one ESS and one ESE (orange bars in Figure 5.13C). Creation of a new ESS could decrease tau exon 10 inclusion in mRNA, decreasing the amount of 4R tau.

HSF also predicted nine potential disruptions of existing ESE sites (purple bars in Figure 5.13C). All these overlapped to some extent with an experimentally determined ESE (D'Souza and Schellenberg, 2005). The nine sequences are predicted to bind the serine/arginine rich (SR) splicing factors SRp40, Tra2-β, SF2/ASF, 9G8, SRp55, and SC35. All but SRp40 are reported to have a role in tau exon 10 splicing (Yu et al., 2004).

Tra2β and SF2/ASF increase exon 10 inclusion through binding to the poly-purine enhancer (PPE) towards the 5' end of exon 10 (Figure 5.13C) (D'Souza and Schellenberg, 2006; Jiang et al., 2003; Kondo et al., 2004). The effect of Tra2β is abolished by the delta 280K MAPT mutation, and the effect of SF2/ASF is greatly reduced (D'Souza and Schellenberg, 2006). Delta 280K is the deletion of nucleotides AAG at positions 16-18 in Figure 5.13C. The effect of this deletion on both Tra2β- and SF2/ASF-mediated splicing suggests that the main binding sites of these two splicing factors are not disrupted by the silent mutations.

SRp55 has been reported to increase (Yin et al., 2012) or decrease (Wang et al., 2005) exon 10 inclusion in tau transcripts in two different studies. However, Wang et al. found that deleting nucleotides 8-15 (counting from the first nucleotide of exon 10) prevented SRp55 decreasing exon 10 inclusion, suggesting that SRp55's main binding site is not the ESE site disrupted by the silent mutations. Disruption of the potential ESE by the silent mutations may therefore not affect tau splicing.

Overexpression of 9G8 is reported to decrease exon 10 inclusion (Gao et al., 2007). However, deletion of intron 10 nucleotides +11 to +22 (counting from the first nucleotide of intron 10 as one) prevented a 9G8-induced decrease in exon 10 inclusion, suggesting that 9G8 binds in intron 10, not exon 10 (Gao et al., 2007), so alteration of the ESE site towards the 3' end of exon 10 may not alter tau splicing.

SC35 is implicated in exon 10 inclusion (Qian and Liu, 2014). However, SC35 primarily interacts with the SC35-like binding sequence at the 5' end of exon 10, since when this sequence is deleted, SC35 no longer increases exon 10 inclusion in tau mRNA (Qian et al., 2011). The disruption of a possible SC35 binding sequence towards the 3' end of exon 10 may therefore not affect exon 10 splicing.

Altogether, the results from HSF suggest that the silent blocking mutations in the P301Lhet and P301Lhom iPSC lines used in this Chapter may activate a cryptic splice acceptor site (potentially producing truncated tau exon 10), create an ESS (potentially decreasing tau exon 10 inclusion), and disrupt existing ESEs (potentially decreasing tau exon 10 inclusion). Of these possible changes, the creation of an ESS and of a splice acceptor site are the most likely to alter tau splicing, since the splicing factors predicted to bind the

disrupted potential ESEs have been shown to influence tau splicing primarily by binding to other sequences.

In conclusion, tau expression in neurons derived from these isogenic lines should be investigated further. This is done in Chapter 6.

5.5 Discussion

I was not able to induce or correct the N279K mutation in iPSCs. Some loci are more amenable to editing by CRISPR than others, due in part to closed versus open chromatin (Daer et al., 2017) and it is possible that tau exon 10 is not amenable to gene editing. However, this is unlikely: indels in CTRL2 colonies indicate that Cas9 cut the DNA, and the N279K mutation has been corrected in iPSC-derived NPCs by Hallmann et al. (2017), who used two Cas9wt nucleases to target the intron 9/exon 10 and exon 10/intron 10 boundaries, and an ssODN as a repair template. Therefore, the lack of CRISPR-edited iPSCs suggests methodological problems. In this section, I discuss the shortfalls of CRISPR strategies 2 and 3, and some alternative strategies.

5.5.1 Improvements to CRISPR 2

In the second strategy I designed (CRISPR 2, Section 5.4.2), I screened 30 CTRL2 iPSC colonies for the PAM mutation by restriction digest. There are several potential explanations for why this strategy did not work: gRNA positioning, using Cas9 nickase, and screening insufficient colonies.

gRNA positioning

The CRISPR 2 gRNAs were upstream of the N279K locus and the closest nick site was 29bp away. Trevino and Zhang (2013) suggest that one nick should be within 20bp of the mutation locus for HDR, so my CRISPR 2 design may be inefficient. In addition, Ran et al. (2013a) showed that gRNAs for Cas9n are efficient when they either flank the mutation locus, or have one nick site within 1bp of the mutation locus. Although Ran et al. did not explore the efficiency of Cas9n pairs further from the mutation locus, this indicates that a better design would have the Cas9n pairs flanking the mutation site.

Cas9 nickase

Cas9n is reported to be at least as efficient as Cas9wt for gene editing (Gopalappa et al., 2018) and may be more efficient for HDR (Mali et al., 2013). However, my Cas9n strategy depended on electroporating three components (left and right Cas9n plasmids and the ssODN) into the same iPSC, which is less likely than electroporating in two components (Cas9wt and the ssODN) required for Cas9wt. Therefore, using Cas9n in CRISPR 2 may have decreased the probability of successful editing, which caused me to use Cas9wt for CRISPR 3.

I used Cas9n to decrease the chance of off-target effects, despite reports that these are rare in iPSCs (Smith et al., 2014; Veres et al., 2014), because high levels of off-target editing had been reported in cultured cells (Fu et al., 2013). Using Cas9n was more cautious than necessary, at the expense of decreasing CRISPR efficiency and this was another factor which led me to use Cas9wt for CRISPR 3.

Screening insufficient colonies

I screened only 30 colonies after CRISPR 2, so I would not have detected edited colonies if the editing efficiency was less than 3.3%. I screened so few colonies because I decided to redesign my CRISPR strategy, rather than continue with a flawed strategy. I screened colonies for the PAM mutation, not the N279K mutation, because digestion with BsaH1 (which digests the control but not the PAM mutant sequence) gave cleaner differentiation between digested and undigested bands than AseI (which digests the control but not the N279K mutant sequence). This strategy produced the possibility that an undigested band (indicating the presence of the PAM mutation) would be present due to incomplete digestion rather than successful editing. For this reason, both positive (known to be digested) and negative (known not to be digested) controls were included in screening by restriction digest in Section 5.4.4.

Since the PAM mutation was closer to the nick sites, it was more likely to be induced by HDR than the more distal N279K mutation (Elliott et al., 1998; Paquet et al., 2016). Screening for the PAM mutation was therefore a poor proxy for the N279K mutation and would have over-predicted the number of edited colonies.

Furthermore, I did not sequence any colonies from CRISPR 2 since I did not consider the possibility of non-clonal colonies, like those found after CRISPR 3. To detect mutations in non-clonal colonies, I could have run digested next to undigested DNA samples and compared the relative ratios, as I did in Section 5.4.4.

5.5.2 Improvements to CRISPR 3

In the third strategy I designed (CRISPR 3, Section 5.4.4), I screened 99 colonies for the N279K mutation by restriction digest and Sanger sequencing. Although I detected indels in some CTRL2 colonies, no indels were detected in the N279K2 colonies and the N279K mutation locus was not edited. There are several possible reasons why this strategy did not work: insufficient screening, no blocking mutations, and not optimising transfection conditions for both iPSC lines.

Insufficient screening

CRISPR-induced point mutations are inefficient in iPSCs, with frequencies as low as 1% (Yang et al., 2014). Screening only 99 colonies means I would not have detected editing at frequencies below 2%, so the simplest improvement to this strategy would be screening more colonies. I did not do this because picking individual colonies, expanding them, screening them and keeping the duplicates in culture whilst interpreting the screening results was time consuming and labour intensive. In addition, not all colonies survived picking, which limited the number of colonies available for screening: some did not attach to the feeder layer, some attached but then differentiated, and some attached but failed to grow.

Non-clonal colonies

Some colonies had mixed sequences after CRISPR, which made screening difficult. This may be because I electroporated iPSCs in 2-3 cell clumps, or because Cas9 was active during colony expansion: Merkle et al. (2015) observed heterogeneously edited colonies after CRISPR and reduced (but did not eliminate) heterogeneity by limiting the Cas9 activity window with a doxycycline-inducible Cas9. To produce fewer non-clonal colonies, I could have combined Merkle et al.'s method with that of Byrne et al. (2014a), who electroporated iPSCs with GFP-labelled Cas9, then FACs sorted single GFP-positive iPSCs into individual wells of a 96-well plate.

Another way to increase the proportion of clonal colonies is using NPCs, which grow more easily from single cells than iPSCs (Reinhardt et al., 2013). Hallmann et al. (2017) used this method and although they did induce the N279K mutation, they only used NPCs from one differentiation in their experiments. CRISPR editing of NPCs leaves two options: differentiate and edit three sets of NPCs independently generated from iPSCs, or count three independent differentiations of NPCs to neurons as three independent experiments. CRISPR editing three times would be extremely time consuming and disregarding the importance of

the iPSC to NPC transition could skew results. In addition, editing only NPCs narrows the potential uses of the edited cell line for other researchers. For these reasons, I chose to edit iPSCs.

I could have increased the number of clonal colonies with a different antibiotic selection method. To increase the number of iPSCs surviving puromycin selection which were edited, rather than just expressing the puromycin resistance gene in the Cas9 plasmid, I could have used a repair template which inserted a puromycin-resistance cassette next to the mutation. Imamura et al. (2016) used this method to edit iPSCs at the MAPT exon 10+14 locus and excised the cassette using the piggyBac transposon system. I did not consider this method because transposon insertion and excision can leave scars but Imamura et al. isolated scarless edited iPSCs, indicating that this is a viable alternative.

Given that CRISPR 2 and 3 produced mixed colonies, I could have used the protocol of Miyaoka et al. (2014), who adapted the yeast cloning sib-selection method for iPSCs. This method involves dissociating iPSCs to single cells, using nucleases and repair templates to make a desired point mutation, and then plating iPSCs into two duplicate 96-well plates after editing. DNA is then harvested from each well of one 96-well plate, and digital droplet PCR is performed to identify the well containing the highest proportion of edited iPSCs. The corresponding well of iPSCs in the duplicate 96-well plate is then re-plated into two new 96-well plates. Repeated rounds of digital droplet PCR and expansion of the most promising wells led to isolation of scarlessly corrected iPSC clones - in Miyaoka et al.'s paper, the corrected iPSCs isolated using this method were present as 1:2000 of the initial population. I used a similar method: picking the most promising colonies, dissociating them to small clumps and expanding them. However, I picked individual colonies, some of which did not survive. Miyaoka et al.'s protocol avoids plating individual iPSCs or small iPSC clumps, which is likely to improve iPSC survival. In addition, Miyaoka et al.'s iPSCs were feeder-free, whereas the CTRL2 and N279K2 iPSCs are feeder-dependent and did not adapt well to feeder-free conditions. CRISPR editing is twice as efficient with feeder-free rather than feeder-dependent iPSCs (Byrne et al., 2014a) and this is another factor that may have lowered the efficiency of my CRISPR strategy. If I were to edit iPSCs by CRISPR again, I would use feeder-free iPSCs and the iPSC sib-selection method, as described above.

Blocking mutations

Indels were detected in 6 out of 58 CTRL2 colonies (10.3%), indicating that Cas9 cut the DNA, although this does not show whether HDR took place: DSBs could have been repaired

by HDR and re-cut by Cas9 before repair by NHEJ to make indels, or simply repaired by NHEJ to make indels.

Re-cutting by Cas9 could be reduced by blocking mutations (Cho et al., 2014; Hsu et al., 2013) but as discussed in Section 5.4.4, mutations in this region may alter exon 10 splicing. Paquet et al. (2016) overcame this problem by using CRISPR to insert the desired mutation and a blocking mutation, expanding iPSC colonies and then using CRISPR to correct the blocking mutation, leaving only the desired mutation. However, this method is impractically slow: Paquet et al. CRISPR-edited, expanded, screened and karyotyped the iPSCs and then repeated the entire process. A more practical alternative would be to assess changes in exon 10 splicing caused by silent blocking mutations using exon trapping (Duyk et al., 1990): if the blocking mutations did not change exon 10 splicing, they would be safe to use. I designed exon trapping plasmids to test two blocking mutations which would have increased the efficiency of gene editing at the N279K locus, but the isogenic P301L iPSC lines became available shortly afterwards.

Repair template design

Indels may have occurred because Cas9 cut the DNA but the HDR template did not make repairs. This could have been due to low template availability. I tested two ssODN concentrations declared optimal in relevant literature (Section 5.3.3) but these were similar and since I saw no difference in cell death between the two concentrations, I chose the higher concentration. A more thorough approach would have been to test a larger range of ssODN concentrations and to use the highest concentration which did not cause noticeable cell death.

Additionally, my ssODN templates were not complementary to the gRNA and therefore not optimal. Intuitively, non-complementary ssODNs are a logical choice: they cannot bind the gRNA, so they cannot be cut by Cas9, or occupy Cas9 and reduce target DNA cutting. However, after Cas9wt makes a DSB, the Cas9 complex releases the non-target strand (the strand not bound to gRNA) first, before the entire complex dissociates from the DNA (Richardson et al., 2016). Cas9 can cut DNA and then remain bound for five hours, during which time the non-target strand is available for binding with a gRNA-complementary repair template but the target strand is bound to Cas9 and cannot bind a gRNA-non-complementary repair template. Since the non-target strand is more available for binding after Cas9 cleavage, ssODNs complementary to the gRNA may be more efficient, which is supported by some studies (Yang et al., 2013) but not others (Kan et al., 2017). Richardson et al.'s research was not published when I was designing the ssODNs, which is why I designed them not complementary to the gRNA.

Optimisation of transfection conditions

There were fewer N279K2 than CTRL2 colonies after electroporation and puromycin selection, perhaps because I optimised the electroporation program, puromycin concentration and ssODN concentration for CTRL2 iPSCs only. To get more surviving clones, I should have optimised the parameters for both iPSC lines. I could also have tried other transfection components, such as recombinant Cas9 protein and *in vitro* transcribed gRNA, which cause more DNA cleavage in iPSCs than Cas9 and gRNA plasmids (Liang et al., 2015). Synchronising iPSCs in M phase also increases CRISPR efficiency (Lin et al., 2014), and small molecules including the DNA ligase inhibitor Scr7 can increase HDR up to 19-fold (Maruyama et al., 2015).

As well as optimising the transfection conditions, I could have assessed CRISPR efficiency in easier to culture cells, such as HEK293 cells before iPSCs. Since iPSCs are delicate relative to HEK293 cells, I decided to optimise the method once, on iPSCs, rather than twice, on HEK293 cells and then iPSCs. However, I could have used methods such as a T7 endonuclease assay to check the cutting ability and efficiency of my Cas9wt and Cas9n strategies before transfecting iPSCs with the CRISPR components, to avoid using inefficient gRNAs.

5.5.3 Summary

In this Chapter, I designed three CRISPR strategies to make isogenic iPSC lines. Two of the CRISPR strategies were attempted, but only the third CRISPR strategy produced cells with edited DNA. The DNA changes were indels, and no colonies containing a base change at the N279K mutation locus were found.

The difficulties inherent in performing CRISPR on iPSCs (outlined in this section) meant that I was unable to make isogenic iPSC lines. Since isogenic control iPSC lines for other MAPT mutations were available, I focussed my efforts on making iPSC-derived cerebral organoids (described in Chapter 6) rather than continuing to attempt to edit the N279K mutation locus.

Chapter 6

Cerebral organoids

6.1 Aims

Differentiating iPSC-derived neurons in a 3D environment may provide advantages over a 2D environment, including enhanced survival and maturation. 3D culture may also provide an advantage over 2D cultures for modelling neurodegenerative diseases: a study of iPSC-derived neurons with AD-relevant mutations showed disease-like changes in 3D, but not in 2D (Choi et al., 2014). This suggests that 3D culture may also enhance the phenotypes of MAPT-mutant iPSC-derived neurons.

Cerebral organoids (COs) are 3D structures which differentiate over time to produce neurons and astrocytes (Lancaster and Knoblich, 2014a). Unlike some 3D culture systems (which consist of neurons embedded in a thick matrigel layer), COs are generated through directed differentiation. Beginning as embryoid bodies made of iPSCs, COs recapitulate some features of the developing brain, including generation of neurons from all six cortical layers, and the generation of astrocytes. The addition of patterning factors can be used to make brain-region specific COs (Lancaster et al., 2017).

Variability between iPSC lines can contribute to variability between COs. This variability can be decreased by using isogenic iPSCs, which share the same genetic background (Giandomenico and Lancaster, 2017; Lancaster et al., 2017). Although I was not able to make a pair of isogenic iPSC lines from patient-derived iPSCs with the N279K mutation (in Chapter 5), I obtained three isogenic iPSC lines (isogenic control, P301L heterozygous, P301L homozygous). I used these three isogenic lines alongside an FTDP-17T patient-derived iPSC line with the P301L MAPT mutation to make cerebral organoids.

The aim of the work described in this Chapter is to make cerebral organoids from control and MAPT-mutant iPSCs, to characterise them, and to investigate disease-relevant changes. This aim will be fulfilled by:

1. Differentiating iPSCs into cerebral organoids, and determining the proportion of astrocytes and neurons in the 3D cultures. The emergence of astrocytes by day 100 is expected, and indicates maturation of the culture. Determining the proportion of astrocytes will also allow me to see whether there is FTDP-17T-relevant astrocyte overgrowth.

2. Examining synaptic protein expression. Synapses are expected to form by day 100, and examining synaptic protein levels will also indicate if there is FTDP-17T relevant synapse loss.

3. Assessing tau isoform expression to determine the maturity of the neurons with respect to tau isoform expression, since 3D culture may increase expression of 4R tau. 4R tau expression is particularly important for neurons with the P301L mutation, since it is only present in 4R tau.

4. Examining tau phosphorylation at the AT8 epitope and tau conformational changes with the MC-1 antibody, to determine whether 3D culture enhances the development of FTDP-17T-relevant changes.

6.2 Introduction

The first 3D pluripotent stem cell (PSC)-derived cultures were optic cup structures made from mouse embryonic stem cells (mESCs) (Eiraku et al., 2011). Later, Lancaster and Knoblich (2014a) used induced pluripotent stem cells (iPSCs) to make "minibrains" or COs in which proliferative NPCs differentiated to produce a mixture of brain areas. At the time of writing, COs have been produced to model brain areas including the forebrain (Kadoshima et al., 2013), midbrain (Qian et al., 2016), cerebellum (Muguruma, 2018), hippocampus and choroid plexus (Sakaguchi et al., 2015), and hypothalamus (Qian et al., 2016), to name a few. COs can be made using patterning factors, which increases batch-to-batch reproducibility and brain area specificity (Lancaster et al., 2017; Qian et al., 2016), or COs can develop through intrinsic cues including morphogens such as Wnt and Nodal, which can be spontaneously released in culture (Eiraku and Sasai, 2012). This gives more complex, less reproducible COs, containing a variety of brain areas (Lancaster et al., 2013).

The work described in this Chapter used forebrain-specific COs, generated from iPSCs with the heterozygous or homozygous P301L MAPT mutation, and an isogenic control.

6.2.1 Cerebral cortex development

iPSC differentiation to COs recreates aspects of human brain development, which is briefly described here.

During fetal development the future brain and spinal cord develop from one of three germ layers called the ectoderm. The ectoderm forms the neural plate, which folds to make the neural tube: a layer of neuroepithelial cells (NECs, also known as primary progenitors or neural stem cells) radially arranged around a central cavity that becomes a ventricle. The neural tube receives patterning cues (as described in Chapter 1) and develops rostral-caudal and dorsal-ventral axes - the rostral part of the neural tube forms the telencephalon, which gives rise to the future forebrain (Petros et al., 2011; Wilson and Houart, 2004).

NECs in the neural tube divide symmetrically, expanding the NEC population. When neurogenesis begins NECs transition to radial glial cells: radially orientated, polarised cells whose processes span from the apical side (proximal to the ventricle) to the basal side (distal to the ventricle) of the developing tissue, forming a scaffold along which neurons migrate (Bystron et al., 2008; Kriegstein and Alvarez-Buylla, 2009).

Radial glia are the precursors of almost all CNS cells, as demonstrated by experiments labelling radial glia and finding almost all brain regions labelled after development (Anthony et al., 2004). During cortical neurogenesis radial glia divide asymmetrically to produce a radial glial cell and either a neuron, a glial cell, or an intermediate cell: an intermediate progenitor or an outer radial glial cell (Hansen et al., 2010; Kriegstein and Alvarez-Buylla, 2009). Intermediate progenitors divide symmetrically to produce either two neurons or two intermediate progenitors (Kriegstein and Alvarez-Buylla, 2009), whereas outer radial glial cells can divide symmetrically to proliferate, or divide asymmetrically to produce an outer radial glial cell and an intermediate progenitor (Hansen et al., 2010). Intermediate progenitors are lineage-restricted: in mice they divide to produce neurons found in all six cortical layers, but their progeny is not found in interneurons which are from a different lineage (Mihalas et al., 2016).

The first neurons in the developing cortex are Cajal-Retzius neurons in the developing pre-plate which originate in adjacent areas and migrate into the cortex. They help guide newly generated neurons but disappear during development (Bystron et al., 2008). Subsequently generated neurons form the cortical plate which splits the preplate to make the transient

subplate and the marginal zone (the future layer I) (Mountcastle, 1997). Neurons destined for the future layers 2-6 are made in an inside-out temporal sequence in which their birthdate determines their future identity and cortical layer position, such that early-born neurons populate the lower cortical layers and late-born neurons populate the upper layers (Angevine and Sidman, 1961). These neurons can be identified by expression of specific transcription factors (reviewed by Molyneaux et al., 2007). They are predominantly glutamatergic; GABAergic cortical interneurons form in the caudal and medial ganglionic eminences and migrate into the cortex later in development (Wonders and Anderson, 2006). After neurogenesis, radial glia generate astrocytes and oligodendrocyte precursors (Kriegstein and Alvarez-Buylla, 2009; Rakic, 2003).

6.2.2 Cerebral organoids as models of the brain

Some aspects of cerebral cortex development are recapitulated by COs (reviewed by Heide et al., 2018). For example, COs contain proliferative NECs and radial glia which undergo inter-kinetic nuclear migration: movement of the radial glial cell body such that cell division happens close to the ventricle (Lancaster et al., 2013). The radial glia in COs produce neurons, astrocytes, and oligodendrocytes in a time-dependent manner (Lancaster et al., 2013; Monzel et al., 2017; Renner et al., 2017). Neurons in COs form synaptic connections, are electrophysiologically active (Paşca et al., 2015), and represent populations from all six cortical layers (Lancaster et al., 2013). Although the cortical layers are not spatially separated as they are in the fetal brain, some separation of upper and lower layers has been observed (Kadoshima et al., 2013; Lancaster et al., 2013; Paşca et al., 2015; Qian et al., 2016).

However, some aspects of the human brain are not present in COs. COs made without patterning factors contain multiple brain areas which are not organised in terms of where the areas develop relative to each other (Lancaster et al., 2013), perhaps because COs lack axes across the entire tissue (Kelava and Lancaster, 2016). COs also lack other tissues found in the developing brain, such as vasculature. This can lead to necrotic cores if COs become too large for diffusion to adequately deliver oxygen and nutrients (Kelava and Lancaster, 2016; Raja et al., 2016) and this has been compensated for by gently agitating CO cultures (Lancaster et al., 2013; Qian et al., 2016). Cell types such as microglia, which develop from the yolk sac - a different lineage from the rest of the brain (reviewed by Ginhoux and Prinz, 2015), are also absent. This may have implications for synaptic pruning, which is carried out by microglia in postnatal brains (Schafer et al., 2012), and for modelling diseases where microglia are implicated.

Other features of the human brain not recapitulated by COs include the extracellular matrix which is required to support a continuous neuroepithelium rather than individual neural rosettes (Nasu et al., 2012). In COs this is compensated for by the addition of matrigel (Lancaster and Knoblich, 2014b; Lancaster et al., 2013). COs also lack cortical folding into gyri and sulci. Some folding has been observed in COs with a PTEN mutation linked to autism (Li et al., 2017) and neuroepithelial wrinkling has been reported (Karzbrun et al., 2018) although the relevance of this to cortical folding in the human brain is unclear (Lancaster, 2018).

As might be expected given the development-mimicking nature of COs, CO gene expression profiles are like those of the fetal brain. Gene expression studies have found comparable expression between 75 day-old COs and 19-24 week-old fetal brain (Paşca et al., 2015), between day 40 and day 60 COs and 12-16 week-old fetal brain (Luo et al., 2016), and between 60 day-old forebrain-specific COs and 8-9 week-old fetal brain (Lancaster et al., 2017) .

6.2.3 Advantages of 3D neural cultures over 2D cultures

The 3D culture of COs may provide advantages over 2D cell cultures with respect to microenvironment and maturity, which are outlined below. However, all the studies discussed used 3D matrigel or hydrogel cell cultures, in which neurons or NPCs are disorganised, rather than self-organising COs. To date, no studies have compared neuronal maturity (by RNA profiling, for example) between 2D monolayer cell cultures and 3D COs.

Cell microenvironment

Neurons in 3D cultures have a more brain-like environment than those in 2D cultures. Instead of the flat, stiff surface of a cell culture dish, cells inside a CO are in contact with other cells or with matrigel, which more closely resembles brain stiffness (Ranjan et al., 2018). In addition, NPCs and neurons in self-organising cultures can determine their own polarity, whereas a 2D surface forces an apical-basal polarity which may affect cell function and signalling (reviewed by Baker and Chen, 2012).

Culture maturity

One of the field-wide challenges in using PSC-derived neurons to examine the effects of mutations which cause disease in adult or aged human brains is the relative immaturity of the neurons. Therefore, the finding that 3D culture of neural cells can hasten maturity is

particularly important. Culture in a 3D hydrogel layer (as compared to a traditional 2D monolayer) has been shown to increase differentiation of immortalised human NPCs (ReN cells) (Choi et al., 2014; Liedmann et al., 2012; Ortinau et al., 2010; Park et al., 2018), SHSY-5Y cells (Seidel et al., 2012), and iPSC-derived NPCs (Muratore et al., 2014; Zhang et al., 2016) to neurons. In the case of the ReN cell-derived NPCs (Ortinau et al., 2010) and iPSC-derived NPCs (Zhang et al., 2016), the increased differentiation to mature neurons may have been partly because more NPCs survived in 3D relative to 2D culture.

In addition, 3D hydrogel-cultured SHSY-5Y-derived neurons (Seidel et al., 2012) and iPSC-derived neurons (Zhang et al., 2016) expressed more synaptic markers than those in 2D cultures, suggesting greater maturity. Three-D iPSC-derived NPC cultures have also been shown to enhance electrophysiological maturity as compared to 2D cultures: neurons from 3D cultures fired more mature action potentials, and expressed higher levels of voltage-activated sodium and potassium channels (Zhang et al., 2016).

Three-dimensional cultures of ReN cells also seem to mature faster with respect to astrocyte production. Choi et al. (2014) reported higher levels of GFAP and S100β mRNA in 3D as compared to 2D culture, and Park et al. (2018) detected more GFAP in 3D as compared to 2D cultures by Western blotting. Since astrocytes are produced after neurons in the sequence of NPC differentiation (Kriegstein and Alvarez-Buylla, 2009; Rakic, 2003), this suggests greater maturity in the 3D cultures. However, Zhang et al. (2016) found fewer astrocytes in differentiated 3D iPSC-derived cultures than in 2D cultures, suggesting that the 3D cultures were less mature compared to those in 2D. The finding that 3D cultured neurons were more mature in electrophysiological and synapse development, would contradict Zhang et al.'s conclusion, indicating that the 3D substrate may have favoured neuronal differentiation relative to the 2D substrate.

Tau expression

Human tau isoform expression can be used as indication of an iPSC-derived neural culture's maturity, since the shortest 0N3R tau isoform is expressed during development, and the remaining five isoforms (0N4R, 1N3R, 1N4R, 2N3R, 2N4R) are co-expressed with the 0N3R isoform post-natally (Goedert and Jakes, 1990; Goedert and Spillantini, 1990). There is some evidence that 3D culture enhances adult-like tau splicing. Choi et al. (2014) found higher 4R tau and total tau mRNA levels in 49 day-old 3D ReN cell cultures as compared to 2D cultures, although mRNA changes were not corroborated at the protein level.

Inducing mature expression of tau isoforms is particularly important for studying some MAPT mutations which cause FTDP-17T, such as the P301L mutation. P301L is a mutation

in tau exon 10 (Hutton et al., 1998; Poorkaj et al., 1998; Spillantini et al., 1998b), the exon which is transcribed and translated in the three four-repeat (4R) tau isoforms (0N4R, 1N4R, 2N4R), which are only expressed post-natally.

6.2.4 Tau dysfunction in 3D PSC-derived cultures

COs are becoming an increasing popular way to model the human brain *in vitro* but relatively few studies have used this system to examine the effects of FTDP-17T-relevant MAPT mutations. Seo et al. (2017) used patient-derived iPSCs with the P301L MAPT mutation to produce two isogenic iPSC lines using CRISPR. The iPSC lines were with and without a delta-p35 mutation, which prevents p35 cleavage to make p25. p25 can activate cyclin-dependent kinase 5 (Cdk5) which may have a role in tau phosphorylation in AD (Sengupta et al., 2006; Yamaguchi et al., 1996). Eighty day-old COs derived from delta-p35 P301L mutant iPSCs showed a trend towards a lower phosphorylated tau (pSer202 and pThr181) over total tau ratio, and expressed more synaptophysin than COs from P301L mutant iPSCs. This suggests a possible role for p25 in FTDP-17T, but P301L mutant COs were not compared with control COs, making these results difficult to interpret.

Other groups have studied the effects of familial AD mutations on tau phosphorylation in COs, reporting increases in tau phosphorylation at Ser202 and Thr205 (detected with the AT8 antibody). For example, Yan et al. (2018) found an increased proportion of AT8 positive COs derived from iPSCs with an AD-relevant presenilin 1 mutation as compared to controls after 28 days in culture. Similarly, Gonzalez et al. (2018) found higher levels of AT8 positive and PHF1 (detecting pSer396 and pSer404) positive tau in COs made from iPSCs with trisomy 21 (from a donor with Down's syndrome) and from COs with an AD-relevant presenilin 1 mutation as compared to controls. Although these findings are not directly relevant to FTDP-17T, they demonstrate that differences in tau phosphorylation can be induced by endogenous mutations and are detectable in COs.

As well as being aberrantly phosphorylated, tau forms aggregates in FTDP-17T and tauopathies including AD (Foster et al., 1997; Spillantini et al., 1998a). However, protein aggregation is only recapitulated to a limited extent in iPSC-derived cultures. Gonzalez et al. (2018) have detected Gallyas silver positive cells in 110 day-old trisomy 21 and presenilin 1 mutant COs. Gallyas silver staining is a sensitive method used to detect tau in neurofibrillary tangles in AD, corticobasal degeneration (CBD) and progressive supranuclear palsy (PSP), amongst other diseases (Uchihara, 2007). Gonzalez et al. also extracted protein from COs with PBS, and then, from the PBS-insoluble pellet, they extracted protein in formic acid. The

results showed more tau in the formic acid soluble fraction of presenilin mutant and trisomy 21 COs than from that of control COs.

Gallyas silver positive cells have also been detected in ReN cell-derived neurons cultured in thick matrigel layers, which over-expressed mutant β-amyloid (due to the presence of three AD-related mutations in amyloid precursor protein) and expressed presenilin 1 with one AD-related mutation (Choi et al., 2014). Choi et al. also found an increase in sarkosyl-insoluble tau in the AD mutant cultures, and detected extracellular β-amyloid accumulation in 3D but not 2D cultures. They suggested this is because the 3D matrigel layer trapped β-amyloid released by the neurons, whereas β-amyloid released from 2D cultures diffused into the media and was removed during media changes.

These results indicate that insoluble, abnormal tau can be detected in some COs and 3D neural cultures, and that protein accumulation may be favoured in 3D cultures relative to 2D cultures. Again, these findings are not from cultures with MAPT mutations, but they do demonstrate the potential for observing FTDP-17T-relevant tau changes in COs.

6.3 Materials and Methods

6.3.1 iPSC culture and differentiation

iPSCs were thawed and cultured as described in Chapter 2.

iPSCs were differentiated to COs following the method of Lancaster et al. (2017) for forebrain-patterned COs (also known as microfilament-engineered cerebral organoids: enCORs). The method is described in detail in Section 2.4 and Table 6.1 in Chapter 2. I differentiated COs from the isogenic iPSC lines IsoCon, P301Lhet, and P301Lhom, and from the patient-derived iPSC line P301Lpat. However, not all iPSC lines differentiated to COs with the same efficiency: IsoCon, P301Lhet, and P301Lhom COs shared the same genetic background and differentiated more easily, although P301Lhet iPSCs could not be maintained in culture; P301Lpat COs were more difficult to differentiate. The number of differentiations and the characteristics of the iPSCs are shown in Table 6.1.

I made at least one batch of COs from each of the iPSC lines, aiming to culture them for at least 100 days. However, bacterial infections meant I had to discard some batches. When bacterial infections occurred, I kept all unaffected COs until the media needed to be changed, checked under the microscope for the absence of infection, and cut short the differentiation. Since some differentiations were cut short, COs were 84-100 days old.

‘

Table 6.1 **Differentiation of iPSCs to COs**

iPSC line	Number of differentiations	iPSC culture surface
IsoCon	3	Feeder-free
P301Lhet	1	Feeder-free
P301Lhom	3	Feeder-free
P301Lpat	3	Feeder-dependent

The forebrain CO method is from Lancaster et al. (2017). The number of differentiations denotes how many differentiations produced COs after 100 days, not how many differentiations were attempted: one differentiation each of forebrain-patterned IsoCon, P301Lhom, CTRL1 and P301Lpat COs became infected during culture and could not be used. I was unable to maintain the P301Lhet iPSC line in culture after the first differentiation.

6.3.2 Immunostaining, Western blotting and statistical analysis

Immunostaining was performed as described in Section 2.5.1 and Western blots were performed as described in Section 2.6. Statistical analysis was performed as described in Section 2.7.

Quantification of immunostaining

AT8 and MC-1 staining were quantified using ImageJ. In both cases, COs were co-stained with the total tau antibody tau DAKO. The mean AT8, MC-1, and total tau fluorescence intensities were measured using the mean grey value function of the Measure menu in ImageJ. Background fluorescence intensity was measured in AT8, MC-1, and total tau images by selecting an area of the image which did not contain the CO, and using the mean grey value function of the Measure menu. Background fluorescence intensity was subtracted from the intensity of the whole image for each of the AT8, MC-1, and total tau images. AT8 and MC-1 values were normalised to the total tau fluorescence intensities in the corresponding images.

6.4 Results

6.4.1 Cell types present in cerebral organoids

To determine the proportion of neurons and astrocytes in COs from each iPSC line, I quantified the amount of βIII-tubulin and GFAP detected in Western blots, and normalised these to the amount of GAPDH. Although GFAP detects radial glia as well as astrocytes

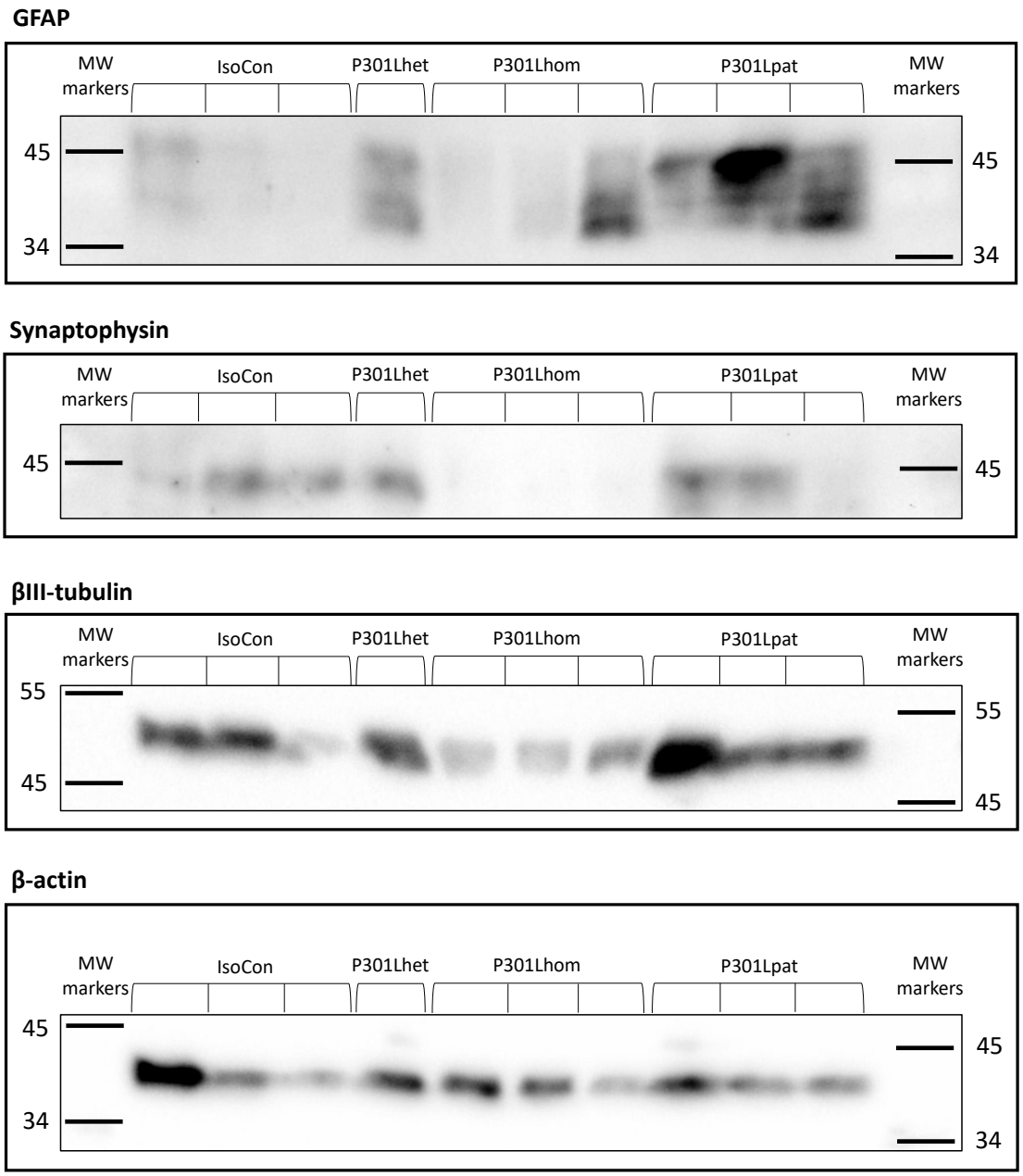

Fig. 6.1 **Western blots for GFAP, synaptophysin, βIII-tubulin, and GAPDH in iPSC-derived COs.** A representative blot. Each lane contained protein from at least six COs derived from the indicated iPSC line in one independent differentiation round. Molecular weights, in kDa, are indicated. This blot was repeated to ensure that the results were reproducible, and to improve on the blurred staining. The second blot confirmed the results of the first and the staining was clearer, however, there was no protein in the third P301Lhom lane due to a loading error. Therefore, the first iteration of the blot is shown.

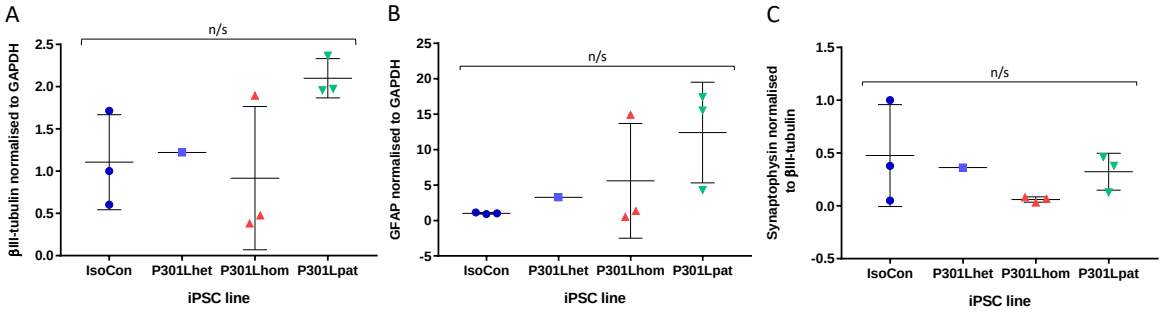

Fig. 6.2 **There is no significant difference in the amount of βIII-tubulin positive neurons, in the amount of GFAP-expressing astrocytes, or in the amount of the synaptic protein synaptophysin between IsoCon, P301Lhet, P301Lhom and P301Lpat iPSC-derived COs at day 84-100. A)** βIII-tubulin normalised to GAPDH. There was no significant difference in the amount of βIII-tubulin between COs from the different iPSC lines, as determined by one-way ANOVA. **B)** GFAP normalised to GAPDH. There was no significant difference in the amount of GFAP between COs from the different iPSC lines, as determined by one-way ANOVA. **C)** Synaptophysin normalised to βIII-tubulin. There was no significant difference in the amount of synaptophysin between COs from the different iPSC lines, as determined by one-way ANOVA. All results are relative to the amount of βIII-tubulin (**A**), GFAP (**B**), or synaptophysin (**C**) in IsoCon COs derived in the third differentiation round, which was set to 1. Each point shows normalised chemiluminescence intensity from one of one (P301Lhet) or three (IsoCon, P301Lhom, P301Lpat) independent differentiations; bars show the mean$\pm$SD.

(Raponi et al., 2007), the number of radial glia (which can be identified by their radial arrangement around a central ventricle) was low in my COs at day 84-100. Western blots were performed using protein extracts made from at least six COs from each differentiation of each iPSC line, meaning that each Western blot lane contained protein from at least six COs which had all been grown together. The blot was repeated twice with the same samples, and similar results were obtained each time. A representative blot is show in Figure 6.1, and quantification of the Western blot is show in Figure 6.2.

I compared the amount of βIII-tubulin (normalised to GAPDH) in IsoCon, P301Lhet, P301Lhom, and P301Lpat COs using a one-way ANOVA, which showed no significant difference between the mean values ($F(3,6)=2.242$, $p=0.1836$, Figure 6.2A). Comparing the amount of GFAP (normalised to GAPDH) in the COs using a one-way ANOVA also showed no significant differences ($F(3,6)=1.777$, $p=0.2513$, Figure 6.2B).

I also compared the amount of βIII-tubulin and GFAP between COs by immunostaining at least two sections from each batch of COs from each iPSC line. Most COs contained large areas of βIII-tubulin positive neurons (Figure 6.3). GFAP positive astrocytes were sometimes packed into one area, or spread throughout βIII-tubulin positive neurons (Figure 6.3).

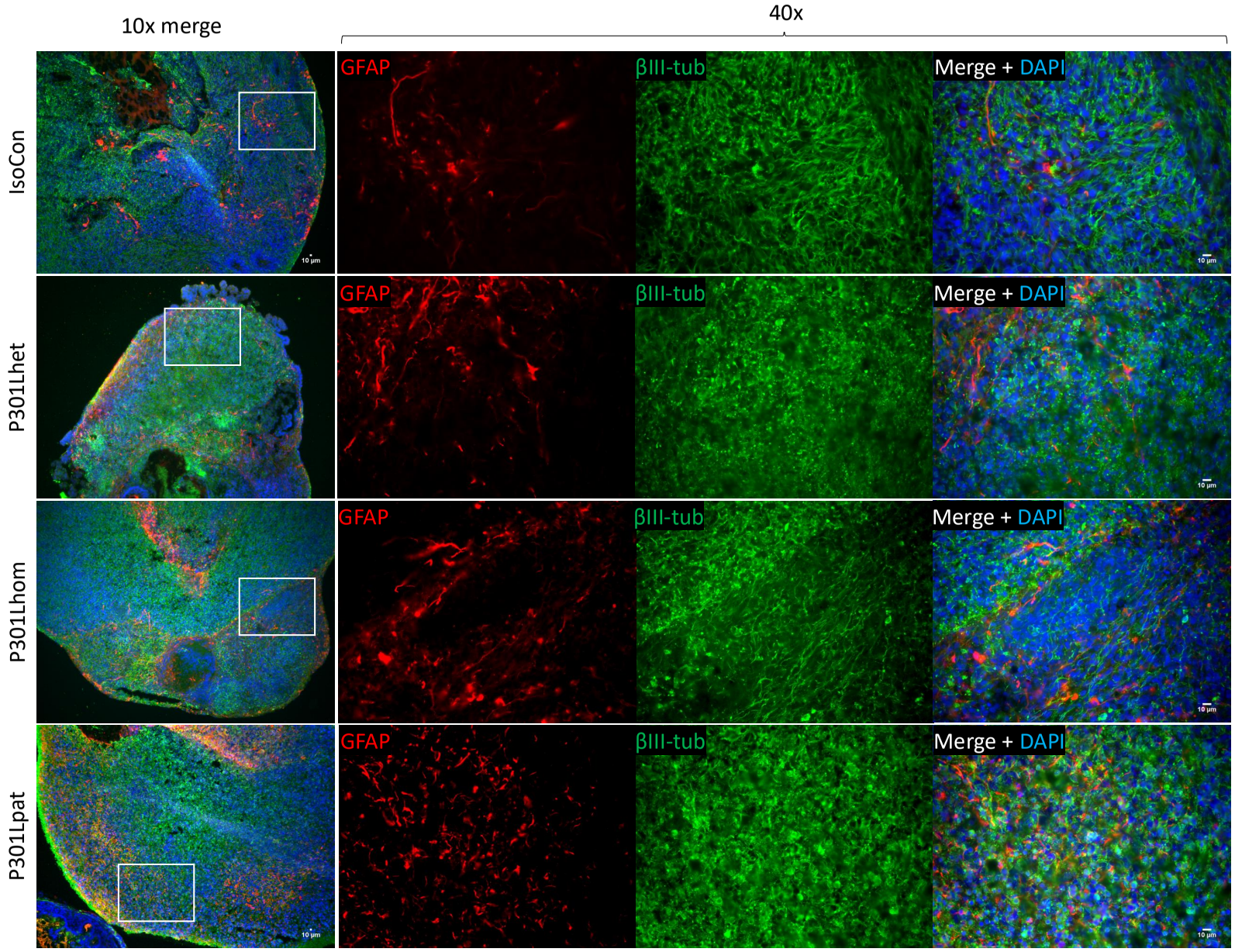

Fig. 6.3 **IsoCon, P301Lhet, P301Lhom, and P301Lpat iPSC-derived COs all express GFAP and βIII-tubulin at day 84-100.** Quantification by Western blot showed that there was no significant difference in the amount of GFAP or the amount of βIII-tubulin (both normalised to GAPDH) between COs from the four iPSC lines. This is reflected in the immunofluorescence images, and suggests that COs from all four iPSC lines were maturing at similar rates, and that there was no astrogliosis-like proliferation of astrocytes. Representative images of areas containing GFAP and βIII-tubulin positive cells. At least six COs from each differentiation (at day 84-100) were cryosectioned together for immunostaining. White boxes in the merged images on the left indicate the areas which are magnified in the subsequent three images. Scale bar = 10µm.

As an estimate of the number of synapses, I measured the amount of synaptophysin in protein extracts from all COs. Synaptophysin is a pre-synaptic protein which has been shown to be a good proxy for synapse number in the human brain (Bigio et al., 2001). Synaptophysin detected in protein extracts from IsoCon, P301Lhet, P301Lhom and P301Lpat COs is shown in Figures 6.1 and 6.2. Comparing the amount of synaptophysin (normalised to βIII-tubulin) using a one-way ANOVA showed no significant difference between the mean values ($F(3,6)=1.027$, $p=0.4448$).

Overall, these results show no significant differences in the amount of synaptophysin, βIII-tubulin, or GFAP between COs made from different iPSC lines.

6.4.2 Layer markers

To determine whether the COs contained cortical forebrain neurons, and to establish the relative maturity of the COs, I examined the expression of cortical layer markers by immunofluorescence. I used the layer markers Tbr2 (expressed by intermediate progenitors, Bulfone et al., 1995), Tbr1 (layer 6 pre-plate neurons, Bulfone et al., 1995), and Cux1/2 (layer 2-4 neurons, Nieto et al., 2004). Initially, one section from each batch of COs from each iPSC line was stained. If layer markers were not detected, one or two further sections were stained. The number of differentiations in which each layer marker was detected is summarised in Table 6.2.

A small number of Tbr2 positive intermediate progenitors were detected in IsoCon, P301Lhom, and P301Lpat COs from one or two of three differentiations, but not in P301Lhet COs (Figure 6.4). However, P301Lhet COs contained layer 6 Tbr1 positive neurons, and therefore presumably contained intermediate progenitors at some point, since Tbr2 and Tbr1 are expressed sequentially (Englund, 2005). A small number of Tbr1 positive (layer 6)

Table 6.2 **COs expressing the layer markers Tbr2, Tbr1, and Cux1/2**

iPSC line	**Tbr2** Intermediate progenitors	**Tbr1** Layer 6 neurons	**Cux 1/2** Layer 2-4 neurons
IsoCon	++	+++	++
P301Lhet	-	+	-
P301Lhom	++	++	++
P301Lpat	+	++	+

Symbols denote whether layer markers were detected in no differentiations (-), one differentiation (+), two differentiations (++) or three differentiations (+++) of CO from the three iPSC lines.

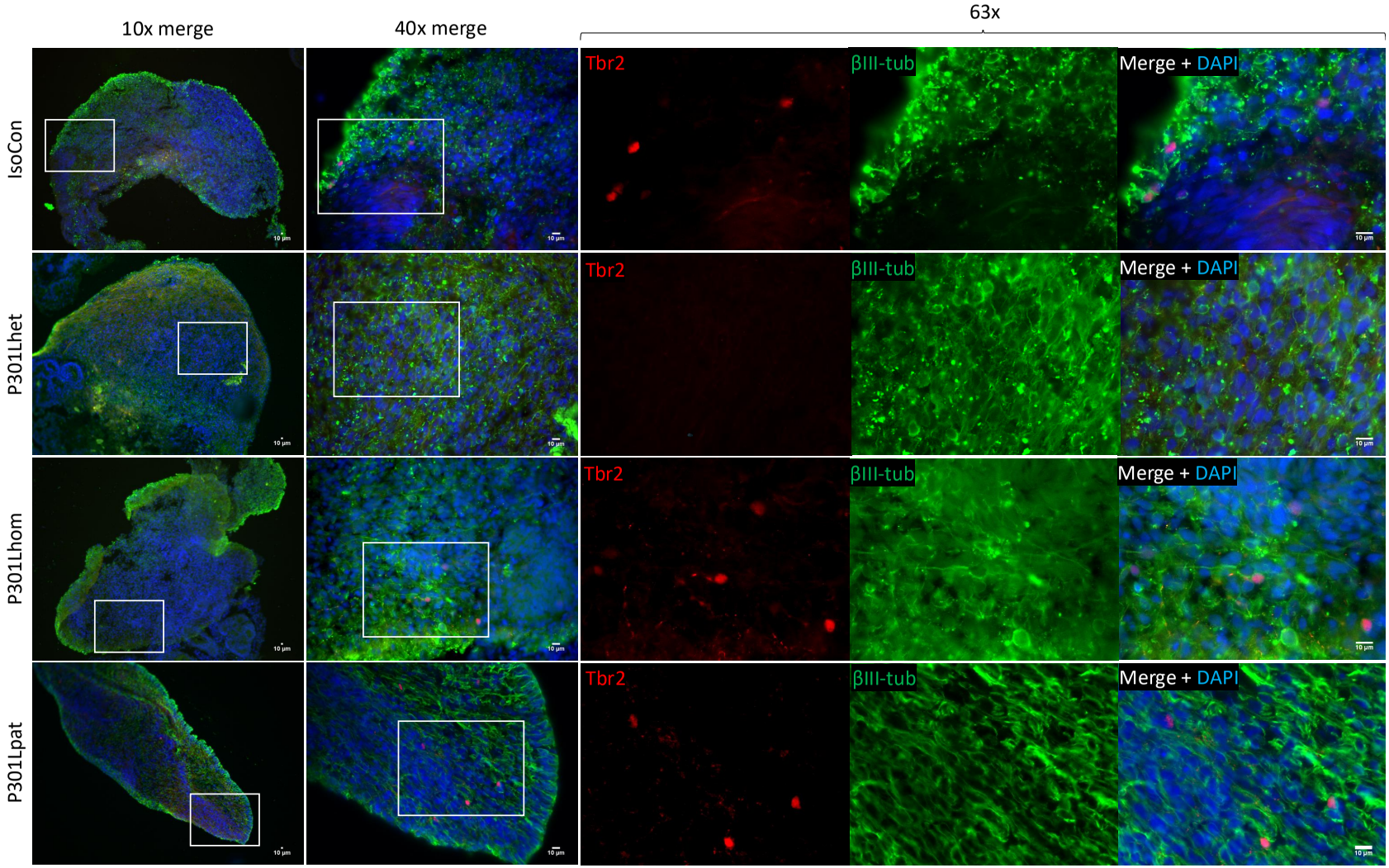

Fig. 6.4 **Tbr2 positive intermediate progenitor cells were detected in IsoCon, P301Lhom, and P301Lpat (but not P301Lhet) iPSC-derived COs at day 84-100.** A small number of Tbr2 positive intermediate progenitors was expected in COs from all iPSC lines, since intermediate progenitors are produced early in neurogenesis. By day 100, most intermediate progenitors were expected to have divided to produce neurons, or to have died due to necrosis at the CO centre. The lack of intermediate progenitors detected in P301Lhet COs was not expected. Tbr1 positive cells were observed in P301Lhet COs, indicating that P301Lhet COs must have contained intermediate progenitors at some point, since Tbr1 and Tbr2 are expressed sequentially. At least six COs from each of three differentiation rounds (IsoCon, P301Lhom, P301Lpat) or one differentiation round (P301Lhet) were cryosectioned together and stained simultaneously. One, two or three sections from each batch of COs were stained. White boxes in the merged images on the left indicate magnified areas, shown in merged images on the right. Scale bar = 10μm.

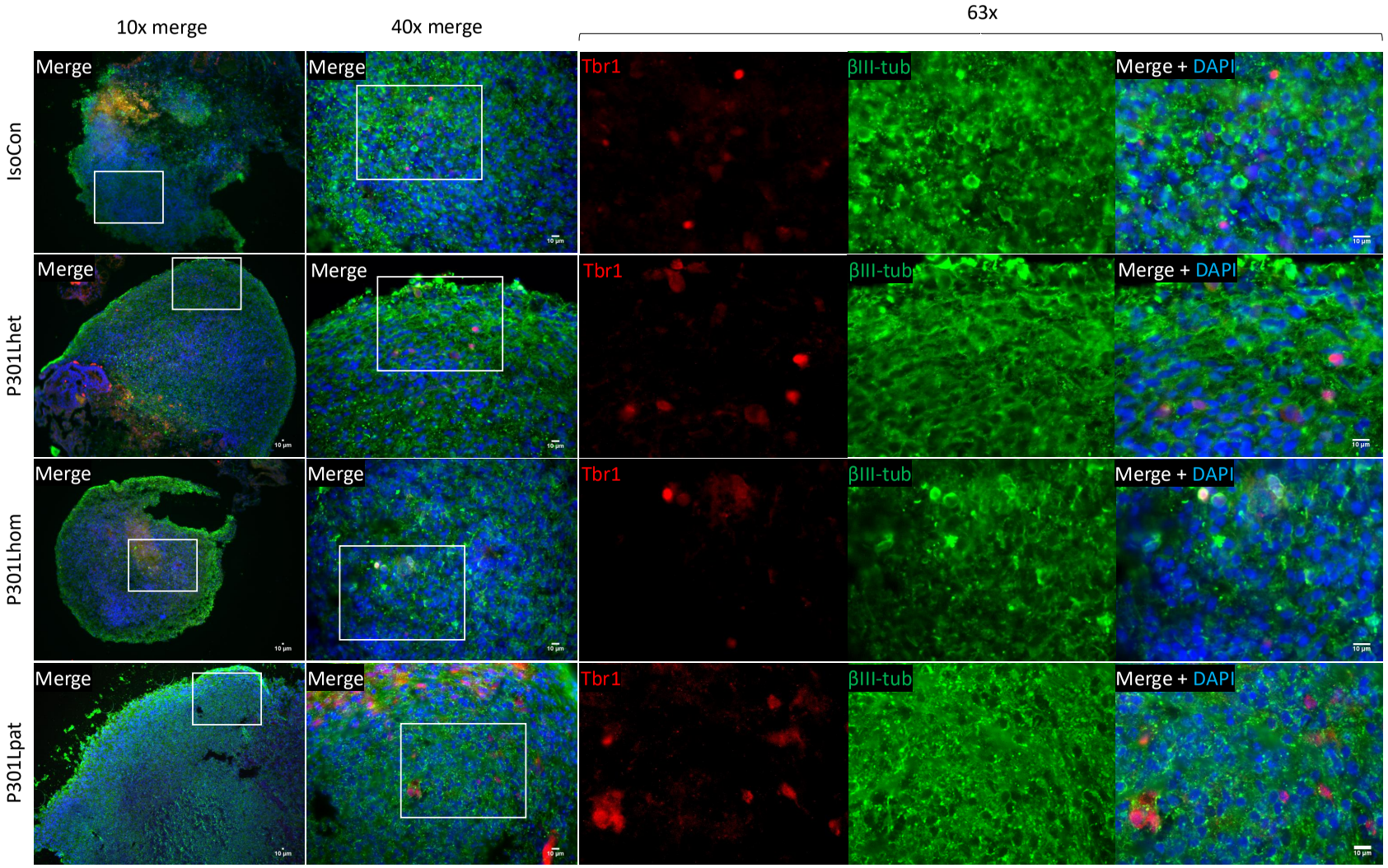

Fig. 6.5 **Tbr1 positive layer 6 neurons were detected in IsoCon, P301Lhet, P301Lhom, and P301Lpat iPSC-derived COs at day 84-100.** This was an expected result, since layer 6 neurons were expected in COs from all four iPSC lines. At least six COs from each of three differentiation rounds (IsoCon, P301Lhom, P301Lpat) or one differentiation round (P301Lhet) were cryosectioned together and stained simultaneously. One, two or three sections from each batch of COs were stained. White boxes in the merged images on the left indicate magnified areas, shown in merged images on the right. Scale bar = 10µm.

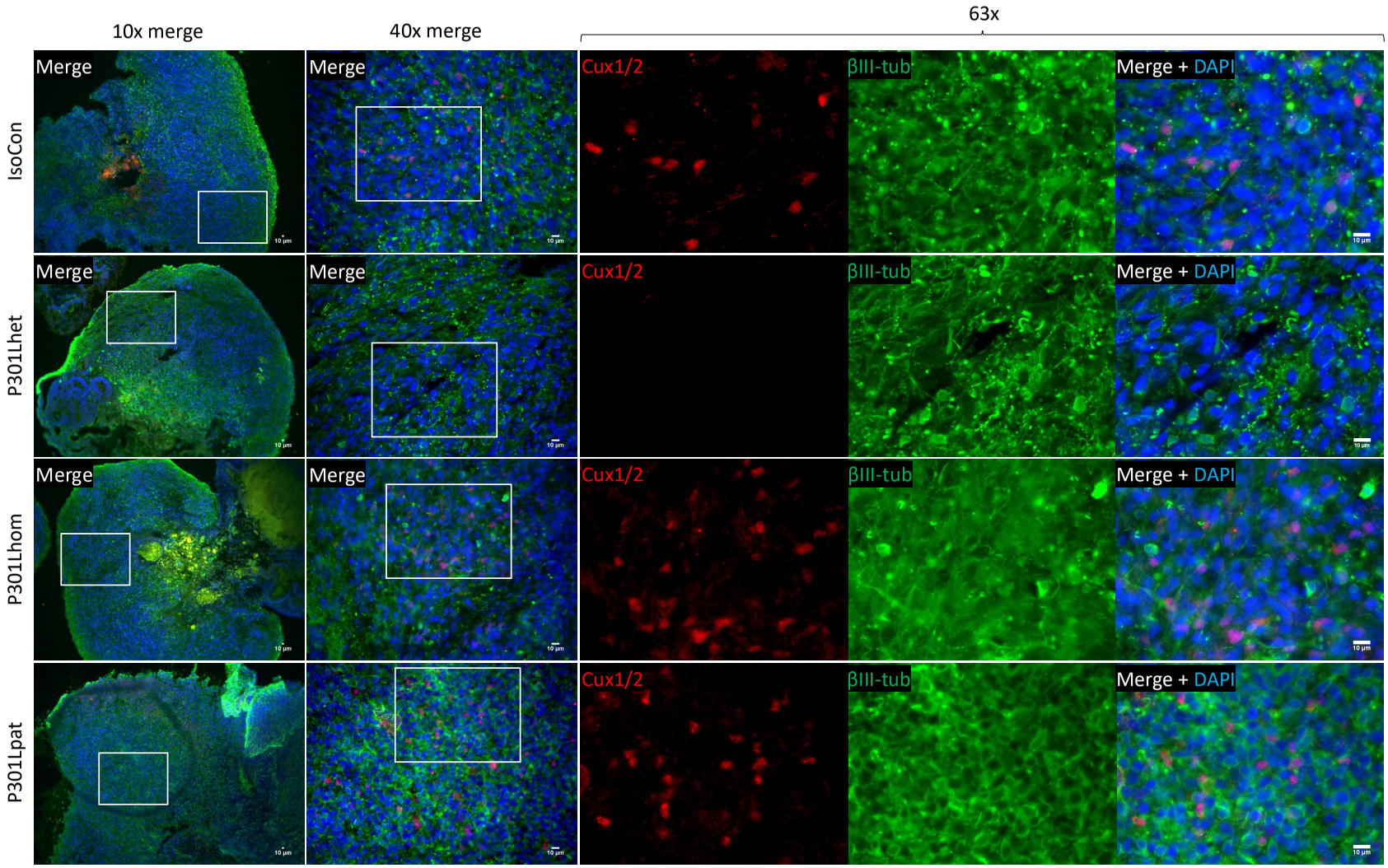

Fig. 6.6 **Cux1/2 positive layer 2-4 neurons were detected in IsoCon, P301Lhom, and P301Lpat (but not P301Lhet) iPSC-derived COs at day 84-100.** Layer 2-4 neurons were expected in COs from all four iPSC lines. The absence of layer 2-4 neurons in P301Lhet COs was unexpected, and suggests that these COs were developing more slowly than the other COs, or did not contain much forebrain-like tissue. At least six COs from each of three differentiation rounds (IsoCon, P301Lhom, P301Lpat) or one differentiation round (P301Lhet) were cryosectioned together and stained simultaneously. One, two or three sections from each batch of COs were stained. White boxes in the merged images on the left indicate magnified areas, shown in merged images on the right. Scale bar = 10μm.

neurons were found in IsoCon COs from three of three differentiation rounds, in P301Lhom and P301Lpat COs from two of three differentiation rounds, and in P301Lhet COs from one of one differentiation rounds (Figure 6.5). Cux1/2 positive (layer 2-4) neurons were found in IsoCon COs from two of three differentiation rounds, in P301Lhom COs from two of three differentiation rounds, and in P301Lpat COs from one of three differentiation rounds, but not in P301Lhet COs (Figure 6.6).

These results show that most COs contained at least one marker indicating the presence of cortical neurons, although some areas within each CO did not contain any of these markers. The timing of layer marker expression was also in line with other studies on iPSC-derived neural cultures: Tbr1 positive layer 6 neurons have been detected in 30-110 day-old COs (Gonzalez et al., 2018; Lancaster et al., 2013), and Cux1/2 positive layer 2-4 neurons have been detected in 70 day-old monolayer cortical neuron cultures (Shi et al., 2012a).

6.4.3 Tau isoform expression in cerebral organoids

I assessed 3R and 4R tau isoform expression in my COs by Western blotting and immunofluorescence. Representative Western blots using protein from day 84-100 IsoCon, P301Lhet, P301Lhom, and P301Lpat COs are shown in Figure 6.7, and a summary of the tau isoforms detected is shown in Figure 6.3. Western blots were repeated at least twice and at most three times per independently differentiated batch of COs.

The 0N3R tau isoform was detected in protein extracts from COs derived from each iPSC line, in each independent differentiation (blue asterisks in Figure 6.7). This was also the predominant isoform, suggesting a high proportion of immature neurons. The 0N4R tau isoform (red asterisks in Figure 6.7) was detected in IsoCon COs (in three differentiations), P301Lhet COs (one differentiation), P301Lhom COs (two of three differentiations) and P301Lpat COs (three of three differentiations). However, the prominence of the 0N3R tau isoform band may have obstructed detection of some 0N4R isoform bands, since longer exposure of the Western blot to detect weaker 0N4R bands increased the size of the 0N3R band detected. The 1N3R tau isoform bands (green asterisks in Figure 6.7) were detected in IsoCon COs (in two of three differentiations), P301Lhet COs (one differentiation), P301Lhom COs (one of three differentiations), and P301Lpat COs (one of three differentiations).

The detection of 0N4R in most COs with the P301L mutation is particularly important since P301L is only present in 4R tau (Hasegawa et al., 1999; Hong, 1998). Since some 4R tau is present, effects of the P301L mutation may be present.

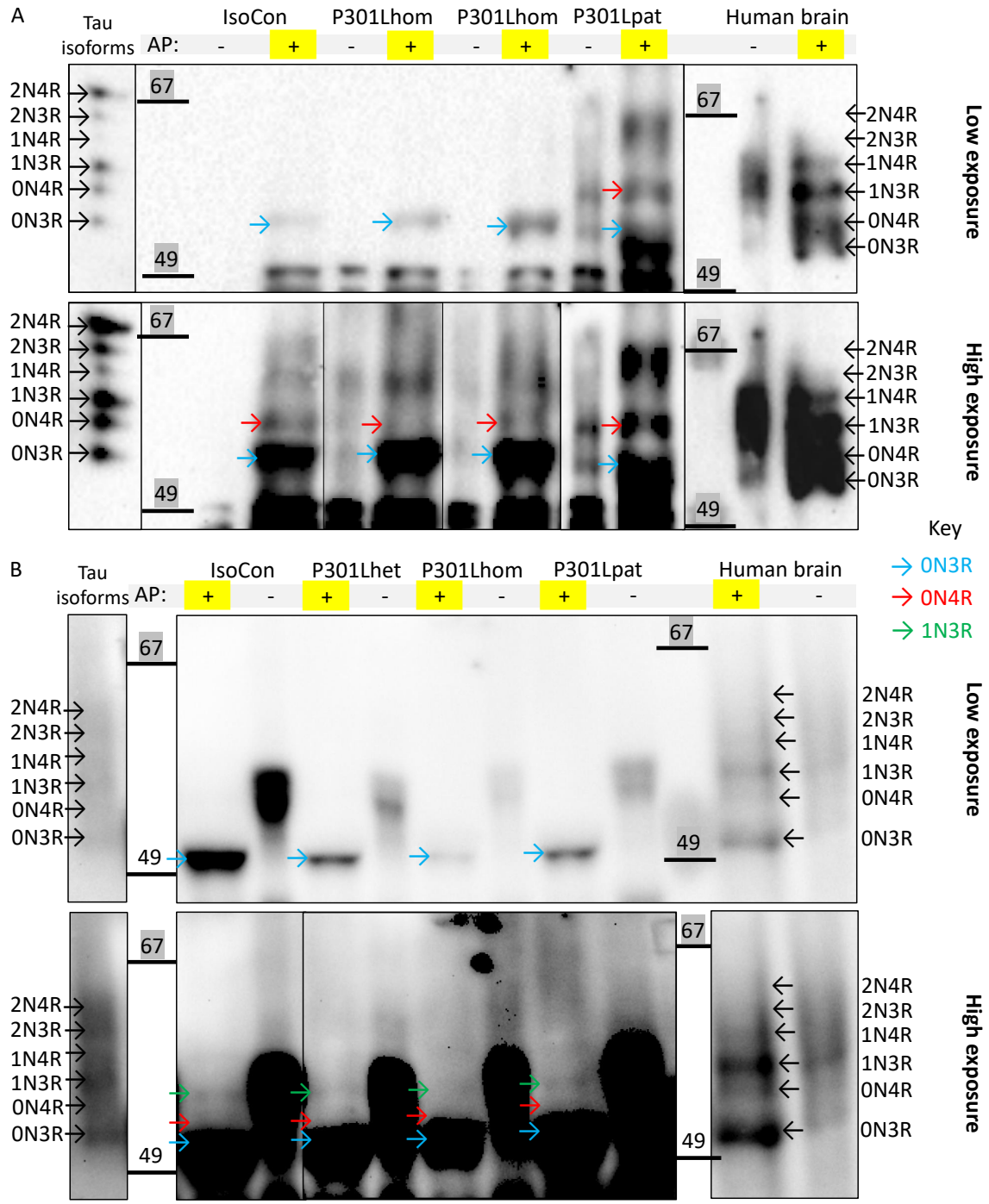

Fig. 6.7 **Western blots for tau isoforms show expression of 0N3R, 0N4R and some 1N3R tau in IsoCon, P301Lhet, P301Lhom and P301Lpat iPSC-derived COs at day 84-100.** Representative blots probed for all tau isoforms using the total tau antibody tau DAKO. Each lane contained protein from at least six COs derived from the indicated iPSC line in one independent differentiation round. "+", highlighted in yellow, indicates lanes containing protein which was dephosphorylated with alkaline phosphatase (AP), to visualise the tau isoforms as distinct bands. "-" indicates lanes containing protein not treated with alkaline phosphatase, where tau is phosphorylated, and runs as a smear. The size of the molecular weight markers (kDa) are shown. Recombinant tau isoforms and control adult human brain are included as positive controls, and each isoform is labelled. Low **A)** and high **B)** exposures of the same membrane are shown. Arrows in blue (0N3R), red (0N4R), or green (1N3R) indicate tau isoforms present in protein from COs (see Key). Black vertical lines indicate that the two parts of the same blot are shown at different exposures.

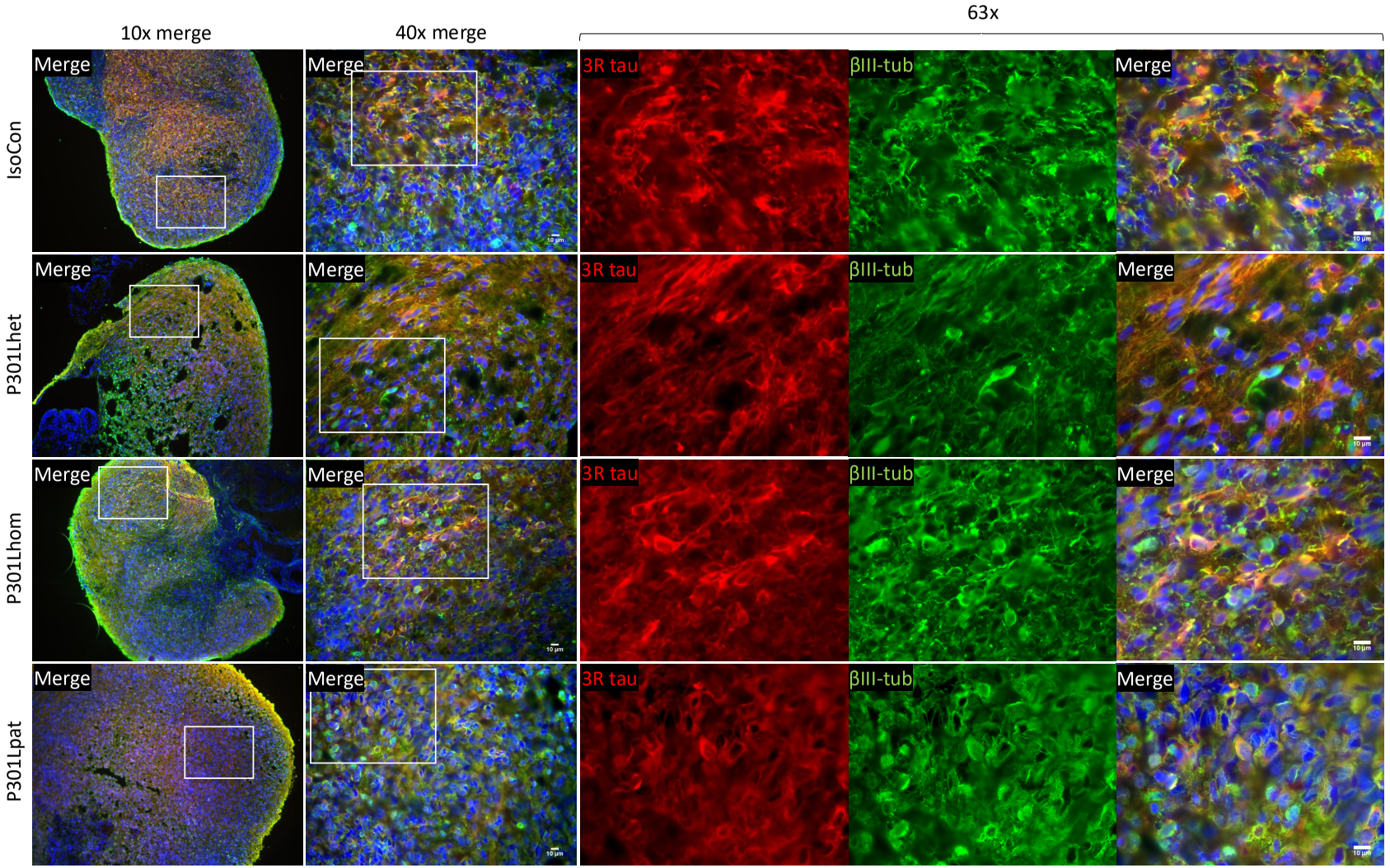

Fig. 6.8 **3R tau expression was detected in IsoCon, P301Lhet, P301Lhom, and P301Lpat iPSC-derived COs at day 84-100.** 3R tau was visible in the cell bodies and in some processes in COs from all four iPSC lines. The majority of the 3R protein detected was 0N3R, with a small amount of 1N3R, as determined by Western blot. The expression of 0N3R tau was expected, since 0N3R tau is expressed in human neurons pre-natally, as well as alongside the other five isoforms in the adult human brain. 1N3R tau expression was not expected, since it is expressed only in the post-natal human brain. The large amount of 0N3R and small amount of 1N3R tau suggests a large proportion of immature neurons, and a small proportion of maturing neurons. Representative images of βIII-tubulin positive, 3R tau positive neurons in COs. 3R tau was detected with the RD3 antibody. At least six COs from each differentiation were cryosectioned together for immunostaining. White boxes in the merged images on the left indicate magnified areas, shown in merged images on the right. Scale bar = 10µm.

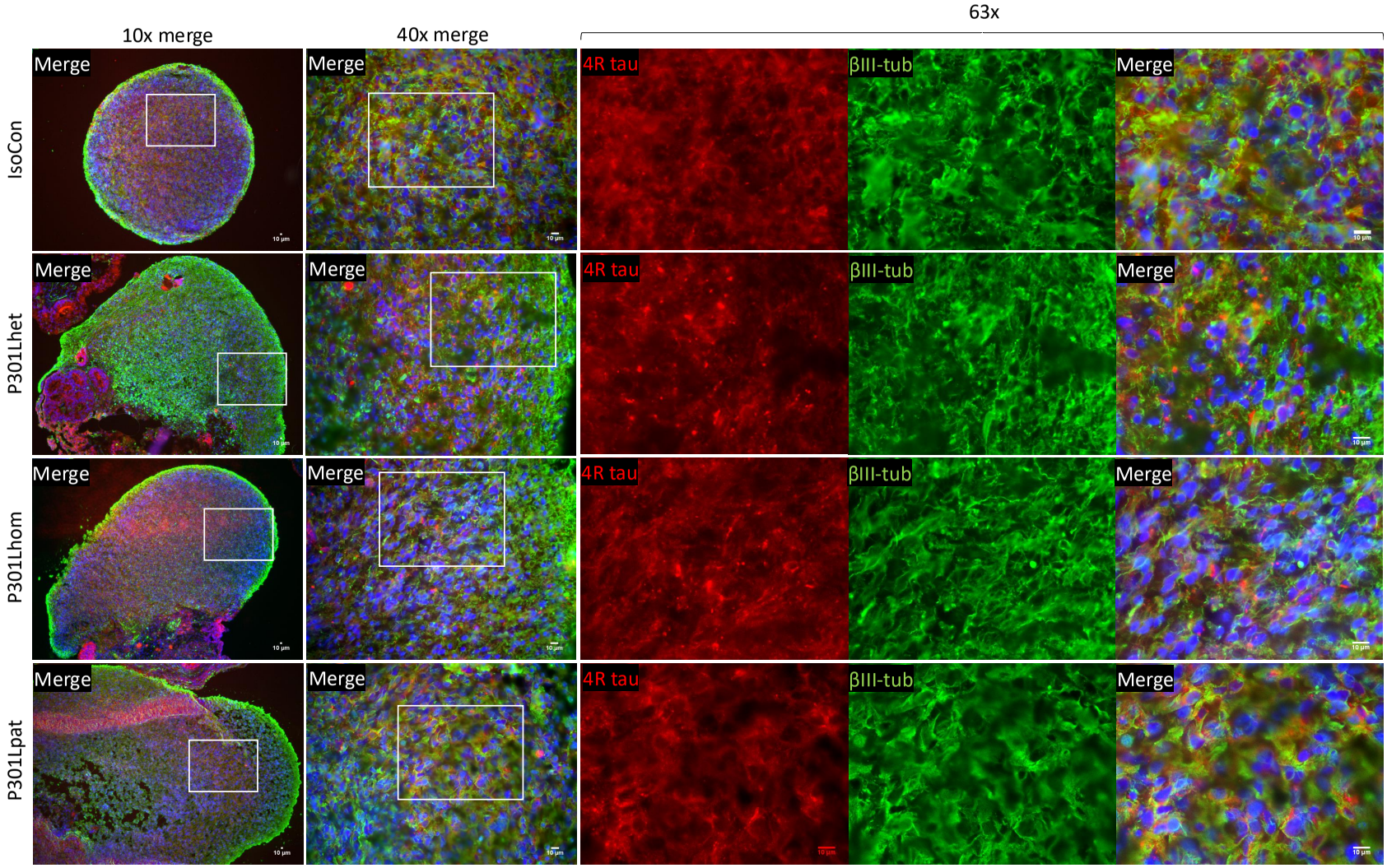

Fig. 6.9 **4R tau expression detected in IsoCon, P301Lhet, P301Lhom, and P301Lpat iPSC-derived COs at day 84-100.** 4R tau was visible in cell bodies of COs from all four iPSC lines. The majority of the 4R tau protein detected was 0N4R, according to Western blots. The expression of 0N4R tau indicates that some neurons in the COs were maturing, since 0N4R tau is only expressed in the post-natal human brain. This also suggests that the COs were more mature with respect to tau expression than the monolayer cultures described in Chapters 3 and 4. Expression of 0N4R tau also indicates that some P301L mutant tau was present in the P301L mutant COs, since this mutation is present in 4R, but not 3R tau. Representative images of βIII-tubulin positive, 4R tau positive neurons in COs. 4R tau was detected with the RD4 antibody, then signal was amplified with biotinylated anti-mouse IgG and a streptavidin Alexa Fluor conjugate. At least six COs from each differentiation were cryosectioned together for immunostaining. White boxes in the merged images on the left indicate magnified areas, shown in merged images on the right. An area of necrosis is visible in the merged image of P301Lpat. This occurred in the centres of some larger COs, or in some COs which fused with each other in culture, due to the CO's size exceeding that at which diffusion of oxygen and nutrients into its centre was sufficient to sustain cells. This was an expected phenomenon (Lancaster et al., 2017). Scale bar = 10µm.

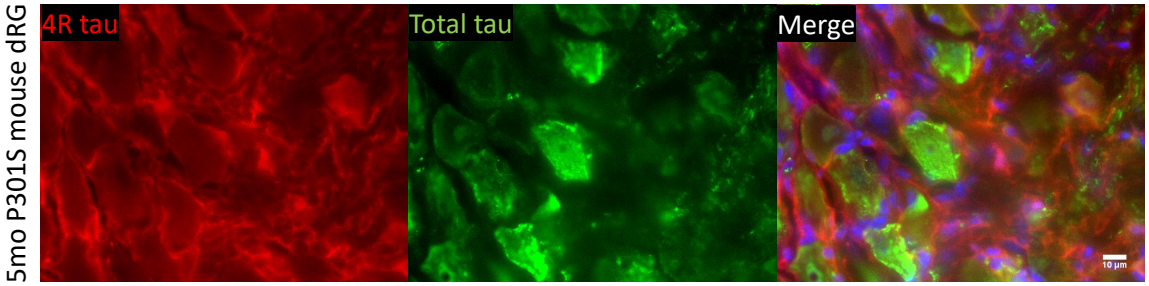

Fig. 6.10 **Positive control for 4R tau immunostaining: dRG from a 5 month-old P301S mouse.** 4R tau was detected with the RD4 antibody, then signal was amplified with biotinylated anti-mouse IgG and a streptavidin Alexa Fluor conjugate. All tau isoforms were detected with the tau DAKO antibody. Some cells show bright tau DAKO staining, which is expected: it indicates the presence of tau accumulations (Mellone et al., 2013). Scale bar = 10µm.

Table 6.3 **Tau isoforms in day 84-100 IsoCon, P301Lhet, P301Lhom, and P301Lpat COs detected by Western blotting**

	IsoCon	**P301Lhet**	**P301Lhom**	**P301Lpat**
0N3R	3/3	1/1	3/3	3/3
0N4R	3/3	1/1	2/3	3/3
1N3R	2/3	1/1	1/3	1/3

Western blots were performed using COs from each independent differentiation round. The table indicates which tau isoforms were observed in COs from each iPSC line as a proportion of the total number of independent differentiations. For example, 1/3 means the isoform was seen in one of three differentiations.

I corroborated the results of Western blots by immunostaining with antibodies against 3R or 4R tau, and co-staining βIII-tubulin, to identify neurons. 3R tau was detected in cell bodies and in processes (Figure 6.8). The 4R tau signal was amplified using biotin and streptavidin during immunostaining, and 5-month-old P301S mouse dorsal root ganglia (dRGs) were used as a positive control (Figure 6.10) . The 4R tau isoform was detected mostly in cell bodies (Figure 6.9).

There was no clear difference in the overall brightness of 4R tau immunofluorescence between the COs. This is expected, since the P301L mutation does not alter 4R tau splicing (Hasegawa et al., 1999; Hong, 1998; Hutton et al., 1998), and 0N4R tau was detected in COs from each of the iPSC lines by Western blotting.

Together, the Western blots and immunostaining experiments to detect tau isoforms show that the 0N3R tau isoform was strongly expressed in COs from all iPSC lines, and that lower amounts of 0N4R and 1N3R tau were also present. This indicates mature tau splicing in some neurons. Since 0N4R and 1N3R tau bands were stronger in Western blots using protein from COs than in Western blots using protein from monolayer neurons (Chapter 3) my results suggest that 3D culture as COs increases maturation with respect to tau expression in iPSC-derived neurons. However, to determine that this is due to 3D culture and not differences between the iPSC lines used for monolayer culture and those used for 3D culture, cerebral organoids and monolayer neurons would need to be grown from the same iPSCs at the same time, and the tau isoforms present would need to be assessed on the same Western blots.

When the P301Lhet and P301Lhom iPSC lines were generated from the IsoCon line using CRISPR, silent mutations were introduced to increase gene editing efficiency. It is possible that these mutations could alter exon 10 splicing, changing the amount of 4R tau present (discussed in Chapter 5). Since the IsoCon and P301Lpat COs do not contain the silent mutations, but the P301Lhet and P301Lhom COs do, comparing the tau isoforms expressed is one way to determine the effects of the silent mutations on exon 10 splicing. The detection of similar amounts of 0N4R tau in COs without the silent mutations (IsoCon and P301Lpat) and with the silent mutations (P301Lhet and P301Lhom) suggests that the silent mutations had a minimal effect on exon 10 splicing.

6.4.4 Tau phosphorylation at Ser202 and Thr205 (the AT8 epitope)

Tau phosphorylation at Ser202 and Thr205 (detected with the AT8 antibody) occurs in both the fetal human brain (Goedert et al., 1993) and in disease, including in the brains of people with FTDP-17T, but not in normal adult human brains (Han et al., 2009; Miklossy et al., 2007; Spillantini et al., 1996b). To determine the extent of Ser202 and Thr205 phosphorylation in my COs, I immunostained with the AT8 antibody and the tau DAKO antibody, which detects all tau isoforms and is referred to as “total tau”.

Cryosectioned dRGs from 5-month-old P301S mice were used as positive controls for tau staining (Figure 6.11). AT8 positive and negative cells were visible, indicating that phosphorylated and total tau could be detected by immunofluorescence. In the COs, AT8 staining (detected at 647nm) overlapped with total tau staining (detected at 488nm), indicating that AT8 staining was specific for tau. AT8 was visible in cell bodies and processes in the COs (Figure 6.11).

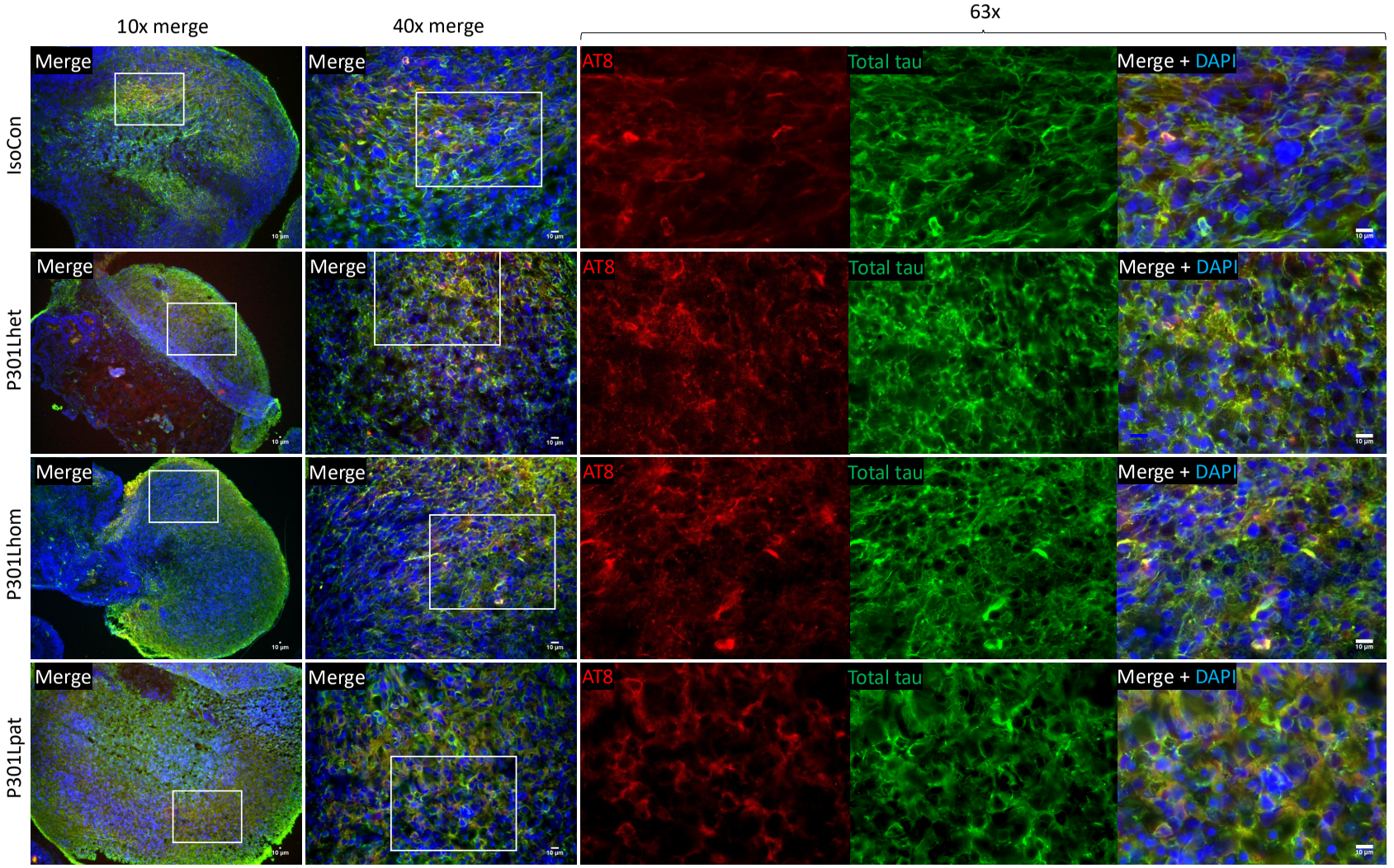

Fig. 6.11 **Tau phosphorylated at Ser202 and Thr205 (detected with the AT8 antibody) is found in IsoCon, P301Lhet, P301Lhom, and P301Lpat COs at day 84-100.** AT8 positive tau was detected in cell bodies and in some processes in COs from all iPSC lines. Quantification of these and other images showed that there was no significant difference in the amount of AT8 staining between COs from control and P301L iPSC lines, suggesting that no FTDP-17T-relevant phosphorylation at the AT8 epitope was present. Representative images of COs containing tau positive neurons (stained with the tau DAKO antibody, which detects all tau isoforms), some of which contained tau phosphorylated at Ser202 and Thr205 (detected with the AT8 antibody). At least six COs from each differentiation were cryosectioned together for immunostaining. White boxes in the merged images on the left indicate magnified areas, shown in merged images on the right. Scale bar = 10µm.

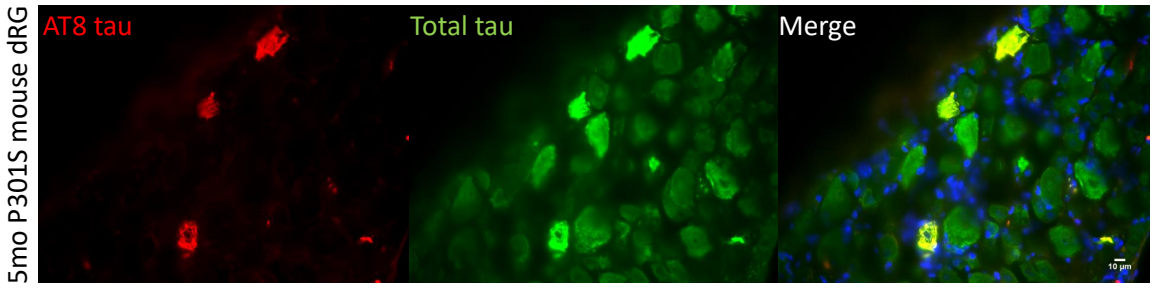

Fig. 6.12 **Positive control for AT8 immunostaining: dRG from a 5 month-old P301S mouse.** Tau phosphorylated at Ser202 and Thr205 was detected with the AT8 antibody. All tau isoforms were detected with the tau DAKO antibody. Some cells show bright tau DAKO staining, which is expected and indicates the presence of tau accumulations (Mellone et al. 2013). In a subset of these cells, the accumulated tau is phosphorylated at Ser202 and Thr205, and is therefore AT8 positive. Scale bar = 10µm.

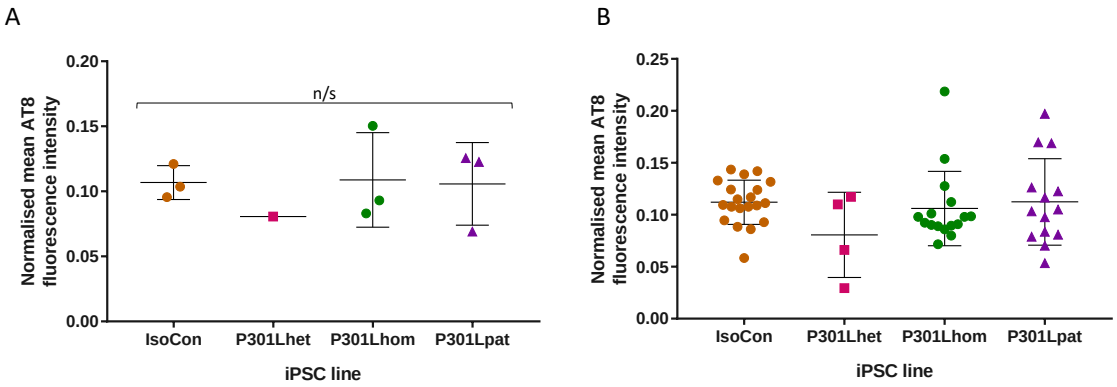

Fig. 6.13 **There is no significant difference in AT8 immunofluorescence intensity between IsoCon, P301Lhet, P301Lhom, and P301Lpat iPSC-derived COs at day 84-100.** Mean AT8 fluorescence, minus background fluorescence (measured in areas outside the CO), normalised to total tau fluorescence. **A)** Each point represents the average AT8 fluorescence (normalised to total tau fluorescence) of COs made in three independent differentiations. Error bars show the mean± SD. A significance bar indicates the results of a one-way ANOVA: there was no significant difference in the amount of AT8 staining in COs made from different iPSC lines. **B)** shows the data which was summarised in **A)**. In **B)**, each point represents the AT8 fluorescence (normalised to total tau fluorescence) of one CO (which is an average of two representative images from each CO). Error bars show mean±SD, considering all individual points.

Two sections from each batch of at least six COs (at least 90μm apart) were stained and analysed. Staining both sets of sections gave similar results, and results from the second set of sections stained are presented here. I quantified AT8 staining by measuring fluorescence intensity and subtracting background fluorescence (fluorescence visible outside the COs, in empty areas), then normalising to total tau fluorescence intensity. Images for quantification were taken at 40x (shown in Figure 6.11), from two representative areas per CO. At least six COs from each batch were stained for AT8 and total tau, and images were taken of every CO which had large lobes of total tau positive neurons.

Figure 6.13A shows the mean AT8 fluorescence (normalised to total tau fluorescence) for each batch of independently differentiated COs, and 6.13B shows the mean AT8 fluorescence intensity (normalised to total tau fluorescence) of individual COs. A one-way ANOVA comparing the mean AT8 fluorescence intensities presented in 6.13A found no significant difference between COs derived from IsoCon, P301Lhet, P301Lhom, and P301Lpat iPSCs ($F(3,6)=0.2568$, $p=0.8541$).

These results show no difference in tau phosphorylation at Ser202 and Thr205 between COs derived from the isogenic iPSC lines IsoCon, P301Lhet and P301Lhom, suggesting that AT8 immunoreactivity in these COs is development-like, rather than related to FTDP-17T-linked MAPT mutations.

6.4.5 Conformational changes in tau

The MC-1 antibody detects misfolded tau, with an epitope consisting of tau amino acids 7–9 and 312–342 (Jicha et al., 1996). MC-1 positive tau is detected in the brains of several mouse models expressing mutant tau (Decker et al., 2015; Maeda et al., 2016; Xu et al., 2014), and in the brains of people with AD and other tauopathies (Bouras et al., 2003), where it is thought to represent a pathological conformation of tau associated with aggregation (Jeganathan et al., 2008).

MC-1 positive tau has so far only been reported in iPSC-derived neural cultures exposed to external cues, such as tau fibrils (Usenovic et al., 2015), tau fibrils and tau overexpression (Medda et al., 2016), or transplantation of iPSC-derived neurons into an AD mouse brain (Espuny-Camacho et al., 2017). For example, Medda et al. (2016) transduced control iPSC-derived NPCs with a virus containing P301L-mutant 2N4R tau, then seeded the cultures with a pro-aggregation tau fragment (containing the P301L mutation), and found MC-1 immunoreactivity after 32 days. However, the spontaneous appearance of MC-1 positive tau

has not yet been reported in neural cultures derived from iPSCs whose donors carry MAPT mutations.

To determine whether misfolded tau was present in my COs, I immunostained for MC-1 (detected at 647nm in the far-red channel) and all tau isoforms, referred to here as "total tau" (detected with the tau DAKO antibody, at 488nm in the green channel). Very low levels of fluorescence were detected at 568nm (in the red channel), indicating that MC-1 staining was not bleed-through from total tau staining. A positive control for MC-1 staining (cell bodies in dRGs from a five month-old P301S mouse) is shown in Figure 6.14, indicating that staining technique itself was sufficient to detect misfolded tau.

Representative images from IsoCon, P301Lhet, P301Lhom, and P301Lpat COs are shown in Figure 6.14. Some MC-1 staining was visible in COs from all iPSC lines, including in IsoCon COs, and it was localised to cell bodies and processes. In each case, MC-1 staining overlapped with total tau staining, suggesting that it was specific for tau. However, similar patterns and levels of MC-1 staining were in detected control (IsoCon) as well as MAPT mutant (P301Lhet, P301Lhom, and P301Lpat) COs. Since MC-1 staining is not detected in control human brain (Weaver et al., 2000), and since the MC-1 staining detected in COs was much dimmer than in the positive control (Figure 6.15) it is possible that MC-1 staining in COs was background staining, and that mis-folded tau was not present.

Two sections from each batch of at least six COs (at least 90μm apart) were stained and analysed. Staining both sets of sections gave similar results, and results from the second set of sections stained are presented here. I quantified MC-1 staining by measuring fluorescence intensity and subtracting background fluorescence (measured in empty areas outside the COs), and normalising to total tau fluorescence intensity. Images for quantification were taken at 40x (shown in Figure 6.14), from two representative areas per CO.

Figure 6.16A shows the mean MC-1 fluorescence (normalised to total tau fluorescence) in COs from three independently differentiations, and Figure 6.16B shows MC-1 fluorescence (normalised to total tau fluorescence) from each individual CO. A one-way ANOVA showed no significant difference between the mean MC-1 fluorescence intensity from IsoCon, P301Lhet, P301Lhom, and P301Lpat COs ($F(3,6)=0.9078$, $p=0.4909$).

The immunofluorescence results suggest that misfolded tau was present in all COs, including IsoCon COs. This finding was not expected, since MC-1 does not react with control human brain (Weaver et al., 2000). Further work is needed to clarify whether the MC-1 staining in IsoCon COs is specific.

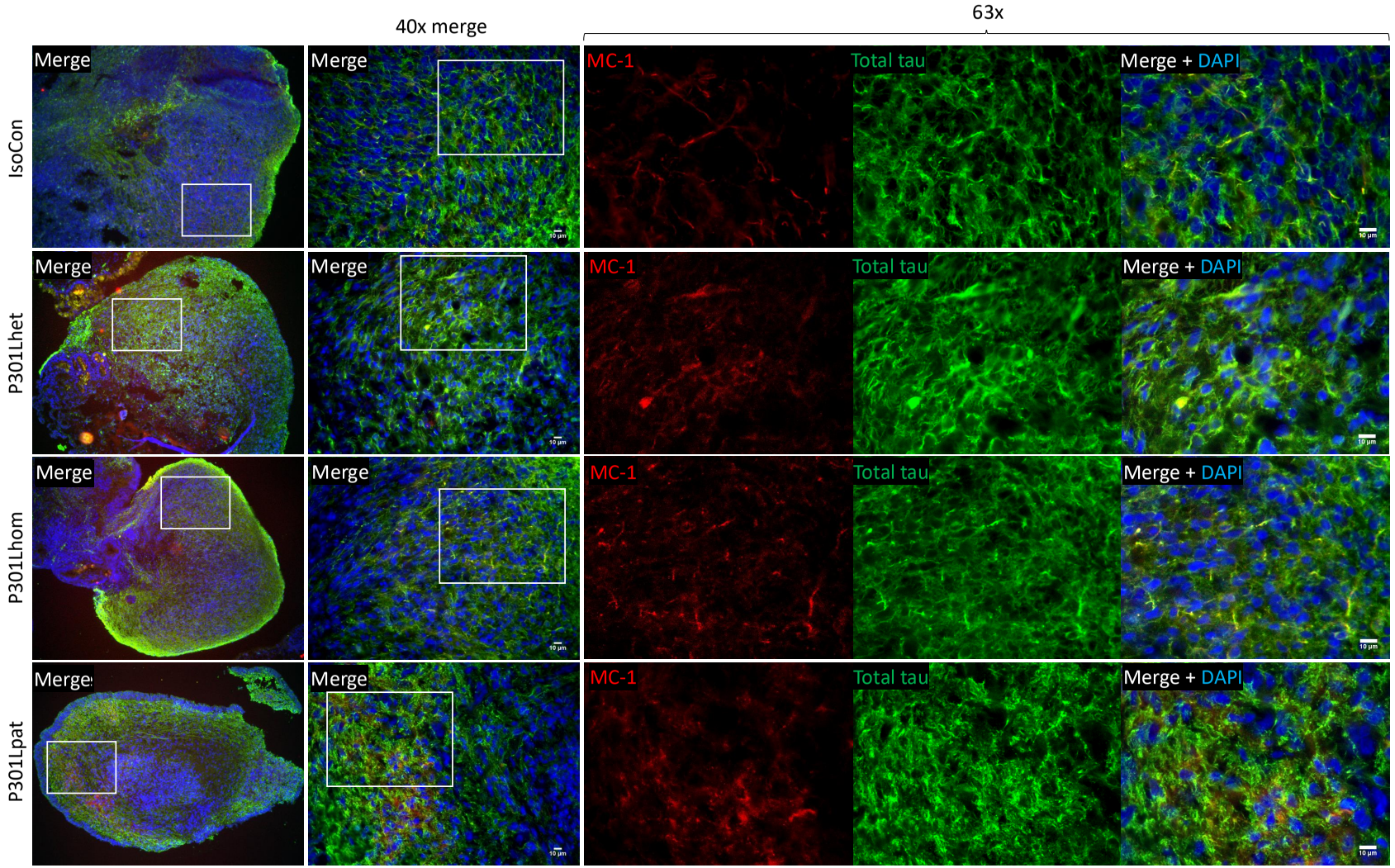

Fig. 6.14 **Possible background staining with the MC-1 antibody against mis-folded tau is detected in IsoCon, P301Lhet, P301Lhom, and P301Lpat COs at day 84-100.** MC-1 staining was detected in occasional cell bodies and in structures that resemble processes in COs from all iPSC lines. MC-1 positive tau in control COs was not expected, since MC-1 staining is not found in the brains of healthy adult humans. This, and the dim MC-1 immunofluorescence in the COs as compared to the positive control suggests that MC-1 staining was not specific for misfolded tau, and that there was no tau misfolding in the COs. Representative images of COs containing tau positive neurons (stained with the tau DAKO antibody, which detects all tau isoforms), some of which contained misfolded tau (detected with the MC-1 antibody). At least six COs from each differentiation were cryosectioned together for immunostaining. White boxes in the merged images on the left indicate magnified areas, shown in merged images on the right. Scale bar = 10µm.

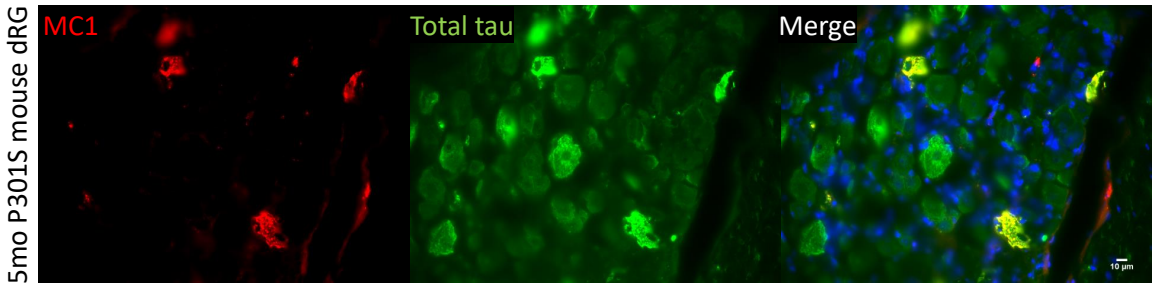

Fig. 6.15 **Positive control for MC1 immunostaining: dRG from a 5 month-old P301S mouse.** Misfolded tau was detected with the MC1 antibody. All tau isoforms were detected with the tau DAKO antibody. All tau isoforms were detected with the tau DAKO antibody. Some cells show bright tau DAKO staining, which is expected and indicates the presence of tau accumulations (Mellone et al. 2013). In a subset of these cells, the accumulated tau is MC1 positive, indicating that it is misfolded. Scale bar = 10µm.

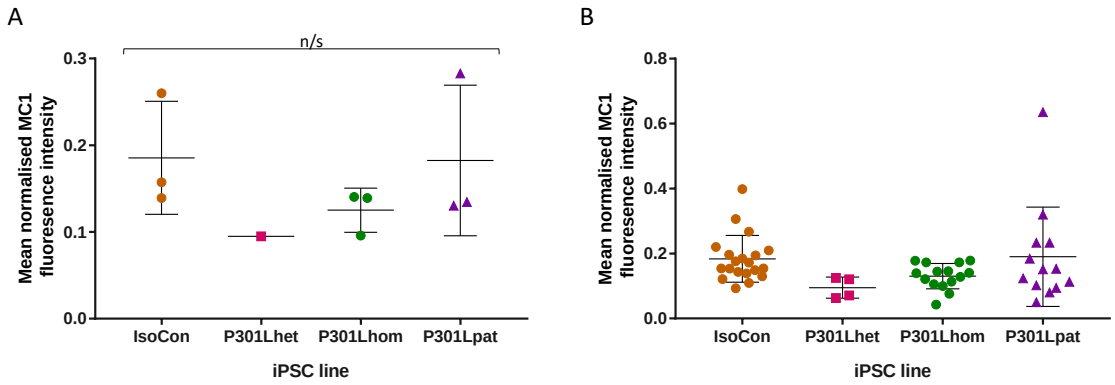

Fig. 6.16 **There is no significant difference in MC-1 immunofluorescence intensity between IsoCon, P301Lhet, P301Lhom, and P301Lpat iPSC-derived COs at day 84-100.** Mean MC-1 fluorescence, minus background fluorescence, was normalised to mean total tau (tau DAKO) fluorescence. **A)** Each point represents the average MC-1 fluorescence (normalised to total tau fluorescence) from at least four COs made in the same differentiation round. Bars show mean±SD. A significance bar indicates the results of a one-way ANOVA: there was no significant difference in the amount of MC-1 between COs made from the control and P301L mutant iPSC lines. This is likely to be because the MC-1 staining observed is non-specific. **B** shows the data which was summarised in **A**. In **B**, each point represents the mean MC-1 fluorescence value (normalised to total tau fluorescence) for each CO imaged. Values for each CO were obtained by averaging two readings from different areas of the same CO, where possible. Bars show mean±SD of the data, considering all individual points.

6.5 Discussion

6.5.1 Cell types detected

I detected βIII-tubulin positive neurons, the synaptic protein synaptophysin, and GFAP positive astrocytes in COs derived from the IsoCon, P301Lhet, P301Lhom, and P301Lpat iPSCs, and there was no significant difference in the amount of βIII-tubulin, GFAP, or synaptophysin detected between COs from the different iPSC lines. The detection of these proteins in 84-100 day-old COs was expected, since synapses have been detected in iPSC-derived COs from day 28 onwards (Mariani et al., 2012; Paşca et al., 2015; Yan et al., 2018), astrocytes are expressed from approximately day 45 onwards in forebrain monolayer iPSC-derived neural cultures (Shi et al., 2012a), and from approximately day 30 in ESC-derived COs (Matsui et al., 2018). Using GFAP to detect astrocytes may have over-estimated the proportion present, since radial glia also express GFAP (Raponi et al., 2007). However, I found few neural rosette-like radially arranged areas when immunostaining. Neural rosettes are sites of neurogenesis analogous to the neural tube, which are populated by neural precursors including radial glia (Elkabetz et al., 2008). Finding few neural rosettes in the COs indicates that the number of radial glia present was relatively low. By only immunostaining for neurons and astrocytes, I did not detect other cell types that may have been present in the COs, such as oligodendrocytes or oligodendrocyte precursors (Renner et al., 2017). Further characterisation of these cultures could include immunostaining for these cells.

Astrocyte proliferation has been observed in cortical and sub-cortical brain areas in people with MAPT mutations including P301L (Miyasaka et al., 2001). To see if this phenotype is recapitulated in COs, I could have aged the COs for longer. However, control COs contain mostly astrocytes at later timepoints (229 days) (Renner et al., 2017), so any astrocyte proliferation in MAPT-mutant COs would probably be masked by similar overgrowth in control COs as part of normal CO culture.

Synapse loss is a feature of human tauopathies including PSP and Pick's disease (Bigio et al., 2001; Callahan and Coleman, 1995; Masliah et al., 1989). It is also found in FTDP-17T mouse models, including in three-month-old mice expressing human P301S tau (Xu et al., 2014; Yoshiyama et al., 2007). However, significant synapse loss has not been detected in iPSC-derived neural cultures in the presence of an endogenous MAPT mutation alone (Silva et al., 2016). Decreased synapse density in iPSC-derived neurons has been observed after overexpression of the tau repeat domain containing both P301L and V337M MAPT mutations (Reilly et al., 2017), and after addition of recombinant tau fibrils (Usenovic et al., 2015). The requirement for exogenous or abnormal tau suggests that synapse loss is unlikely

to occur spontaneously in COs, or that it might require extended time in culture. Future experiments could include adding tau fibrils and measuring synapse density as one parameter which may be affected.

Early electrophysiological activity compared to controls has been observed in iPSC-derived P301L (and N279K) MAPT mutant neurons (Iovino et al., 2015), and in hippocampal neurons from mice expressing human P301L mutant tau (Crimins et al., 2012). Although I did not find evidence of synaptic loss in COs with the P301L MAPT mutation, it may be interesting to investigate electrophysiological activity in COs from the isogenic control and P301L iPSCs, particularly since COs are amenable to acute slice electrophysiology (Paşca et al., 2015).

6.5.2 Layer markers detected

COs from most differentiations contained cortical layer markers, indicating a cortical fate. This was expected, since the default state of NPCs differentiating without patterning cues is rostral forebrain (Tropepe et al., 2001; Watanabe et al., 2005), and because the forebrain-patterned COs were subjected to patterning factors to induce differentiation towards a forebrain fate (Lancaster et al., 2017). However, most COs also contained areas in which cortical neuron markers were not detected, and cortical neuron markers were not detected in some COs. This suggests that neurons from non-cortical brain areas may have been present, despite the COs having been differentiated by a protocol designed to produce mostly forebrain tissues. It could have been interesting to investigate this further using markers for other brain areas, such as hypothalamus, choroid plexus, retina, ventral forebrain, hindbrain, or spinal cord, which have been detected in non-patterned COs (Lancaster et al., 2013), but this was outside of the scope of my project. Future work on identifying the brain areas within COs could include immunostaining for cortical lobe markers. This would allow analysis of tau phosphorylation or misfolding focussed on frontal and temporal lobe-like tissue, which is most affected in FTDP-17T (Foster et al., 1997).

The similarity in layer marker expression between COs from the isogenic iPSC lines suggests that the P301L mutation does not alter layer marker expression, although a more detailed examination of the number of cells expressing each layer marker, and the timing of layer marker expression would be required to definitively determine this.

Exploring spontaneous NPC proliferation and the relative quantities of layer-specific neurons produced in P301L COs may be of interest, since two studies in iPSCs have identified effects on these parameters in the presence of MAPT mutations. García-León et al. (2018)

found a trend towards fewer proliferative cells and higher levels of neuron markers in spontaneously differentiating NPC cultures made from iPSCs with all three of the P301L, N279K, and intron 10+16 MAPT mutations as compared to controls. Although the presence of three MAPT mutations is non-physiological, it does suggest that MAPT mutations may affect NPC differentiation, although the effects may be more subtle with only one MAPT mutation. In addition, Verheyen et al. (2018) found that monolayer neural cultures derived from iPSCs with either the intron 10+16 mutation or both the intron 10+16 and the P301S mutations contained significantly fewer proliferative cells than control cultures, as well as significantly fewer Tbr1 positive neurons than control cultures after 50 days. It may be worth investigating this result in COs using isogenic iPSC lines.

6.5.3 Tau isoform expression in cerebral organoids

Western blotting and immunofluorescence results show that 3R tau, specifically 0N3R tau, was strongly expressed in COs from all iPSC lines, suggesting that immature neurons predominated. A few radially arranged rosette-like structures were visible in COs, as were intermediate progenitors, indicating that new neurons were being generated, even at day 84-100. To minimise the proportion of immature neurons, I could have maintained the COs for longer in culture, until neurogenesis was complete. Sloan et al. (2017) have maintained COs for 590 days, indicating that it is possible to grow these cultures for longer, but older COs contain predominantly astrocytes (Renner et al., 2017), so optimal aging of COs to detect tau isoforms may involve a trade-off between CO age and neuron content.

The 0N4R tau isoform was detected in COs from each of the iPSC lines by immunofluorescence and Western blotting. Since the P301L mutation is in tau exon 10 (Hong, 1998; Spillantini et al., 1998b), it is present in 4R (but not 3R) tau. Detecting some 4R tau in the COs indicates that P301L-mutant tau was present, and that effects of the P301L mutation could potentially be observed. However, Western blots indicated that there was much less 0N4R tau than 0N3R tau.

Bands indicating the presence of 1N3R tau were also detected by Western blot. Expression of 0N3R, 0N4R, and 1N3R tau in the COs indicates some adult-like tau splicing, which has previously been observed in both control and P301L-mutation iPSC-derived monolayer neurons (Iovino et al., 2015). To observe the tau isoforms present more clearly, I could have made larger batches of COs, so that protein extracts could be made using RIPA and perchloric acid independently. Tau can be selectively solubilised in perchloric acid (Goedert

and Jakes, 1990; Lindwall and Cole, 1984), giving Western blots with lower background in which tau isoforms can be more clearly observed.

My results suggest that 3D culture as COs (rather than 2D culture as monolayer neurons) increases maturity with respect to tau isoform expression. This is supported by the work of Choi et al. (2014), who found an increase in 4R tau and total tau mRNA in 3D as compared to 2D ReN cell-derived matrigel-based neuron cultures. Future work could include comparing tau expression between day 100 monolayer neurons and COs from the same iPSC lines, to more thoroughly examine the effect of 3D culture on tau expression in COs.

6.5.4 Tau phosphorylation

There was no significant difference in tau phosphorylation at Ser202 and Thr205 between IsoCon, P301Lhet, and P301Lhom COs, as measured by fluorescence intensity of AT8 staining. The lack of a difference in AT8 positive tau between MAPT-mutant and control COs was not expected, since increased AT8 staining relative to control has been detected in N279K (Ehrlich et al., 2015; Iovino et al., 2015), P301L (Iovino et al., 2015), V337M (Ehrlich et al., 2015) and A152T (Fong et al., 2013; Silva et al., 2016) MAPT-mutant iPSC-derived neurons. However, the AT8 epitope is also phosphorylated during fetal development (Goedert et al., 1993). The similarity in AT8 staining observed between the COs may have been caused by development-like AT8 phosphorylation in control and MAPT-mutant COs

The method I used to quantify AT8 positive neurons may not have been sensitive enough to detect small differences between COs. This was shown in Chapter 4, in which measuring the AT8 positive area in day 50 monolayer neurons was not sufficient to detect differences in the proportion of AT8 positive cells found when counting cells. However, measuring AT8 positive area was sensitive enough to detect an increase in the proportion of AT8 positive neurons over time (from day 50 to day 80-100), indicating that the method is appropriate for detecting larger differences between cultures.

Tau phosphorylation in other CO studies has been quantified using methods similar to the one I chose. For example, Raja et al. (2016) measured tau phosphorylation at Ser396 and Thr181 by measuring mean fluorescence intensity, and plotted it as fold increase compared to control. Other studies have included images of phosphorylated tau immunofluorescence without attempting quantification, demonstrating the difficulty in appropriately quantifying apparent differences.

A more sensitive detection method might be flow cytometry, as used by Yan et al. (2018), who detected a significant difference in the number of AT8 positive cells from COs with a

presenilin 1 mutation as compared to control COs. However, COs must be dissociated to single cells for this, meaning that neuronal processes (and any AT8 positive tau they contain) may be lost. Another alternative would be detecting AT8 positive tau by Western blot. I did detect AT8 positive tau in Western blots using IsoCon, P301Lhet, P301Lhom, and P301Lpat COs, but the amount of total tau detected varied greatly between different samples, making quantification impossible.

6.5.5 Tau misfolding

MC-1 positive tau in iPSC-derived neural cultures has previously been detected after addition of tau fibrils (Usenovic et al., 2015), tau overexpression and tau fibrils (Medda et al., 2016), or grafting into an AD mouse brain (Espuny-Camacho et al., 2017), but not in aging cultures expressing endogenous MAPT mutations. For these reasons, I did not expect to detect MC-1 positive tau.

There was no difference in tau misfolding between IsoCon, P301Lhet, and P301Lhom COs, as measured by the fluorescence intensity of MC-1 staining. I detected some MC-1 staining in all COs (including IsoCon COs) and this staining overlapped with total tau staining, suggesting that it was specific for tau. However, this would mean there was tau misfolding in IsoCon COs, which was not expected, since MC-1 positive tau is absent from the normal human brain (Spillantini et al., 1996b; Weaver et al., 2000). MC-1 staining in COs was much dimmer than that in the positive control, indicating that MC-1 staining in COs was background staining, and that mis-folded tau was not present. This result was expected, particularly since there was no significant difference in the amount of AT8 positive tau detected in the COs.

Future work could include further assessment of tau misfolding in COs, for example by native blotting - since MC-1 is a conformation-dependent epitope (Jicha et al., 1996), native blotting would need to be used, to avoid the denaturation which occurs during Western blotting.

6.5.6 Limitations and improvements

Variability between CO cultures

Variability of CO cultures is a recognised phenomenon which may be caused in part by incomplete neural induction (Lancaster et al., 2017): forebrain-patterned COs are more reproducible than their non-patterned counterparts, but still show variability between batches

(Lancaster et al., 2017). Batch variability and variability between cell lines may mask subtle phenotypes (Giandomenico and Lancaster, 2017).

My results show some variability between COs, which may have been enhanced by the relatively small sample sizes: a minimum of six COs from the same differentiation round were used for each of Western blotting and immunostaining. However, given the heterogeneity of the COs, samples for immunostaining and Western blotting may have been dissimilar, leading to different results from immunostaining and Western blotting experiments. Although at least six COs per batch were cryosectioned for immunofluorescence, not all were imaged. Some COs peeled away from the slide surface during staining and were lost, and some COs contained very few βIII-tubulin positive neurons. Variability between COs and between batches could be reduced by producing larger CO batches, perhaps in a 96-well format (Schukking et al., 2018), or using a scaled-up version of the spinning bio-reactor method (Qian et al., 2016).

Differences between iPSC lines may have also accounted for some variation between COs. For example, the three isogenic iPSC lines and the patient iPSC line were derived using different methods to make iPSCs, cultured in different iPSC culture systems (mTeSR and vitronectin versus KSR medium and feeder cells, Chapter 2) and were at different passage numbers when used (less than 15 for the isogenic iPSCs, unknown for the other iPSC lines).

Imaging

Immunostaining experiments were performed on at least two slices containing at least six COs. Although the two slices were at least 90µm apart, this may not have given results representative of the whole CO, since COs were not homogenous throughout. To quantify tau phosphorylation with AT8 and MC-1 immunostaining, I took two images per CO, although this still may not have been sufficient to represent all the variation of each CO. A good alternative might be high-content imaging, to measure the fluorescence intensity in more fields per CO. However, in COs containing non-neuronal cells or non-cortical brain areas, this method would also have drawbacks. To counteract this, I could have immunostained serial sections for cortical layers markers and for markers of interest (AT8, MC-1, 3R tau, 4R tau, total tau), then excluded from my analysis all non-forebrain-like tissue, and any rosette-like structures, as done by (Renner et al., 2017).

6.5.7 Summary

In this Chapter, I

1. Differentiated iPSCs into cerebral organoids, and determined that the proportion of astrocytes (GFAP) and neurons (βIII-tubulin) were not significantly different between control or P301L COs. No FTDP-17T-relevant astrocyte overgrowth was detected in the P301L COs.

2. Examined synaptic protein expression. Similar levels of synaptophysin were expressed by control and P301L COs, and there was no FTDP-17T relevant synapse loss in P301L COs.

3. Assessed tau isoform expression. 0N3R, 0N4R and 1N3R tau were detected by Western blotting in COs from all iPSC lines. Although 0N3R tau predominated, indicating a large number of immature neurons, the expression of some 0N4R and 1N3R tau suggests that some mature neurons were present. This result suggests that 3D culture does increase neuronal maturity with respect to tau isoform expression, and indicates that 3D COs may be a good model method for making mature neurons.

4. Examined tau phosphorylation at the AT8 epitope. There was no significant difference in the amount of AT8 staining between control and P301L COs, indicating that FTDP-17T-relevant changes in phosphorylation were not occurring by day 100.

5. Examined tau conformational changes with the MC-1 antibody. There was no significant different in the amount of MC-1 staining between control and P301L COs, and the MC-1 staining detected across all COs is likely to have been background staining.

In conclusion, the results in this Chapter provide ample avenues for future work on COs with MAPT mutations. In particular, examination of tau isoforms suggests that 3D COs may be more mature in terms of tau splicing than monolayer cultures. This finding merits further investigation, since it suggests that COs are a promising method for maturing neurons in culture. Although limited disease-relevant changes were examined, the presence of AT8 immunoreactivity indicates that tau phosphorylation occurs in COs. Longer culture times may be needed to detect FTDP-17T-relevant differences between control and P301L COs, and to increase neuronal maturity.

Chapter 7

Discussion

My project aimed to study the effects of the MAPT mutations N279K and V337M in 2D monolayer neural cultures, to generate isogenic iPSC lines with the N279K MAPT mutation, and to investigate the P301L MAPT mutation in 3D cerebral organoids (COs). In contrast to other studies using iPSC-derived MAPT-mutant neurons, this project made COs from isogenic iPSC lines. There was some variability between monolayer cultures and COs made in independent differentiations, which may have hindered my ability to detect subtle differences between control and MAPT-mutant neurons. The monolayer neural cultures matured over time, but I detected only one significant change in an FTDP-17T-relevant parameter: an increase in tau phosphorylation at Ser202 and Thr205 (detected with the AT8 antibody), which has already been published (Iovino et al., 2015). In both control COs and COs with the P301L mutation, I detected some tau phosphorylation (with the AT8 antibody) and some tau misfolding (with the MC-1 antibody). Although this is an interesting result, I did not corroborate or investigate it further due to time constraints.

7.1 Characterisation of control and MAPT-mutant iPSC-derived cultures

7.1.1 Monolayer cultures

The 2D neural cultures matured between day 50 and day 80-100. At day 50 the cultures contained mostly βIII-tubulin positive neurons and few S100β positive astrocytes, but by day 80-100, the proportion of astrocytes had significantly increased and the contribution of neurons to total protein had fallen. The increase in astrocyte number over time indicates

normal maturation of the cultures, since astrocytes are produced after neurons (Kriegstein and Alvarez-Buylla, 2009; Rakic, 2003). The amount of synaptophysin (normalised to the amount of βIII-tubulin) increased over time, suggesting ongoing synapse formation in the cultures. Tau splicing also matured over time: in the control cultures 0N3R tau and occasionally 0N4R was visible at day 50, whereas 0N3R, some 0N4R and occasional 1N3R tau appeared by day 80-100.

7.1.2 COs

COs from each of the iPSC lines IsoCon, P301Lhet, P301Lhom and P301Lpat contained βIII-tubulin positive neurons, although the amount detected varied between CO batches. Most COs contained some GFAP positive astrocytes, although some COs contained mostly astrocytes and very little βIII-tubulin, whereas others contained undetectable amounts of GFAP. Most COs also expressed synaptophysin, indicating synapse formation, although synaptophysin levels were variable. COs from all iPSC lines contained at least one marker indicating the presence of cortical neurons.

7.2 FTDP-17T-relevant phenotypes detected

7.2.1 Comparison of my work with other findings

My results from monolayer neurons are compared with previous work using the same iPSC lines but a different method (Iovino et al., 2015) in Table 7.1. My results from COs from the isogenic control, P301Lhet, P301Lhom and P301Lpat iPSC lines are compared with results from the same isogenic control and P301Lhet iPSCs grown as monolayers neurons (Appendix 2), and with results from previous work using a different control but the same P301Lpat iPSCs grown as monolayer neurons (Iovino et al., 2015) in Table 7.2.

7.2.2 Tau splicing

N279K

The N279K mutation increases tau exon 10 inclusion in mRNA and therefore increases 4R tau expression (D'Souza et al., 1999; Hong, 1998), and there was evidence of this in my cultures. The tau isoforms 0N3R, 0N4R and occasionally 1N3R and 1N4R were detected by Western blotting in N279K cultures at day 50 and day 80-100. This is compared to the

Table 7.1 **Comparison of results from control, N279K and V337M iPSC-derived neurons from my work in monolayer neurons with Iovino et al.'s results in control and N279K monolayer neurons made from the same iPSC lines using a different method**

	Monolayer neurons Iovino et al. (2015)			Monolayer neurons in this project	
	D50	**D150**		**D50**	**D80-100**
βIII-tubulin	✓	✓		✓	✓↓ from D50
Astrocytes	-	-		✓(few)	✓↑ from D50
Synapses	-	-		✓	✓↑ from D50
Tau isoforms					
Control	0N3R, some 0N4R	All 6 isoforms	**CTRL1**	0N3R, 0N4R	0N3R, 0N4R, 1N3R
			CTRL2	0N3R	0N3R, 0N4R
N279K	0N3R, 0N4R	All 6 isoforms	**N279K1**	0N3R, 0N4R, 1N3R, 1N4R	0N3R, 0N4R, 1N3R
			N279K2	0N3R, 0N4R	0N3R, 0N4R, 1N3R, 1N4R
V337M	-	-	**V337M**	0N3R, 0N4R	0N3R, 0N4R, 1N3R, 1N4R
Tau phosphorylation (AT8)					
Control	✓	-	**CTRL1**	✓	✓
			CTRL2	✓	✓
N279K	✓↑ vs control	-	**N279K1**	✓↑ vs control	✓→ vs control
			N279K2	✓→ vs control	✓→ vs control
V337M	-	-	**V337M**	✓→ vs control	✓→ vs control
Tau mis-folding (MC-1)					
Control	-	-	**CTRL1**	-	X
			CTRL2	-	X
N279K	-	-	**N279K1**	-	X
			N279K2	-	X
V337M	-	-	**V337M**	-	X
Fibrillar tau (pFTAA)					
Control	-	-	**CTRL1**	-	X
			CTRL2	-	X
N279K	-	-	**N279K1**	-	X
			N279K2	-	X
V337M	-	-	**V337M**	-	X

✓= indicated immunofluorescence positive; X = indicated immunofluorescence negative; - = indicated immunofluorescence not attempted; → = no change; ↑ = increase; ↓ = decrease.

Table 7.2 **Comparison of results from control and P301L iPSC-derived neurons from my work in monolayer neurons, Iovino et al.'s work in monolayer neurons, and my work in cerebral organoids**

	Monolayer neurons Iovino et al. (2015)			Monolayer neurons (Axol)	Cerebral Organoids
	D50	D150		D41	D84-100
βIII-tubulin	✓	✓		✓	✓variable
Astrocytes	-	-		X	✓variable
Synapses	-	-		-	✓variable
Tau isoforms					
Control	0N3R, some 0N4R	All 6 isoforms	**IsoCon**	0N3R	0N3R, 0N4R, 1N3R
P301L	0N3R	All 6 isoforms	**P301Lpat**	-	0N3R, 0N4R, 1N3R
			P301Lhet	0N3R	0N3R, 0N4R, 1N3R
			P301Lhom	-	0N3R, 0N4R, 1N3R
Tau phosphorylation (AT8)					
Control	✓	-	**IsoCon**	✓	✓
P301L	✓↑ vs control	-	**P301Lpat**	-	✓→ vs control
			P301Lhet	✓→ vs control	✓→ vs control
			P301Lhom	-	✓→ vs control
Tau mis-folding (MC-1)					
Control	-	-	**IsoCon**	X	Low
P301L	-	-	**P301Lpat**	-	✓→ vs control
			P301Lhet	-	✓→ vs control
			P301Lhom	-	✓→ vs control
Fibrillar tau (pFTAA)					
Control	-	-	**IsoCon**	X	X
P301L	-	-	**P301Lpat**	-	X
			P301Lhet	-	-
			P301Lhom	-	-

✓ = indicated immunofluorescence positive; X = indicated immunofluorescence negative; - = indicated immunofluorescence not attempted; → = no change; ↑ = increase; ↓ = decrease; Axol = NPCs obtained from Axol.

control cultures, which expressed 0N3R tau with occasional 0N4R tau at day 50, and 0N3R tau with some 0N4R and 1N3R tau at day 80-100. In addition, 4R tau immunofluorescence was brighter in N279K1 and N279K2 cultures at day 100, suggesting increased levels of 4R tau relative to the controls.

V337M

The V337M mutation does not alter tau exon 10 splicing (Hong, 1998). In my V337M cultures 0N3R and 0N4R tau were detected at day 50, and 0N3R, with occasional 0N4R, 1N3R and 1N4R were detected at day 80-100. However, in control cultures, 0N3R tau with occasional 0N4R tau was detected at day 50, and 0N3R tau with some 0N4R and 1N3R tau was found at day 80-100. This may suggest that more adult-like tau splicing was taking place earlier in V337M cultures, although a comprehensive comparison of tau splicing would require iPSC lines isogenic for the V337M mutation.

P301L

The P301L mutation does not alter tau exon 10 splicing (Hasegawa et al., 1999; Hong, 1998) but the P301Lhet and P301Lhom iPSCs contained silent mutations in tau exon 10 (the scars of editing by CRISPR) which may have affected tau splicing. I detected 0N3R and 0N4R tau in control and P301L COs in all three differentiations (with the exception of P301Lhom: 0N4R was detected in two of three differentiations). 1N3R tau was detected in control and P301L COs from one or two differentiations. These results indicate tau splicing in P301L-mutant COs was like that in the control, even when additional silent mutations were present. However, the effects of the silent mutations on tau splicing may merit further investigation.

7.2.3 Tau phosphorylation

I detected an increase in tau phosphorylation at Ser202 and Thr205 (detected with the AT8 antibody) in 50 day-old N279K monolayer neurons (pooled results from N279K1 and N279K2) relative to controls (pooled results from CTRL1 and CTRL2), which has already been reported in different experiments using neurons from the same iPSC lines (Iovino et al., 2015) but a different differentiation method. However, when each of the N279K lines were compared to controls, the difference in the proportion of AT8 positive neurons was significant for the N279K1 but not the N279K2 cultures. This may have been due to differences between the two iPSC lines and variability between the differentiations.

In addition, there was a significant difference in the proportion of AT8 positive neurons in N279K as compared to control neurons at day 50, but not at day 80-100. Phosphorylation at the AT8 epitope increased from day 50 to day 80-100 (comparing all cultures at day 50 to all cultures at day 80-100), so changes in phosphorylation related to the N279K mutation visible in the N279K1 cultures at day 50 may have been hidden by an increase AT8 phosphorylation in control cultures, particularly in CTRL1 cultures, where the increase in the proportion of AT8 positive cells between day 50 and day 80-100 was significant.

There was no significant difference in the proportion of AT8 positive neurons between control and V337M monolayer cultures at day 50 or day 80-100.

In addition, there was no significant difference in AT8 fluorescence intensity between IsoCon, P301Lhet, P301Lhom and P301Lpat COs at day 84-100.

The lack of a difference in phosphorylation at the AT8 epitope between MAPT-mutant and control monolayer neurons and COs may have occurred because AT8 detects tau phosphorylated in the fetal human brain (Brion et al., 1993; Matsuo et al., 1994; Milenkovic et al., 2018), as well as in FTDP-17T and other tauopathies (de Silva et al., 2006; Spillantini et al., 1996a). Therefore, normal development-like AT8 phosphorylation may have hindered my ability to detect MAPT mutation-related phosphorylation. One way to minimise this would be to use isogenic iPSC lines which differ only at the MAPT mutation locus, or to use antibodies which do not detect tau phosphorylated in the developing brain, such as AT100 (Ksiezak-reding et al., 2000; Matsuo et al., 1994), or AP422 (Miyasaka et al., 2001; Morishima-Kawashima et al., 1995).

7.2.4 Tau misfolding

No MC-1 positive tau was detected in MAPT-mutant or control monolayer cultures at day 80-100. Some pFTAA positive structures were detected in preliminary stainings of CTRL2, N279K1 and V337M cultures, but these did not overlap with total tau staining, indicating that they did not represent filamentous tau.

MC-1 staining, indicating mis-folded tau, was detected in COs derived from the IsoCon, P301Lhet, P301Lhom and P301Lpat iPSC lines. However, there was no significant difference in MC-1 fluorescence intensity between IsoCon, P301Lhet, P301Lhom and P301Lpat COs. Since MC-1 staining is not found in the brains of control subjects (Weaver et al., 2000), this finding merits further investigation.

7.2.5 Other phenotypes in monolayer cultures

There was no significant difference in the number of αB-crystallin positive neurons in MAPT-mutant as compared to control cultures at day 80-100, although there was a trend towards an increased number in N279K1 cultures. There was no significant difference in spontaneous cell death between control and MAPT-mutant cultures, and no significant change in cell death between day 30 and day 100.

7.2.6 Protective factors

The detection of FTDP-17T relevant phenotypes may have been hindered by protective culture conditions. For example, the maintenance medium for monolayer cultures contained cAMP and BDNF which support neuronal survival in culture (Dugan et al., 1999; Yoshii and Constantine-Paton, 2010). Maintenance media for the monolayer cultures and COs also contained antioxidants as part of the B27 supplement, which may mask tau-related deficits in culture: Mertens et al. (2013) found that ESC-derived neurons expressing psuedo-phosphorylated 2N4R tau cultured without B27 formed axonal varicosities and died in culture at higher rates than neurons expressing normal 2N4R tau. Removing protective factors may have allowed more FTDP-17T-relevant phenotypes to be detected.

7.3 Generation of isogenic N279K iPSC lines

I was unable to make isogenic N279K iPSC lines using CRISPR. Whilst screening for the N279K mutation, I detected small deletions in some edited iPSCs, indicating that Cas9 was cutting DNA, and suggesting that editing with the repair template was inefficient. This may be because I did not increase CRISPR efficiency by including silent blocking mutations in the repair template, which would have prevented Cas9 re-cutting DNA with the desired mutation after editing (Cho et al., 2014; Hsu et al., 2013; Jinek et al., 2012). I did not use blocking mutations because they would have fallen within tau exon 10 or the proximal parts of intron 9 or 10, all of which contain sequences involved in exon 10 splicing (D'Souza and Schellenberg, 2000, 2002). Tau exon 10 contains multiple weak splice sites, splicing silencers, modulators and enhancers which work together to control exon 10 inclusion and exclusion (D'Souza and Schellenberg, 2002), making it difficult to determine the effects of a silent mutation on splicing without splicing assays. The potential of silent mutations to disrupt splicing *in vivo* is evidenced by the FTDP-17T-linked mutations S305I, S305N and

S305S (in exon 10); and +3, +4, +11, +12, +13, +14, +15 and +16 (in intron 10), all of which alter exon 10 splicing (Ghetti et al., 2015; McCarthy et al., 2015).

Making isogenic iPSCs without blocking mutations is two- to ten-fold less efficient (Flynn et al., 2015; Paquet et al., 2016). To get around this inefficiency, I could have screened more iPSC colonies after CRISPR, but this was a time- and labour-intensive process. Alternatively, I could have used digital droplet PCR after CRISPR, in which edited iPSCs are screened for the desired mutation in bulk following rounds of replating and expansion in a manner similar to sib-selection. This method has been used to obtain isogenic iPSCs without blocking mutations (Miyaoka et al., 2014).

Another option would have been making isogenic iPSCs with blocking mutations and assessing exon 10 splicing in splicing assays. I designed exon trapping plasmids to do this before being gifted the three isogenic iPSC lines (control, heterozygous and homozygous P301L knock-in) from Axol. The two P301L lines contained blocking mutations which may alter tau splicing (Figure 5.13 in Chapter 6). I did not see evidence of altered 4R inclusion relative to the control in Western blots, but, having not tested the effects of the blocking mutations on splicing, an effect on 4R tau expression cannot be discounted.

7.4 Limitations and improvements

7.4.1 Choice of control and sample size

Experiments with iPSC-derived neurons have many levels at which differences can arise when cultures are compared. For example: people donating tissue for iPSC production have different genetic backgrounds; tissue choice for iPSC generation may affect the iPSC transcriptome (Hargus et al., 2014); iPSC clones from the same individual may differ due to re-programming-induced mutations (Gore et al., 2011), or in aberrant re-programming factor expression (Boulting et al., 2011), or in their ability to differentiate into neurons (Boulting et al., 2011); and iPSC lines (from the same or different donors) do not differentiate into different lineages with the same efficiency (Bock et al., 2011; Boulting et al., 2011; Hu et al., 2010). Options for controls include multiple iPSC clones derived from the same individual (to minimise variation associated with iPSC derivation, culture and differentiation), isogenic iPSC lines (to minimise genetic background effects), or multiple iPSC lines from unrelated individuals (to model variation in the population).

This problem is further compounded by the question of what a reasonable replicate is. Most studies using iPSC-derived neurons present data from at least three temporally

independent experiments per iPSC line, but some studies use one batch of NPCs, terminally differentiated three times (Hallmann et al., 2017). Repeatedly differentiating neurons from iPSCs can control for chance occurrences during differentiation, but this approach may also increase variability between the batches of neurons produced. In contrast, differentiating iPSCs to NPCs once and using the same NPC pool to generate multiple rounds of neurons decreases variation due to differentiation but increases the probability that chance differences during NPC differentiation are carried through the experiment and mistaken for results. I performed three independent differentiations from iPSCs to neurons, so the differences between control and MAPT cultures cannot be attributed to differences in one differentiation from iPSCs to neurons and subsequent expansion of the NPCs.

The data in this project represents a small number of individuals. I used the statistically significant FTDP-17T-relevant phenotype detected during this project to calculate the number of iPSC lines necessary to get power of at least 80% and $p<0.05$. 80% power is generally accepted as appropriate, and means that the probability of correctly rejecting the null hypothesis is 80% (Button et al., 2013). For the monolayer neural cultures, nine control and nine N279K iPSC lines from different donors would be required for 80% power (calculated from the significant increase in AT8 positive neurons in N279K cultures at day 50). A total of 18 iPSC lines cultured and differentiated simultaneously would require at least two people working on the cell cultures, but a bigger challenge might be obtaining nine iPSC lines with the appropriate MAPT mutations from different donors.

7.4.2 Variability between iPSC lines

Genetic background differences between the iPSC lines may have contributed to variation in my neural cultures. iPSC lines from the same or different donors differentiate into neurons with different efficiencies (Bock et al., 2011; Boulting et al., 2011; Hu et al., 2010), and neurons produced from different PSC lines using the same protocol exhibit different properties (Wu et al., 2007). This may have contributed to variability in monolayer cultures and COs (apart from those using the isogenic iPSC lines).

Genetic background has also been shown to influence tau phosphorylation in rats expressing truncated human tau (Stozicka et al., 2010), so it is possible that the genetic backgrounds of the two N279K lines contributed to the difference in tau phosphorylation at day 50. Isogenic iPSC lines may provide a way around this, but creating isogenic lines from control iPSCs may not be the answer, since people with the same FTDP-17T-related MAPT mutations

do not always experience the same symptoms, leading to the suggestion that as-yet-unknown environmental or genetic influences may be present (Foster et al., 1997).

As well as genetic background differences, differences in culture conditions could have affected my experiments. The CTRL1, CTRL2, N279K1, N279K2, V337M and P301Lpat iPSCs were cultured on feeder cells with KSR media, whereas IsoCon, P301Lhet and P301Lhom COs were feeder-free, cultured on vitronectin with E8 media. This meant that the iPSCs used to make monolayer cultures were maintained in comparable conditions, but the iPSCs used to make COs were not, since the P301Lpat iPSCs did not adapt to feeder-free culture. In addition, the P301Lhet iPSCs differentiated quickly in feeder-free and feeder conditions, and I was unable to maintain the line. The loss of the P301Lhet, but not the P301Lhom or IsoCon lines suggests that gene editing may have introduced some unwanted changes in P301Lhet iPSCs, although these had a normal karyotype.

The contribution of differences between the iPSC lines to variability between the COs could have been minimised by adapting the P301Lpat iPSCs to feeder-free conditions, and culturing them on vitronectin with E8 media before making COs. However, since the P301Lpat COs did not share a genetic background with the isogenic IsoCon, P301Lhet and P301Lhom lines, the ideal solution would have been to make an isogenic control for the P301Lpat line. This was not attempted, due to the time involved in gene editing experiments.

7.4.3 Variability between cultures

Variability between each differentiation to monolayer neurons or COs may have contributed to the detection of relatively few FTDP-17T-relevant phenotypes by hiding subtle differences. Variability between monolayer cultures could have been minimised by making large batches of NPCs from iPSCs, expanding them, and differentiating the NPCs to neurons three independent times. However, as discussed in Section 7.4.2, any errors in the initial differentiation to NPCs would be carried through to the neurons and may be mis-interpreted as an FTDP-17T-relevant result.

Variation occurring due to genetic background differences was minimised by using three isogenic iPSC lines to make COs. In addition, I differentiated the COs using a method which produces forebrain-specific cortical tissue (Lancaster et al., 2017), rather than an earlier method which produces a variety of brain areas in unpredictable proportions (Lancaster et al., 2013). Nevertheless, there was some variability between the CO batches which may have hidden subtle FTDP-17T-related phenotypes. Variability between CO batches and between COs from different cell lines is a recognised issue (Giandomenico and Lancaster, 2017) and

indicates that particular care needs to be taken to identify FTDP-17T-relevant changes in COs.

7.4.4 Specificity of brain areas modelled

FTDP-17T affects primarily the frontal and temporal cortex (Foster et al., 1997). To make my cultures as relevant as possible to these brain areas, I differentiated monolayer cultures from NPCs with a forebrain fate which was confirmed by immunostaining for Pax6, Otx2 and FoxG1. However, FoxG1 staining was cytoplasmic rather than nuclear, suggesting that the NPCs were differentiating towards neurons (Pancrazi et al., 2015; Regad et al., 2007). Pax6, Otx2 and FoxG1 positive cells correspond to those in the developing telecephalon and diencephalon (Larsen et al., 2010; Tao and Lai, 1992; Terzić and Saraga-Babić, 1999), which develop into a large number of areas in the adult brain including the thalamus, hypothalamus, epithalamus and subthalamus (from the diencephalon), and the cerebral cortex, basal ganglia, hippocampus, amygdala, and hypothalamus (from the telencephalon) (Augustine, 2017).

To confirm the identity of my COs, I immunostained for the cortical layer markers Tbr1 and Cux1/2, and the intermediate progenitor marker Tbr2 - the presence of other brain areas was not investigated. At least one of these markers were detected in COs derived from the IsoCon, P301Lhet, P301Lhom and P301Lpat iPSCs, indicating the presence of some cortical tissue. However, the cerebral cortex contains many different areas, and methods for making specific cortical areas from iPSCs have not yet been published. To detect the most disease-relevant subset of neurons in my COs and monolayer cultures, I could have used cortical lobe markers to detect neurons corresponding to the most relevant brain areas: frontal and temporal cortex.

One way to decrease variability in my results would be to only analyse tau phosphorylation and misfolding in specific brain areas of the COs. To do this, I could have stained serial sections with cortical lobe markers on the first slide of the series (to identify frontal and temporal cortex-like areas), antibodies against phosphorylated or misfolded tau (to detect tau pathology) on the second slide of the series, and layer markers (to further elucidate the relevant subsets of cells) on the third slice of the series. Parts of the CO corresponding to frontal or temporal cortex-like tissue could then be examined, and compared across COs and across cell lines. However, this was not done due to time restrictions.

7.5 Future directions

iPSC-derived neuron maturity

One limitation of using iPSC-derived neurons to study a neurodegenerative disease is the relative immaturity of these cultures. Therefore, future work could include artificially aging immature neurons using progerin, for example. This has been done by Miller et al. (2013), who expressed progerin in iPSC-derived neurons with Parkinson's disease-related mutations, and found that it enhanced phenotypes including cell death and a decrease in dendrite length. However, the physiological relevance of these findings are unclear (Ichida and Kiskinis, 2015).

Alternatively, future work could include exploring options to recreate the mature, adult-like expression of all six tau isoforms in iPSC-derived neurons. This could include methods such as trans-splicing, which has been used to drive the expression of 4R tau in ESC-derived neurons and mice (Avale et al., 2013; Lacovich et al., 2017), although it has not been used to recapitulate the splicing of all six tau isoforms as seen in the adult human brain. Another potential avenue is making induced neurons (iNs), which may express 0N4R tau and mature MAP isoforms earlier than traditionally differentiated neurons (Imamura et al., 2016), although this has not yet been extensively characterised.

Another alternative would be culturing iPSC-derived COs for much longer. Since they are in suspension, COs do not suffer from the detachment problems encountered in long term monolayer culture, and have been cultured for as long as 590 days (Sloan et al., 2017). This should be ample time for mature tau splicing to develop, since it has been reported in monolayer cultures after 150 (Iovino et al., 2015), 190 (Beevers et al., 2017), and 365 (Sposito et al., 2015) days.

Yet another possible avenue would be to obtain induced neurons by transdifferentiation of fibroblasts, which has been shown to produce neurons with retain age-dependent transcriptome features (Mertens et al., 2015). Hu et al. (2015) reported that induced neurons made from fibroblasts obtained from AD sufferers had higher Aβ40 or Aβ42 levels than those from controls, indicating disease-relevant changes may be enhanced in induced neurons as compared to those from directed differentiation. Since FTDP-17T emerges in adult humans, but the iPSC-derived neurons I studied were very young compared to those in an adult brain, retaining age-related signatures may have allowed me to see disease-relevant changes in tau.

However, not all fibroblasts are converted to neurons during transdifferentiation (Mertens et al., 2015; Treutlein et al., 2016), and transdifferentiation efficiency decreases for fibroblasts which have been kept in culture for longer (Sun et al., 2014), so the number of neurons which

can be produced from one donor fibroblast sample is limited. This issue could be avoided by using transdifferentiation to produce proliferative NPCs (Han et al., 2012; Sheng et al., 2012), so that the number of neurons produced would no longer be limited by the number of initial fibroblasts. NPCs from transdifferentiation could be gene edited to produce isogenic NPCs, and cultured in 3D, in a manner similar to COs.

Work on the iPSC lines used in this project

Future work using the isogenic IsoCon, P301Lhet and P301Lhom iPSC lines could include testing the effects of the three silent mutations on exon 10 splicing. This is necessary because testing the silent mutations *in silico* suggests that they may decrease tau exon 10 splicing, potentially decreasing the amount of 4R tau, which contains the P301L mutation.

Generation of isogenic iPSCs from the N279K iPSC lines would also be a good next step, since this would minimise variation between monolayer cultures or COs produced from the iPSCs, which would allow more subtle phenotypes to be investigated. Isogenic N279K iPSC lines could be differentiated to forebrain-specific COs and cultured for at least 150 days to allow tau splicing to mature. Serial cryosections of these COs could be immunostained for cortical lobe markers (to detect frontal and temporal lobe-like tissue), cortical layer markers (to determine maturity), and antibodies against abnormal tau such as MC-1 and AT100. Analysis of only the areas corresponding to frontal and temporal lobe cortical neurons may allow relevant and subtle phenotypes to be detected. These experiments could also be performed with the isogenic control and P301Lhom iPSCs, although the physiologically-relevant P301Lhet line would be absent.

Alternatively, the FTDP-17T-relevant phenotypes seen in COs could be enhanced by seeding the COs with pre-formed tau fibrils to induce tau aggregation. I attempted this but the COs became infected shortly after injection. If this technique is optimised, it could be used to investigate tau aggregation and even spreading in 3D. In addition, microglia could be added to COs to extend work done in mouse models (Brelstaff et al., 2018) to a human brain-like system.

7.6 Conclusions

In this project, the following were achieved:

1. **Forebrain-specific neurons were differentiated from patient-derived iPSCs with the N279K and V337M MAPT mutations, and from control subject-derived iP-**

SCs. This allowed a previously reported increase in tau phosphorylation at the AT8 epitope to be observed again, using the same iPSCs but a different method of neuronal differentiation.

2. **Forebrain-patterned COs were differentiated** from patient-derived iPSCs with the P301L MAPT mutation, and from a set of three isogenic control subject-derived iPSCs, expressing normal tau, the heterozygous P301L MAPT mutation, and the homozygous P301L MAPT mutation. The 0N3R tau isoform was strongly expressed in COs from all iPSC lines, and lower amounts of 0N4R and 1N3R tau were also present. This indicates mature tau splicing in some neurons, and suggests that 3D culture may enhance neuronal maturation with respect to tau expression. No differences in tau phosphorylation (detected with the AT8 antibody) or tau mis-folding (detected with the MC-1 antibody) were detected between control and P301L MAPT-mutant iPSC-derived COs.

3. **Silent mutations introduced during CRISPR which may alter tau splicing were identified**. Determining whether the affected isogenic iPSC lines express 4R tau differently may be important in deciding whether or not to use them in future studies.

One statistically significant result relating to a FTDP-17T-relevant phenotype was detected in this project: an increase in the proportion of AT8 positive neurons with the N279K mutation relative to controls at day 50. This confirms previous results from the same iPSC lines using a different differentiation method. Detection of other phenotypes may have been hindered by the variability of the cultures created and by maintenance media containing protective factors.

The most important finding from this project is that 3D culture may enhance neuronal maturity with respect to tau isoform expression, as compared to monolayer cultures, making it a potentially valuable method for studying tauopathies. Overall, this project highlights the need for the development of methods that allow increased reproducibility in iPSC studies, as well as appropriate numbers of iPSC lines and the use of isogenic iPSC lines.

References

Adams, S. J., DeTure, M. A., McBride, M., Dickson, D. W., and Petrucelli, L. (2010). Three repeat isoforms of tau inhibit assembly of four repeat tau filaments. *PloS one*, 5(5):e10810.

Agholme, L., Lindström, T., Kågedal, K., Marcusson, J., and Hallbeck, M. (2010). An In Vitro Model for Neuroscience: Differentiation of SH-SY5Y Cells into Cells with Morphological and Biochemical Characteristics of Mature Neurons. *Journal of Alzheimer's Disease*, 20(4):1069–82.

Ahmed, T., Van der Jeugd, A., Blum, D., Galas, M. C., D'Hooge, R., Buee, L., and Balschun, D. (2014). Cognition and hippocampal synaptic plasticity in mice with a homozygous tau deletion. *Neurobiology of Aging*, 35(11):2474–8.

Alberici, A., Gobbo, C., Panzacchi, A., Nicosia, F., Ghidoni, R., Benussi, L., Hock, C., Papassotiropoulos, A., Liberini, P., Growdon, J. H., Frisoni, G. B., Villa, A., Zanetti, O., Cappa, S., Fazio, F., and Binetti, G. (2004). Frontotemporal dementia: impact of P301L tau mutation on a healthy carrier. *Journal of neurology, neurosurgery, and psychiatry*, 75(11):1607–10.

Alonso, A. d. C., Mederlyova, A., Novak, M., Grundke-Iqbal, I., and Iqbal, K. (2004). Promotion of Hyperphosphorylation by Frontotemporal Dementia Tau Mutations. *Journal of Biological Chemistry*, 279(33):34873–81.

Alonso, A. d. C., Zaidi, T., Novak, M., Grundke-Iqbal, I., and Iqbal, K. (2001). Hyperphosphorylation Induces Self-Assembly of Tau into Tangles of Paired Helical Filaments/Shraight Filaments. *Proceedings of the National Academy of Sciences*, 98(12):6923–8.

Andorfer, C., Acker, C. M., Kress, Y., Hof, P. R., Duff, K., and Davies, P. (2005). Cell-cycle reentry and cell death in transgenic mice expressing nonmutant human tau isoforms. *The Journal of neuroscience : the official journal of the Society for Neuroscience*, 25(22):5446–54.

Anfossi, M., Vuono, R., Maletta, R., Virdee, K., Mirabelli, M., Colao, R., Puccio, G., Bernardi, L., Frangipane, F., Gallo, M., Geracitano, S., Tomaino, C., Curcio, S. A. M., Zannino, G., Lamenza, F., Duyckaerts, C., Spillantini, M. G., Losso, M. A., and Bruni, A. C. (2011). Compound heterozygosity of 2 novel MAPT mutations in frontotemporal dementia. *Neurobiology of aging*, 32(4):757.e1–11.

Angevine, J. B. and Sidman, R. L. (1961). Autoradiographic Study of Cell Migration during Histogenesis of Cerebral Cortex in the Mouse. *Nature*, 192(4804):766–8.

Anthony, T. E., Klein, C., Fishell, G., and Heintz, N. (2004). Radial Glia Serve as Neuronal Progenitors in All Regions of the Central Nervous System. *Neuron*, 41(6):881–90.

Aoki, K., Uchihara, T., Nakamura, A., Komori, T., Arai, N., and Mizutani, T. (2003). Expression of apolipoprotein E in ballooned neurons?Comparative immunohistochemical study on neurodegenerative disorders and infarction. *Acta Neuropathologica*, 106(5):436–40.

Aoyagi, H., Hasegawa, M., and Tamaoka, A. (2007). Fibrillogenic nuclei composed of P301L mutant tau induce elongation of P301L tau but not wild-type tau. *Journal of Biological Chemistry*, 282(28):20309–18.

Arai, T., Ikeda, K., Akiyama, H., Shikamoto, Y., Tsuchiya, K., Yagishita, S., Beach, T., Rogers, J., Schwab, C., and McGeer, P. L. (2001). Distinct isoforms of tau aggregated in neurons and glial cells in brains of patients with Pick's disease, corticobasal degeneration and progressive supranuclear palsy. *Acta neuropathologica*, 101(2):167–73.

Arendt, T., Stieler, J., Strijkstra, A. M., Hut, R. a., Rüdiger, J., Van der Zee, E. a., Harkany, T., Holzer, M., and Härtig, W. (2003). Reversible paired helical filament-like phosphorylation of tau is an adaptive process associated with neuronal plasticity in hibernating animals. *The Journal of neuroscience : the official journal of the Society for Neuroscience*, 23(18):6972–81.

Arvanitakis, Z., Witte, R. J., Dickson, D. W., Tsuboi, Y., Uitti, R. J., Slowinski, J., Hutton, M. L., Lin, S.-C., Boeve, B. F., Cheshire, W. P., Pooley, R. A., Liss, J. M., Caviness, J. N., Strongosky, A. J., and Wszolek, Z. K. (2007). Clinical-pathologic study of biomarkers in FTDP-17 (PPND family with N279K tau mutation). *Parkinsonism & Related Disorders*, 13(4):230–9.

Ashe, K. H. and Zahs, K. R. (2010). Probing the biology of Alzheimer's disease in mice. *Neuron*, 66(5):631–45.

Ashman, J. B., Hall, E. S., Eveleth, J., and Boekelheide, K. (1992). Tau, the Neuronal Heat-Stable Microtubule-Associated Protein, is also Present in the Cross-Linked Microtubule Network of the Testicular Spermatid Manchette1. *Biology of Reproduction*, 46(1):120–9.

Astick, M. and Vanderhaeghen, P. (2018). From Human Pluripotent Stem Cells to Cortical Circuits. *Current Topics in Developmental Biology*, 129:67–98.

Augustine, J. R. (2017). *Human Neuroanatomy*. Wiley Blackwell, Hoboken, New Jersey, 2nd edition.

Avale, M. E., Rodríguez-Martín, T., and Gallo, J. M. (2013). Trans-splicing correction of tau isoform imbalance in a mouse model of tau mis-splicing. *Human Molecular Genetics*, 22(13):2603–11.

Bachiller, D., Klingensmith, J., Kemp, C., Belo, J. A., Anderson, R. M., May, S. R., McMahon, J. A., McMahon, A. P., Harland, R. M., Rossant, J., and De Robertis, E. M. (2000). The organizer factors Chordin and Noggin are required for mouse forebrain development. *Nature*, 403(6770):658–61.

Baker, B. M. and Chen, C. S. (2012). Deconstructing the third dimension – how 3D culture microenvironments alter cellular cues. *Journal of Cell Science*, 125(13):3015–24.

Baker, M., Litvan, I., Houlden, H., Adamson, J., Dickson, D., Perez-Tur, J., Hardy, J., Lynch, T., Bigio, E., and Hutton, M. (1999). Association of an extended haplotype in the tau gene with progressive supranuclear palsy. *Human Molecular Genetics*, 8(4):711–5.

Baker, M., Mackenzie, I. R., Pickering-Brown, S. M., Gass, J., Rademakers, R., Lindholm, C., Snowden, J., Adamson, J., Sadovnick, A. D., Rollinson, S., Cannon, A., Dwosh, E., Neary, D., Melquist, S., Richardson, A., Dickson, D., Berger, Z., Eriksen, J., Robinson, T., Zehr, C., Dickey, C. A., Crook, R., McGowan, E., Mann, D., Boeve, B., Feldman, H., and Hutton, M. (2006). Mutations in progranulin cause tau-negative frontotemporal dementia linked to chromosome 17. *Nature*, 442(7105):916–9.

Barghorn, S., Zheng-Fischhöfer, Q., Ackmann, M., Biernat, J., von Bergen, M., Mandelkow, E.-M., and Mandelkow, E. (2000). Structure, Microtubule Interactions, and Paired Helical Filament Aggregation by Tau Mutants of Frontotemporal Dementias †. *Biochemistry*, 39(38):11714–21.

Barrangou, R., Fremaux, C., Deveau, H., Richards, M., Boyaval, P., Moineau, S., Romero, D. A., and Horvath, P. (2007). CRISPR provides acquired resistance against viruses in prokaryotes. *Science*, 315(5819):1709–12.

Beagle, A. J., Darwish, S. M., Ranasinghe, K. G., La, A. L., Karageorgiou, E., and Vossel, K. A. (2017). Relative Incidence of Seizures and Myoclonus in Alzheimer's Disease, Dementia with Lewy Bodies, and Frontotemporal Dementia. *Journal of Alzheimer's Disease*, 60(1):211–23.

Beevers, J. E., Lai, M. C., Collins, E., Booth, H. D., Zambon, F., Parkkinen, L., Vowles, J., Cowley, S. A., Wade-Martins, R., and Caffrey, T. M. (2017). MAPT Genetic Variation and Neuronal Maturity Alter Isoform Expression Affecting Axonal Transport in iPSC-Derived Dopamine Neurons. *Stem Cell Reports*, 9(2):587–99.

Belinsky, G. S., Rich, M. T., Sirois, C. L., Short, S. M., Pedrosa, E., Lachman, H. M., and Antic, S. D. (2014). Patch-clamp recordings and calcium imaging followed by single-cell PCR reveal the developmental profile of 13 genes in iPSC-derived human neurons. *Stem cell research*, 12(1):101–18.

Bergström, P., Agholme, L., Nazir, F. H., Satir, T. M., Toombs, J., Wellington, H., Strandberg, J., Bontell, T. O., Kvartsberg, H., Holmström, M., Boreström, C., Simonsson, S., Kunath, T., Lindahl, A., Blennow, K., Hanse, E., Portelius, E., Wray, S., and Zetterberg, H. (2016). Amyloid precursor protein expression and processing are differentially regulated during cortical neuron differentiation. *Scientific Reports*, 6(October):29200.

Bhat, S. P. and Nagineni, C. N. (1989). αB subunit of lens-specific protein α-crystallin is present in other ocular and non-ocular tissues. *Biochemical and Biophysical Research Communications*, 158(1):319–25.

Bigio, E. H., Vono, M. B., Satumtira, S., Adamson, J., Sontag, E., Hynan, L. S., White, C. L., Baker, M., and Hutton, M. (2001). Cortical synapse loss in progressive supranuclear palsy. *Journal of Neuropathology and Experimental Neurology*, 60(5):403–10.

Binder, L. I., Frankfurter, A., and Rebhun, L. I. (1985). The distribution of tau in the mammalian central nervous system. *The Journal of cell biology*, 101(4):1371–8.

Birnbaum, J. H., Wanner, D., Gietl, A. F., Saake, A., Kündig, T. M., Hock, C., Nitsch, R. M., and Tackenberg, C. (2018). Oxidative stress and altered mitochondrial protein expression in the absence of amyloid-β and tau pathology in iPSC-derived neurons from sporadic Alzheimer's disease patients. *Stem Cell Research*, 27:121–30.

Black, M. M., Slaughter, T., Moshiach, S., Obrocka, M., and Fischer, I. (1996). Tau is enriched on dynamic microtubules in the distal region of growing axons. *The Journal of neuroscience : the official journal of the Society for Neuroscience*, 16(11):3601–19.

Blennow, K. and Hampel, H. (2003). CSF markers for incipient Alzheimer's disease. *Lancet Neurology*, 2(10):605–13.

Bloemendal, H., de Jong, W., Jaenicke, R., Lubsen, N. H., Slingsby, C., and Tardieu, A. (2004). Ageing and vision: structure, stability and function of lens crystallins. *Progress in Biophysics and Molecular Biology*, 86(3):407–85.

Bock, C., Kiskinis, E., Verstappen, G., Gu, H., Boulting, G., Smith, Z. D., Ziller, M., Croft, G. F., Amoroso, M. W., Oakley, D. H., Gnirke, A., Eggan, K., and Meissner, A. (2011). Reference maps of human es and ips cell variation enable high-throughput characterization of pluripotent cell lines. *Cell*, 144(3):439–52.

Boiko, T., Van Wart, A., Caldwell, J. H., Levinson, S. R., Trimmer, J. S., and Matthews, G. (2003). Functional specialization of the axon initial segment by isoform-specific sodium channel targeting. *The Journal of neuroscience : the official journal of the Society for Neuroscience*, 23(6):2306–13.

Boulting, G. L., Kiskinis, E., Croft, G. F., Amoroso, M. W., Oakley, D. H., Wainger, B. J., Williams, D. J., Kahler, D. J., Yamaki, M., Davidow, L., Rodolfa, C. T., Dimos, J. T., Mikkilineni, S., MacDermott, A. B., Woolf, C. J., Henderson, C. E., Wichterle, H., and Eggan, K. (2011). A functionally characterized test set of human induced pluripotent stem cells. *Nature Biotechnology*, 29(3):279–87.

Bouras, C., Riederer, B. M., Hof, P. R., and Giannakopoulos, P. (2003). Induction of MC-1 immunoreactivity in axons after injection of the Fc fragment of human immunoglobulins in macaque monkeys. *Acta neuropathologica*, 105(1):58–64.

Braak, H. and Braak, E. (1991). Neuropathological stageing of Alzheimer-related changes. *Acta Neuropathologica*, 82:239–59.

Braak, H. and Del Tredici, K. (2011). The pathological process underlying Alzheimer's disease in individuals under thirty. *Acta Neuropathologica*, 121(2):171–81.

Braak, H., Del Tredici, K., Sandmann-Kiel, D., Rüb, U., and Schultz, C. (2001). Nerve cells expressing heat-shock proteins in Parkinson's disease. *Acta neuropathologica*, 102(5):449–54.

Bramblett, G. T., Goedert, M., Jakes, R., Merrick, S. E., Trojanowski, J. Q., and Lee, V. M. (1993). Abnormal tau phosphorylation at Ser396 in Alzheimer's disease recapitulates development and contributes to reduced microtubule binding. *Neuron*, 10(6):1089–99.

Brandt, R., Hundelt, M., and Shahani, N. (2005). Tau alteration and neuronal degeneration in tauopathies: Mechanisms and models. *Biochimica et Biophysica Acta - Molecular Basis of Disease*, 1739(2):331–54.

Brandt, R., Léger, J., and Lee, G. (1995). Interaction of tau with the neural plasma membrane mediated by tau's amino-terminal projection domain. *Journal of Cell Biology*, 131(5):1327–40.

Brelstaff, J., Ossola, B., Neher, J. J., Klingstedt, T., Nilsson, K. P. R., Goedert, M., Spillantini, M. G., and Tolkovsky, A. M. (2015). The fluorescent pentameric oligothiophene pFTAA identifies filamentous tau in live neurons cultured from adult P301S tau mice. *Frontiers in Neuroscience*, 9:184.

Brelstaff, J., Tolkovsky, A. M., Ghetti, B., Goedert, M., and Spillantini, M. G. (2018). Living Neurons with Tau Filaments Aberrantly Expose Phosphatidylserine and Are Phagocytosed by Microglia. *Cell reports*, 24(8):1939–48.e4.

Brion, J. P., Smith, C., Couck, A. M., Gallo, J. M., and Anderton, B. H. (1993). Developmental changes in tau phosphorylation: fetal tau is transiently phosphorylated in a manner similar to paired helical filament-tau characteristic of Alzheimer's disease. *Journal of neurochemistry*, 61(6):2071–80.

Brix, J., Zhou, Y., and Luo, Y. (2015). The Epigenetic Reprogramming Roadmap in Generation of iPSCs from Somatic Cells. *Journal of genetics and genomics = Yi chuan xue bao*, 42(12):661–70.

Broustal, O., Camuzat, A., Guillot-Noël, L., Guy, N., Millecamps, S., Deffond, D., Lacomblez, L., Golfier, V., Hannequin, D., Salachas, F., Camu, W., Didic, M., Dubois, B., Meininger, V., Le Ber, I., and Brice, A. (2010). FUS mutations in frontotemporal lobar degeneration with amyotrophic lateral sclerosis. *Journal of Alzheimer's disease : JAD*, 22:765–9.

Bulfone, A., Smiga, S. M., Shimamura, K., Peterson, A., Puelles, L., and Rubenstein, J. L. (1995). T-Brain-1: A homolog of Brachyury whose expression defines molecularly distinct domains within the cerebral cortex. *Neuron*, 15(1):63–78.

Bullmann, T., de Silva, R., Holzer, M., Mori, H., and Arendt, T. (2007). Expression of Embryonic Tau Protein Isoforms Persist During Adult Neurogenesis in the Hippocampus. *Hippocampus*, 17(9):98–102.

Button, K. S., Ioannidis, J. P. A., Mokrysz, C., Nosek, B. A., Flint, J., Robinson, E. S. J., and Munafò, M. R. (2013). Power failure: why small sample size undermines the reliability of neuroscience. *Nature reviews. Neuroscience*, 14(5):365–76.

Byrne, S. M., Mali, P., and Church, G. M. (2014a). *Genome Editing in Human Stem Cells*, volume 546. Elsevier Inc., 1 edition.

Byrne, S. M., Ortiz, L., Mali, P., Aach, J., and Church, G. M. (2014b). Multi-kilobase homozygous targeted gene replacement in human induced pluripotent stem cells. *Nucleic acids research*, 43(3):e21.

Bystron, I., Blakemore, C., and Rakic, P. (2008). Development of the human cerebral cortex: Boulder Committee revisited. *Nature Reviews Neuroscience*, 9(2):110–22.

Caceres, A. and Kosik, K. S. (1990). Inhibition of neurite polarity by tau antisense oligonucleotides in primary cerebellar neurons. *Nature*, 343(6257):461–3.

Caffrey, T. M., Joachim, C., Paracchini, S., Esiri, M. M., and Wade-Martins, R. (2006). Haplotype-specific expression of exon 10 at the human MAPT locus. *Human Molecular Genetics*, 15(24):3529–37.

Caffrey, T. M., Joachim, C., and Wade-Martins, R. (2008). Haplotype-specific expression of the N-terminal exons 2 and 3 at the human MAPT locus. *Neurobiology of Aging*, 29(12):1923–9.

Cahan, P., Li, H., Morris, S. A., Lummertz da Rocha, E., Daley, G. Q., and Collins, J. J. (2014). CellNet: network biology applied to stem cell engineering. *Cell*, 158(4):903–15.

Caiazzo, M., Giannelli, S., Valente, P., Lignani, G., Carissimo, A., Sessa, A., Colasante, G., Bartolomeo, R., Massimino, L., Ferroni, S., Settembre, C., Benfenati, F., and Broccoli, V. (2015). Direct conversion of fibroblasts into functional astrocytes by defined transcription factors. *Stem cell reports*, 4(1):25–36.

Callahan, L. M. and Coleman, P. D. (1995). Neurons bearing neurofibrillary tangles are responsible for selected synaptic deficits in Alzheimer's disease. *Neurobiology of Aging*, 16(3):311–4.

Caminsky, N. G., Mucaki, E. J., and Rogan, P. K. (2014). Interpretation of mRNA splicing mutations in genetic disease: review of the literature and guidelines for information-theoretical analysis. *F1000Research*.

Camp, J. G., Badsha, F., Florio, M., Kanton, S., Gerber, T., Wilsch-Bräuninger, M., Lewitus, E., Sykes, A., Hevers, W., Lancaster, M., Knoblich, J. A., Lachmann, R., Pääbo, S., Huttner, W. B., and Treutlein, B. (2015). Human cerebral organoids recapitulate gene expression programs of fetal neocortex development. *Proceedings of the National Academy of Sciences*, 112(51):201520760.

Campbell, K. H. S., McWhir, J., Ritchie, W. A., and Wilmut, I. (1996). Sheep cloned by nuclear transfer from a cultured cell line. *Nature*, 380(6569):64–66.

Carlier, M. F., Simon, C., Cassoly, R., and Pradel, L. A. (1984). Interaction between microtubule-associated protein tau and spectrin. *Biochimie*, 66(4):305–11.

Chai, X., Dage, J. L., and Citron, M. (2012). Constitutive secretion of tau protein by an unconventional mechanism. *Neurobiology of Disease*, 48(3):356–66.

Chambers, S. M., Fasano, C. A., Papapetrou, E. P., Tomishima, M., Sadelain, M., and Studer, L. (2009). Highly efficient neural conversion of human ES and iPS cells by dual inhibition of SMAD signaling. *Nature biotechnology*, 27(3):275–80.

Chan, F. K. M., Moriwaki, K., and De Rosa, M. J. (2013). Detection of necrosis by release of lactate dehydrogenase activity. *Methods in Molecular Biology*, 979:65–70.

Chanda, S., Ang, C. E., Davila, J., Pak, C., Mall, M., Lee, Q. Y., Ahlenius, H., Jung, S. W., Südhof, T. C., and Wernig, M. (2014). Generation of induced neuronal cells by the single reprogramming factor ASCL1. *Stem cell reports*, 3(2):282–96.

Chang, H. H. Y., Pannunzio, N. R., Adachi, N., and Lieber, M. R. (2017). Non-homologous DNA end joining and alternative pathways to double-strand break repair. *Nature Reviews Molecular Cell Biology*, 18(8):495–506.

Chen, F., Pruett-Miller, S. M., Huang, Y., Gjoka, M., Duda, K., Taunton, J., Collingwood, T. N., Frodin, M., and Davis, G. D. (2011). High-frequency genome editing using ssDNA oligonucleotides with zinc-finger nucleases. *Nature Methods*, 8(9):753–5.

Chen, J., Kanai, Y., Cowan, N. J., and Hirokawa, N. (1992). Projection domains of MAP2 and tau determine spacings between microtubules in dendrites and axons. *Nature*, 360(6405):674–7.

Cheng, A., Coksaygan, T., Tang, H., Khatri, R., Balice-Gordon, R. J., Rao, M. S., and Mattson, M. P. (2007). Truncated tyrosine kinase B brain-derived neurotrophic factor receptor directs cortical neural stem cells to a glial cell fate by a novel signaling mechanism. *Journal of neurochemistry*, 100(6):1515–30.

Cho, S. W., Kim, S., Kim, Y., Kweon, J., Kim, H. S., Bae, S., and Kim, J. S. (2014). Analysis of off-target effects of CRISPR/Cas-derived RNA-guided endonucleases and nickases. *Genome Research*, 24(1):132–41.

Choi, S. H., Kim, Y. H., Hebisch, M., Sliwinski, C., Lee, S., D'Avanzo, C., Chen, H., Hooli, B., Asselin, C., Muffat, J., Klee, J. B., Zhang, C., Wainger, B. J., Peitz, M., Kovacs, D. M., Woolf, C. J., Wagner, S. L., Tanzi, R. E., and Kim, D. Y. (2014). A three-dimensional human neural cell culture model of Alzheimer's disease. *Nature*, 515(7526):274–8.

Christopherson, K. S., Ullian, E. M., Stokes, C. C., Mullowney, C. E., Hell, J. W., Agah, A., Lawler, J., Mosher, D. F., Bornstein, P., and Barres, B. A. (2005). Thrombospondins are astrocyte-secreted proteins that promote CNS synaptogenesis. *Cell*, 120(3):421–33.

Chung, W.-S., Allen, N. J., and Eroglu, C. (2015). Astrocytes Control Synapse Formation, Function, and Elimination. *Cold Spring Harbor Perspectives in Biology*, 7(9):a020370.

Clark, L. N., Poorkaj, P., Wszolek, Z., Geschwind, D. H., Nasreddine, Z. S., Miller, B., Li, D., Payami, H., Awert, F., Markopoulou, K., Andreadis, A., D'Souza, I., Lee, V. M.-Y., Reed, L., Trojanowski, J. Q., Zhukareva, V., Bird, T., Schellenberg, G., and Wilhelmsen, K. C. (1998). Pathogenic implications of mutations in the tau gene in pallido-ponto-nigral degeneration and related neurodegenerative disorders linked to chromosome 17. *Proceedings of the National Academy of Sciences*, 95(22):13103–7.

Clavaguera, F., Bolmont, T., Crowther, R. A., Abramowski, D., Frank, S., Probst, A., Fraser, G., Stalder, A. K., Beibel, M., Staufenbiel, M., Jucker, M., Goedert, M., and Tolnay, M. (2009). Transmission and spreading of tauopathy in transgenic mouse brain. *Nature Cell Biology*, 11(7):909–13.

Clavaguera, F., Hench, J., Lavenir, I., Schweighauser, G., Frank, S., Goedert, M., and Tolnay, M. (2014). Peripheral administration of tau aggregates triggers intracerebral tauopathy in transgenic mice. *Acta Neuropathologica*, 127(2):299–301.

Colman, A. and Dreesen, O. (2009). Induced pluripotent stem cells and the stability of the differentiated state. *EMBO reports*, 10(7):714–21.

Combs, B. and Gamblin, T. C. (2012). FTDP-17 tau mutations induce distinct effects on aggregation and microtubule interactions. *Biochemistry*, 51(43):8597–607.

Cong, L., Ran, F. A., Cox, D., Lin, S., Barretto, R., Habib, N., Hsu, P. D., Wu, X., Jiang, W., Marraffini, L. A., and Zhang, F. (2013). Multiplex genome engineering using CRISPR/Cas systems. *Science (New York, N.Y.)*, 339(6121):819–23.

Cowan, C. M. and Mudher, A. (2013). Are tau aggregates toxic or protective in tauopathies? *Frontiers in Neurology*, 4:1–13.

Crimins, J. L., Rocher, A. B., and Luebke, J. I. (2012). Electrophysiological changes precede morphological changes to frontal cortical pyramidal neurons in the rTg4510 mouse model of progressive tauopathy. *Acta Neuropathologica*, 124(6):777–95.

Cruts, M., Gijselinck, I., Van Der Zee, J., Engelborghs, S., Wils, H., Pirici, D., Rademakers, R., Vandenberghe, R., Dermaut, B., Martin, J. J., Van Duijn, C., Peeters, K., Sciot, R., Santens, P., De Pooter, T., Mattheijssens, M., Van Den Broeck, M., Cuijt, I., Vennekens, K., De Deyn, P. P., Kumar-Singh, S., and Van Broeckhoven, C. (2006). Null mutations in progranulin cause ubiquitin-positive frontotemporal dementia linked to chromosome 17q21. *Nature*, 442(7105):920–4.

Cuylen, S., Blaukopf, C., Politi, A. Z., Müller-Reichert, T., Neumann, B., Poser, I., Ellenberg, J., Hyman, A. A., and Gerlich, D. W. (2016). Ki-67 acts as a biological surfactant to disperse mitotic chromosomes. *Nature*, 535(7611):308–12.

Dabir, D. V., Trojanowski, J. Q., Richter-Landsberg, C., Lee, V. M.-Y., and Forman, M. S. (2004). Expression of the Small Heat-Shock Protein αB-Crystallin in Tauopathies with Glial Pathology. *The American Journal of Pathology*, 164(1):155–66.

Daer, R. M., Cutts, J. P., Brafman, D. A., and Haynes, K. A. (2017). The Impact of Chromatin Dynamics on Cas9-Mediated Genome Editing in Human Cells. *ACS Synthetic Biology*, 6(3):428–38.

Dang, J., Tiwari, S. K., Lichinchi, G., Qin, Y., Patil, V. S., Eroshkin, A. M., and Rana, T. M. (2016). Zika Virus Depletes Neural Progenitors in Human Cerebral Organoids through Activation of the Innate Immune Receptor TLR3. *Cell Stem Cell*, 19(2):258–65.

Davis, R. L., Weintraub, H., and Lassar, A. B. (1987). Expression of a single transfected cDNA converts fibroblasts to myoblasts. *Cell*, 51(6):987–1000.

Dawson, H. N., Cantillana, V., Chen, L., and Vitek, M. P. (2007). The Tau N279K Exon 10 Splicing Mutation Recapitulates Frontotemporal Dementia and Parkinsonism Linked to Chromosome 17 Tauopathy in a Mouse Model. *Journal of Neuroscience*, 27(34):9155–68.

Dawson, H. N., Cantillana, V., Jansen, M., Wang, H., Vitek, M. P., Wilcock, D. M., Lynch, J. R., and Laskowitz, D. T. (2010). Loss of tau elicits axonal degeneration in a mouse model of Alzheimer's disease. *Neuroscience*, 169(1):516–31.

Dawson, H. N., Ferreira, A., Eyster, M. V., Ghoshal, N., Binder, L. I., and Vitek, M. P. (2001). Inhibition of neuronal maturation in primary hippocampal neurons from tau deficient mice. *Journal of cell science*, 114(Pt 6):1179–87.

Dayanandan, R., Van Slegtenhorst, M., Mack, T. G. A., Ko, L., Yen, S. H., Leroy, K., Brion, J. P., Anderton, B. H., Hutton, M., and Lovestone, S. (1999). Mutations in tau reduce its microtubule binding properties in intact cells and affect its phosphorylation. *FEBS Letters*, 446(2-3):228–32.

de Calignon, A., Polydoro, M., Suárez-Calvet, M., William, C., Adamowicz, D. H., Kopeikina, K. J., Pitstick, R., Sahara, N., Ashe, K. H., Carlson, G. A., Spires-Jones, T. L., and Hyman, B. T. (2012). Propagation of tau pathology in a model of early Alzheimer's disease. *Neuron*, 73(4):685–97.

de Silva, R., Lashley, T., Strand, C., Shiarli, A. M., Shi, J., Tian, J., Bailey, K. L., Davies, P., Bigio, E. H., Arima, K., Iseki, E., Murayama, S., Kretzschmar, H., Neumann, M., Lippa, C., Halliday, G., MacKenzie, J., Ravid, R., Dickson, D., Wszolek, Z., Iwatsubo, T., Pickering-Brown, S. M., Holton, J., Lees, A., Revesz, T., and Mann, D. M. (2006). An immunohistochemical study of cases of sporadic and inherited frontotemporal lobar degeneration using 3R- and 4R-specific tau monoclonal antibodies. *Acta Neuropathologica*, 111(4):329–40.

Decker, J. M., Krüger, L., Sydow, A., Zhao, S., Frotscher, M., Mandelkow, E., and Mandelkow, E.-M. (2015). Pro-aggregant Tau impairs mossy fiber plasticity due to structural changes and Ca++ dysregulation. *Acta neuropathologica communications*, 3(1):23.

DeJesus-Hernandez, M., Mackenzie, I. R., Boeve, B. F., Boxer, A. L., Baker, M., Rutherford, N. J., Nicholson, A. M., Finch, N. C. A., Flynn, H., Adamson, J., Kouri, N., Wojtas, A., Sengdy, P., Hsiung, G. Y. R., Karydas, A., Seeley, W. W., Josephs, K. A., Coppola, G., Geschwind, D. H., Wszolek, Z. K., Feldman, H., Knopman, D. S., Petersen, R. C., Miller, B. L., Dickson, D. W., Boylan, K. B., Graff-Radford, N. R., and Rademakers, R. (2011). Expanded GGGGCC Hexanucleotide Repeat in Noncoding Region of C9ORF72 Causes Chromosome 9p-Linked FTD and ALS. *Neuron*, 72(2):245–56.

Delisle, M. B., Murrell, J. R., Richardson, R., Trofatter, J. A., Rascol, O., Soulages, X., Mohr, M., Calvas, P., and Ghetti, B. (1999). A mutation at codon 279 (N279K) in exon 10 of the Tau gene causes a tauopathy with dementia and supranuclear palsy. *Acta neuropathologica*, 98(1):62–77.

Deloulme, J. C., Raponi, E., Gentil, B. J., Bertacchi, N., Marks, A., Labourdette, G., and Baudier, J. (2004). Nuclear expression of S100B in oligodendrocyte progenitor cells correlates with differentiation toward the oligodendroglial lineage and modulates oligodendrocytes maturation. *Molecular and Cellular Neuroscience*, 27(4):453–65.

Desmet, F. O., Hamroun, D., Lalande, M., Collod-Bëroud, G., Claustres, M., and Béroud, C. (2009). Human Splicing Finder: An online bioinformatics tool to predict splicing signals. *Nucleic Acids Research*, 37(9):1–14.

Despres, C., Byrne, C., Qi, H., Cantrelle, F.-X., Huvent, I., Chambraud, B., Baulieu, E.-E., Jacquot, Y., Landrieu, I., Lippens, G., and Smet-Nocca, C. (2017). Identification of the Tau

phosphorylation pattern that drives its aggregation. *Proceedings of the National Academy of Sciences of the United States of America*, 114(34):9080–5.

Di, J., Cohen, L. S., Corbo, C. P., Phillips, G. R., El Idrissi, A., and Alonso, A. D. (2016). Abnormal tau induces cognitive impairment through two different mechanisms: Synaptic dysfunction and neuronal loss. *Scientific Reports*, 6(January):1–12.

Dianov, G. L. and Hübscher, U. (2013). Mammalian Base Excision Repair: the Forgotten Archangel. *Nucleic Acids Research*, 41(6):3483–90.

Ding, Q., Regan, S. N., Xia, Y., Oostrom, L. A., Cowan, C. A., and Musunuru, K. (2013). Enhanced efficiency of human pluripotent stem cell genome editing through replacing TALENs with CRISPRs. *Cell Stem Cell*, 12(4):393–4.

Dixit, R., Ross, J. L., Goldman, Y. E., and Holzbaur, E. L. F. (2008). Differential regulation of dynein and kinesin motor proteins by tau. *Science (New York, N.Y.)*, 319(5866):1086–9.

Drechsel, D. N., Hyman, A. A., Cobb, M. H., and Kirschner, M. W. (1992). Modulation of the dynamic instability of tubulin assembly by the microtubule-associated protein tau. *Molecular Biology of the Cell*, 3(10):1141–54.

Drubin, D. G. and Kirschner, M. W. (1986). Tau protein function in living cells. *The Journal of cell biology*, 103(6 Pt 2):2739–46.

D'Souza, I., Poorkaj, P., Hong, M., Nochlin, D., Lee, V. M., Bird, T. D., and Schellenberg, G. D. (1999). Missense and silent tau gene mutations cause frontotemporal dementia with parkinsonism-chromosome 17 type, by affecting multiple alternative RNA splicing regulatory elements. *Proceedings of the National Academy of Sciences of the United States of America*, 96(10):5598–603.

D'Souza, I. and Schellenberg, G. D. (2000). Determinants of 4-repeat tau expression. Coordination between enhancing and inhibitory splicing sequences for exon 10 inclusion. *Journal of Biological Chemistry*, 275(23):17700–9.

D'Souza, I. and Schellenberg, G. D. (2002). Tau Exon 10 Expression Involves a Bipartite Intron 10 Regulatory Sequence and Weak 5' and 3' Splice Sites. *Journal of Biological Chemistry*, 277(29):26587–99.

D'Souza, I. and Schellenberg, G. D. (2005). Regulation of tau isoform expression and dementia. *Biochimica et Biophysica Acta (BBA) - Molecular Basis of Disease*, 1739(2-3):104–15.

D'Souza, I. and Schellenberg, G. D. (2006). Arginine/serine-rich protein interaction domain-dependent modulation of a tau exon 10 splicing enhancer: Altered interactions and mechanisms for functionally antagonistic FTDP-17 mutations Δ280K and N279K. *Journal of Biological Chemistry*, 281(5):2460–9.

Dugan, L. L., Kim, J. S., Zhang, Y., Bart, R. D., Sun, Y., Holtzman, D. M., and Gutmann, D. H. (1999). Differential Effects of cAMP in Neurons and Astrocytes. *the Journal of Biological Chemistry*, 274(36):25842–8.

Dujardin, S., Lï¿½colle, K., Caillierez, R., Bï¿½gard, S., Zommer, N., Lachaud, C., Carrier, S., Dufour, N., Aurï¿½gan, G., Winderickx, J., Hantraye, P., Dï¿½glon, N., Colin, M., and Buï¿½e, L. (2014). Neuron-to-neuron wild-type Tau protein transfer through a trans-synaptic mechanism: Relevance to sporadic tauopathies. *Acta Neuropathologica Communications*, 2(1):1–14.

Duyk, G. M., Kim, S. W., Myers, R. M., and Cox, D. R. (1990). Exon trapping: a genetic screen to identify candidate transcribed sequences in cloned mammalian genomic dna. *Proceedings of the National Academy of Sciences*, 87(22):8995–9.

Ehrlich, M., Hallmann, A. L., Reinhardt, P., Araúzo-Bravo, M. J., Korr, S., Röpke, A., Psathaki, O. E., Ehling, P., Meuth, S. G., Oblak, A. L., Murrell, J. R., Ghetti, B., Zaehres, H., Schöler, H. R., Sterneckert, J., Kuhlmann, T., and Hargus, G. (2015). Distinct neurodegenerative changes in an induced pluripotent stem cell model of frontotemporal dementia linked to mutant tau protein. *Stem Cell Reports*, 5(1):83–96.

Eiraku, M. and Sasai, Y. (2012). Self-formation of layered neural structures in three-dimensional culture of ES cells. *Current opinion in neurobiology*, 22(5):768–77.

Eiraku, M., Takata, N., Ishibashi, H., Kawada, M., Sakakura, E., Okuda, S., Sekiguchi, K., Adachi, T., and Sasai, Y. (2011). Self-organizing optic-cup morphogenesis in three-dimensional culture. *Nature*, 472(7341):51–6.

Elkabetz, Y., Panagiotakos, G., G., A., Socci, N. D., Tabar, V., and Studer, L. (2008). Human ES cell-derived neural rosettes reveal a functionally dinstinct early neural stem cell stage. *Genes & Development*, 22(2):152–65.

Elliott, B., Richardson, C., Winderbaum, J., Nickoloff, J. A., and Jasin, M. (1998). Gene conversion tracts from double-strand break repair in mammalian cells. *Molecular and cellular biology*, 18(1):93–101.

Ellis, P., Fagan, B. M., Magness, S. T., Hutton, S., Taranova, O., Hayashi, S., McMahon, A., Rao, M., and Pevny, L. (2004). SOX2, a persistent marker for multipotential neural stem cells derived from embryonic stem cells, the embryo or the adult. *Developmental Neuroscience*, 26(2-4):148–65.

Englund, C. (2005). Pax6, Tbr2, and Tbr1 Are Expressed Sequentially by Radial Glia, Intermediate Progenitor Cells, and Postmitotic Neurons in Developing Neocortex. *Journal of Neuroscience*, 25(1):247–51.

Er, J. C., Leong, C., Teoh, C. L., Yuan, Q., Merchant, P., Dunn, M., Sulzer, D., Sames, D., Bhinge, A., Kim, D., Kim, S. M., Yoon, M. H., Stanton, L. W., Je, S. H., Yun, S. W., and Chang, Y. T. (2015). Neuo: A fluorescent chemical probe for live neuron labeling. *Angewandte Chemie - International Edition*, 54(8):2442–6.

Espíndola, S. L., Damianich, A., Alvarez, R. J., Sartor, M., Belforte, J. E., Ferrario, J. E., Gallo, J. M., and Avale, M. E. (2018). Modulation of Tau Isoforms Imbalance Precludes Tau Pathology and Cognitive Decline in a Mouse Model of Tauopathy. *Cell Reports*, 23(3):709–15.

Espuny-Camacho, I., Arranz, A. M., Fiers, M., Snellinx, A., Ando, K., Munck, S., Bonnefont, J., Lambot, L., Corthout, N., Omodho, L., Vanden Eynden, E., Radaelli, E., Tesseur, I., Wray, S., Ebneth, A., Hardy, J., Leroy, K., Brion, J.-p., Vanderhaeghen, P., and De Strooper, B. (2017). Hallmarks of Alzheimer's Disease in Stem-Cell-Derived Human Neurons Transplanted into Mouse Brain. *Neuron*, 93(5):1066–81.e8.

Falcon, B., Cavallini, A., Angers, R., Glover, S., Murray, T. K., Barnham, L., Jackson, S., O'Neill, M. J., Isaacs, A. M., Hutton, M. L., Szekeres, P. G., Goedert, M., and Bose, S. (2015). Conformation determines the seeding potencies of native and recombinant Tau aggregates. *The Journal of biological chemistry*, 290(2):1049–65.

Ferrer, I., López-González, I., Carmona, M., Arregui, L., Dalfó, E., Torrejón-Escribano, B., Diehl, R., and Kovacs, G. G. (2014). Glial and Neuronal Tau Pathology in Tauopathies. *Journal of Neuropathology & Experimental Neurology*, 73(1):81–97.

Fitzpatrick, A. W. P., Falcon, B., He, S., Murzin, A. G., Murshudov, G., Garringer, H. J., Crowther, R. A., Ghetti, B., Goedert, M., and Scheres, S. H. W. (2017). Cryo-EM structures of tau filaments from Alzheimer's disease. *Nature*, 547(7662):185–90.

Flynn, R., Grundmann, A., Renz, P., Hänseler, W., James, W. S., Cowley, S. A., and Moore, M. D. (2015). CRISPR-mediated genotypic and phenotypic correction of a chronic granulomatous disease mutation in human iPS cells. *Experimental Hematology*, 43(10):838–48.

Fong, H., Wang, C., Knoferle, J., Walker, D., Balestra, M. E., Tong, L. M., Leung, L., Ring, K. L., Seeley, W. W., Karydas, A., Kshirsagar, M. A., Boxer, A. L., Kosik, K. S., Miller, B. L., and Huang, Y. (2013). Genetic correction of tauopathy phenotypes in neurons derived from human induced pluripotent stem cells. *Stem Cell Reports*, 1(3):226–34.

Forman, M. S. (2005). Transgenic Mouse Model of Tau Pathology in Astrocytes Leading to Nervous System Degeneration. *Journal of Neuroscience*, 25(14):3539–50.

Forrest, S. L., Kril, J. J., Stevens, C. H., Kwok, J. B., Hallupp, M., Kim, W. S., Huang, Y., McGinley, C. V., Werka, H., Kiernan, M. C., Götz, J., Spillantini, M. G., Hodges, J. R., Ittner, L. M., and Halliday, G. M. (2018). Retiring the term FTDP-17 as MAPT mutations are genetic forms of sporadic frontotemporal tauopathies. *Brain : a journal of neurology*, 141(2):521–34.

Foster, N. L., Wilhelmsen, K., Sima, a. a., Jones, M. Z., D'Amato, C. J., and Gilman, S. (1997). Frontotemporal dementia and parkinsonism linked to chromosome 17: a consensus conference. Conference Participants. *Annals of neurology*, 41(6):706–15.

Francesconi, M., Di Stefano, B., Berenguer, C., de Andrés-Aguayo, L., Plana-Carmona, M., Mendez-Lago, M., Guillaumet-Adkins, A., Rodriguez-Esteban, G., Gut, M., Gut, I. G., Heyn, H., Lehner, B., and Graf, T. (2019). Single cell RNA-seq identifies the origins of heterogeneity in efficient cell transdifferentiation and reprogramming. *eLife*, 8.

Freiesleben, W., Söylemezoglu, F., Lowe, J., Janzer, R. C., and Kleihues, P. (1997). Wernicke's encephalopathy with ballooned neurons in the mamillary bodies: an immunohistochemical study. *Neuropathology and applied neurobiology*, 23(1):36–42.

Fu, Y., Foden, J. a., Khayter, C., Maeder, M. L., Reyon, D., Joung, J. K., and Sander, J. D. (2013). High-frequency off-target mutagenesis induced by CRISPR-Cas nucleases in human cells. *Nature biotechnology*, 31(9):822–6.

Fu, Y., Sander, J. D., Reyon, D., Cascio, V. M., and Joung, J. K. (2014). Improving CRISPR-Cas nuclease specificity using truncated guide RNAs. *Nature Biotechnology*, 32(3):279–84.

Fujino, Y., DeLucia, M. W., Davies, P., and Dickson, D. W. (2004). Ballooned neurones in the limbic lobe are associated with Alzheimer type pathology and lack diagnostic specificity. *Neuropathology and Applied Neurobiology*, 30(6):676–82.

Fujio, K., Sato, M., Uemura, T., Sato, T., Sato-Harada, R., and Harada, A. (2007). 14-3-3 Proteins and protein phosphatases are not reduced in tau-deficient mice. *NeuroReport*, 18(10):1049–52.

Furman, J. L., Vaquer-Alicea, J., White, C. L., Cairns, N. J., Nelson, P. T., and Diamond, M. I. (2017). Widespread tau seeding activity at early Braak stages. *Acta neuropathologica*, 133(1):91–100.

Gaj, T., Gersbach, C. A., and Barbas, C. F. (2013). ZFN, TALEN, and CRISPR/Cas-based methods for genome engineering. *Trends in Biotechnology*, 31(7):397–405.

Galiano, M. R., Jha, S., Ho, T. S. Y., Zhang, C., Ogawa, Y., Chang, K. J., Stankewich, M. C., Mohler, P. J., and Rasband, M. N. (2012). A distal axonal cytoskeleton forms an intra-axonal boundary that controls axon initial segment assembly. *Cell*, 149(5):1125–39.

Gao, L., Wang, J., Wang, Y., and Andreadis, A. (2007). SR protein 9G8 modulates splicing of tau exon 10 via its proximal downstream intron, a clustering region for frontotemporal dementia mutations. *Molecular and cellular neurosciences*, 34(1):48–58.

García-León, J. A., Cabrera-Socorro, A., Eggermont, K., Swijsen, A., Terryn, J., Fazal, R., Nami, F., Ordovás, L., Quiles, A., Lluis, F., Serneels, L., Wierda, K., Sierksma, A., Kreir, M., Pestana, F., Van Damme, P., De Strooper, B., Thorrez, L., Ebneth, A., and Verfaillie, C. M. (2018). Generation of a human induced pluripotent stem cell-based model for tauopathies combining three microtubule-associated protein tau mutations which displays several phenotypes linked to neurodegeneration. *Alzheimer's & dementia : the journal of the Alzheimer's Association*, (July):Accepted.

Gaspard, N., Bouschet, T., Hourez, R., Dimidschstein, J., Naeije, G., van den Ameele, J., Espuny-Camacho, I., Herpoel, A., Passante, L., Schiffmann, S. N., Gaillard, A., and Vanderhaeghen, P. (2008). An intrinsic mechanism of corticogenesis from embryonic stem cells. *Nature*, 455(7211):351–7.

Georgieff, I. S., Liem, R. K., Couchie, D., Mavilia, C., Nunez, J., and Shelanski, M. L. (1993). Expression of high molecular weight tau in the central and peripheral nervous systems. *Journal of cell science*, 105 pt 3:729–37.

Gerdes, J., Lemke, H., Baisch, H., Wacker, H. H., Schwab, U., and Stein, H. (1984). Cell cycle analysis of a cell proliferation-associated human nuclear antigen defined by the monoclonal antibody Ki-67. *Journal of immunology*, 133(4):1710–5.

Ghetti, B., Oblak, A. L., Boeve, B. F., Johnson, K. a., Dickerson, B. C., and Goedert, M. (2015). Invited review: Frontotemporal dementia caused by microtubule-associated protein tau gene (MAPT) mutations: a chameleon for neuropathology and neuroimaging. *Neuropathology and Applied Neurobiology*, 41(1):24–46.

Giandomenico, S. L. and Lancaster, M. A. (2017). Probing human brain evolution and development in organoids. *Current opinion in cell biology*, 44:36–43.

Ginhoux, F. and Prinz, M. (2015). Origin of Microglia: Current Concepts and Past Controversies. *Cold Spring Harbor Perspectives in Biology*, 7(8):a020537.

Goedert, M. (2016). The ordered assembly of tau is the gain-of-toxic function that causes human tauopathies. *Alzheimer's and Dementia*, 12(10):1040–50.

Goedert, M. and Jakes, R. (1990). Expression of separate isoforms of human tau protein: correlation with the tau pattern in brain and effects on tubulin polymerization. *The EMBO journal*, 9(13):4225–30.

Goedert, M., Jakes, R., Crowther, R. A., Cohen, P., Vanmechelen, E., Vandermeeren, M., and Cras, P. (1994). Epitope mapping of monoclonal antibodies to the paired helical filaments of Alzheimer's disease: identification of phosphorylation sites in tau protein. *Biochemical Journal*, 301(3):871–7.

Goedert, M., Jakes, R., Crowther, R. A., Six, J., Lübke, U., Vandermeeren, M., Cras, P., Trojanowski, J. Q., and Lee, V. M. (1993). The abnormal phosphorylation of tau protein at Ser-202 in Alzheimer disease recapitulates phosphorylation during development. *Proceedings of the National Academy of Sciences of the United States of America*, 90(11):5066–70.

Goedert, M., Jakes, R., Spillantini, M. G., Hasegawa, M., Smith, M. J., and Crowther, R. A. (1996). Assembly of microtubule-associated protein tau into Alzheimer-like filaments induced by sulphated glycosaminoglycans. *Nature*, 383(6600):550–53.

Goedert, M., Jakes, R., and Vanmechelen, E. (1995). Monoclonal antibody AT8 recognises tau protein phosphorylated at both serine 202 and threonine 205. *Neuroscience Letters*, 189(3):167–70.

Goedert, M. and Spillantini, M. G. (1990). Molecular neuropathology of Alzheimer's disease: in situ hybridization studies. *Cell Mol.Neurobiol.*, 10(0272-4340):159–74.

Goedert, M. and Spillantini, M. G. (2001). Tau gene mutations and neurodegeneration. *Biochem Soc Symp*, 1(67):59–71.

Goedert, M., Spillantini, M. G., and Crowther, R. A. (1992). Cloning of a big tau microtubule-associated protein characteristic of the peripheral nervous system. *Proceedings of the National Academy of Sciences*, 89(5):1983–7.

Goedert, M., Spillantini, M. G., Jakes, R., Rutherford, D., and Crowther, R. A. (1989a). Multiple isoforms of human microtubule-associated protein tau: sequences and localization in neurofibrillary tangles of Alzheimer's disease. *Neuron*, 3(4):519–26.

Goedert, M., Spillantini, M. G., Potier, M. C., Ulrich, J., and Crowther, R. A. (1989b). Cloning and sequencing of the cDNA encoding an isoform of microtubule-associated protein tau containing four tandem repeats: differential expression of tau protein mRNAs in human brain. *The EMBO journal*, 8(2):393–9.

Goedert, M., Wischik, C. M., Crowther, R. A., Walker, J. E., and Klug, A. (1988). Cloning and sequencing of the cDNA encoding a core protein of the paired helical filament of Alzheimer disease: identification as the microtubule-associated protein tau. *Proceedings of the National Academy of Sciences*, 85(11):4051–5.

Gonzalez, C., Armijo, E., Bravo-Alegria, J., Becerra-Calixto, A., Mays, C. E., and Soto, C. (2018). Modeling amyloid beta and tau pathology in human cerebral organoids. *Molecular Psychiatry*.

Goode, B. L. and Feinstein, S. C. (1994). Identification of a novel microtubule binding and assembly domain in the developmentally regulated inter-repeat region of tau. *Journal of Cell Biology*, 124(5):769–81.

Gopalappa, R., Suresh, B., Ramakrishna, S., and Kim, H. H. (2018). Paired D10A Cas9 nickases are sometimes more efficient than individual nucleases for gene disruption. *Nucleic Acids Research*, page gky222.

Gore, A., Li, Z., Fung, H.-L., Young, J. E., Agarwal, S., Antosiewicz-Bourget, J., Canto, I., Giorgetti, A., Israel, M. A., Kiskinis, E., Lee, J.-H., Loh, Y.-H., Manos, P. D., Montserrat, N., Panopoulos, A. D., Ruiz, S., Wilbert, M. L., Yu, J., Kirkness, E. F., Belmonte, J. C. I., Rossi, D. J., Thomson, J. A., Eggan, K., Daley, G. Q., Goldstein, L. S. B., and Zhang, K. (2011). Somatic coding mutations in human induced pluripotent stem cells. *Nature*, 471(7336):63–7.

Götz, J. and Ittner, L. M. (2008). Animal models of Alzheimer's disease and frontotemporal dementia. *Nature reviews. Neuroscience*, 9(7):532–44.

Götz, J., Probst, A., Spillantini, M. G., Schäfer, T., Jakes, R., Bürki, K., and Goedert, M. (1995). Somatodendritic localization and hyperphosphorylation of tau protein in transgenic mice expressing the longest human brain tau isoform. *The EMBO journal*, 14(7):1304–13.

Granic, A., Padmanabhan, J., Norden, M., and Potter, H. (2010). Alzheimer Aβ Peptide Induces Chromosome Mis-Segregation and Aneuploidy, Including Trisomy 21: Requirement for Tau and APP. *Molecular Biology of the Cell*, 21(4):511–20.

Griffith, L. M. and Pollard, T. D. (1982). The interaction of actin filaments with microtubules and microtubule-associated proteins. *Journal of Biological Chemistry*, 257(15):9143–51.

Grundke-Iqbal, I., Iqbal, K., Quinlan, M., Tung, Y. C., Zaidi, M. S., and Wisniewski, H. M. (1986). Microtubule-associated protein tau. A component of Alzheimer paired helical filaments. *The Journal of biological chemistry*, 261(13):6084–9.

Gu, Y., Oyama, F., and Ihara, Y. (1996). Tau is widely expressed in rat tissues. *Journal of neurochemistry*, 67(3):1235–44.

Gunawardana, C. G., Mehrabian, M., Wang, X., Mueller, I., Lubambo, I. B., Jonkman, J. E. N., Wang, H., and Schmitt-Ulms, G. (2015). The Human Tau Interactome: Binding to the Ribonucleoproteome, and Impaired Binding of the Proline-to-Leucine Mutant at Position 301 (P301L) to Chaperones and the Proteasome. *Molecular & Cellular Proteomics*, 14(11):3000–14.

Guo, J. L., Narasimhan, S., Changolkar, L., He, Z., Stieber, A., Zhang, B., Gathagan, R. J., Iba, M., McBride, J. D., Trojanowski, J. Q., and Lee, V. M. Y. (2016). Unique pathological tau conformers from Alzheimer's brains transmit tau pathology in nontransgenic mice. *The Journal of experimental medicine*, 213(12):2635–54.

Gurdon, J. B. (1962). The developmental capacity of nuclei taken from intestinal epithelium cells of feeding tadpoles. *Journal of embryology and experimental morphology*, 10(4):622–40.

Haase, C., Stieler, J. T., Arendt, T., and Holzer, M. (2004). Pseudophosphorylation of tau protein alters its ability for self-aggregation. *Journal of Neurochemistry*, 88(6):1509–20.

Habela, C. W., Song, H., and li Ming, G. (2015). Modeling synaptogenesis in schizophrenia and autism using human iPSC derived neurons. *Molecular and Cellular Neuroscience*.

Hachem, S., Aguirre, A., Vives, V., Marks, A., Gallo, V., and Legraverend, C. (2005). Spatial and temporal expression of S100B in cells of oligodendrocyte lineage. *GLIA*, 51(2):81–97.

Hallmann, A.-L., Araúzo-Bravo, M. J., Mavrommatis, L., Ehrlich, M., Röpke, A., Brockhaus, J., Missler, M., Sterneckert, J., Schöler, H. R., Kuhlmann, T., Zaehres, H., and Hargus, G. (2017). Astrocyte pathology in a human neural stem cell model of frontotemporal dementia caused by mutant TAU protein. *Scientific Reports*, 7(May 2016):42991.

Hampton, D. W., Webber, D. J., Bilican, B., Goedert, M., Spillantini, M. G., and Chandran, S. (2010). Cell-Mediated Neuroprotection in a Mouse Model of Human Tauopathy. *Journal of Neuroscience*, 30(30):9973–83.

Han, D., Qureshi, H. Y., Lu, Y., and Paudel, H. K. (2009). Familial FTDP-17 missense mutations inhibit microtubule assembly-promoting activity of tau by increasing phosphorylation at Ser202in vitro. *Journal of Biological Chemistry*, 284(20):13422–13433.

Han, D. W., Tapia, N., Hermann, A., Hemmer, K., Höing, S., Araúzo-Bravo, M. J., Zaehres, H., Wu, G., Frank, S., Moritz, S., Greber, B., Yang, J. H., Lee, H. T., Schwamborn, J. C., Storch, A., and Schöler, H. R. (2012). Direct Reprogramming of Fibroblasts into Neural Stem Cells by Defined Factors. *Cell Stem Cell*, 10(4):465–72.

Handel, A. E., Chintawar, S., Lalic, T., Whiteley, E., Vowles, J., Giustacchini, A., Argoud, K., Sopp, P., Nakanishi, M., Bowden, R., Cowley, S., Newey, S., Akerman, C., Ponting, C. P., and Cader, M. Z. (2016). Assessing similarity to primary tissue and cortical layer identity in induced pluripotent stem cell-derived cortical neurons through single-cell transcriptomics. *Human molecular genetics*, 25(5):989–1000.

Hanger, D. P., Hughes, K., Woodgett, J. R., Brion, J. P., and Anderton, B. H. (1992). Glycogen synthase kinase-3 induces Alzheimer's disease-like phosphorylation of tau: Generation of paired helical filament epitopes and neuronal localisation of the kinase. *Neuroscience Letters*, 147(1):58–62.

Hanger, D. P. and Noble, W. (2011). Functional Implications of Glycogen Synthase Kinase-3-Mediated Tau Phosphorylation. *International Journal of Alzheimer's Disease*, 2011:1–11.

Hansen, D. V., Lui, J. H., Parker, P. R. L., and Kriegstein, A. R. (2010). Neurogenic radial glia in the outer subventricular zone of human neocortex. *Nature*, 464(7288):554–61.

Harada, A., Oguchi, K., Okabe, S., Kuno, J., Terade, S., Ohshima, T., Sato-Yoshitake, R., Takei, Y., Noda, T., and Hirokawa, N. (1994). Altered microtubule organization in small-calibre axons of mice lacking tau protein. *Letters to Nature*, 369:488–91.

Hargus, G., Ehrlich, M., Araúzo-Bravo, M. J., Hemmer, K., Hallmann, A.-L., Reinhardt, P., Kim, K.-P., Adachi, K., Santourlidis, S., Ghanjati, F., Fauser, M., Ossig, C., Storch, A., Kim, J. B., Schwamborn, J. C., Sterneckert, J., Schöler, H. R., Kuhlmann, T., and Zaehres, H. (2014). Origin-dependent neural cell identities in differentiated human iPSCs in vitro and after transplantation into the mouse brain. *Cell reports*, 8(6):1697–1703.

Hasegawa, M., Jakes, R., Crowther, R. A., Lee, V. M., Ihara, Y., and Goedert, M. (1996). Characterization of mAb AP422, a novel phosphorylation-dependent monoclonal antibody against tau protein. *FEBS Letters*, 384(1):25–30.

Hasegawa, M., Smith, M. J., and Goedert, M. (1998). Tau proteins with FTDP-17 mutations have a reduced ability to promote microtubule assembly. *FEBS Letters*, 437(3):207–10.

Hasegawa, M., Smith, M. J., Iijima, M., Tabira, T., and Goedert, M. (1999). FTDP-17 mutations N279K and S305N in tau produce increased splicing of exon 10. *FEBS Letters*, 443(2):93–6.

He, Z., Proudfoot, C., Whitelaw, C. B. A., and Lillico, S. G. (2016). Comparison of CRISPR/Cas9 and TALENs on editing an integrated EGFP gene in the genome of HEK293FT cells. *SpringerPlus*, 5(1).

Heide, M., Huttner, W. B., and Mora-Bermúdez, F. (2018). Brain organoids as models to study human neocortex development and evolution. *Current Opinion in Cell Biology*, 55:8–16.

Higurashi, N., Uchida, T., Lossin, C., Misumi, Y., Okada, Y., Akamatsu, W., Imaizumi, Y., Zhang, B., Nabeshima, K., Mori, M. X., Katsurabayashi, S., Shirasaka, Y., Okano, H., and Hirose, S. (2013). A human Dravet syndrome model from patient induced pluripotent stem cells. *Molecular Brain*, 6(1):19.

Hirokawa, N., Shiomura, Y., and Okabe, S. (1988). Tau Proteins: The Molecular Structure and Mode of Binding on Microtubules. *The journal of cell biology*, 107(October):1449–59.

Hochedlinger, K. and Jaenisch, R. (2015). Induced Pluripotency and Epigenetic Reprogramming. *Cold Spring Harbor perspectives in biology*, 7(12):a019448.

Hockfield, S. and McKay, R. D. (1985). Identification of major cell classes in the developing mammalian nervous system. *The Journal of neuroscience : the official journal of the Society for Neuroscience*, 5(12):3310–28.

Holmes, B. B., DeVos, S. L., Kfoury, N., Li, M., Jacks, R., Yanamandra, K., Ouidja, M. O., Brodsky, F. M., Marasa, J., Bagchi, D. P., Kotzbauer, P. T., Miller, T. M., Papy-Garcia, D., and Diamond, M. I. (2013). Heparan sulfate proteoglycans mediate internalization and propagation of specific proteopathic seeds. *Proceedings of the National Academy of Sciences*, 110(33):E3138–47.

Hong, M. (1998). Mutation-Specific Functional Impairments in Distinct Tau Isoforms of Hereditary FTDP-17. *Science*, 282(5395):1914–1917.

Horwitz, J. (2003). Alpha-crystallin. *Experimental eye research*, 76(2):145–53.

Houlden, H., Baker, M., Morris, H., MacDonald, N., Pickering-Brown, S., Adamson, J., Lees, A., Rossor, M., Quinn, N., Kertesz, A., Khan, M., Hardy, J., Lantos, P., St. George-Hyslop, P., Munoz, D., Mann, D., Lang, A., Bergeron, C., Bigio, E., Litvan, I., Bhatia, K., Dickson, D., Wood, N., and Hutton, M. (2001). Corticobasal degeneration and progressive supranuclear palsy share a common tau haplotype. *Neurology*, 56(12):1702–6.

Hsu, P. D., Scott, D. A., Weinstein, J. A., Ran, F. A., Konermann, S., Agarwala, V., Li, Y., Fine, E. J., Wu, X., Shalem, O., Cradick, T. J., Marraffini, L. A., Bao, G., and Zhang, F. (2013). DNA targeting specificity of RNA-guided Cas9 nucleases. *Nature biotechnology*, 31(9):827–32.

Hu, B.-Y., Weick, J. P., Yu, J., Ma, L.-X., Zhang, X.-Q., Thomson, J. A., and Zhang, S.-C. (2010). Neural differentiation of human induced pluripotent stem cells follows developmental principles but with variable potency. *Proceedings of the National Academy of Sciences of the United States of America*, 107(9):4335–40.

Hu, W., Qiu, B., Guan, W., Wang, Q., Wang, M., Li, W., Gao, L., Shen, L., Huang, Y., Xie, G., Zhao, H., Jin, Y., Tang, B., Yu, Y., Zhao, J., and Pei, G. (2015). Direct Conversion of Normal and Alzheimer's Disease Human Fibroblasts into Neuronal Cells by Small Molecules. *Cell Stem Cell*, 17(2):204–12.

Hu, W., Zhang, X., Tung, Y. C., Xie, S., Liu, F., and Iqbal, K. (2016). Hyperphosphorylation determines both the spread and the morphology of tau pathology. *Alzheimer's & dementia : the journal of the Alzheimer's Association*, 12(10):1066–77.

Hua, Q. and He, R. (2000). Human neuronal tau promoting the melting temperature of DNA. *Chinese Science Bulletin*, 45(11):999–1002.

Hutton, M., Lendon, C. L., Rizzu, P., Baker, M., Froelich, S., Houlden, H., Pickering-Brown, S., Chakraverty, S., Isaacs, A., Grover, A., Hackett, J., Adamson, J., Lincoln, S., Dickson, D., Davies, P., Petersen, R. C., Stevens, M., de Graaff, E., Wauters, E., van Baren, J., Hillebrand, M., Joosse, M., Kwon, J. M., Nowotny, P., Che, L. K., Norton, J., Morris, J. C., Reed, L. A., Trojanowski, J., Basun, H., Lannfelt, L., Neystat, M., Fahn, S., Dark, F., Tannenberg, T., Dodd, P. R., Hayward, N., Kwok, J. B., Schofield, P. R., Andreadis, A., Snowden, J., Craufurd, D., Neary, D., Owen, F., Oostra, B. A., Hardy, J., Goate, A., van Swieten, J., Mann, D., Lynch, T., and Heutink, P. (1998). Association of missense and 5'-splice-site mutations in tau with the inherited dementia FTDP-17. *Nature*, 393(6686):702–5.

Iba, M., Guo, J. L., McBride, J. D., Zhang, B., Trojanowski, J. Q., and Lee, V. M.-Y. (2013). Synthetic Tau Fibrils Mediate Transmission of Neurofibrillary Tangles in a Transgenic Mouse Model of Alzheimer's-Like Tauopathy. *Journal of Neuroscience*, 33(3):1024–37.

Ichida, J. K. and Kiskinis, E. (2015). Probing disorders of the nervous system using reprogramming approaches. *The EMBO Journal*, 34(11):1456–77.

Ikegami, S., Harada, A., and Hirokawa, N. (2000). Muscle weakness, hyperactivity, and impairment in fear conditioning in tau-deficient mice. *Neuroscience Letters*, 279(3):129–32.

Imamura, K., Sahara, N., Kanaan, N. M., Tsukita, K., Kondo, T., Kutoku, Y., Ohsawa, Y., Sunada, Y., Kawakami, K., Hotta, A., Yawata, S., Watanabe, D., Hasegawa, M., Trojanowski, J. Q., Lee, V. M.-Y., Suhara, T., Higuchi, M., and Inoue, H. (2016). Calcium dysregulation contributes to neurodegeneration in FTLD patient iPSC-derived neurons. *Scientific reports*, 6:34904.

Iovino, M., Agathou, S., González-Rueda, A., Del Castillo Velasco-Herrera, M., Borroni, B., Alberici, A., Lynch, T., O'Dowd, S., Geti, I., Gaffney, D., Vallier, L., Paulsen, O., Káradóttir, R. T., and Spillantini, M. G. (2015). Early maturation and distinct tau pathology in induced pluripotent stem cell-derived neurons from patients with MAPT mutations. *Brain*, 138(11):3345–59.

Iovino, M., Pfisterer, U., Holton, J. L., Lashley, T., Swingler, R. J., Calo, L., Treacy, R., Revesz, T., Parmar, M., Goedert, M., Muqit, M. M. K., and Spillantini, M. G. (2014). The novel MAPT mutation K298E: mechanisms of mutant tau toxicity, brain pathology and tau expression in induced fibroblast-derived neurons. *Acta neuropathologica*, 127(2):283–95.

Irwin, D. J., Lee, V. M.-Y., and Trojanowski, J. Q. (2013). Parkinson's disease dementia: convergence of α-synuclein, tau and amyloid-β pathologies. *Nature Reviews Neuroscience*, 14(9):626–36.

Ishihara, T., Hong, M., Zhang, B., Nakagawa, Y., Lee, M. K., Trojanowski, J. Q., and Lee, V. M. (1999). Age-Dependent Emergence and Progression of a Tauopathy in Transgenic Mice Overexpressing the Shortest Human Tau Isoform. *Neuron*, 24(3):751–62.

Ishino, Y., Shinagawa, H., Makino, K., Amemura, M., and Nakata, A. (1987). Nucleotide sequence of the iap gene, responsible for alkaline phosphatase isozyme conversion in Escherichia coli, and identification of the gene product. *Journal of bacteriology*, 169(12):5429–33.

Israel, M. a., Yuan, S. H., Bardy, C., Reyna, S. M., Mu, Y., Herrera, C., Hefferan, M. P., Van Gorp, S., Nazor, K. L., Boscolo, F. S., Carson, C. T., Laurent, L. C., Marsala, M., Gage, F. H., Remes, A. M., Koo, E. H., and Goldstein, L. S. B. (2012). Probing sporadic and familial Alzheimer's disease using induced pluripotent stem cells. *Nature*, 482(7384):216–20.

Ittner, L. M., Ke, Y. D., Delerue, F., Bi, M., Gladbach, A., van Eersel, J., Wölfing, H., Chieng, B. C., Christie, M. J., Napier, I. A., Eckert, A., Staufenbiel, M., Hardeman, E., and Götz, J. (2010). Dendritic function of tau mediates amyloid-beta toxicity in Alzheimer's disease mouse models. *Cell*, 142(3):387–97.

Iwaki, T., Kume-Iwaki, A., and Goldman, J. E. (1990). Cellular Distribution of aB-Crystallin Tissues in Non-lenticular Tissues. *The Journal of Histochemistry and Cytochemistry*, 38(1):31–9.

Jackson, S. J., Kerridge, C., Cooper, J., Cavallini, A., Falcon, B., Cella, C. V., Landi, A., Szekeres, P. G., Murray, T. K., Ahmed, Z., Goedert, M., Hutton, M., O'Neill, M. J., and Bose, S. (2016). Short Fibrils Constitute the Major Species of Seed-Competent Tau in the Brains of Mice Transgenic for Human P301S Tau. *Journal of Neuroscience*, 36(3):762–72.

Jakob, U., Gaestel, M., Engel, K., and Buchner, J. (1993). Small heat shock proteins are molecular chaperones. *The Journal of biological chemistry*, 268(3):1517–20.

Jeganathan, S., Hascher, A., Chinnathambi, S., Biernat, J., Mandelkow, E.-M., and Mandelkow, E. (2008). Proline-directed pseudo-phosphorylation at AT8 and PHF1 epitopes induces a compaction of the paperclip folding of Tau and generates a pathological (MC-1) conformation. *The Journal of biological chemistry*, 283(46):32066–76.

Jiang, Z., Tang, H., Havlioglu, N., Zhang, X., Stamm, S., Yan, R., and Wu, J. Y. (2003). Mutations in Tau Gene Exon 10 Associated with FTDP-17 Alter the Activity of an Exonic Splicing Enhancer to Interact with Tra2β. *Journal of Biological Chemistry*, 278(21):18997–19007.

Jicha, G. A., Bowser, R., Kazam, I. G., and Davies, P. (1996). Alz-50 and MC-1, a new monoclonal antibody raised to paired helical filaments, recognize conformational epitopes on recombinant tau. *J. Neurosci. Res*, 48:128–32.

Jinek, M., Chylinski, K., Fonfara, I., Hauer, M., Doudna, J. A., and Charpentier, E. (2012). A Programmable Dual-RNA–Guided DNA Endonuclease in Adaptive Bacterial Immunity. *Science*, 337:816–22.

Johnson, M. A., Weick, J. P., Pearce, R. A., and Zhang, S.-C. (2007). Functional Neural Development from Human Embryonic Stem Cells: Accelerated Synaptic Activity via Astrocyte Coculture. *Journal of Neuroscience*, 27(12):3069–77.

Kadoshima, T., Sakaguchi, H., Nakano, T., Soen, M., Ando, S., Eiraku, M., and Sasai, Y. (2013). Self-organization of axial polarity, inside-out layer pattern, and species-specific progenitor dynamics in human ES cell-derived neocortex. *Proceedings of the National Academy of Sciences*, 110(50):20284–9.

Kan, Y., Ruis, B., Lin, S., and Hendrickson, E. A. (2014). The Mechanism of Gene Targeting in Human Somatic Cells. *PLoS Genetics*, 10(4).

Kan, Y., Ruis, B., Takasugi, T., and Hendrickson, E. A. (2017). Mechanisms of precise genome editing using oligonucleotide donors. *Genome Research*, 27(7):1099–111.

Kang, L., Wang, J., Zhang, Y., Kou, Z., and Gao, S. (2009). iPS cells can support full-term development of tetraploid blastocyst-complemented embryos. *Cell stem cell*, 5(2):135–8.

Kara, E., Ling, H., Pittman, A. M., Shaw, K., de Silva, R., Simone, R., Holton, J. L., Warren, J. D., Rohrer, J. D., Xiromerisiou, G., Lees, A., Hardy, J., Houlden, H., and Revesz, T. (2012). The MAPT p.A152T variant is a risk factor associated with tauopathies with

atypical clinical and neuropathological features. *Neurobiology of Aging*, 33(9):2231.e7–2231.e14.

Karzbrun, E., Kshirsagar, A., Cohen, S. R., Hanna, J. H., and Reiner, O. (2018). Human brain organoids on a chip reveal the physics of folding. *Nature Physics*, 14(5):515–22.

Kelava, I. and Lancaster, M. A. (2016). Stem Cell Models of Human Brain Development. *Cell Stem Cell*, 18(6):736–48.

Kenessey, A. and Yen, S. H. C. (1993). The extent of phosphorylation of fetal tau is comparable to that of PHF-tau from Alzheimer paired helical filaments. *Brain Research*, 629(1):40–6.

Kettenmann, H. and Verkhratsky, A. (2016). Glial Cells: Neuroglia. In *Neuroscience in the 21st Century*, pages 547–78. Springer New York, New York, NY.

Kim, Y. D., Choi, H., Lee, W. J., Park, H., Kam, T. I., hoon Hong, S., Nah, J., Jung, S., Shin, B., Lee, H., Choi, T. Y., Choo, H., Kim, K. K., Choi, S. Y., Kayed, R., and Jung, Y. K. (2016). Caspase-cleaved tau exhibits rapid memory impairment associated with tau oligomers in a transgenic mouse model. *Neurobiology of Disease*, 87:19–28.

Kirkeby, A., Nelander, J., and Parmar, M. (2012). Generating regionalized neuronal cells from pluripotency, a step-by-step protocol. *Frontiers in cellular neuroscience*, 6:64.

Klein, C., Kramer, E.-M., Cardine, A.-M., Schraven, B., Brandt, R., and Trotter, J. (2002). Process outgrowth of oligodendrocytes is promoted by interaction of fyn kinase with the cytoskeletal protein tau. *The Journal of neuroscience : the official journal of the Society for Neuroscience*, 22(3):698–707.

Klemenz, R., Fröhli, E., Steiger, R. H., Schäfer, R., and Aoyama, A. (1991). Alpha B-crystallin is a small heat shock protein. *Proceedings of the National Academy of Sciences of the United States of America*, 88(9):3652–6.

Kobayashi, S., Tanaka, T., Soeda, Y., Almeida, O. F., and Takashima, A. (2017). Local Somatodendritic Translation and Hyperphosphorylation of Tau Protein Triggered by AMPA and NMDA Receptor Stimulation. *EBioMedicine*, 20:120–6.

Koffie, R. M., Hyman, B. T., and Spires-Jones, T. L. (2011). Alzheimer's disease: synapses gone cold. *Molecular Neurodegeneration*, 6(1):63.

Kole, M. H. P. and Stuart, G. J. (2012). Signal processing in the axon initial segment. *Neuron*, 73(2):235–47.

Kondo, S., Yamamoto, N., Murakami, T., Okumura, M., Mayeda, A., and Imaizumi, K. (2004). Tra2β, SF2/ASF and SRp30c modulate the function of an exonic splicing enhancer in exon 10 of tau pre-mRNA. *Genes to Cells*, 9(2):121–30.

Kondo, T., Funayama, M., Miyake, M., Tsukita, K., Era, T., Osaka, H., Ayaki, T., Takahashi, R., and Inoue, H. (2016). Modeling Alexander disease with patient iPSCs reveals cellular and molecular pathology of astrocytes. *Acta neuropathologica communications*, 4(1):69.

Koolen, D. A., Kramer, J. M., Neveling, K., Nillesen, W. M., Moore-Barton, H. L., Elmslie, F. V., Toutain, A., Amiel, J., Malan, V., Tsai, A. C. H., Cheung, S. W., Gilissen, C., Verwiel, E. T., Martens, S., Feuth, T., Bongers, E. M., De Vries, P., Scheffer, H., Vissers, L. E., De Brouwer, A. P., Brunner, H. G., Veltman, J. A., Schenck, A., Yntema, H. G., and De Vries, B. B. (2012). Mutations in the chromatin modifier gene KANSL1 cause the 17q21.31 microdeletion syndrome. *Nature Genetics*, 44(6):639–41.

Kopeikina, K. J., Polydoro, M., Tai, H.-C., Yaeger, E., Carlson, G. A., Pitstick, R., Hyman, B. T., and Spires-Jones, T. L. (2013). Synaptic alterations in the rTg4510 mouse model of tauopathy. *Journal of Comparative Neurology*, 521(6):1334–53.

Kosik, K. S. and Finch, E. a. (1987). MAP2 and tau segregate into dendritic and axonal domains after the elaboration of morphologically distinct neurites: an immunocytochemical study of cultured rat cerebrum. *The Journal of neuroscience : the official journal of the Society for Neuroscience*, 7(10):3142–53.

Krencik, R. and Ullian, E. M. (2013). A cellular star atlas: using astrocytes from human pluripotent stem cells for disease studies. *Frontiers in Cellular Neuroscience*, 7(March):25.

Kriegstein, A. and Alvarez-Buylla, A. (2009). The Glial Nature of Embryonic and Adult Neural Stem Cells. *Annual Review of Neuroscience*, 32(1):149–84.

Kril, J. J., Patel, S., Harding, A. J., and Halliday, G. M. (2002). Neuron loss from the hippocampus of Alzheimer's disease exceeds extracellular neurofibrillary tangle formation. *Acta Neuropathologica*, 103(4):370–6.

Ksiezak-reding, H., He, D., Gordon-krajcer, W., Kress, Y., Lee, S., and Dickson, D. W. (2000). Induction of Alzheimer-Specific Tau Epitope AT100 in Apoptotic Human Fetal Astrocytes. *Cell Motility and the Cytoskeleton*, 47(February):236–52.

Kuan, C.-Y., Roth, K. A., Flavell, R. A., and Rakic, P. (2000). Mechanisms of programmed cell death in the developing brain. *Trends in Neurosciences*, 23(7):291–7.

Kwolek, B. and Kepski, M. (2015). Improving fall detection by the use of depth sensor and accelerometer. *Neurocomputing*, 168(8):637–45.

Lacovich, V., Espindola, S. L., Alloatti, M., Pozo Devoto, V., Cromberg, L. E., Čarná, M. E., Forte, G., Gallo, J.-M., Bruno, L., Stokin, G. B., Avale, M. E., and Falzone, T. L. (2017). Tau Isoforms Imbalance Impairs the Axonal Transport of the Amyloid Precursor Protein in Human Neurons. *The Journal of neuroscience : the official journal of the Society for Neuroscience*, 37(1):58–69.

Lagui, D., Probst, A., and Ulrich, J. (1995). Alzheimer's changes in non-demented and demented patients: a statistical approach to their relationships. *Acta Neuropathologica*, 89(1):57–62.

Lancaster, M. A. (2018). Crinkle-Cut Brain Organoids. *Cell Stem Cell*, 22(5):616–8.

Lancaster, M. A., Corsini, N. S., Wolfinger, S., Gustafson, E. H., Phillips, A. W., Burkard, T. R., Otani, T., Livesey, F. J., and Knoblich, J. A. (2017). Guided self-organization and cortical plate formation in human brain organoids. *Nature biotechnology*, 35(7):659–66.

Lancaster, M. A. and Knoblich, J. A. (2014a). Generation of cerebral organoids from human pluripotent stem cells. *Nature protocols*, 9(10):2329–40.

Lancaster, M. a. and Knoblich, J. a. (2014b). Organogenesis in a dish: Modeling development and disease using organoid technologies. *Science*, 345(6194):1247125–1–9.

Lancaster, M. A., Renner, M., Martin, C.-a., Wenzel, D., Bicknell, L. S., Hurles, M. E., Homfray, T., Penninger, J. M., Jackson, A. P., and Knoblich, J. A. (2013). Cerebral organoids model human brain development and microcephaly. *Nature*, 501(7467):373–9.

Lang, E., Szendrei, G. I., Lee, V. M., and Otvos, L. (1992). Immunological and conformational characterization of a phosphorylated immunodominant epitope on the paired helical filaments found in Alzheimer's disease. *Biochemical and Biophysical Research Communications*, 187(2):783–90.

Larsen, K. B., Lutterodt, M. C., Møllgård, K., and Møller, M. (2010). Expression of the Homeobox Genes OTX2 and OTX1 in the Early Developing Human Brain. *Journal of Histochemistry & Cytochemistry*, 58(7):669–78.

Lasagna-Reeves, C. A., Castillo-Carranza, D. L., Sengupta, U., Sarmiento, J., Troncoso, J., Jackson, G. R., and Kayed, R. (2012). Identification of oligomers at early stages of tau aggregation in Alzheimer's disease. *The FASEB Journal*, 26(5):1946–59.

Le Corre, S., Klafki, H. W., Plesnila, N., Hübinger, G., Obermeier, A., Sahagún, H., Monse, B., Seneci, P., Lewis, J., Eriksen, J., Zehr, C., Yue, M., McGowan, E., Dickson, D. W., Hutton, M., and Roder, H. M. (2006). An inhibitor of tau hyperphosphorylation prevents severe motor impairments in tau transgenic mice. *Proceedings of the National Academy of Sciences of the United States of America*, 103(25):9673–8.

Le Guennec, K., Quenez, O., Nicolas, G., Wallon, D., Rousseau, S., Richard, A. C., Alexander, J., Paschou, P., Charbonnier, C., Bellenguez, C., Grenier-Boley, B., Lechner, D., Bihoreau, M. T., Olaso, R., Boland, A., Meyer, V., Deleuze, J. F., Amouyel, P., Munter, H. M., Bourque, G., Lathrop, M., Frebourg, T., Redon, R., Letenneur, L., Dartigues, J. F., Martinaud, O., Kalev, O., Mehrabian, S., Traykov, L., Ströbel, T., Le Ber, I., Caroppo, P., Epelbaum, S., Jonveaux, T., Pasquier, F., Rollin-Sillaire, A., Génin, E., Guyant-Maréchal, L., Kovacs, G. G., Lambert, J. C., Hannequin, D., Campion, D., and Rovelet-Lecrux, A. (2017). 17q21.31 duplication causes prominent tau-related dementia with increased MAPT expression. *Molecular Psychiatry*, 22(8):1119–25.

Leak, R. K. (2014). Heat shock proteins in neurodegenerative disorders and aging. *Journal of Cell Communication and Signaling*, 8(4):293–310.

Lee, G., Thangavel, R., Sharma, V. M., Litersky, J. M., Bhaskar, K., Fang, S. M., Do, L. H., Andreadis, A., Van Hoesen, G., and Ksiezak-Reding, H. (2004). Phosphorylation of Tau by Fyn: Implications for Alzheimer's Disease. *Journal of Neuroscience*, 24(9):2304–12.

Lei, P., Ayton, S., Finkelstein, D. I., Spoerri, L., Ciccotosto, G. D., Wright, D. K., Wong, B. X., Adlard, P. A., Cherny, R. A., Lam, L. Q., Roberts, B. R., Volitakis, I., Egan, G. F., McLean, C. A., Cappai, R., Duce, J. A., and Bush, A. I. (2012). Tau deficiency induces parkinsonism with dementia by impairing APP-mediated iron export. *Nature Medicine*, 18(2):291–5.

Li, H. L., Fujimoto, N., Sasakawa, N., Shirai, S., Ohkame, T., Sakuma, T., Tanaka, M., Amano, N., Watanabe, A., Sakurai, H., Yamamoto, T., Yamanaka, S., and Hotta, A. (2014a). Precise Correction of the Dystrophin Gene in Duchenne Muscular Dystrophy Patient Induced Pluripotent Stem Cells by TALEN and CRISPR-Cas9. *Stem Cell Reports*, 4(1):143–54.

Li, K., Wang, G., Andersen, T., Zhou, P., and Pu, W. T. (2014b). Optimization of Genome Engineering Approaches with the CRISPR/Cas9 System. *PloS one*, 9(8):e105779.

Li, W., Cavelti-Weder, C., Zhang, Y., Zhang, Y., Clement, K., Donovan, S., Gonzalez, G., Zhu, J., Stemann, M., Xu, K., Hashimoto, T., Yamada, T., Nakanishi, M., Zhang, Y., Zeng, S., Gifford, D., Meissner, A., Weir, G., and Zhou, Q. (2014c). Long-term persistence and development of induced pancreatic beta cells generated by lineage conversion of acinar cells. *Nature biotechnology*, 32(12):1223–30.

Li, Y., Muffat, J., Omer, A., Bosch, I., Lancaster, M. A., Sur, M., Gehrke, L., Knoblich, J. A., and Jaenisch, R. (2017). Induction of Expansion and Folding in Human Cerebral Organoids. *Cell Stem Cell*, 20(3):385–96.e3.

Liang, X., Potter, J., Kumar, S., Ravinder, N., and Chesnut, J. D. (2017). Enhanced CRISPR/Cas9-mediated precise genome editing by improved design and delivery of gRNA, Cas9 nuclease, and donor DNA. *Journal of Biotechnology*, 241:136–46.

Liang, X., Potter, J., Kumar, S., Zou, Y., Quintanilla, R., Sridharan, M., Carte, J., Chen, W., Roark, N., Ranganathan, S., Ravinder, N., and Chesnut, J. D. (2015). Rapid and highly efficient mammalian cell engineering via Cas9 protein transfection. *Journal of Biotechnology*, 208:44–53.

Liedmann, A., Frech, S., Morgan, P. J., Rolfs, A., and Frech, M. J. (2012). Differentiation of Human Neural Progenitor Cells in Functionalized Hydrogel Matrices. *BioResearch Open Access*, 1(1):16–24.

Lin, S., Staahl, B. T., Alla, R. K., and Doudna, J. A. (2014). Enhanced homology-directed human genome engineering by controlled timing of CRISPR/Cas9 delivery. *eLife*, 3:e04766.

Lindwall, G. and Cole, R. D. (1984). The purification of tau protein and the occurrence of two phosphorylation states of tau in brain. *Journal of Biological Chemistry*, 259(19):12241–5.

Liu, C. W. A., Lee, G., and Jay, D. G. (1999). Tau is required for neurite outgrowth and growth cone motility of chick sensory neurons. *Cell Motility and the Cytoskeleton*, 43(3):232–42.

Liu, L., Drouet, V., Wu, J. W., Witter, M. P., Small, S. A., Clelland, C., and Duff, K. (2012). Trans-Synaptic Spread of Tau Pathology In Vivo. *PLoS ONE*, 7(2):e31302.

Loomis, P. A., Howard, T. H., Castleberry, R. P., and Binder, L. I. (1990). Identification of nuclear tau isoforms in human neuroblastoma cells. *Proceedings of the National Academy of Sciences*, 87(21):8422–6.

López-González, I., Carmona, M., Arregui, L., Kovacs, G. G., and Ferrer, I. (2014). αB-crystallin and HSP27 in glial cells in tauopathies. *Neuropathology*, 34(6):517–26.

LoPresti, P., Szuchet, S., Papasozomenos, S. C., Zinkowski, R. P., and Binder, L. I. (1995). Functional implications for the microtubule-associated protein tau: localization in oligodendrocytes. *Proceedings of the National Academy of Sciences*, 92(22):10369–73.

Lorincz, A. and Nusser, Z. (2008). Cell-Type-Dependent Molecular Composition of the Axon Initial Segment. *Journal of Neuroscience*, 28(53):14329–40.

Lowell, S., Benchoua, A., Heavey, B., and Smith, A. G. (2006). Notch promotes neural lineage entry by pluripotent embryonic stem cells. *PLoS biology*, 4(5):e121.

Lund, R. J., Närvä, E., and Lahesmaa, R. (2012). Genetic and epigenetic stability of human pluripotent stem cells. *Nature reviews. Genetics*, 13(10):732–44.

Luo, C., Lancaster, M. A., Castanon, R., Nery, J. R., Knoblich, J. A., and Ecker, J. R. (2016). Cerebral Organoids Recapitulate Epigenomic Signatures of the Human Fetal Brain. *Cell Reports*, 17(12):3369–84.

Ma, Q.-L., Zuo, X., Yang, F., Ubeda, O. J., Gant, D. J., Alaverdyan, M., Kiosea, N. C., Nazari, S., Chen, P. P., Nothias, F., Chan, P., Teng, E., Frautschy, S. A., and Cole, G. M. (2014). Loss of MAP Function Leads to Hippocampal Synapse Loss and Deficits in the Morris Water Maze with Aging. *Journal of Neuroscience*, 34(21):7124–36.

Mackenzie, I. R., Munoz, D. G., Kusaka, H., Yokota, O., Ishihara, K., Roeber, S., Kretzschmar, H. A., Cairns, N. J., and Neumann, M. (2011). Distinct pathological subtypes of FTLD-FUS. *Acta Neuropathologica*, 121(2):207–18.

Mackenzie, I. R. A., Neumann, M., Bigio, E. H., Cairns, N. J., Alafuzoff, I., Kril, J., Kovacs, G. G., Ghetti, B., Halliday, G., Holm, I. E., Ince, P. G., Kamphorst, W., Revesz, T., Rozemuller, A. J. M., Kumar-Singh, S., Akiyama, H., Baborie, A., Spina, S., Dickson, D. W., Trojanowski, J. Q., and Mann, D. M. A. (2009). Nomenclature for neuropathologic subtypes of frontotemporal lobar degeneration: Consensus recommendations. *Acta Neuropathologica*, 117(1):15–8.

Maeda, S., Djukic, B., Taneja, P., Yu, G.-q., Lo, I., Davis, A., Craft, R., Guo, W., Wang, X., Kim, D., Ponnusamy, R., Gill, T. M., Masliah, E., and Mucke, L. (2016). Expression of A152T human tau causes age-dependent neuronal dysfunction and loss in transgenic mice. *EMBO reports*, 17(4):530–51.

Magnani, E., Fan, J., Gasparini, L., Golding, M., Williams, M., Schiavo, G., Goedert, M., Amos, L. A., and Spillantini, M. G. (2007). Interaction of tau protein with the dynactin complex. *EMBO Journal*, 26(21):4546–54.

Majounie, E., Cross, W., Newsway, V., Dillman, A., Vandrovcova, J., Morris, C. M., Nalls, M. A., Ferrucci, L., Owen, M. J., O'Donovan, M. C., Cookson, M. R., Singleton, A. B., de Silva, R., and Morris, H. R. (2013). Variation in tau isoform expression in different brain regions and disease states. *Neurobiology of Aging*, 34(7):1922.e7–e12.

Makarova, K. S., Wolf, Y. I., Alkhnbashi, O. S., Costa, F., Shah, S. A., Saunders, S. J., Barrangou, R., Brouns, S. J. J., Charpentier, E., Haft, D. H., Horvath, P., Moineau, S., Mojica, F. J. M., Terns, R. M., Terns, M. P., White, M. F., Yakunin, A. F., Garrett, R. A., van der Oost, J., Backofen, R., and Koonin, E. V. (2015). An updated evolutionary classification of CRISPR-Cas systems. *Nature reviews. Microbiology*, 13(11):722–36.

Mali, P., Yang, L., Esvelt, K. M., Aach, J., Guell, M., Dicarlo, J. E., Norville, J. E., and Church, G. M. (2013). RNA-Guided Human Genome Engineering via Cas9. (February):823–7.

Malkani, R., D'Souza, I., Gwinn-Hardy, K., Schellenberg, G. D., Hardy, J., and Momeni, P. (2006). A MAPT mutation in a regulatory element upstream of exon 10 causes frontotemporal dementia. *Neurobiology of disease*, 22(2):401–3.

Mandelkow, E. M., Stamer, K., Vogel, R., Thies, E., and Mandelkow, E. (2003). Clogging of axons by tau, inhibition of axonal traffic and starvation of synapses. *Neurobiology of Aging*, 24(8):1079–85.

Marciniak, E., Leboucher, A., Caron, E., Ahmed, T., Tailleux, A., Dumont, J., Issad, T., Gerhardt, E., Pagesy, P., Vileno, M., Bournonville, C., Hamdane, M., Bantubungi, K., Lancel, S., Demeyer, D., Eddarkaoui, S., Vallez, E., Vieau, D., Humez, S., Faivre, E., Grenier-Boley, B., Outeiro, T. F., Staels, B., Amouyel, P., Balschun, D., Buee, L., and Blum, D. (2017). Tau deletion promotes brain insulin resistance. *The Journal of Experimental Medicine*, 214(8):2257–69.

Mariani, J., Coppola, G., Zhang, P., Abyzov, A., Provini, L., Tomasini, L., Amenduni, M., Szekely, A., Palejev, D., Wilson, M., Gerstein, M., Grigorenko, E. L., Chawarska, K., Pelphrey, K. A., Howe, J. R., and Vaccarino, F. M. (2015). FOXG1-Dependent Dysregulation of GABA/Glutamate Neuron Differentiation in Autism Spectrum Disorders. *Cell*, 162(2):375–90.

Mariani, J., Vittoria, M., Palejev, D., and Tomasini, Livia; Coppola, G.; Szekely, A.M.; Horvath, T.L.; Vaccarino, M. (2012). Modeling human cortical development in vitro using induced pluripotent stem cells. *Proceedings of the National Academy of Sciences*, 109(31):12770–5.

Martin, L., Latypova, X., and Terro, F. (2011). Post-translational modifications of tau protein: Implications for Alzheimer's disease. *Neurochemistry International*, 58(4):458–71.

Maruyama, T., Dougan, S. K., Truttmann, M. C., Bilate, A. M., Ingram, J. R., and Ploegh, H. L. (2015). Increasing the efficiency of precise genome editing with CRISPR-Cas9 by inhibition of nonhomologous end joining. *Nature Biotechnology*, 33(5):538–42.

Masliah, E., Terry, R. D., DeTeresa, R. M., and Hansen, L. A. (1989). Immunohistochemical quantification of the synapse-related protein synaptophysin in Alzheimer disease. *Neuroscience Letters*, 103(2):234–9.

Matsui, T. K., Matsubayashi, M., Sakaguchi, Y. M., Hayashi, R. K., Zheng, C., Sugie, K., Hasegawa, M., Nakagawa, T., and Mori, E. (2018). Six-month cultured cerebral organoids from human ES cells contain matured neural cells. *Neuroscience Letters*, 670(February):75–82.

Matsumoto, S., Udaka, F., Kameyama, M., Kusaka, H., Ito, H., and Imai, T. (1996). Subcortical neurofibrillary tangles, neuropil threads, and argentophilic glial inclusions in corticobasal degeneration. *Clinical neuropathology*, 15(4):209–14.

Matsuo, E. S., Shin, R. W., Billingsley, M. L., Van deVoorde, A., O'Connor, M., Trojanowski, J. Q., and Lee, V. M. (1994). Biopsy-derived adult human brain tau is phosphorylated at many of the same sites as Alzheimer's disease paired helical filament tau. *Neuron*, 13(4):989–1002.

McCarthy, A., Lonergan, R., Olszewska, D. A., O'Dowd, S., Cummins, G., Magennis, B., Fallon, E. M., Pender, N., Huey, E. D., Cosentino, S., O'Rourke, K., Kelly, B. D., O'Connell, M., Delon, I., Farrell, M., Spillantini, M. G., Rowland, L. P., Fahn, S., Craig, P., Hutton, M., and Lynch, T. (2015). Closing the tau loop: The missing tau mutation. *Brain*, 138(10):3100–9.

McCoy, M. J., Paul, A. J., Victor, M. B., Richner, M., Gabel, H. W., Gong, H., Yoo, A. S., and Ahn, T.-H. (2018). LONGO: an R package for interactive gene length dependent analysis for neuronal identity. *Bioinformatics*, 34(13):i422–8.

Medda, X., Mertens, L., Versweyveld, S., Diels, A., Barnham, L., Bretteville, A., Buist, A., Verheyen, A., Royaux, I., Ebneth, A., and Cabrera-Socorro, A. (2016). Development of a Scalable, High-Throughput-Compatible Assay to Detect Tau Aggregates Using iPSC-Derived Cortical Neurons Maintained in a Three-Dimensional Culture Format. *Journal of Biomolecular Screening*, 21(8):804–15.

Mellone, M., Kestoras, D., Andrews, M. R., Dassie, E., Crowther, R. A., Stokin, G. B., Tinsley, J., Horne, G., Goedert, M., Tolkovsky, A. M., and Spillantini, M. G. (2013). Tau pathology is present in vivo and develops in vitro in sensory neurons from human P301S tau transgenic mice: a system for screening drugs against tauopathies. *The Journal of neuroscience : the official journal of the Society for Neuroscience*, 33(46):18175–89.

Mercken, M., Vandermeeren, M., Lübke, U., Six, J., Boons, J., Van de Voorde, A., Martin, J. J., and Gheuens, J. (1992). Monoclonal antibodies with selective specificity for Alzheimer Tau are directed against phosphatase-sensitive epitopes. *Acta Neuropathologica*, 84(3):265–72.

Merkle, F. T., Neuhausser, W. M., Santos, D., Valen, E., Gagnon, J. A., Maas, K., Sandoe, J., Schier, A. F., and Eggan, K. (2015). Efficient CRISPR-Cas9-Mediated Generation of Knockin Human Pluripotent Stem Cells Lacking Undesired Mutations at the Targeted Locus. *Cell Reports*, 11(6):875–83.

Mertens, J., Paquola, A. C., Ku, M., Hatch, E., Böhnke, L., Ladjevardi, S., McGrath, S., Campbell, B., Lee, H., Herdy, J. R., Gonçalves, J. T., Toda, T., Kim, Y., Winkler, J., Yao, J., Hetzer, M. W., and Gage, F. H. (2015). Directly Reprogrammed Human Neurons Retain Aging-Associated Transcriptomic Signatures and Reveal Age-Related Nucleocytoplasmic Defects. *Cell Stem Cell*, 17(6):705–18.

Mertens, J., Stüber, K., Poppe, D., Doerr, J., Ladewig, J., Brüstle, O., and Koch, P. (2013). Embryonic Stem Cell–Based Modeling of Tau Pathology in Human Neurons. *The American Journal of Pathology*, 182(5):1769–79.

Mietelska-Porowska, A., Wasik, U., Goras, M., Filipek, A., and Niewiadomska, G. (2014). Tau protein modifications and interactions: Their role in function and dysfunction. *International Journal of Molecular Sciences*, 15(3):4671–713.

Mihalas, A. B., Elsen, G. E., Bedogni, F., Daza, R. A., Ramos-Laguna, K. A., Arnold, S. J., and Hevner, R. F. (2016). Intermediate Progenitor Cohorts Differentially Generate Cortical Layers and Require Tbr2 for Timely Acquisition of Neuronal Subtype Identity. *Cell Reports*, 16(1):92–105.

Miklossy, J., Qing, H., Guo, J. P., Yu, S., Wszolek, Z. K., Calne, D., McGeer, E. G., and McGeer, P. L. (2007). Lrrk2 and chronic inflammation are linked to pallido-ponto-nigral degeneration caused by the N279K tau mutation. *Acta Neuropathologica*, 114(3):243–54.

Milenkovic, I., Jarc, J., Dassler, E., Aronica, E., Iyer, A., Adle-Biassette, H., Scharrer, A., Reischer, T., Hainfellner, J. A., and Kovacs, G. G. (2018). The physiological phosphorylation of tau is critically changed in fetal brains of individuals with Down syndrome. *Neuropathology and Applied Neurobiology*, 44(3):314–27.

Miller, D. M., Thomas, S. D., Islam, A., Muench, D., and Sedoris, K. (2012). c-Myc and Cancer Metabolism. *Clinical Cancer Research*, 18(20):5546–53.

Miller, J. C., Tan, S., Qiao, G., Barlow, K. A., Wang, J., Xia, D. F., Meng, X., Paschon, D. E., Leung, E., Hinkley, S. J., Dulay, G. P., Hua, K. L., Ankoudinova, I., Cost, G. J., Urnov, F. D., Zhang, H. S., Holmes, M. C., Zhang, L., Gregory, P. D., and Rebar, E. J. (2011). A TALE nuclease architecture for efficient genome editing. *Nature Biotechnology*, 29(2):143–50.

Miller, J. D., Ganat, Y. M., Kishinevsky, S., Bowman, R. L., Liu, B., Tu, E. Y., Mandal, P. K., Vera, E., Shim, J.-w., Kriks, S., Taldone, T., Fusaki, N., Tomishima, M. J., Krainc, D., Milner, T. A., Rossi, D. J., and Studer, L. (2013). Human iPSC-based modeling of late-onset disease via progerin-induced aging. *Cell stem cell*, 13(6):691–705.

Mirbaha, H., Holmes, B. B., Sanders, D. W., Bieschke, J., and Diamond, M. I. (2015). Tau Trimers Are the Minimal Propagation Unit Spontaneously Internalized to Seed Intracellular Aggregation. *The Journal of biological chemistry*, 290(24):14893–903.

Miyaoka, Y., Chan, A. H., Judge, L. M., Yoo, J., Huang, M., Nguyen, T. D., Lizarraga, P. P., So, P.-L., and Conklin, B. R. (2014). Isolation of single-base genome-edited human iPS cells without antibiotic selection. *Nature Methods*, 11(3):291–3.

Miyasaka, T., Morishima-Kawashima, M., Ravid, R., Kamphorst, W., Nagashima, K., and Ihara, Y. (2001). Selective deposition of mutant tau in the FTDP-17 brain affected by the P301L mutation. *Journal of Neuropathology and Experimental Neurology*, 60(9):872–84.

Mizuno, Y., Takeuchi, T., Takatama, M., and Okamoto, K. (2003). Expression of nestin in Purkinje cells in patients with Creutzfeldt-Jakob disease. *Neuroscience Letters*, 352(2):109–12.

Molyneaux, B. J., Arlotta, P., Menezes, J. R. L., and Macklis, J. D. (2007). Neuronal subtype specification in the cerebral cortex. *Nature Reviews Neuroscience*, 8(6):427–37.

Momeni, P., Pittman, A., Lashley, T., Vandrovcova, J., Malzer, E., Luk, C., Hulette, C., Lees, A., Revesz, T., Hardy, J., and de Silva, R. (2009). Clinical and pathological features of an Alzheimer's disease patient with the MAPT ΔK280 mutation. *Neurobiology of Aging*, 30(3):388–93.

Monzel, A. S., Smits, L. M., Hemmer, K., Hachi, S., Moreno, E. L., van Wuellen, T., Jarazo, J., Walter, J., Brüggemann, I., Boussaad, I., Berger, E., Fleming, R. M., Bolognin, S., and Schwamborn, J. C. (2017). Derivation of Human Midbrain-Specific Organoids from Neuroepithelial Stem Cells. *Stem Cell Reports*, 8(5):1144–54.

Mori, H., Oda, M., and Mizuno, Y. (1996). Cortical ballooned neurons in progressive supranuclear palsy. *Neuroscience letters*, 209(2):109–12.

Morishima-Kawashima, M., Hasegawa, M., Takio, K., Suzuki, M., Yoshida, H., Titani, K., and Ihara, Y. (1995). Proline-directed and Non-proline-directed Phosphorylation of PHF-tau. *Journal of Biological Chemistry*, 270(2):823–9.

Morris, M., Hamto, P., Adame, A., Devidze, N., Masliah, E., and Mucke, L. (2013). Age-appropriate cognition and subtle dopamine-independent motor deficits in aged Tau knock-out mice. *Neurobiology of Aging*, 34(6):1523–9.

Morsch, R., Simon, W., and Coleman, P. D. (1999). Neurons May Live for Decades with Neurofibrillary Tangles. *Journal of Neuropathology and Experimental Neurology*, 58(2):188–97.

Mountcastle, V. (1997). The columnar organization of the neocortex. *Brain*, 120(4):701–22.

Mudher, A., Colin, M., Dujardin, S., Medina, M., Dewachter, I., Naini, S. M. A., Mandelkow, E.-M., Mandelkow, E., Buée, L., Goedert, M., and Brion, J.-P. (2017). What is the evidence that tau pathology spreads through prion-like propagation? *Acta Neuropathologica Communications*, 5(1):99.

Muguruma, K. (2018). Self-Organized Cerebellar Tissue from Human Pluripotent Stem Cells and Disease Modeling with Patient-Derived iPSCs. *The Cerebellum*, 17(1):37–41.

Mukrasch, M. D., Bibow, S., Korukottu, J., Jeganathan, S., Biernat, J., Griesinger, C., Mandelkow, E., and Zweckstetter, M. (2009). Structural polymorphism of 441-residue tau at single residue resolution. *PLoS biology*, 7(2):e34.

Muñoz-Sanjuán, I. and Brivanlou, A. H. (2002). Neural induction, the default model and embryonic stem cells. *Nature reviews. Neuroscience*, 3(4):271–80.

Muratore, C. R., Srikanth, P., Callahan, D. G., and Young-Pearse, T. L. (2014). Comparison and Optimization of hiPSC Forebrain Cortical Differentiation Protocols. *PLoS ONE*, 9(8):e105807.

Nacharaju, P., Lewis, J., Easson, C., Yen, S., Hackett, J., Hutton, M., and Yen, S.-h. (1999). Accelerated filament formation from tau protein with specific FTDP-17 missense mutations. *FEBS Letters*, 447:195–9.

Nassif, N., Penney, J., Pal, S., Engels, W. R., and Gloor, G. B. (1994). Efficient copying of nonhomologous sequences from ectopic sites via P-element-induced gap repair. *Molecular and cellular biology*, 14(3):1613–25.

Nasu, M., Takata, N., Danjo, T., Sakaguchi, H., Kadoshima, T., Futaki, S., Sekiguchi, K., Eiraku, M., and Sasai, Y. (2012). Robust Formation and Maintenance of Continuous Stratified Cortical Neuroepithelium by Laminin-Containing Matrix in Mouse ES Cell Culture. *PLoS ONE*, 7(12):e53024.

Neary, D., Snowden, J. S., Gustafson, L., Passant, U., Stuss, D., Black, S., Freedman, M., Kertesz, A., Robert, P. H., Albert, M., Boone, K., Miller, B. L., Cummings, J., and Benson, D. F. (1998). Frontotemporal lobar degeneration: A consensus on clinical diagnostic criteria. *Neurology*, 51(6):1546–54.

Neve, R. L., Harris, P., Kosik, K. S., Kurnit, D. M., and Donlon, T. A. (1986). Identification of cDNA clones for the human microtubule-associated protein tau and chromosomal localization of the genes for tau and microtubule-associated protein 2. *Molecular Brain Research*, 1(3):271–80.

Nicholl, D. J., Greenstone, M. A., Clarke, C. E., Rizzu, P., Crooks, D., Crowe, A., Trojanowski, J. Q., Lee, V. M. Y., and Heutink, P. (2003). An English Kindred with a Novel Recessive Tauopathy and Respiratory Failure. *Annals of Neurology*, 54(5):682–6.

Nieto, M., Monuki, E. S., Tang, H., Imitola, J., Haubst, N., Khoury, S. J., Cunningham, J., Gotz, M., and Walsh, C. A. (2004). Expression of Cux-1 and Cux-2 in the subventricular zone and upper layers II-IV of the cerebral cortex. *The Journal of Comparative Neurology*, 479(2):168–80.

Nieweg, K., Andreyeva, A., van Stegen, B., Tanriöver, G., and Gottmann, K. (2015). Alzheimer's disease-related amyloid-β induces synaptotoxicity in human iPS cell-derived neurons. *Cell death & disease*, 6:e1709.

Nimsanor, N., Kitiyanant, N., Poulsen, U., Rasmussen, M. A., Clausen, C., Mau-Holzmann, U. A., Nielsen, J. E., Nielsen, T. T., Hyttel, P., Holst, B., and Schmid, B. (2016a). Generation of an isogenic, gene-corrected iPSC line from a symptomatic 57-year-old female patient with frontotemporal dementia caused by a P301L mutation in the microtubule associated protein tau (MAPT) gene. *Stem cell research*, 17(3):556–9.

Nimsanor, N., Poulsen, U., Rasmussen, M. A., Clausen, C., Mau-Holzmann, U. A., Nielsen, J. E., Nielsen, T. T., Hyttel, P., Holst, B., and Schmid, B. (2016b). Generation of an isogenic, gene-corrected ipsc line from a pre-symptomatic 28-year-old woman with an r406w mutation in the microtubule associated protein tau (mapt) gene. *Stem Cell Research*, 17(3):600 – 602.

Nimsanor, N., Poulsen, U., Rasmussen, M. A., Clausen, C., Mau-Holzmann, U. A., Nielsen, J. E., Nielsen, T. T., Hyttel, P., Holst, B., and Schmid, B. (2016c). Generation of an isogenic, gene-corrected ipsc line from a symptomatic 59-year-old female patient with frontotemporal dementia caused by an r406w mutation in the microtubule associated protein tau (mapt) gene. *Stem Cell Research*, 17(3):576 – 579.

Niwa, H., Miyazaki, J. I., and Smith, A. G. (2000). Quantitative expression of Oct-3/4 defines differentiation, dedifferentiation or self-renewal of ES cells. *Nature Genetics*, 24(4):372–6.

Odawara, A., Katoh, H., Matsuda, N., and Suzuki, I. (2016). Physiological maturation and drug responses of human induced pluripotent stem cell-derived cortical neuronal networks in long-term culture. *Scientific Reports*, 6(April):26181.

Ogaki, K., Li, Y., Takanashi, M., Ishikawa, K. I., Kobayashi, T., Nonaka, T., Hasegawa, M., Kishi, M., Yoshino, H., Funayama, M., Tsukamoto, T., Shioya, K., Yokochi, M., Imai, H., Sasaki, R., Kokubo, Y., Kuzuhara, S., Motoi, Y., Tomiyama, H., and Hattori, N. (2013).

Analyses of the MAPT, PGRN, and C9orf72 mutations in Japanese patients with FTLD, PSP, and CBS. *Parkinsonism and Related Disorders*, 19(1):15–20.

O'Geen, H., Yu, A. S., and Segal, D. J. (2015). How specific is CRISPR/Cas9 really? *Current opinion in chemical biology*, 29:72–8.

Orii, K. E., Lee, Y., Kondo, N., and McKinnon, P. J. (2006). Selective utilization of nonhomologous end-joining and homologous recombination DNA repair pathways during nervous system development. *Proceedings of the National Academy of Sciences of the United States of America*, 103(26):10017–22.

Ortinau, S., Schmich, J., Block, S., Liedmann, A., Jonas, L., Weiss, D. G., Helm, C. A., Rolfs, A., and Frech, M. J. (2010). Effect of 3D-scaffold formation on differentiation and survival in human neural progenitor cells. *BioMedical Engineering OnLine*, 9(1):70.

Ossola, B., Zhao, C., Compston, A., Pluchino, S., Franklin, R. J. M., and Spillantini, M. G. (2016). Neuronal expression of pathological tau accelerates oligodendrocyte progenitor cell differentiation. *Glia*, 64(3):457–71.

Paşca, A. M., Sloan, S. A., Clarke, L. E., Tian, Y., Makinson, C. D., Huber, N., Kim, C. H., Park, J.-Y., O'Rourke, N. A., Nguyen, K. D., Smith, S. J., Huguenard, J. R., Geschwind, D. H., Barres, B. A., and Paşca, S. P. (2015). Functional cortical neurons and astrocytes from human pluripotent stem cells in 3D culture. *Nature Methods*, 12(7):671–8.

Pancrazi, L., Di Benedetto, G., Colombaioni, L., Della Sala, G., Testa, G., Olimpico, F., Reyes, A., Zeviani, M., Pozzan, T., and Costa, M. (2015). Foxg1 localizes to mitochondria and coordinates cell differentiation and bioenergetics. *Proceedings of the National Academy of Sciences of the United States of America*, 112(45):13910–5.

Panda, D., Samuel, J. C., Massie, M., Feinstein, S. C., and Wilson, L. (2003). Differential regulation of microtubule dynamics by three- and four-repeat tau: implications for the onset of neurodegenerative disease. *Proceedings of the National Academy of Sciences of the United States of America*, 100(16):9548–53.

Pandis, D. and Scarmeas, N. (2012). Seizures in Alzheimer Disease: Clinical and Epidemiological Data. *Epilepsy Currents*, 12(5):184–7.

Papasozomenos, S. C. and Binder, L. I. (1987). Phosphorylation determines two distinct species of Tau in the central nervous system. *Cell motility and the cytoskeleton*, 8(3):210–26.

Paquet, D., Kwart, D., Chen, A., Sproul, A., Jacob, S., Teo, S., Olsen, K. M., Gregg, A., Noggle, S., and Tessier-Lavigne, M. (2016). Efficient introduction of specific homozygous and heterozygous mutations using CRISPR/Cas9. *Nature*, 533(7601):1–18.

Park, J., Wetzel, I., Marriott, I., Dréau, D., D'Avanzo, C., Kim, D. Y., Tanzi, R. E., and Cho, H. (2018). A 3D human triculture system modeling neurodegeneration and neuroinflammation in Alzheimer's disease. *Nature Neuroscience*, 21(7):941–51.

Passarella, D. and Goedert, M. (2018). Beta-sheet assembly of Tau and neurodegeneration in Drosophila melanogaster. *Neurobiology of Aging*, 72:98–105.

Pastor, P., Ezquerra, M., Muñoz, E., Martí, M. J., Blesa, R., Tolosa, E., and Oliva, R. (2000). Significant association between the tau gene A0/A0 genotype and Parkinson's disease. *Annals of Neurology*, 47(2):242–5.

Patani, R., Lewis, P. A., Trabzuni, D., Puddifoot, C. A., Wyllie, D. J., Walker, R., Smith, C., Hardingham, G. E., Weale, M., Hardy, J., Chandran, S., and Ryten, M. (2012). Investigating the utility of human embryonic stem cell-derived neurons to model ageing and neurodegenerative disease using whole-genome gene expression and splicing analysis. *Journal of Neurochemistry*, 122(4):738–51.

Peeraer, E., Bottelbergs, A., Van Kolen, K., Stancu, I. C., Vasconcelos, B., Mahieu, M., Duytschaever, H., Ver Donck, L., Torremans, A., Sluydts, E., Van Acker, N., Kemp, J. A., Mercken, M., Brunden, K. R., Trojanowski, J. Q., Dewachter, I., Lee, V. M., and Moechars, D. (2015). Intracerebral injection of preformed synthetic tau fibrils initiates widespread tauopathy and neuronal loss in the brains of tau transgenic mice. *Neurobiology of Disease*, 73:83–95.

Pérez, M., Valpuesta, J. M., Medina, M., Montejo de Garcini, E., and Avila, J. (1996). Polymerization of tau into filaments in the presence of heparin: the minimal sequence required for tau-tau interaction. *Journal of neurochemistry*, 67(3):1183–90.

Petersen, R., Lambourne, J. J., Javierre, B. M., Grassi, L., Kreuzhuber, R., Ruklisa, D., Rosa, I. M., Tomé, A. R., Elding, H., van Geffen, J. P., Jiang, T., Farrow, S., Cairns, J., Al-Subaie, A. M., Ashford, S., Attwood, A., Batista, J., Bouman, H., Burden, F., Choudry, F. A., Clarke, L., Flicek, P., Garner, S. F., Haimel, M., Kempster, C., Ladopoulos, V., Lenaerts, A.-S., Materek, P. M., McKinney, H., Meacham, S., Mead, D., Nagy, M., Penkett, C. J., Rendon, A., Seyres, D., Sun, B., Tuna, S., van der Weide, M.-E., Wingett, S. W., Martens, J. H., Stegle, O., Richardson, S., Vallier, L., Roberts, D. J., Freson, K., Wernisch, L., Stunnenberg, H. G., Danesh, J., Fraser, P., Soranzo, N., Butterworth, A. S., Heemskerk, J. W., Turro, E., Spivakov, M., Ouwehand, W. H., Astle, W. J., Downes, K., Kostadima, M., and Frontini, M. (2017). Platelet function is modified by common sequence variation in megakaryocyte super enhancers. *Nature communications*, 8:16058.

Petros, T. J., Tyson, J. A., and Anderson, S. A. (2011). Pluripotent Stem Cells for the Study of CNS Development. *Frontiers in Molecular Neuroscience*, 4(October):1–12.

Phatnani, H. and Maniatis, T. (2015). Astrocytes in Neurodegenerative Disease: Table 1. *Cold Spring Harbor Perspectives in Biology*, 7(6):a020628.

Pickering-Brown, S. M., Baker, M., Nonaka, T., Ikeda, K., Sharma, S., Mackenzie, J., Simpson, S. A., Moore, J. W., Snowden, J. S., De Silva, R., Revesz, T., Hasegawa, M., Hutton, M., and Mann, D. M. (2004). Frontotemporal dementia with Pick-type histology associated with Q336R mutation in the tau gene. *Brain*, 127(6):1415–26.

Pierfelice, T., Alberi, L., and Gaiano, N. (2011). Notch in the Vertebrate Nervous System: An Old Dog with New Tricks. *Neuron*, 69(5):840–55.

Polanco, J. C., Scicluna, B. J., Hill, A. F., and Götz, J. (2016). Extracellular Vesicles Isolated from the Brains of rTg4510 Mice Seed Tau Protein Aggregation in a Threshold-dependent Manner. *The Journal of biological chemistry*, 291(24):12445–66.

Poorkaj, P., Bird, T. D., Wijsman, E., Nemens, E., Garruto, R. M., Anderson, L., Andreadis, A., Wiederholt, W. C., Raskind, M., and Schellenberg, G. D. (1998). Tau is a candidate gene for chromosome 17 frontotemporal dementia. *Annals of neurology*, 43(6):815–25.

Poorkaj, P., Kas, A., D'Souza, I., Zhou, Y., Pham, Q., Stone, M., Olson, M. V., and Schellenberg, G. D. (2001). A genomic sequence analysis of the mouse and human microtubule-associated protein tau. *Mammalian Genome*, 12(9):700–12.

Preuss, U. and Mandelkow, E. M. (1998). Mitotic phosphorylation of tau protein in neuronal cell lines resembles phosphorylation in Alzheimer's disease. *European Journal of Cell Biology*, 76(3):176–84.

Qian, W., Liang, H., Shi, J., Jin, N., Grundke-Iqbal, I., Iqbal, K., Gong, C.-X., and Liu, F. (2011). Regulation of the alternative splicing of tau exon 10 by SC35 and Dyrk1A. *Nucleic Acids Research*, 39(14):6161–71.

Qian, W. and Liu, F. (2014). Regulation of alternative splicing of tau exon 10. *Neuroscience bulletin*, 30(2):367–77.

Qian, X., Nguyen, H. N., Song, M. M., Hadiono, C., Ogden, S. C., Hammack, C., Yao, B., Hamersky, G. R., Jacob, F., Zhong, C., Yoon, K.-j., Jeang, W., Lin, L., Li, Y., Thakor, J., Berg, D. A., Zhang, C., Kang, E., Chickering, M., Nauen, D., Ho, C.-Y., Wen, Z., Christian, K. M., Shi, P.-Y., Maher, B. J., Wu, H., Jin, P., Tang, H., Song, H., and Ming, G.-l. (2016). Brain-Region-Specific Organoids Using Mini-bioreactors for Modeling ZIKV Exposure. *Cell*, 165(5):1238–54.

Radecke, S., Radecke, F., Peter, I., and Schwarz, K. (2006). Physical incorporation of a single-stranded oligodeoxynucleotide during targeted repair of a human chromosomal locus. *Journal of Gene Medicine*, 8(2):217–28.

Raja, W. K., Mungenast, A. E., Lin, Y.-T., Ko, T., Abdurrob, F., Seo, J., and Tsai, L.-H. (2016). Self-Organizing 3D Human Neural Tissue Derived from Induced Pluripotent Stem Cells Recapitulate Alzheimer's Disease Phenotypes. *PLOS ONE*, 11(9):e0161969.

Rakic, P. (2003). Developmental and Evolutionary Adaptations of Cortical Radial Glia. *Cerebral Cortex*, 13(6):541–9.

Ran, F. A., Hsu, P. D., Lin, C.-Y., Gootenberg, J. S., Konermann, S., Trevino, A. E., Scott, D. A., Inoue, A., Matoba, S., Zhang, Y., and Zhang, F. (2013a). Double nicking by RNA-guided CRISPR Cas9 for enhanced genome editing specificity. *Cell*, 154(6):1380–9.

Ran, F. A., Hsu, P. D., Wright, J., Agarwala, V., Scott, D. a., and Zhang, F. (2013b). Genome engineering using the CRISPR-Cas9 system. *Nature protocols*, 8(11):2281–308.

Ranjan, V. D., Qiu, L., Tan, E. K., Zeng, L., and Zhang, Y. (2018). Modeling Alzheimer's Disease: Insights from In vivo to In vitro 3D Culture Platforms. *Journal of tissue engineering and regenerative medicine*.

Ranjha, L., Howard, S. M., and Cejka, P. (2018). Main steps in DNA double-strand break repair: an introduction to homologous recombination and related processes. *Chromosoma*, pages 1–28.

Raponi, E., Agenes, F., Delphin, C., Assard, N., Baudier, J., Legraverend, C., and Deloulme, J. C. (2007). S100B expression defines a state in which GFAP-expressing cells lose their neural stem cell potential and acquire a more mature developmental stage. *GLIA*, 55(2):165–77.

Rapoport, M., Dawson, H. N., Binder, L. I., Vitek, M. P., and Ferreira, A. (2002). Tau is essential to -amyloid-induced neurotoxicity. *Proceedings of the National Academy of Sciences*, 99(9):6364–9.

Rasband, M. N. (2010). The axon initial segment and the maintenance of neuronal polarity. *Nature Reviews Neuroscience*, 11(8):552–62.

Reed, L. (2001). Phenotypic correlations in FTDP-17. *Neurobiology of Aging*, 22(1):89–107.

Regad, T., Roth, M., Bredenkamp, N., Illing, N., and Papalopulu, N. (2007). The neural progenitor-specifying activity of FoxG1 is antagonistically regulated by CKI and FGF. *Nature Cell Biology*, 9(5):531–40.

Reilly, P., Winston, C. N., Baron, K., Trejo, M., Rockenstein, E. M., Akers, J. C., Kfoury, N., Diamond, M., Masliah, E., Rissman, R. A., and Yuan, S. H. (2017). Novel human neuronal tau model exhibiting neurofibrillary tangles and transcellular propagation. *Neurobiology of Disease*.

Reinhardt, P., Glatza, M., Hemmer, K., Tsytsyura, Y., Thiel, C. S., Höing, S., Moritz, S., Parga, J. A., Wagner, L., Bruder, J. M., Wu, G., Schmid, B., Röpke, A., Klingauf, J., Schwamborn, J. C., Gasser, T., Schöler, H. R., and Sterneckert, J. (2013). Derivation and Expansion Using Only Small Molecules of Human Neural Progenitors for Neurodegenerative Disease Modeling. *PLoS ONE*, 8(3).

Renner, M., Lancaster, M. A., Bian, S., Choi, H., Ku, T., Peer, A., Chung, K., and Knoblich, J. A. (2017). Self-organized developmental patterning and differentiation in cerebral organoids. *The EMBO Journal*, 36(10):1316–29.

Renton, A. E., Majounie, E., Waite, A., Simón-Sánchez, J., Rollinson, S., Gibbs, J. R., Schymick, J. C., Laaksovirta, H., van Swieten, J. C., Myllykangas, L., Kalimo, H., Paetau, A., Abramzon, Y., Remes, A. M., Kaganovich, A., Scholz, S. W., Duckworth, J., Ding, J., Harmer, D. W., Hernandez, D. G., Johnson, J. O., Mok, K., Ryten, M., Trabzuni, D., Guerreiro, R. J., Orrell, R. W., Neal, J., Murray, A., Pearson, J., Jansen, I. E., Sondervan, D., Seelaar, H., Blake, D., Young, K., Halliwell, N., Callister, J. B., Toulson, G., Richardson, A., Gerhard, A., Snowden, J., Mann, D., Neary, D., Nalls, M. A., Peuralinna, T., Jansson, L., Isoviita, V.-M., Kaivorinne, A.-L., Hölttä-Vuori, M., Ikonen, E., Sulkava, R., Benatar, M., Wuu, J., Chiò, A., Restagno, G., Borghero, G., Sabatelli, M., Heckerman, D., Rogaeva, E., Zinman, L., Rothstein, J. D., Sendtner, M., Drepper, C., Eichler, E. E., Alkan, C., Abdullaev, Z., Pack, S. D., Dutra, A., Pak, E., Hardy, J., Singleton, A., Williams, N. M., Heutink, P., Pickering-Brown, S., Morris, H. R., Tienari, P. J., and Traynor, B. J. (2011). A Hexanucleotide Repeat Expansion in C9ORF72 Is the Cause of Chromosome 9p21-Linked ALS-FTD. *Neuron*, 72(2):257–68.

Richardson, C. D., Ray, G. J., DeWitt, M. A., Curie, G. L., and Corn, J. E. (2016). Enhancing homology-directed genome editing by catalytically active and inactive CRISPR-Cas9 using asymmetric donor DNA. *Nature Biotechnology*, 34(3):339–44.

Rizzini, C., Goedert, M., Hodges, J. R., Smith, M. J., Jakes, R., Hills, R., Xuereb, J. H., Crowther, R. A., and Spillantini, M. G. (2000). Tau gene mutation K257T causes a tauopathy similar to Pick's disease. *Journal of neuropathology and experimental neurology*, 59(11):990–1001.

Rizzu, P., Joosse, M., Ravid, R., Hoogeveen, a., Kamphorst, W., van Swieten, J. C., Willemsen, R., and Heutink, P. (2000). Mutation-dependent aggregation of tau protein and its selective depletion from the soluble fraction in brain of P301L FTDP-17 patients. *Human molecular genetics*, 9(20):3075–82.

Roberson, E. D., Scearce-Levie, K., Palop, J. J., Yan, F., Cheng, I. H., Wu, T., Gerstein, H., Yu, G.-Q., and Mucke, L. (2007). Reducing Endogenous Tau Ameliorates Amyloid b–Induced Deficits in an Alzheimer's Disease Mouse Model. *Biochemistry*, 316(May):750–4.

Rohrer, J. D., Guerreiro, R., Vandrovcova, J., Uphill, J., Reiman, D., Beck, J., Isaacs, A. M., Authier, A., Ferrari, R., Fox, N. C., MacKenzie, I. R., Warren, J. D., De Silva, R., Holton, J., Revesz, T., Hardy, J., Mead, S., and Rossor, M. N. (2009). The heritability and genetics of frontotemporal lobar degeneration. *Neurology*, 73(18):1451–6.

Rösner, H., Rebhan, M., Vacun, G., and Vanmechelen, E. (1995). Developmental expression of tau proteins in the chicken and rat brain: Rapid down-regulation of a paired helical filament epitope in the rat cerebral cortex coincides with the transition from immature to adult tau isoforms. *International Journal of Developmental Neuroscience*, 13(6):607–17.

Rossi, G., Dalprà, L., Crosti, F., Lissoni, S., Sciacca, F. L., Catania, M., Mangieri, M., Giaccone, G., Croci, D., and Tagliavini, F. (2008). A new function of microtubule-associated protein tau: Involvement in chromosome stability. *Cell Cycle*, 7(12):1788–94.

Rossi, G. and Tagliavini, F. (2015). Frontotemporal lobar degeneration: Old knowledge and new insight into the pathogenetic mechanisms of tau mutations. *Frontiers in Aging Neuroscience*, 7(OCT):1–15.

Rouhani, F., Kumasaka, N., de Brito, M. C., Bradley, A., Vallier, L., and Gaffney, D. (2014). Genetic background drives transcriptional variation in human induced pluripotent stem cells. *PLoS genetics*, 10(6):e1004432.

Rovelet-Lecrux, A., Lecourtois, M., Thomas-Anterion, C., Le Ber, I., Brice, A., Frebourg, T., Hannequin, D., and Campion, D. (2009). Partial deletion of the MAPT gene: A novel mechanism of FTDP-17. *Human Mutation*, 30(4):E591–E602.

Sahara, N., Maeda, S., Yoshiike, Y., Mizoroki, T., Yamashita, S., Murayama, M., Park, J.-M., Saito, Y., Murayama, S., and Takashima, A. (2007). Molecular chaperone-mediated tau protein metabolism counteracts the formation of granular tau oligomers in human brain. *Journal of Neuroscience Research*, 85(14):3098–108.

Sakaguchi, H., Kadoshima, T., Soen, M., Narii, N., Ishida, Y., Ohgushi, M., Takahashi, J., Eiraku, M., and Sasai, Y. (2015). Generation of functional hippocampal neurons from self-organizing human embryonic stem cell-derived dorsomedial telencephalic tissue. *Nature Communications*, 6(1):8896.

Sakurai, A., Okamoto, K., Fujita, Y., Nakazato, Y., Wakabayashi, K., Takahashi, H., and Gonatas, N. K. (2000). Fragmentation of the Golgi apparatus of the ballooned neurons in patients with corticobasal degeneration and Creutzfeldt-Jakob disease. *Acta neuropathologica*, 100(3):270–4.

Saleh-Gohari, N. (2004). Conservative homologous recombination preferentially repairs DNA double-strand breaks in the S phase of the cell cycle in human cells. *Nucleic Acids Research*, 32(12):3683–8.

Sander, J. D. and Joung, J. K. (2014). CRISPR-Cas systems for editing, regulating and targeting genomes. *Nature biotechnology*, 32(4):347–55.

Santacruz, K., Lewis, J., Spires, T., Paulson, J., Kotilinek, L., Ingelsson, M., Guimaraes, A., DeTure, M., Ramsden, M., McGowan, E., Forster, C., Yue, M., Orne, J., Janus, C., Mariash, A., Kuskowski, M., Hyman, B., Hutton, M., and Ashe, K. H. (2005). Tau suppression in a neurodegenerative mouse model improves memory function. *Science (New York, N.Y.)*, 309(5733):476–81.

Santiváñez Pérez, J. A. (2017). Phd thesis: Effect of parkinson's disease-related alpha synuclein abnormalities on the maturation of distinct ipsc-derived neuronal populations. *University of Cambridge*.

Schafer, D. P., Jha, S., Liu, F., Akella, T., McCullough, L. D., and Rasband, M. N. (2009). Disruption of the axon initial segment cytoskeleton is a new mechanism for neuronal injury. *The Journal of neuroscience : the official journal of the Society for Neuroscience*, 29(42):13242–54.

Schafer, D. P., Lehrman, E. K., Kautzman, A. G., Koyama, R., Mardinly, A. R., Yamasaki, R., Ransohoff, R. M., Greenberg, M. E., Barres, B. A., and Stevens, B. (2012). Microglia Sculpt Postnatal Neural Circuits in an Activity and Complement-Dependent Manner. *Neuron*, 74(4):691–705.

Schneider, A., Biernat, J., Von Bergen, M., Mandelkow, E., and Mandelkow, E. M. (1999). Phosphorylation that detaches tau protein from microtubules (Ser262, Ser214) also protects it against aggregation into Alzheimer paired helical filaments. *Biochemistry*, 38(12):3549–58.

Schoch, K. M., DeVos, S. L., Miller, R. L., Chun, S. J., Norrbom, M., Wozniak, D. F., Dawson, H. N., Bennett, C. F., Rigo, F., and Miller, T. M. (2016). Increased 4R-Tau Induces Pathological Changes in a Human-Tau Mouse Model. *Neuron*, 90(5):941–7.

Scholzen, T. and Gerdes, J. (2000). The Ki-67 protein: From the known and the unknown. *Journal of Cellular Physiology*, 182(3):311–22.

Schukking, M., Miranda, H. C., Trujillo, C. A., Negraes, P. D., and Muotri, A. R. (2018). Direct Generation of Human Cortical Organoids from Primary Cells. *Stem Cells and Development*, (858):scd.2018.0112.

Schwartzentruber, J., Foskolou, S., Kilpinen, H., Rodrigues, J., Alasoo, K., Knights, A. J., Patel, M., Goncalves, A., Ferreira, R., Benn, C. L., Wilbrey, A., Bictash, M., Impey, E., Cao, L., Lainez, S., Loucif, A. J., Whiting, P. J., Gutteridge, A., and Gaffney, D. J. (2018). Molecular and functional variation in iPSC-derived sensory neurons. *Nature Genetics*.

Seelaar, H., Kamphorst, W., Rosso, S. M., Azmani, A., Masdjedi, R., De Koning, I., Maat-Kievit, J. A., Anar, B., Kaat, L. D., Breedveld, G. J., Dooijes, D., Rozemuller, J. M., Bronner, I. F., Rizzu, P., and Van Swieten, J. C. (2008). Distinct genetic forms of frontotemporal dementia. *Neurology*, 71(16):1220–6.

Seidel, D., Krinke, D., Jahnke, H.-G., Hirche, A., Kloß, D., Mack, T. G. A., Striggow, F., and Robitzki, A. (2012). Induced Tauopathy in a Novel 3D-Culture Model Mediates Neurodegenerative Processes: A Real-Time Study on Biochips. *PLoS ONE*, 7(11):e49150.

Sengupta, A., Novak, M., Grundke-Iqbal, I., and Iqbal, K. (2006). Regulation of phosphorylation of tau by cyclin-dependent kinase 5 and glycogen synthase kinase-3 at substrate level. *FEBS letters*, 580(25):5925–33.

Seo, J., Kritskiy, O., Watson, L. A., Barker, S. J., Dey, D., Raja, W. K., Lin, Y.-T., Ko, T., Cho, S., Penney, J., Silva, M. C., Sheridan, S. D., Lucente, D., Gusella, J. F., Dickerson, B. C., Haggarty, S. J., and Tsai, L.-H. (2017). Inhibition of p25/Cdk5 Attenuates Tauopathy in Mouse and iPSC Models of Frontotemporal Dementia. *The Journal of Neuroscience*, 37(41):9917–24.

Seubert, P., Mawal-Dewan, M., Barbour, R., Jakes, R., Goedert, M., Johnson, G. V. W., Litersky, J. M., Schenk, D., Lieberburg, I., Trojanowski, J. Q., and Lee, V. M. (1995). Detection of Phosphorylated Ser 262 in Fetal Tau, Adult Tau, and Paired Helical Filament Tau. *Journal of Biological Chemistry*, 270(32):18917–22.

Shahani, N., Subramaniam, S., Wolf, T., Tackenberg, C., and Brandt, R. (2006). Tau aggregation and progressive neuronal degeneration in the absence of changes in spine density and morphology after targeted expression of Alzheimer's disease-relevant tau constructs in organotypic hippocampal slices. *The Journal of neuroscience : the official journal of the Society for Neuroscience*, 26(22):6103–14.

Shaw-Smith, C., Pittman, A. M., Willatt, L., Martin, H., Rickman, L., Gribble, S., Curley, R., Cumming, S., Dunn, C., Kalaitzopoulos, D., Porter, K., Prigmore, E., Krepischi-Santos, A. C., Varela, M. C., Koiffmann, C. P., Lees, A. J., Rosenberg, C., Firth, H. V., De Silva, R., and Carter, N. P. (2006). Microdeletion encompassing MAPT at chromosome 17q21.3 is associated with developmental delay and learning disability. *Nature Genetics*, 38(9):1032–7.

Sheng, C., Zheng, Q., Wu, J., Xu, Z., Sang, L., Wang, L., Guo, C., Zhu, W., Tong, M., Liu, L., Li, W., Liu, Z.-H., Zhao, X.-Y., Wang, L., Chen, Z., and Zhou, Q. (2012). Generation of dopaminergic neurons directly from mouse fibroblasts and fibroblast-derived neural progenitors. *Cell Research*, 22(4):769–72.

Shi, Y., Kirwan, P., and Livesey, F. J. (2012a). Directed differentiation of human pluripotent stem cells to cerebral cortex neurons and neural networks. *Nature protocols*, 7(10):1836–46.

Shi, Y., Kirwan, P., Smith, J., Maclean, G., Orkin, S. H., and Livesey, F. J. (2012b). A Human Stem Cell Model of Early Alzheimer's Disease Pathology in Down Syndrome. *Sci Transl Med*, 4(124):124–9.

Shi, Y., Kirwan, P., Smith, J., Robinson, H. P. C., and Livesey, F. J. (2012c). Human cerebral cortex development from pluripotent stem cells to functional excitatory synapses. *Nature neuroscience*, 15(3):477–86.

Shipton, O. A., Leitz, J. R., Dworzak, J., Acton, C. E. J., Tunbridge, E. M., Denk, F., Dawson, H. N., Vitek, M. P., Wade-Martins, R., Paulsen, O., and Vargas-Caballero, M. (2011). Tau Protein Is Required for Amyloid -Induced Impairment of Hippocampal Long-Term Potentiation. *Journal of Neuroscience*, 31(5):1688–92.

Sieben, A., Van Langenhove, T., Engelborghs, S., Martin, J.-J., Boon, P., Cras, P., De Deyn, P.-P., Santens, P., Van Broeckhoven, C., and Cruts, M. (2012). The genetics and neuropathology of frontotemporal lobar degeneration. *Acta Neuropathologica*, 124(3):353–72.

Sillen, A., Barbier, P., Landrieu, I., Lefebvre, S., Wieruszeski, J. M., Leroy, A., Peyrot, V., and Lippens, G. (2007). NMR investigation of the interaction between the neuronal protein Tau and the microtubules. *Biochemistry*, 46(11):3055–64.

Silva, M. C., Cheng, C., Mair, W., Almeida, S., Fong, H., Biswas, M. H. U., Zhang, Z., Huang, Y., Temple, S., Coppola, G., Geschwind, D. H., Karydas, A., Miller, B. L., Kosik, K. S., Gao, F.-B., Steen, J. A., and Haggarty, S. J. (2016). Human iPSC-Derived Neuronal Model of Tau-A152T Frontotemporal Dementia Reveals Tau-Mediated Mechanisms of Neuronal Vulnerability. *Stem cell reports*, 7(3):325–40.

Skibinski, G., Parkinson, N. J., Brown, J. M., Chakrabarti, L., Lloyd, S. L., Hummerich, H., Nielsen, J. E., Hodges, J. R., Spillantini, M. G., Thusgaard, T., Brandner, S., Brun, A., Rossor, M. N., Gade, A., Johannsen, P., Sørensen, S. A., Gydesen, S., Fisher, E. M., and Collinge, J. (2005). Mutations in the endosomal ESCRTIII-complex subunit CHMP2B in frontotemporal dementia. *Nature Genetics*, 37(8):806–8.

Sloan, S. A., Darmanis, S., Huber, N., Khan, T. A., Birey, F., Caneda, C., Reimer, R., Quake, S. R., Barres, B. A., and Paşca, S. P. (2017). Human Astrocyte Maturation Captured in 3D Cerebral Cortical Spheroids Derived from Pluripotent Stem Cells. *Neuron*, 95(4):779–90.e6.

Slowinski, J., Dominik, J., Uitti, R. J., Ahmed, Z., Dickson, D. D., and Wszolek, Z. K. (2007). Frontotemporal dementia and parkinsonism linked to chromosome 17 with the N279K tau mutation. *Neuropathology*, 27(1):73–80.

Smith, C., Gore, A., Yan, W., Abalde-Atristain, L., Li, Z., He, C., Wang, Y., Brodsky, R. A., Zhang, K., Cheng, L., and Ye, Z. (2014). Whole-Genome Sequencing Analysis Reveals High Specificity of CRISPR/Cas9 and TALEN-Based Genome Editing in Human iPSCs. *Cell Stem Cell*, 15(1):12–13.

Son, E. Y., Ichida, J. K., Wainger, B. J., Toma, J. S., Rafuse, V. F., Woolf, C. J., and Eggan, K. (2011). Conversion of mouse and human fibroblasts into functional spinal motor neurons. *Cell stem cell*, 9(3):205–18.

Sperfeld, A. D., Collatz, M. B., Baier, H., Palmbach, M., Storch, A., Schwarz, J., Tatsch, K., Reske, S., Joosse, M., Heutink, P., and Ludolph, A. C. (1999). FTDP-17: An early-onset phenotype with parkinsonism and epileptic seizures caused by a novel mutation. *Annals of Neurology*, 46(5):708–15.

Spillantini, M. G., Bird, T. D., and Ghetti, B. (1998a). Frontotemporal dementia and Parkinsonism linked to chromosome 17: a new group of tauopathies. *Brain pathology (Zurich, Switzerland)*, 8(2):387–402.

Spillantini, M. G., Crowther, R. A., and Goedert, M. (1996a). Comparison of the neurofibrillary pathology in Alzheimer's disease and familial presenile dementia with tangles. *Acta Neuropathologica*, 92(1):42–8.

Spillantini, M. G., Crowther, R. A., and Goedert, M. (1996b). Comparison of the neurofibrillary pathology in Alzheimer's disease and familial presenile dementia with tangles. *Acta Neuropathologica*, 92(1):42–8.

Spillantini, M. G., Crowther, R. A., Kamphorst, W., Heutink, P., and van Swieten, J. C. (1998b). Tau pathology in two Dutch families with mutations in the microtubule-binding region of tau. *The American journal of pathology*, 153(5):1359–63.

Spillantini, M. G. and Goedert, M. (2013). Tau pathology and neurodegeneration. *Lancet neurology*, 12(6):609–22.

Spillantini, M. G., Murrell, J. R., Goedert, M., Farlow, M. R., Klug, A., and Ghetti, B. (1998c). Mutation in the tau gene in familial multiple system tauopathy with presenile dementia. *Proceedings of the National Academy of Sciences*, 95(13):7737–41.

Spina, S., Schonhaut, D. R., Boeve, B. F., Seeley, W. W., Ossenkoppele, R., O'Neil, J. P., Lazaris, A., Rosen, H. J., Boxer, A. L., Perry, D. C., Miller, B. L., Dickson, D. W., Parisi, J. E., Jagust, W. J., Murray, M. E., and Rabinovici, G. D. (2017). Frontotemporal dementia with the V337M MAPT mutation. *Neurology*, 88(8):758–66.

Sposito, T., Preza, E., Mahoney, C. J., Setó-Salvia, N., Ryan, N. S., Morris, H. R., Arber, C., Devine, M. J., Houlden, H., Warner, T. T., Bushell, T. J., Zagnoni, M., Kunath, T., Livesey, F. J., Fox, N. C., Rossor, M. N., Hardy, J., and Wray, S. (2015). Developmental regulation of tau splicing is disrupted in stem cell-derived neurons from frontotemporal dementia patients with the 10 + 16 splice-site mutation in MAPT. *Human Molecular Genetics*, 24(18):5260–9.

Stanford, P. M., Shepherd, C. E., Halliday, G. M., Brooks, W. S., Schofield, P. W., Brodaty, H., Martins, R. N., Kwok, J. B. J., and Schofield, P. R. (2003). Mutations in the tau gene that cause an increase in three repeat tau and frontotemporal dementia. *Brain*, 126(4):814–26.

Stefansson, H., Helgason, A., Thorleifsson, G., Steinthorsdottir, V., Masson, G., Barnard, J., Baker, A., Jonasdottir, A., Ingason, A., Gudnadottir, V. G., Desnica, N., Hicks, A., Gylfason, A., Gudbjartsson, D. F., Jonsdottir, G. M., Sainz, J., Agnarsson, K., Birgisdottir, B., Ghosh, S., Olafsdottir, A., Cazier, J. B., Kristjansson, K., Frigge, M. L., Thorgeirsson, T. E., Gulcher, J. R., Kong, A., and Stefansson, K. (2005). A common inversion under selection in Europeans. *Nature Genetics*, 37(2):129–37.

Steiner, B., Mandelkow, E. M., Biernat, J., Gustke, N., Meyer, H. E., Schmidt, B., Mieskes, G., Söling, H. D., Drechsel, D., and Kirschner, M. W. (1990). Phosphorylation of microtubule-associated protein tau: identification of the site for Ca2(+)-calmodulin dependent kinase and relationship with tau phosphorylation in Alzheimer tangles. *The EMBO journal*, 9(11):3539–44.

Steinhilb, M. L., Dias-Santagata, D., Fulga, T. A., Felch, D. L., and Feany, M. B. (2007). Tau phosphorylation sites work in concert to promote neurotoxicity in vivo. *Molecular biology of the cell*, 18(12):5060–8.

Sternberg, S. H. and Doudna, J. A. (2015). Expanding the Biologist's Toolkit with CRISPR-Cas9. *Molecular Cell*, 58(4):568–74.

Stozicka, Z., Zilka, N., Novak, P., Kovacech, B., Bugos, O., and Novak, M. (2010). Genetic background modifies neurodegeneration and neuroinflammation driven by misfolded human tau protein in rat model of tauopathy: implication for immunomodulatory approach to Alzheimer's disease. *Journal of neuroinflammation*, 7(1):64.

Sultan, A., Nesslany, F., Violet, M., Bégard, S., Loyens, A., Talahari, S., Mansuroglu, Z., Marzin, D., Sergeant, N., Humez, S., Colin, M., Bonnefoy, E., Buée, L., and Galas, M. C. (2011). Nuclear Tau, a key player in neuronal DNA protection. *Journal of Biological Chemistry*, 286(6):4566–75.

Sun, C.-k., Zhou, D., Zhang, Z., He, L., Zhang, F., Wang, X., Yuan, J., Chen, Q., Wu, L.-G., and Yang, Q. (2014). Senescence impairs direct conversion of human somatic cells to neurons. *Nature Communications*, 5(1):4112.

Sun, H. and Chasin, L. A. (2000). Multiple Splicing Defects in an Intronic False Exon. *Molecular and Cellular Biology*, 20(17):6414–25.

Synofzik, M., Born, C., Rominger, A., Lummel, N., Schöls, L., Biskup, S., Schüle, C., Grasshoff, U., Klopstock, T., and Adamczyk, C. (2014). Targeted high-throughput sequencing identifies a TARDBP mutation as a cause of early-onset FTD without motor neuron disease. *Neurobiology of Aging*, 35(5).

Tacik, P., Sanchez-Contreras, M., DeTure, M., Murray, M. E., Rademakers, R., Ross, O. A., Wszolek, Z. K., Parisi, J. E., Knopman, D. S., Petersen, R. C., and Dickson, D. W. (2017). Clinicopathologic heterogeneity in frontotemporal dementia and parkinsonism linked to chromosome 17 (FTDP-17) due to microtubule-associated protein tau (MAPT) p.P301L mutation, including a patient with globular glial tauopathy. *Neuropathology and Applied Neurobiology*, 43(3):200–14.

Takahashi, K., Tanabe, K., Ohnuki, M., Narita, M., Ichisaka, T., Tomoda, K., and Yamanaka, S. (2007). Induction of pluripotent stem cells from adult human fibroblasts by defined factors. *Cell*, 131(5):861–72.

Takahashi, K. and Yamanaka, S. (2006). Induction of Pluripotent Stem Cells from Mouse Embryonic and Adult Fibroblast Cultures by Defined Factors. *Cell*, 126(4):663–76.

Takamori, S., Holt, M., Stenius, K., Lemke, E. A., Grønborg, M., Riedel, D., Urlaub, H., Schenck, S., Brügger, B., Ringler, P., Müller, S. A., Rammner, B., Gräter, F., Hub, J. S., De Groot, B. L., Mieskes, G., Moriyama, Y., Klingauf, J., Grubmüller, H., Heuser, J., Wieland, F., and Jahn, R. (2006). Molecular Anatomy of a Trafficking Organelle. *Cell*, 127(4):831–46.

Takano, T., Rutka, J. T., and Becker, L. E. (1996). Overexpression of nestin and vimentin in ependymal cells in hydrocephalus. *Acta Neuropathologica*, 92(1):90–7.

Takuma, H., Arawaka, S., and Mori, H. (2003). Isoforms changes of tau protein during development in various species. *Developmental Brain Research*, 142(2):121–7.

Tan, D. C. S., Yao, S., Ittner, A., Bertz, J., Ke, Y. D., Ittner, L. M., and Delerue, F. (2018). Generation of a New Tau Knockout (tauΔex1) Line Using CRISPR/Cas9 Genome Editing in Mice. *Journal of Alzheimer's disease : JAD*, 62(2):571–8.

Tao, W. and Lai, E. (1992). Telencephalon-restricted expression of BF-1, a new member of the HNF-3/fork head gene family, in the developing rat brain. *Neuron*, 8(5):957–66.

Tashiro, K., Hasegawa, M., Ihara, Y., and Iwatsubo, T. (1997). Somatodendritic localization of phosphorylated tau in neonatal and adult rat cerebral cortex. *Neuroreport*, 8(12):2797–2801.

Terry, R. D., Masliah, E., Salmon, D. P., Butters, N., DeTeresa, R., Hill, R., Hansen, L. A., and Katzman, R. (1991). Physical basis of cognitive alterations in alzheimer's disease: Synapse loss is the major correlate of cognitive impairment. *Annals of Neurology*, 30(4):572–80.

Terzić, J. and Saraga-Babić, M. (1999). Expression pattern of PAX3 and PAX6 genes during human embryogenesis. *International Journal of Developmental Biology*, 43(6):501–8.

The International Stem Cell Initiative, X. (2007). Characterization of human embryonic stem cell lines by the International Stem Cell Initiative. *Nature Biotechnology*, 25:803–16.

Thoma, E. C., Wischmeyer, E., Offen, N., Maurus, K., Sirén, A.-L., Schartl, M., and Wagner, T. U. (2012). Ectopic Expression of Neurogenin 2 Alone is Sufficient to Induce Differentiation of Embryonic Stem Cells into Mature Neurons. *PLoS ONE*, 7(6):e38651.

Thomson, J. A., Itskovitz-Eldor, J., Shapiro, S. S., Waknitz, M. A., Swiergiel, J. J., Marshall, V. S., and Jones, J. M. (1998). Embryonic stem cell lines derived from human blastocysts. *Science (New York, N.Y.)*, 282(5391):1145–7.

Thurston, V. C., Zinkowski, R. P., and Binder, L. I. (1996). Tau as a nucleolar protein in human nonneural cells in vitro and in vivo. *Chromosoma*, 105(1):20–30.

Togo, T. and Dickson, D. W. (2002). Ballooned neurons in progressive supranuclear palsy are usually due to concurrent argyrophilic grain disease. *Acta neuropathologica*, 104(1):53–6.

Tolnay, M. and Probst, A. (1998). Ballooned neurons expressing αB-crystallin as a constant feature of the amygdala in argyrophilic grain disease. *Neuroscience Letters*, 246(3):165–8.

Trabzuni, D., Wray, S., Vandrovcova, J., Ramasamy, A., Walker, R., Smith, C., Luk, C., Gibbs, J. R., Dillman, A., Hernandez, D. G., Arepalli, S., Singleton, A. B., Cookson, M. R., Pittman, A. M., De silva, R., Weale, M. E., Hardy, J., and Ryten, M. (2012). MAPT expression and splicing is differentially regulated by brain region: Relation to genotype and implication for tauopathies. *Human Molecular Genetics*, 21(18):4094–103.

Treutlein, B., Lee, Q. Y., Camp, J. G., Mall, M., Koh, W., Shariati, S. A. M., Sim, S., Neff, N. F., Skotheim, J. M., Wernig, M., and Quake, S. R. (2016). Dissecting direct reprogramming from fibroblast to neuron using single-cell RNA-seq. *Nature*, 534(7607):391–5.

Trevino, A. E. and Zhang, F. (2013). *Genome Editing Using Cas9*, volume 546. Elsevier Inc., 1 edition.

Tropepe, V., Hitoshi, S., Sirard, C., Mak, T. W., Rossant, J., and Van Der Kooy, D. (2001). Direct neural fate specification from embryonic stem cells: A primitive mammalian neural stem cell stage acquired through a default mechanism. *Neuron*, 30(1):65–78.

Tsai, S. Q., Zheng, Z., Nguyen, N. T., Liebers, M., Topkar, V. V., Thapar, V., Wyvekens, N., Khayter, C., Iafrate, A. J., Le, L. P., Aryee, M. J., and Joung, J. K. (2015). GUIDE-seq enables genome-wide profiling of off-target cleavage by CRISPR-Cas nucleases. *Nature Biotechnology*, 33(2):187–97.

Tucker, K. L., Meyer, M., and Barde, Y.-A. (2001). Neurotrophins are required for nerve growth during development. *Nat Neurosci.*, 4(1):29–37.

Uchihara, T. (2007). Silver diagnosis in neuropathology: principles, practice and revised interpretation. *Acta Neuropathologica*, 113(5):483–99.

Usenovic, M., Niroomand, S., Drolet, R. E., Yao, L., Gaspar, R. C., Hatcher, N. G., Schachter, J., Renger, J. J., and Parmentier-Batteur, S. (2015). Internalized Tau Oligomers Cause Neurodegeneration by Inducing Accumulation of Pathogenic Tau in Human Neurons Derived from Induced Pluripotent Stem Cells. *The Journal of Neuroscience*, 35(42):14234–50.

Vallier, L., Touboul, T., Brown, S., Cho, C., Bilican, B., Alexander, M., Cedervall, J., Chandran, S., Ahrlund-Richter, L., Weber, A., and Pedersen, R. A. (2009). Signaling pathways controlling pluripotency and early cell fate decisions of human induced pluripotent stem cells. *Stem Cell*, 27(11):2655–66.

Van Hummel, A., Bi, M., Ippati, S., Van Der Hoven, J., Volkerling, A., Lee, W. S., Tan, D. C., Bongers, A., Ittner, A., Ke, Y. D., and Ittner, L. M. (2016). No overt deficits in aged tau-deficient C57Bl/6.Mapttm1(EGFP)kitGFP knockin mice. *PLoS ONE*, 11(10):1–14.

van Swieten, J. C., Stevens, M., Rosso, S. M., Rizzu, P., Joosse, M., de Koning, I., Kamphorst, W., Ravid, R., Spillantini, M. G., Niermeijer, and Heutink, P. (1999). Phenotypic variation in hereditary frontotemporal dementia with tau mutations. *Annals of neurology*, 46(4):617–26.

Vanamee, É. S., Santagata, S., and Aggarwal, A. K. (2001). FokI requires two specific DNA sites for cleavage. *Journal of Molecular Biology*, 309(1):69–78.

Veres, A., Gosis, B. S., Ding, Q., Collins, R., Ragavendran, A., Brand, H., Erdin, S., Talkowski, M. E., and Musunuru, K. (2014). Low Incidence of Off-Target Mutations in Individual CRISPR-Cas9 and TALEN Targeted Human Stem Cell Clones Detected by Whole-Genome Sequencing. *Cell stem cell*, 15(1):27–30.

Verheyen, A., Diels, A., Reumers, J., Van Hoorde, K., Van den Wyngaert, I., van Outryve d'Ydewalle, C., De Bondt, A., Kuijlaars, J., De Muynck, L., De Hoogt, R., Bretteville, A., Jaensch, S., Buist, A., Cabrera-Socorro, A., Wray, S., Ebneth, A., Roevens, P., Royaux, I., and Peeters, P. J. (2018). Genetically Engineered iPSC-Derived FTDP-17 MAPT Neurons Display Mutation-Specific Neurodegenerative and Neurodevelopmental Phenotypes. *Stem Cell Reports*, 11(2):363–79.

von Bergen, M., Friedhoff, P., Biernat, J., Heberle, J., Mandelkow, E.-M., and Mandelkow, E. (2000). Assembly of tau protein into Alzheimer paired helical filaments depends on a local sequence motif (306VQIVYK311) forming beta structure. *Proceedings of the National Academy of Sciences*, 97(10):5129–34.

Wang, J.-Z. and Liu, F. (2008). Microtubule-associated protein tau in development, degeneration and protection of neurons. *Progress in neurobiology*, 85(2):148–75.

Wang, J. Z., Xia, Y. Y., Grundke-Iqbal, I., and Iqbal, K. (2012). Abnormal hyperphosphorylation of tau: Sites, regulation, and molecular mechanism of neurofibrillary degeneration. *Advances in Alzheimer's Disease*, 3:123–39.

Wang, Y., Balaji, V., Kaniyappan, S., Krüger, L., Irsen, S., Tepper, K., Chandupatla, R., Maetzler, W., Schneider, A., Mandelkow, E., and Mandelkow, E.-M. (2017). The release and trans-synaptic transmission of Tau via exosomes. *Molecular Neurodegeneration*, 12(1):5.

Wang, Y. and Mandelkow, E. (2015). Tau in physiology and pathology. *Nature reviews. Neuroscience*, 17(1):22–35.

Wang, Y., Wang, J., Gao, L., Lafyatis, R., Stamm, S., and Andreadis, A. (2005). Tau exons 2 and 10, which are misregulated in neurodegenerative diseases, are partly regulated by silencers which bind a SRp30c.SRp55 complex that either recruits or antagonizes htra2beta1. *The Journal of biological chemistry*, 280(14):14230–9.

Ward, S. M., Himmelstein, D. S., Lancia, J. K., Fu, Y., Patterson, K. R., and Binder, L. I. (2013). TOC1: Characterization of a selective oligomeric tau antibody. *Journal of Alzheimer's Disease*, 37(3):593–602.

Warmus, B. a., Sekar, D. R., McCutchen, E., Schellenberg, G. D., Roberts, R. C., McMahon, L. L., and Roberson, E. D. (2014). Tau-Mediated NMDA Receptor Impairment Underlies Dysfunction of a Selectively Vulnerable Network in a Mouse Model of Frontotemporal Dementia. *Journal of Neuroscience*, 34(49):16482–95.

Warren, N. M. and Burn, D. J. (2007). Progressive supranuclear palsy. *Practical Neurology*, 7:16–23.

Watanabe, K., Kamiya, D., Nishiyama, A., Katayama, T., Nozaki, S., Kawasaki, H., Watanabe, Y., Mizuseki, K., and Sasai, Y. (2005). Directed differentiation of telencephalic precursors from embryonic stem cells. *Nature Neuroscience*, 8(3):288–96.

Watts, G. D., Wymer, J., Kovach, M. J., Mehta, S. G., Mumm, S., Darvish, D., Pestronk, A., Whyte, M. P., and Kimonis, V. E. (2004). Inclusion body myopathy associated with Paget disease of bone and frontotemporal dementia is caused by mutant valosin-containing protein. *Nature Genetics*, 36(4):377–81.

Weaver, C. L., Espinoza, M., Kress, Y., and Davies, P. (2000). Conformational change as one of the earliest alterations of tau in Alzheimer's disease. *Neurobiology of aging*, 21(5):719–27.

Weingarten, M. D., Lockwood, A. H., Hwo, S.-Y., and Kirschner, M. W. (1975). A Protein Factor Essential for Microtubule Assembly. *Proc Natl Acad Sci USA.*, 72(5):1858–62.

Whitwell, J. L., Jack, C. R., and Ivnik, R. J. (2009). Atrophy patterns in IVS10+16, IVS10+3, N279K, S305N, P301L, and V337M MAPT mutations. *Neurology*, 73:1058–65.

Wilson, S. W. and Houart, C. (2004). Early Steps in the Development of the Forebrain. *Developmental Cell*, 6(2):167–81.

Wischik, C. M., Novak, M., Thøgersen, H. C., Edwards, P. C., Runswick, M. J., Jakes, R., Walker, J. E., Milstein, C., Roth, M., and Klug, a. (1988). Isolation of a fragment of tau derived from the core of the paired helical filament of Alzheimer disease. *Proceedings of the National Academy of Sciences of the United States of America*, 85(12):4506–10.

Wittmann, C. W. (2001). Tauopathy in Drosophila: Neurodegeneration Without Neurofibrillary Tangles. *Science*, 293(5530):711–4.

Wonders, C. P. and Anderson, S. A. (2006). The origin and specification of cortical interneurons. *Nature Reviews Neuroscience*, 7(9):687–96.

Wren, M. C., Zhao, J., Liu, C.-C., Murray, M. E., Atagi, Y., Davis, M. D., Fu, Y., Okano, H. J., Ogaki, K., Strongosky, A. J., Tacik, P., Rademakers, R., Ross, O. A., Dickson, D. W., Wszolek, Z. K., Kanekiyo, T., and Bu, G. (2015). Frontotemporal dementia-associated N279K tau mutant disrupts subcellular vesicle trafficking and induces cellular stress in iPSC-derived neural stem cells. *Molecular Neurodegeneration*, 10(1):46.

Wu, H., Xu, J., Pang, Z. P., Ge, W., Kim, K. J., Blanchi, B., Chen, C., Sudhof, T. C., and Sun, Y. E. (2007). Integrative genomic and functional analyses reveal neuronal subtype differentiation bias in human embryonic stem cell lines. *Proceedings of the National Academy of Sciences*, 104(34):13821–6.

Wu, J. W., Herman, M., Liu, L., Simoes, S., Acker, C. M., Figueroa, H., Steinberg, J. I., Margittai, M., Kayed, R., Zurzolo, C., Di Paolo, G., and Duff, K. E. (2013). Small misfolded tau species are internalized via bulk endocytosis and anterogradely and retrogradely transported in neurons. *Journal of Biological Chemistry*, 288(3):1856–70.

Wu, X., Scott, D. A., Kriz, A. J., Chiu, A. C., Hsu, P. D., Dadon, D. B., Cheng, A. W., Trevino, A. E., Konermann, S., Chen, S., Jaenisch, R., Zhang, F., and Sharp, P. A. (2014). Genome-wide binding of the CRISPR endonuclease Cas9 in mammalian cells. *Nature Biotechnology*, 32(7).

Xu, H., Rösler, T. W., Carlsson, T., de Andrade, A., Bruch, J., Höllerhage, M., Oertel, W. H., and Höglinger, G. U. (2014). Memory deficits correlate with tau and spine pathology in P301S MAPT transgenic mice. *Neuropathology and Applied Neurobiology*, 40(7):833–43.

Yamaguchi, H., Ishiguro, K., Uchida, T., Takashima, A., Lemere, C. A., and Imahori, K. (1996). Preferential labeling of Alzheimer neurofibrillary tangles with antisera for tau protein kinase (TPK) I/glycogen synthase kinase-3β and cyclin-dependent kinase 5, a component of TPK II. *Acta Neuropathologica*, 92(3):232–41.

Yan, Y., Song, L., Bejoy, J., Zhao, J., Kanekiyo, T., Bu, G., Zhou, Y., and Li, Y. (2018). Modeling Neurodegenerative Microenvironment Using Cortical Organoids Derived from Human Stem Cells. *Tissue Engineering Part A*, 24(13-14):1125–37.

Yang, L., Guell, M., Byrne, S., Yang, J. L., De Los Angeles, A., Mali, P., Aach, J., Kim-Kiselak, C., Briggs, A. W., Rios, X., Huang, P. Y., Daley, G., and Church, G. (2013). Optimization of scarless human stem cell genome editing. *Nucleic Acids Research*, 41(19):9049–61.

Yang, L., Yang, J. L., Byrne, S., Pan, J., and Church, G. M. (2014). CRISPR/Cas9-Directed Genome Editing of Cultured Cells. *Current protocols in molecular biology*, 107(July):31.1.1–17.

Yang, S., Kuan, W.-L., and Spillantini, M. G. (2016). Progressive tauopathy in P301S tau transgenic mice is associated with a functional deficit of the olfactory system. *European Journal of Neuroscience*, 44(6):2396–403.

Yao, T.-M. (2003). Aggregation Analysis of the Microtubule Binding Domain in Tau Protein by Spectroscopic Methods. *Journal of Biochemistry*, 134(1):91–9.

Yin, X., Jin, N., Gu, J., Shi, J., Zhou, J., Gong, C.-X., Iqbal, K., Grundke-Iqbal, I., and Liu, F. (2012). Dual-specificity tyrosine phosphorylation-regulated kinase 1A (Dyrk1A) modulates serine/arginine-rich protein 55 (SRp55)-promoted Tau exon 10 inclusion. *The Journal of biological chemistry*, 287(36):30497–506.

Yoshii, A. and Constantine-Paton, M. (2010). Postsynaptic BDNF-TrkB signaling in synapse maturation, plasticity, and disease.

Yoshiyama, Y., Higuchi, M., Zhang, B., Huang, S. M., Iwata, N., Saido, T. C. C., Maeda, J., Suhara, T., Trojanowski, J. Q., and Lee, V. M. (2007). Synapse Loss and Microglial Activation Precede Tangles in a P301S Tauopathy Mouse Model. *Neuron*, 53(3):337–51.

Yu, J., Vodyanik, M., Smuga-Otto, K., Antosiewicz-Bourget, J., Frane, J. L., Tian, S., Nie, J., Jonsdottir, G. a., Ruotti, V., Stewart, R., Slukvin, I. I., and Thomson, J. a. (2007). Induced pluripotent stem cell lines derived from human somatic cells. *Science*, 318(5858):1917–20.

Yu, Q., Guo, J., and Zhou, J. (2004). A minimal length between tau exon 10 and 11 is required for correct splicing of exon 10. *Journal of Neurochemistry*, 90(1):164–72.

Zempel, H., Dennissen, F. J., Kumar, Y., Luedtke, J., Biernat, J., Mandelkow, E. M., and Mandelkow, E. (2017). Axodendritic sorting and pathological missorting of Tau are isoform-specific and determined by axon initial segment architecture. *Journal of Biological Chemistry*, 292(29):12192–207.

Zempel, H. and Mandelkow, E. (2014). Lost after translation: Missorting of Tau protein and consequences for Alzheimer disease. *Trends in Neurosciences*, 37(12):721–32.

Zhang, X. H.-F., Kangsamaksin, T., Chao, M. S. P., Banerjee, J. K., and Chasin, L. A. (2005). Exon inclusion is dependent on predictable exonic splicing enhancers. *Molecular and cellular biology*, 25(16):7323–32.

Zhang, Y., Pak, C. H., Han, Y., Ahlenius, H., Zhang, Z., Chanda, S., Marro, S., Patzke, C., Acuna, C., Covy, J., Xu, W., Yang, N., Danko, T., Chen, L., Wernig, M., and Südhof, T. C. (2013). Rapid single-step induction of functional neurons from human pluripotent stem cells. *Neuron*, 78(5):785–98.

Zhang, Z.-N., Freitas, B. C., Qian, H., Lux, J., Acab, A., Trujillo, C. A., Herai, R. H., Nguyen Huu, V. A., Wen, J. H., Joshi-Barr, S., Karpiak, J. V., Engler, A. J., Fu, X.-D., Muotri, A. R., and Almutairi, A. (2016). Layered hydrogels accelerate iPSC-derived neuronal maturation and reveal migration defects caused by MeCP2 dysfunction. *Proceedings of the National Academy of Sciences*, 113(12):3185–90.

Zheng-Fischhofer, Q., Biernat, J., Mandelkow, E.-M., Illenberger, S., Godemann, R., and Mandelkow, E. (1998). Sequential phosphorylation of Tau by glycogen synthase kinase-3beta and protein kinase A at Thr212 and Ser214 generates the Alzheimer-specific epitope of antibody AT100 and requires a paired-helical-filament-like conformation. *European Journal of Biochemistry*, 252(3):542–52.

Zheng-Fischhöfer, Q., Biernat, J., Mandelkow, E. M., Illenberger, S., Godemann, R., and Mandelkow, E.-m. (1998). Sequential phosphorylation of Tau by glycogen synthase kinase-3beta and protein kinase A at Thr212 and Ser214 generates the Alzheimer-specific epitope of antibody AT100 and requires a paired-helical-filament-like conformation. *European journal of biochemistry*, 252(3):542–52.

Zhong, Q., Congdon, E. E., Nagaraja, H. N., and Kuret, J. (2012). Tau isoform composition influences rate and extent of filament formation. *Journal of Biological Chemistry*, 287(24):20711–9.

Zollino, M., Orteschi, D., Murdolo, M., Lattante, S., Battaglia, D., Stefanini, C., Mercuri, E., Chiurazzi, P., Neri, G., and Marangi, G. (2012). Mutations in KANSL1 cause the 17q21.31 microdeletion syndrome phenotype. *Nature Genetics*, 44(6):636–8.

Appendix A

Off-target matches with CRISPR 3

top 20 genome-wide off-target sites

sequence	score	mismatches	locus
GCAGATTATTAATAAGAAACTGG	2.2	2MMs [7:19]	chr1:-181032461
AAAGATAATTAATAAGAAGTCAG	1.5	3MMs [1:2:20]	chr2:-141666720
GTAGATATTTATTAAGAAGCAGG	1.4	3MMs [2:8:12]	chr6:-151579733
GCAGATAGAGAATAAGAAGCAGG	1.3	3MMs [8:9:10]	chr4:-90762062
ATAGATAATTAAAAAGAAGCTGG	1.2	3MMs [1:2:13]	chr4:+141154072
ACAAATAATTAATAAGAATCCAG	1.1	3MMs [1:4:19]	chr3:-82054462
TGGGCCCATGGCACGTGTGAGGG	0.4	4MMs [1:2:6:12]	chr17:+79066042
ACAGAGCAGGGAACGTGTGAGGG	0.4	4MMs [3:5:9:12]	chr10:-46526565
ACAGAGCAGGGAACGTGTGAGGG	0.4	4MMs [3:5:9:12]	chr10:-48713910
AGGGTGCATAGGACATGTGACAG	0.4	4MMs [2:5:10:15]	chr12:-6888430
ACCGTGCAGGGGTCGTGTGACAG	0.3	4MMs [3:5:9:13]	chr15:+69223364
ACGGTGTAAGGGACGTGTGCCGG	0.3	4MMs [5:7:9:20]	chr15:+93631863
ACCCCGGATGGGACCTGTGACAG	0.3	4MMs [3:4:7:15]	chr15:+85427656
AAGCCTCATGGGACATGTGATGG	0.2	4MMs [2:4:6:15]	chr21:-24382838
ACGCCGCACGTGACGTGTGCTGG	0.2	4MMs [4:9:11:20]	chr9:-96793030
ACGGCCCAAAGGACGTGTCAAGG	0.2	4MMs [6:9:10:19]	chr6:+35458132
ACGGAAGATGGGACCTGTGAAGG	0.2	4MMs [5:6:7:15]	chr9:+138282512
GCAGCGCATGGGGCCTGTGAAAG	0.2	4MMs [1:3:13:15]	chr7:+157021752
ATGGAGCATGGGCCTTGTGATAG	0.2	4MMs [2:5:13:15]	chr2:-129255057
ACACCGCAAGGGAAGTGTGAGAG	0.1	4MMs [3:4:9:14]	chr4:-130315571
ACAGCGCTTGGGACGTGGGGAGG	0.1	4MMs [3:8:18:20]	chr16:+89373360
ACAGTCCATGGGAGGTGTGAAGG	0.1	4MMs [3:5:6:14]	chr8:+134229566
ACGGCGCAGGGGACGCGTGGGGG	0.1	3MMs [9:16:20]	chr11:+65547883
ACAGTGCATGGGATGTGTGGGAG	0.1	4MMs [3:5:14:20]	chr8:+93859512
ACAGTGCATGGGAAGTGTGGGGG	0.1	4MMs [3:5:14:20]	chr11:-126134824
ACGGCCAGTGGGAAGTGTGATGG	0.1	4MMs [6:7:8:14]	chr16:+81751752
ACTGAGCATGGGCGGTGTGACGG	0.1	4MMs [3:5:13:14]	chr2:-129231264
ACGGCTCAAGAGACTTGTGAAAG	0.1	4MMs [6:9:11:15]	chr2:+102966539
ACGGCACCTGAGATGTGTGAGAG	0.1	4MMs [6:8:11:14]	chr4:+60404216
ACGGCAGATGGGACTTTTGAGAG	0.1	4MMs [6:7:15:17]	chr11:+62437246
ACGGTGTATGGGACCTGGGAGGG	0.1	4MMs [5:7:15:18]	chr16:+12219312
ACGGCACAGGTGATGTGTGATGG	0.0	4MMs [6:9:11:14]	chr1:-151545272
ACGGTGCCTGGGAGGGGTGATGG	0.0	4MMs [5:8:14:16]	chrY:-10038484
ACGGGGCATGGGAGGTTTGCAGG	0.0	4MMs [5:14:17:20]	chr20:-896519
ACGGACCATGGGAGATGTGAGAG	0.0	4MMs [5:6:14:15]	chr9:-100122790
ACGGCTCCTGGGATCTGTGACAG	0.0	4MMs [6:8:14:15]	chr4:-189515141
ACGTCCCATGGGATGTGGGAAAG	0.0	4MMs [4:6:14:18]	chr20:-25202030
AGGGCACATGGGAGGCGTGAGGG	0.0	4MMs [2:6:14:16]	chr7:-44257760
ACGGCGCAGGGTACCTGAGACAG	0.0	4MMs [9:12:15:18]	chr9:+137520053
ACGGCGCAGGGTACACGTGAGAG	0.0	4MMs [9:12:15:16]	chr8:+124630075
ACGGCGCAGGTGATGTGAGAGGG	0.0	4MMs [9:11:14:18]	chr1:+19792962

Fig. A.1 **Top 20 predicted off-target sites for CRISPR 3 gRNA.** The sequence and chromosomal location of the 20 closest matches to CRISPR 3 gRNA, excluding the intended target, tau exon 10. The number and location of mismatches between the gRNA and the endogenous DNA are indicated. Higher scores indicate higher predicted likelyhood of off-target effects at the listed locus. Off-target predictions are from MIT CRISPR design tool.

Appendix B

NPC-derived monolayer neurons from IsoCon and P301Lhet iPSCs

Isogenic control (IsoCon), the corresponding knock-in P301L-heterozgyous (P301Lhet), and unrelated non-isogenic control 6 (Con6) iPSC-derived NPCs were gifted by Axol. The NPCs were differentiated to neurons and maintained in culture for 21 days (approximately 41 days after iPSCs, referred to here as day 41) or 40 days (approximately 60 days after iPSCs, referred to here as day 60). The aim was to compare the knock-in P301Lhet neuron phenotype with that of neurons carrying the same mutation obtained from an individual suffering from FTDP-17T (Iovino et al., 2015), and to compare the effects of two types of maturation media on the Con6 neurons (data not shown).

B.1 Confirmation of genotype in IsoCon and P301Lhet neurons

To confirm the presence of the heterozygous P301L mutation in the P301Lhet neurons, and to confirm its absence in the IsoCon and Con6 neurons, DNA was extracted from neurons derived from the first set of NPCs received, and a 650bp fragment containing tau exon 10 was amplified by PCR. DNA was subjected to restriction digest with Sma1, which digests wild-type, but not P301L mutant DNA. IsoCon and Con6 DNA from the first set of cells received was completely digested to 350 and 300bp fragments by Sma1 (see Figure B.1A), indicating the absence of the P301L mutation. P301L DNA from the first set of cells was partially digested by Sma1, confirming the presence of the heterozygous P301L mutation (see Figure B.1A).

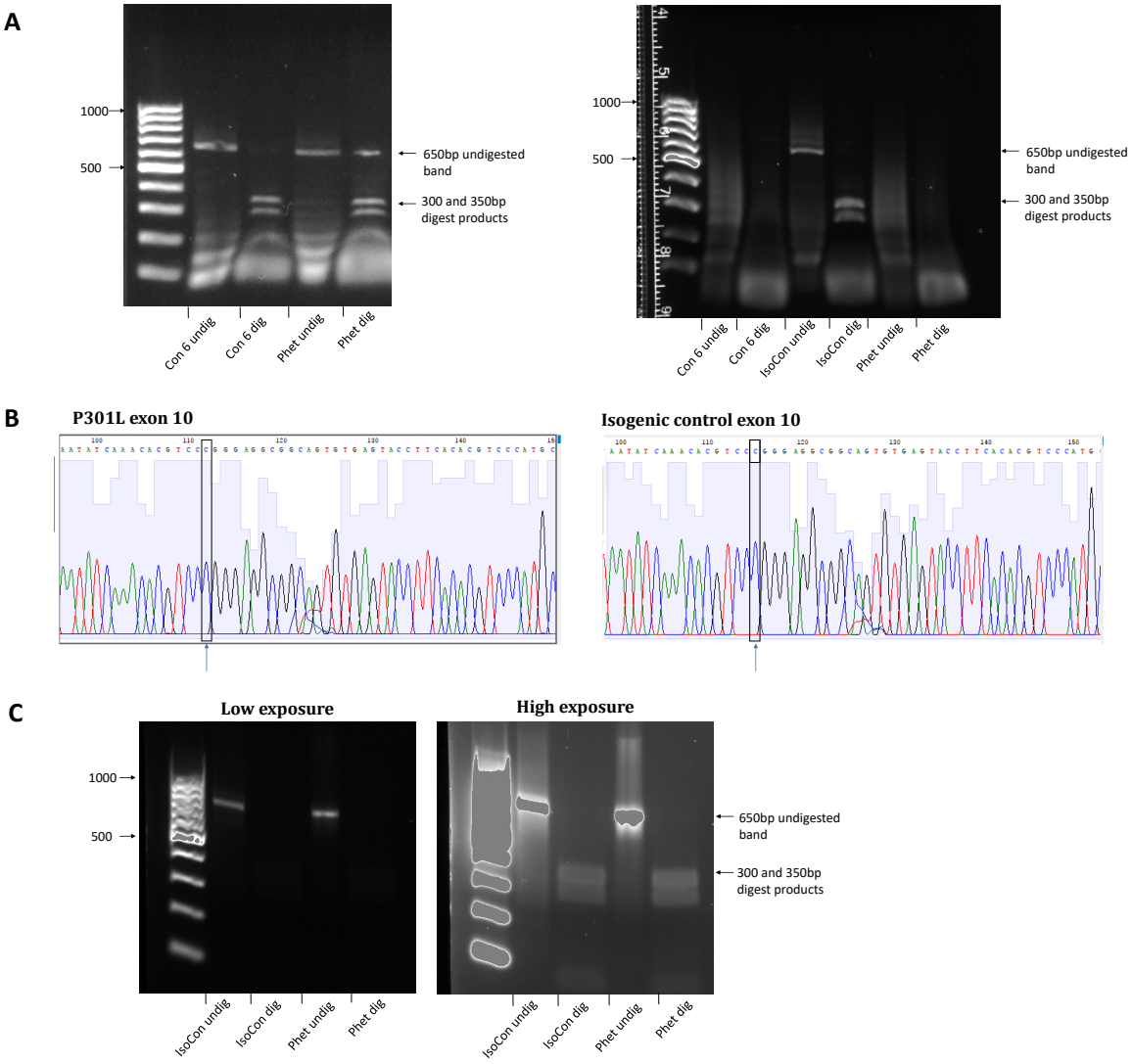

Fig. B.1 **Sanger sequencing and restriction digest to assess the P301L mutation locus in IsoCon, P301Lhet and Con6 neurons. A)** 650 base pairs (bps) of DNA containing exon 10 amplified from neurons derived from the first set of Con6, IsoCon and P301Lhet cells received, digested with Sma1. **B)** Sanger sequencing results from DNA amplified from neurons derived from the second set of Con6, IsoCon and P301Lhet cells received. **C)** 650bps of DNA containing exon 10 amplified from neurons derived from the second set of Con6, IsoCon and P301Lhet cells received, digested with Sma1.

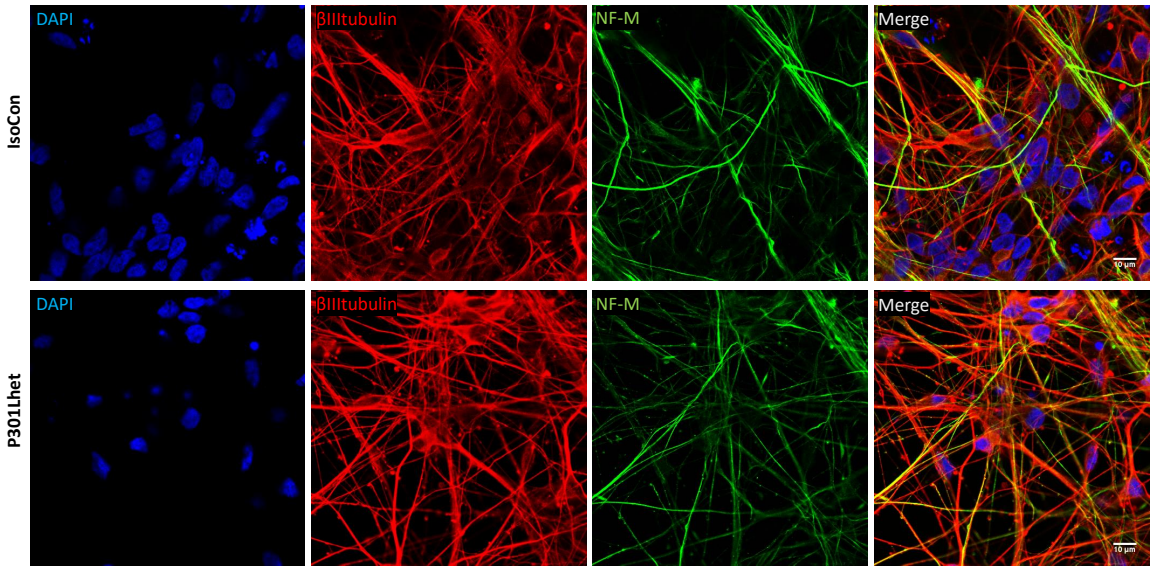

Fig. B.2 **The cytoskeletal proteins neurofilament-M and βIII-tubulin in 41 day-old IsoCon and P301Lhet NPC-derived neurons.** IsoCon and P301Lhet neurons immunostained for βIII-tubulin and neurofilament-M (NF-M). Scale bar = 10µm.

This procedure was repeated using DNA extracted from neurons derived from the second set of NPCs received. IsoCon and P301Lhet DNA was completely digested to 350 and 300bp fragments by Sma1 (see Figure B.1C), indicating the absence of the P301L mutation. DNA from neurons derived from the second set of NPCs was amplified again by PCR and sequenced by Sanger sequencing. Both control and P301L sequences showed a control sequence without the P301L mutation (see Figure B.1B). In the P301L case, base C (indicated by an arrow in Figure B.1B) should be accompanied by base T. DNA preparation and sequencing was repeated twice and gave the same result.

This indicates that the P301L mutation was present in neurons derived from NPCs provided for the first set of experiments, but not the second set. Therefore, all IsoCon and P301Lhet results presented are from the same differentiation round, and no independent differentiation rounds can corroborate results from P301Lhet neurons.

B.2 Cytoskeleton proteins in IsoCon and P301Lhet neurons

The cytoskeletal proteins neurofilament-M and βIII-tubulin were present in IsoCon and P301Lhet neuronal processes after 21 days in culture (41 days after iPSCs), indicating the differentiation of NPCs to neurons (see Figure B.2).

B.3 Tau isoforms in IsoCon and P301Lhet neurons

At day 41, 3R tau was detected in cell bodies and processes in both IsoCon and P301Lhet neurons by immunofluorescence (see Figure B.3A). 4R tau was detected in cell bodies and some processes in both IsoCon and P301Lhet neurons by immunofluorescence (see Figure B.3B). 4R tau was present in low amounts, so signal was amplified using biotin and fluorescently-conjugated streptavidin. There was no clear difference in fluorescence intensity between IsoCon and P301Lhet neurons. This was expected, since the P301L mutation does not alter exon 10 inclusion (Hasegawa et al., 1999; Hong, 1998; Hutton et al., 1998).

Immunofluorescence results were corroborated by Western blotting. Tau was extracted from 41 day-old IsoCon and P301Lhet neurons using perchloric acid, in which tau is selectively soluble (Lindwall and Cole, 1984), and extracts were dialysed in Tris-HCl. Samples from each protein extract were dephosphorylated with alkaline phosphatase from E.coli (dephos in Figure B.4) and loaded next to phosphorylated samples (phos in Figure B.4). Faint bands corresponding to 0N3R tau were visible in the P301Lhet and IsoCon lanes at low exposure (Figure B.4A), and at higher exposure Figure B.4B and C), but no other tau isoforms were visible. This suggests that mostly immature neurons, expressing the fetal 0N3R tau isoform, were present at day 41, and that levels of 4R tau were too low to detect by Western blot.

B.4 Tau phosphorylation at Ser202 and Thr205 (AT8) in IsoCon and P301Lhet neurons

Tau phosphorylation at the AT8 epitope (at Ser202 and Thr205) occurs in both FTDP-17T and fetal brains (Brion et al., 1993; Spillantini et al., 1996a). AT8 positive tau was assessed by immunostaining (amplifying AT8 signal with biotin and fluorescently-conjugated streptavidin) and counting the proportion of AT8 positive neurons. Some AT8 positive

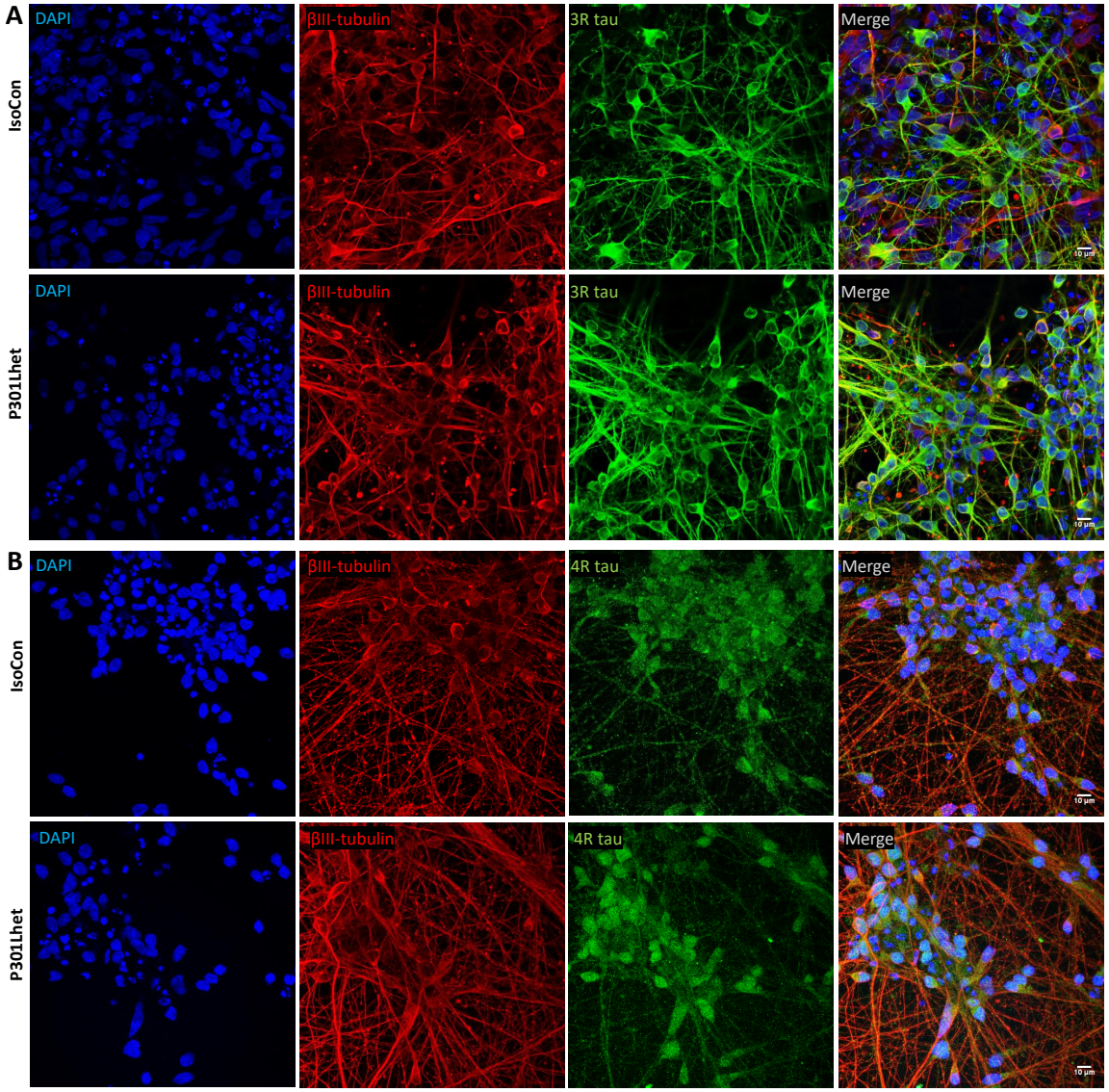

Fig. B.3 **3R and 4R tau in day 41 IsoCon and P301Lhet neurons. A)** 3R tau or **B)** 4R tau in day 41 IsoCon and P301Lhet neurons after 41 day-old neurons, co-stained for βIII-tubulin. Scale bar = 10µm.

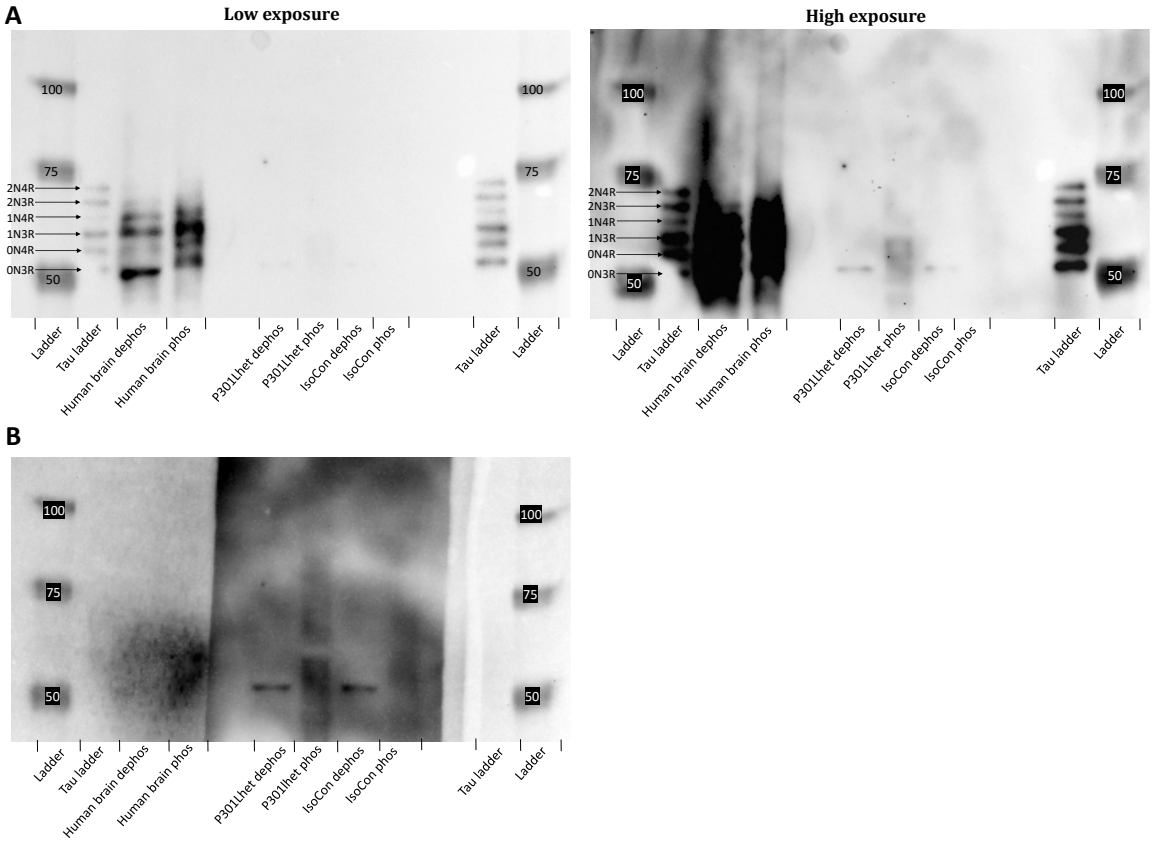

Fig. B.4 **Tau isoforms in 41 day-old IsoCon and P301Lhet neurons detected by Western blot. A)** Low exposure, **B)** higher exposure, and **C)** highest exposure of the same blot. Dephosphorylated samples were loaded next to phosphorylated samples, and recombinant tau isoforms (tau ladder) and control human brain extract were used as positive controls for tau isoforms. The membrane was probed with an antibody against total tau.

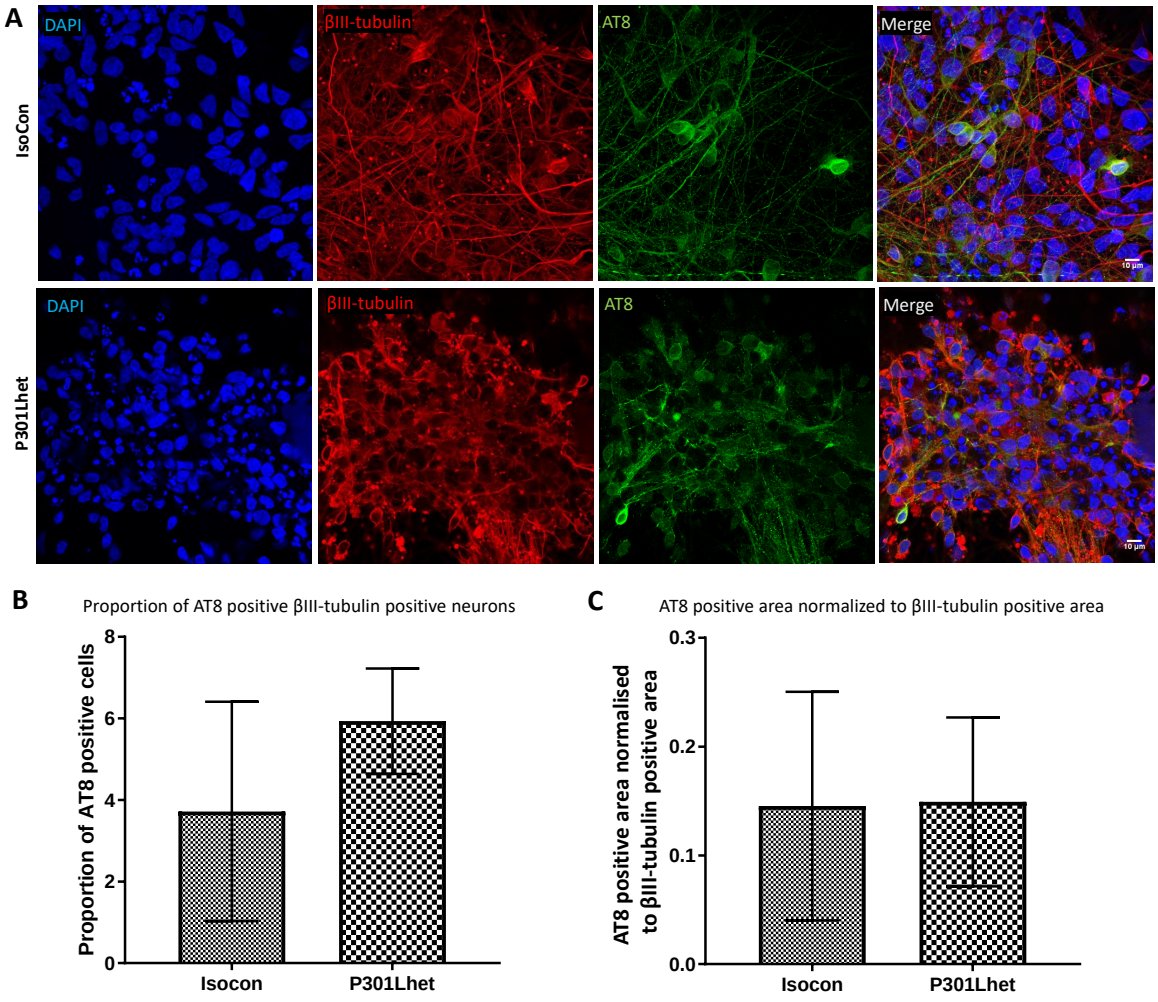

Fig. B.5 **Tau phosphorylation at the AT8 epitope in IsoCon and P301Lhet neurons. A)** 41 day-old IsoCon and P301Lhet neurons stained for AT8 and βIII-tubulin. Scale bar = 10 µm. **B)** The proportion of AT8 positive, βIII-tubulin positive neurons in IsoCon and P301Lhet cultures. Bars show the average of 3 technical replicates, error bars show the standard deviation. **C)** The ratio of the AT8 positive area to the βIII-tubulin positive area measured in IsoCon and P301Lhet cultures. Bars show the average of 3 technical replicates, error bars show SD.

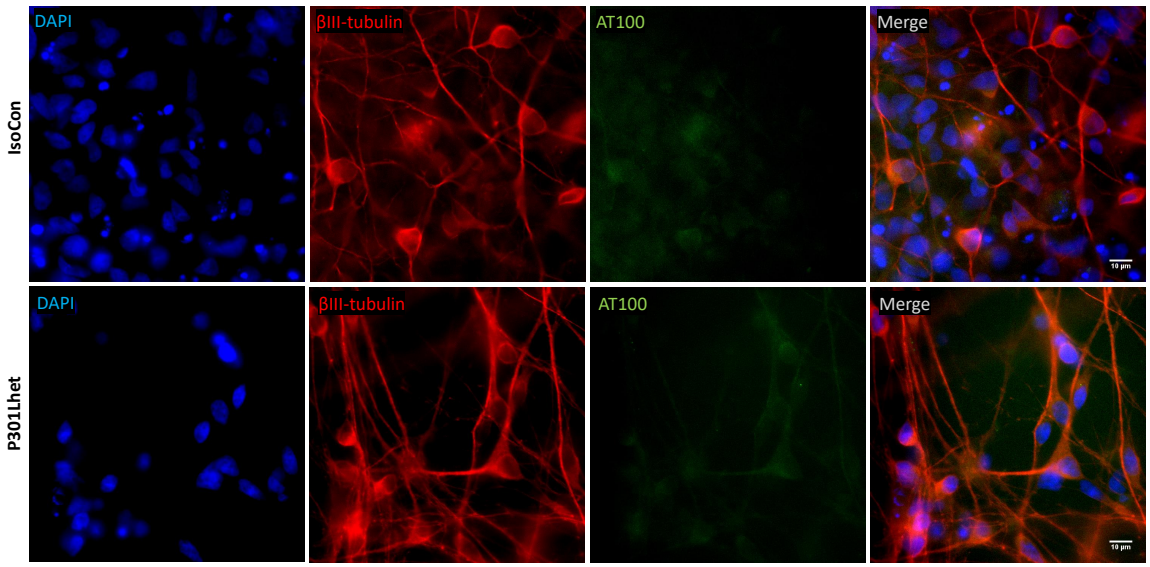

Fig. B.6 **No tau phosphorylation at the AT100 epitope in IsoCon and P301Lhet neurons.** IsoCon and P301Lhet neurons immunostained for AT100 and βIII-tubulin. Scale bar = 10µm.

neurons were detected in both IsoCon and P301Lhet cultures, mostly in cell bodies (see Figure B.5A). The proportion of AT8 positive neurons and the AT8 positive areas was not significantly different between the IsoCon and P301Lhet neurons (see Figure B.5B and C).

This is at odds with findings using 55 day-old neurons derived from a different control iPSC line and a different P301L iPSC line, in which there were significantly more AT8 positive P301L neurons (Iovino et al., 2015). However, results presented here were from only one differentiation, and would require replicating to confidently reach a conclusion.

B.5 Tau phosphorylation at Thr212 and Ser214 (AT100) in IsoCon and P301Lhet neurons

Phosphorylation and conformational changes which result in the AT100 epitope (Thr212 and Ser214) being presented occur in tauopathies, but not fetal brains (Matsuo et al., 1994; Rizzini et al., 2000). Tau phosphorylation at the AT100 epitope was not detected in 41 day-old IsoCon or P301Lhet neurons by immunofluorescence (see Figure B.6). This was expected, since AT100 positive tau was not observed in P301L mutant neurons from another iPSC line, even after 150 days (Iovino et al., 2015).

B.6 α-synuclein and βIII-tubulin positive puncta and loops in neuronal processes of IsoCon and P301Lhet neurons

α-synuclein positive, βIII-tubulin positive puncta and loops in neuronal processes were detected in P301L cultures by Iovino et al. (2015). To see if this phenotype was also present in P301Lhet cultures, I immunostained 41 day-old P301Lhet and IsoCon cultures for α-synuclein and βIII-tubulin, and counted the number of positive puncta (see Figure B.7A). More α-synuclein positive, βIII-tubulin positive puncta were found in P301Lhet neuronal processes than in IsoCon, but the number of "loops" in neuronal processes was similar between the two lines (see Figure B.7B).

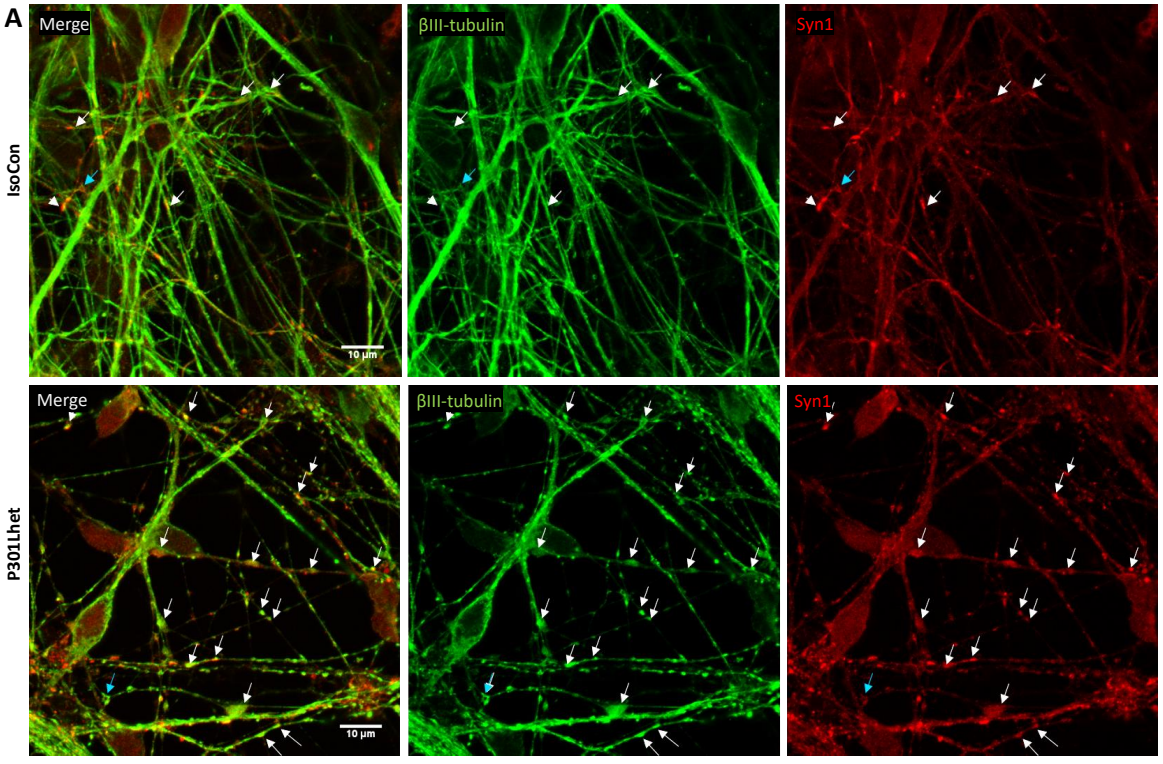

B

NPC-derived neuron genotype	Average number of βIII-tubulin and syn1 positive puncta	Average number of βIII-tubulin and syn1 positive loops
P301L-heterozygous	13.7	2
Isogenic control	1.3	1

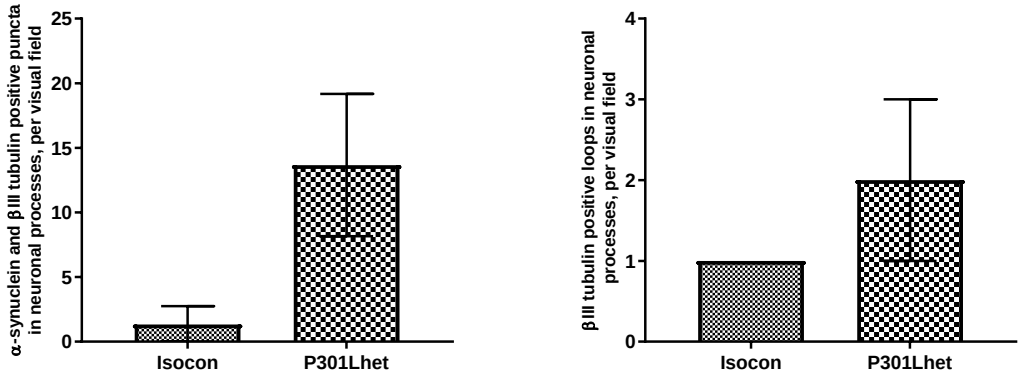

Fig. B.7 **α-synuclein positive, βIIItubulin positive puncta and loops in processes. A)** IsoCon) and P301Lhet neurons immunostained to show α-synuclein (Syn1) positive, βIII-tubulin positive puncta (white arrows) and loops (blue arrows) in neuronal processes. Scale bar = 10µm. **B)** The number of α-synuclein and βIII-tubulin positive puncta and loops were counted, blinded to genotype, in z-stack images taken 0.2 µm apart on a confocal microscope. The table shows the average of 3 technical replicates. Graphs show the average of the 3 technical (bar) and standard deviation (error bars).